

**BIRLA CENTRAL LIBRARY**

**PILANI (Rajasthan)**

Class No.: 621.384185

Book No.: M86R

Accession No.: 50563







**INTERNATIONAL MONOGRAPHS  
ON RADIO**

*General Editors*

**SIR EDWARD APPLETON *and* HENRY G. BOOKER**



# RADIO AERIALS

BY

E. B. MOULLIN, M.A., Sc.D.

FELLOW OF KING'S COLLEGE, CAMBRIDGE AND  
PROFESSOR OF ELECTRICAL ENGINEERING  
IN THE UNIVERSITY  
FORMERLY FELLOW OF MAGDALEN COLLEGE,  
OXFORD

OXFORD  
AT THE CLARENDON PRESS  
1949

*Oxford University Press, Amen House, London E.C.4*

GLASGOW NEW YORK TORONTO MELBOURNE WELLINGTON

BOMBAY CALCUTTA MADRAS CAPE TOWN

*Geoffrey Cumberlege, Publisher to the University*

PRINTED IN GREAT BRITAIN

## PREFACE

I HAVE been writing this book, off and on, for the last six years. Now that it is all in print, the preface must be written and should describe my aims in writing the book. It is hard to recall now precisely why I embarked on this stupendous task in 1943. Probably it was due to exasperation at not having the various standard cases of aerial design set out in a book, either for the convenience of my own reference or to assist in explanation to others.

The general scheme is to set out very fully the solution of a large number of special solutions of Maxwell's equations and to show how they can be used to guide the experimental work on which all practical designs of aerials must ultimately rest.

It is bad practice to start on experimental work before having thought out what the experiment is likely to show: unless this is done much time will be wasted and it is likely that the experimental results will not be capable of general interpretation. The performance of most aerials approximates very closely to the known solution of some idealized problem, and therefore the standard solutions set out here are a great help in practice.

This work is intended mainly as a hand-book to assist in the design and testing of short-wave aerials and it contains a large amount of experimental work. But in addition to this use, much of the earlier chapters should be helpful to students of electromagnetic theory, independently of whether or not they expect to do practical work on aerials: thus it is intended, in part, as a students' text-book.

Though this is a large book it does not attempt to cover all aspects of aerial design and it does not even cover the whole of the aspects with which it does deal. I have always been disinclined to write about anything of which I have not had personal experience and for this reason I have scarcely touched on problems I have not worked at.

The book contains a great deal of mathematical analysis: all of it is straightforward work which could have been done any time these last sixty years: though sometimes rather intricate, it is all elementary in the sense of not requiring any special skill or novelty of method. There is no reason to expect that there is any of it which has not been worked out, at least in part, by someone else previously. Because it is proper to regard the analysis as elementary I have not attempted to search out previous publications of the solutions I have derived myself. But I

believe I have not failed to make acknowledgement of every occasion on which I have obtained help from previously published work.

When the book had been completed, the Editors of this series suggested that I should convert all the analysis into M.K.S. units. Though quite willing in principle to do so I found it was impracticable to do it at that late stage: had the attempt been made I feel sure that many slips and errors would have crept in. Thus it was decided to leave it as it had been written.

This book was started and most of it was written in the Trafford Park Laboratories of Messrs. Metropolitan-Vickers Electrical Co. Ltd. Without the ideal conditions, the experimental facilities, and the kindness and help of my colleagues at Trafford Park it never could have been written. I take this opportunity to record my ever-grateful thanks to the Company and especially to Sir Arthur Fleming for the encouragement he gave me and for allowing me the privilege of spending three extremely happy years working under his direction.

E. B. M.

ENGINEERING LABORATORY,  
CAMBRIDGE

*April, 1949*

# CONTENTS

## CHAPTER I. ELECTROMAGNETIC FIELD OF CURRENT FILAMENT AND PLANES

1.1. Preliminary	1
1.2. Brief survey of the steady current problem	1
1.3. The Maxwell hypothesis	7
1.4. Maxwell's equations in free space	13
1.5. Lorentz's equation and retarded potentials	15
1.6. Fields due to a very small closed circuit	21
1.7. Field of a long filament carrying a current $I \sin pt$	28
1.8. Field of a tubular current of any radius	37
1.9. Field of a filament carrying current $I \cos(\pi y/g) \sin pt$	38
1.10. Field of a current $I \cos by \sin pt$ distributed round a tube of radius $R$	44
1.11. Vector potential of a blade of current	44
1.12. Field of a pair of like current filaments	45
1.13. Field of a pair of oppositely directed filaments	48
1.14. Field of an isolated filament referred to an origin not on the wire	50
1.15. Field of a long solenoid	51
1.16. Field of a line doublet	54

### PLANAR PROBLEMS

1.17. Field of an infinite sheet carrying uniform current density	55
1.18. Field of infinite sheet carrying current density which varies periodically across its width	58
1.19. Infinite plane grid of parallel wires	62
1.20. Current filament between two parallel conducting planes.	64

### SUNDRY PROBLEMS IN THREE DIMENSIONS

1.21. Field of an electric doublet	66
1.22. Radiation resistance of a half-wave aerial	70
1.23. Circle of radius $R$	72
1.24. Two similar and coaxial circles with planes parallel	78
1.25. Field of a ring doublet	78

## CHAPTER II. CERTAIN STANDARD DIFFRACTION PATTERNS AND POLAR DIAGRAMS AND POWER GAIN OF CERTAIN ARRAYS

2.1. The basic idea	81
2.2. Curtain array with side spacing $\frac{1}{2}\lambda$	82
2.3. Curtain array with non-uniform cophased loading	85
2.4. Curtain array with 'triangular' loading	86
2.5. Curtain array with sinusoidal loading	89
2.6. Curtain array with spacing $\frac{1}{2}\lambda$ and binomial loading	90
2.7. Method of turning the main beam away from the normal	93
2.8. In-line arrays	97
2.9. Pattern at any angle of elevation for curtain array	99
2.10. The power gain of aerials	100
2.11. Power gain of two parallel half-wave aerials separated by $\frac{1}{2}\lambda$ carrying equal and cophased current	101
2.12. Power gain of two parallel half-wave aerials with equal currents in phase quadrature	102



2.13. Power gain of three parallel and cophased half-wave aerials . . . . .	103
2.14. Power gain of four parallel cophased half-wave aerials . . . . .	104
2.15. Power gain of eight parallel cophased half-wave aerials . . . . .	104
2.16. Limiting output for very wide curtain of half-wave aerials . . . . .	105
2.17. Empirical formula for power gain of curtain of $N$ half-wave aerials . . . . .	105
2.18. Power gain when loading is not uniform . . . . .	105
2.19. Power gain of in-line arrays . . . . .	106
2.20. Power gain of a high curtain . . . . .	110
2.21. Curtain of single half-wave aerials in which alternate elements are in anti-phase: prototype of Yagi arrays. . . . .	111
2.22. Poynting's theorem . . . . .	113

### CHAPTER III. AERIALS IN THE PRESENCE OF INFINITELY EXTENDED FLAT SHEET REFLECTORS

3.1. Introduction . . . . .	118
3.2. Current filament parallel to an infinite and perfectly conducting plane . . . . .	119
(a) Density of current induced in the sheet . . . . .	122
3.3. Pair of reflecting sheets at right angles . . . . .	125
3.4. Reflecting plates inclined at any angle . . . . .	127
3.5. The curves of forward field . . . . .	133
(a) The general form of the Bessel function $J_n(z)$ . . . . .	137
(b) Curve of forward field expressed in a Bessel series . . . . .	139
3.6. Radiation resistance of a filament in a Vee reflector . . . . .	144
3.7. Power gain of long in-line array in a Vee reflector . . . . .	150
3.8. The shape of the diffraction pattern . . . . .	154
3.9. Principle of improving the shape of the pattern by addition of a 'parasitic' aerial . . . . .	160
3.10. Method of turning aside the main beam produced by a Vee reflector . . . . .	161
3.11. The diffraction pattern at a finite distance. . . . .	165
3.12. Reciprocal properties of Vee mirrors: . . . . .	167
(a) Two simple reciprocities . . . . .	167
(b) Less simple reciprocities . . . . .	168
(c) Reciprocity in power gain . . . . .	168

### CHAPTER IV. HALF-WAVE AERIAL COMBINED WITH VEE REFLECTOR

4.1. Introduction . . . . .	171
4.2. The radiation figure at a great distance . . . . .	171
4.3. Radiation resistance as a function of $k$ . . . . .	172
4.4. Power gain as a function of $k$ . . . . .	175
4.5. Some solid models of radiation figures . . . . .	177
4.6. Half-wave aerial with axis perpendicular to the junction line of reflecting sheets . . . . .	181
4.7. Frequency consciousness of aerials in Vee reflectors . . . . .	183
4.8. Line doublets in Vee reflectors . . . . .	184
(a) Line doublet parallel to an infinite conducting sheet . . . . .	184
(b) Line doublet referred to any origin . . . . .	186
4.9. An aerial in a rectangular wave guide . . . . .	186

### CHAPTER V. THE SEMI-INFINITE SHEET: NETWORK REFLECTORS

5.1. Introduction . . . . .	188
5.2. Long current filament in the presence of a half-plane . . . . .	188
5.3. Curtain array parallel to a half-plane . . . . .	196
5.4. Effect of bounding edge on the forward field . . . . .	199

# CONTENTS

ix

5.5. Density of current induced in each side of the sheet . . . . .	199
5.6. Screening properties of a grid of parallel wires . . . . .	203
5.7. Screening qualities of a squirrel cage of wires . . . . .	207
5.8. Three simple problems of rod reflectors: . . . . .	210
(a) Aerial with one parallel rod as a reflector . . . . .	210
(b) Aerial and two parallel reflecting rods . . . . .	212
(c) Aerial $\frac{1}{2}\lambda$ in front of a three-rod grating . . . . .	214
(d) Currents induced in a grid of three wires by an incident plane wave . . . . .	216
(e) Currents induced in a grid of four wires by an incident plane wave . . . . .	218
5.9. Current induced in a thin rod placed perpendicular to the electric vector . . . . .	218
5.10. Grating of thin wires perpendicular to the electric vector . . . . .	220
5.11. Netting with square mesh of side $g$ . . . . .	220

## CHAPTER VI. SOME PROBLEMS OF CYLINDERS

6.1. Introduction . . . . .	222
6.2. Field of a sinusoidal distribution of current density flowing along a cylinder . . . . .	222
6.3. Tube with sinusoidal distribution of axially* flowing current density surrounded by a perfectly conducting tube . . . . .	227
6.4. Current filament parallel to a metal cylinder . . . . .	228
(a) Numerical example of distribution of current density . . . . .	230
(b) The external field of the current in the presence of the cylinder . . . . .	232
(c) Numerical examples of the external field and of the power gain . . . . .	233
(d) Numerical example of the field quite close to the cylinder . . . . .	238
(e) Attempt to use the optical image treatment for estimating the forward field . . . . .	240
6.5. Reciprocal properties with cylinders . . . . .	240
6.6. Plane wave incident on a cylinder parallel to the electric vector . . . . .	241
(a) The external field of the currents induced in the cylinder . . . . .	245
6.7. The resultant field close to the cylinder . . . . .	251
6.8. The rate of working in re-radiation and the pressure of radiation . . . . .	255
6.9. Field of currents flowing round the circumference of a cylinder . . . . .	258
6.10. Plane wave incident on a cylinder whose axis is perpendicular to the electric vector . . . . .	261
6.11. The external field of the currents induced in the cylinder . . . . .	263

## CHAPTER VII. FURTHER PROBLEMS OF CYLINDERS AND FLAT SHEETS

7.1. Current filament parallel to and directly above a half-cylindrical boss rising out of an infinite plane; and the limiting case when the incident field is a plane wave . . . . .	265
7.2. Current filament anywhere in the presence of an infinite plane having a half-cylindrical boss . . . . .	275
7.3. Any Vee reflector with cylindrical back . . . . .	278
7.4. Filament anywhere in a Vee reflector with cylindrical back . . . . .	283
7.5. The density of current induced at the apex of the Vee . . . . .	286
7.6. Method of producing a non-reflecting chamber . . . . .	288
7.7. Extension of §§ 7.3 and 7.6 to include rectangular wave guides and their correct termination . . . . .	295

## FURTHER PROBLEMS OF HALF-PLANES

7.8. Plane wave incident on a half-plane having a cylinder at its bounding edge . . . . .	300
7.9. Current induced in a half-plane when the coplanar current filament is very distant . . . . .	301
7.10. Current density induced in a half-plane when a plane wave is incident normally on it . . . . .	303

7.11. Resultant field due to a plane wave incident normally on a half-plane . . . . .	307
7.12. Plane wave incident normally on an infinite sheet in which there is a parallel-sided aperture . . . . .	321

#### CHAPTER VIII. THE SINGLE ISOLATED AERIAL

8.1. The electric doublet and the thin linear aerial . . . . .	324
8.2. Radiation resistance of a linear aerial . . . . .	329
8.3. The resonant length and the $Q$ of a half-wave aerial . . . . .	332
8.4. A brief survey of refined analytical solutions . . . . .	337
8.5. Aerials with a large capacitance roof . . . . .	338
8.6. Inductance and capacitance per unit length of an aerial . . . . .	340

### EXPERIMENTAL SECTION

#### CHAPTER IX. GENERAL EXPERIMENTAL METHODS AND EQUIPMENT

9.1. . . . .	341
9.2. The monitor aerial . . . . .	349
(a) The impedance of a short thin aerial . . . . .	350
9.3. Monitor aerial used to explore the equatorial field of a half-wave aerial . . . . .	358

#### CHAPTER X. TESTS OF VEE REFLECTORS

10.1. Preliminary . . . . .	363
10.2. Forward field tests . . . . .	363
10.3. The equatorial pattern . . . . .	369
(a) General survey . . . . .	369
(b) Pattern at the first station . . . . .	372
(c) Pattern at the second station . . . . .	375
(d) Patterns for the third station . . . . .	383

#### CHAPTER XI. PERFORMANCE OF HALF-WAVE AERIAL AND FLAT SHEET: PERFORMANCE OF NETWORK REFLECTORS

11.1. Aerial opposite the middle of a rectangular sheet . . . . .	386
11.2. Aerial in the plane of the sheet . . . . .	389
11.3. Aerial level with edge of sheet ( $\alpha = 90^\circ$ ) . . . . .	392
11.4. Continuous sheets compared with sheets of netting . . . . .	393
11.5. Half-wave aerial and two coplanar untuned parasite rods . . . . .	397

#### CHAPTER XII. TURNING THE BEAM OFF CENTRE: USE OF VEE REFLECTORS SIDE BY SIDE: TROUGH REFLECTORS

12.1. Further analysis of turning the beam off centre . . . . .	401
12.2. Pair of Vee reflectors side by side . . . . .	409
12.3. Trough-shaped reflectors . . . . .	415
12.4. Analysis of a $45^\circ$ Vee with circular back . . . . .	423
12.5. Vee reflectors used to curb the side lobes of curtain arrays . . . . .	425

#### CHAPTER XIII. PARABOLIC REFLECTORS

13.1. Introduction . . . . .	429
13.2. Experiments with parabolic cylinders . . . . .	430
(a) Forward-field tests . . . . .	431
(b) Relation between aperture and width of main beam . . . . .	434
(c) Attempt to turn the beam by offsetting the aerial . . . . .	437
(d) The complete diffraction pattern for $d/F = 1$ . . . . .	437

# CONTENTS

xi

13.3. Comparison of parabola with a Vee . . . . .	440
13.4. Use of parasitic aerial with reflector . . . . .	447
13.5. Parabola excited by means of a wave guide . . . . .	449
13.6. Difficulties in understanding the optical behaviour of a parabola . . . . .	453
13.7. The field of a semicircular cylinder . . . . .	457
(a) Current density uniform . . . . .	457
(b) Sinusoidal distribution of current density . . . . .	460
(c) Current density $I_n \sin n(\alpha + \theta)$ , with $n$ odd . . . . .	461
(d) Current density $I_n \cos n(\alpha + \theta)$ , with $n$ even . . . . .	461
(e) General expression for the electric force at the cylinder . . . . .	461
(f) The field of a circular arc with uniform density . . . . .	461
CHAPTER XIV. IN-LINE AND CURTAIN ARRAYS. YAGI AERIALS	
14.1. The performance of separately fed arrays . . . . .	463
14.2. Examples of patterns when the loading is symmetrical but not necessarily cophased . . . . .	470
14.3. Examples of patterns when the phase distribution is not symmetrical . . . . .	476
14.4. An example of a 16-member curtain in front of a flat reflector . . . . .	479
14.5. Measured performance of horizontal dipole arrays at $\lambda$ about 20 m. . . . .	482
14.6. Analysis of the effect of ground slope . . . . .	486
(a) Uniform slope . . . . .	486
(b) Two uniform slopes . . . . .	488
14.7. The field close to a curtain: method of estimating the power output . . . . .	489
14.8. Measurement of the power output from a Vee reflector . . . . .	495
14.9 Yagi arrays . . . . .	504
TABLES OF BESSEL FUNCTIONS . . . . .	508
A SHORT LIST OF FORMULAE . . . . .	510
INDEX . . . . .	512

Figs. 4.9, 4.10, 4.11, 4.12, 4.13, 4.14 and 9.1, 9.2, appear between pages 176-7.



## ELECTROMAGNETIC FIELD OF CURRENT FILAMENT AND PLANES

### 1.1. Preliminary

IN studying electromagnetism the student is soon introduced to certain standard problems whose solution is straightforward: typically these are the distribution of magnetic field due to a steady current flowing in (a) a very long straight wire, (b) a very long solenoid, (c) an infinite flat sheet. In this chapter we shall solve these problems for a current which is alternating simple harmonically at any frequency. We shall include a few associated problems which can be solved by superposition of these three standard cases. In this way we provide ourselves with a set of tools which can be used to solve, either completely or approximately, other more complicated problems which are the main study of this book.

In this chapter our concern is only to find the solution to certain precisely specified and hypothetical problems: it is no part of our business *now* to discuss whether these problems are precisely realizable in the physical world: that will come later and such matters are discussed at length through the remainder of the book. Suffice it to say now that the reader need not fear he is being asked to watch the solution of certain pedantic and pedagogic exercises: if he will learn to do these exercises he can then be taught to solve many practical problems which arise continually in the practice of radio communication. These preliminary exercises may be likened to the essential grammar, if not the very alphabet, of the language. Those who would speak and read this language must know these preliminaries, there is no other way. The alternative is not a language but is gesture and dumb show: this is not to say, however, that some communication cannot be carried out by the process of gesture and dumb show, for much is done that way.

In teaching these preliminaries the reader's attention will not be distracted by discussions of practical ways and means, though an aside remark may sometimes be made; the writer does not propose to justify each choice of theme now but asks for an act of faith from the reader.

### 1.2. Brief survey of the steady current problem

In the eighteenth century men sought to establish experimentally a connexion between electrical phenomena, as produced by the frictional type of generator, and the magnetic phenomena of the lodestone.

Systematic description of the first had been helped enormously by the invention of a hypothetical and imponderable stuff called electricity, which served as a sort of mental focus for the 'virtues' observed; it described, without attempting to explain, these 'virtues'. Similarly, the concept of magnetic pole had correlated the observed phenomena of magnetism and served to provide a way for calculating the net result of any combination of specified lodestones. Then came the discoveries of the Italian physiologist Galvani (1737-98) and the invention by Volta (1745-1827) of the voltaic pile, now called an electric battery. The voltaic pile produced sparks and shocks and attractions, and therefore was indistinguishable in effect from a frictional electric machine, but had the additional property that its 'virtue' was long lived and not immediately discharged by a shock or spark. It was a new and better source with which to seek for magnetic effects. Many people sought a connexion between electricity and magnetism, and Hans Christian Oersted (1777-1851) found it, in Copenhagen, in the year 1820. Within a year of the notification of Oersted's discovery the French mathematician André Marie Ampère (1775-1836) had established a full and complete quantitative description of the whole phenomenon. His work is an everlasting glory of logical thought, systematic experiment, and experimental genius: it left nothing which could possibly be added to the quantitative statement of steady current magnetic phenomena, so long as man finds it convenient to describe electrical phenomena in terms of charges, inverse square law, and magnetic fields. Ampère started with the guess, better called hypothesis, that the magnetic field which results when the ends of a single turn of wire are connected to the two terminals of a voltaic pile is indistinguishable from that of a bar magnet with axis normal to the plane of the turn, provided always the comparison is made at an infinite distance and, moreover, that the moment of this said equivalent magnet would be equal to the area of the turn (whatever its shape) multiplied by the electric current flowing in it. It should be noted that his hypothesis is formulated in a way which forbids all possibility of exact and direct experimental verification, since the comparison must be made at infinity. A magnetic field was known to be associated with an electric circuit and therefore any circuit must be represented by some equivalent system of bar magnets. The genius of Ampère lay in postulating comparison at an infinite distance: the power of his logical argument lay in discovering how strong the field should be at a finite distance. In effect he had conceived the elementary circuit, corresponding to the elementary magnetic

particle. The pure logic of his argument made it possible to design experiments by which his hypothesis could be tested; these experiments he conceived and made, no subsequent experiment has yielded the faintest suggestion that Ampère's hypothesis is not a complete and accurate description of the whole phenomenon. The hypothesis is expressed most conveniently in a derived form, as follows: If a unit magnetic pole is taken round any circuit path which threads a current, then work is done whose amount equals  $4\pi$  times the current flowing in the circuit which is threaded. It is expressed algebraically by the symbols  $\oint H dl = 4\pi i$ , or by the 'short-hand' description  $\text{curl } H = 4\pi i$ . The inclusion of the factor  $4\pi$  seems clumsy, but if it is left out here it causes trouble elsewhere and cannot be avoided everywhere. We shall refer to this statement of the hypothesis as Ampère's Law or as the Work Law.†

To obtain a magnetic field it is essential to connect each end of the coil to one terminal of the battery, in modern parlance to close the switch: that was the discovery which Oersted made and which others had failed to make. The existing nomenclature and ideas of electricity insisted that a current of this imponderable hypothetical fluid must be flowing from the battery. There was no need to suppose it flowed anywhere except through the material of the wire itself, and to suppose more than this would be to introduce an unhelpful complication. Yet the associated magnetic field is found everywhere through the whole of space. Thus have we associated something which is found throughout a volume with something which occurs only locally; namely, a flow of current which is concentrated entirely within a fine wire. It is important to have this concept clear in the mind.

Though the work law (when couched in its magnetic-shell form) suffices to calculate the magnetic field due to any circuit or coil whatsoever, it is not a convenient tool for calculation. Calculation would be simplified enormously if the circuit could be treated as elements of length rather than elements of area. But an isolated elementary length of circuit has no physical meaning whatever because it has ceased to be a circuit: the concept of cutting the wire into lengths is obviously and inescapably equivalent to 'opening the switch'. We owe it to the clarity of thought of Oliver Heaviside (1850–1925) to give us a rational

† In rationalized M.K.S. units we should write  $\oint H dl = i$ , where  $i$  is the current in amperes,  $dl$  is measured in metres, and  $H$  is the force in newtons on the unit magnetic pole, the unit magnetic pole being defined as one which repels a similar pole 1 metre away with a force of  $\frac{1}{4}\pi\mu_0$  Nw, where  $\mu_0 = 4\pi/10^7$ . Thus this unit pole is  $10^8/4\pi$  times as large as the classic unit in the c.g. system.



method of forging the tool required for computation. Because his concept bears a striking resemblance to the alternating-current doublet, used repeatedly in this book, it is appropriate to develop the Heaviside element here, even at the cost of a small delay in our main quest.

Suppose a cylindrical 'torch battery' (having the usual insulation round its curved sides) is immersed in an infinite ocean of some conducting liquid, say sea-water. Then current will flow out radially and

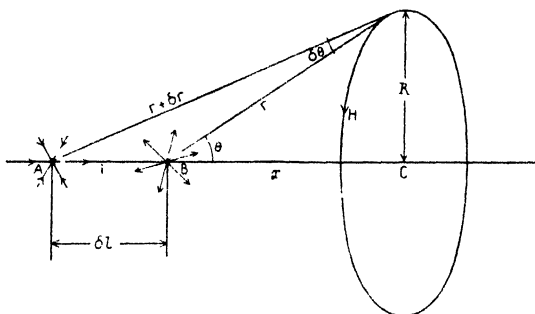


FIG. 1.1. Diagram of Heaviside element.

uniformly from its positive pole and converge similarly into its negative pole. In Fig. 1.1 the battery is represented diagrammatically by  $AB$ . Because current flow is symmetrical about the axis  $AB$  the lines of magnetic force must all be circles centred on this axis. One such is indicated in Fig. 1.1 by the circle whose centre is  $C$  and radius  $R$ . If the field be  $H$  round this circle then, by Ampère's work law,  $H \times 2\pi R = 4\pi \times \text{current flowing through the circle}$ . This said current must be equal numerically to the difference between the outwardly flowing current diverging radially from  $B$  and the like inward flow converging on  $A$ . The current density  $i$  at radius  $r$ , due to a total current  $I$  diverging radially, is  $I/4\pi r^2$ . Hence the total current flowing outwards through the ring of radius  $R$  is this density multiplied by the area of the spherical cap bounded by the circle of radius  $R$ . This area is well known to be equal to  $2\pi r(r - r \cos \theta)$ , and thus the outflowing current equals

$$\frac{I}{4\pi r^2} \times 2\pi r^2 (1 - \cos \theta) = \frac{I}{2} (1 - \cos \theta).$$

Hence the net current =  $\frac{I}{2} [(1 - \cos \theta) - \{1 - \cos(\theta - \delta\theta)\}] = \frac{I}{2} \sin \theta \delta\theta$ .

$$\therefore H \times 2\pi R = \frac{4\pi I}{2} \sin \theta \delta\theta.$$

$$\therefore H = \frac{I \delta \theta \sin \theta}{R} = \frac{I \delta \theta}{r} = \frac{I \delta l \sin \theta}{r^2} \cdot \dagger \quad (1.1)$$

The magnetic field at any point in the ocean is thus described in terms of the length of the battery and the total current flowing through it. Though current is flowing everywhere throughout the whole ocean, yet the magnetic field is described in terms of the current flowing only in that one place where all of it is constrained to gather together and pass through a very narrow tube, the battery. The calculation is much simpler than could possibly have been expected at first sight. Any number of batteries may be joined end to end, each joint being then insulated to prevent current flowing from it. The magnetic field which will then result is to be calculated by evaluating  $I \delta l \sin \theta / r^2$  along the chain of batteries, but the integration must start and finish with this chain. Strange to say, the magnetic effect of the current flow which is diffused everywhere is reckoned correctly in this process. Such a process might be needed in practice to calculate the strength of a magnetic field intended to explode magnetic mines. Heaviside called his concept 'a rational current element' and described it on p. 502 of vol. ii of his *Collected Papers*. If the two open ends of his 'cable of batteries' are joined together, then flow in the ocean will cease and the ocean plays no more part: a closed wire circuit has been formed and now the conducting ocean can be drained away. The process has shown that the magnetic field of a closed circuit can be calculated at any point by performing the integral of  $I \delta l \sin \theta / r^2$  round the circuit: it has provided a new tool for calculation and that is all there is to be said about it. It does not say and cannot say that a particular element makes a particular contribution to the total result, in the sense that the total result would be that much smaller if that element were snipped out. If the element were snipped out current would cease to flow and there would be no magnetic field anywhere. Magnetic field would reappear if the ocean was poured back again and then the field would be short of the previous total by the contribution from the missing element; but it would not be the original current flow.

The intrinsic interest of Heaviside's element is very great: its interest here is to show that fields due to a flow which occurs throughout the whole of space can be calculated in terms of the current flow in that one tiny element of volume where all the current is constrained to pass. We are leading up to aërials and are hoping to calculate the field at a

† In rationalized M.K.S. units (1.1) would be written  $H = I \delta l \sin \theta / 4\pi r^2$  oersteds, where  $I$  is in amperes,  $l$  and  $r$  in metres.

distant point in terms of the current where it flows through the aerial itself. That is why Heaviside's element matters to us here, it is a hopeful portent: it may now be stored in our memory and we may proceed.

Armed with the Heaviside element it is a simple matter to evaluate the field outside a long straight current filament, inside an infinite solenoid or outside an infinite plane: the result is well known to be  $H = 2I/r$ ,  $4\pi I$ ; or  $2\pi I$  respectively. These results are true only if the current is steady, and it is then only that Ampère's law applies.

In 1831 Michael Faraday (1791–1867) discovered that a current is produced in a closed circuit while it is moving in a magnetic field: the effect ceases with the motion.

The flow of current in a wire can be caused only by the existence of an electric field: it seems unlikely that this field depends on the presence of the material circuit. To be a little less positive, we will put it this way: though a material circuit is necessary for a current flow, yet an electric field could be discovered at any point of space by means other than the flow of a current, say, by a charged pith ball or a gold-leaf electroscope. A charged pith ball moved relative to a magnet will, in principle, disclose the existence of an electric field. A detector sensitive enough to show the force at a point did not then exist. The only detector which worked was a galvanometer recording the current induced in a wire circuit, and this could only disclose the electric force integrated round the closed circuit. Neumann formulated the discovery quantitatively and his formulation may be written

$$\oint E \, dl = -d\phi/dt \dagger$$

or

$$\text{curl } E = -dH/dt.$$

The negative sign describes the sense of the 'electromotive force', according to right-handed axes or the 'right-hand screw rule'. We shall call it the Faraday Law or the Electromotive Force Law. Though inadequate experimental facilities may have demanded a material circuit, it can scarcely be doubted that  $\text{curl } E = -dH/dt$  round any circuitual line drawn in space, whether current is allowed to flow or not. Experience showed currents were induced in a circuit during the change of current in another circuit, relative movement of the circuits not being essential. Thus, current was induced in a search coil placed inside a

† In rationalized M.K.S. units  $E$  would be in volts per metre and  $\phi$  in the units appropriate to the unit pole of that system: thus the familiar factor  $10^{-8}$  is avoided.

long solenoid in which an alternating current flowed. More significant still, current was induced in a 'search coil' which embraced the long solenoid externally: in such circumstances the induced electromotive force is independent of the area of the search coil, provided only it embraces the solenoid. It would thus seem that an electric force can be produced even at places where there is no magnetic field. The suspicions of the thoughtful reader will be aroused here, and rightly so. He will suspect the magnetic field is not zero outside a solenoid carrying an alternating current, and he will be right. He will suspect that more precise measurements will show the e.m.f. is not independent of the area of the search coil, and again he will be right. He is perceiving that Faraday's and Ampère's laws are not strictly consistent and that in using the relation  $\text{curl } E = -dH/dt$  it will not suffice to calculate  $H$  by Ampère's method. Ampère's law applies only to steady currents: it needs extending to include changing currents. Without such extension this book cannot proceed.

We here remind the reader of a mathematical tool useful in describing magnetic fields. It is a tool which describes the flux through an area in terms of a line integral round its bounding edge: it is denoted by the symbol  $A$  and is defined by the equation  $\oint A dl = \phi$  or  $\text{curl } A = H$ . It is called the vector potential because the inverse square law demands that  $A = i dl/r + \text{constant}$ , and this is reminiscent of the electrostatic potential of a charge element, for which  $V = q/r + \text{constant}$ . Arbitrary convention takes the constant in  $V$  as zero. If we choose to do so we can take the constant in  $A$  as zero, but with no more and no less reason than mere convenience. We believe that  $\text{curl } E = -dH/dt$  and we define  $\text{curl } A = H$ . Thus we obtain  $E = -dA/dt + d/dt$  (unknown constant). The value we derive for  $E$  will depend on this unknown constant and the issue cannot be evaded. Faraday's law cannot possibly suffice, by any device of introducing a new function, to disclose the value of  $E$  at a point. For it relates only to  $\text{curl } E$ , and not to  $E$  itself at any point of the curl. Suffice it here to remind the reader of the mathematical tool called vector potential: a function, like scalar potential, defined only by its space rate of change in relation to a static field.

### 1.3. The Maxwell hypothesis

Consider a flat plate condenser having plates of area  $A$  separated a distance  $d$  and *in vacuo* and carrying a charge  $Q$ : then the electric force  $E$  between the plates has the value  $4\pi(Q/A)$  everywhere. If the condenser is in the process of charging, or discharging, the current  $I$

flowing in the wires connecting the plates to the source of voltage is related to  $Q$  by the relation  $I = dQ/dt = (A/4\pi)(dE/dt)$ . This relationship between  $I$  and  $dE/dt$  shows we may trace round a complete circuit of current flow by introducing the device of reckoning a changing electric force as equivalent to a current: round one part of the circuital path the flow consists of moving electric charges confined to a wire, and in the other part it consists of a time changing electric force. It is a device for making current flow circuital; for tracing round a circuit.

Between 1863 and 1875 James Clerk Maxwell (1831–79) conceived the idea that this equivalence might be complete and that a changing electric field could never be distinguished from the current flow conceived by Ampère. In other words, it must be accompanied by a magnetic field: and hence that the magnetic field associated with the current flow which is charging a condenser would be calculated correctly by the ‘Heaviside rational current element’ process. It was an idea which was not then susceptible to direct experimental verification: it is essential, just as it was with Ampère’s idea, to derive the logical consequences of the idea and find therefrom an experiment capable of verification. The idea of current flow as something which can occur only in a wire is gone for ever; now it is something which may occur everywhere; in places it may be a conduction current and elsewhere a displacement current, but they are only alternative aspects of a coherent and indistinguishable whole. Steady flow is a particular case where the current flow is restricted to the wire; at any rate this is so on a time average and a not too detailed view of the phenomenon.

Apply the concept to a charged particle moving uniformly in a straight line. All space is filled with electric field which is changing at every point because the charge is moving. If there is magnetic field, then symmetry shows its lines must be circles centred on the axis of movement: Fig. 1.1 will suffice to describe the problem if the torch battery  $AB$  is replaced by a charge  $q$  moving with speed  $v$  in the direction  $AB$ . According to the inverse square law the flux of electric force through the circle of radius  $R$  is readily seen to be equal to  $2\pi q/r^2 \times r^2(1 - \cos \theta)$ : hence the time rate of change of this electric flux is

$$\begin{aligned} -2\pi q \frac{d}{dt}(\cos \theta) &= -2\pi q \frac{d}{dt} \left\{ \frac{x}{(x^2 + R^2)^{1/2}} \right\} = 2\pi q \frac{vR^2}{(R^2 + x^2)^{3/2}} \\ &= 2\pi q \frac{vR^2}{r^3} = 2\pi q \frac{vR}{r^2} \sin \theta. \end{aligned}$$

Now applying the Ampère law we find  $H = qv \sin \theta / r^2$ , and this is the same as would result from a Heaviside element  $I \delta l = qv$  at  $AB$ , immersed in a conducting ocean. Once more the magnetic effect of a current which is distributed through all space is to be calculated in terms of the current flowing at the one point where it is all constrained together, in this case the only point where charged matter is in motion. The previous calculation of  $H$  cannot be correct because no cognizance has been taken of the Faraday law:  $E$  was stated from the inverse square law and consequently  $\text{curl } E$  must be zero, whereas in fact  $\text{curl } E$  must equal  $-dH/dt$ . Thus it was incorrect to write  $E = q/r^2$  when  $q$  is in motion, and the expression for  $H$  is only an approximately correct derivation from the Maxwell hypothesis.

So far we have deliberately worked in inconsistent units.  $Q$  in the expression  $E = Q/4\pi A$  or  $q/r^2$  is in electrostatic units, whereas  $i$  in  $\text{curl } H = 4\pi i$  is in electromagnetic units. We ought to have written  $E = Q/4\pi c A$  or  $q/cr^2$ , where  $c$  is the number of electrostatic units in one electromagnetic unit of charge. Accordingly we write the Maxwell hypothesis as

$$\text{curl } H = 4\pi \times \frac{1}{4\pi c} \frac{dE}{dt} = \frac{1}{c} \frac{dE}{dt},$$

and shall call it the Maxwell law. If the path curled round includes also a charge  $q$  moving with speed  $v$  we have

$$\text{curl } H = \frac{1}{c} \left( 4\pi qv + \frac{dE}{dt} \right) \equiv \frac{1}{c} \left( 4\pi i + \frac{dE}{dt} \right),$$

where  $i$  is the conduction current reckoned in E.S. units.

The whole concept of current is now much enlarged and is included in a definition once given by Faraday:† 'By a current I mean anything progressive, whether it be a fluid of electricity, or two fluids moving in opposite directions, or merely vibrations, or, speaking more generally, progressive forces.'

Many electricians continue to find that Maxwell's concept of displacement current is repugnant to them and it would seem that Lord Kelvin was always among that number. Perhaps the reason for that distaste is somewhat as follows. The science of electricity advanced enormously as soon as men invented the 'stuff electricity' and concentrated their attention on the charges situated at points in space; charges which, in a sense, they had just then invented. This was in contrast to devoting their attention to the whole 'orb of virtue' surrounding an 'electrified

† See Faraday's *Researches*, vol. 1, 19.

body'. The concept that the charge was the cause and the orb of virtue was the result seems to have marked the real birth of the science and to have paved the way for Priestley's suggestion of inverse square law. The dictum 'never rest until you have located the charges which are producing the electric field' is one of the soundest precepts which an applied electrician can have.

In using Ampère's law we curl round charges which are supposed to be moving along a wire and thus here we know and remember where the charges are located. But in using Maxwell's law we do not curl round our supposedly ultimate concept, the charge, but only curl round a path which encloses a field (the effect of a charge) which is changing. Looked at in this way, the electrician may well feel repugnance and feel he has abandoned the precious and hard-won charge to play, as of old, with a nebulous 'orb of virtue' or 'electric effluvium'. But Maxwell was much influenced by Faraday and it seems now as if Faraday's mind worked more, on the whole, with orbs of virtue than with point charges. It must surely be rather a matter of arbitrary choice whether the charge or the field is regarded as the ultimate reality; the old dictum that a charge is the end of a tube of force seems to abandon the cause and effect notion and to regard the charge and the tube as inseparable parts of a whole unity.

Let us now return to the condenser of our supposed experiment and let it be furnished with a material dielectric, such as paraffin wax. In our determination to try to describe everything in terms of electric charges, we endow the particles of this wax with electric doublets whose electric moment is attained by the slight straining apart of a normally coincident positive and negative charge under the influence of the attractions and repulsions arising from the charges situated on the metal plates of the condenser. This idea has been very successful and has served to describe all the main phenomena of dielectric polarization while still permitting the retention of an inverse square law which is unmodified by the properties of the medium surrounding the charges. And, moreover, in due course, it has helped to lead on to the extremely fruitful concepts of valency electrons in a molecule. The idea of the formation of doublets in the material dielectric is firmly entrenched in our system and is a valuable addition to it. Accordingly, in curling round a path in the paraffin wax, while the condenser is charging, we certainly do presume that we are curling round electric charges which are in motion, restricted though this motion is. A microscopic view of what is happening in the wax differs from a microscopic view of what

is happening in the wire only in that we are apt to suppose that a given electron can progress along the whole length of the wire, whereas a given electron in the wax must always oscillate about a fixed point in space and can never emerge from the wax and pass on to a plate of the condenser. But when we allow ourselves to go so far as to speak about a given electron, to mark one with a spot of paint so to speak, we are pretty certain to be talking nonsense. If all electrons are identical, how can any one be endowed with recognizable identity? It has to be admitted that, whether we are curling round a path in the wax or curling round the wire, a current of moving charges is threaded and that there does not seem to be any significant difference in the mechanism of current flow. And thus Maxwell's law does not appear to be any new concept when applied to a material dielectric and in such circumstances there does not appear to be any real distinction between conduction and displacement currents. However, there does remain one important point which must be taken into account. The electric charge which appears on the surfaces of the wax is smaller than the charge on the contiguous plate of the condenser and therefore the current due to moving charges in the wax is smaller than the current of moving charges flowing in the wires through which the condenser is being charged; and this means the current is not continuous in magnitude round the whole circuit, even though it consists of moving charges in all parts of the circuit. The current due to the oscillating charges in the wax is too small; to bring it up to strength there must be added something which is not current in the sense that it consists of moving charges. The amount which has to be added is equal in numerical value to the rate of change of the force in a 'pipe hole' drilled through the wax from one plate to the other; it has this value because this force is obviously proportional to the differences between the charge on the plates and the charge on the surfaces of the wax. So, notwithstanding the current of oscillating charges in the wax, we shall have to reckon as current something which is not movement of charge, at that place, if we are to obtain the same value of magnetic force at the surface of the plate whether we curl round a path in the wax and parallel to the plate and close to it or whether we curl round the plate itself. Thus the Maxwell hypothesis seems to be inescapable, whether we like it or not. The idea of oscillating doublets in the dielectric, thereby seeming to be a current just like a conduction current, does much to stimulate the notion of a current through the dielectric. Having once visualized this mechanism for current through a material dielectric, surely every



electrician would feel compelled to treat the current of oscillating charges as the equivalent of a conduction current, in that Ampère's work law must surely be applicable to it, and therefore he feels prepared to calculate the magnetic field at a point in the wax. But the known value of the magnetic field at the surface of the plate shows that the current through the dielectric must be made continuous with the current in the plate by the seemingly fictitious process of reckoning as current something which is not attributable to charges moving through the circuit curled round. And, moreover, the ideas which are prompted very naturally by the doublet mechanism of a material dielectric demand, through a general sense of continuity, to be applied when no material dielectric is present and the component of current due to oscillating electric charges has vanished.

In thinking of the formation of doublets in a material dielectric it is natural to think of the displacement of valency electrons, and then the term displacement current seems particularly appropriate to that current which consists of the oscillatory movements of charges; it would be a term which was appropriate to and descriptive of the slightly different mechanism from that obtaining in a genuine conduction current in a wire or an electrolyte. But in fact the term is used to describe the total current through the dielectric whether or not this happens to include a component arising from oscillatory movement of charges, such being present only when the dielectric consists of material particles. The term 'displacement current' dates from Maxwell and it does not seem that he paid any special attention to a particle mechanism of solid or liquid dielectrics. In his determination to make currents continuous, something had to happen in the dielectric and that something could not be a conduction of the ordinary and familiar kind; therefore let it be called a displacement without yet bothering what it was a displacement of or bothering about any particular mechanism. Seemingly, all dielectrics to him were continuous structures; some dielectrics 'displaced' more than others under the action of a given electric field, just as some materials yield more than others to a given mechanical force. One of the very great advantages of our doublet theory of material dielectrics is that it allows us to make inverse square law independent, in its magnitude, of the material surrounding the charges. When we say that the force is  $ee'/Kr^2$  we know that the use of  $K$  is merely a very convenient way of allowing for the force due to a multitude of electric charges which were already in the wax and have disclosed their presence by being strained apart slightly by the

forces from the charges  $e$  and  $e'$ . From this point of view the dielectric constant of a vacuum is unity by the very nature of things, and the idea of the dielectric constant of free space becomes a repugnant notion, even though it may be desirable to swallow it as a convenient fiction in the interests of making a system which is consistent dimensionally. Maybe it is desirable, from some points of view, to write the force between charges as  $ee'/K_0 r^2$ , where  $K_0$  is some undiscovered, and presumably undiscoverable property of free space which shall be called, perhaps rather unfortunately, the dielectric constant of free space. Then the dielectric constant of, say, paraffin wax, must be written as  $KK_0$ , where  $K$  is purely a ratio. The doublet description of a material dielectric gives us a complete understanding of how and why  $K$  arises; but we have no physical conceptions of the meaning of  $K_0$  and scent the possibility of its existence only through our ideas of dimensions. Of course, if the doublet description of material dielectrics had not emerged, then  $K$  would be just as mystifying as  $K_0$ ; but the said theory has emerged and was bound to do so, and thus the whole meaning of the ratio  $K$  is well understood, and the effect it describes could have been predicted before it was discovered experimentally. The theory of dielectrics has made the seemingly necessary retention of  $K_0$  more than ever artificial, and perhaps we may be allowed to say both irritating and repugnant.

In order to test Maxwell's hypothesis experimentally we must discover its logical implications and need an algebraic statement of it to help in this task.

#### 1.4. Maxwell's equations in free space

For any region of space which does not include charged matter we propose that

$$\left. \begin{aligned} \text{curl } H &= \frac{1}{c} \dot{E} \\ \text{and} \quad \text{curl } E &= -\frac{1}{c} \dot{H} \end{aligned} \right\} \quad (1.2)$$

and retain Gauss's theorem of inverse square law, which gives

$$\left. \begin{aligned} \text{div } E &= 0 \\ \text{and} \quad \text{div } H &= 0 \end{aligned} \right\}^{\dagger} \quad (1.3)$$

<sup>†</sup> We do not propose to retain here the dielectric constant and the permeability of free space, concepts discussed at the end of the last section. Electric force is measured in the electrostatic system of units and hence the displacement current must be written as  $(1/c) \dot{E}$  when using it in the work law.

Writing these in Cartesian form gives

$$\left. \begin{aligned} \frac{1}{c} \frac{\partial E_1}{\partial t} &= \frac{\partial H_3}{\partial y} - \frac{\partial H_2}{\partial z} \\ \frac{1}{c} \frac{\partial E_2}{\partial t} &= \frac{\partial H_1}{\partial z} - \frac{\partial H_3}{\partial x} \\ \frac{1}{c} \frac{\partial E_3}{\partial t} &= \frac{\partial H_2}{\partial x} - \frac{\partial H_1}{\partial y} \end{aligned} \right\}, \quad (1.4)$$

$$\left. \begin{aligned} -\frac{1}{c} \frac{\partial H_1}{\partial t} &= \frac{\partial E_3}{\partial y} - \frac{\partial E_2}{\partial z} \\ -\frac{1}{c} \frac{\partial H_2}{\partial t} &= \frac{\partial E_1}{\partial z} - \frac{\partial E_3}{\partial x} \\ -\frac{1}{c} \frac{\partial H_3}{\partial t} &= \frac{\partial E_2}{\partial x} - \frac{\partial E_1}{\partial y} \end{aligned} \right\}, \quad (1.5)$$

$$\left. \begin{aligned} \frac{\partial E_1}{\partial x} + \frac{\partial E_2}{\partial y} + \frac{\partial E_3}{\partial z} &= 0 \\ \frac{\partial H_1}{\partial x} + \frac{\partial H_2}{\partial y} + \frac{\partial H_3}{\partial z} &= 0 \end{aligned} \right\}. \quad (1.6)$$

Differentiating the first of (1.4) with respect to  $t$  gives

$$\begin{aligned} \frac{1}{c} \frac{\partial^2 E_1}{\partial t^2} &= \frac{\partial}{\partial t} \left( \frac{\partial H_3}{\partial y} \right) - \frac{\partial}{\partial t} \left( \frac{\partial H_2}{\partial z} \right) \\ &= \frac{\partial}{\partial y} \left( \frac{\partial H_3}{\partial t} \right) - \frac{\partial}{\partial z} \left( \frac{\partial H_2}{\partial t} \right) \\ &= -c \left\{ \frac{\partial}{\partial y} \left( \frac{\partial E_2}{\partial x} - \frac{\partial E_1}{\partial y} \right) - \frac{\partial}{\partial z} \left( \frac{\partial E_1}{\partial z} - \frac{\partial E_3}{\partial x} \right) \right\}, \quad \text{from (1.5),} \\ &= -c \left\{ \frac{\partial^2 E_2}{\partial y \partial x} + \frac{\partial^2 E_3}{\partial z \partial x} - \frac{\partial^2 E_1}{\partial y^2} - \frac{\partial^2 E_1}{\partial z^2} \right\} \\ &= c \left\{ \frac{\partial^2 E_1}{\partial x^2} + \frac{\partial^2 E_1}{\partial y^2} + \frac{\partial^2 E_1}{\partial z^2} - \frac{\partial}{\partial x} \left( \frac{\partial E_1}{\partial x} + \frac{\partial E_2}{\partial y} + \frac{\partial E_3}{\partial z} \right) \right\} \\ &= c \left\{ \frac{\partial^2 E_1}{\partial x^2} + \frac{\partial^2 E_1}{\partial y^2} + \frac{\partial^2 E_1}{\partial z^2} \right\}, \quad \text{by (1.6).} \\ \therefore \nabla^2 E_1 &= \frac{1}{c^2} \frac{\partial^2 E_1}{\partial t^2}, \end{aligned} \quad (1.7)$$

with similar equations for  $E_2$  and  $E_3$ ; also for  $H_1$ ,  $H_2$ , and  $H_3$ . Equations of the form (1.7) will be called the wave equation.

Equations typified by (1.7) have a solution of the form  $E = f(t-r/c)$ ,†

† See, for example, Jeans's *Electricity and Magnetism*, § 579, Liouville.

which may be interpreted as stating that an observer travelling with uniform speed  $c$  would perceive fields which differed markedly from those he would perceive if he was travelling with any speed other than  $c$ . The idea of a certain velocity has thus emerged, but we purposely do not discuss the matter further at present: the magnitude of this velocity is equal numerically to the ratio of the electromagnetic to the electrostatic unit of charge.

### 1.5. Lorentz's equation and retarded potentials

Maxwell's equations relate to free space and therefore do not help directly to discover the fields in free space due to a specified disturbance at the origin. We must derive fresh equations for paths which curl round moving charges and closed conducting circuits. In a given volume element  $d\tau$ , let there be a charge  $q$  moving with component velocities  $v_1$ ,  $v_2$ , and  $v_3$ : then  $qv_1 = i_1$ , etc. Equations (1.4) must now be written

$$\frac{4\pi}{c} \left( qv_1 + \frac{\dot{E}_1}{4\pi} \right) = \frac{\partial H_3}{\partial y} - \frac{\partial H_2}{\partial z}, \quad \text{etc.}^\dagger \quad (1.8)$$

We now use the vector potential, the full definition of this function being that  $\text{curl } A = H$ : a definition which defines  $\partial A/\partial x$  but does not define the magnitude of  $A$ . Accordingly we have

$$H_2 = \frac{\partial A_1}{\partial z} - \frac{\partial A_3}{\partial x} \quad \text{and} \quad H_3 = \frac{\partial A_2}{\partial x} - \frac{\partial A_1}{\partial y}.$$

Whence

$$\begin{aligned} \frac{4\pi}{c} \left( qv_1 + \frac{\dot{E}_1}{4\pi} \right) &= \frac{\partial^2 A_2}{\partial y \partial x} - \frac{\partial^2 A_1}{\partial y^2} - \frac{\partial^2 A_1}{\partial z^2} + \frac{\partial^2 A_3}{\partial z \partial x} \\ &= \frac{\partial^2 A_1}{\partial x^2} + \frac{\partial^2 A_2}{\partial y \partial x} + \frac{\partial^2 A_3}{\partial z \partial x} - \frac{\partial^2 A_1}{\partial x^2} - \frac{\partial^2 A_1}{\partial y^2} - \frac{\partial^2 A_1}{\partial z^2} \\ &= \frac{\partial}{\partial x} \left( \frac{\partial A_1}{\partial x} + \frac{\partial A_2}{\partial y} + \frac{\partial A_3}{\partial z} \right) - \nabla^2 A_1 \\ &= \frac{\partial}{\partial x} (\text{div } A) - \nabla^2 A_1, \end{aligned} \quad (1.9)$$

$$\text{also} \quad \frac{\partial E_3}{\partial y} - \frac{\partial E_2}{\partial z} = -\frac{1}{c} \frac{\partial H_1}{\partial t} = -\frac{1}{c} \frac{\partial}{\partial t} \left( \frac{\partial A_3}{\partial y} - \frac{\partial A_2}{\partial z} \right). \quad (1.10)$$

The form of (1.10) suggests that  $E_3 = -\frac{1}{c} \frac{\partial A_3}{\partial t}$ , etc.: but suppose  $E_3 = -\frac{1}{c} \frac{\partial A_3}{\partial t} - \frac{\partial V}{\partial z}$ , etc., where  $V$  is some function of  $x$ ,  $y$ ,  $z$ , and  $t$ .

<sup>†</sup> In this,  $q$  is reckoned in electrostatic units of charge and hence the current is  $(1/c)qv_1$  reckoned in electromagnetic units of current.

Then (1.10) will be satisfied if  $-\frac{\partial^2 V}{\partial y \partial z} + \frac{\partial^2 V}{\partial z \partial y} = 0$ : that is, provided  $V$  is any function which has no curl, such, for instance, as the scalar potential of charges. Accordingly we have

$$E_1 = -\frac{1}{c} \frac{\partial^2 A_1}{\partial t^2} - \frac{\partial^2 V}{\partial t \partial x}. \quad (1.11)$$

Substituting (1.11) in (1.9) gives

$$\frac{4\pi q v_1}{c} - \frac{1}{c^2} \frac{\partial^2 A_1}{\partial t^2} - \frac{1}{c} \frac{\partial^2 V}{\partial t \partial x} = \frac{\partial}{\partial x} (\text{div } A) - \nabla^2 A_1,$$

$$\text{or} \quad \nabla^2 A_1 - \frac{1}{c^2} \frac{\partial^2 A_1}{\partial t^2} = -\frac{4\pi q v_1}{c} + \frac{\partial}{\partial x} \left( \text{div } A + \frac{1}{c} \frac{\partial V}{\partial t} \right). \quad (1.12)$$

The left-hand side of (1.12) has now the form of the wave equation. Remember, however, that  $V$  and  $A$  are two subsidiary mathematical tools which have been defined only by the relations  $\text{curl } V = 0$  and  $\text{curl } A = H$ , definitions which define only the slopes and not the values of the functions. The value of the function can be reckoned from any convenient datum level without upsetting the definition, and it remains only to decide what datum is the most convenient. For scalar potential of charges it is commonly found convenient to say arbitrarily that the potential at infinity is zero. It is permissible here to impose any datum on the value of  $A$  and  $V$  since no datum can alter the value of their curl. Equation (1.12) will be simplified enormously if we impose the extra condition, on the magnitude of  $A$  and  $V$ , that  $\text{div } A + \frac{1}{c} \frac{\partial V}{\partial t} = 0$ : then we have

$$\nabla^2 A_1 = \frac{1}{c^2} \frac{\partial^2 A_1}{\partial t^2} - \frac{4\pi q v_1}{c}, \quad (1.13)$$

and similar equations for  $A_2$  and  $A_3$ .

Now by Gauss's theorem

$$\begin{aligned} 4\pi q &= \frac{\partial E_1}{\partial x} + \frac{\partial E_2}{\partial y} + \frac{\partial E_3}{\partial z} \equiv \text{div } E \\ &= -\frac{1}{c^2} \frac{\partial}{\partial t} \left( \frac{\partial A_1}{\partial x} + \frac{\partial A_2}{\partial y} + \frac{\partial A_3}{\partial z} \right) - \frac{\partial^2 V}{\partial x^2} - \frac{\partial^2 V}{\partial y^2} - \frac{\partial^2 V}{\partial z^2} \\ &= +\frac{1}{c^2} \frac{\partial^2 V}{\partial t^2} - \nabla^2 V, \quad \text{since} \quad \text{div } A = -\frac{1}{c} \frac{\partial V}{\partial t}. \\ \therefore \quad \nabla^2 V &= \frac{1}{c^2} \frac{\partial^2 V}{\partial t^2} - 4\pi q. \end{aligned} \quad (1.14)$$

Thus the arbitrary but permissible decision imposed on  $A$  and  $V$ , namely, that  $\text{div } A + \frac{1}{c} \frac{\partial V}{\partial t} = 0$ , has resulted in similar equations for  $A$  and  $V$ , as shown in (1.13) and (1.14) and which have the form of the wave equation plus an extra term involving charges at a specified point; they may be compared to Poisson's equation of electrostatics.

It may be found that the solution of (1.13) and (1.14) is

$$\left. \begin{aligned} A_1 &= \frac{1}{c} \int \frac{[qv_1] d\tau}{r} \\ A_2 &= \frac{1}{c} \int \frac{[qv_2] d\tau}{r} \\ A_3 &= \frac{1}{c} \int \frac{[qv_3] d\tau}{r} \end{aligned} \right\} \quad V = \int \frac{[q] d\tau}{r}, \quad (1.15)$$

where  $[q]$  and  $[qv_1]$ , etc., denote that the charge and current supposed to be in a given volume element of  $d\tau$  (distant  $r$  from the point where  $A_1$ , etc., and  $V$  are being calculated) at time  $t$  is not that obtaining in the element at that time but is to be taken as that which obtained in the element at the earlier time  $t - r/c$ . This may be put as follows: If current and charge are indicated by meters visible from the distant point, then the distant observer is to use in his calculations the values he reads now, his perception being late by time  $t = r/c$ . Such quantities are often called 'retarded functions';  $A$  and  $V$  are called the retarded vector and scalar electromagnetic potentials respectively. Retarded functions are due to L. Lorentz (1829-91) of Copenhagen.

Hence, if  $q$  and  $qv$  are postulated at all points where  $q$  exists, then  $A$  and  $V$  can be calculated at any point of space; and from them the fundamental quantities  $E$  and  $H$  can be calculated, by means of the relations

$$\left. \begin{aligned} E_1 &= -\frac{1}{c} \frac{\partial A_1}{\partial t} - \frac{\partial V}{\partial x} \\ &= -\frac{1}{c} \frac{\partial}{\partial t} \int \frac{[qv_1] d\tau}{r} - \frac{\partial}{\partial x} \int \frac{[q] d\tau}{r}, \quad \text{etc.} \\ \text{and} \quad H_1 &= \frac{\partial A_3}{\partial y} - \frac{\partial A_2}{\partial z}, \quad \text{etc.} \end{aligned} \right\} \quad (1.16)$$

By this process it has been made possible to calculate  $E$  at any point of space in terms only of the movement of electric charges supposed to be located at certain points; and without reference to the fields in all the rest of space. If we choose to take the view that an electron has

material substance which is located at a point, then everything is reckoned from these electrons and from them alone: the whole system is bound to the idea, or invention, of electric charge and electric fluid. Put analytically, the process of integration is one from points and not a volume integration through all space: in this way the evaluation is greatly simplified. This approach is the very opposite of that implied in the Huygens (1629–95) process, where the origin of the disturbance is distributed through all space or at any rate moves along: here the immediate cause of disturbance is tied to electric charges constrained to move on fixed conductors† and it is not the displacement currents filling space. It may well be argued that the existence of an electron is inferred only by observing an electric field: and that since such field can be perceived everywhere, every electron, in a sense, fills all space and is not located at a point. Granted this is a reasonable point of view, then if it is adhered to, the Lorentz equations have no meaning since they postulate charge *in* an element of volume: it all depends on what we mean by charge. The field of a charged particle has a convergence point at the particle and this convergence point we call the charge. Lorentz's equations do disclose the fields set up by any number of charged bodies when they are moved about. The only uncertainty is whether the movement of small charged beads along a path does produce the same effect as is produced by what we call a current in a conductor.

Throughout this book the writer will relate fields at a given point to currents flowing in fixed conductors,† his conception of current having just been explained: to him the fields (i.e. displacement currents) in the remainder of space are irrelevant. To him propagation velocity arises only in that the distant observer must use local time for reckoning the magnitudes of the currents in distant conductors, and even then he shrinks from the physical concept of the velocity. The algebraic relation of  $f(t-r/c)$  can be interpreted in terms of something proceeding with velocity  $c$ , but the relation appears only in the expressions to be used for calculating  $A$  or  $V$  and these two vectors are not observable quantities, being only algebraic tools. To say that  $A$  and  $V$  are propagated with velocity  $c$  has no physical meaning, since  $A$  and  $V$  are not quantities which are recognizable directly, and it seems to be straining unduly to seek an analogy in order to identify  $c$  with a velocity, when it is but the ratio of two systems of units. The writer's approach is a consistent, logical, and possible approach, but presumably it is not the

† Or possibly charges oscillating about a mean position in a material dielectric, see § 1.3.

only approach possible. Presumably it must be possible to take account of what is happening everywhere and the process should give the same answer if the volume integration is performed correctly. The relations

$\text{curl } H = \frac{1}{c} \dot{E}$  and  $\text{curl } E = -\frac{1}{c} \dot{H}$  relate essentially to quantities located

at a given point. Thus, at a given point,  $H$  does not depend on the integrated effects of the displacement currents filling all space, but depends only on the displacement current at the point where  $H$  is to be reckoned. The rest of space matters only to the extent that what is happening throughout it does determine what the displacement current is at the point where we are making observations.

This approach appears to conflict with the approach which develops naturally from the classic methods of physical optics. It is helpful to give here a brief historical review. Study of the phenomena of light goes far back into antiquity, at any rate as far as Hipparchus in 200 B.C. Narrow shafts of light appearing through cracks and holes are obvious to all, likewise the hard edge of shadows. These familiar experiences readily suggest material particles travelling in straight lines; a flight of arrows or of bullets according as we are living in old or in modern days. On this concept, laws of reflection and refraction are discovered by experimentation, and optical technology has been born. The Dutchman, Christian Huygens (1629–95), exercised his imagination on the manner in which the arrows flew and with what propelled them. In some ways it seems possible his imagination may really have been playing more with the propagation of sound than of light and his ideas very appropriate to propagation by collision between molecules having an agitation velocity. Be this as it may, he invented a geometrical construction which led to an advancing surface which we will call a wave-front. Everyone has the perception that sound travels comparatively slowly and appears to have a definite velocity. Something advances and brings to a point of space some virtue which did not appear to exist there just previously. Huygens produced a geometrical construction which described how a virtue might creep along or propagate: it dealt with the very front edge of the virtue, be that virtue light or sound. The construction comprehended the known laws of reflection and refraction but could not describe the hard edge of shadows. Mainly for this reason, most natural scientists (Newton in particular) concluded that Huygens had done no more than invent a certain geometrical technique which had no particular foundation in reality. In 1801 Thomas Young (1773–1829) was struck by observing



trains of wavelets traversing a surface of water: he recognized they could be led into a pair of canals and reunited in such a way as to produce smooth water by means of the destructive interference of wave crests. He succeeded in observing this effect from the small shafts of light emerging from two holes in a screen, and thus established a correspondence between the phenomena of light and that of waves on the surface of a pond. His startling discovery revived Huygens's construction, which had long been in obscurity.

In 1821 Young's ideas were put into mathematical form by Auguste Jean Fresnel (1788-1827), who formulated a wave equation. Presumably it was the indirect influence of the work of Fourier, and of Euler before him, which helped Fresnel to reduce his equations to a manageable form by the simple but all-important device of making his quantities vary harmonically with time. This step made possible the imposing mathematical analysis developed by men such as Stokes in the first half of the nineteenth century. All that analysis is interpreted and described in terms of Huygens's principle and construction: no doubt this was very natural, more especially when we remember that Maxwell's interpretation of light in terms of electricity did not emerge till about 1870. But it does seem to the writer that the habits of thought which prevailed between 1820 and 1880 can be somewhat confusing to-day and be accompanied by hidden pitfalls. Huygens was not thinking of harmonic variation in time but was thinking of short-lived pulses, which may be likened to bubbles which expand till they burst suddenly and thus cease to exist, or even to the flight of a molecule brought to an end by a collision. The writer feels that when Fresnel's harmonic excitation came in, Huygens's ideas ought to have gone out for good; but in fact they did not. Huygens's ideas are very suggestive in respect of occurrences at a wave-front, meaning by that the hard front edge of an advancing disturbance. Once Fresnel's harmonic variation is admitted there is no wave-front in the sense just defined because the disturbance has existed for infinite time already, all transient effects having died out. A wave-front now becomes the more recondite notion of a surface of equal phase; it is this which advances with a constant velocity and not the front edge of the wave train, since that is already at infinity. The equi-phase-front can be considered to propagate itself locally, and at itself, by molecular collisions if molecules enter into the process, as they do in a sound wave. Once light was described in terms of electric forces it seems to the writer that Huygens's ideas were inadmissible in an equi-phase-front, and that it then became essential

to relate the disturbance to those places where electrons were located. But the formulae and technique of optics were built up before Maxwell's time, and concentrated attention on a wave-front and hence logically on an aperture. There are no electrons in an aperture, and hence the aperture ideas can be made to work only by the device of filling it with fictitious equivalent electrons; the process of finding this equivalent stratum is very difficult and often insoluble.

Many who have been brought up in the techniques of physical optics do not consciously realize the necessity for this equivalent stratum and in consequence use the 'aperture concepts' more freely than is quite justifiable. It is very difficult for one who uses electrical concepts to converse with one who uses optical concepts because the two languages are not the same, even though they have a common root and some similarity. A point is reached where the two men realize they are talking different languages and then the attempted conversation has to be given up. Readers are asked to realize that this book is written in the electrical language and insists on trying to relate fields to currents flowing in conductors.† It starts with the alphabet and simple grammar of the language, and thus does not assume this knowledge in its readers. But if readers are not willing to face the effort of learning the grammar, and of using it, the book cannot be of much use to them.

### 1.6. Fields due to a very small closed circuit

We shall always presume currents in the conductors pulsate simple harmonically: it is the state of greatest interest in the problems we have mostly in mind and is general, in the formal sense, by the application of Fourier's theorem.

Let a planar circuit of thin wire carry a current  $i = I \sin pt$ : it is postulated the current has the same magnitude and phase at every point of the circuit and we do not stop to discuss here whether this is physically possible. Let Fig. 1.2(a) be a close view of the circuit. It is required to find the field at a very distant point  $P$  described with reference to Fig. 1.2(b). The point  $P$  must be very distant; so here our investigation bears a likeness to that of Ampère. Because it is laid down that the current is uniform round the circuit, there is no charge anywhere on the wire, and accordingly the delayed scalar potential  $V$  in (1.15) is zero everywhere, and the electric field, by (1.16), is due only to the delayed vector potential of the currents.

Imagine the wire crenellated into short steps parallel to and per-

† Or, if need be, to charges oscillating in a dielectric, see § 1.3.

pendicular to the direction  $OB$ . Two representative parallel steps are shown by  $ef$  and  $gh$ : two perpendicular steps by  $ab$  and  $cd$ . The parallel steps  $ef$  and  $gh$  are equidistant from the very distant point  $P$  and carry oppositely directed currents: hence the net contribution from them to  $A$  at point  $P$  is zero. The perpendicular element  $ab$  is more distant by

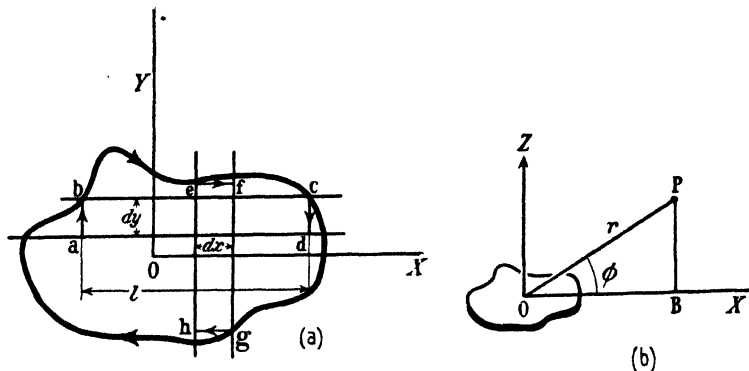


FIG. 1.2.

$l \cos \phi$  from  $P$  than is the perpendicular element  $cd$ . The delayed vector potential at  $P$  due to these two elements is thus given by

$$\frac{c \delta A}{I \delta y} \equiv \frac{1}{(r - \frac{1}{2} l \cos \phi)} \sin \left( pt - \frac{pr}{c} + \frac{pl}{2c} \cos \phi \right) - \frac{1}{(r + \frac{1}{2} l \cos \phi)} \sin \left( pt - \frac{pr}{c} - \frac{pl}{2c} \cos \phi \right).$$

We now impose a condition not needed by Ampère, namely, that  $pl/2c$  is very small; then

$$\begin{aligned} \frac{c \delta A}{I \delta y} &\doteq \frac{\sin(pt - pr/c) + (pl \cos \phi / 2c) \cos(pt - pr/c)}{r - \frac{1}{2} l \cos \phi} \\ &\quad - \frac{\sin(pt - pr/c) - (pl \cos \phi / 2c) \cos(pt - pr/c)}{r + \frac{1}{2} l \cos \phi}, \quad \text{if } \frac{pl}{2c} \ll 1 \\ &\doteq l \cos \phi \left( \frac{\sin(pt - pr/c)}{r^2} + \frac{p}{cr} \cos \left( pt - \frac{pr}{c} \right) \right), \quad \text{since } \frac{l}{r} \ll 1. \end{aligned}$$

The condition that  $pl/2c \ll 1$  is the same as saying that  $\pi l / \lambda \ll 1$ , where  $\lambda$  is the wavelength defined by  $c = f\lambda$ : hence here  $P$  must not only be very distant from the circuit, but the dimensions of the circuit must also be vanishingly small compared with  $\lambda$ .

But  $l \delta y$  is the area of the strip  $abcd$ : if a similar calculation is made for any other pair of perpendicular steps and all are added, it should

be clear that  $l \, dy$  becomes replaced by  $S$ , the area of the circuit of any shape.

Hence

$$\begin{aligned} A &= \frac{IS}{c} \cos \phi \left\{ \left( \frac{\cos pr/c}{r^2} + \frac{p \sin pr/c}{cr} \right) \sin pt + \right. \\ &\quad \left. + \left( -\frac{\sin pr/c}{r^2} + \frac{p \cos pr/c}{rc} \right) \cos pt \right\} \\ &\equiv \frac{a^2 IS}{c} \cos \phi \left\{ \left( \frac{\cos ar}{a^2 r^2} + \frac{\sin ar}{ar} \right) + j \left( -\frac{\sin ar}{a^2 r^2} + \frac{\cos ar}{ar} \right) \right\}, \\ &\quad \text{where } a \equiv p/c. \quad (1.17) \end{aligned}$$

$$\therefore E_2 = -\frac{1}{c} \frac{\partial A_2}{\partial t} \equiv \frac{a^3 IS}{c} \cos \phi \left\{ \left( -\frac{\sin ar}{a^2 r^2} + \frac{\cos ar}{ar} \right) - j \left( \frac{\cos ar}{a^2 r^2} + \frac{\sin ar}{ar} \right) \right\}. \quad (1.18)$$

Equation (1.18) shows that there is a component of  $E_2$  in phase with the current in the wire and also a component in quadrature thereto. At certain distances either component can be zero, but never both zero simultaneously. If one is zero at distance  $r$  it will again be zero at distance  $r + \frac{1}{2}\lambda$ ,  $r + \lambda$ , etc. The phase of the resultant field repeats cyclically with wavelength  $\lambda$ , where  $c = f\lambda$ .

It should be noticed that it is only the area  $S$  and not the shape of the circuit which enters into (1.18); and in this respect it is like Ampère's hypothesis for the magnetic moment of a small circuit. Accordingly the electric field is disposed in circular lines centred on the axis  $OZ$ ; always provided that  $P$  is very distant and  $l/\lambda \ll 1$ .

We will now use the vector potential to calculate the magnetic field. We will use polar coordinates and then there will be a radial component of magnetic field  $H_r$  and a tangential component  $H_\theta$ . The equi-vector-potential lines will be small circles of a sphere centred at the circuit and with a normal to this circuit pointing to the pole of this sphere. To find the radial component of magnetic field we must find the curl of  $A$  round a path consisting of short arcs of two neighbouring small circles and two short arcs of great circles. Consider a point  $P(r, \phi)$  on a sphere of radius  $r$ . Then the radius of the small circle through  $P$  is  $r \cos \phi$  and the length of a short arc of it is  $r \cos \phi \, \delta\theta$ . The contribution to the curl from this arc is  $A r \cos \phi \, \delta\theta$ . The contribution to the curl from a portion of the path along an arc of a great circle is zero, because  $A$  in this direction is zero. Accordingly the required curl of  $A$  is

$$\frac{\partial}{\partial \phi} (A r \cos \phi \, \delta\theta) \, \delta\phi.$$

The area within the curl is

$$r \cos \phi \delta \theta r \delta \phi.$$

Accordingly  $H_r r \cos \phi \delta \theta r \delta \phi = \frac{\partial}{\partial \phi} (Ar \cos \phi \delta \theta) \delta \phi.$

$$\therefore r H_r \cos \phi = \frac{\partial}{\partial \phi} (A \cos \phi), \quad \text{since } r \text{ and } \delta \theta \text{ are constants.}$$

To find  $H_\theta$  we must traverse short arcs of small circles on spheres of radii  $r$  and  $r + \delta r$ , both of them at elevation  $\phi$ . Accordingly

$$\begin{aligned} H_\theta r \cos \phi \delta \theta \delta r &= \frac{\partial}{\partial r} (Ar \cos \phi \delta \theta) \delta r \\ &= \cos \phi \delta \theta \frac{\partial}{\partial r} (Ar) \delta r. \end{aligned}$$

$$\therefore H_\theta = \frac{\partial A}{\partial r} + \frac{A}{r}.$$

Accordingly it follows from (1.17) that

$$H_r = -\frac{2IS}{cr^3} \sin \phi \{(\cos ar + ar \sin ar) + j(-\sin ar + ar \cos ar)\}$$

and

$$H_\theta = \frac{IS \cos \phi}{cr^3} [(a^2 r^2 - 1) \cos ar - ar \sin ar - j\{(a^2 r^2 - 1) \sin ar + ar \cos ar\}].$$

If  $ar \ll 1$ , we may write  $\sin ar \doteq ar - \frac{a^3 r^3}{3!}$  and  $\cos ar \doteq 1 - \frac{a^2 r^2}{2}$ , then

$$H_r = -\frac{2IS}{cr^3} \sin \phi \left( 1 + \frac{a^2 r^2}{2} - j \frac{a^3 r^3}{3} \right)$$

and 
$$H_\theta = -\frac{IS \cos \phi}{cr^3} \left[ 1 - \frac{a^2 r^2}{2} + \frac{a^4 r^4}{3} + j \frac{2a^3 r^3}{3} \right].$$

When  $ar$  tends to zero these expressions are the components of the field due to a magnetic particle of moment  $IS/c$  and hence they then agree with Ampère's expression for the field of a small circuit carrying a steady current. Note, however, that the requirement is only that  $2\pi r/\lambda$  should be very small, and this can still obtain even when  $r$  tends to infinity compared with the physical dimensions of the circuit. Thus, suppose  $p/2\pi$  equals 50 cycles/sec. and  $r = 1$  km., then  $ar \doteq 1/10^3$ ; then for distances up to 1 km. from the circuit the inphase component of magnetic field will differ by less than one part in  $10^6$  from the value it would have if the current were 'frozen' steady at its instantaneous value.

Though all space is filled with displacement current, yet the field at any given point can be calculated in terms of the conduction current in the wire, and in terms of this alone. In this approach to the problem it is the only thing which matters, the rest of space does not enter explicitly into the calculation.

It should be remembered that the Lorentz equations are constructed on the supposition of moving charged particles, and we have tacitly but inevitably supposed a current is such a stream. Yet, in the limit, we arrive at Ampère's hypothesis, which was not bound to so narrow a description of current flow.

On making  $ar$  small in (1.18) we obtain

$$E_2 = \frac{a^3 IS \cos \phi}{c} \left\{ \left( -\frac{ar}{3} + \frac{4}{5!} a^3 r^3 \right) - j \left( \frac{1}{2} - \frac{1}{8} a^2 r^2 + \frac{1}{a^2 r^2} \right) \right\} \quad (1.18a)$$

and accordingly note it is only the quadrature term which tends to infinity when  $ar$  tends to zero. This is a key to an essential factor in the problem, but this aspect is better treated by starting close up to the circuit.

It is important to recognize that equations (1.15) are correct for all values of  $r$ , even down to zero; this follows from the statement of (1.8); hence they may be used to find the field at points very close indeed to the conductors.

Let the circuit discussed in relation to Fig. 1.2 be the rectangle shown in Fig. 1.3: it is desired to find the electric field at any point  $P$  on the perimeter. The process consists in finding the delayed vector potential at  $P$  due to the elements of current round the perimeter. At  $P$  the component of field along the wire arises only from the current in  $OA$  and in  $CB$ , since the vector potential is everywhere parallel to the current. At distance  $r$  from a current element  $I dl \sin pt$  we have

$$\begin{aligned} \frac{c \delta A}{I \delta l} &= \frac{\sin(pt - ar)}{r} = a \left( \frac{\cos ar}{ar} - j \frac{\sin ar}{ar} \right) \\ &= a \left\{ \left( \frac{1}{ar} - \frac{ar}{2!} \dots \right) - j \left( 1 - \frac{a^2 r^2}{3!} + \dots \right) \right\}. \end{aligned}$$

Consider first the quadrature component of  $A$  at  $P$ ; then the elements at  $R$  and  $Q$  together contribute

$$\begin{aligned} \frac{c \delta A}{I \delta l} &= -ja \left\{ - \left( 1 - \frac{a^2 PR^2}{3!} \right) + \left( 1 - \frac{a^2 PQ^2}{3!} \right) \right\} \\ &= -j \frac{a^3}{3!} (PR^2 - PQ^2) = -j \frac{a^3}{3!} RQ^2. \end{aligned}$$

Hence the total  $A$  at  $P$ , due to the sides  $CB$  and  $OA$ , is

$$A = -j \frac{I a^3 b h^2}{c^3 3!}, \text{ whence } \dagger E_P = -\frac{I p^4 b h^2}{c^4 3!} \sin pt, \text{ since } E = -\frac{I}{c} A.$$

This is independent of  $x$ , the coordinate of the point  $P$ , and hence  $E_P$

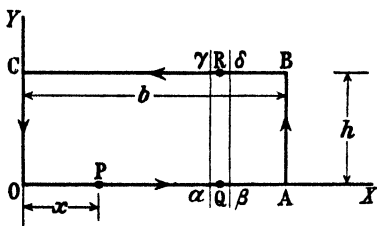


FIG. 1.3

has the same value at all points along  $OA$ . Accordingly, the voltage difference between  $O$  and  $A$  equals  $-\frac{I p^4 b^2 h^2}{c^4 3!}$ , and the e.m.f. round the complete rectangle is four times this amount; note that this e.m.f. is in antiphase with the current and therefore represents an output of work. The rate of working is given by  $P = (I^2/c) \frac{2}{3} a^4 S^2 \sin^2 pt$  and thus it is as though the circuit had a resistance equal to  $2a^4 S^2/3c$ . This apparent resistance is not associated with imperfect conductivity of the wire and therefore must represent power leaving the circuit. In other words, the circuit radiates energy and has a radiation resistance

$$R = 20a^4 S^2 = \frac{320\pi^4 S^2}{\lambda^4} \text{ ohms.}$$

Though the circuit in Fig. 1.3 was rectangular, brief consideration will show the same result would have been arrived at for a circuit of any shape, provided that terms in  $a^4 r^4$ , etc., are ignored.

The quadrature component of field is dominated by the term  $1/r$ , and evaluation of this leads to the familiar expression for self-inductance and need not detain us here.

If in (1.18a) the small circuit be supposed circular,‡ then it follows the e.m.f. round it equals

$$\frac{2}{3} \frac{S^2 a^4 I}{c} = \frac{2}{3} \frac{I p^4}{c^4} S^2,$$

a result in agreement with that we have just found: however, it was not

† The symbols  $E_P$  and  $E_Q$  are used to denote respectively the component of  $E$  which is in phase with or in phase quadrature with the current in the circuit.

‡ For circle of any radius see p. 74 and equation (1.84a).

obvious the inphase component in (1.18a) would hold correct right down to the circuit itself.

It follows from (1.18) that

$$E = \frac{a^3 IS \cos \theta}{c} \frac{\sqrt{(1 + 1/a^2 r^2)}}{ar} \sin(pt - \alpha), \quad (1.19)$$

where

$$\begin{aligned} \tan \alpha &= \frac{1 + ar \tan ar}{ar - \tan ar} \\ &= \tan \left( ar + \tan^{-1} \frac{1}{ar} \right). \\ \therefore \alpha &= ar + \tan^{-1} \frac{1}{ar}. \end{aligned} \quad (1.20)$$

Equation (1.19) shows that  $E$  becomes rapidly asymptotic to  $1/ar$ , the discrepancy being only 5 per cent. even when  $r/\lambda = \frac{1}{2}$ . Equation (1.20) shows that  $\alpha$  becomes rapidly asymptotic to  $ar$ , that is  $\alpha \rightarrow 2\pi(r/\lambda)$ . Hence the phase of the field will be the same as the phase of the current whenever the distance is a whole number of wavelengths, provided  $ar$  is large. When  $ar = 0$ ,  $\alpha = \frac{1}{2}\pi$ , and when  $r/\lambda = \frac{1}{2}$ ,  $\alpha = 197.4^\circ$ .

We will here call the reader's attention explicitly to the outstanding feature of the field described by (1.18) and by the expression for the magnetic field. That outstanding feature is not so much that the magnetic field is very much larger, at great distances, than we should have calculated by applying Ampère's hypothesis to an alternating current, as that the phase of the field changes progressively and regularly with a substantially constant wavelength. This change of phase is something quite new and unexpected, and is surely more remarkable than a mere discrepancy of magnitude, since it is a change in kind and not only in degree. The picture of a field which is already established and existing everywhere, but has the essential characteristic that its phase changes with a constant wavelength is, the writer suggests, a more helpful picture to the reader than that of a field which is travelling outwards with a constant speed. It is not the field which travels with a constant speed, but it is a hypothetical observer who would have to travel with this speed if he is to experience a field which does not alternate, but merely decreases smoothly in magnitude as the distance increases. When calculating the resultant field due to two separate coils the reader will readily perceive that in adding the contributions provided by the two separate coils he must allow for the difference in phase between these two contributions: a difference which depends only on the number of wavelengths which separate the two



coils, both of which are very distant from the point where the field is to be calculated. This description comes to the same thing numerically as saying that allowance must be made for the difference in time which the field of either coil takes to reach a given point in space; but no very precise meaning can be attached to the statement that a field takes a given time to reach a given place. Precision is attained only by introducing a hypothetical observer, who has to travel in a particular manner so that he does not experience any alternation of force. If the reader is subconsciously thinking of an experience like seeing the flash of a gun and hearing an explosion after an interval of time, then he is thinking of the real front of a disturbance, and is not thinking about continuing to listen to the steady howl of a siren. It is important to realize that equations like (1.18) do not apply until the initial front of the disturbance has spread beyond the point where the field is being observed. This is implicit in the solution, and has entered into it when it is supposed that the field at a given point alternates simple harmonically with the frequency of the source; this is tantamount to saying that the steady state has been reached and any transient effect has died out. The appropriate analysis for dealing with the transient effect does not appear to have been worked out.

If we have made our point that it is in general best to think of a field which has been established everywhere and which changes its phase with a constant wavelength, then we remind the reader that the product of the wavelength and the frequency is constant, and that the numerical value of this constant is  $c$ , the ratio between the electromagnetic and the electrostatic unit of charge. It is true that the product has the dimensions of a velocity and that if a hypothetical observer moves with this velocity he will not perceive an alternating field; but is this hypothetical experiment very illuminating? It is true that ranges can be calculated correctly by presuming that Radar pulses travel with velocity  $c$ , but do not let us bother about that here.

### 1.7. Field of a long filament carrying a current $I \sin pt$

Let a current  $I \sin pt$  flow along a thin wire of infinite length: it is thus postulated that there is no change of magnitude or of phase from point to point along the filament. Infinite length and absence of return current may offend the reader's sense of what constitutes a realizable problem; just as his senses were probably offended when he was first confronted with the similar problem for a steady current. Then it turned out he was being asked to do one stage only in evaluating an

integral round a complete circuit; the problem was soon made realizable by placing a return current parallel to the first. He is asked to accept the present problem as an act of faith and not demand more justification now; he will be shown later that, when the current is alternating, the

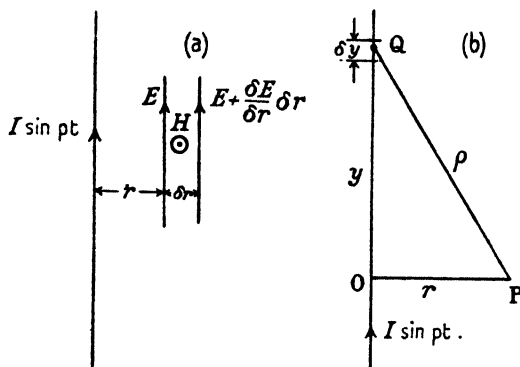


FIG. 1.4.

analysis represents far more than one step of a circuital integration, and is a realizable problem as it stands.

Because the filament has infinite length the field distribution is in two dimensions only: symmetry demands that the magnetic field is disposed in circles centred on the wire, and the electric field is everywhere parallel to the wire, without radial component anywhere. Since this field distribution is a very simple one, it is easy to derive the relevant equations *de novo*, without adapting them from (1.7), and to do so will give the reader experience of the general process. Curling right-handedly round a rectangle of unit height and radial width  $\delta r$  (see Fig. 1.4) gives  $\frac{\partial E}{\partial r} = \frac{1}{c} \frac{\partial H}{\partial t}$ , if  $H$  has the sense shown in the figure.

Curling right-handedly along magnetic lines gives

$$-2\pi(r+\delta r)\left(H + \frac{\partial H}{\partial r} \delta r\right) + 2\pi r H = \frac{4\pi}{c} \left\{ -\frac{2\pi r \delta r}{4\pi} \frac{\partial E}{\partial t} \right\},$$

$$\text{i.e.} \quad \frac{\partial H}{\partial r} + \frac{H}{r} = \frac{1}{c} \frac{\partial E}{\partial t}.$$

$$\therefore \frac{\partial^2 H}{\partial t \partial r} + \frac{1}{r} \frac{\partial H}{\partial t} = \frac{1}{c} \frac{\partial^2 E}{\partial t^2},$$

whence elimination of  $H$  gives

$$\frac{\partial^2 E}{\partial r^2} + \frac{1}{r} \frac{\partial E}{\partial r} = \frac{1}{c^2} \frac{\partial^2 E}{\partial t^2}.$$

In this problem  $E$  must pulsate harmonically everywhere, and accordingly

$$\frac{1}{c} \frac{\partial^2 E}{\partial t^2} = -\frac{p^2 E}{c^2} \equiv -a^2 E,$$

whence

$$\frac{d^2 E}{dr^2} + \frac{1}{r} \frac{dE}{dr} + a^2 E = 0. \quad (1.21)$$

A straightforward process shows this equation has a solution which is the infinite series

$$E = 1 - \frac{(\frac{1}{2}z)^2}{1!} + \frac{(\frac{1}{2}z)^4}{(2!)^2} - \frac{(\frac{1}{2}z)^6}{(3!)^2} + \dots \equiv J_0(z),$$

or the infinite series

$$E = \frac{2}{\pi} \left\{ (\log \frac{1}{2}z + \gamma) J_0(z) + (\frac{1}{2}z)^2 - \frac{(\frac{1}{2}z)^4}{(2!)^2} (1 + \frac{1}{2}) + \right. \\ \left. + \frac{(\frac{1}{2}z)^6}{(3!)^2} (1 + \frac{1}{2} + \frac{1}{3}) + \dots \right\} \equiv Y_0(z),$$

where  $z \equiv ar$ ,  $\gamma = 0.5772\dots$  (Euler's constant). The two infinite series are represented by the symbols  $J_0(z)$  and  $Y_0(z)$  respectively: they have been evaluated and tabulated. When  $z$  tends to zero we see that  $J_0(z)$  tends to unity and  $Y_0(z)$  tends logarithmically to minus infinity. Numerical evaluation will show that  $J_0(z)$  passes through zero between  $z = 2$  and  $z = 3$  and that  $Y_0(z)$  is positive when  $z$  is unity. The ratio of the  $(n+1)$ th to the  $n$ th term (starting with  $n = 0$ ) of  $J_0(z)$  is equal to  $\{z/2(n+1)\}^2$ , and this is less than unity provided  $n+1$  exceeds  $\frac{1}{2}z$ . Suppose, for example,  $z = 6$ , then the third term is the largest, and we can write

$$J_0(z) = 1 - (\frac{1}{2}z)^2 + \frac{(\frac{1}{2}z)^4}{(2!)^2} - \frac{(\frac{1}{2}z)^6}{(3!)^2} \left\{ 1 - \left(\frac{1}{4} \frac{z}{2}\right)^2 + \left(\frac{1}{4.5} \frac{z}{2}\right)^4 - \dots \right\}.$$

The infinite series in the curled brackets is less term by term than the series  $1 - (\frac{3}{4})^2 + (\frac{3}{4})^4 - \dots = 1/\{1 + (\frac{3}{4})^2\}$ , and is still less than the series  $1 + (\frac{3}{4})^2 + (\frac{3}{4})^4 - \dots$ . Thus the series is convergent and would still be convergent if all the terms were positive, instead of alternatively positive and negative. Thus the series is what is called absolutely convergent and it is permissible to differentiate it term by term. The convergence is not conditional on the alternations of sign, and hence the finite sum is not the finite difference between two infinite quantities. The series  $Y_0(z)$  is also absolutely convergent. A rough plot of  $J_0(z)$  and  $Y_0(z)$  (or plotting from tables) will show each is zero repeatedly and sensibly with period  $\pi$ . The solution for the small circuit was of the form  $\sin ar$  and  $\cos ar$ , and has thus led us to expect a solution of periodic form here.

We found there was an output of energy from the small circuit, and that it had a field whose R.M.S. value varied inversely as the distance and did not increase with time. The total energy associated with the field is obtained by integrating  $E^2/8\pi$  per unit volume through all space. Since  $E$  varies as  $1/r$ , the steady output of energy means that the field must be contained within a sphere of finite radius, and, moreover, a radius which is increasing uniformly with time, thus implying a wave-front in the old Huygensian sense. To use a seventeenth-century expression, the source is surrounded by an ever-expanding 'orb of virtue'. The idea of the uniformly expanding orb of virtue leads us to expect that the field will vary as  $r^{-1}$  in the cylindrical problem, and accordingly we expect that  $\sin z/z^{\frac{1}{2}}$  is either a solution of (1.21) or at least an approximate solution when  $z$  is large. If  $E = (\cos z + \sin z)/z^{\frac{1}{2}}$ , then substitution shows the right-hand side of (1.21) is equal to  $(\cos z + \sin z)/4z^{\frac{3}{2}} = E/4z^2$ , and this quantity gets smaller and smaller as  $z$  becomes large: thus we have obviously found an approximate solution when  $z$  is large. It is well known that

$$J_0(z) \doteq \sqrt{(1/\pi z)}(\cos z + \sin z) = \sqrt{(2/\pi z)}\cos(z - \tfrac{1}{4}\pi)$$

and  $Y_0(z) \doteq \sqrt{(2/\pi z)}\sin(z - \tfrac{1}{4}\pi)$ , when  $z$  is large.

We have now found the solution of Maxwell's equations appropriate to this problem, in a form suitable for numerical evaluation; and, moreover, see it has the character natural to expect.

Equation (1.21) is well known, and is called Bessel's equation: the generalized theory of it was published by the German astronomer F. W. Bessel in 1824, particular cases having been known during the previous century. The functions  $J_0(z)$  and  $Y_0(z)$  are called Bessel functions of the first and second kind respectively, and of zero order; later on we shall meet Bessel functions of higher order. Suffice it for the present to recognize  $J_0(z)$  and  $Y_0(z)$  as the symbols for a pair of infinite series which, when plotted, are reminiscent of  $\cos z$  and  $\sin z$  respectively, and more especially of  $\cos z/z^{\frac{1}{2}}$  and  $\sin z/z^{\frac{1}{2}}$ : they are tabulated in a form reminiscent of the tables of  $\cos z$  and  $\sin z$ .

Accordingly  $E = \{AJ_0(z) + BY_0(z)\}\sin pt$  is a possible solution of (1.21), where the constants  $A$  and  $B$  must be found so as to correspond with a current filament at the origin. Similarly

$$E = \{CJ_0(z) + DY_0(z)\}\cos pt$$

is a possible solution: hence the most complete solution is

$$E = \{AJ_0(z) + BY_0(z)\} + j\{CJ_0(z) + DY_0(z)\}. \quad (1.22)$$

In this problem some of the constants may be zero; to find them we

must use the delayed functions of equation (1.15). If, by using delayed functions, we can calculate  $E$  at one point, we shall thereby fix the values of  $A$ ,  $B$ , etc., and hence know  $E$  everywhere. Because the current is uniform in magnitude and phase there is no electric charge anywhere on the filament, and therefore the contribution arising from  $V$ , the delayed scalar potential, is zero. But the charge cannot be zero at the ends of the wire, even though these are at infinity: the wire must terminate, even though at infinity, and at these terminations conduction current ceases and charge accumulates. The charge which accumulates there is  $\int i dt = (I/p)\cos pt$ ; thus the two charges at infinity depend only on  $I$  and  $p$ , and not on the length of the wire, and thus its infinite length does not involve an infinite charge. The delayed scalar potential of this finite charge is, by (1.15), of the form  $[Q]/r$ , and thus tends to zero as  $r$  tends to infinity. Hence, as the two ends are pushed farther and farther away, the effect of the charges at them gets steadily less and less at points in the mid-equatorial plane of the filament and near its surface. Accordingly we are ignoring the contribution from, and not the existence of, the charges; and thus the statement of the problem is compatible with the essential requirements of electricity and of current flow.

Accordingly we calculate  $E$  from  $A$  alone: since conduction current flows only in the wire,  $A$  is everywhere parallel to the filament. Thus, with reference to Fig. 1.4(b), we have to evaluate

$$\frac{I}{c} \int_0^{\infty} \frac{\sin\{pt - a\sqrt{(r^2 + y^2)}\}}{\sqrt{(r^2 + y^2)}} dy,$$

and hence

$$-E = \frac{aI}{c} \int_{-\infty}^{+\infty} \left( \frac{\sin a\rho}{a\rho} + j \frac{\cos a\rho}{a\rho} \right) dy.$$

The inphase component can be evaluated without difficulty at  $r = 0$

because  $\int_{-\infty}^{+\infty} \frac{\sin ay}{ay} dy$  is known to be finite and equal to  $\pi$ . The quadra-

ture component is troublesome to evaluate because that integral tends, logarithmically, to infinity when  $r = 0$ . When  $ar = 0$ ,  $J_0(ar) = 1$  and  $Y_0(ar) = -\infty$ . Hence, using the inphase component only of (1.22), we have now found that

$$-\frac{aI\pi}{c} = (A \times 1 + B \times -\infty);$$

hence we must make  $B$  zero and  $A$  equal to  $-aI\pi/c$ .

The impasse with the quadrature term disappears when allowance is made for the small finite radius  $b$  of the wire. We must find the field at a point on the surface of this thin round wire, and to do so must evaluate the integral in two portions: the first from  $y = 0$  up to a value of  $y$  which is very large compared with  $b$  and yet very small compared with  $\lambda$ ; the second, from this point on to infinity.

Now

$$\begin{aligned} \int_0^y \frac{\cos a\rho}{a\rho} dy &= \int_0^y \left( \frac{1}{a\rho} - \frac{a\rho}{2} + \dots \right) dy \\ &\doteq \int_0^y \left\{ \frac{1}{a(b^2+y^2)^{\frac{1}{2}}} - \frac{1}{2}a(b^2+y^2)^{\frac{1}{2}} \right\} dy, \quad \text{if } a\rho \ll 1 \\ &= \left[ \frac{1}{a} \log\{y + \sqrt{(b^2+y^2)}\} - \frac{1}{4}a\{y\sqrt{(b^2+y^2)} + b^2 \log \frac{y + \sqrt{(y^2+b^2)}}{b} \right]_0^y \\ &= \frac{1}{a} \log \frac{y + \sqrt{(b^2+y^2)}}{b} - \frac{1}{4}a \left\{ y\sqrt{(b^2+y^2)} + b^2 \log \frac{y + \sqrt{(y^2+b^2)}}{b} \right\} \\ &\doteq \frac{1}{a} \log \frac{2y}{b} - \frac{1}{4}a \left( y^2 + b^2 \log \frac{2y}{b} \right), \quad \text{if } y \gg b \\ &\doteq \frac{1}{a} \left( \log \frac{2y}{b} - \frac{a^2 y^2}{4} \right). \end{aligned}$$

It is known that

$$\int_y^\infty \frac{\cos ay}{ay} dy = \frac{1}{a} \left( -\gamma - \log ay + \frac{a^2 y^2}{4} \dots \right).$$

Hence 
$$\int_{-\infty}^{+\infty} \frac{\cos a\rho}{a\rho} dy = -\frac{2}{a} \left( \gamma + \log \frac{ab}{2} \right), \quad \text{when } ab \ll 1.$$

Hence, from (1.22),

$$\frac{\pi a I}{c} Y_0(ab) = C \times 1 + D Y_0(ab),$$

whence  $C = 0$  and  $D = a\pi I/c$ , and accordingly

$$\frac{cE}{a\pi I} = -J_0(ar) + jY_0(ar) \quad (1.23)$$

and

$$-\frac{cA}{\pi I} = Y_0(ar) + jJ_0(ar). \quad (1.23a)$$

These two equations, very simple in form, are of fundamental importance, and are in constant use: they should be memorized.†

Now

$$H = -\frac{\partial A}{\partial r}.$$

$$\therefore H = \frac{a\pi I}{c} \{Y'_0(ar) + jJ'_0(ar)\}. \quad (1.24)$$

The same result can be achieved from the relation  $\frac{\partial E}{\partial r} = \frac{1}{c} \frac{\partial H}{\partial t}$ .

† Equation (1.23) can be derived directly by means of a known integral, as follows:

$$-\frac{cE}{I} = \int_{-\infty}^{+\infty} \left( \frac{\sin a\rho}{\rho} + j \frac{\cos a\rho}{\rho} \right) dy, \quad \text{where } \rho^2 = y^2 + r^2.$$

Put  $\rho = r \cosh \theta$  and  $y = r \sinh \theta$ , then

$$\begin{aligned} -\frac{cE}{I} &= \int_{-\infty}^{+\infty} \{ \sin(ar \cosh \theta) + j \cos(ar \cosh \theta) \} d\theta \\ &= a\pi \{ J_0(ar) - j Y_0(ar) \}. \end{aligned}$$

See Watson, p. 180, equations (12) and (13). The writer is indebted to Mr. M. Gardiner for drawing his attention to the integral form of  $J_\nu(z)$  and to its application here.

However, there is much to be said for the longer derivation we have used since it avoids a recondite property of Bessel functions. But it is satisfactory to have this known property of Bessel functions to use since by it we do derive the field of a current filament directly from the delayed potentials without the intervening step of using Maxwell's equations, a step which must be unnecessary in principle, since it has entered into the derivation of the delayed potentials.

An alternative approach by known integrals is as follows:

$$\begin{aligned} A &= \frac{2I}{c} \int_0^\infty \frac{\sin(pt - a\rho)}{\rho} dy \\ &= \frac{2I}{c} \int_0^\infty \left( \frac{\cos a\rho}{\rho} - j \frac{\sin a\rho}{\rho} \right) dy. \end{aligned}$$

Put  $\rho^2 = r^2 + y^2 = r^2 \theta^2$ , then  $y = r(\theta^2 - 1)^{\frac{1}{2}}$  and  $dy = \frac{r\theta d\theta}{y} = \frac{r\theta d\theta}{(\theta^2 - 1)^{\frac{1}{2}}}$ .

$$\therefore A = \frac{2I}{c} \int_1^\infty \left\{ \frac{\cos(ar\theta)}{(\theta^2 - 1)^{\frac{1}{2}}} - j \frac{\sin(ar\theta)}{(\theta^2 - 1)^{\frac{1}{2}}} \right\} d\theta.$$

$$\text{Now} \quad \int_1^\infty \frac{\cos(ar\theta) d\theta}{(\theta^2 - 1)^{\frac{1}{2}}} = -\frac{1}{2}\pi Y_0(ar) \quad \text{and} \quad \int_1^\infty \frac{\sin(ar\theta) d\theta}{(\theta^2 - 1)^{\frac{1}{2}}} = \frac{1}{2}\pi J_0(ar),$$

see McLachlan, *Bessel Functions for Engineers*, formulae (66) and (29).

$$\therefore A = -\frac{I\pi}{c} \{ Y_0(ar) + j J_0(ar) \}.$$

$$\therefore \frac{cE}{I} = a\pi \{ -J_0(ar) + j Y_0(ar) \}.$$

Since the series for  $J_0$  and  $Y_0$  are absolutely convergent, they can be differentiated term by term, and hence it may be found that

$$-J'_0(z) = \frac{1}{2}z \left\{ 1 - \frac{(\frac{1}{2}z)^2}{2} + \frac{(\frac{1}{2}z)^4}{3(2!)^2} - \frac{(\frac{1}{2}z)^6}{4(3!)^2} + \frac{(\frac{1}{2}z)^8}{5(4!)^2} - \dots \right\},$$

a series reminiscent of  $J_0(z)$ . It is the Bessel function of order unity and is written  $J_1(z)$ . Hence  $J'_0(z) = -J_1(z)$  and also  $Y'_0(z) = -Y_1(z)$ , and thus we write

$$H = \frac{a\pi I}{c} \{Y_1(ar) + jJ_1(ar)\}. \quad (1.25)$$

But

$$Y_1(z) \equiv -Y'_0(z) = -\frac{2}{\pi} \left\{ \frac{1}{z} J_0(z) + (\log \frac{1}{2}z + \gamma) J'_0(z) + z + \dots \right\}$$

$$\doteq -\frac{2}{\pi z} (1 - \frac{1}{2}z^2 \log z), \quad \text{when } z \rightarrow 0.$$

$$\therefore H \doteq -\frac{a\pi I}{c} \left\{ -\frac{2}{\pi ar} - j\frac{ar}{2} \right\}, \quad \text{when } ar \rightarrow 0$$

$$= \frac{2I}{rc} \left( 1 + j\frac{\pi a^2 r^2}{4} \right),$$

and this reduces to the familiar expression, for a steady current, when  $ar$  tends to zero; again, the general expression for the field reduces to that derived from Ampère's hypothesis when the frequency tends to zero. Suppose the frequency is 50 cycles/sec., then  $ar \doteq 1/10^3$  at a distance of 1 km. from the wire. There the fractional value of the quadrature component of  $H$  is less than one part in a million.

At the surface of the wire (1.23) gives  $cE/a\pi I = -1 + jY_0(ab)$ . Hence there is an antiphase field at the surface of the wire and this represents an output of power equivalent to a resistance  $a\pi/c$  per unit length, which is  $30\pi^2$  ohms per half wavelength. This is the radiation resistance per half wavelength of a filament in which the current is constant in magnitude and phase. The reactive field is

$$-\frac{\pi a I}{c} Y_0(ab) = -\frac{2pI}{c^2} (\log ab - 0.1159) = \frac{2pI}{c^2} \log \left( \frac{0.18\lambda}{b} \right).$$

Hence the inductance per unit length of a fine wire filament is equal to that of a coaxial cable whose outer conductor has a radius  $0.18\lambda$  and inner conductor a radius  $b$ . Fig. 1.5 depicts the manner in which the two components of  $E$  vary with distance from the centre of a tubular filament of radius  $b/\lambda = 1/100$ . When  $ar$  is large (1.23) reduces to

$$\frac{cE}{a\pi I} = -\sqrt{\left(\frac{2}{\pi ar}\right)} \cos(pt - ar - \frac{1}{4}\pi), \quad (1.26)$$



and this shows the phase of the wave is such that it is as though the filament were  $\frac{1}{2}\lambda$  nearer the observation point than it really is. This is in interesting contrast to the magnetic field of a very small circuit, where we found the phase corresponded precisely with the distance from the elementary circuit.

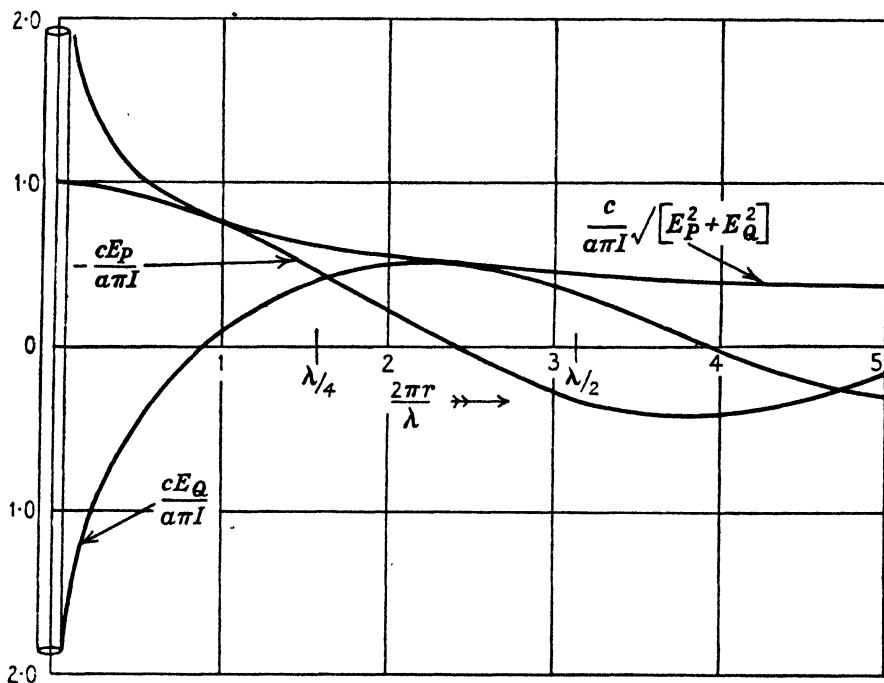


FIG. 1.5. Distribution of electric field of a current filament.

Since  $\oint H dl = 4\pi \times (\text{conduction current plus displacement current})$ , it follows this total current is zero at that radius at which  $H$  is zero. There is no radius at which  $|H|$  is zero, but there are successive radii at which either one or other component of  $H$  is zero. Hence the first radius at which the inphase component of  $H$  is zero marks the boundary where the total inphase displacement current is equal and opposite to the conduction current in the wire. By equation (1.25), this occurs when  $Y_1(ar)$  is zero for the first time, and this is when  $ar = 2.18$  or  $r/\lambda = 0.347$ . This radius may be regarded as the boundary of the original current flow in the wire, though this concept is not very helpful, since the essence of the Maxwell concept is that current flows everywhere. However, it may help the reader to realize that the conduction current flowing in the wire is made circuital by displacement currents which

are generated by that said conduction current and not generated by electric charges accumulating on the surface of the wire. The presence of an electric force does not necessarily depend on the accumulation of electric charge. If the reader insists on inquiring how the current could be produced in the filament he can be given a convincing reply: it could be generated by an incident plane wave. There are, however, other methods of even greater interest.

### 1.8. Field of a tubular current of any radius

Equation (1.21) must represent the field of a current flowing along a tube of any radius and distributed uniformly round the circumference, and the solution given in (1.22) must be applicable in such circumstances. We have found the constants  $A$ ,  $B$ , etc., appropriate to a filament, now we must find them for a tube of any radius  $R$ : we shall write  $2\pi R/\lambda \equiv k$ . The current flowing along the tube and distributed uniformly round the circumference of the tube may be decomposed into current filaments. The centre of the tube is equidistant from all such filaments, and therefore the field at the centre is, by (1.23), given by the relation

$$\frac{cE}{a\pi I} = -J_0(k) + jY_0(k).$$

Hence substitution in (1.22) gives

$$\frac{a\pi I}{c} \{-J_0(k) + jY_0(k)\} = (A' + B' \times -\infty) + j(C' + D' \times -\infty).$$

Accordingly  $B'$  and  $D'$  must be zero;

$$A' = -\frac{a\pi I}{c} J_0(k) \quad \text{and} \quad C' = \frac{a\pi I}{c} Y_0(k),$$

whence 
$$\frac{cE}{a\pi I} = \{-J_0(k) + jY_0(k)\} J_0(ar), \quad (1.27)$$

and this equation gives the field at all internal points.

The field at the surface of the very thin tube is given by

$$\frac{cE}{a\pi I} = \{-J_0(k) + jY_0(k)\} J_0(k). \quad (1.27 a)$$

Using (1.23) for external points gives

$$\begin{aligned} \frac{a\pi I}{c} \{-J_0(k) + jY_0(k)\} J_0(k) \\ = \{-A'' J_0(k) + B'' Y_0(k)\} + j\{-C'' J_0(k) + D'' Y_0(k)\}. \end{aligned}$$

Accordingly  $B''$  and  $C''$  must be zero, whence the external field is given by

$$\frac{cE}{a\pi I} = J_0(k)\{-J_0(ar) + jY_0(ar)\}. \quad (1.28)$$

This shows the external field is the same as that of a current filament of strength  $J_0(k)I$ .

Now  $J_0(k) = 0$  when  $k = 2.405, 5.520, 8.654$ , etc. (values whose difference approaches more and more closely to  $\pi$  but is never precisely equal to  $\pi$ ), which is when  $R/\lambda = 0.382, 0.88$ , etc. If the very thin tube has any one of these critical radii, then the external field is precisely zero everywhere, and the conduction current in its walls cannot be detected by any external test; this discovery of a non-radiating current is very interesting and perhaps surprising. The mechanism by which the external field becomes zero will become apparent in the next chapter, where that aspect of the problem is discussed.

The inphase component of field at the surface is proportional to  $J_0^2(k)$ : it follows the radiation resistance, is  $30\pi^2 J_0^2(k)$  ohms per half wavelength, and the apparent inductance is  $2J_0(k)Y_0(k)$  cm. per cm. of length. The inductance is zero when  $Y_0(k) = 0$ , and this occurs when  $R/\lambda = 0.142, 0.63$ , etc.; in such circumstances a condition is attained which corresponds with a 'rejector circuit' resonance. If  $R/\lambda$  lies between 0.142 and 0.63 the reactance is capacitive. The reader should recognize that a capacitive reactance can arise even though there are no charges present: this is another aspect of the general thesis that a quadrature electric field need not imply the presence of charge: whether such field is in leading or lagging phase quadrature may depend only on physical dimensions and not on accumulation of charge.

The internal magnetic field is given by the equation

$$\begin{aligned} H &= -\frac{a\pi I}{c}\{-J_0(k) + jY_0(k)\}J_1(ar) \\ &\doteq \frac{2\pi^3}{\lambda} \frac{r}{\lambda}\{J_0(k) - jY_0(k)\}, \quad \text{when } r/\lambda \ll 1. \end{aligned}$$

This shows there is always magnetic field inside a tube, the quadrature component being the more important when  $k$  is small; it reduces to zero for a steady current.

### 1.9. Field of a filament carrying current $I \cos(\pi y/g) \sin pt$

The next case to consider is a filament in which the current is constant in phase along the infinite length, but has a magnitude which varies harmonically with distance. This is a more complex problem, because

now there must be charge on the filament, and this may well contribute to the field, and accordingly it may seem to be essential to evaluate the delayed scalar potential. The current distribution is illustrated diagrammatically in Fig. 1.6; the current is always zero at points typified by *C*, *D*, *E*, *F*, etc., separated from one another by distance *g*. If at any

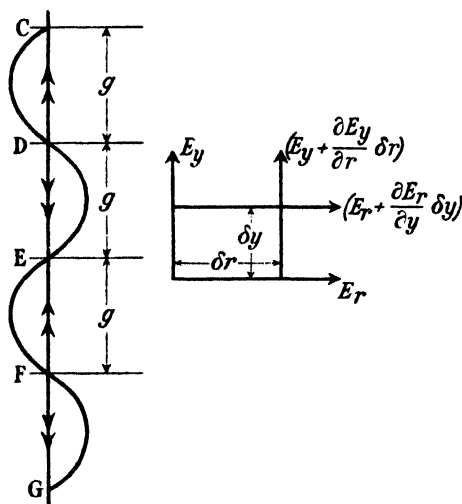


FIG. 1.6.

instant of time current is flowing upwards along all the lengths *DC* and *FE*, then it is flowing downwards along all the length of *DE* and *FG*, etc. If the filament were of length  $2g$ ,  $4g$ , etc., the field would be zero at a distant point in the equatorial plane because the field of *DE* would cancel that of *CD*; it would be appreciable only at points high above or below the equatorial plane. But here we have the analytical abstraction of a filament of infinite length, and it is not superficially apparent whether the field will be finite or zero at a large distance; only complete analysis can give the answer. If the charge density were constant along the length, the field due to it would be purely radial; it is unlikely the sinoidal distribution of charge will annul the radial component of electric field completely. There will certainly be an axial component of *E* because this will arise from the vector potential, which is purely axial; it will be a very special case if the net axial field is zero, and this can happen only if the axial component arising from the charges just neutralizes, at all points, the axial component due to  $dA/dt$ .

The axial symmetry demands that *H* must be disposed in circles centred on the wire. Since we now have to allow for a radial component  $E_r$  of electric force there will be a radial component of displacement

current, and hence the curl of  $H$  round it will not be zero; hence, at any given radius,  $H$  is a function of  $y$  such that  $\frac{\partial H}{\partial y} = -\frac{1}{c} \frac{\partial E_r}{\partial t}$ . Curling right-handedly round the rectangle inset in Fig. 1.6 gives

$$\frac{\partial E_y}{\partial r} - \frac{\partial E_r}{\partial y} = \frac{1}{c} \frac{\partial H}{\partial t}.$$

These two relations show that  $E_r$  and  $E_y$  can be found if  $H$  is known. But  $H$  can be found from the vector potential alone, since  $\text{curl } A = H$ ; but  $A$  depends only on the current, and hence  $H$  can be calculated without reference to the charges. Thus it is not essential to perform direct integration from the charges to calculate  $E_r$  and  $E_y$  (even though  $E_r$  can arise only from the charges), since they can be derived from  $H$ , which depends only on the current. It is not essential to make explicit reference to the charges, though implicit reference is made to them through the current distribution, which involves a distribution of charge.

The vector potential at any point in a plane perpendicular to the filament and crossing it at points such as  $C$ ,  $D$ ,  $E$ , etc., in Fig. 1.6 must be zero, since it is equidistant from similar and oppositely directed current elements. Accordingly, at any radius,  $A$  must be zero in planes separated by  $g$  and must be periodic, and thus it is natural to expect that  $A/I = f(r)\cos\pi y/g$  when the origin is on the filament and midway between the nodes of current. Now  $A$  is an analytical tool which has been fashioned so that each of its three rectangular components satisfies the wave equation, see (1.12) and (1.13). Here there is only one component of  $A$ , and that is parallel to the current. Accordingly

$$\frac{\partial^2 A}{\partial r^2} + \frac{1}{r} \frac{\partial A}{\partial r} + \frac{\partial^2 A}{\partial y^2} + a^2 A = 0.$$

If  $A$  varies as  $\cos\pi y/g \equiv \cos by$  we have

$$\frac{\partial^2 A}{\partial r^2} + \frac{1}{r} \frac{\partial A}{\partial r} + (a^2 - b^2)A = 0,$$

which we write

$$\frac{\partial^2 A}{\partial r^2} + \frac{1}{r} \frac{\partial A}{\partial r} + a'^2 A = 0, \quad \text{where } a'^2 \equiv a^2 - b^2.$$

Hence, as in (1.22), we now have

$$A = \{BJ_0(a'r) + jCY_0(a'r)\}\cos by,$$

provided  $a > b$ , which is  $g > \frac{1}{2}\lambda$ .

To find  $B$  and  $C$  we must evaluate  $A$  at the surface of the filament: at the origin we have

$$\begin{aligned}\frac{cA}{I} &= \int_{-\infty}^{+\infty} \frac{\cos by \sin(pt - py/c)}{y} dy \\ &= \int_{-\infty}^{+\infty} \frac{\cos by \cos ay}{y} dy - j \int_{-\infty}^{+\infty} \frac{\cos by \sin ay}{y} dy,\end{aligned}$$

therefore

$$\begin{aligned}\frac{2cA}{I} &= \int_{-\infty}^{+\infty} \frac{\cos(a+b)y + \cos(a-b)y}{y} dy - j \int_{-\infty}^{+\infty} \frac{\sin(a+b)y + \sin(a-b)y}{y} dy \\ &\equiv \int_{-\infty}^{+\infty} \left( \frac{\cos u \, du}{u} + \frac{\cos w \, dw}{w} \right) - j \int_{-\infty}^{+\infty} \left( \frac{\sin u \, du}{u} + \frac{\sin w \, dw}{w} \right).\end{aligned}$$

Now  $\int_{-\infty}^{+\infty} (\sin u \, du)/u = \frac{1}{2}\pi$ : if  $b > a$  (i.e.  $g < \frac{1}{2}\lambda$ ), then  $w$  is negative and the quadrature component of  $A$  is zero: a truly startling discovery of great importance.

If  $a > b$ , then the quadrature integral equals  $2\pi$ . It should be noted that the sign of the inphase integral does not change if  $w$  is negative: we have found it already, with much labour, just before arriving at (1.23). Hence at the origin  $-cA/\pi I = Y_0(a'b) + jJ_0(a'b)$ , and at  $y = -\frac{1}{2}g$  it is obviously zero. If we shift the origin a distance  $z$  along the axis we can write the current distribution as  $I \cos bz \cos by + I \sin bz \sin by$ . Now  $A$  is zero at point  $z$  for the second term in this distribution, and hence it follows that  $-cA/\pi I = \{Y_0(a'b) + jJ_0(a'b)\} \cos by$  along the surface of the filament, and this shows the general expression is

$$-\frac{cA}{\pi I} = \{Y_0(a'r) + jJ_0(a'r)\} \cos by, \quad (1.29)$$

which differs from (1.23a) only in the term  $\cos by$  and in that  $a'$  has replaced  $a$ ; it degenerates to (1.23a) when  $b$  tends to zero. Since  $H = -\partial A/\partial r$  we have

$$-\frac{cH}{a'\pi I} = \{Y_1(a'r) + jJ_1(a'r)\} \cos by. \quad (1.30)$$

Since  $\frac{\partial H}{\partial y} = -\frac{1}{c} \frac{\partial E_r}{\partial t}$ ,

we have  $\frac{caE_r}{ba'\pi I} = \{J_1(a'r) + jY_1(a'r)\} \sin by,$  (1.31)

and from the relation

$$\frac{\partial E_y}{\partial r} - \frac{\partial E_r}{\partial y} = \frac{1}{c} \frac{\partial H}{\partial t},$$

we have 
$$\frac{cE_y}{a\pi I} = \left(1 - \frac{b^2}{a^2}\right) \{-J_0(a'r) + jY_0(a'r)\} \cos by,$$

or 
$$\frac{acE_y}{a'^2\pi I} = \{-J_0(a'r) + jY_0(a'r)\} \cos by. \quad (1.32)$$

(1.32) degenerates into (1.23) and (1.30) into (1.25) when  $b$  tends to zero, and then  $E_r$  tends to zero as  $b^2$ . Before interpreting equations (1.30) to (1.32) we will consider the case where  $b > a$ , which is  $g < \frac{1}{2}\lambda$ . We now write  $a''^2 \equiv b^2 - a^2 = -a'^2$ , so that

$$\frac{\partial^2 A}{\partial r^2} + \frac{1}{r} \frac{\partial A}{\partial r} - a''^2 A = 0,$$

and the solution of this is

$$A = BI_0(a''r) + jCK_0(a''r),$$

where  $I_0$  and  $K_0$  are the modified Bessel functions such that

$$I_0(z) = J_0(jz).$$

We have seen that the quadrature component of  $A$  is zero at the surface if  $g < \frac{1}{2}\lambda$ , and hence  $C$  in the above is zero. But even when  $g < \frac{1}{2}\lambda$  the inphase component at the surface remains unchanged in value when  $a-b$  is negative. When  $z$  is very small  $Y_0(z) \doteq (2/\pi) \log z$  and  $K_0(z) \doteq -\log z$ . When  $g > \frac{1}{2}\lambda$ ,  $A = (\pi I/c)Y_0(a'b)$  at the surface, and this we may write as  $A = -(2I/c)K_0(a''b)$ . Accordingly, the general expression is

$$\frac{cA}{I} = 2K_0(a''r) \cos by, \quad (1.33)$$

and this leads to 
$$\frac{cH}{a''I} = 2K_1(a''r) \cos by, \quad (1.34)$$

$$-\frac{acE_r}{a''bI} = 2jK_1(a''r) \sin by, \quad (1.35)$$

and 
$$\frac{acE_y}{a''^2I} = 2jK_0(a''r) \cos by. \quad (1.36)$$

When  $z$  exceeds about 2,  $K_0(z) \doteq \sqrt{(\pi/2z)}e^{-z}$  and hence, provided  $g < \frac{1}{2}\lambda$ , the fields do tend rapidly to zero as the distance from the filament increases. It was pointed out initially that it was not obvious that the field would be appreciable, since one loop of current must

tend to neutralize the next: we have found it does fall rapidly to zero unless  $g > \frac{1}{2}\lambda$ , and this is an essential condition for the field to be appreciable at a large distance. If  $g < \frac{1}{2}\lambda$ , then  $H$  is everywhere in phase with  $I$ , and both  $E_r$  and  $E_y$  are in phase quadrature with  $I$ : if  $g > \frac{1}{2}\lambda$  then, from (1.31), etc., the fields fall off as  $r^{-1}$ , and their phase changes with a wavelength  $\lambda\{1 - (2\lambda/g)^2\}^{-1/2}$ . It is surely as unexpected to find the wavelength of the disturbance is increased as it is surprising to find the field can be finite at large distances. An observer travelling with speed  $c\{1 - (2\lambda/g)^2\}^{-1/2}$  would experience a force on his test charge which decreased continuously as the distance increased but did not pulsate. But the mass of the test charge would have passed through infinity in attaining this speed, so it would seem the hypothetical observation is meaningless. It is another example of the difficulties encountered in the concepts of propagation velocity. It is well to remember that the presence of a solid dielectric would decrease the wavelength, and the manner in which this shortening comes about is as difficult to visualize as the lengthening we have encountered in this problem.

Now consider the special case where  $b$  tends to the value  $a$ , i.e.  $g = \frac{1}{2}\lambda$ , so that  $a'r$  tends to zero for all values of  $r$ . Then we may write (1.32) as

$$\frac{acE_y}{\pi I} = \frac{1}{r^2} \left\{ -a'^2 r^2 + j \frac{2}{\pi} a'^2 r^2 \log a'r \right\} \cos by;$$

since  $x \log x$  tends to zero with  $x$  it follows that  $E_y$  tends to zero as  $a'$  tends to zero. Since there is now no axial displacement current it follows at once that  $H \times 2\pi r = 4\pi I \cos by$ , and this result also follows from (1.30), since  $J_1(a'r) = 0$  when  $a'r = 0$  and  $Y_1(a'r) \rightarrow -2/\pi a'r$ .

Similarly

$$-\frac{cE_r}{I} = \frac{2b}{ar} \sin by \cos pt = -\frac{2q}{r},$$

since  $dq/dt = di/dy = bI \sin by$ . Accordingly the fields at any given section are precisely the same as they would be if the current were steady, or the charge static and continued to infinity along the filament, at the local value. In this very special case the fields fall off as  $1/r$ , and the electric field is purely radial everywhere, even at the surface, and this means no work is done on the current:  $E$  and  $H$  are in phase quadrature, and their phase does not change with distance.

It follows from (1.32) that the output of work equals  $(a'^2 \pi / ac) I^2 \cos^2 by$  per unit length, and hence the radiation resistance per unit length is constant and equal to  $a'^2 \pi / a$ : hence the radiation resistance per loop



of current, measured from the middle of the loop, is  $30\pi^2(2g/\lambda - \lambda/2g)$  ohms.

### 1.10. Field of a current $I \cos by \sin pt$ distributed round a tube of radius $R$

Proceeding as in § 1.8 it can readily be shown that

$$-\frac{cH}{a'\pi I} = J_0(k)\{Y_1(a'r) + jJ_1(a'r)\}\cos by, \quad \text{for } r > R, \quad (1.37)$$

$$\text{or} \quad = J_1(ar)\{Y_0(k) + jJ_0(k)\}\cos by, \quad \text{for } R > r,$$

and to obtain  $E_r$  and  $E_y$  it is necessary only to place  $J_0(k)$  in front of the curled bracket in (1.31) and (1.32), remembering that  $k = a'R$ . When  $g < \frac{1}{2}\lambda$ , (1.33) to (1.36) become

$$\frac{cA}{I} = 2I_0(k)K_0(a''r)\cos by, \quad \text{for } r > R \quad (1.38)$$

$$\text{or} \quad = 2K_0(k)I_0(a''r)\cos by, \quad \text{for } R > r,$$

$$\frac{cH}{a''I} = 2I_0(k)K_1(a''r)\cos by, \quad \text{for } r > R \quad (1.39)$$

$$\text{or} \quad = -2K_0(k)I_1(a''r)\cos by, \quad \text{for } R > r,$$

$$-\frac{acE_r}{a''bI} = 2jI_0(k)K_1(a''r)\sin by, \quad \text{for } r > R \quad (1.40)$$

$$\text{or} \quad = -2jK_0(k)I_1(a''r)\sin by, \quad \text{for } R > r,$$

$$\frac{acE_y}{a''^2I} = 2jI_0(k)K_0(a''r)\cos by, \quad \text{for } r > R \quad (1.41)$$

$$\text{or} \quad = 2jK_0(k)I_0(a''r)\cos by, \quad \text{for } R > r.$$

If  $a''$  is small (1.39) gives  $cH/I = (2I/R)\cos by$  at the outside surface, as it should do, and  $cH/I = (k^2 \log k)/R$  at the inside surface. If  $g \ll \frac{1}{2}\lambda$ , then  $a'' \doteq b$ ; then if  $k$  is large, which means  $\pi R/g$  greater than, say, unity, we find  $cH/I = 1/R$  at the outside surface and  $-1/R$  at the inside surface.

### 1.11. Vector potential of a blade of current

We shall often need the vector potential of a blade of current, by which we mean a narrow strip of infinite length with current flowing transversely to the length. Of course there must be charges along the edges of the blade; but here we are concerned only with the vector potential which depends only on the current. We may use Fig. 1.4 if

we suppose the current is flowing transversely to the filament and hence across a blade of width  $\delta l$ . Then

$$\frac{A}{c} = \int_{-\infty}^{+\infty} \frac{[i] \delta l}{\rho} dy;$$

this is the same integral we had to evaluate for the current filament save that now  $I \delta l$  must replace  $I$ ; accordingly, by (1.23 a),

$$-\frac{cA}{\pi I \delta l} = Y_0(ar) + jJ_0(ar). \quad (1.42)$$

Though the extension is very obvious, it is convenient for reference to give it a special section here, because we often have to make use of it. If the current is  $I \cos by$  along the length, then (1.42) will become (1.29) or (1.33), remembering that  $I$  must be replaced by  $I \delta l$  in them. It must be remembered that although  $A$  is a function of  $r$  only, its direction is always parallel to the blade.

### 1.12. Field of a pair of like current filaments

Let a pair of filaments be separated a distance  $2R$  and carry equal currents flowing in like sense: in Fig. 1.7 a cross-section of the filaments is represented by the points  $A$  and  $B$ . To simplify the algebra we shall suppose the current is constant in magnitude along the length; if this magnitude varies as  $\cos by$  we have but to replace  $a$  by  $a'$  or  $a''$  and to use the results of § 1.9. The field pattern must be symmetrical about the line  $AB$  and also about the normal to it through  $O$ : accordingly, at the point  $P(r, \theta)$  its equation must be of the form

$$E = f(r) + \phi(r) \cos 2\theta + \psi(r) \cos 4\theta + \dots$$

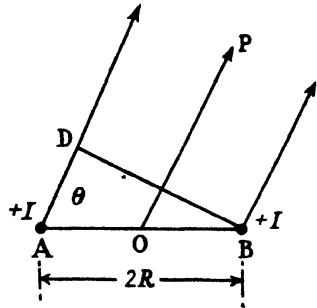


FIG. 1.7.

Expressing (1.7) in polar form shows the axial component of  $E$  (and there is no other component if the magnitude of current is constant along the filaments) must satisfy the equation

$$\frac{\partial^2 E}{\partial r^2} + \frac{1}{r} \frac{\partial E}{\partial r} + \frac{1}{r^2} \frac{\partial^2 E}{\partial \theta^2} + a^2 E = 0. \quad (1.43)$$

If this has a solution of the form  $E = F(ar) \cos n\theta$ , substitution shows that

$$\frac{\partial^2 F}{\partial r^2} + \frac{1}{r} \frac{\partial F}{\partial r} + \left( a^2 - \frac{n^2}{r^2} \right) F = 0.$$

This is Bessel's equation of order  $n$ , and its solution is

$$E = [\{AJ_n(ar) + BY_n(ar)\} + j\{CJ_n(ar) + DY_n(ar)\}]\cos n\theta,$$

since symmetry has shown that terms involving  $\sin n\theta$  are inadmissible here.

When  $ar$  tends to infinity the form of solution is straightforward, since either filament alone would produce at  $P$  a field of the same magnitude  $E_0$ . The distance from  $P$  to filament  $A$  tends to exceed that from  $B$  by  $2R \cos \theta$ : this difference is too small compared with  $r$  to have appreciable effect on the magnitude, but does have appreciable effect on the relative phase of the contributions to the resultant field made by each of the two separated filaments. The resultant field is the vector sum of the two contributions, and this differs insensibly from  $2 \cos(k \cos \theta) E_0$ , when  $R/r$  tends to zero. Hence, when  $ar$  tends to infinity, the solution of (1.43) must degenerate into

$$\frac{cE}{2a\pi I} = \{-J_0(ar) + jY_0(ar)\} \cos(k \cos \theta). \quad (1.44)$$

A well-known Fourier expansion for  $\cos(k \cos \theta)$  is

$$\cos(k \cos \theta) = J_0(k) - 2\{J_2(k) \cos 2\theta - J_4(k) \cos 4\theta + \dots\}. \quad (1.45)$$

Substitution of (1.45) in (1.44) would be of the form of the general solution if  $-J_0(ar) + jY_0(ar)$  could be replaced by  $-J_n(ar) + jY_n(ar)$ . The recurrence formula of Bessel functions is

$$J_{n+1}(z) = -J_{n-1}(z) + \frac{2n}{z} J_n(z)$$

and 
$$Y_{n+1}(z) = -Y_{n-1}(z) + \frac{2n}{z} Y_n(z),$$

and this shows that  $J_0(z) = -J_2(z) = J_4(z)$ , etc., and  $Y_0(z) = -Y_2(z)$ , etc., when  $z$  tends to infinity. Hence at infinity it is permissible to write

$$\begin{aligned} \frac{cE}{2a\pi I} = \{-J_0(ar) + jY_0(ar)\} J_0(k) + \\ + 2\{-J_2(ar) + jY_2(ar)\} J_2(k) \cos 2\theta + \dots, \end{aligned} \quad (1.46)$$

and this is a solution of (1.43). Accordingly it is the solution of our problem, and we have found an expression for the field of two like filaments with respect to an origin midway between them. When  $ar < k$ , then  $k$  and  $ar$  must be interchanged in (1.46).

The general term is  $\{-J_{2n}(ar) + jY_{2n}(ar)\} J_{2n}(k) \cos 2n\theta$ , and it is neces-

sary to consider the value this assumes when  $n$  is infinite and  $ar$  has any value. Now

$$J_n(ar) = \frac{(ar/2)^n}{n!} \left\{ 1 - \frac{(ar/2)^2}{n+1} + \dots \right\},$$

and this tends to  $\frac{(ar/2)^n}{n!}$  for sufficiently large  $n$  for any value of  $ar$ .

Hence  $J_{2n}(k)J_{2n}(ar)$  tends to  $(ark/4)^{2n}/\{(2n)!\}^2$ , and it is easy to show this is an absolutely convergent series for all values of  $ark$ . Since  $\cos 2n\theta$  is never greater than unity it follows, *a fortiori*, the real part of (1.46) is absolutely convergent. For sufficiently large  $n$  the dominant term in  $Y_n(z)$  is  $-(1/\pi)(n-1)!(2/z)^n$ , and thus  $Y_n(z)$  then increases without limit. But for large enough  $n$  we have

$$J_{2n}(k)Y_{2n}(ar) = -\frac{1}{\pi} \frac{1}{2n} \left( \frac{k}{ar} \right)^{2n},$$

and this is an absolutely convergent series for all values of  $ar$  greater than  $k$ .

At  $k = ar$  and  $\theta = 0$  or  $\pi$  the series degenerates ultimately into the form  $\sum 1/n$ , and this diverges logarithmically to infinity. This is what is required, because at these two points there are current filaments, and at them the quadrature component of force is proportional to  $Y_0(0) + Y_0(2k)$ . Now  $\sum (1/n)\cos n\theta$  is known to be convergent, though not absolutely convergent, and thus (1.46) is valid everywhere except at the two filaments, and may be differentiated term by term except at the radius  $r = R$ .

It should be noted explicitly that the inphase component of  $E$  is absolutely convergent even at the filaments themselves, and this is a characteristic of all our problems: then it is the field against which the currents do work. At either filament its value is

$$-\frac{cE_P}{a\pi I} = 2[J_0^2(k) + 2\{J_2^2(k) + J_4^2(k) + \dots\}],$$

and the right-hand side of this gives the radiation resistance relative to an isolated filament. Also it is clear from Fig. 1.7 that at either wire

$$-\frac{cE_P}{a\pi I} = J_0(0) + J_0(2k):$$

and thus is found an expansion for  $J_0(2k)$  in terms of  $J_n^2(k)$ .

Equation (1.46) is the first appearance of a form we shall soon generalize and use repeatedly. Its absolute convergence renders it

valid for numerical computation in all circumstances, though computation is very cumbersome if  $k$  is large and  $r \gg R$ . Fortunately the sum converges very rapidly to the limit given by (1.44) and (1.45), and in most cases it is the value for  $ar$  very large which chiefly concerns us. The writer feels he ought to point out one step which has caused him much misgiving. The recurrence formula has been used to show that  $J_0(z) = J_2(z)$ , etc., when  $z$  is very large, but there we ignored the obvious condition that  $z$  must be very large compared with  $n$ : we are dealing with an infinite series, and thus it is not permissible to limit  $n$  in that way. Now (1.46) is a solution of Maxwell's equation, it has the required degrees of symmetry, and its sum runs logarithmically to infinity at the two currents, and accordingly there is strong reason to suppose it is the solution of our problem. Also, there is no doubt the solution we require must tend to degenerate into (1.44) when  $ar$  is very large, even though it cannot do so accurately since (1.44) is not a solution of (1.43). The two solutions are identical, term by term, when  $n/ar$  is small; but corresponding terms are very discrepant when  $n/ar$  is not small. Perhaps the process we have used has been no more than a hint for a lucky guess in spotting (1.46). However, this equation can be derived in several other ways, and undoubtedly is the solution we require, and its sum must tend to (1.44) when  $R/r \ll 1$ : we need have no qualms about it.

### 1.13. Field of a pair of oppositely directed filaments

The disposition is described by Fig. 1.8, which differs from Fig. 1.7 only in that the current at  $A$  is negative. Considerations of symmetry show that now the field must be expressed by an equation of the form

$$E = f(r)\cos\theta + \phi(r)\cos 3\theta + \psi(r)\cos 5\theta + \dots,$$

and it follows, from the last section, that

$$\begin{aligned} \frac{cE}{4\pi aI} = \{ -J_1(ar) + jY_1(ar) \} J_1(k) \cos\theta + \\ + \{ -J_3(ar) + jY_3(ar) \} J_3(k) \cos 3\theta + \dots \end{aligned} \quad (1.47)$$

When  $ar$  tends to infinity  $-J_1(ar) = +J_3(ar) = -J_5(ar)$ , etc., and then (1.47) takes the form

$$\frac{cE}{4\pi aI} = \{ -J_1(ar) + jY_1(ar) \} \{ J_1(k) \cos\theta - J_3(k) \cos 3\theta + J_5(k) \cos 5\theta - \dots \}.$$

Moreover, at infinity,  $J_1(ar) = Y_0(ar)$  and  $Y_1(ar) = -J_0(ar)$ ; also it is

known that  $\frac{1}{2}\sin(k\cos\theta) = J_1(k)\cos\theta - J_3(k)\cos 3\theta + \dots$ . Hence, at infinity (1.47) can be written

$$\frac{cE}{4\pi aI} = j\{-J_0(ar) + jY_0(ar)\} \times \frac{1}{2}\sin(k\cos\theta). \quad (1.48)$$

Now consider the field at a very distant point  $P$  in Fig. 1.8: it is the vector difference of two equal vectors whose phase differs by an amount corresponding to a path difference  $2R\cos\theta$ , which is an angle

$$\phi = (4\pi R/\lambda)\cos\theta.$$

The appropriate vector diagram is inset in Fig. 1.8 and shows the resultant is  $2\sin\phi/2 = 2\sin(k\cos\theta)$  times a single vector, and is in leading phase quadrature with the field which would arise from a hypothetical current at  $O$ . Thus the field should have the value shown in (1.48), and thus we have shown that (1.47) fits the problem at infinity and is a solution of the problem.

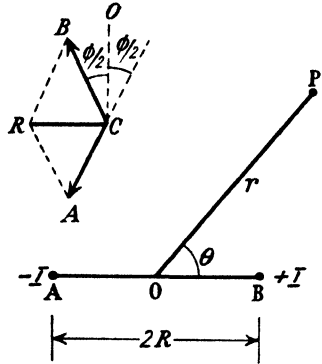


FIG. 1.8.

If  $k > ar$  it is necessary to interchange  $k$  and  $ar$  in (1.47), which then shows the field is zero at  $O$ , as it should be, since  $J_1(0) = J_3(0) = 0$ . Discussions similar to those in the last section show that (1.47) is convergent everywhere save at the two points  $(k, 0)$  and  $(k, \pi)$ , where it diverges logarithmically to plus or minus infinity, and is absolutely convergent save on the circle  $ar = k$ . We have now shown it describes the particular problem (a) at infinity, (b) at each wire, (c) at the origin: hence it must be the solution of the problem.

For the inphase component of field at  $B$  we have

$$-\frac{cE_P}{\pi aI} = 4[J_1^2(k) + J_3^2(k) + \dots];$$

the right-hand side of this gives the radiation resistance relative to an isolated filament. Also it is clear from Fig. 1.8 that this ratio is equal to  $1 - J_0(2k)$  and accordingly find that

$$J_0(2k) = 1 - 4\{J_1^2(k) + J_3^2(k) + \dots\}.$$

By means of the expression for  $J_0(2k)$  in the last section we find that

$$1 = J_0^2(k) + 2 \sum_{n=1}^{\infty} J_n^2(k) \text{ for all values of } k.$$

If each wire has a very small radius  $b$  then, from (1.23 a), the line

integral of the vector potential round a path up the surface of one wire, normally across to the surface of the other, down it and normally across again is

$$-\frac{2\pi I}{c}\{Y_0(ab)-Y_0(2k)+jJ_0(ab)-jJ_0(2k)\}.$$

Accordingly the magnetic flux passing between the wires is

$$\frac{2I}{c}\left(\log \frac{2k}{b}-k^2\right) \quad \text{when } 2k \ll 1:$$

this reduces to the steady current value when  $k$  is zero and also gives the order of approximation to the limit when  $k$  is small.

If the reader has been inclined to doubt the reality of the problems we are studying he is now in at least as good a position as in steady current problems, since he now has a go and return wire, even though the rectangular circuit is indefinitely long.

#### 1.14. Field of an isolated filament referred to an origin not on the wire

By means of equations (1.46) and (1.47) we can now relate the field of an isolated filament to an origin at any distance from the wire: this facility is very helpful in solving many problems.

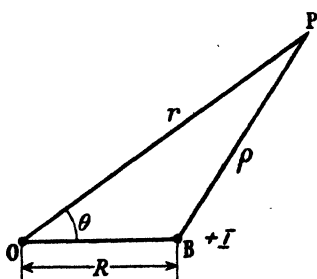


FIG. 1.9.

Thus let  $B$  in Fig. 1.9 represent a filament  $I \sin pt$  perpendicular to the plane of the paper. Its field is given by (1.23) when the origin is at  $B$ : now we wish to have the origin at  $O$ , and this places the filament at the point  $(R, 0)$ .

On superposing Figs. 1.7 and 1.8 we obtain a current  $2I$  at  $B$  and zero current at  $A$ , and the field referred to  $O$  would be given by the sum of (1.46) and (1.47), and accordingly the field of current  $I \sin pt$  at  $B$  is given by

$$\frac{cE}{\pi I} = \{-J_0(ar) + jY_0(ar)\}J_0(k) + 2 \sum_{n=1}^{\infty} \{-J_n(ar) + jY_n(ar)\}J_n(k) \cos n\theta. \quad (1.49)$$

When  $R > r$ , interchange  $k$  and  $ar$  in (1.49). Equation (1.49) is very important later and is needed now. The series is convergent, save at  $(k, 0)$  where it diverges logarithmically to infinity, and is absolutely convergent save on the circle of radius  $k$ .

It is known as Neumann's addition theorem.†

If the current is on the left-hand side of  $A$  (that is, at point  $(k, \pi)$ ), then we must write  $(-1)^n$  inside the  $\Sigma$  sign: it is a disposition which we shall use at times.

With reference to Fig. 1.9, comparison of (1.49) with (1.23) shows that

$$-J_0(a\rho) + jY_0(a\rho) = \{-J_0(ar) + jY_0(ar)\}J_0(k) + \\ + 2 \sum_1^{\infty} \{-J_n(ar) + jY_n(ar)\}J_n(k) \cos n\theta,$$

where  $\rho \equiv (r^2 + R^2 - 2Rr \cos \theta)^{\frac{1}{2}}$  and  $r > R$ .

### 1.15. Field of a long solenoid

Suppose a current of uniform density and constant phase is flowing circumferentially round a tube of radius  $R$  and infinite length; the familiar problem of a circular solenoid (current sheet and not a helix). The current crossing unit axial length of a generator of the cylinder is  $I \sin pt$ . Consider an element  $IR \delta\theta \sin pt$  situated at  $Q$  (see Fig. 1.10). We require the vector potential at  $P$  of an infinitely long strip of very small width with current flowing perpendicular to the length: this has been found in § 1.11, the strip being then called a blade.

By (1.42) the vector potential at  $P$  due to the blade at  $Q$  is

$$-\frac{c \delta A}{\pi I R \delta \theta} = Y_0(a\rho) + jJ_0(a\rho),$$

and is directed perpendicular to  $OQ$ : we require the component perpendicular to  $OP$ , and hence

$$-\frac{cA}{\pi I} = R \int_0^{2\pi} \{Y_0(a\rho) + jJ_0(a\rho)\} \cos \theta \, d\theta \\ = R \int_0^{2\pi} [\{Y_0(ar) + jJ_0(ar)\}J_0(k) + \\ + 2 \sum_1^{\infty} \{Y_n(ar) + jJ_n(ar)\}J_n(k) \cos n\theta] \cos \theta \, d\theta \quad (1.50)$$

$$= 2\pi R \{Y_1(ar) + jJ_1(ar)\}J_1(k). \quad (1.51)$$

$$\therefore E = -\frac{A}{c} = \frac{2\pi k I}{c} \{-J_1(ar) + jY_1(ar)\}J_1(k). \quad (1.52)$$

And thus  $A$  is disposed in circles centred at  $O$ : if  $r < R$ , interchange  $r$  and  $R$  in (1.52). It is postulated that the density is uniform and

† See *Bessel Functions*, G. N. Watson, p. 358, or *Modern Analysis*, Whittaker and Watson, p. 380, example 15.



accordingly there are no charges, and hence  $E = -\dot{A}/c$ : the charges which necessarily resided along the edges of each component blade have vanished by neutralization from the next element. The magnetic field is obtained from the circuital relation  $-H = A/r + \partial A/\partial r$ .

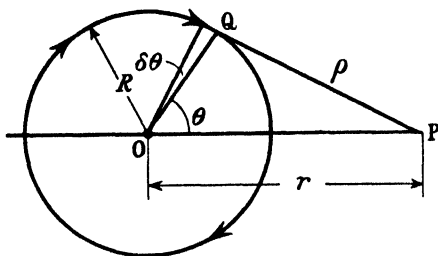


FIG. 1.10. Section across circular current sheet.

$$\begin{aligned} \therefore H &= \frac{2\pi^2 RI}{c} \left\{ \frac{Y_1(ar)}{r} + j \frac{J_1(ar)}{r} + aY_1'(ar) + jaJ_1'(ar) \right\} J_1(k) \\ &= \frac{2\pi^2 kI}{c} \{Y_0(ar) + jJ_0(ar)\} J_1(k), \quad \text{since } J_1'(z) = -\frac{J_1(z)}{z} + J_0(z), \end{aligned} \quad (1.53)$$

or

$$= \frac{2\pi^2 kI}{c} \{Y_1(k) + jJ_1(k)\} J_0(ar)$$

for internal points.

It is worth noting that in this problem  $H$  is axial and a function of  $r$  only, and hence must satisfy Bessel's equation of zero order and accordingly must vary as  $J_0(ar)$  and  $Y_0(ar)$ : thus (1.53) is seen to be essentially correct in form, our method of approach having served to find the constants of integration. Internally and with small  $k$

$$\begin{aligned} H &\doteq \frac{2\pi^2 kI}{c} \left( -\frac{2}{\pi k} + j \frac{k}{2} \right) \left\{ 1 - \left( \frac{ar}{2} \right)^2 \right\} \\ &= -\frac{4\pi I}{c} \left( 1 - j \frac{\pi k^2}{4} \right) \left( 1 - \frac{a^2 r^2}{4} \right), \end{aligned}$$

and this shows the degree of approximation to the limiting value  $4\pi I/c$ . It should be noted consciously that there is magnetic field outside a solenoid which carries an alternating current, unless the radius has a special value which makes  $J_1(k) = 0$ ; then the external field is zero everywhere, just as though the current were steady: such special radii are  $R/\lambda = 0.606, 1.118$ , etc. Note also that the internal magnetic field is everywhere in phase quadrature with the current when  $Y_1(k) = 0$ ; this occurs first when  $R/\lambda = 0.347$ .

It follows from (1.52) that the 'radiation resistance' is  $120\pi^3 S J_1^2(k)$  ohms per half wavelength of axial length: this reduces to  $120\pi^4 S^2/\lambda^4$  ohms when  $k$  is very small. The radiation resistance of a small coil is (see § 1.6)  $320\pi^4 S^2/\lambda^4$  ohms: accordingly the output from a very small solenoid per half wave of axial length is three-eighths of the output of a small coil having the same ampere turns per unit length as the solenoid.

It follows from (1.53) that the phase of the external magnetic field tends to correspond to a distance  $\lambda/8$  less than the distance between the observation point and the axis of the solenoid.

The electric field tends, by (1.52), to the value

$$\begin{aligned}\frac{cE}{I} &= -2\pi k J_1(k) \sqrt{\left(\frac{2}{\pi ar}\right)} \cos(pt - ar + \tfrac{1}{4}\pi) \\ &= +2\pi k J_1(k) \sqrt{\left(\frac{2}{\pi ar}\right)} \sin(pt - ar - \tfrac{1}{4}\pi),\end{aligned}$$

and this shows the phase corresponds to a distance greater than  $r$  by  $\lambda/8$ , in contrast with the small coil for which, equation (1.20) shows, the phase of  $E$  corresponds precisely with  $r$ . If the current density varies as  $\cos by$  along the axis of the solenoid there will be a radial component of  $H$  in addition to the axial component. As in § 1.9 it is necessary to replace  $a$  by  $a'$ , where  $a'^2 \equiv a^2 - b^2$ . With this modification (1.52) and (1.53) remain unchanged except that each must be multiplied by  $\cos by$ . In addition we have

$$\frac{cH_r}{\pi^2 b R I} = J_1(k) \{Y_1(a'r) + jJ_1(a'r)\} \sin by. \quad (1.54)$$

In the special case when  $g = \frac{1}{2}\lambda$  this reduces to

$$\frac{cH_r}{I} = -\frac{\pi^2 R^2}{gr} \sin by \quad \text{or} \quad -\frac{\pi^2 r}{g} \sin by$$

for external and internal points respectively: also  $H_y = (4\pi I/c) \cos by$  for internal points, a result reminiscent of steady currents.

If  $g < \frac{1}{2}\lambda$  then (1.51) becomes

$$\frac{cA}{\pi I R} = 4I_1(k) K_1(a'r) \cos by, \quad \text{for } r > R, \quad (1.55)$$

or  $\quad \quad \quad = 4K_1(k) I_1(a'r) \cos by, \quad \text{for } R > r,$

whence  $\frac{cE}{I} = -j4\pi a R I_1(k) K_1(a'r) \cos by, \quad (1.56)$

or  $\quad \quad \quad = -j4\pi a R K_1(k) I_1(a'r) \cos by.$

It should be noticed that there is now no inphase component of  $E$  and

thus the output is zero. Equation (1.55) is very useful in problems of coils enclosed in metal screening cans with closed ends, but this application will not be developed here.

### 1.16. Field of a line doublet

Take Fig. 1.16 to represent a normal cross-section through a line doublet of infinite length and carrying a current  $I$  per unit length. This is a two-dimensional problem, and we have already found in § 1.11 that the vector potential of a blade of current is

$$-\frac{cA}{\pi I \delta l} = Y_0(ar) + jJ_0(ar).$$

In this  $A$  is everywhere parallel to the blade. The magnetic field must be everywhere perpendicular to the plane of the paper and

$$H = -\frac{\partial A}{\partial x},$$

accordingly, 
$$-\frac{cH}{\pi Il} = -a\{Y_1(ar) + jJ_1(ar)\} \frac{\partial r}{\partial x}.$$

$$\therefore \frac{cH}{a\pi Il} = \{Y_1(ar) + jJ_1(ar)\} \cos \phi. \quad (1.57)$$

Now 
$$\frac{1}{c} \frac{\partial E_t}{\partial t} = -\frac{\partial H}{\partial r} = -\frac{a^2 \pi Il}{c} \cos \phi \{Y'_1(ar) + jJ'_1(ar)\}.$$

$$\begin{aligned} \therefore -\frac{cE_t}{a\pi Il} &= \cos \phi \{J'_1(ar) - jY'_1(ar)\} \\ &= \cos \phi \left[ \left\{ -\frac{J_1(ar)}{ar} + J_0(ar) \right\} - j \left\{ -\frac{Y_1(ar)}{ar} + Y_0(ar) \right\} \right] \\ &= \frac{1}{2} \cos \phi \{ [J_0(ar) - J_2(ar)] - j[Y_0(ar) - Y_2(ar)] \}. \end{aligned} \quad (1)$$

Again, 
$$\frac{\partial H}{\partial \theta} = -\frac{r}{c} \frac{\partial E_r}{\partial t}.$$

$$\therefore \frac{cE_r}{a\pi Il} = \frac{\sin \phi}{ar} \{-J_1(ar) + jY_1(ar)\}. \quad (1)$$

When  $ar \rightarrow 0$

$$\begin{aligned} -\frac{cE_t}{a\pi Il} &\doteq \cos \phi \left[ -\frac{1}{2} + 1 - j\frac{2}{\pi} \left( \frac{1}{a^2 r^2} - \log ar \right) \right] \\ &\doteq \cos \phi \left( \frac{1}{2} - j\frac{2}{\pi} \times \frac{1}{a^2 r^2} \right) \end{aligned}$$

and 
$$\frac{cE_r}{a\pi Il} \doteq \sin \phi \left( -\frac{1}{2} + j\frac{2}{\pi} \times \frac{1}{a^2 r^2} \right).$$

Hence at the line doublet,  $E_p = -a\pi Il/2c$ , in contrast with  $-\frac{2}{3}(a^2 I'l/c)$  for a single doublet. If we choose  $I$  so that  $\frac{1}{2}\lambda I = I'$  (i.e. the line doublet

has the same number of metre amperes per half wavelength of its length as the single doublet), then the output per half wavelength is

$$\frac{2\pi^2}{c} \left( \frac{l}{\lambda} \right)^2 I'^2$$

as compared with

$$\frac{4}{3} \frac{2\pi^2}{c} \left( \frac{l}{\lambda} \right)^2 I'^2$$

for the isolated doublet.

We can also write  $E_P = -(\pi^2/c)(l/\lambda)I$ , and should compare this with the expression  $E_P = -2\pi i/c$  for an infinite sheet, see (1.60); these are identical if  $l/\lambda = 2/\pi$ .

### PLANAR PROBLEMS

#### 1.17. Field of an infinite sheet carrying uniform current density

Let  $AB$  in Fig. 1.11 be the trace of an infinite plane sheet standing perpendicular to the paper and carrying a uniform current density  $i \sin pt$  flowing upwards. Because the sheet is infinite in both directions the field at any point  $P$  must be independent of distance in respect of magnitude, though not necessarily in respect of phase. The magnetic field must be parallel to the plane of the paper: curling round an elementary circuital path close to the sheet and threading it twice gives  $H = (2\pi i/c) \sin pt$  at the surface.

In this problem equation (1.7) takes the form  $d^2H/dx^2 = -a^2H$  and the solution is

$$H = (A \cos ax + B \sin ax) + j(C \cos ax + D \sin ax),$$

where the constants  $A$ ,  $B$ , etc., must be found to

suit the current density in the sheet. When  $x = 0$  we have found that  $H$  is in phase with  $i$ : accordingly  $C$  must be zero and  $A = 2\pi i/c$ . Now divide the sheet into filaments parallel to the current flow, a typical filament being  $i \delta y$  at  $Q$  in Fig. 1.11. Then for the field at  $P$  we have

$$\begin{aligned} \frac{cE}{a\pi i} &= 2 \int_0^\infty \{-J_0(a\rho) + jY_0(a\rho)\} dy \\ &= 2 \int_0^\infty \{-J_0(ay) + jY_0(ay)\} dy, \quad \text{if } P \text{ is at } O, \\ &= \frac{2}{a}(-1 + j \times 0). \end{aligned}$$

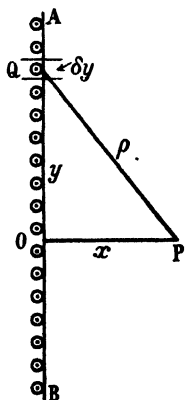


FIG. 1.11.

Hence  $E = -(2\pi i/c)\sin pt$  at the surface of the sheet.

Since 
$$c \frac{\partial H}{\partial x} = \frac{\partial E}{\partial t},$$

we have 
$$\frac{\partial E}{\partial t} = \frac{a}{c} \left( -\frac{2\pi i}{c} \sin ax + B \cos ax \right) + jD \cos ax.$$

$$\therefore E = D \cos ax - j \left( -\frac{2\pi i}{c} \sin ax + B \cos ax \right).$$

Since we have found that the quadrature component of  $E$  is zero at the surface it follows that  $B$  must be zero and  $D = -2\pi i/c$ .

$$\therefore \left. \begin{aligned} \frac{cH}{2\pi i} &= \cos ax - j \sin ax = \sin(pt - ax) \\ \text{and } -\frac{cE}{2\pi i} &= \cos ax - j \sin ax = \sin(pt - ax) \end{aligned} \right\} \quad (1.60)$$

Accordingly  $E = H$  numerically at all points and at every instant of time: at any point the phase of both  $E$  and  $H$  corresponds exactly with the distance of the point from the sheet.

It is helpful and instructive to solve the problem completely from the field of a filament: it follows from (1.49) that

$$J_0(a^2x^2 + a^2y^2)^{\frac{1}{2}} = J_0(ax)J_0(ay) - 2\{J_2(ax)J_2(ay) - J_4(ax)J_4(ay) + \dots\}.$$

Hence at point  $P$  in Fig. 1.11 the inphase component of  $E$  is given by

$$-\frac{cE_P}{a\pi i} = J_0(ax) \int_{-\infty}^{+\infty} J_0(ay) dy - 2J_2(ax) \int_{-\infty}^{+\infty} J_2(ay) dy + \dots$$

It is known that 
$$\int_0^{\infty} J_n(z) dz = 1.$$

$$\therefore -\frac{cE_P}{2\pi i} = J(ax) - 2\{J_2(ax) - J_4(ax) + J_6(ax) \dots\} \\ = \cos ax.$$

Alternatively we could have used (1.46) instead of proceeding from (1.49). It does not appear possible to evaluate the quadrature component of field in the same manner because a typical term in it is  $J_n(ax)Y_n(ay)$  when  $y > x$  and  $J_n(ay)Y_n(ax)$  when  $x > y$ . Hence a typical term in the integration is

$$J_n(ax) \int_x^{\infty} Y_n(ay) dy + Y_n(ax) \int_0^x J_n(ay) dy$$

and this does not seem to be integrable. It is known from (1.46) that

$$\frac{cE_Q}{2\pi i} = \sin ax = 2\{J_1(ax) - J_3(ax) + \dots\},$$

and this must give the value of the unknown integrals. The solution of some problems in this book depends on being able to make a suitable change of origin. As an example of this process we will calculate the field at point  $Q(0, z)$  in the sheet, using the origin  $O$  in Fig. 1.11. Then by (1.49)

$$\begin{aligned} -\frac{cE_P}{a\pi i} &= J_0(az) \int_z^\infty J_0(ay) dy + J_0(az) \int_0^z J_0(ay) dy + \\ &\quad + 2\left\{J_2(az) \int_z^\infty J_2(ay) dy + J_2(az) \int_0^z J_2(ay) dy\right\} + \dots \\ \therefore -\frac{cE_P}{a\pi i} &= J_0(az) + 2J_2(az) + 2J_4(az) + \dots \\ &= \cos(az \cos \tfrac{1}{2}\pi) = 1. \end{aligned}$$

Since the plane is infinite, the field at  $Q$  must necessarily equal that at  $O$ , and hence the calculation we have just made is pointless save as an example of the use of a fresh origin. It is not possible to calculate the quadrature component at  $Q$ , working from  $O$  as origin, because this involves

$$\int_z^\infty Y_n(ay) dy, \text{ etc.}$$

The analytical concept of infinite sheets is not only artificial but must always tend to be a little suspect: the reader should be inquiring how wide a sheet must be to count as sensibly infinite. Here the sheet need not be infinitely wide, though it must be infinitely high. If its width is  $2z$ , then in the midline

$$\frac{cE_P}{2a\pi i} = - \int_0^z J_0(ay) dy + j \int_0^z Y_0(ay) dy.$$

It can be readily shown that, provided  $z$  is large,

$$\int_0^z J_0(ay) dy \doteq 1 - Y_0(az) \quad \text{and} \quad \int_0^z Y_0(ay) dy \doteq -J_0(az).$$

Hence 
$$\frac{cE}{2a\pi i} \doteq \{-1 + Y_0(az)\} - jJ_0(az)$$

$$\doteq \left\{-1 + \sqrt{\left(\frac{2}{\pi az}\right)} \sin(az - \tfrac{1}{4}\pi) - j \sqrt{\left(\frac{2}{\pi az}\right)} \cos(az - \tfrac{1}{4}\pi)\right\}.$$

Hence  $z/\lambda$  must exceed  $200\pi$  before the fluctuations of  $E_P$  fall to 3 per cent.: they are, however, only about 20 per cent. when  $z/\lambda = 3$ . Thus we have found the rate of approach to infinite width for the force at a point on the sheet: for a point not on the sheet see Chapters VII and VIII. We remember there must be line charges along the top and bottom edges of the sheet but know the force contributed by them is negligible, since we have seen it was negligible for each elementary vertical filament. However, we can build up the strip from horizontal line doublets: their charges will neutralize by superposition save along the bounding edges. The field of a line doublet is given in (1.58) and (1.59). Hence, from (1.59), the force at a point on the surface of the sheet is

$$\begin{aligned}\frac{cE}{a\pi i} &= 2 \int_0^z \left\{ -\frac{J_1(ay)}{ay} + j\frac{Y_1(ay)}{ay} \right\} dy \\ &= 2 \int_0^z \left[ -\frac{1}{2}\{J_2(ay) + J_0(ay)\} + j\frac{1}{2}\{Y_2(ay) + Y_0(ay)\} \right] dy. \\ \therefore \frac{cE_P}{\pi i} &= \int_0^z \{J_2(ay) + J_0(ay)\} d(ay) = 2,\end{aligned}$$

when  $z$  tends to infinity. This, however, gives accurately the force in the midline of a sheet of vertical height  $2z$  and infinite width and includes the contribution from the line charges along the edges. The quadrature term becomes divergent at the origin, because there we are in the middle of a doublet. It is not worth while to go through all the moves of unravelling the tangle because we know already that  $E_Q$  is in fact zero. Using the approximate expressions for  $\int J_0(z) dz$ , we have

$$\begin{aligned}\frac{cE_P}{2\pi i} &\doteq 1 - \frac{1}{2}Y_2(az) - \frac{1}{2}Y_0(az) \\ &= 1 - \frac{Y_1(az)}{az}.\end{aligned}$$

Hence here the fluctuations fall off as  $(az)^{\frac{1}{2}}$ , thus showing the approach to the limit is very rapid and much more rapid than in respect of width.

### 1.18. Field of infinite sheet carrying current density which varies periodically across its width

Let  $ABC$  be the trace of an infinite flat sheet standing perpendicular to the paper: current flows perpendicular to the paper and is cophased everywhere. Let the density be  $I \cos(\pi y/g) \sin pt \equiv I \cos by \sin pt$ : then,

with reference to Fig. 1.12, the density is always zero at points  $A$ ,  $B$ ,  $C$ , etc. Note that the density is constant along the direction of flow and accordingly the sheet can be divided into current filaments of infinite length. Consideration will show that the vector potential  $A$  and the electric force  $E$  must be zero in a plane typified by  $BD$ , because any point in this plane is equidistant from similarly situated filaments of unlike sense. In this two-dimensional problem,  $A$  must satisfy the equation

$$\frac{\partial^2 A}{\partial x^2} + \frac{\partial^2 A}{\partial y^2} + a^2 A = 0.$$

Since  $A$  must repeat itself periodically in the  $y$ -direction, the distribution in a plane distant  $x$  from the sheet can be expressed as a Fourier series and accordingly the solution must be of the form  $A = f(x)\cos nby$ , when the origin is at  $O$ . Accordingly we have

$$\frac{d^2 A}{dx^2} + (a^2 - n^2 b^2)A = 0. \quad (1.61)$$

If  $a > nb$  (i.e.  $g > n\lambda/2$ ) the solution is of the form

$$A = \sin mx \cos nby:$$

but if  $a < nb$  it will be of the form

$$A = e^{-mx} \cos nby$$

and thus diminishes rapidly with distance without being periodic. We have to find the solution appropriate to the density  $I \cos by$  in the sheet and expect to proceed as in the last section by dividing the sheet into long filaments: this approach works, but it is very cumbersome. If, however, we divide the plane into horizontal strips (i.e. blades transverse to the direction of flow), the complete solution is very straightforward. It follows readily from § 1.11 combined with § 1.9, that if the density varies as  $\cos by$  along the blade, then (1.42) becomes

$$-\frac{cA}{\pi I \delta z} = \{Y_0(a'\rho) + jJ_0(a'\rho)\} \cos by,$$

where  $a'^2 \equiv a^2 - b^2$  and the origin is at a maximum of density. Then, with reference to Fig. 1.13, the vector potential at  $P$  is the sum of

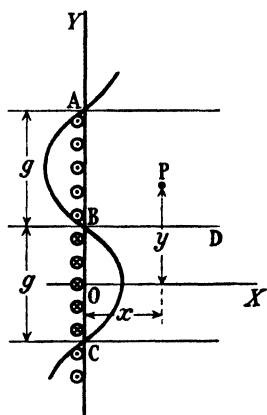


FIG. 1.12.



contributions from blades typified by  $BQC$  at height  $z$  above the  $(x, y)$ -plane and is parallel to the sheet. Accordingly

$$-\frac{cA}{\pi I} = 2 \cos by \int_0^{\infty} \{Y_0(a'\rho) + jJ_0(a'\rho)\} dz.$$

Had the density been uniform across the sheet the corresponding

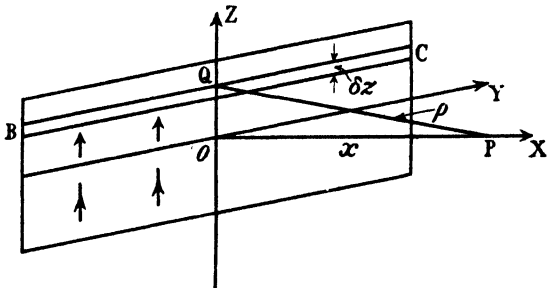


FIG. 1.13.

integral would have differed from the foregoing only in that  $a$  would have replaced  $a'$ , and thus it follows readily from (1.60), since

$$E = -\frac{1}{c} \frac{dA}{dt},$$

that we should have had

$$-\frac{acA}{2\pi i} = \sin ax + j \cos ax.$$

Whence, in our present problem, we must have

$$-\frac{a'cA}{2\pi I} = (\sin a'x + j \cos a'x) \cos by.$$

$$\begin{aligned} \therefore \frac{a'cE}{2\pi aI} &= (-\cos a'x + j \sin a'x) \cos by \\ &= -\epsilon^{-ja'x} \cos by, \end{aligned} \quad (1.62)$$

$$\begin{aligned} -\frac{cH_y}{2\pi I} &= (-\cos a'x + j \sin a'x) \cos by \\ &= -\epsilon^{-ja'x} \cos by, \end{aligned} \quad (1.63)$$

$$\begin{aligned} -\frac{ca'H_x}{2\pi bI} &= (\sin a'x + j \cos a'x) \sin by \\ &= j\epsilon^{-ja'x} \sin by. \end{aligned} \quad (1.64)$$

This shows that  $|E|$  and  $|H|$  are independent of  $x$ , but that the phase changes with wavelength  $\lambda\{1-(\lambda/2g)^2\}^{-\frac{1}{2}}$ . This accords with the over-

riding requirements of (1.61), but in addition shows that for the particular density distribution we have chosen the only admissible value of  $n$  is unity. At the surface of the sheet (1.62) gives

$$\frac{a'cE}{2\pi aI} = -\cos by.$$

Now approach the problem by dividing the sheet into vertical strips as in Fig. 1.11 and proceeding as in § 1.17 for a point on the surface.

Then we have

$$\frac{cE}{2\pi aI} = \int_0^\infty \{-J_0(ay) + jY_0(ay)\} \cos by \, dy.$$

Comparison of the two approaches shows that, when  $a > b$ ,

$$\int_0^\infty J_0(ay) \cos by \, dy = \frac{1}{(a^2 - b^2)^{\frac{1}{2}}}$$

and 
$$\int_0^\infty Y_0(ay) \cos by \, dy = 0.$$

The first integral is very well known and is due to Weber; the second integral is less well known.

When  $g < \frac{1}{2}\lambda$  the vector potential of a blade (compare 1.55) is

$$\frac{cA}{I \, dz} = 2K_0(mr) \cos by,$$

where  $m^2 \equiv b^2 - a^2$ , and this leads to

$$\left. \begin{aligned} -\frac{mcE}{2\pi aI} &= j\epsilon^{-mx} \cos by, \\ \frac{cH_y}{2\pi I} &= \epsilon^{-mx} \cos by, \\ \text{and} \quad \frac{mcH_x}{2\pi bI} &= \epsilon^{-mx} \sin by, \end{aligned} \right\} \quad (1.65)$$

and these follow directly from (1.62)–(1.64) by writing  $m = +ja'$ . Equations (1.65) are also in accordance with the overruling requirements (1.61) in showing the field is not periodic and decreases exponentially with distance when  $g < \frac{1}{2}\lambda$ , and that for density  $\cos by$  the only permissible value of  $n$  is unity. Note that  $E$  is now everywhere in quadrature with  $I$  and hence the power output is zero; and this is to be expected, since the field attenuates very rapidly.

Comparison of the approaches by the horizontal and vertical division shows that when  $a < b$ ,

$$\int_0^{\infty} J_0(ay) \cos by \, dy = 0$$

and 
$$\int_0^{\infty} Y_0(ay) \cos by \, dy = \frac{1}{(b^2 - a^2)^{\frac{1}{2}}}.$$

Returning to (1.62), we see the fields are akin to a plane wave in that  $E$  and  $H_y$  are everywhere cophased, but here  $H_y = E\{1 - (\lambda/2g)^2\}^{\frac{1}{2}}$ : the so-called 'propagation velocity' exceeds  $c$ , but it is still possible to regard the Poynting vector as travelling with speed  $c$ . It should be noted that the quadrature component of field is zero at the surface of the sheet and that the phase corresponds precisely with the distance; or in short, that (1.62)–(1.64) reduce to (1.60) when  $g$  is infinite.

We have now a measure of the effect of inequalities of distribution across an infinite sheet. Provided the inequalities are periodic they can be expressed as a Fourier series: if the pitch of the inequality is less than  $\lambda$ , then the field at a large distance is precisely the same as if the density were uniform and equal to the mean value of the actual distribution, the effect of the inequality is limited to a region near the sheet and appears only in the quadrature component. If the pitch exceeds  $\lambda$ , then the field at a large distance will be that due to the mean density together with a term given by (1.62): the two components have the same frequency but different wavelengths, and thus there will be interference maxima and minima in the  $x$ -direction as well as a superposed ripple in the  $y$ -direction.

### 1.19. Infinite plane grid of parallel wires

Let adjacent filaments be spaced a distance  $g$  apart, the origin of rectangular coordinates being taken at one wire, as shown in Fig. 1.14: each wire carries a current  $I \sin pt$  throughout its length. The current distribution is shown inset in the figure and consists of rectangles of height  $I'$  and width  $2\alpha$ . When expressed as a Fourier series this distribution is

$$\frac{i}{I'} = \frac{2\alpha}{g} \left( 1 + 2 \sum_1^{\infty} \frac{\sin(2\pi n\alpha/g)}{(2\pi n\alpha/g)} \cos \frac{2\pi ny}{g} \right), \quad \text{with } n \text{ odd.}$$

$$\therefore \quad \frac{i}{I} = \frac{1}{g} \left( 1 + 2 \sum_1^{\infty} \cos \frac{2\pi ny}{g} \right),$$

if  $\alpha \rightarrow 0$ , and where  $I$  is the current in each wire. If  $g < \lambda$  the distance

between the current nodes of every harmonic component is less than  $\frac{1}{2}\lambda$  and accordingly each one produces a field which varies as  $e^{-a'x}$ . Hence at a large distance the field will be precisely the same as that of an infinite sheet with uniform density  $I/g$ : it is precisely the same as if the concentrated currents had been smeared uniformly over the

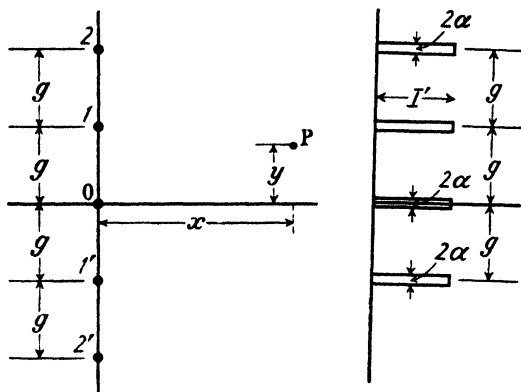


FIG. 1.14.

plane. If  $g > \frac{1}{2}\lambda$  the field will be that of a uniform density  $I/g$  together with the fields of those harmonic components for which  $g > n\lambda$ . Accordingly at each wire

$$-cE_P = \frac{2\pi I}{g} \left[ 1 + 2 \sum_{n=1}^{n=g/\lambda} \frac{1}{\{1 - (n\lambda/g)^2\}^{\frac{1}{2}}} \right]. \quad (1.66)$$

It must not be forgotten that when  $g > \lambda$  the field will have a component whose wavelength exceeds  $\lambda$ .

Since  $cE/a\pi I = -J_0(ar) + jY_0(ar)$ , it follows directly from Fig. 1.14 that at the surface of a wire

$$-\frac{cE_P}{a\pi I} = 1 + 2 \sum_1^{\infty} J_0(nag):$$

hence by comparison with the result obtained by the Fourier process we find that

$$\sum_1^{\infty} J_0(nz) = \frac{1}{z} - \frac{1}{2},$$

if  $z < \pi$ , a result which can be obtained directly from the theory of Bessel functions (see Watson, p. 632, 19.4). If  $g = \lambda$ , then

$$\begin{aligned} \frac{cE}{a\pi I} \doteq 1 + 2 \left[ J_0(2\pi) + J_0(4\pi) + \frac{1}{\pi\sqrt{2}} \left\{ \frac{1}{3^{\frac{1}{2}}} + \frac{1}{4^{\frac{1}{2}}} + \frac{1}{5^{\frac{1}{2}}} + \dots \right\} \right] + \\ + jY_0(ab') + 2j \left[ Y_0(2\pi) + Y_0(4\pi) - \frac{1}{\pi\sqrt{2}} \left\{ \frac{1}{3^{\frac{1}{2}}} + \frac{1}{4^{\frac{1}{2}}} + \dots \right\} \right]. \end{aligned}$$

These series diverge logarithmically to infinity; but  $\sum_1^{\infty} J_0(nz)$  and  $\sum_1^{\infty} Y_0(nz)$  are convergent, though not absolutely, for all values of  $z$  save the special and isolated values  $2\pi, 4\pi$ , etc. If  $g/\lambda = 3/2$  then, by (1.66),

$$-\frac{cE_P g}{2\pi I} = 1 + \frac{2}{(1-\frac{1}{3})^{\frac{1}{2}}} = 3.68 \quad \text{or} \quad -\frac{cE_P}{a\pi I} = 0.78.$$

The quadrature field at the surface cannot be evaluated from (1.62) because it is saved from being infinite only because the small radius  $b'$  is finite. It is better to proceed from

$$\frac{cE_Q}{a\pi I} = Y_0(ab') + 2 \sum_1^{\infty} Y_0(nag).$$

When  $g/\lambda$  has the values 0.16,  $\frac{1}{4}$ ,  $\frac{1}{2}$ , and  $\frac{3}{4}$  we have estimated that  $\sum_1^{\infty} Y_0(nag)$  equals 0.62, 0.56, 0.20, and -0.32 respectively.

However, (1.62) shows that the contribution to  $E_Q$  from the fundamental component of density is zero, and hence by (1.65)

$$-\frac{cE_Q}{2\pi a I} = j \left( \frac{\epsilon^{-m_3 x}}{m_3} + \frac{\epsilon^{-m_5 x}}{m_5} + \dots \right),$$

where  $m_3^2 = 9b^2 - a^2$ ,  $m_5^2 = 25b^2 - a^2$ , etc.

We defer a more detailed consideration of  $E_Q$  until Chapter V and Fig. 5.16, where it is required to estimate the screening qualities of wire netting.

## 1.20. Current filament between two parallel conducting planes

Reverting to Fig. 1.12 and equations (1.62) or (1.65) it will be seen that  $E$  and  $H_y$  are zero in planes separated by a distance  $g$ , and accordingly infinitely extended and perfectly conducting sheets may be situated in these planes, and then we have a sinoidally loaded current sheet across a corridor of width  $g$ ; in technical parlance this is called a 'rectangular wave guide'. Currents will be induced in the walls having a density given by  $4\pi i = cH_x$ , whence by (1.64)

$$\frac{2i}{I} = j \frac{b}{a'} \epsilon^{-j a' x},$$

since  $\sin by = 1$  at the walls. This shows the walls are sinoidally loaded with two component densities which are in quadrature in both time and space.

Fig. 1.15 represents a cross-section, in which  $AB$  is the sinoidally loaded driving sheet and the sinusoid represents the quadrature component of induced density, successive nodes of current being separated

a distance  $\pi/a'$ . We have seen in (1.62) that density  $\cos by$  radiates a field perpendicular to the sheet with wavelength  $(a/a')\lambda$ : hence density  $\cos a'y$  radiates a field with wavelength

$$\frac{a'}{b} \times \frac{a}{a'} \lambda = \frac{a}{b} \lambda = 2g.$$

But here there are two similar sheets separated a distance  $g$  and each radiating a field of wavelength  $2g$ , consequently their net field is zero

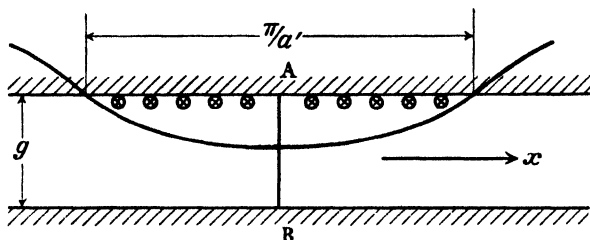


FIG. 1.15.

in a direction perpendicular to the walls and outside them. This shows the induced densities do in fact produce zero external field. The field of the sheet  $AB$  decreases as  $x^{-1}$  in the  $x$ -direction and thus is negligible ultimately, and then we may say the field in the guide is due only to the currents induced in its walls: but these are induced by the driving sheet  $AB$ , and the actual field is always given by (1.62). The sheet  $AB$  has all the attributes of what an engineer calls a generator. If the sheet  $AB$  is replaced by a single central wire, then we have but to use the Fourier series of the last section, omitting its constant term. It then follows readily that, if  $g/\lambda$  lies between  $\frac{1}{2}$  and  $\frac{3}{2}$ ,

$$\frac{cE}{I} = \frac{4\pi}{g} \left[ \frac{a}{a'} (-\cos a'x + j \sin a'x) \cos by - \frac{ja}{m_3} \epsilon^{-m_3 x} \cos 3by - \frac{ja}{m_5} \epsilon^{-m_5 x} \cos 5by - \dots \right], \quad (1.67)$$

where  $m_3^2 = (3b)^2 - a^2$ , etc., and this is also the field of a wire grating in which the currents alternate in sense. Proceeding from that system we have

$$\frac{cE}{a\pi I} = -\{1 - 2J_0(ag) + 2J_0(2ag) - 2J_0(3ag) + \dots\} + j\{Y_0(ab') - 2Y_0(ag) + 2Y_0(2ag) - \dots\}$$

at the surface of a wire. Comparison with (1.67) shows

$$1 + 2 \sum_{n=1}^{\infty} (-1)^n J_0(nag) = 0$$

if  $g < \pi$ , a well-known result called the Schlömilch null function (see Watson, p. 634), and if  $g$  lies between  $\pi$  and  $3\pi$ , the sum of the series is

$$\frac{4}{ga'} = \frac{4}{ag\{1 - (\pi^2/a^2g^2)\}^{\frac{1}{2}}}.$$

Relative to the isolated value, the radiation resistance of each wire is  $\frac{4}{\pi\{(2g/\lambda)^2 - 1\}^{\frac{1}{2}}}$  provided  $g/\lambda < 3/2$ . The quadrature field at the surface can best be evaluated from (1.67), or computed from values in  $Y_0(nag)$  taken from tables. When  $g = 1$  we find  $cE_Q/a\pi I = Y(ab') + 0.27$ . Since  $Y(ab')$  is negative we see that neighbouring wires then reduce the effective self-inductance of the wire. When  $g/\lambda$  is small, say less than  $1/5$ , (1.67) becomes

$$\begin{aligned} -\frac{cE}{I} &\div \frac{4p}{c}j(\epsilon^{-m_1x} + \frac{1}{3}\epsilon^{-3m_1x} + \frac{1}{5}\epsilon^{-5m_1x} + \dots) \\ &= \frac{2p}{c}j \log \tanh m_1x, \end{aligned} \quad (1.68)$$

and this gives the field in what is commonly called an attenuator. It is perhaps advisable to point out explicitly that it is permissible to place metal cover plates across the two infinite walls, thereby producing a rectangular tube: currents will be induced in these cover plates and will have axial and transverse components obtained by dividing (1.63) and (1.64) by  $4\pi$ . Since the transverse component dwindles to zero at the midline there must also be a charge density on the cover plates: the induced charges and currents together produce a field equivalent to that contributed by the currents in the, previously, infinitely high walls and driving filament.

In these last two sections we have derived all the analysis essential for solving problems of wave guides, attenuators, and wire netting screens. We leave their more detailed and practical interpretation to later chapters.

## SUNDRY PROBLEMS IN THREE DIMENSIONS

### 1.21. Field of an electric doublet

Let there be a doublet of moment  $Ql \cos pt$  at the origin and pointing along the axis of  $z$  (see Fig. 1.16). By a doublet is meant here a fine wire of length  $l$  terminated by large capacitances;  $l$  will then be shrunk to zero while maintaining  $Ql$  finite. It corresponds to the Heaviside current element of § 1.2 (Fig. 1.1): here there is no need to provide an

infinite conducting ocean because the current is not steady but is alternating. It is required to find the field at a point  $P$  distant  $r$  from the doublet and at an angle of elevation  $\phi$  above the equatorial plane

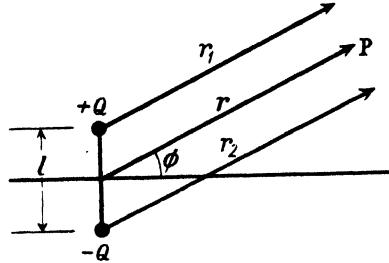


FIG. 1.16. Electric doublet.

(see Fig. 1.16). When  $P$  is very distant the retarded potential there due to charge  $+Q$  will be

$$\frac{V}{Q} = \frac{\cos(pt - pr/c)}{r_1} = \frac{\cos ar_1}{r_1} + j \frac{\sin ar_1}{r_1}.$$

Hence the retarded potential at  $P$  due to both charges is

$$\begin{aligned} \frac{V}{Q} &= \left( \frac{\cos ar_1}{r_1} - \frac{\cos ar_2}{r_2} \right) + j \left( \frac{\sin ar_1}{r_1} - \frac{\sin ar_2}{r_2} \right) \\ &\doteq \left( \frac{\cos ar_1}{r_1} - \frac{\cos a(r_1 + l \sin \phi)}{r_1 + l \sin \phi} \right) + j \left( \frac{\sin ar_1}{r_1} - \frac{\sin a(r_1 + l \sin \phi)}{r_1 + l \sin \phi} \right) \\ &\doteq \left\{ \left( \frac{1}{r} - \frac{1}{r + l \sin \phi} \right) \cos ar + \frac{al \sin \phi \sin ar}{r} \right\} + \\ &\quad + j \left\{ \left( \frac{1}{r} - \frac{1}{r + l \sin \phi} \right) \sin ar - \frac{al \sin \phi \cos ar}{r} \right\} \\ &\doteq l \sin \phi \left[ \left( \frac{\cos ar}{r^2} + \frac{a \sin ar}{r} \right) + j \left( \frac{\sin ar}{r^2} - \frac{a \cos ar}{r} \right) \right], \\ \therefore \frac{1}{r} \frac{\partial V}{\partial \phi} &= Ql \cos \phi \left\{ \left( \frac{\cos ar}{r^3} + \frac{a \sin ar}{r^2} \right) + j \left( \frac{\sin ar}{r^3} - \frac{a \cos ar}{r^2} \right) \right\} \end{aligned}$$

and

$$\begin{aligned} \frac{\partial V}{\partial r} &= Ql \sin \phi \left\{ \left( -\frac{2 \cos ar}{r^3} - \frac{2a \sin ar}{r^2} + \frac{a^2 \cos ar}{r} \right) + \right. \\ &\quad \left. + j \left( -\frac{2 \sin ar}{r^3} + \frac{2a \cos ar}{r^2} + \frac{a^2 \sin ar}{r} \right) \right\}. \end{aligned}$$

$$A = -\frac{Qpl \sin(pt - pr/c)}{r^2} = \frac{Qpl}{r^2} (\sin ar - j \cos ar),$$



$$\therefore \frac{1}{c} \frac{\partial A_z}{\partial t} = -\frac{Qa^2 l}{r} (\cos ar + j \sin ar).$$

$$\begin{aligned} E_t &= -\frac{1}{r} \frac{\partial V}{\partial \phi} - \frac{1}{c} \frac{\partial A_z}{\partial t} \cos \phi \\ &= -\frac{Ql \cos \phi}{r^3} \{(\cos ar + ar \sin ar - a^2 r^2 \cos ar) + \\ &\quad + j(\sin ar - ar \cos ar - a^2 r^2 \sin ar)\}, \end{aligned} \quad (1.69)$$

$$\begin{aligned} E_r &= -\frac{\partial V}{\partial r} - \frac{1}{c} \frac{\partial A_z}{\partial t} \sin \phi \\ &= \frac{2Ql \sin \phi}{r^3} \{(\cos ar + ar \sin ar) + j(\sin ar - ar \cos ar)\}. \end{aligned} \quad (1.70)$$

$$\therefore |E_t| = \frac{Ql \cos \phi}{r^3} (1 - a^2 r^2 + a^4 r^4)^{\frac{1}{2}} \quad (1.71)$$

$$\text{and} \quad |E_r| = \frac{2Ql \sin \phi}{r^3} (1 + a^2 r^2)^{\frac{1}{2}}. \quad (1.72)$$

Writing these in terms of current, where  $I = -pQ$ ,

$$\begin{aligned} \frac{c|E_t|}{a^2 Il} &= -\frac{\cos \phi}{ar} \left(1 - \frac{1}{a^2 r^2} + \frac{1}{a^4 r^4}\right)^{\frac{1}{2}} \\ \text{and} \quad \frac{c|E_r|}{a^2 Il} &= -\frac{2 \sin \phi}{a^2 r^2} \left(1 + \frac{1}{a^2 r^2}\right)^{\frac{1}{2}} \end{aligned} \quad (1.73)$$

$$\begin{aligned} H &= -\frac{\partial A}{\partial x} = -\frac{Il}{c} \frac{\partial}{\partial x} \left( \frac{\cos ar}{r} - j \frac{\sin ar}{r} \right) \\ &= -\frac{Il}{c} \left\{ -\frac{\cos ar}{r^2} - \frac{a \sin ar}{r} - j \left( -\frac{\sin ar}{r^2} + \frac{a \cos ar}{r} \right) \right\} \frac{\partial r}{\partial x} \\ &= \frac{aIl}{cr} \cos \phi \left\{ \sin ar + \frac{\cos ar}{ar} + j \left( \cos ar - \frac{\sin ar}{ar} \right) \right\} \\ &= \frac{aIl \cos \phi}{cr} \left(1 + \frac{1}{a^2 r^2}\right)^{\frac{1}{2}} \sin(pt - \beta), \end{aligned} \quad (1.74)$$

$$\text{where} \quad \tan \beta = \frac{\tan ar - ar}{1 + ar \tan ar} = \tan(\tan^{-1} ar - ar).$$

$$\therefore \beta = ar - \tan^{-1} ar.$$

Accordingly, when  $ar$  is large, the phase of  $H$  tends to correspond with the doublet being  $\frac{1}{4}\lambda$  closer than it really is to the point where  $H$  is being observed.

It will be noted that  $H$  is derived from the current alone and remembered that  $E$  can always be derived from  $H$  by means of the circuital

relations. Hence  $E$  could have been derived without explicit reference to the charges and to  $V$ , as indeed it was done in §§ 1.9 and 1.16. Here it has been derived explicitly by use of  $V$ , as an example of that method.

Now

$$A = \frac{aIl}{c} \left( \frac{\cos ar}{ar} - j \frac{\sin ar}{ar} \right),$$

and it is known that

$$J_1(ar) = \sqrt{\left(\frac{2}{\pi ar}\right)} \sin ar \quad \text{and} \quad Y_1(ar) = -\sqrt{\left(\frac{2}{\pi ar}\right)} \cos ar,$$

and hence we may write  $A$  in the form

$$-\frac{cA}{aIl} \sqrt{\frac{2}{\pi}} = \frac{1}{\sqrt{(ar)}} \{Y_1(ar) + jJ_1(ar)\} \quad (1.75)$$

and this is very reminiscent of (1.23). Also we can write

$$\frac{cH}{a^2Il} \sqrt{\left(\frac{2}{\pi}\right)} = \frac{\cos \phi}{\sqrt{(ar)}} \{Y_1(ar) - jJ_1(ar)\} \quad (1.76)$$

and this is very reminiscent of (1.24) when  $Y'_0$  is replaced by  $Y_1$ .

In this problem  $E_r$ ,  $E_\phi$ , and  $H$  are functions of  $\phi$  but not of  $\theta$ , the bearing. Maxwell's equation now takes the form

$$r^2 \frac{\partial^2 H}{\partial r^2} + 2r \frac{\partial H}{\partial r} + \frac{1}{\sin \phi} \frac{\partial}{\partial \phi} \left( \sin \phi \frac{\partial H}{\partial \phi} \right) + a^2 r^2 H = 0, \quad (1.77)$$

and the general solution of this is known to be

$$H = \frac{1}{r^{\frac{1}{2}}} \{A J_{n+\frac{1}{2}}(ar) + B J_{-n-\frac{1}{2}}(ar)\} P_n(\mu), \quad (1.78)$$

where  $\mu \equiv \cos \theta$  and  $P(\mu)$  is a surface harmonic (Legendre function): it is well known that  $P_0(\mu) = 1$  and  $P_1(\mu) = \cos \theta$ , and accordingly (1.76) is seen to conform with (1.78).

On writing  $\sin ar = ar - \frac{a^3 r^3}{3!} + \dots$  and  $\cos ar = 1 - \frac{a^2 r^2}{2!} + \dots$  in the quadrature term of (1.69) and (1.70) we obtain

$$-\frac{cE_\phi}{a^2Il} = \left( \frac{2}{3} - \frac{4}{5} \frac{a^2 r^2}{3!} + \frac{6}{7} \frac{a^4 r^4}{5!} - \frac{8}{9} \frac{a^6 r^6}{7!} + \dots \right) \cos \phi \quad (1.79)$$

$$\text{and} \quad \frac{cE_r}{a^2Il} = 2 \left( \frac{2}{3!} - \frac{4}{5!} a^2 r^2 + \frac{6}{7!} a^4 r^4 - \frac{8}{9!} a^6 r^6 + \dots \right) \sin \phi. \quad (1.79a)$$

These equations show that when  $ar$  tends to zero the component of electric field which is in phase with the current is parallel to the doublet,

directed oppositely to the current, and independent of distance. It has the value

$$E_P = -\frac{2}{3} \frac{a^2 I l}{c}$$

along the axis of the doublet, and hence the rate of working is

$$W = \frac{2}{3} \frac{a^2 l^2}{c} I^2 \sin^2 pt,$$

and this may be expressed in terms of a radiation resistance. The quadrature component of field tends to infinity at the doublet: these correspond to  $J_0(ar) = 1$  and  $Y_0(ar) = \infty$  when  $ar \rightarrow 0$ , in our previous problems.

### 1.22. Radiation resistance of a half-wave aerial

Because this result is required in the next chapter it must be derived here though it belongs more properly to Chapter VIII, which is devoted to the isolated fine wire aerial. Unfortunately the precise current distribution along a finite wire cannot be calculated; the reasons for this will become apparent in Chapter VIII. Therefore it is necessary to take a general distribution, and we shall assume only one thing, namely, that the phase of the current is constant at all points along the length. This simplification is almost certainly not correct. Let the length of the thin straight wire be  $2h$ . It is required to calculate the field at point  $P$  (see Fig. 1.17) due to charge elements  $+q \delta y$  and  $-q \delta y$  at the points  $B$  and  $B'$  respectively. We shall concern ourselves only with the component of field which is in phase with the current. For the vector potential at  $P$  we have

$$\begin{aligned} \frac{cA}{i \delta y} &= \frac{1}{r_1} \sin(pt - ar_1) + \frac{1}{r_2} \sin(pt - ar_2). \\ \therefore \frac{A}{ai \delta y} &= \left( \frac{\sin ar_1}{r_1} + \frac{\sin ar_2}{r_2} \right) \sin pt + \text{term in } \cos pt. \\ \therefore -\frac{cA}{a^2 i \delta y} &= \left\{ 2 - \frac{a^2}{6} (r_1^2 + r_2^2) + \frac{a^4}{120} (r_1^4 + r_2^4) + \dots \right\} \\ &= 2 \left\{ 1 - \frac{a^2}{6} (z^2 + y^2) + \frac{a^4}{120} (z^4 + 6y^2 z^2 + y^4) - \dots \right\}. \end{aligned}$$

This is the contribution to  $A$  at  $P$  provided by current elements at  $B$  and  $B'$ . To find the total value of  $A$  at  $P$  contributed by all the elements along the wire we must integrate this expression with respect

to  $y$ . On doing this and writing  $\int_0^h i dz = X_0$  and  $\int_0^h iz^n dz = X_n$  we obtain

$$-\frac{cA}{2a^2} = X_0 - \frac{a^2}{6}(y^2X_0 + X_2) + \frac{a^4}{120}(y^4X_0 + 6y^2X_2 + X_4) - \dots$$

To find the electric field at  $P$  we must also find there the contribution which arises through the space rate of change of the delayed potential

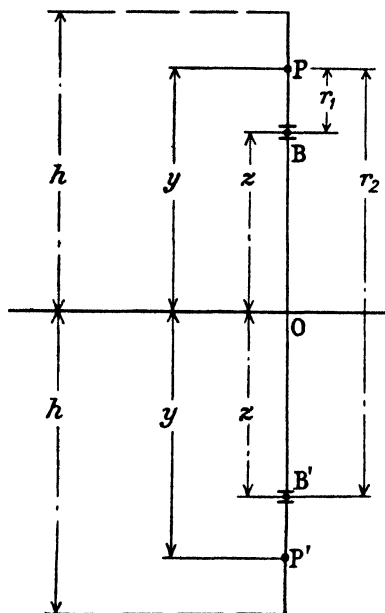


FIG. 1.17.

of the charges: this can be found by a similar process and details need not be given.† On doing this we find

$$-\frac{cE_P}{2a^2} = \frac{2}{3} \left[ \left( X_0 - \frac{a^2X_2}{10} + \frac{a^4X_4}{280} - \dots \right) - \frac{a^2y^2}{10} \left( X_0 - \frac{3}{14}a^2X_2 + \dots \right) + \frac{a^4y^4}{280} \left( X_0 - \frac{5}{18}a^2X_2 + \dots \right) - \dots \right]. \quad (1.80)$$

This shows that  $E_P$  varies along the length of the wire. To find the rate of working it is necessary to evaluate  $2 \int_0^h iE_P dy$ , and on doing

† For full details of the algebra of these steps see *Journal I.E.E.* (Proceedings Wireless Section), 11 (1936), 95.

this we obtain

$$\frac{cP}{4a^2} = \frac{2}{3} X_0^2 \left[ 1 - \frac{a^2}{5} \frac{X_2}{X_0} + \frac{a^4}{140} \left( \frac{X_4}{X_0} + \frac{3X_2^2}{X_0^2} \right) - \frac{a^6}{7560} \left( \frac{X_6}{X_0} + \frac{15X_2X_4}{X_0^2} \right) + \dots \right]. \quad (1.80a)$$

This expression is general for any distribution of current having a constant phase along the wire. If  $h = \frac{1}{2}\lambda$  and if  $i = I \sin(2\pi y/\lambda)$ , then it may be found that

$$-\frac{cP}{4a^2} = 0.6095 X_0^2. \quad (1.81)$$

Thus in respect of the output it is as though  $E_p$  were constant along the aerial, of total length  $\frac{1}{2}\lambda$ , and having the value

$$E_p = -\frac{2}{3} \times \frac{2X_0^2 a^2}{c},$$

and thus there is a small reduction in the mean effective inphase field. If  $2h = \frac{1}{2}\lambda$ , and if the current distribution is triangular, vice sinoidal, then evaluation shows the factor 0.6095 becomes 0.616. Accordingly we may have great confidence in taking the value of this numerical factor as 0.61 for any aerial whose total length is  $\frac{1}{2}\lambda$ . Accordingly we have

$$P = 240 \frac{\pi^2}{\lambda^2} \times 0.61 X_0^2 \text{ watts}. \quad (1.82)$$

If the distribution is sinoidal, then the radiation resistance of a half-wave aerial is 73 ohms. We shall continue this discussion in detail in Chapter VIII.

### 1.23. Circle of radius $R$

In some respects we can now generalize the problem of a very small circuit, solved in § 1.6. Let a current  $I \sin pt$  flow, in a thin wire, round a circle of radius  $R$ . It should be noted that the current is constant in magnitude and phase at all points round the circumference for any value of  $R$ . We do not discuss here how such a current could be produced in practice, since we are concerned now only with the field which would result from such a current. The more complex distribution which would obtain in practice can be dealt with by a Fourier series corresponding to that used in § 1.19: here we are concerned only with the field due to the constant term in such a series.

Since the current is constant in magnitude and phase there is no charge on the wire, and accordingly the electric field can be derived

from the vector potential only. The vector potential at point  $P$ , in Fig. 1.18, due to an element  $IR \delta\theta \sin pt$  at  $B$  is

$$\frac{c \delta A}{I} = \left( \frac{\cos ar}{r} - j \frac{\sin ar}{r} \right) \cos \theta R \delta\theta.$$

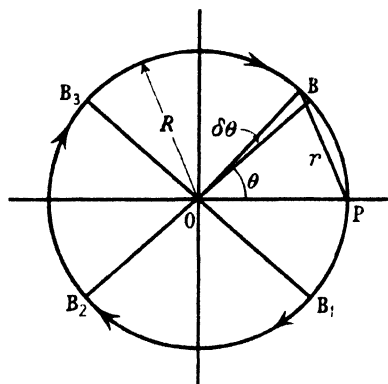


FIG. 1.18.

Consider first the quadrature component of  $A$ , then

$$\begin{aligned} \frac{j c A}{I} &= 2 \int_0^{\pi} \frac{\sin(2k \sin \frac{1}{2}\theta)}{2 \sin \frac{1}{2}\theta} \cos \theta d\theta, \quad \text{where } aR \equiv k, \\ &= 2 \int_0^{\pi} \left\{ \frac{\sin(2k \sin \frac{1}{2}\theta)}{2 \sin \frac{1}{2}\theta} - \sin(2k \sin \frac{1}{2}\theta) \sin \frac{1}{2}\theta \right\} d\theta \\ &= 4 \int_0^{\frac{1}{2}\pi} \left\{ \frac{\sin(2k \sin \phi)}{2 \sin \phi} - \sin(2k \sin \phi) \sin \phi \right\} d\phi, \quad \text{where } \frac{1}{2}\theta \equiv \phi, \\ &= 4 \int_0^{\frac{1}{2}\pi} \left[ \frac{J_1(2k) \sin \phi + J_3(2k) \sin 3\phi + \dots}{\sin \phi} - \right. \\ &\quad \left. - \{ (1 - \cos 2\phi) J_1(2k) + (\cos 2\phi - \cos 4\phi) J_3(2k) + \dots \} \right] d\phi \\ &= 4 \int_0^{\frac{1}{2}\pi} \left\{ J_3(2k) \frac{\sin 3\phi}{\sin \phi} + J_5(2k) \frac{\sin 5\phi}{\sin \phi} + \dots \right\} d\phi \\ &= 2\pi \{ J_3(2k) + J_5(2k) + \dots \}, \quad \text{since } \int_0^{\frac{1}{2}\pi} \frac{\sin n\phi}{\sin \phi} d\phi = \frac{1}{2}\pi, \quad \text{if } n \text{ is odd,} \\ &= \pi \int_0^{2k} J_2(z) dz. \end{aligned}$$

$$\therefore \frac{cE_P}{a\pi I} = - \int_0^{2k} J_2(z) dz. \quad (1.83)$$

$$\begin{aligned} \therefore \frac{P}{I^2} &\equiv \frac{2\pi RE_P}{I} = \frac{2\pi^2 k}{c} \int_0^{2k} J_2(z) dz \\ &= \frac{2\pi^2 k^4}{3c} \left( 1 - \frac{k^2}{5} + \frac{k^4}{56} - \frac{k^6}{720} + \dots \right). \end{aligned} \quad (1.84) \quad (1.84a)$$

Equation (1.84) gives the radiation resistance for a circle of any radius, while (1.84a) shows that when  $k$  is very small the expression reduces to that found already in § 1.6, for a very small circuit. We now find, from (1.84a), that the well-known and limiting value is correct to closer than 5 per cent. so long as  $k < \frac{1}{2}$ , which is  $R/\lambda < \frac{1}{18}$ .

Since  $\int_0^\infty J_n(z) dz = 1$ , equation (1.83) shows that  $E_P = -a\pi I/c$  when  $R \rightarrow \infty$ , and thus reduces to the value appropriate to a straight filament; see (1.23).

The radiation resistance passes through maxima and minima when  $J_2(k) = 0$  and this occurs when  $R/\lambda = 0.813, 1.34, 1.85$ , etc. Fig. 1.19 shows radiation resistance plotted as a function of  $2R/\lambda$ : the dotted line is the asymptote for  $2R/\lambda$  very large, and the dotted curve is the asymptote for  $2R/\lambda$  very small. It may be seen that the curve of radiation resistance is climbing much the same general gradient as the straight asymptote, but with pauses at maxima and minima: it should be noted that the curve is everywhere below the asymptote, and thus the radiation resistance is always less than  $(120\pi^3 R)/\lambda$  ohms.

It follows from (1.78) that the value of  $A$  at distance  $r$  from the centre of the circle and at elevation  $\phi$  above its plane must be given by

$$j \frac{cA}{I} = \sqrt{\left(\frac{\pi}{2ar}\right)} \sum \{A_n J_{n+\frac{1}{2}}(ar)\} P_n(\mu), \quad \text{with } n \text{ odd.}$$

When  $\phi = 0$ ,  $P_n(\mu) = 1$ : hence in the plane of the circle

$$j \frac{cA}{I} = \sqrt{\left(\frac{\pi}{2ar}\right)} \{A_1 J_{\frac{1}{2}}(ar) + A_3 J_{\frac{3}{2}}(ar) + \dots\}. \quad (1.85)$$

Equation (1.17), for a very small circle, may be written

$$\frac{cA}{\pi k^2 I} = \sqrt{\left(\frac{\pi}{2ar}\right)} \{Y_{\frac{1}{2}}(ar) - jJ_{\frac{1}{2}}(ar)\} P_1(\mu). \quad (1.85a)$$

Comparison of (1.85) and (1.85a) shows that  $A_1 = \pi k^2$ . Expansion of (1.85) with  $ar = k$  gives

$$j \frac{cA}{I} = \frac{A_1 k}{3} \left( 1 - \frac{k^2}{10} + \frac{k^4}{2 \cdot 4 \cdot 5 \cdot 7} - \dots \right) + \\ + \frac{A_3 k^3}{3 \cdot 5 \cdot 7} \left( 1 - \frac{k^2}{2 \cdot 9} + \frac{k^4}{2 \cdot 4 \cdot 9 \cdot 11} - \dots \right) + \dots$$

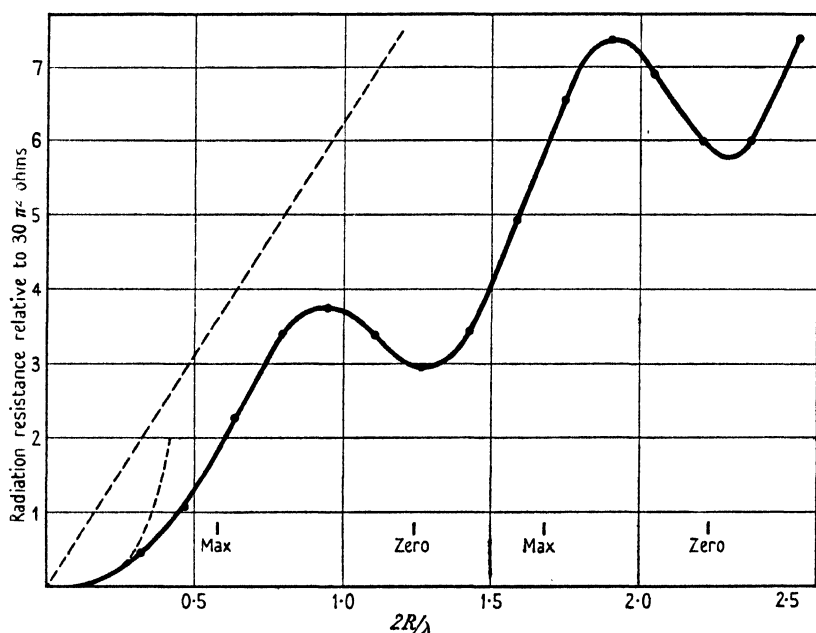


FIG. 1.19. Uniform current flowing round a circle of radius  $R$ .

Comparison of this with (1.84a) gives

$$A_1 = \pi k^2, \quad A_3 = -\frac{1}{2}\pi k^2, \quad A_5 = \frac{121}{4}\pi k^2, \quad \text{etc.}$$

$$\therefore \frac{j c A}{\pi k^2 I} = \sqrt{\left( \frac{\pi}{2 a r} \right) \{ J_1(ar) P_1(\mu) - \frac{1}{2} J_3(ar) P_3(\mu) + \frac{121}{4} J_5(ar) P_5(\mu) + \dots \}}, \quad (1.86)$$

and this equation serves to evaluate the mutual radiation resistance between two parallel and coaxial circles. The mutual radiation resistance between two similar coaxial circles whose planes are separated a distance  $z$  is given by the readily derivable expression

$$-\frac{c E_P}{a \pi^2 I} = 2 \{ J_3(2k) + J_5(2k) + \dots \} - \\ - \frac{a^2 z^2 k^3}{30} \left\{ 1 - \frac{a^2 z^2}{28} + \frac{a^4 z^4}{1512} - \frac{k^2}{7} + a^2 k^2 \frac{(2z^2 + 5R^2)}{504} \right\} + \dots \quad (1.87)$$



More terms will be needed in this expression if it is to be used for computation when  $k$  exceeds about 2.

To calculate the effective inductance of the circle we require the inphase component of vector potential at point  $P$  in Fig. 1.18. In the notation of this figure we have

$$\begin{aligned}
 \frac{cA}{2IaR} &= \int_0^\pi \frac{\cos ar}{ar} \cos \theta \, d\theta \\
 &= \int_0^\pi \left( \frac{1}{ar} - \frac{ar}{2!} + \frac{a^3 r^3}{4!} - \dots \right) \cos \theta \, d\theta \\
 &= \int_0^\pi \frac{\cos \theta \, d\theta}{ar} - \int_0^\pi \left[ \left\{ \frac{2k \sin \frac{1}{2}\theta}{2!} - \frac{(2k \sin \frac{1}{2}\theta)^3}{4!} + \dots \right\} - \right. \\
 &\quad \left. - 2 \left\{ -\frac{2k \sin^3 \frac{1}{2}\theta}{2!} + \frac{2^3 k^3 \sin^5 \frac{1}{2}\theta}{4!} - \dots \right\} \right] d\theta. \\
 \therefore \frac{cA}{2I} &= R \int_0^\pi \frac{\cos \theta \, d\theta}{r} + x^2 \left( \frac{1}{3 \cdot 2!} - \frac{2x^2}{5 \cdot 4!} + \frac{2^2 x^4}{7 \cdot 3 \cdot 6!} - \frac{2^3 x^6}{7! \cdot 6!} + \dots \right), \\
 &\quad \text{where } x \equiv 2k, \\
 &= R \int \frac{\cos \theta \, d\theta}{r} + \frac{2k^2}{3} \left( 1 - \frac{2k^2}{5} + \frac{8k^4}{315} - \frac{4k^6}{4725} + \dots \right). \quad (1.88)
 \end{aligned}$$

The integral term in (1.88) is the vector potential for a steady current and is well known to be equal to  $\{\log(8R/b) - 2.00\}$ , where  $b$  is the small radius of the wire: if  $R/\lambda = \frac{1}{2}$  and  $\lambda/b = 100$ , the value of this term is 4, and if  $R/\lambda = 2$  and  $\lambda/b = 100$ , its value is 6.4. The series portion of (1.88) is approximately equal to +0.4 when  $k = 1$  and -0.675 when  $k = 2$ , thus showing it passes through zero near  $k = 1.5$ . In other words, the self-inductance passes through the steady current value when  $R/\lambda$  is approximately equal to  $\frac{1}{4}$ .

Since, as we have seen, the quadrature component of  $A$  tends in the limit to the value appropriate to a straight filament, it is natural to suppose the inphase component will also tend to the limit for a straight filament, and this is

$$A = -\frac{\pi I}{c} Y_0(ab) \doteq \frac{2I}{c^2} \log\left(\frac{0.18\lambda}{b}\right).$$

Thus it seems improbable that the reactance of a circle of fine wire can ever tend to zero, but is always inductive.

The magnitude of  $A$  at infinity can be calculated as follows. Consider a very distant point in the plane of the circle and in the direction  $OP$  in Fig. 1.18. Consider first the elements  $IR\delta\theta$  at  $B$  and  $B_1$  and resolve them into components parallel to  $OP$  and perpendicular thereto. The parallel components are opposite in sense and hence make no net contribution at the distant point in the direction  $OP$ : the same is true of the horizontal components of elements at  $B_2$  and  $B_3$ . Thus we are left with unlike perpendicular components  $IR\delta\theta \cos \theta$  at  $B$  and  $B_3$  also at  $B_1$  and  $B_2$ . Hence, as in § 1.13, Fig. 1.8, the vector sum of such a pair will be  $2j \sin(k \cos \theta)$  times the contribution of one element, the phase of the resultant being that of an element at  $O$ . Hence, consideration will show that at a very large distance  $r$  we have

$$\begin{aligned} \frac{cA}{I} &= 4j \left( \frac{\cos ar}{ar} - j \frac{\sin ar}{r} \right) \int_0^{\frac{1}{2}\pi} \sin(k \cos \theta) R \cos \theta \, d\theta \\ &= 4k \sqrt{\left( \frac{\pi}{2ar} \right)} \{J_{\frac{1}{2}}(ar) - jY_{\frac{1}{2}}(ar)\} \int_0^{\frac{1}{2}\pi} \{J_1(k) \cos^2 \theta - J_3(k) \cos \theta \cos 3\theta\} \, d\theta \\ &= \sqrt{\left( \frac{\pi}{2ar} \right)} \{J_{\frac{1}{2}}(ar) - jY_{\frac{1}{2}}(ar)\} \pi k J_1(k). \end{aligned} \quad (1.89)$$

If the point is at an angle of elevation  $\phi$  from the plane of the circle, then we must write  $J_1(k \cos \phi)$  in (1.89) above. Hence it follows that  $A$  is zero whenever  $J_1(k \cos \phi)$  is zero. When  $ar \rightarrow \infty$ ,  $Y_{\frac{1}{2}} = J_{\frac{1}{2}} = -J_{\frac{1}{2}}$ , etc., and so (1.89) is compatible in form with (1.85).

Converting to electric field, by the relation  $E = -\frac{1}{c} \frac{dA}{dt}$ , we have

$$-\frac{cE}{2\pi akI} = \left( \frac{\cos ar}{ar} - j \frac{\sin ar}{ar} \right) J_1(k \cos \phi), \quad (1.90)$$

$$\text{or} \quad -\frac{cE}{aI} = \frac{4\pi^3 R^2}{\lambda^2} \cos \phi \left( 1 - \frac{k^2 \cos^2 \phi}{8} \right) \left( \frac{\cos ar}{ar} - j \frac{\sin ar}{ar} \right),$$

$$\text{if} \quad \frac{R}{\lambda} \ll \frac{\sqrt{6}}{\pi} = 0.78. \quad (1.90a)$$

Equation (1.90a) shows that (1.90) reduces, when  $k$  is very small, to the well-known expression for the field of a very small circle, as given already in (1.18). But (1.90a) shows the limiting form is substantially correct, even in the equatorial plane, so long as  $2R/\lambda$  is less than, say,  $1/3$ .

Since  $J_1(z)$  passes through zero when  $z = 3.83, 7.02, 10.16$ , etc., it follows from (1.90) that the field can be made zero at any desired

angle of elevation by appropriate choice of the radius: the larger the radius the greater the number of extinction angles which will occur, and we are reminded thereby of a broadside array and how the number of its side lobes increases with the width of the curtain. An example will illustrate this point. Let  $2R/\lambda = 3.83/\pi = 1.22$ , then the field in the equatorial plane will be zero, but will not be zero at elevation  $\phi$  because  $k \cos \phi$  will then be always less than 3.83. The first maximum of  $J_1(z)$  occurs when  $z = 1.8$ , and has the value 0.581; accordingly the field will be a maximum when  $3.83 \cos \phi = 1.8$ , which is  $\phi = 62^\circ$ . In the general case the field will be zero at elevation  $\phi$  when  $k \cos \phi = 10.16, 7.02, 3.83$ , etc.

Bearing Poynting's theorem in mind, we realize the total output will be small when the field is zero in the equatorial plane, because the equatorial belt contributes much to the area of a Poynting sphere. Accordingly we shall expect the radiation resistance to be a minimum at radii near those which make the equatorial field zero and vice versa. The radii for maximum and zero equatorial field are marked in Fig. 1.19, and it may be seen that these agree approximately with the maxima and minima of radiation resistance, and thus explain why these minima must exist.

#### 1.24. Two similar and coaxial circles with planes parallel

If there are two similar coaxial circles in planes separated a distance  $2h$  and carrying equal and cophased currents, then it follows, as in (1.44), from (1.90) that

$$-\frac{cE}{4\pi akI} = \left( \frac{\cos ar}{ar} - j \frac{\sin ar}{ar} \right) J_1(k \cos \phi) \cos(k' \sin \phi), \quad (1.91)$$

where  $k' \equiv 2\pi h/\lambda$ .

By suitable choice of both  $k$  and  $k'$  it must be possible to make the total output very small, though never zero. Thus, if  $k = 3.83$ , the equatorial field is zero and the field of one circle alone would be a maximum at  $\phi = 62^\circ$ . The field at this elevation will be zero if  $k'$  is chosen so that  $k' \sin 62^\circ = \frac{1}{2}\pi$ , which is  $2h/\lambda = 0.57$ . Accordingly with such an arrangement the field will be small, save near  $\phi = 30^\circ$ , and is zero at  $\phi = 0, 62^\circ$ , and  $90^\circ$ .

#### 1.25. Field of a ring doublet

Let the circle in Fig. 1.20 represent a ring of doublets standing perpendicular to the plane of the paper: thus, if the ring of electric charge just above the paper is positive, the corresponding ring just

below the plane is negative, the two rings of charge being joined by a short cylinder of conduction current flowing perpendicular to the paper. We will calculate the vector potential, which is everywhere parallel to the conduction current and therefore perpendicular to the paper: the radial component of  $A$  does not exist. Each element of the ring makes the same contribution to  $A$  at a very distant point  $Q$ , in

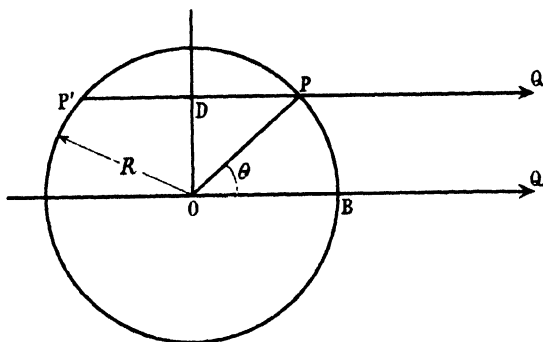


FIG. 1.20.

direction  $OB$ , and we have only to make allowance for the path difference between typical components. The pair of similarly situated elements at  $P$  and  $P'$ , when acting together, produce at  $Q$  a resultant which is  $2 \cos\{(2\pi R/\lambda)/\cos \theta\} \equiv 2 \cos(k \cos \theta)$  times either contribution alone (compare 1.44). Hence if  $A_0$  be the vector potential at the point  $Q$  due to the current in unit arc we have

$$\begin{aligned} \frac{A}{A_0} &= 2 \int_0^{\frac{1}{2}\pi} 2 \cos(k \cos \theta) R d\theta \\ &= 4R \int_0^{\frac{1}{2}\pi} \{J_0(k) - 2J_2(k) \cos 2\theta + 2J_4(k) \cos 4\theta + \dots\} d\theta \\ &= 2\pi R J_0(k). \end{aligned} \tag{1.92}$$

Hence the resultant vector potential of the whole ring is  $J_0(k)$  times what it would be if the ring of short aeriels were collapsed into a single aerial at its centre. This result is reminiscent of a tubular current, see (1.27), and indeed describes why it is that a tube produces no external field if  $J(k) = 0$ . But the field of a ring doublet cannot be zero everywhere: we have been reckoning  $A$  at a point in the plane of the ring.

but had the point  $Q$  been at elevation  $\phi$  the typical path difference would have been  $\cos \theta \cos \phi$  and then (1.92) would have been

$$\frac{A}{A_0} = 2\pi RJ(k \cos \phi), \quad (1.93)$$

and this shows that, for a given  $k$ ,  $A$  cannot be zero for all values of  $\phi$ .

The inphase component of field at the ring can be found by the process corresponding to that used in § 1.22: this will not be developed here, but the reader is referred to *Journal I.E.E.* **88**, Part III, 1941, p. 50, and to equation (15): for a ring doublet this equation is

$$\frac{cP}{4a^2} = \frac{2}{3} X_0^2 \left( 1 - \frac{2k^2}{5} + \frac{9k^4}{140} - \frac{k^6}{189} + \dots \right). \quad (1.94)$$

Comparison with (1.81) shows that the infinite series in brackets represents the factor by which the output is reduced when a simple doublet is expanded into a ring doublet. The number of terms is insufficient to evaluate the output accurately when  $k = 2.405$ , but the factor seems then to be of the order of  $\frac{1}{4}$ . It follows from this discussion that a metal ring cannot have a natural mode of oscillation if it is excited by an electric field parallel to its axis; for there is no radius which makes the radiated field zero, though the radiated energy will be near a minimum if  $2\pi R/\lambda = 2.405$ .

The magnetic field at a great distance is obtained by differentiating (1.92) with respect to  $x$  in the manner of (1.74).

## II

### CERTAIN STANDARD DIFFRACTION PATTERNS AND POLAR DIAGRAMS AND POWER GAIN OF CERTAIN ARRAYS

#### 2.1. The basic idea

SOMETIMES we wish an aerial to broadcast equally in all directions; in other circumstances we wish it to provide a communication service to one fixed point only: then we are glad to constrain its radiation to a narrow path both as a means of conserving power and of reducing unnecessary interference with other stations. A narrow beam of radiation can be attained by using an array of many aerials spaced apart a distance comparable with a wavelength. Consider two parallel aerials carrying equal cophased currents and spaced apart a distance  $2R$ , as shown diagrammatically in Fig. 1.7. At a very distant point the resultant field will be the vector sum of two components which are sensibly equal in magnitude. Reference to the figure shows the path difference from  $P$  to the two aerials tends to equal  $2R \cos \theta$ : hence the phase-angle  $\beta$  between the two sensibly equal component vectors is

$$\beta = \frac{2\pi}{\lambda} \times 2R \cos \theta.$$

If each aerial alone would produce at  $P$  a field  $E_0$ , then the two together will produce a field (see also p. 46)

$$2E_0 \cos \frac{\beta}{2} = 2E_0 \cos \left( \frac{2\pi R}{\lambda} \cos \theta \right) \equiv 2E_0 \cos(k \cos \theta).$$

If on some bearing  $\theta$  the path difference is  $\frac{1}{2}\lambda$ , then the two components will be in antiphase, and in that particular direction the field will be zero. Thus suppose the two aerials are spaced apart a distance  $\lambda$ : then when  $\theta = 60^\circ$ , the path difference will be  $\frac{1}{2}\lambda$  and thus on bearings  $\pm 60^\circ$  and  $\pm 120^\circ$  to the direction  $AB$  the resultant field will be zero. We are utilizing the principle which, in the study of optics, is called destructive interference. If the relation between intensity and bearing is plotted in polar coordinates, the resulting diagram in this case has four petals or lobes each with maximum intensity  $2E_0$ : two have a width, zero to zero, of  $120^\circ$  and two a width  $60^\circ$ . When plotted in polar coordinates the intensity distribution will be referred to as a polar diagram: when plotted in Cartesian coordinates it will be called a diffraction pattern.

Now consider the case when the two currents are not necessarily equal or cophased, differing in time phase by the angle  $\alpha$ . Then on bearing  $\theta$  the two component fields will differ in phase by the angle  $\beta$  resulting from the path difference plus the angle  $\alpha$  which is the arbitrary phase difference of the two currents. If the resultant field on bearing  $\theta$  be  $R_1$ , then

$$R_1^2 = E_1^2 + E_2^2 + 2E_1 E_2 \cos(\beta + \alpha).$$

In this relation we suppose the left-hand current,  $A$  in Fig. 1.7, lags  $\alpha$  in phase with respect to current  $B$ . Then on bearing  $180^\circ + \theta$  the angle between the two component vectors will be  $\beta - \alpha$  and then we have

$$\begin{aligned} R_2^2 &= E_1^2 + E_2^2 + 2E_1 E_2 \cos(\beta - \alpha) \\ &= (E_1 - E_2)^2 + 2E_1 E_2 \{1 + \cos(\beta - \alpha)\} \\ &= (E_1 - E_2)^2 + 4E_1 E_2 \cos^2 \frac{\beta - \alpha}{2}. \end{aligned} \quad (2.1)$$

This shows  $R_2$  can be zero provided  $E_1$  is equal to  $E_2$  and if in addition  $\beta - \alpha = \pi, 3\pi$ , etc.: if both these conditions are fulfilled, then

$$R_1 = 2E \sin \alpha$$

and generally  $R^2 = 2E^2 \{1 + \sin(\frac{1}{2}\pi \cos \theta)\}$ .

A well-known application of this principle is when the spacing is  $\frac{1}{4}\lambda$  and the phase angle is  $90^\circ$ . Thus with reference to Fig. 1.7, suppose current  $A$  leads a quarter cycle on current  $B$ . Consider the field in the direction  $AB$ . The field of  $A$  lags that of  $B$  by a quarter cycle in respect of path difference, but this lag of quarter cycle is compensated for by the lead of quarter cycle in the current  $A$ . Hence the field is  $2E$  in direction  $AB$  and is zero in direction  $BA$ : when  $\theta = \pm 90^\circ$ ,  $R = \sqrt{2}E$ : the polar diagram is a heart-shaped figure. These two examples serve as an introduction to certain standard cases.

## 2.2. Curtain array with side spacing $\frac{1}{2}\lambda$

Consider an array of  $N$  parallel aeriels carrying equal and cophased currents, forming a grating with spacing  $\frac{1}{2}\lambda$ . We will consider now only the pattern in the equatorial plane of the grating and thus need not discuss whether each member is a doublet, half-wave aerial, or long filament. We may use Fig. 1.14 to illustrate this problem. Then on any bearing the components due to currents 2 and 2' will lead and lag the component due to current  $O$  by the same angle: accordingly the phase of the resultant field must be the same as the phase of the

component due to the middle wire of the grating. The resultant field at a very distant point is the vector sum of  $N$  equal vectors each inclined at an angle  $2\beta = (2\pi g/\lambda)\sin\theta$  to its neighbour, where  $\theta$  is the bearing with respect to the *normal* to the grating. The vector polygon is typified by Fig. 2.1: the resultant is  $FA$  and is parallel to  $DC$ , the component due to the middle member. It follows from simple trigonometry that

$$\frac{FA}{N \times AB} = \frac{\sin N\beta}{N \sin \beta} = \frac{\sin\{(\pi g N/\lambda)\sin\theta\}}{N \sin\{(\pi g/\lambda)\sin\theta\}}. \quad (2.2)$$

A precisely corresponding problem arises in calculating the e.m.f. of an alternating current dynamo, and we shall adopt here its long-established nomenclature and term expression (2.2), the 'breadth factor' of the array. It is highly convenient to visualize the array in terms of a single equivalent aerial placed at its middle point and carrying a current whose magnitude is  $N$  times the 'breadth factor'; we note this single equivalent current is a function of the bearing angle. Conscious recognition of this principle and artifice makes it simple to add vectorially the fields of any number of arrays, which need not even be coplanar.

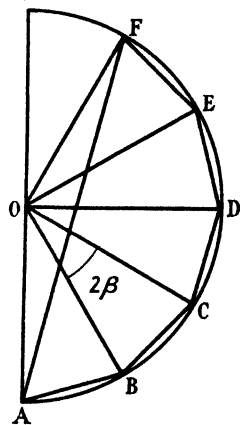


FIG. 2.1.

We note from (2.2) that the resultant field is zero when

$$\frac{\pi g N}{\lambda} \sin\theta = \pi, 2\pi, \text{etc.}; \quad \text{or} \quad \sin\theta = \frac{\lambda}{Ng}, \frac{2\lambda}{Ng}, \text{etc.} \quad (2.3)$$

In many of our applications  $g/\lambda = \frac{1}{2}$  and then  $\sin\theta = 2/N, 4/N, 6/N$ , etc. If  $b$  is the total breadth of the array,  $b = (N-1)g \doteq Ng$ : accordingly the bearings for zero field are given approximately by

$$\sin\theta \doteq \frac{\lambda}{b}, \frac{2\lambda}{b}, \frac{3\lambda}{b}. \quad (2.3a)$$

Since the field passes through zero on all the bearings for which  $N\beta = \pi, 2\pi$ , etc., the field must be a maximum on bearings very near those for which  $N\beta = 3\pi/2, 5\pi/2$ , etc. Now when  $g/\lambda$  is not greater than  $\frac{1}{2}$  the path difference between consecutive members must be less than  $\frac{1}{2}\lambda$  and hence  $\beta$ , which is half the phase angle between two consecutive members, can attain to  $\frac{1}{2}\pi$  only when the bearing is verging on  $90^\circ$ . We are interested mainly in the field on bearings less than, say,  $30^\circ$  away from the normal, and in such circumstances may



write  $\sin \beta \doteq \beta$  in (2.2). Then it follows that when  $N\beta = 3\pi/2, 5\pi/2$ , etc., the breadth factor is approximately equal to  $1/N\beta$  and hence successive maxima are substantially in the ratio  $1, 2/3\pi, 2/5\pi, 2/7\pi$ , etc.; i.e.  $1, 0.21, 0.13, 0.09, 0.07, 0.06, 0.05$ , etc. Fig. 2.2 shows the diffraction pattern in the equatorial plane of a curtain array having 16 equal

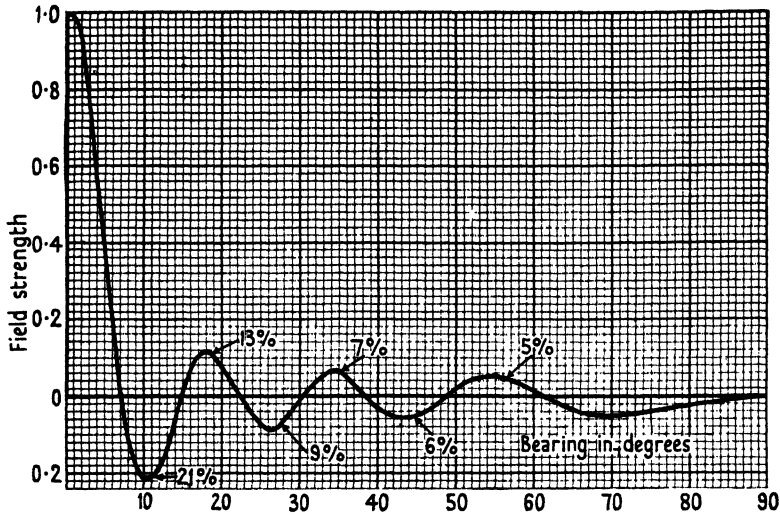


FIG. 2.2. Relating to curtain-array; current loading uniform and cophased.  
Power gain 21.8.

and cophased members spaced  $\frac{1}{2}\lambda$  apart. It is typical of the pattern of the large directive arrays which are to be seen in this country and which carry out the point-to-point services of the G.P.O. and of commercial communication companies.

The pattern is commonly said to consist of a central beam and side lobes: it is important to realize that increasing the width of the array does not decrease the fractional amplitude of the side lobes. Increasing the width merely narrows the main beam and adds more side lobes, the first of which always has an amplitude which is 21 per cent. of the amplitude of the main beam.

It is important to realize some zeros occur in a way we may call absolute while others are not absolute in the sense we mean here. Thus consider a pair of aerials separated by  $2\lambda$ : then the path difference for such a pair will be  $\frac{1}{2}\lambda$  when the bearing is  $\arcsin \frac{1}{2}$ , which is  $14.5^\circ$ . The curtain of 16 members can be decomposed into 8 such pairs separated by  $2\lambda$  and thus the net resultant field must be zero on a bearing of  $14.5^\circ$  (see Fig. 2.2), and such a zero we call an absolute zero.

This condition will occur again when  $\theta = \arcsin \frac{3}{4} = 48.55^\circ$ , and hence this bearing is also an absolute zero. Again, a pair of aerials separated by  $\lambda$  will have a path difference of  $\frac{1}{2}\lambda$  when the bearing is  $30^\circ$  and there are 8 such pairs in a curtain of 16 members, and hence  $\theta = 30^\circ$  is also an absolute zero. It will be appreciated that alternate zeros are absolute, while the remainder become zero for a less absolute reason. When the distance between the members is very small the curtain degenerates ultimately into a uniformly loaded continuous sheet. Then extension of the argument respecting absolute zeros will show the first zero of field must occur on that bearing for which the path difference between the midline of the sheet and either of its two edges is  $\frac{1}{2}\lambda$ ; this also follows from (2.3a). The other absolute zeros occur when this path difference is  $3\lambda/2$ ,  $5\lambda/2$ , etc., and give half the total number of zeros.

In considering a single curtain, spacings greater than  $\frac{1}{2}\lambda$  are not of interest. In the problem of the optical grating we have to consider a curtain of curtains and then  $g$  will stand for the distance between the midpoints of neighbouring wide current sheets, and in such circumstances  $g/\lambda$  is large, usually of the order of 20. Having fixed in our minds that the side lobes of a curtain or current sheet are of the order of 21 per cent., 13 per cent., etc., we must remember this applies only to a curtain for which  $g/\lambda$  is not greater than  $\frac{1}{2}$ . When  $g/\lambda$  is large there will be bearings for which  $2\beta = 2\pi$ ,  $4\pi$ , etc., and then consideration will show the breadth factor must be unity. The pattern would consist of a series of equal main beams with small side lobes between them.

### 2.3. Curtain array with non-uniform cophased loading

In certain circumstances the side lobes are objectionable; not because of the waste of power they represent, since that is small, but because they may cause troublesome interference at a comparatively short range. It is well known that some side lobes can be decreased in relative magnitude by concentrating the current in the middle of the curtain, at the expense, however, of increasing the width of the main beam. The mechanism of the action is readily understood by remembering that the phase of the resultant field on any bearing is the phase of the component from the middle member, provided only that all currents are cophased. Suppose now the current in the 8 central members of a 16-member curtain is twice that in the outside 4 at each end. This may be thought of as the superposition of a 16-member uniformly loaded curtain and an 8-member uniformly loaded curtain.

In virtue of the property just described the resulting diffraction pattern is the *arithmetic* sum of the patterns appropriate to a 16-member and to an 8-member curtain. Now refer to Fig. 2.2: had this depicted the pattern of an 8-member curtain the maximum of the first side lobe would have occurred very near a bearing of  $20^\circ$  and of the second near  $36^\circ$ , and so on. Hence, on bearing  $20^\circ$  the 8-member

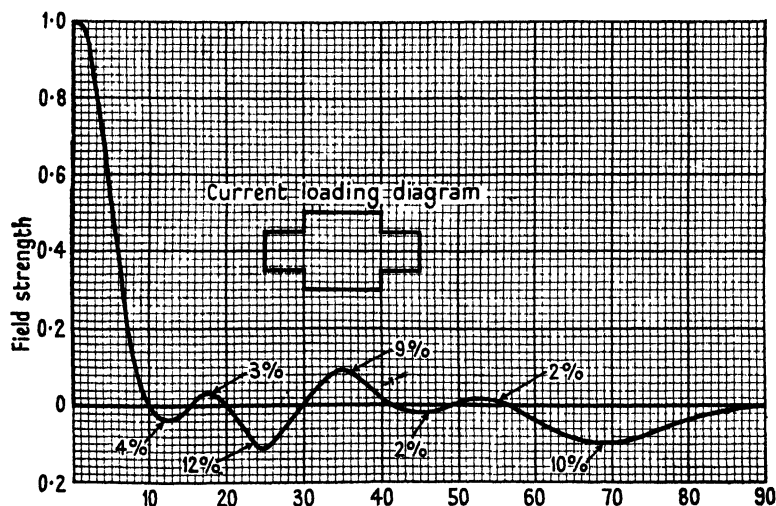


FIG. 2.3. Curtain-array: current loading 1:2:2:1, cophased. Power gain 17.3.

contributes a negative field of 21 per cent. and the 16-member a positive field of about 13 per cent., and thus the result will be a negative field of some 8 per cent. and is therefore a substantial reduction of the largest lobe. Fig. 2.3 shows the whole resultant pattern and is typical of the general principle involved. Comparing these two figures we see that in Fig. 2.3 the first zero occurs on a bearing of  $10^\circ$  instead of  $7\frac{1}{2}^\circ$ , but the first two side lobes have become small; on the other hand, the third and fourth have been enhanced slightly.

## 2.4. Curtain array with 'triangular' loading

By this we mean a load curve which is symmetrical about the middle member and in which there is a constant difference in current from member to member: thus if the curtain had 16 members, then the currents in them, reckoning from the extreme towards the middle, would be 1, 2, 3, 4, 5, 6, 7, 8, 8, 7, 6, ..., 1. All currents are supposed to be cophased. Accordingly the pattern can be built up by arithmetic addition of component patterns. We will consider first a 16-member

curtain and proceed by induction to a general formula. Accordingly we have to add the pattern for a uniformly loaded array of 16 members to that of 14 members and then to that of 12 members, and so on. Let  $2\beta$  be the phase angle between any two consecutive members on

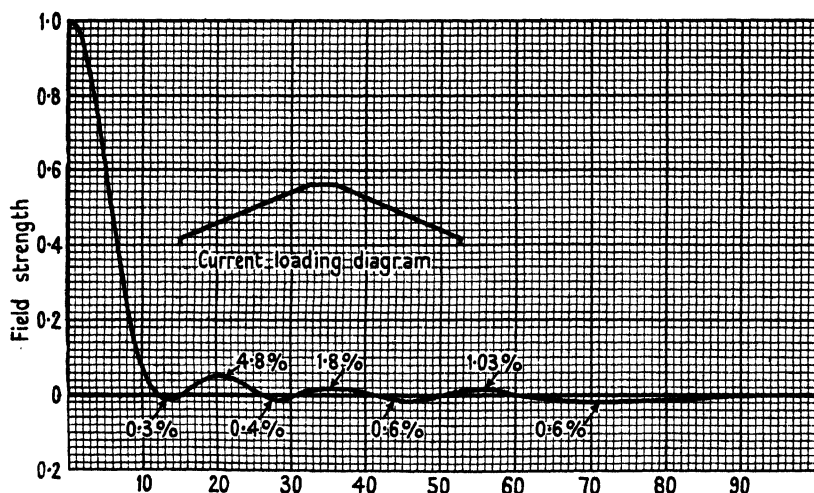


FIG. 2.4. Current loading, triangular and cophased. Power gain 13.3.

bearing  $\theta$ . Then if  $R$  is the resultant field and  $E_0$  the field per unit current for an isolated member, we have by (2.2)

$$\begin{aligned} \frac{R}{E_0} &= \frac{\sin 16\beta}{\sin \beta} + \frac{\sin 14\beta}{\sin \beta} + \dots + \frac{\sin 2\beta}{\sin \beta} \\ &= \frac{\sin 9\beta \sin 8\beta}{\sin^2 \beta} \\ &= \left( \sin \frac{N+2}{2} \beta \sin \frac{N}{2} \beta \right) / \sin^2 \beta. \end{aligned}$$

When  $\beta = 0$  we have  $R_0 = \frac{N(N+2)}{2} E_0$ , and accordingly

$$\text{Breadth factor} = \frac{\sin\left(\frac{N+2}{2}\right)\beta}{\left(\frac{N+2}{2}\right)\sin \beta} \times \frac{\sin(N/2)\beta}{(N/2)\sin \beta}, \quad (2.4)$$

and this shows the pattern is the product of the pattern of a uniformly loaded array having  $(N+2)/2$  members with the pattern of a uniformly loaded array having  $N/2$  members. Fig. 2.4 shows the pattern for an array with 16 members and should be compared with Fig. 2.2. It will

be seen that the largest side lobe is now 4.8 per cent. as compared with 21 per cent.

Now let  $N$  become large and  $g$  small, but the product  $Ng = b$  remains constant: that is to say, an array of given width in which the number of component members is increased without limit. Then

$$\frac{N+2}{2} \beta = \frac{N+2}{2} \frac{\pi g}{\lambda} \sin \theta \doteq \frac{\pi b}{2\lambda} \sin \theta,$$

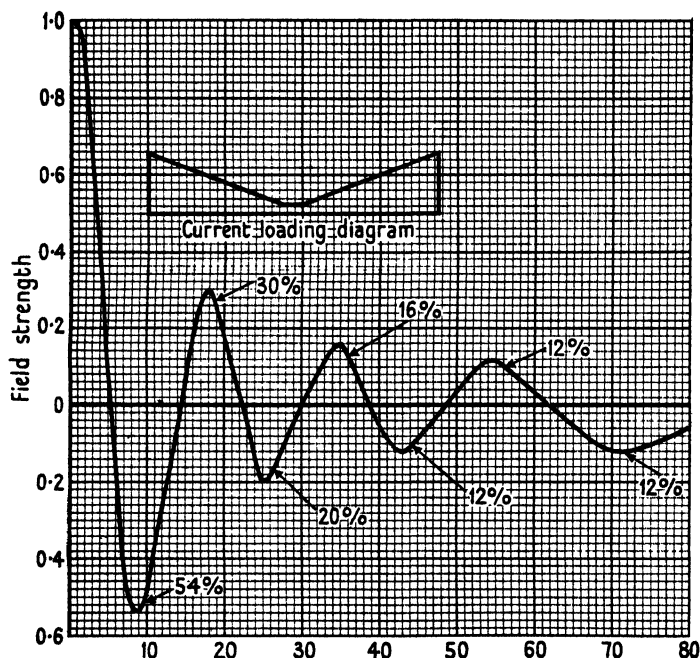


FIG. 2.5. Loading outward-triangular, cophased. Power gain 13.3.

and accordingly (2.4) becomes

$$\text{Breadth factor} = \left\{ \frac{\sin\{(\pi b/2\lambda)\sin\theta\}}{(\pi b/2\lambda)\sin\theta} \right\}^2, \quad (2.4a)$$

and this is the square of the breadth factor of a uniformly loaded continuous sheet of width  $\frac{1}{2}b$ . Accordingly it has  $b/\lambda$  bearings of zero field, whereas the uniformly loaded sheet of the same width would have twice this number. The breadth factor is always positive and hence there is no change of phase in passing through a bearing for zero field. The maxima of the side lobes are given by the series  $1, (2/3\pi)^2, (2/5\pi)^2, \dots$ , i.e. 100, 4.5, 1.63, 0.82, 0.5, 0.34 per cent., etc. Though the

angle for the first zero is twice as great with triangular as with uniform loading this does not mean the main beam is twice as wide at half-height. Thus in Fig. 2.2 this width is  $4.5^\circ$  and in Fig. 2.4 it is  $6^\circ$ .

The pattern appropriate to a loading which increases uniformly from the centre outwards can obviously be obtained from the difference between Figs. 2.2 and 2.4 provided that the ordinate scale of 2.2 is twice that of 2.4. The result is shown in Fig. 2.5: here the side lobes are enormous and the main beam is decreased in width. The pattern for any polygonal loading can be derived by appropriate combinations of Figs. 2.2 and 2.4, and these figures should be regarded as the constructional units for any symmetrical cophased loadings.

### 2.5. Curtain array with sinusoidal loading

Let  $N$  be odd, and let the current in the middle member be  $I$ ; then it is to be  $I \cos \alpha$ ,  $I \cos 2\alpha$ , etc., in successive members on each side of the middle,  $\alpha$  being such that  $(N+1)\alpha = \pi$ . Then if  $2\beta$  be the phase angle due to path difference between any consecutive pair of currents on an assigned bearing  $\theta$  and numbering from an extreme member of the array, we shall have

$$\frac{R}{E_0} = \sin \alpha \sin pt + \sin 2\alpha \sin(pt + 2\beta) + \dots$$

After considerable reduction, the breadth factor is found to be

$$\text{Breadth factor} = \frac{2 \cos(N+1)\beta \sin^2(\alpha/2)}{\cos 2\beta - \cos \alpha}. \quad (2.5)$$

Close scrutiny shows (2.5) has the value  $\frac{1}{4}\pi$  when  $2\beta = \alpha$ . The field is zero when  $(b/\lambda)\sin \theta = 3/2, 5/2$ , etc., and this shows the first bearing for zero field is about 1.5 times as great as for uniform loading of the same width.

Sinusoidal loading of members separated by a finite distance  $g$  is rather a pedagogic problem and therefore has not been expounded in detail. On the other hand, a continuous sheet of width  $b = \frac{1}{2}\lambda$  with sinusoidal loading is of great practical importance. The appropriate expression can be obtained by taking (2.5) to the limit; but because this example is of great practical importance it is worth while to derive the expression *ab initio*. Let the flow of current be perpendicular to the breadth  $b$  and have density  $\cos(\pi x/b)$ , where  $x$  is the distance of an elementary strip of width  $\delta x$  from the middle of the array. Then the resultant field due to elements  $\cos(\pi x/b) \delta x$  at  $\pm x$  will be proportional

to  $2 \cos \frac{\pi x}{b} \cos \left( \frac{2\pi x}{\lambda} \sin \theta \right) \delta x$  on bearing  $\theta$  from the normal to the plane of the array. Accordingly

$$\begin{aligned}
 R &= 2 \int_0^{b/2} \cos \frac{\pi x}{b} \cos \left( \frac{2\pi x}{\lambda} \sin \theta \right) dx \\
 &= 2 \int_0^{\frac{1}{2}\lambda} \cos \frac{2\pi x}{\lambda} \cos \left( \frac{2\pi x}{\lambda} \sin \theta \right) dx, \quad \text{since } b = \frac{1}{2}\lambda, \\
 &= \int_0^{\frac{1}{2}\lambda} \left[ \cos \left\{ \frac{2\pi x}{\lambda} (1 + \sin \theta) \right\} + \cos \left\{ \frac{2\pi x}{\lambda} (1 - \sin \theta) \right\} \right] dx \\
 &= \frac{\lambda}{2\pi} \left\{ \frac{\sin \left\{ \frac{1}{2}\pi (1 + \sin \theta) \right\}}{1 + \sin \theta} + \frac{\sin \left\{ \frac{1}{2}\pi (1 - \sin \theta) \right\}}{1 - \sin \theta} \right\} \\
 &= \frac{\lambda}{\pi} \frac{\cos(\frac{1}{2}\pi \sin \theta)}{\cos^2 \theta}.
 \end{aligned}$$

When  $\theta = 0$ ,  $R_0 = \lambda/\pi$ , and hence

$$\text{Breadth factor} = \frac{R}{R_0} = \frac{\cos(\frac{1}{2}\pi \sin \theta)}{\cos^2 \theta}. \quad (2.6)$$

This attains the value  $\frac{1}{2}\pi$  when  $\theta = \frac{1}{2}\pi$ : hence the polar diagram of a sheet of width  $\frac{1}{2}\lambda$  with sinusoidal loading is not far from a circle. When  $b/\lambda = \frac{1}{2}$ , then (2.4) reduces to

$$\frac{16 \sin^2(\frac{1}{2}\pi \sin \theta)}{\pi^2 \sin^2 \theta}, \quad (2.7)$$

and the value of this is 0.81 when  $\theta = \frac{1}{2}\pi$ .

## 2.6. Curtain array with spacing $\frac{1}{2}\lambda$ and binomial loading

The previous sections have shown the size of the lobes depends on the distribution of current across the array: we have found that a concentration in the middle reduces the lobes to a small value and they are virtually removed by triangular loading. There is, however, a loading for which the field never falls to zero save when  $\theta = 90^\circ$ , and then ripples do not exist on the skirts of the diffraction pattern. Consider a pair of equal cophased currents separated by  $\frac{1}{2}\lambda$ : their resultant field can be zero only when  $\theta = 90^\circ$ . The pair can be replaced by a single equivalent aerial half-way between them and supposed to bear a current of strength  $2 \cos(\frac{1}{2}\pi \sin \theta)$ . Now arrange two such pairs as in Fig. 2.6(a) with their planes very close together: the left-hand pair can be replaced by a single equivalent aerial at *A* and the second by an equivalent at *B*. The two equivalents are separated by  $\frac{1}{2}\lambda$  and

have equal strengths on any assigned bearing, and accordingly their field falls to zero only at  $\theta = 90^\circ$ . Because their planes are very close they degenerate into a 3-member curtain with loading 1, 2, 1. Now take two such 3-element curtains disposed as in Fig. 2.6(b): each of these two can be replaced by a single equivalent at its middle point and these two equivalents are separated by  $\frac{1}{2}\lambda$ .

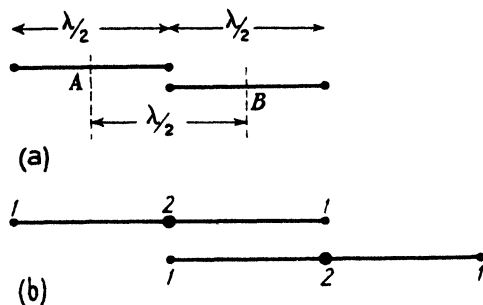


FIG. 2.6.

Accordingly it follows that the field of a 4-element curtain with loading 1, 3, 3, 1 will fall to zero only when  $\theta = 90^\circ$ . We can now take two such 4-element curtains to build one with 5 elements and loading 1, 4, 6, 4, 1. We can proceed indefinitely in this manner and so arrive at an array in which each member, reckoning from one extreme, carries a current proportional to the coefficients in the expansion of  $(1+x)^{N-1}$ : accordingly we shall term this a binomial loading. It follows readily that

$$\text{Breadth factor} = \cos^{N-1}(\tfrac{1}{2}\pi \sin \theta). \quad (2.7 a)$$

Had the loading been uniform the field would have been zero for the first time when  $\sin \theta = 2/N$ : if  $N = 6$ , then on this bearing the field of an array in which the loading is 1, 5, 10, 10, 5, 1 is, from (2.7 a),

$$(0.866)^5 = 0.486.$$

Thus it is seen the main beam slopes rather gradually away to zero, and this must be so because the performance is obviously dominated by the large current in the middle pair of members. When  $N$  is large it follows readily from (2.7 a) that the fractional reduction when  $\sin \theta = 2/N$  approaches the value  $\pi^2/2N$ . Binomial loading is an elegant device,<sup>†</sup> but of little practical value: it does remove side lobes in the sense that the field nowhere passes through zero, but it replaces them by giving the pattern a gently falling skirt. For all practical purposes triangular loading is the best for avoiding side lobes.

<sup>†</sup> It may be well known, but was shown to me by Mr. R. V. Alred in September 1940; compare also p. 94 of *Studies in Optics* by A. A. Michelson.



As a final example we give Fig. 2.7, which shows the pattern for a 16-member equally loaded array save that the current is zero in the two middle members. Here we note the absent currents have increased the first side lobe from 21 to 37 per cent. and exemplify once more the great importance of the central members. Those who have had much practical experience of adjusting arrays will know how hard it

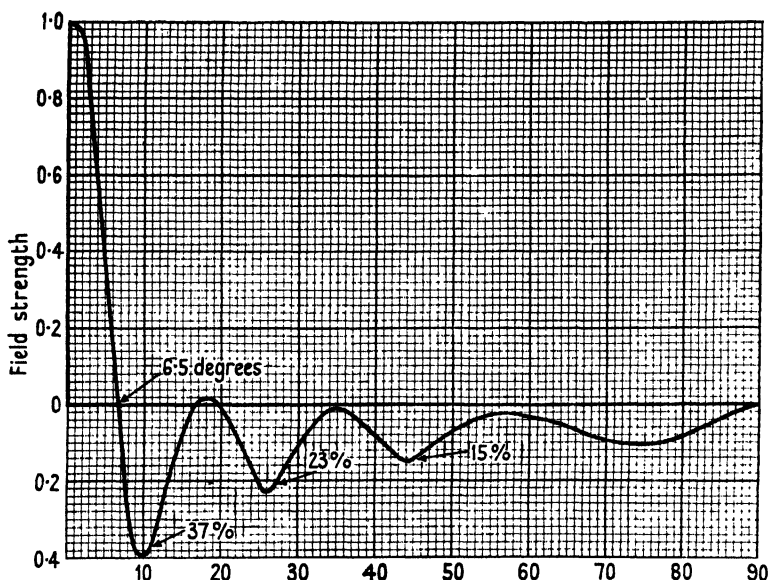


FIG. 2.7. Loading cophased and uniform save that the two central members are absent. Power gain 21.4.

often is to attain side lobes as small as 21 per cent. even when steps have been taken to encourage concentration of current in the central members. This difficulty does not appear to arise in the vast panels such as are used for world services operating at a wavelength of some 20 m. Presumably this is because it is comparatively easy to regulate the feeding to each member at such comparatively long wavelengths. For wavelengths less than about 2 m. it is difficult to control the feeding and still more difficult to ascertain the current in each member; and it is at such wavelengths that the side lobes have the unpleasant habit of being larger than they ought to be. We will reserve these practical considerations to a later chapter, but will interpolate the following dictum here: if the side lobes are larger than they should be, then it is almost certain that two or three members near the middle of the curtain have less than their proper share of current. Inadequacy of current is far more likely to be the cause of the trouble than incorrect-

ness of phase. The tester should not rest till he is quite certain the middle members have their proper share of current; when, and only when, he is satisfied that they have should he allow himself to be deflected by the suggestion that phasing is incorrect. That explanation is always put forward and is almost always wrong: an infinity of time can be wasted in shortening individual cables slightly, remaking joints, and doing much incidental permanent damage. But it is a more obvious and direct occupation than measuring the current in each member: repeated failures seem to damp little the hopefulness which is inherent in junior testers: the remote chance of a fortunate occurrence is in general more attractive than the stern discipline of systematic and ordered work. We will renew this discussion in Chapter XIV.

### 2.7. Method of turning the main beam away from the normal

Sometimes it is required to change the direction of the main beam of a curtain array and it may well be impossible, as, for example, with the great panels of the G.P.O., to turn the array physically as a whole. We must seek to turn the beam by electrical means, and it is necessary to assess the possibility of doing so by adjustment of the phase of the component members. Thus suppose the phase of one extreme quarter is advanced by a quarter cycle with respect to the central half and the phase of the other extreme quarter is retarded by a quarter cycle. Then the result must be somewhat as though the plane of the whole array had been turned through an angle whose tangent equals  $\frac{1}{2}\lambda$  divided by the total width. If the spacing is  $\frac{1}{2}\lambda$ , then this angle is  $1/(N-1)$  radians, or, say,  $4^\circ$  if  $N = 16$ . Since the distance of the middle of the array to the middle of an outer quarter is  $\frac{3}{8}b$  it may be more proper to compare the angle with  $4/3(N-1)$ , but this must certainly be an upper limit which cannot be attained. The process of deriving the pattern is best described by a numerical example and we will take  $N = 16$ . Each outer 4 has a breadth coefficient

$$\frac{\sin\{4(2\pi d/\lambda)\sin\theta\}}{4\sin\{(2\pi d/\lambda)\sin\theta\}} = \frac{\sin(4\pi\sin\theta)}{4\sin(\pi\sin\theta)}$$

and can be replaced by a single equivalent aerial at the middle point of an outer quarter. These two equivalent aerials are in antiphase with one another and are separated a distance  $6\lambda$ . Hence the two together will produce a field strength

$$2\sin(6\pi\sin\theta)\frac{\sin(4\pi\sin\theta)}{\sin(\pi\sin\theta)},$$

and this will be in phase quadrature with the current in the outer



quarters and therefore in phase with the field from the middle half (compare § 1.13). The middle half will produce a field given by

$$\frac{\sin(4\pi \sin \theta)}{\sin(\pi \sin \theta)}.$$

These two component patterns must be plotted separately and added *arithmetically*. The first component is zero when  $\theta = 0$  and when  $\theta = \pm 9.6^\circ$ , and hence presumably is near its maximum when  $\theta = \pm 4.8^\circ$ , one maximum being positive and the other negative. The second component is a maximum when  $\theta = 0$  and zero when  $\theta = \pm 14.5^\circ$ , and hence must be far short of its maximum when  $\theta = 4.8^\circ$ . Thus we are adding a decreasing and an increasing function, and the maximum will occur before the maximum of the increasing function, and hence the beam must be turned through less than  $4.8^\circ$ . The firm line curve in Fig. 2.8 shows the resulting pattern, while the dotted curve is the pattern when all 16 currents are cophased. The beam is turned off centre by about  $4^\circ$ : it will be noted that the side lobes are modified profoundly and enhanced.

Fig. 2.9 shows the component patterns when only the two extreme currents are in leading and lagging phase quadrature with the other 14: it serves to illustrate the process underlying all such calculations; in this case the main beam is turned through nearly  $1^\circ$ .

It can be shown that when  $N$  is large the main beam is turned off centre through an angle which is approximately equal to (a)  $3/\pi \times 2/N$  of the first zero angle when only the extreme members are in leading and lagging phase quadrature with the remainder, (b) half the first zero angle when the outer quarters are in leading and lagging quadrature, (c) three-eighths of the first zero angle when the two halves of the array are in phase quadrature. (d) If the two halves are in antiphase the main beam is bifurcated (the forward field being zero) and each of the two equal maxima is off centre by an angle just greater than  $3/2N$ .

We see it is not possible to rotate the beam through more than a few degrees by appropriate adjustment of phase: this limitation may be distressing when it is desired so to turn the beam, but it has a very fortunate aspect which is of immense practical benefit. For if it is very hard to turn the beam off centre by deliberate and co-operative phase adjustment then it means the beam will not be turned off centre appreciably by small maladjustments of phase of individual members. The main beam is, as it were, very rigid, and will always be almost

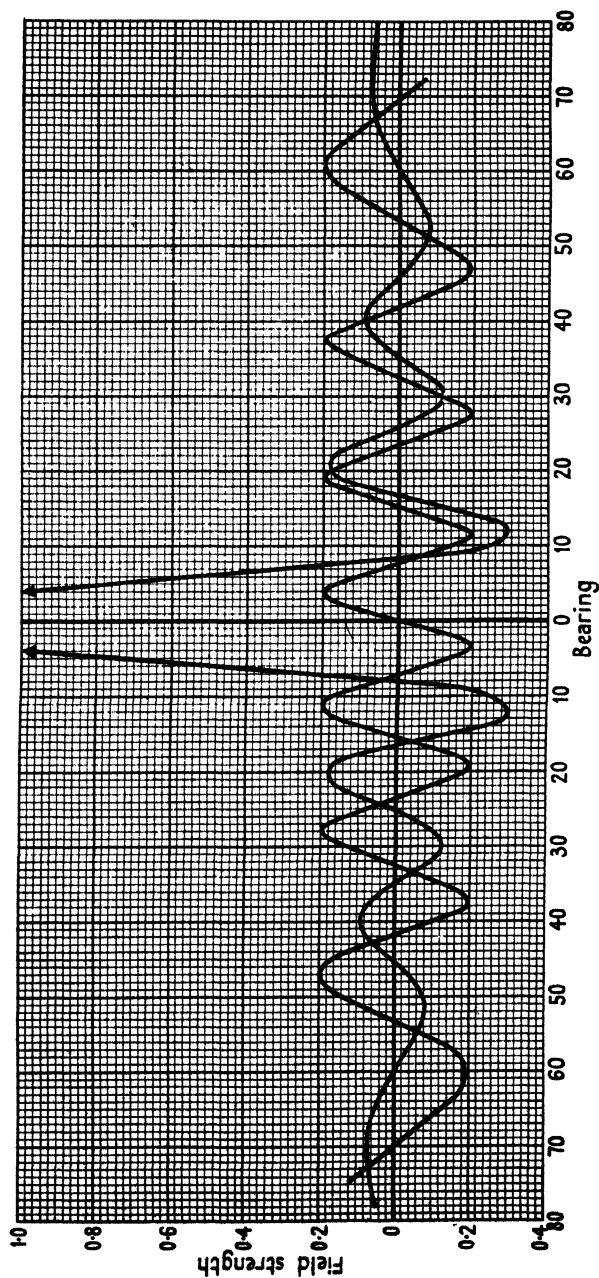


FIG. 2.9. Pattern for 14 equal cophased currents, spaced  $\frac{1}{2}\lambda$  apart, and pattern for two antiphased currents spaced  $7\frac{1}{2}\lambda$  apart. Resultant pattern is the sum of these two components. Note that the two sets of ripples tend to augment one another on the R.H.S. and tend to neutralize one another on the L.H.S.

perfectly on centre, no matter how much the array as a whole is out of adjustment. This property cannot be over-emphasized and it seems almost impossible to make the young test-hand appreciate it. That the main beam is on centre is no criterion whatever that the array is in reasonably correct adjustment: the difficulty is not to get it on centre but to get it off centre. The side lobes, however, are very sensitive to maladjustment of phase and are as 'flexible' as the main beam is 'rigid'. To support this statement see Fig. 2.8. Unsymmetrical side lobes certainly denote maladjustment of phase: large side lobes are not likely to be due to maladjustment of phase but to maladjustment of magnitude. These practical points will be taken up fully in Chapter XIV. It is, however, well to interpolate these remarks here, since bitter experience shows they are principles which are extremely difficult to inculcate in the heads of many whose business is to adjust aerial curtains.

## 2.8. In-line arrays

The reader must not forget that the diffraction patterns discussed in the last section are valid only in the equatorial plane of a curtain. We now consider the radiation figure for an isolated straight wire of any length, called hereafter an in-line array: when this has been done we can complete the problem of a curtain.

The radiation figure of an in-line array is obviously a solid of revolution about the array as axis. In Chapter I we derived the field of a doublet aerial, and equation (1.71) shows that the electric field is tangential at large distances and varies as the cosine of the angle of elevation above the equatorial plane. Any in-line array can be built up by superposing a distribution of doublets appropriate to the current distribution in the array. Here the informed reader will interject that the current distribution is never known exactly, the only certainty being that the current is zero at each end of the wire: he states truly, but will soon find the lack of precise knowledge makes a very small uncertainty in the radiation figure. Consider first a wire half a wavelength long with a current distribution which is sinusoidal: it can be built up of a sinusoidal distribution of doublets. At angle of elevation  $\phi$  every component doublet will make a contribution to the field proportional to  $\cos \phi$  and to the strength of that component. The resultant field will be the vector sum of all these contributions, each one having a phase angle corresponding to the path difference due to its position on the half-wave aerial: the value of this resultant is given by

equation (2.6). Accordingly the field at elevation  $\phi$ , and on any bearing, is given by

$$F_1 = \frac{\cos(\frac{1}{2}\pi \sin \phi)}{\cos^2 \phi} \cos \phi = \frac{\cos(\frac{1}{2}\pi \sin \phi)}{\cos \phi}. \quad (2.8)$$

Some values of  $F_1$  and of  $\cos \phi$  are collected in Table 2.1 below.

TABLE 2.1

$\phi$	0	20	30	40	45	60	70	80	90
$\cos \phi$	1	0.94	0.866	0.77	0.71	0.5	0.34	0.17	0
$F_1$	1	0.91	0.816	0.69	0.62	0.42	0.28	0.14	0

This table shows that  $F_1$  is never much less than  $\cos \phi$ , and this means that  $F_1$  is insensitive to the length of the aerial (provided this does not exceed  $\frac{1}{2}\lambda$ ). It is also insensitive to the current distribution; thus, if the distribution were triangular (instead of sinusoidal)  $F_1$  would be  $\cos \phi$  times (2.7) and then it may be found that  $F_1 = 0.43$  when  $\phi = 60^\circ$ . The query raised by the hypothetical reader has been answered, and it has been shown that the result is insensitive to current distribution.

If there are  $N$  half-wave units in line, all currents being cophased and equal, the resulting breadth factor will be the product of (2.2) and (2.8) and thus

$$\text{Breadth factor} = F_1 \times F_2 = \frac{\cos(\frac{1}{2}\pi \sin \phi)}{\cos \phi} \times \frac{\sin(\frac{1}{2}N\pi \sin \phi)}{N \sin(\frac{1}{2}\pi \sin \phi)}. \quad (2.9)$$

Because the resulting pattern is the product of  $F_1$  and  $F_2$ , uncertainty in the current distribution does not produce a cumulative effect. It is true that (2.9) assumes that all the  $N$  elements carry equal currents similarly distributed: if the currents are not equal, then equation (2.9) must be modified in accordance with § 2.3. If the distribution of equal 'metre-amperes' differs slightly from element to element, this can do no more than 'blur' slightly the value of  $F_1$ , within limits which Table 2.1 shows are very small. Thus (2.9) must be valid for any real in-line array, with great accuracy, provided it is interpreted with full understanding of the factors postulated in the last few sections. It now appears that Figs. 2.2–2.5 have much wider application than was apparent at first and are standard forms which will solve any problem provided only the bearing scale is adjusted to suit the particular value of  $N$ . Thus if Fig. 2.2 is to be applied to a 16-member in-line array it is necessary only to multiply its ordinates by the values of  $F_1$  given in Table 2.1. Note that the in-line disposition has a marked effect in reducing the 'far out' side lobes: thus the 5 per cent. lobe at  $55^\circ$  will be reduced to

about 2.5 per cent. by the in-line disposition. Near-in lobes are scarcely affected, because then  $\cos \phi$  is near unity. Hence Fig. 2.4 will scarcely be changed, taking the practical outlook that the side lobes are negligible anyhow with a triangular distribution. If the reader will ponder these matters he will realize how little the distribution along a member can matter, more especially when there is some concentration of loading towards the middle of the in-line array.

We will not discuss here how the current is fed to the various members: a common method is to place all in series through 'Franklin phasing coils'. Many engineers believe that then the current tends to attenuate along the length, and this is very probable. If this is so it provides an automatic way of concentrating current in the middle of the line and the only appreciable effect on the pattern is reduction of near-in side lobes: we say 'near in' because the 'far out' lobes are made small anyhow by the  $F_1$  or  $\cos \phi$  effect. The pattern will scarcely be changed if individual elements, pitched  $\frac{1}{2}\lambda$  apart, are themselves shorter than  $\frac{1}{2}\lambda$ . If there are gaps between the tips (a necessary provision when each element is fed by a separate cable), then, in the limit,  $F_1$  can but be increased to  $\cos \phi$ .

All that was said in § 2.7. about turning the beam is applicable without modification to an in-line array.

## 2.9. Pattern at any angle of elevation for curtain array

In § 2.2 attention was tacitly restricted to the equatorial plane by taking the typical path difference as  $g \sin \theta$ . Consideration will show that the path difference at angle of elevation  $\phi$  becomes  $g \sin \theta \cos \phi$ . Hence the more general expression for the breadth coefficient becomes

$$F_3 = \frac{\sin\{(N\pi g/\lambda)\sin \theta \cos \phi\}}{\sin\{(\pi g/\lambda)\sin \theta \cos \phi\}}, \quad (2.10)$$

this is zero when  $\sin \theta \cos \phi = 2/N, 4/N$ , etc., if  $g/\lambda = \frac{1}{2}$ .

The beams and lobes are narrowest in the equatorial plane. In other words, a ship proceeding on a given bearing towards the curtain can remain in zero field; but an aeroplane flying vertically above that ship would not be in zero field. Or take a numerical example in which  $N = 16$ , the bearings of zero field in the equatorial plane are shown in Fig. 2.2: the fourth zero is given by  $\sin \theta = 8/(16 \cos \phi)$  and accordingly the fourth and higher zeros cannot occur at elevations above  $60^\circ$ .

A curtain array is usually several half wavelengths high and then the pattern is given by the relation

$$F = F_1 \times F_2 \times F_3, \quad (2.11)$$



where these factors are defined by (2.8), (2.9), and (2.10). It should be obvious the radiation figure then consists dominantly of a beam normal to the array: it is approximately a solid of revolution, which is always waisted slightly in the equatorial plane.

The shape of the main beam, when plotted as a diffraction pattern, is always very nearly sinusoidal: it is convenient to defer close consideration of this shape until the next chapter.

## 2.10. The power gain of aerials

So far we have considered only the directive properties of arrays without explicit reference to the saving of power which must accrue thereby. The saving of power is defined relative to a half-wave aerial which necessarily radiates equally on all bearings. Let an array produce a certain field  $E$  on an assigned bearing at a given large distance: let it then be replaced by a single half-wave aerial, and let the power input to this be adjusted till it produces the same field  $E$  at that distant point. When this adjustment has been attained, let the power input to the half-wave aerial be  $G$  times that required by the array. Then the 'power gain' of the array is said to be equal to  $G$ . We note that this definition leaves  $G$  a function of bearing (and elevation): unless otherwise stated it will be assumed the bearing chosen was normal to the plane of the curtain or to the axis of the in-line array and this will be called the 'forward gain'. The standard of reference has been chosen arbitrarily as a half-wave aerial: it would have been more logical, though less convenient, to have chosen a doublet. The factor  $F_1$  and Table 2.1 show the half-wave aerial possesses slightly more directive properties than a doublet in the sense that it gives a slightly smaller field at high angles of elevation (thus 0.42 as compared with 0.5 at  $\phi = 60^\circ$ ). Therefore it has a power gain with respect to a doublet; but according to ordinary convention the doublet would be said to have a power loss with respect to a half-wave aerial. In equation (1.79) we found the inphase component of field along a doublet was

$$-\frac{cE_P}{a^2} = \frac{2}{3}Il$$

and thus the output was

$$P = \int_0^l E_P i \, dx = \frac{2}{3} \frac{4a^2 X_0^2}{c},$$

where  $X_0$  is the area under the current distribution curve from the middle of the doublet to its tip. In equation (1.80) we found the

inphase component of field along a finite aerial decreased slightly from the middle to the tips. The output was given by (1.80a): when the length was  $\frac{1}{2}\lambda$  and the current distribution was sinusoidal this reduced to

$$P = 0.6095 \times \frac{4a^2 X_0^2}{c}.$$

Accordingly the 'power loss' of a doublet with respect to a half-wave aerial is  $0.6095 \times \frac{3}{2} = 0.9142$ , and this is about 0.4 of a dB.

The power gain can best be calculated by means of the inphase field: a few examples should make the process clear.

### 2.11. Power gain of two parallel half-wave aerials separated by $\frac{1}{2}\lambda$ carrying equal and cophased current

The inphase component of field along each of the two aerials will now consist of one portion due to the current in itself and another portion due to the current in the neighbouring aerial. If the neighbour were a doublet its field would be given by (1.69) which is repeated here and referred to the current

$$-\frac{cE_l}{2a^2 X_0} = \frac{\cos \phi}{a^3 r^3} \{(\sin ar - ar \cos ar - a^2 r^2 \sin ar) + \\ + j(\cos ar + ar \sin ar - a^2 r^2 \cos ar)\}. \quad (2.12)$$

Here we are concerned only with the inphase component, in the equatorial plane, at  $r/\lambda = \frac{1}{2}$ , which is  $ar = \pi$ : hence, then,

$$\frac{cE_P}{2a^2 X_0} = -\frac{1}{\pi^2}.$$

It is a toilsome argument to show that  $E_P$  is almost constant in the range of height  $\pm \frac{1}{4}\lambda$  and would be still more nearly constant if the doublet were replaced by a half-wave aerial. For details the reader is referred to Chapter VIII, where the assumption is justified fully. Accordingly the electric field along each aerial is

$$\frac{cE_P}{2a^2 X_0} = -0.6095 + \frac{1}{\pi^2} = -0.5081,$$

hence 
$$P = 0.5081 \times \frac{4a^2 X_0^2}{c}.$$

If the reader is suspicious of the approximation in taking the 'mutual force' constant along the length  $\frac{1}{2}\lambda$  he will be reassured by remembering the work is dominated by the contribution from the large current near the middle: even if the force decreases slightly near the tips, this will

have a second-order effect on the work (which is the product of current and field) because the current itself must decrease smoothly to zero at the tips. The 'forward field' of the two aerials is the same as the field of a single aerial carrying the sum of their two equal currents. Accordingly the output of the single half-wave aerial which would produce a field in the 'forward direction' equal to that of the pair is

$$P = 0.6095 \times \frac{4a^2 X_0^2}{c} \times 4.$$

The output of the two aerials together is

$$P = 0.5081 \times \frac{4a^2 X_0^2}{c} \times 2$$

and hence the power gain is

$$G = \frac{0.6095 \times 4}{0.5081 \times 2} = 2.40. \quad (2.13)$$

Concurrently the radiation resistance of each aerial is reduced by the presence of the other in the ratio  $0.508/0.609 = 0.84$ , and thus is about 62 ohms.

### 2.12. Power gain of two parallel half-wave aerials with equal currents in phase quadrature

Here it is the quadrature field of one aerial which will be in phase with the current in the other aerial; but consideration will show that if the mutual field is in phase with the current in the one aerial then it will be in antiphase with the current in the other aerial. The mutual interaction causes one aerial to radiate more power than the other, but the total output from the two together is precisely the same as it would be if the pair were separated by an infinite distance. A case of great interest is that considered in § 2.1, where the separation is  $\frac{1}{2}\lambda$ : then the far distant field in the plane of the pair in one direction is twice that due to one alone, while in the opposite sense it is zero. Hence, for equal field strength, the output of a single half-wave aerial would need to be four times the average of the pair, while the total output of the pair is twice that of each member in isolation. The forward power gain therefore is two, and will remain two no matter what the separation, so long as it is not less than  $\frac{1}{2}\lambda$ .

At distance  $\frac{1}{2}\lambda$  the quadrature field of a doublet is  $E_Q = 0.4 \times 2a^2 X_0/c$ : hence the inphase field along one aerial is proportional to

$$0.609 + 0.4 = 1.009$$

and along the other it is  $0.609 - 0.4 = 0.209$ . Accordingly the output and radiation resistance of one is about five times that of the other, the resistances being in the neighbourhood of 120 and 24 ohms. It is of great practical importance to be conscious of this large inequality of resistance, for it will affect profoundly the conditions required for feeding the pair. Unless due precautions are taken the two currents will not be equal even if they are in phase quadrature, and then it is impossible to obtain zero field in one direction in the plane of the pair (see (2.1)).

### 2.13. Power gain of three parallel and cophased half-wave aeriols

Here the mutual action of the outer pair on the middle member is not the same as the mutual action on an outer member from the other two. Reference to (2.12) will show that when  $ar = 2\pi$  then

$$-\frac{cE_P}{2a^2X_0} = +\frac{1}{4\pi^2}.$$

Hence for the middle member we have

$$-\frac{cE_P}{2a^2X_0} = 0.6095 - \frac{2}{\pi^2} = 0.407,$$

and for each outer member

$$-\frac{cE_P}{2a^2X_0} = 0.6095 - \frac{1}{\pi^2} + \frac{1}{4\pi^2} = 0.533;$$

accordingly the total output is proportional to  $0.407 + 2 \times 0.533 = 1.473$ . The forward field is three times that of a single aerial and so the output of the single aerial for equal field is proportional to  $9 \times 0.6095 = 5.485$ , and thus

$$G = \frac{5.485}{1.473} = 3.72. \quad (2.14)$$

Note that the resistance of each outer member exceeds that of the middle member in the ratio  $0.533/0.407 = 1.3$ , the resistances being approximately 49 and 64 ohms. Here we meet, for the first time, a factor which is of great practical importance: namely, that current will not naturally tend to distribute itself equally between the members of a curtain unless steps are taken to force it to do so. There is a tendency for current to concentrate in the middle, and we have seen this tends to reduce the side lobes.

The mutual reaction of the quadrature component of field will affect the tuning conditions: a different tuning condition is required by each

member. It is clear that impedance measurements must be made with the whole array excited.

### 2.14. Power gain of four parallel cophased half-wave aerials

Let the four aerials, carrying equal cophased currents, be represented by Fig. 2.10. Then the output from aerials 2 or 3 is proportional to

$$0.6095 - \frac{2}{\pi^2} + \frac{1}{4\pi^2} = 0.4315,$$

while the output from 1 or 4 is proportional to

$$0.6095 - \frac{1}{\pi^2} + \frac{1}{4\pi^2} - \frac{1}{9\pi^2} = 0.522.$$

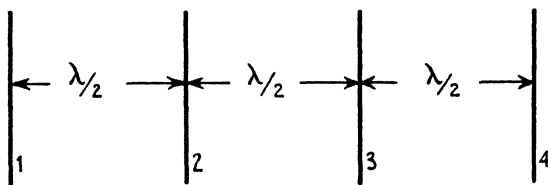


FIG. 2.10.

The forward field is four times that of a single aerial, and hence it follows that

$$G = \frac{16 \times 0.6095}{2(0.4315 + 0.522)} = 5.1. \quad (2.15)$$

The radiation resistances are approximately 52 ohms for the inner and 64 ohms for the outer pair, showing once more that current will tend to concentrate in the inner pair.

### 2.15. Power gain of eight parallel cophased half-wave aerials

Following the same process it can be shown that

$$\begin{aligned} \frac{cP}{4a^2 X_0^2} &= 2 \left\{ 4 \times 0.6095 - \frac{1}{\pi^2} \left( 7 - \frac{6}{2^2} + \frac{5}{3^2} - \frac{4}{4^2} + \frac{3}{5^2} - \frac{2}{6^2} + \frac{1}{7^2} \right) \right\} \\ &= 3.706. \end{aligned}$$

Hence

$$G = \frac{64 \times 0.6095}{3.706} = 10.5. \quad (2.16)$$

The radiation resistance of each end member is near 63 ohms, and that of each of the middle pair near 54 ohms.

### 2.16. Limiting output for very wide curtain of half-wave aerials

When the number of members is infinite the output of any one will tend to the value given by

$$\frac{cP}{4a^2X_0^2} = \left\{ 0.6095 - \frac{2}{\pi^2} \left( 1 - \frac{1}{2^2} + \frac{1}{3^2} - \frac{1}{4^2} + \dots \right) \right\} \\ = (0.6095 - \frac{1}{8}) = 0.4428,$$

since  $1 + \frac{1}{2^2} + \frac{1}{3^2} + \frac{1}{4^2} \dots = \frac{\pi^2}{6}$  and  $1 + \frac{1}{3^2} + \frac{1}{5^2} + \frac{1}{7^2} \dots = \frac{\pi^2}{8}$ .

Accordingly, when  $N$  becomes very large the gain approximates to the expression

$$G = \frac{0.6095N^2}{0.4428N} = 1.38N. \quad (2.17)$$

The output of the extreme member of a semi-infinite curtain is proportional to  $(0.6095 - \frac{1}{8}) = 0.526$ , and accordingly the extreme range of radiation resistance is in the ratio 1.19 and the resistance will be near 53 ohms rising to 63 at the outside members. Pistolcorks calculated such resistances in a classic paper before the Institute of Radio Engineers† and found the limiting value to be near 56 ohms.

### 2.17. Empirical formula for power gain of curtain of $N$ half-wave aerials

In the following table are collected the power gains of curtains composed of various numbers of half-wave aerials.

TABLE 2.2

$N$	1	2	3	4	6	8	very large
$G$	1	2.4	3.7	5.1	7.84	10.5	$1.38N$

The values given in it are related approximately by the empirical relation

$$G = 1.38(N - 0.32), \quad (2.18)$$

which is correct to closer than 4 per cent. from  $N = 2$  upwards.

### 2.18. Power gain when loading is not uniform

The process of calculating the gain when the loading is not uniform should follow obviously from the previous examples of uniform loading. Reference to Figs. 2.2–2.9 will show that each carries a legend stating the power gain: these have been evaluated by the method just described.

† See *Proc. I.R.E.* 17 (1929), 570.

Thus in Fig. 2.2 the gain is 21.8, which accords with (2.18). When the current loading is triangular (Fig. 2.4) the gain is 13.3, and when the loading is 1.2.2.1 (Fig. 2.3) the gain is 17.3; the diminution of gain is due mainly to the increase in width of the main beam, a statement which will be understood better when we have developed and illustrated Poynting's theorem. A caution is needed about calculating the power gain when the beam is turned off centre (see Figs. 2.7 and 2.8) by giving the currents in the outside members a leading and lagging quadrature phase; it is that such members have no net interaction with the central members. The process of evaluating the gain of a 16-member curtain whose two outer quarters are in phase quadrature is as follows. First calculate the output from an 8-member curtain (the central half): this can be derived from (2.18). Then calculate the output from a 4-member curtain in the presence of another 4-member curtain at the other end of the array and carrying antiphased currents: the interaction between these widely separated groups of 4 turns out to be insignificant. We have now found the total output. The forward field must be found from drawing the pattern, and when this has been done  $G$  can be calculated.

In Fig. 2.8 the stated gain is 18.2: this is the gain reckoned with respect to the field on bearing  $+4^\circ$  and not on the much smaller forward field at bearing zero. We will make this more clear as follows:

$$\text{Output} = \frac{0.6095N^2}{G},$$

hence with  $N = 8$  the output is proportional to 3.7, since  $G = 10.5$  (see Table 2.2). When  $N = 4$  the output is found to be 1.9: ignoring the mutual action of the two end groups of four, the total output is proportional to  $3.7 + 2 \times 1.9 = 7.5$ , as compared with 7.16 for a 16-member curtain. Reference to Fig. 2.7 shows the maximum field is 0.94 of what it would be if all the 16 members were cophased, and accordingly

$$G = \frac{0.6095 \times 16^2 \times (0.94)^2}{7.5} = 18.2.$$

Reckoned on the field at bearing zero  $G = 5.2$ .

### 2.19. Power gain of in-line arrays

Here the mutual field is the field along the axis of a half-wave aerial and beyond its tips. The values of this field at various distances from the middle of the aerial are given in Fig. 8.1 and differ very little from the field that would obtain if the half-wave aerial were replaced by a

doublet having the same number of metre-amperes. Consider first two half-wave aerials in line and contiguous. The inphase field along a doublet is  $E_P = \frac{2}{3} \times 2a^2 X_0/c$ , at the midpoint of a half-wave aerial it is  $E_P = 2/\pi \times 2a^2 X_0/c$ : we shall express the force in terms of  $\frac{2}{3} \times a^2 X_0/c$  as a unit. Then by means of Fig. 8.1 we find the field at various distances from the junction of two equal and cophased half-wave aerials has the values shown collected in Table 2.3 below.

TABLE 2.3

$y/\lambda$	0	$\frac{1}{4}$	$\frac{1}{2}$	$\frac{3}{4}$	$\frac{1}{2}$
Field	1.506	1.42	1.29	1.04	0.81

If these values are plotted the resulting curve will be found to differ insensibly from a sinusoid of amplitude  $(1.506 - 0.81) = 0.696$  superposed on a uniform field of magnitude 0.81. Hence, to find the power we have to evaluate

$$\int_0^{\frac{1}{2}\lambda} 0.81 \left( 1 + 0.86 \cos \frac{\pi y}{\lambda} \right) \sin \frac{2\pi y}{\lambda} dy = 1.27 \times \frac{\lambda}{\pi}.$$

The corresponding expression for a single half-wave aerial is  $0.91\lambda/\pi$ : hence the power radiated by each aerial is increased, by the presence of the other, in the ratio  $1.27/0.91 = 1.4$ . Accordingly

$$G = \frac{2^2}{2 \times 1.4} = 1.43. \quad (2.19)$$

Corresponding treatment for three and for four aerials in line gives  $G = 2.06$  and  $2.5$  respectively.

When  $N = 2$  the radiation resistance of each aerial is 102 ohms; when  $N = 3$  the resistance of the middle aerial is 130 ohms and of each outer is 97 ohms, the mean being 108. It should be noted that the resistance of the outer members is less than the middle member and therefore the current will tend to concentrate towards the ends of the array and thereby increase the side lobes. General consideration will show that mutual action between elements separated by distances of the order of a wavelength must be small, because the term  $1/r$  in the field is zero along the axis, see (1.70). We can readily solve the limiting case of this problem by using one of the tools prepared in § 1.7, namely, the current filament of infinite length (Fig. 1.4). Consider first an in-line array of infinite length, the equal and cophased current distribution being that shown in Fig. 2.11 (a) and consisting of half-sinusoids



of height  $I$ . This distribution can be represented by the Fourier series

$$\frac{i}{I} = \frac{4}{\pi} \left( \frac{1}{2} - \frac{\cos(4\pi y/\lambda)}{1.3} - \frac{\cos(8\pi y/\lambda)}{3.5} - \dots \right)$$

and thus consists of ripples superposed on a constant current of magnitude  $2/\pi$ .

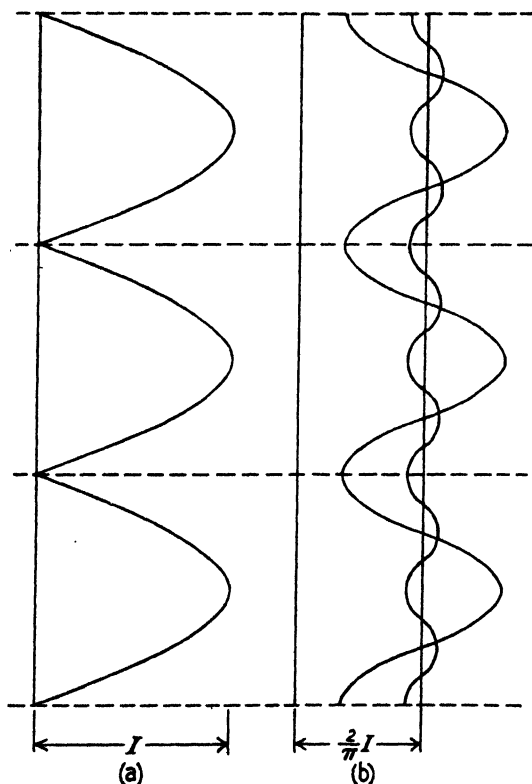


FIG. 2.11.

The forward field due to the ripples on any one half wavelength member is zero because the ripples are a succession of antiphased pairs: even when the length of the array is finite their field at any elevation is very small and must tend to zero when  $N$  tends to infinity. Accordingly the output they contribute tends to zero and the total output will tend to be the same as if the ripples were absent and the current uniform in magnitude and phase throughout the length. Hence, by (1.23) the inphase component of field along the wire would be

$$-E_P = \frac{a\pi}{c} \times \frac{2}{\pi} I = \frac{2aI}{c}.$$

The average value for a single half-wave aerial is

$$-E_P = 0.6095 \times \frac{2a^2 X_0}{c} = 0.6095 \times \frac{2a}{c} \times \frac{2\pi}{\lambda} \times \frac{2}{\pi} \times \frac{\lambda}{4} I = 0.6095 \times \frac{2aI}{c}.$$

From the arithmetic leading to (2.19) we see that the average value of  $E_P$  for two half-wave aerials in line is

$$0.6095 \times \frac{1.27}{0.91} \times \frac{2aI}{c} = 0.85 \times \frac{2aI}{c};$$

when  $N = 3$  it may be found that the average value of  $E_P$  is  $0.9 \times 2aI/c$ . Thus even when  $N$  is only 3, the average value of  $E_P$  has attained 0.9 of its ultimate value, and this shows the rate of approach to the limit is very rapid. We saw in Chapter I that the radiation resistance per half wavelength for a uniform current was  $30\pi^2$  ohms. Hence the radiation resistance per half wavelength of an in-line array, reckoned in terms of the current at its middle point, must tend to the value  $30\pi^2 \times (2/\pi)^2 = 120$  ohms (the average value was 108 ohms when  $N = 3$ ). So for the limiting value we have

$$G = \frac{73.1}{120} N = 0.609N.$$

Some particular values are shown collected in Table 2.4 below.

TABLE 2.4

$N$	1	2	3	4	8	16	very large
$G$	1	1.43	2.06	2.6	5.2	9.8	0.609N

The values stated above are related approximately by the empirical formula

$$G = 0.609(N + 0.4), \quad (2.20)$$

which is correct to about 1 per cent. from  $N = 2$  upwards.

Comparison of (2.20) with (2.18) shows that the gain of a given number of members in curtain is more than twice the gain when the same number is in-line. The radiation figure for the in-line array is a solid of revolution, reminiscent of a flywheel with small cones representing the side lobes. The figure for the curtain may be compared to pears placed stem to stem, and this is obviously more conservative of power.

It is perhaps worth reminding the reader, once more, that the empirical formulae (2.18) and (2.20) are almost independent of the current distribution along each element: provided the currents are cophased and the loading is uniform, both formulae must be correct

to a high degree of accuracy and therefore they are of great practical value and importance. The effect on the power gain of intentional or accidental departures from uniformity of loading can readily be assessed from the values quoted in Figs. 2.3, 2.4, etc., or  $G$  can be evaluated for any assigned loading. The effect of phase difference between members is discussed in §§ 14.2 and 14.3, and is not large. In short, the power gain of an isolated array is a parameter which can be estimated in practice with great confidence and certainty.

## 2.20. Power gain of a high curtain

The curtains considered in §§ 2.12–17 were only one element high. The large curtains to be seen about the country-side are usually 3 elements high above the ground, and so are effectively 6 elements in height. Thus each string of elements is high enough to give each one a radiation resistance near 120 ohms if it were isolated and not a member in a curtain. Neighbouring members of the curtain will reduce the resistance.

The limiting case was solved in § 1.19, where we considered an infinite grid of wires of infinite height. There we found that up to  $g/\lambda = \frac{1}{2}$ ,

$$-cE_P = \frac{2\pi I'}{g} = \frac{4\pi I'}{\lambda},$$

if  $g = \frac{1}{2}\lambda$ . In our case we must make  $I' = (2/\pi)I$  and then

$$-E_P = \frac{2I}{c} = \frac{aI}{c\pi}$$

and it follows, from the foregoing, that the radiation resistance per member must tend to the value  $2/\pi \times 120 = 76.5$  ohms. If the curtain is  $N_1$  elements high (including the image in the ground) and has  $N_2$  strings in the width, then

$$G = \frac{73.1}{76.5} N_1 N_2 = 0.96 N_1 N_2, \quad (2.21)$$

or  $G \doteq 3.8 \times (\text{area of curtain (and image) in } \lambda^2). \quad (2.21a)$

Formula (2.21) may over-estimate  $G$  for very wide curtains which are only about 3 elements high above the ground; for though they are high enough to make the 'self-resistance' 120 ohms per member, they are not high enough (compared with the width) to make the average mutual resistance  $(1 - 2/\pi)$  of 120 ohms. The average resistance will be less than 120 ohms and more than 76.5 ohms, and thus limits are set to the uncertainty in applying (2.21) in practice. One may suggest the gain will not be less than six times the area of the curtain (ignoring

the image), reckoned in square wavelengths. We may note in passing that (2.18) may be written  $G = 5.5 \times (\text{area of curtain in } \lambda^2)$ .

The problem of the wide high curtain is examined more fully in Chapter XIV: its practical aspect is complicated enormously by the reflecting curtain that is usually provided, and this reflector is insoluble precisely for reasons which are associated with practical adjustments only.

### 2.21. Curtain of single half-wave aeriels in which alternate elements are in antiphase: prototype of Yagi arrays

If adjacent members are in antiphase, then the field is zero in the plane normal to the curtain if  $N$  is even, and is that of one member if  $N$  is odd. If the spacing is  $\frac{1}{2}\lambda$ , then brief consideration shows the field is  $N$  times that of one member in the direction of the plane of the array. To calculate the pattern we must divide the array into two groups separated by  $\lambda$ : successive members of either group will be cophased. Each group can be replaced by a single equivalent member at its middle point. If  $N$  is odd the two equivalent members will be coincident: if  $N$  is even they will be separated by  $\frac{1}{2}\lambda$ . We will illustrate by a numerical example and take  $N = 9$ . We then have one group of 4 cophased members separated by  $\lambda$  and another group of 5 cophased members also separated by  $\lambda$ , the two groups being in antiphase with one another. If  $E_0$  be the field due to one member on bearing  $\theta$  to the *normal* to the array, we have

$$\frac{E}{E_0} = \frac{\sin(4\pi \sin \theta)}{\sin(\pi \sin \theta)}$$

for the group of four, and

$$\frac{E}{E_0} = \frac{\sin(5\pi \sin \theta)}{\sin(\pi \sin \theta)}$$

for the group of five, and hence

$$\begin{aligned} \frac{E}{E_0} &= \frac{\sin(5\pi \sin \theta) - \sin(4\pi \sin \theta)}{\sin(\pi \sin \theta)} \\ &= \frac{2 \cos(\frac{3}{2}\pi \sin \theta) \sin(\frac{1}{2}\pi \sin \theta)}{\sin(\pi \sin \theta)} \\ &= \frac{\cos(\frac{3}{2}\pi \sin \theta)}{\cos(\frac{1}{2}\pi \sin \theta)}, \end{aligned} \tag{2.22}$$

an expression reminiscent of the form of (2.2). Had  $N$  been equal to 8

the two equivalent equal and antiphased aerials would have been separated by  $\frac{1}{2}\lambda$  and we should have had (compare § 1.13)

$$\begin{aligned}\frac{E}{E_0} &= 2 \frac{\sin(4\pi \sin \theta)}{\sin(\pi \sin \theta)} \sin(\tfrac{1}{2}\pi \sin \theta) \\ &= \frac{\sin(4\pi \sin \theta)}{\cos(\tfrac{1}{2}\pi \sin \theta)}.\end{aligned}\quad (2.23)$$

$E$  is zero in (2.22) when  $\theta = 6.3^\circ, 19.5^\circ, 33.7^\circ, 51^\circ$ , while in (2.23) it is zero when  $\theta = 0^\circ, 14.5^\circ, 30^\circ, 48.5^\circ$ . Obviously the equatorial pattern resembles that of a cophased curtain turned through  $90^\circ$ . In both cases the main beam is zero when  $\theta$  is near  $50^\circ$  from the *normal* and hence corresponds with a main beam coming to zero at about  $\pm 40^\circ$  from the plane of the array. At an angle of elevation  $\phi$  we must replace  $\sin \theta$  by  $\sin \theta \cos \phi$  in both (2.22) and (2.23). Accordingly when  $\theta = 90^\circ$ , (2.22) is zero when  $\cos \phi = \frac{7}{9}$  or  $\phi = 38.7^\circ$  and (2.23) is zero when  $\phi = 41.5^\circ$ : the radiation figures may be likened to two pears placed stem to stem and in addition some conical hoods for the side lobes.

Following § 2.16, we find the output of any one member of a very wide curtain in which the currents are alternate in sense is given by the expression

$$\frac{cP}{4a^2X_0} = \left\{ 0.6095 + \frac{2}{\pi^2} \left( 1 - \frac{1}{2^2} + \frac{1}{3^2} \dots \right) \right\} = 0.7761.$$

Accordingly, when  $N$  is large the gain approximates to the value

$$G = \frac{0.6095N^2}{0.7761N} = 0.78N \quad (2.24)$$

and the radiation resistance per member tends to

$$\frac{0.776}{0.609} \times 73.1 = 93\Omega.$$

The system we have just described can be realized in practice by feeding each member in such a way that the phase alternates. More commonly, however, only one member is fed with power and current is induced in the other members by the field of the driven member. In such circumstances the magnitude of the current is likely to attenuate along the array, and it is found that no advantage accrues from increasing  $N$  indefinitely. In general there is little advantage in making  $N$  greater than about 10. The system in which successive currents are induced by one member is commonly called a 'Yagi array' and will be discussed briefly later on.

## 2.22. Poynting's theorem

Following Maxwell we assume the energy is located in the medium, and that the total energy is given by

$$W = \frac{1}{8\pi} \iiint \{K(E_1^2 + E_2^2 + E_3^2) + \mu(H_1^2 + H_2^2 + H_3^2)\} dx dy dz.$$

According to our interpretation the region in which a field exists is expanding continuously with time, and hence the total stored energy must be increasing continuously, and it is this which demands an output of work from the source, represented by the parameter we call radiation resistance. If we take any fixed and closed region of space it must be possible to interpret the equations in such a way as to make them describe a constant outflow of energy from the whole closed surface. There can be no grounds for asserting that a certain amount of energy does in fact flow across some assigned piece of the total area, but only that it is as though there were a total flow of a certain amount of energy across the whole surface. We shall not develop the appropriate analysis here, but refer the reader to some treatise on electromagnetism (see, for example, Jeans's Chap. 17, § 576, p. 518). It is proved that the flow is to be reckoned at the rate  $(cEH/4\pi)\sin\theta$  per unit area of the closed surface, where  $\theta$  is the angle between  $E$  and  $H$ : the direction of the supposed flow is perpendicular to both  $E$  and  $H$ .

We will apply this to the radiation from a doublet. As the closed surface, take any very large sphere centred at the doublet. Then we know (see (1.73) and (1.74)) that at any point on this sphere  $E$  lies in lines of longitude and  $H$  in lines of latitude and  $E = H$ , and that  $E$  varies as  $\cos\phi$ . Accordingly the rate of flow across an element of surface is  $cE^2/4\pi$ . If  $E_0$  is the field at radius  $R$  in the equatorial plane we have

$$\begin{aligned} P &= \frac{c}{4\pi} \int_{-\frac{1}{2}\pi}^{\frac{1}{2}\pi} E_0^2 \cos^2\phi \times 2\pi R \cdot R \cos\phi \, d\phi \\ &= cE_0^2 R^2 \int_0^{\frac{1}{2}\pi} \cos^3\phi \, d\phi = \frac{2}{3} cE_0^2 R^2 = \frac{2}{3} \times \frac{4a^2 X_0^2}{c}, \quad \text{by (1.73),} \end{aligned}$$

and this agrees with the value deduced from (1.79). There we deduced it from the inphase electric field acting against the current in the doublet: here we deduce it from the field at the surface of an arbitrary sphere drawn in space. We are getting near the Huygens principle, but at the price of having to make a surface integration: it exemplifies the contrast between two possible means of approach, discussed in

Chapter I. Either we must fix our eyes on the points where we are in the habit of choosing to locate an electron or we must integrate over the whole of a closed surface of space: in general the first is much the simpler operation to perform. It is instructive to use (1.73) to express the whole energy present in all space: if this is done, the total energy in the expanding sphere of field will be found to increase uniformly

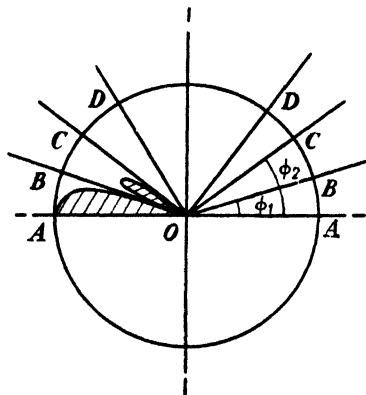


FIG. 2.12.

with time: we leave it as an exercise to the reader (or see *Radio Frequency Measurements*, E. B. Moullin, Chap. I, § 7, p. 23). If the source is a half-wave aerial, then by (2.8)

$$P = cE^2 R^2 \int_0^{\frac{1}{2}\pi} \cos^2(\tfrac{1}{2}\pi \sin \phi) \cos \phi \, d\phi.$$

Possibly this integral can be evaluated in terms of Bessel functions: we know from (1.81) that its value is 0.6095.

The output from an in-line array involves evaluating

$$\int_0^{\frac{1}{2}\pi} \frac{\sin^2(\tfrac{1}{2}N\pi \sin \phi)}{\sin^2(\tfrac{1}{2}\pi \sin \phi)} \cos^2(\tfrac{1}{2}\pi \sin \phi) \cos \phi \, d\phi.$$

Whether or not it is possible to evaluate this directly we prefer to approximate to the answer because this will disclose the structure of the process. Let Fig. 2.12 represent a cross-section of the sphere over whose surface the integration is to be performed. Let the radii  $OB$ ,  $OC$ , etc. be drawn along the extinction angles  $\phi_1$ ,  $\phi_2$ , etc. The angles  $AOB$ ,  $BOC$ , etc., are approximately equal and less than  $15^\circ$  if  $N$  exceeds 8. The obliquity factor  $F_1$  of equation (2.8) remains substan-

tially constant over the small angles  $AOB$ ,  $BOC$ , etc. Hence the error will be small in writing

$$\int_{\phi_1}^{\phi_2} E_1^2 \cos \phi \, d\phi = {}_n F_1^2 \cos \phi_n \int_{\phi_1}^{\phi_2} F_2^2 \, d\phi,$$

where  ${}_n F_1$  and  $\cos \phi_n$  are the values of  $F_1$  and  $\cos \phi$  at the midpoint of the interval. If the main beam and side lobes (when plotted as a diffraction pattern) were sine curves their mean square value would be half the square of their maximum ordinate: if a triangle, one-third of the square of the maximum. Hence the mean square value must be between a half and a third; the mean of these two fractions is  $\frac{5}{12} = 0.416$ . The mean square value of the main beam has been found (by graphical integration) to be 0.466 and 0.472 when  $N = 8$  and 16 respectively: we shall adopt the value 0.47. Also  $AOB \doteq BOC \doteq \frac{2}{N}$ ,

$$\therefore \quad E^2 \int_0^{\frac{1}{2}\pi} \cos \phi \, d\phi \doteq \frac{0.94}{N} ({}_1 F_1^2 \cos \phi_1 + \alpha_2^2 {}_2 F_1^2 \cos \phi_2 + \dots),$$

where  $\alpha_n$  is the fractional amplitude of the  $n$ th side lobe. It is known that (see § 2.2)  $\alpha_2, \alpha_3$ , etc., equal  $2/3\pi, 2/5\pi$ , etc. Moreover,

$$\frac{4}{\pi^2} \left( \frac{1}{3^2} + \frac{1}{5^2} + \frac{1}{7^2} + \dots \right) = \frac{4}{\pi^2} \left( \frac{\pi^2}{8} - 1 \right) = 0.095.$$

Now  ${}_1 F_1^2 \cos \phi_1 + \alpha_2^2 {}_2 F_1^2 \cos \phi_2 + \dots$  must always be less than  $1 + \alpha_2^2 + \alpha_3^2 + \dots$  and hence less than 1.095. It will approach more and more nearly to this value when  $N$  is large because then  ${}_1 F_1^2 \cos \phi_1$  and  ${}_2 F_1^2 \cos \phi_2$  get more and more nearly equal to unity. Accordingly the power gain must tend to the value

$$G = \frac{0.6095N}{0.94 \times 1.095} = 0.6N,$$

and this agrees closely with the value deduced in (2.20), and approximate integration has served its turn. It has, however, disclosed the interesting feature that the power radiated in the side lobes tends to be 9.5 per cent. as an upper limit. It should be noted that the power in the side lobes is relatively less important when  $N$  is small, because then the first and second lobes (which are much the most important) are considerably reduced in size by the obliquity factor  $F_1$  and also because they then 'bathe' a much smaller area of the Poynting sphere. Direct evaluation shows that when  $N = 2, 3, 8$ , and 16 the power in the side lobes is 0.5, 1.0, 4.0, and 6.5 per cent. respectively. Those who are concerned



with making aerials should memorize the result that the power in the side lobes of a uniformly loaded in-line array must be less than 9.5 per cent. If side lobes are objectionable it is not because they radiate a substantial amount of power.

The power radiated by a uniformly loaded curtain can be evaluated by a similar process of approximate integration: it has been done more elegantly in equation (2.18) and will not be done again. Suffice it to say that if the mean square field is taken as 0.47, then the power gain without side lobes is found to be  $1.56N$ . We found in (2.18) that  $G = 1.38N$  and so we deduce that the power in the side lobes is 11 per cent.

The mean square field in the equatorial plane of a uniformly loaded curtain can be found from direct integration, for it is known that

$$\int_0^{\frac{1}{2}\pi} \frac{\sin^2(Ng \sin \theta)}{\sin^2(g \cos \theta)} d\theta = \frac{1}{2}\pi \left\{ N + 2 \sum_{r=1}^{N-1} (N-r) J_0(rg) \right\},$$

this result follows at once, by Poynting's theorem, from the approach to (1.45).†

It has often been thought the power gain can be estimated from the diffraction pattern in the two principal planes. This is true only in the very simplest cases, as a glance at Fig. 4.12 will show. The power gain should be calculated from the inphase component of field along the aerial itself and not by using Poynting's theorem. It may be argued that the diffraction pattern can be measured and the inphase field cannot, and that therefore Poynting's theorem is the only available method of deducing the power gain of an aerial in operation. There is some substance in such an argument, but it needs closer scrutiny. The first process must always be to calculate the power gain and the radiation figure for the idealized array: by idealized is meant that reflecting screens are supposed to extend to infinity and the current distribution between members of an array is postulated (once more we remind the reader that current distribution along a single member is unimportant since it affects the factor  $F_1$  only, and anyhow  $F_1$  is sensibly equal to  $\cos \phi$ ). Then the two principal patterns should be observed for the real array and compared with the ideal patterns. From comparing their mean square values with the ideal it should be possible to estimate how much the power gain falls short of the ideal: provided always there are no significant lobes which do not appear in

† See, for example, McLachlan, *Bessel Functions for Engineers*, § 4, p. 46.

the two principal patterns. In other words, that the radiation figure is not typified by Figs. 4.12–4.14.

We will close this chapter by treating the example of §§ 2.1 and 2.12 by the Poynting method. Here we have two aerials in phase quadrature and separated by  $\frac{1}{4}\lambda$ . Let the field of either aerial alone be  $E_1$  at an angle of elevation  $\phi$ , and let the phase angle due to path difference on a bearing  $\theta$  be  $\beta$ : then the phase difference between the two component fields is  $\beta + \frac{1}{2}\pi$  and the resultant is

$$\begin{aligned} E &= 4E_1^2 \cos^2\left(\frac{\beta + \frac{1}{2}\pi}{2}\right) \\ &= 2E_1^2(1 - \sin \beta). \end{aligned}$$

$$\begin{aligned} \therefore \quad \frac{4\pi P}{c} &= 2 \int_0^{\frac{1}{2}\pi} \int_0^\pi E_1^2 \cos \phi \, d\phi d\theta \\ &= 4 \int_0^{\frac{1}{2}\pi} \int_0^{2\pi} E_1^2 \{1 - \sin(\tfrac{1}{2}\pi \cos \phi \cos \theta)\} \cos \phi \, d\phi d\theta \\ &= 4 \int_0^{\frac{1}{2}\pi} \int_0^{2\pi} E_1^2 \{1 - 2J_1(\tfrac{1}{2}\pi \cos \phi) \cos \theta - 2J_3(\tfrac{1}{2}\pi \cos \phi) \cos 3\theta\} \times \\ &\quad \times \cos \phi \, d\phi d\theta \\ &= 4 \int_0^{\frac{1}{2}\pi} E_1^2 \times 2\pi \cos \phi \, d\phi \\ &= 8\pi \int_0^{\frac{1}{2}\pi} E_1^2 \cos \phi \, d\phi, \end{aligned}$$

and thus is precisely twice the output of one aerial alone. A result we have already shown directly by considering the inphase field along each aerial.

### III

## AERIALS IN THE PRESENCE OF INFINITELY EXTENDED FLAT SHEET REFLECTORS

### 3.1. Introduction

THE curtain arrays discussed in Chapter II have been seen to produce a narrow beam of electric field in both directions along the normal to the array: the in-line arrays produce a thin disk of field bathing the equator of a circumscribing sphere. In general it is required to restrict the radiation from a curtain to one direction along the normal and to restrict the radiation from an in-line array to a sector of the circumscribing sphere. This result can be produced by a second parallel curtain with appropriate spacing and magnitude and phase of current, since any curtain can be replaced by a single equivalent aerial at its middle point. The two equivalent aerials representing the two parallel curtains can produce zero field along one normal if the currents are equal and in phase quadrature and the spacing is  $\frac{1}{2}\lambda$  (see § 2.1), and thus the desired result can be attained. It is more usual to approximate to this result by using one driven curtain to induce current in a second parallel curtain: then the best spacing is a matter for experience and adjustment. It is natural to refer to the second and undriven array as a reflecting curtain. An alternative to an open wire curtain is a very large continuous sheet of metal: such is often preferable in practice because it demands no tuning adjustment provided its area is much larger than the driven curtain. This essential condition will be practicable only if the wavelength is less than, say, 5 metres.

We shall now consider the performance of aerials combined with large flat metal sheets; a system which has enormous practical application when the wavelength is less than about 1.5 m. The problem is idealized at present by supposing the sheets unlimited in extent, and we shall not attempt to discuss here how much these solutions will be modified in practice by the finite size of the sheets: this is discussed analytically in Chapter V and an immense amount of practical observation is scattered through later chapters. Suffice it to say now that quite small sheets do in fact approach very close to the limit of the ideal and thus the solutions we derive here are of great practical value if used with intelligence and understanding.

The problem is much simplified by restricting the field to two dimensions only: in other words, the source is to be thought of as a

very long in-line array. Later we shall replace the long array by a single half-wave aerial. Until further notice, the reader must realize the source is a single filament of infinite length carrying a current  $I \sin pt$ .

### 3.2. Current filament parallel to an infinite and perfectly conducting plane

Consider a filament, carrying a current  $I \sin pt$ , parallel to an infinite and perfectly conducting plane. It follows, from considerations of symmetry, that the electric field must be parallel everywhere to the plane; moreover, it must have zero value at the plane because the conductivity is perfect. The component of magnetic field perpendicular to the plane must be zero at its surface; for if the plane were penetrated by a magnetic field there would be an electromotive force round any circuital path in the plane, and this is impossible since the electric force is zero everywhere in the plane. The penetrating  $H$  can be prevented only by a system of induced currents, flowing parallel to the filament, and having a value and distribution such that they produce a normal component of  $H$  equal and opposite to the normal component of  $H$  which would obtain at any point of the surface if the plane were absent and the filament alone were present. The magnetic force must be parallel to the plane at its surface, and if  $H$  is its magnitude at a point where the current density is  $i$ , then  $H = 4\pi i$ : this result follows by curling round a rectangular path one side of which is just outside the surface and one side is inside it; no displacement current is curled round because  $E$  is zero at the surface, and inside it, and hence the total current curled round is only the conduction current  $i$ ; and moreover, as we have seen,  $H$  is zero along three sides of the rectangular path. Now consider Fig. 3.1 (a), in which  $AB$  and  $F$  represent respectively a section across the plane and the filament, both standing perpendicular to the paper. The induced currents are represented by the dots and crosses in circles lying just inside the trace  $AB$ : it is to be noted that they are shown as crosses in some regions and as dots in others, in order to remind the reader that the induced density is never cophased at all points. The filament would contribute at a point typified by  $P$  an electric force  $E$  depending only on the distance  $r$ : since the net electric force must be zero at the surface, it follows that the distribution of induced currents must be such that the resultant force due to all the filamentary streamlets which compose it is exactly equal to  $-E$  (compare  $cE = 2\pi i$  for a uniform density, see p. 55).

Now consider Fig. 3.1 (b), which depicts a current  $+I$  at  $F$  to the right of a plane  $AB$  and a current  $-I$  at  $F'$  to the left of a second and separate plane  $A'B'$ , the two very thin material planes being placed parallel to one another and close together. The distribution in  $A'B'$  will be similar in form but opposite in sign to that in  $AB$ , and accordingly current densities at  $P$  and  $P'$  will be equal and opposite. Now

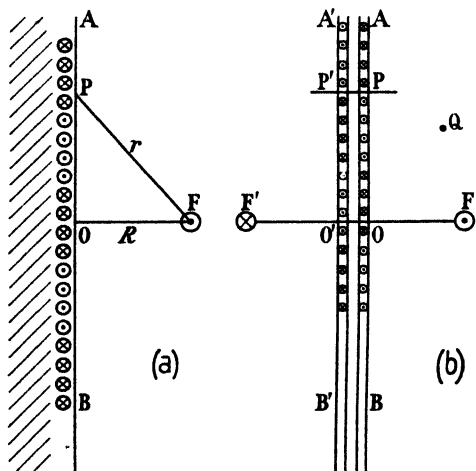


FIG. 3.1.

consider the electric field at a point typified by  $Q$ : it is the resultant of the force due to  $+I$  at  $F$  and to  $-I$  at  $F'$  and to the distribution all over the face  $AB$  and to the distribution all over the face  $A'B'$ . The force due to the two distributors, taken together, will tend to vanish as the two planes are brought ever closer together, because typical streamlets at  $P$  and  $P'$  become more and more nearly coincident, and their contribution to the field will vary as  $2\pi d/\lambda$ , where  $2d$  is the distance between the two faces (see § 1.13). Accordingly, in the limit, the force at  $Q$  will be due to the filaments  $F$  and  $F'$  only, and this is readily calculable. But the field is in no way disturbed by bringing the planes  $AB$  and  $A'B'$  into proximity, since the field between them is zero everywhere. Hence it follows that the field due to the distribution on  $AB$  in Fig. 3.1 (a) is identical with the field due to  $F'$  in Fig. 3.1 (b); and accordingly that the force at any point to the right of  $AB$  in (a) is equal to the force due to current filament  $+I$  at  $F$  together with  $-I$  at its image point  $F'$ , it being supposed that the conducting plane  $AB$  has been removed. Similarly the force at any point to the left of  $AB$  in (a) must be zero because in this region the field due to the induced

density is the same as that of a filament  $-I$  at  $F$ , and hence the total force to the left of  $AB$  is the same as that due to a current  $-I$  at  $F$  together with a current  $+I$  at the same point, making the net current zero.

The magnetic field due to the current and its image is readily calculable in the plane which is midway between them and perpendicular to the plane joining them: consideration will show it is directed along this plane. It is equal in value to the magnetic field due to  $F$  and the distribution on the conducting plane. Since  $H$  is known, the induced density follows from the relation  $H = 4\pi i$  and hence the whole problem is solved. Though the argument has been developed for current filaments, brief consideration will show it is also valid for an electric doublet and hence, by superposition, for any system of doublets in the presence of an infinite and conducting plane.

An image system can be found only for flat sheets: the image systems for spheres and cylinders which are valid in electrostatics are not valid in our problems because we are not now concerned with a scalar potential which varies only as  $1/r$ . Again, the treatment in optics of images due to spherical mirrors is approximate only: if such images are used to obtain solutions of aerial problems it is essential to recognize that such solutions are only approximate.

If the distance between  $F$  and the plane is  $\frac{1}{4}, \frac{3}{4}, \frac{5}{4}$ , etc., of  $\lambda$ , then the distance between  $F$  and  $F'$  is  $\frac{1}{2}, \frac{3}{2}, \frac{5}{2}$ , etc., of  $\lambda$ , and it should be obvious from Fig. 3.1 (b) that the field in the direction  $F'F$  is twice that due to one current alone. If  $OF$  equals  $\frac{1}{2}, 1, \frac{3}{2}$ , etc., of  $\lambda$ , then the field in the direction  $OF$  is zero. It is an essential feature of this and all similar problems that as the aerial  $F$  is moved progressively away from  $O$  the 'forward field' at a distant point will pass successively through maximum and minimum values: in this case zero and  $2E$ . From equation (1.48) the field on bearing  $\theta$  varies as  $2 \sin(k \cos \theta)$ ; it follows from this that there are always one or more bearings on which the field has the value  $2E$  provided  $R$  exceeds  $\frac{1}{4}\lambda$ . As  $R$  is increased from a small value up to  $\frac{1}{4}\lambda$  the polar diagram remains nearly a circle, touching the plane. When  $R$  exceeds  $\frac{1}{4}\lambda$  the circle develops a dimple on bearing zero; when  $R = \frac{1}{2}\lambda$  it has turned into a bifurcated beam whose maxima are at  $\pm 60^\circ$  and which have zero field at  $\theta = 0$  and  $90^\circ$ . When  $R/\lambda = \frac{3}{4}$  the polar diagram consists of three petals of equal length, one centred on  $\theta = 0$  and the other two on  $\theta = \pm 70^\circ$ . When  $R/\lambda = \frac{5}{4}$  there are five petals, and so on. For most practical applications these petals are objectionable and hence we expect to make  $R/\lambda$  near  $\frac{1}{4}$ .

Referred to  $O$  as origin, the field at any distance and for any value of  $R$  is given by (1.47): accordingly the inphase field along the filament  $F$  is given by

$$-\frac{cE_P}{4\pi aI} = J_1^2(k) + J_3^2(k) + J_5^2(k) + \dots \quad (3.1)$$

Also it should be obvious from Figs. 1.8 or 3.1 that

$$-\frac{cE_P}{a\pi I} = 1 - J_0(k), \quad (3.2)$$

and thus by comparing (3.1) and (3.2) we discover an interesting identity. It follows from (3.1) and (1.23) that the radiation resistance per half wavelength of the filament in the presence of the sheet equals  $\{1 - J_0(2k)\} \times 30\pi^2$  ohms, and this equals  $30\pi^2 \times 1.3038$  ohms when  $R/\lambda = \frac{1}{4}$ . If the current distribution is in fact a series of half sinusoids (as in an in-line array), then the resistance, measured from the middle point of any one, will be 157 ohms. Since the forward field is then twice that of the isolated filament the power gain conferred by the reflector is

$$G' = \frac{4 \times 120}{157} = 3.06. \quad (3.3)$$

The general expression is

$$G' = \frac{4 \sin^2 k}{1 - J_0(2k)} = 4(1 - \frac{1}{12}k^2 + \dots). \quad (3.3a)$$

Hence, in respect of gain, it is best to make  $R/\lambda$  less than  $\frac{1}{4}$  and to use the distance as a means of adjusting the radiation resistance to any desired value less than 157 ohms. It follows from (2.20) that the gain of an  $N$ -member in-line array close to a flat sheet is near

$$G = 2.4N. \quad (3.4)$$

(a) *Density of current induced in the sheet*

To find the current density  $i$  we must calculate  $H$ , the magnetic field in the median plane of Fig. 1.8 or 3.1 (b), and then we have  $H = 4\pi i$ .  $H$  can be found most readily from the vector potential  $A$ , since  $\text{curl } A = H$  or  $A = jaE$ : hence from (1.47)

$$-\frac{cA}{4\pi I} = \{Y_1(ar) + jJ_1(ar)\}J_1(k)\cos\theta + \{Y_3(ar) + jJ_3(ar)\}J_3(k)\cos 3\theta + \dots,$$

and

$$H = \frac{1}{r} \frac{\partial A}{\partial \theta},$$

$$\text{thus } \frac{i}{I} = \frac{1}{r} [\{Y_1(ar) + jJ_1(ar)\}J_1(k) - 3\{Y_3(ar) + jJ_3(ar)\}J_3(k) + \dots], \quad (3.5)$$

since here  $\theta = 90^\circ$ .

When  $ar < k$ , interchange  $k$  and  $ar$  in (3.5). When  $ar$  tends to zero

$$J_n(ar) \doteq (\tfrac{1}{2}ar)^n = \frac{1}{n!}$$

and therefore 
$$\frac{i_0}{I} = \tfrac{1}{2}a\{Y_1(k) + jJ_1(k)\}$$

and 
$$\frac{|i_0|}{I} = \tfrac{1}{2}a\sqrt{Y_1^2(k) + J_1^2(k)}$$

$$\doteq \frac{1}{\sqrt{(R\lambda)}}, \quad \text{when } k \text{ exceeds about } 4,$$

or 
$$\doteq \frac{1}{\pi R} \quad \text{when } k \text{ is small.}$$

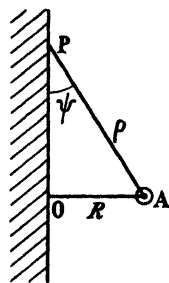


FIG. 3.2.

Equation (3.5) is very cumbersome to evaluate when  $ar$  is large, and in such circumstances it is more convenient to take the origin at the filament. Then with reference to Fig. 3.2, it follows at once from (1.25) that

$$\begin{aligned} \frac{i}{I} &= \tfrac{1}{2}a \sin \psi \{Y_1(a\rho) + jJ_1(a\rho)\} \\ &= \frac{1}{2} \frac{aR}{\rho} \{Y_1(a\rho) + jJ_1(a\rho)\}. \end{aligned} \quad (3.6)$$

When  $a\rho$  is large  $Y_1 = -J_0$  and  $J_1 = Y_0$ , and then

$$i \doteq \tfrac{1}{2}Ia \sin \psi \{-J_0(a\rho) + jY_0(a\rho)\} = \frac{cE \sin \psi}{2\pi}, \quad \text{by (1.23),} \quad (3.6a)$$

where  $E$  is the field which would exist at the point  $P$  if the sheet were absent. It may be seen from (1.60) that if a plane wave of amplitude  $E$  is incident on an infinite sheet it induces a density  $i = cE/2\pi$ . Accordingly the current induced at  $P$  is nearly the same as it would be if the normal component of field incident at this point were incident over the whole plane. This is an important principle of approximation which we shall use in problems where the density cannot be calculated: it is here almost correct in respect of magnitude but never quite correct in respect of phase. The error in magnitude is less than 1 per cent. so long as  $a\rho$  exceeds 4, which is when  $\rho/\lambda > 0.63$ : the phase error is about  $3^\circ$  when  $a\rho = 10$  and about  $1.8^\circ$  when  $a\rho = 16$ . When  $a\rho$  exceeds about 4 we may write

$$\frac{i}{I} \doteq \frac{aR}{2\rho} \sqrt{\left(\frac{2}{\pi a\rho}\right)} \quad \text{or} \quad \frac{i}{i_0} \doteq \left(\frac{R}{\rho}\right)^{\frac{3}{2}}. \quad (3.7)$$

Accordingly  $i/i_0$  decreases rapidly as  $\rho$  increases, and this gives good reason to hope that it will be possible in practice to terminate the sheet



at a finite width without impairing its reflecting properties appreciably: if this is hopeful in the two-dimensional problem it must be still more hopeful if the filament (long in-line array) is replaced by a single half-wave aerial, for then  $i/i_0$  is almost certain to vary as  $(R/\rho)^2$ , as compared with  $(R/\rho)^{\frac{1}{2}}$ .

We have presumed the reflecting sheet is a perfect conductor. If it has a small finite resistivity, of value  $\rho'$  at the operating frequency, the induced current will differ little from the value appropriate to a perfect conductor. Accordingly the energy loss, in unit width of the sheet, is given approximately by

$$\begin{aligned} P &= 2\rho' \int_0^{\infty} |i|^2 dy \doteq 2I^2 \frac{\rho' R^2}{\lambda} \int_0^{\infty} \frac{1}{\rho^3} dy \\ &= \frac{2I^2 \rho'}{\lambda} \int_0^{\frac{1}{2}\pi} \sin \psi d\psi = \frac{2I^2 \rho'}{\lambda}. \end{aligned} \quad (3.8)$$

Accordingly the energy loss in a strip half a wavelength wide equals  $I^2 \rho'$ . This rather surprising result shows the loss in a strip half a wavelength wide is independent of  $\lambda$  (save in so far as  $\rho'$  varies as  $\lambda^{-\frac{1}{2}}$ ) and of  $R$ , provided always that  $R/\lambda$  is not very small. The loss in a strip of infinite width and height  $\frac{1}{2}\lambda$  in the direction of flow is the same as if the aerial current  $I$  flowed through a square piece of reflector of 1 cm. side: this description will help to show the loss is very small. Suppose the aerial wire itself is 1 cm. in circumference and of the same material as the sheet, then the conductor loss in the aerial itself will be  $\frac{1}{2}\lambda$  times as much as the loss in the reflector. This comparison shows clearly that the conductivity of the sheet is not important because the loss in it can scarcely be comparable with the loss in the aerial itself. Resort to tables of  $Y_1$  shows that when  $R/\lambda = \frac{1}{8}$  or  $\frac{1}{4}$  then

$$\frac{\sqrt{(R\lambda)}|i_0|}{I} = 1.18 \quad \text{or} \quad 1.05 \quad \text{respectively,}$$

and accordingly our approximation will not underestimate the loss appreciably.

The effective resistivity of a sheet at frequency  $f$  is  $\rho' = 2\pi\sqrt{(\rho f)}$ , where  $\rho$  is the resistivity of the metal in e.m. units. Accordingly  $\rho' = 2.45 \times 10^{-4} \sqrt{(f \text{ Mc/s})}$  ohms for copper: thus  $\rho' = 6 \times 10^{-3}$  ohms if  $\lambda = 50$  cm. When  $R/\lambda = \frac{1}{4}$  the radiation resistance is 157 ohms, reckoned from the 'loop current', and this is about 400 ohms reckoned on the average current in the array. Accordingly the fractional loss

in a copper reflector is of the order of  $(6 \times 10^{-3})/400$ , which is about 15 parts in a million and is insignificant. It is abundantly clear there is no need to use copper for the reflector: it might just as well be made of painted iron sheet. To use copper or aluminium for electrical reasons discloses a gross lack of understanding and is therefore very bad practice. If the copper aerial wire is 6 mm. diameter and  $\lambda = 50$  cm. its effective resistance (reckoned on average current) will be near 0.1 ohm per member and accordingly the conductor loss in it will be some seventeen times as great as in the whole reflector; though only about one part in 4,000 of the output. If, for reasons of appearance, it is desired to inhibit corrosion by plating the aerial conductor, then significant losses will not result from plating it with a metal whose resistivity is greater than copper. Resistivities, relative to copper, of silver, rhodium, cadmium, and chromium are 0.92, 3.4, 4.2, and 7.8 respectively. When penetration depth is small the effective resistance is proportional to  $\rho^{\frac{1}{2}}$  and accordingly these materials will change the loss, relative to copper, in the ratio 0.96, 1.85, 2.05, and 2.8 respectively. Even chromium plating will not make the loss as much as 0.1 per cent. at  $\lambda = 50$  cm. But it shows a lack of understanding to insist on rhodium-plated aerial rods together with copper reflector sheets. Painted copper rods and painted iron sheet or expanded metal is a construction which shows both an appreciation of the technical aspect of a constructional problem and some regard for its cost.†

Having shown the losses in a flat metal reflecting sheet are negligible, we need scarcely raise this problem again for more complex reflecting systems. If practising engineers insist on trying to reduce a negligible loss, then at least it is to be hoped they will do it by fixing a narrow copper strip, just behind the aerial, to the iron or expanded metal reflector: showing thereby they understand where the dominant fraction of the loss is located. For a full discussion of the effective resistance of plated conductors see the paper by R. Faraday Proctor in the *Wireless Engineer*, 20 (1943), 56.

### 3.3. Pair of reflecting sheets at right angles

The system is illustrated diagrammatically in Fig. 3.3, where  $A$  represents the aerial, standing perpendicular to the plane of the paper.

† *Note:* Teachers of engineering are sometimes accused of paying no attention in their teaching to 'Engineering Economics'. This stricture is not always justified, and indeed it is difficult to conceive how engineering teaching could be arranged to avoid including a perpetual background of economics.

Consideration will show that the four aerials  $A, B, C, D$  must together produce a field in which the electric force is zero along the planes  $OE$

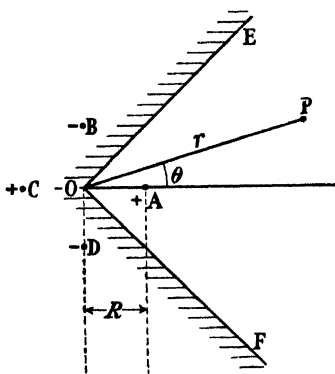


FIG. 3.3.

and  $OF$ . Hence if these planes are replaced by perfect conductors, the aerial  $A$  and the currents induced in said planes will together produce a field in all the region  $EOAF$  which is identical with the field, in this region, due to the aerial  $A$  and the three images. The field at point  $P$  (coordinates  $r, \theta$  with respect to origin  $O$  and initial line  $OA$ ) due to the like pair of aerials  $A$  and  $C$  is given by equation (1.46). The field at  $P$  due to the four aerials  $A, B, C$ , and  $D$  is given by subtracting from (1.46) a similar expression in which  $(\frac{1}{2}\pi - \theta)$  is substituted for  $\theta$ . Accordingly

$$\frac{cE}{8\pi I} = \{-J_2(ar) + jY_2(ar)\}J_2(k)\cos 2\theta + \{-J_6(ar) + jY_6(ar)\}J_6(k)\cos 6\theta + \\ + \{-J_{10}(ar) + jY_{10}(ar)\}J_{10}(k)\cos 10\theta + \dots \quad (3.9)$$

If  $R > r$ , then transpose  $k$  and  $ar$  in (3.9).

When  $ar$  tends to infinity (3.9) degenerates into

$$\frac{E}{8E_0} = J_2(k)\cos 2\theta + J_6(k)\cos 6\theta + \dots, \quad (3.9a)$$

where  $E_0$  is the field at this distance due to an isolated current  $I$ . Consideration of the path difference at a great distance shows also that

$$\frac{E}{2E_0} = \cos(k\cos\theta) - \cos(k\sin\theta). \quad (3.10)$$

And this is an alternative expression for the diffraction pattern. The forward field equals  $2E_0(\cos k - 1) = -4E_0\sin^2 \frac{1}{2}k$ , and this is zero when  $R/\lambda = 1, 2, 3$ , etc., and rises to a maximum value  $4E_0$  when  $R/\lambda = \frac{1}{2}, \frac{3}{2}$ , etc. Thus, as with the single flat sheet,  $R/\lambda$  has an infinite series of values for which the 'forward field' is zero: then the pattern consists of an even number of petals, not all of which necessarily have a maximum  $4E_0$ . We shall delay further discussion of the shape of this pattern till § 3.8. The inphase component of field at the aerial is by (3.9)

$$-\frac{cE_P}{8\pi I} = J_2^2(k) + J_6^2(k) + J_{10}^2(k) + \dots \quad (3.11)$$

It should also be obvious from Fig. 3.3 that

$$-\frac{cE_P}{a\pi I} = 1 - 2J_0(\sqrt{2}k) + J_0(2k), \quad (3.11a)$$

and thus is summed the series in (3.11). Evaluation of numerical values of radiation resistance will be delayed until § 3.6. By Poynting's theorem the output can be derived from the mean square value of (3.9 *a*), and this leads at once to (3.11) since, for example,

$$2 \int_0^{\frac{1}{2}\pi} \cos^2 \theta \, d\theta = \frac{1}{2}\pi.$$

To find the current density induced in the sheets we proceed as in (3.5), and accordingly

$$\frac{i}{I} = \frac{2}{r} [J_2(k)\{Y_2(ar) + jJ_2(ar)\} - 3J_6(k)\{Y_6(ar) + jJ_6(ar)\} + \dots]. \quad (3.12)$$

This expression is cumbersome to evaluate when  $ar$  is large, and we can readily find the asymptotic expression by considering Fig. 3.3. For this shows that  $H$  at the surface of the sheet  $OE$  must be the  $H$  due to the unlike pair of currents  $A, B$  together with the unlike pair  $C, D$ . Hence  $i$  at any point in  $OE$  is the sum of the currents which would be induced in it if it were doubly infinite and excited by the unlike currents  $A$  and  $D$ . To find the resultant it is necessary to add separately the two contributions to the inphase component of current and the two contributions to the quadrature component. Thus, in the notation of Fig. 3.2, we have

$$\begin{aligned} \frac{i}{I} &\doteq \frac{1}{2}a \sin \psi [-J_0(a\rho_1) + J_0(a\rho_2) + j\{Y_0(a\rho_1) - Y_0(a\rho_2)\}] \\ &\doteq \frac{2cE_0 \sin \psi}{2\pi} \sin \frac{k}{\sqrt{2}}. \end{aligned}$$

Here then the induced current does not depend on the normal component of the field due to  $A$  alone, but to that of currents  $+I$  at  $A$  and  $-I$  at  $D$ . If  $AD = \lambda, 2\lambda$ , etc., then the induced current at a distant point will be very small, since the two contributions tend to neutralize one another. Obviously this effect will help to make the performance of finite sheets approximate closely to the ideal limit.

### 3.4. Reflecting plates inclined at any angle

Let the angle between the plates be  $\beta$ , where  $n\beta = \pi$ . When  $n$  is a whole number it is possible to find a system of images (i.e. when  $\beta = 180^\circ, 90^\circ, 60^\circ, 45^\circ, 36^\circ, 30^\circ$ , etc.): then the field can be built up by

appropriate combination of like pairs (for  $n$  even) or unlike pairs ( $n$  odd), and by use of equations (1.43) or (1.47), or by adding by means of (1.49) the fields of currents, alternate in sense, spaced uniformly round a circle of radius  $R$ . On doing this we find the general expression

$$\frac{cE}{a\pi I} = 4n\{[-J_n(ar) + jY_n(ar)]J_n(k)\cos n\theta + \\ + [-J_{3n}(ar) + jY_{3n}(ar)]J_{3n}(k)\cos 3n\theta + \dots\}. \quad (3.13)$$

The inphase component of field at the aerial is always given by the equation

$$\frac{cE_P}{a\pi I} = 4n\{J_n^2(k) + J_{3n}^2(k) + J_{5n}^2(k) + \dots\}. \quad (3.14)$$

As an example let  $\beta = 60^\circ$  and then  $n = 3$ : then we are concerned with  $J_3, J_9, J_{15}$ , etc. When  $ar$  is very large  $Y_3 = -Y_5 = +Y_7 = -Y_9$ , and consequently successive terms in (1.47) must alternate in sign. Also  $Y_3 = -Y_1 = J_0$ . It follows from this example that when  $ar$  tends to infinity

$$\left. \begin{aligned} \frac{E}{4nE_0} &= (-1)^{\frac{1}{2}n}\{J_n(k)\cos n\theta + J_{3n}(k)\cos 3n\theta + \\ &\quad + J_{5n}(k)\cos 5n\theta + \dots\} \quad \text{when } n \text{ is even} \\ \text{and} \\ &= j(-1)^{\frac{1}{2}(n-1)}\{J_n(k)\cos n\theta - J_{3n}(k)\cos 3n\theta + \\ &\quad + J_{5n}(k)\cos 5n\theta - \dots\} \quad \text{when } n \text{ is odd,} \end{aligned} \right\} \quad (3.15)$$

where  $E_0$  is the field at the given distant point due to an isolated filament carrying current  $I$ . Accordingly the magnitude of the forward field is  $J_n(k) + J_{3n}(k) + \dots$  or  $J_n(k) - J_{3n}(k) + \dots$  according as  $n$  is even or odd. It should be noted that (3.15) shows the field at a distant point is always inphase or in antiphase with  $E_0$  when  $n$  is even, and is always in leading or lagging phase quadrature with  $E_0$  when  $n$  is odd.

The forward power gain with respect to an isolated filament is expressed by

$$\left. \begin{aligned} G &= \frac{4n(J_n + J_{3n} + J_{5n} + \dots)^2}{J_n^2 + J_{3n}^2 + \dots}, \quad \text{with } n \text{ even,} \\ \text{or} \\ &= \frac{4n(J_n - J_{3n} + J_{5n} - \dots)^2}{J_n^2 + J_{3n}^2 + \dots}, \quad \text{with } n \text{ odd.} \end{aligned} \right\} \quad (3.16)$$

When  $k$  is small  $J_{3n}$ , etc., are very small compared with  $J_n$  and accordingly  $G$  then tends to the value  $4n$  for all values of  $n$ . We shall see shortly an obvious interpretation of this result in terms of Poynting's theorem. If the filament consists of an in-line array of  $N$  members not

very far from the apex of a Vee reflector of angle  $180^\circ/n$  then, from (2.20),

$$G \doteq 2.4nN. \quad (3.16a)$$

Thus if  $N = 10$  and  $\beta = 45^\circ$ ,  $G = 96$  when  $k$  is small: it can reach a maximum of 460, when  $R/\lambda = 2$ , see Fig. 3.26.

Though equation (3.15) gives the diffraction pattern correctly, an alternative form can be written down directly by consideration of the path difference between component images. Particular cases of such expressions are as follows:

$$n = 1, \quad \beta = 180^\circ: \quad \frac{E}{E_0} = 2 \sin(k \cos \theta). \quad (3.15a)$$

$$n = 2, \quad \beta = 90^\circ: \quad \frac{E}{E_0} = 2\{\cos(k \cos \theta) - \cos(k \sin \theta)\}. \quad (3.15b)$$

$$n = 3, \quad \beta = 60^\circ: \quad \frac{E}{E_0} = 4 \sin\left(\frac{1}{2}k \cos \theta\right)\{\cos\left(\frac{1}{2}k \cos \theta\right) - \cos\left(\frac{1}{2}\sqrt{3}k \sin \theta\right)\}. \quad (3.15c)$$

$$n = 4, \quad \beta = 45^\circ: \quad \frac{E}{E_0} = 2\left\{\cos(k \cos \theta) + \cos(k \sin \theta) - 2 \cos\left(\frac{k}{\sqrt{2}} \cos \theta\right) - \cos\left(\frac{k}{\sqrt{2}} \sin \theta\right)\right\}. \quad (3.15d)$$

Whenever  $n$  is an integer the inphase field at the filament can be found directly by adding the fields due to the images, and thus the sum to infinity of the series  $J_n^2 + J_{3n}^2 + J_{5n}^2 + \dots$  is known, as we have seen already in (3.11a). Thus

$$1 - 2J_0(k) + 2J_0(\sqrt{3}k) - J_0(2k) = 12\{J_3^2(k) + J_9^2(k) + J_{15}^2(k) + \dots\}.$$

We have been careful to stress that  $n$  must be an integer because the formation of (3.13) has been built up from an image system. Consideration, however, appears to show that (3.13) must be the general solution for all values of  $n$ , integral or fractional. Thus it is certainly a solution of the two-dimensional form of Maxwell's equation and makes  $E$  zero when  $\theta = \frac{1}{2}\beta$  since  $n\beta = \pi$ . There is, however, the difficulty that  $E$  is multi-valued when  $n$  is a fraction; thus if  $\theta$  is increased by  $2\pi$ ,  $4\pi$ , etc., then  $\cos n(\theta + 2\pi)$  is not equal to  $\cos n\theta$  unless  $n$  is an integer: accordingly  $E$  can have any value at the point  $r, \theta$  according to the number of multiples of  $2\pi$  by which  $2\theta$  is increased. Thus  $E$  is zero at  $\theta = \frac{1}{2}\beta$  but not at  $\theta = \frac{1}{2}\beta + 2\pi$ , when  $n$  is a fraction. It is true that  $\theta$  cannot exceed  $\frac{1}{2}\beta$  without penetrating the material reflecting sheets: in other words, in our problem the field exists only in

the range of  $\theta$  between  $\pm \frac{1}{2}\beta$ , and hence it seems that larger values have no meaning and that the multiple values are ruled out automatically by the material boundaries we employ. Moreover, the discussion of convergence developed in § 1.9 will hold for any value of  $n$ , and this shows the series is convergent everywhere save at the point  $(k, 0)$  where it diverges logarithmically to infinity, as it ought to do in order to

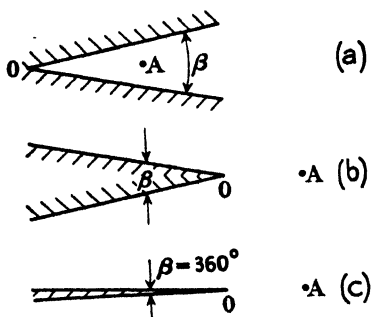


FIG. 3.4.

disclose the current filament of zero radius at this point. There is a distribution of induced current corresponding to  $H$  along the boundary sheets when  $\theta = \frac{1}{2}\beta$ , but it is a little arbitrary to assume this is the distribution which in fact will give zero field at the sheets since a different distribution is appropriate to  $\theta = \frac{1}{2}\beta + 2\pi$ , and this certainly would not make  $E$  zero.

However, for the time being, we shall

assume that the existence of the material boundaries rules out the possibility of multiple values here and thus makes the difficulty purely one of mathematical analysis of no concern in the physical problem. Thus we shall presume that (3.13) describes the field of a thin filament on the bisector of a Vee reflector of any angle and distant  $\lambda k/2\pi$  from the apex, valid for all values of  $n$ . Accordingly it solves the problems typified by Fig. 3.4 (a), (b), and (c). The limiting case, Fig. 3.4 (c), is when  $n = \frac{1}{2}$  and corresponds to a semi-infinite sheet. Solutions for  $n$  less than  $\frac{1}{2}$  do not appear to have a physical interpretation, though some method may be found of interpreting them. Equation (3.14) is valid for all values of  $n$ , but (3.15) needs attention before it can be generalized; this is foreshadowed by its two forms, according as  $n$  is odd or even. Equations of the form (3.15 a-d) can be found only when  $n$  is an integer, because it is only then that a system of images exists. When  $n$  is a fraction,  $E_P$  must be evaluated by the laborious process of adding sufficient terms of the infinite series. When  $z$  is sufficiently large

$$J_n(z) \doteq \sqrt{\left(\frac{2}{\pi z}\right)} \cos\left(z - \frac{1}{2}\pi - \frac{1}{2}n\pi\right) \equiv B \cos(D - \frac{1}{2}n\pi)$$

and

$$Y_n(z) \doteq B \sin(D - \frac{1}{2}n\pi).$$

$$\begin{aligned} \therefore -J_{2n}(z) + jY_{2n}(z) &= B(\cos \frac{1}{2}n\pi + j \sin \frac{1}{2}n\pi)(-\cos D + j \sin D) \\ &= e^{jn\pi}\{-J_0(z) + jY_0(z)\}. \end{aligned}$$

Accordingly, when  $ar$  tends to infinity (3.13) reduces to

$$\frac{E}{E_0} = 4n\{\epsilon^{nj\pi}J_n(k)\cos n\theta + \epsilon^{nj\pi}J_{3n}(k)\cos 3n\theta + \dots\}, \quad (3.13a)$$

valid for all values of  $n$ , integral and fractional, and interpretable physically for all positive real values of  $n$  greater than and including  $\frac{1}{2}$ .

When  $n = \frac{1}{2}$ , then

$$\frac{E}{E_0} = \sqrt{2}[\{J_{\frac{1}{2}}(k)\cos\theta - J_{\frac{1}{2}}(k)\cos 3\theta + J_{\frac{1}{2}}(k)\cos 5\theta - \dots\} + \\ + j\{J_{\frac{1}{2}}(k)\cos\theta + J_{\frac{1}{2}}(k)\cos 3\theta + J_{\frac{1}{2}}(k)\cos 5\theta + \dots\}]. \quad (3.17)$$

We now see this has two components of field in phase quadrature, and this is true for all fractional values of  $n$ : accordingly it is only when the system can be replaced by images that the phase of the field is independent of bearing and is either in phase or in antiphase with  $E_0$ . This comes about in the image system because there are always two images on one line through the apex: if the general case can be described in terms of an infinite set of images, then these are not located in such a manner.

The forward field will fall to zero periodically only if each of the two quadrature components is zero simultaneously for some value of  $k$ . For this to happen in (3.17) it would be necessary that

$$J_{\frac{1}{2}}(k) + J_{\frac{1}{2}}(k) + J_{\frac{1}{2}}(k) + \dots = 0.$$

It is known, however, that the sum of this series is

$$\frac{1}{2} \int_0^k J_{-\frac{1}{2}}(k) dk = (2\pi)^{-\frac{1}{2}} \int_0^k \frac{\cos k}{k^{\frac{1}{2}}} dk,$$

and this integral is never zero. Accordingly there is no value of  $k$  which makes the forward field zero when  $\beta = 360^\circ$  ( $n = \frac{1}{2}$ ), and this is characteristic of all fractional values of  $n$ . For all values of  $n$  the forward field fluctuates periodically as  $k$  is continuously increased, but it is only when  $n$  is an integer that the field falls to zero for particular values of  $k$ .

The general expression for the density of the current induced in the reflector is

$$\frac{i}{I} = \frac{4n^2}{r} [\{Y_n(ar) + jJ_n(ar)\}J_n(k) - 3\{Y_{3n}(ar) + jJ_{3n}(ar)\}J_{3n}(k) + \\ + 5\{Y_{5n}(ar) + jJ_{5n}(ar)\}J_{5n}(k) - \dots] \quad (3.18)$$

valid for all values of  $n$ : when  $r < R$ , interchange  $ar$  and  $k$  above.

The convergence of (3.18) must be examined. When  $n+1 \gg \frac{1}{2}z^2$ ,



then  $J_n(z) \doteq \frac{(\frac{1}{2}z)^n}{\Gamma(n+1)}$ , hence for sufficiently large  $n$  a typical term of the real portion of the series is

$$\frac{n}{\{\Gamma(n+1)\}^2} \left( \frac{ark}{2} \right)^n,$$

and this will certainly be absolutely convergent since the terms are smaller than those of the series represented by  $e^{iark}$ . For sufficiently large  $n$ ,  $J_n(z)Y_n(z) = -1/n$  for all values of  $z$ , whether  $n$  is integral or fractional. Hence a typical term of the imaginary part of (3.18) tends ultimately to  $\pm 1/\pi$ , when  $ar = k$ . Hence at this distance the series is divergent but oscillates finitely. It is conditionally convergent when  $ar$  is just greater or just less than  $k$ , and accordingly it may be used to evaluate the current everywhere save exactly at the distance  $ar = k$ : even there the current is finite, though it may be large. When  $ar$  tends to zero

$$\begin{aligned} \frac{i}{I} &\doteq \frac{4n^2 J_n(ar)}{r} \{Y_n(k) + jJ_n(k)\} \\ &\doteq \frac{2an^2}{\Gamma(n+1)} \left( \frac{ar}{2} \right)^{n-1} \{Y_n(k) + jJ_n(k)\}. \end{aligned}$$

Hence at  $r = 0$ ,  $i$  is zero if  $n > 1$ : it is finite if  $n = 1$  (infinite plane) and is infinite if  $n$  is less than unity. The infinity arises because of the sharp convex angle and would not occur if it had a finite radius of curvature. We shall see later that it causes no serious trouble in analysis and could not occur in any practical structure.

The current density at the apex needs a little further consideration as follows: The lines of magnetic force are parallel to the boundary at its surface; but at the sharp apex the boundary has two directions and therefore the magnetic field must have two directions at this point. But a field cannot have two directions at a point unless the field has the particular value zero and hence this requirement demands that the current density shall be zero at the apex. This explains why  $i$  is zero at  $r = 0$  when  $n$  exceeds unity: but according to our analysis  $i$  should be infinite when  $n$  is less than unity, and this means that  $H$  is infinite and has then two directions at the origin. Moreover, the tangential component of  $H$  is equal to  $A/r$  and hence is proportional to

$$\{Y_n(k) + jJ_n(k)\} J'_n(ar) \cos \theta + \dots$$

But  $2J'_n = J_{n-1} - J_{n+1}$  and hence  $J'_n(ar)$  is infinite when  $ar$  is zero if  $n$  is less than unity. Accordingly, the component of  $H$  perpendicular to the sheets at the origin is of the form  $\infty \times 0$  and its limit is not zero, and

thus the solution breaks down. It is true that the singularity disappears if the apex is furnished with a cylinder of very small radius; but it is suspicious this attention is not required when  $n$  exceeds unity. At present we shall ignore this rather unsatisfactory state of affairs though we shall not forget it.

### 3.5. The curves of forward field

We have seen physical reasons why the forward field for a flat sheet or right-angled reflector must go periodically through zero as  $R$  is increased continuously: in essence this property is general for any angle between the sheets, either acute or obtuse, but when the angle is other than  $180^\circ$ ,  $90^\circ$ ,  $60^\circ$ ,  $45^\circ$ , etc., the field falls to a minimum and does not pass through or reach zero. It is an essential property of reflectors which the reader must never lose sight of, though he may easily lose sight of it if he thinks loosely in terms of optical experience. A comprehensive family of curves of forward field is shown in Figs. 3.5–3.13: this selection is of great practical use since it suffices to cover, by interpolation, almost all cases of practical interest and it represents a great deal of laborious evaluation. Consider first Figs. 3.7 and 3.9: these are simple in their periodicity, and all zero points succeed one another at regular intervals. Fig. 3.11, for a  $60^\circ$  mirror, is periodic in the wave form shown in the figure. When  $\beta = 60^\circ$ ,  $45^\circ$ ,  $30^\circ$ , etc., the forward field must be periodic, though it may be necessary to increase  $R$  through an enormous range before the wave form repeats. It may be compared to a heterodyne pattern (see eq. 3.15*d*); the ripples will not tend to die out, however large  $R$  may be. For example, when  $\beta = 45^\circ$ ,  $E/E_0 = 8$  when  $R/\lambda = 5$ : the ratio  $E/E_0$  will continue to attain the value 8 at large regular intervals no matter how large  $R$  may be. Figs. 3.8 and 3.10 ( $\beta = 120^\circ$  and  $72^\circ$  respectively) are typical of cases where  $n$  is not an integer ( $\frac{2}{3}$  and  $\frac{5}{8}$  respectively) and it is to be noted that now the forward field never reaches zero and  $E/E_0$  is seldom less than unity. Fig. 3.10 is instructive in showing the manner in which Fig. 3.9 changes into Fig. 3.11 as the angle  $\beta$  is decreased from  $90^\circ$  to  $60^\circ$ . It seems probable the curve of Fig. 3.10 must repeat itself for larger values of  $R$ , but the labour of evaluation is prohibitive for  $R/\lambda$  greater than about 4. Similarly the process by which Fig. 3.8 merges into Fig. 3.10 is illustrated by Fig. 3.9, and again we must conclude this figure will repeat itself ultimately. The general trend of these curves, as  $n$  increases, can be understood by the help of (3.15). Provided  $n$  is an integer, a trigonometrical expression can always be found for the curve of forward field

and then its evaluation is straightforward, though sometimes the process is very laborious: thus the equation for  $\beta = 30^\circ$  ( $n = 6$ ), corre-

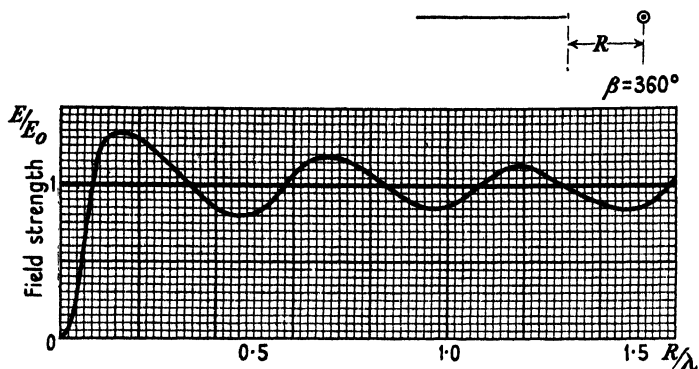


FIG. 3.5.

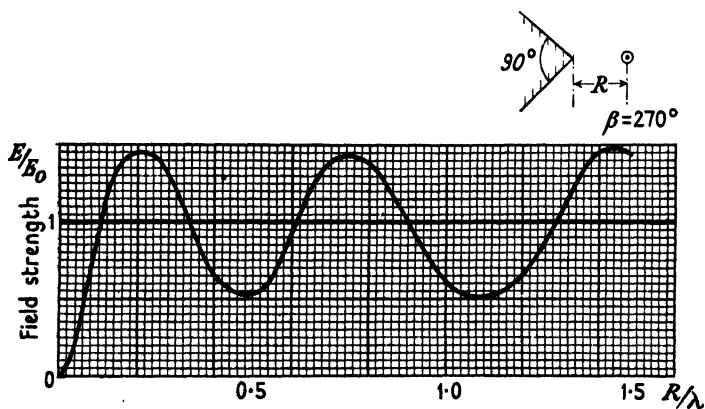


FIG. 3.6.

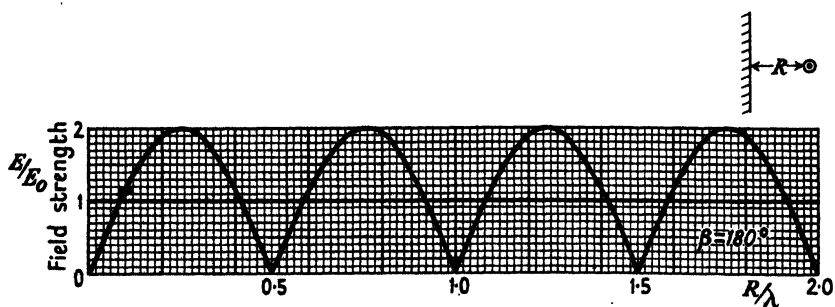


FIG. 3.7.

sponding to (3.15d) for  $\beta = 45^\circ$  ( $n = 4$ ), is very tedious to evaluate, and for larger values of  $n$  the work is intolerable. When  $n$  is a fraction the forward field must be calculated from the infinite series of Bessel

functions given by (3.15) and hence the Bessel process cannot be avoided. But if the reader knows clearly the form of Bessel functions he will at once realize that the Bessel series is a peculiarly elegant method of

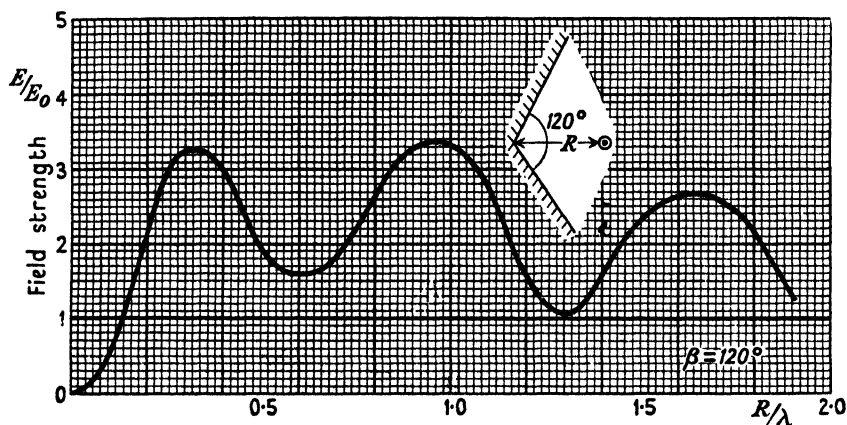


FIG. 3.8.

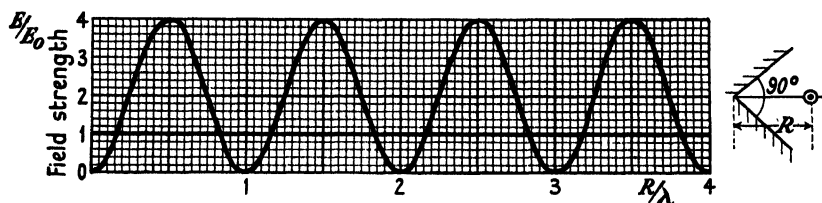


FIG. 3.9.

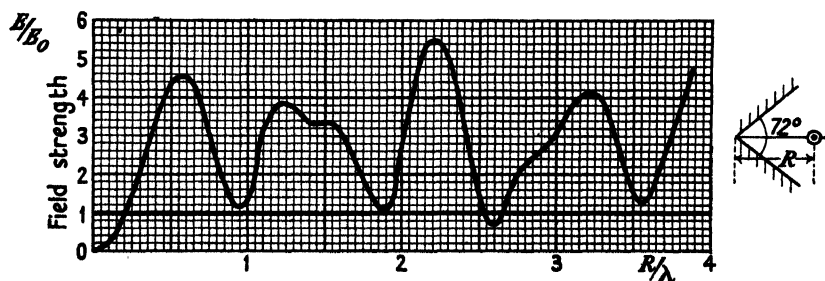


FIG. 3.10.

representation which conveys the whole story graphically to those who know how to read the chart: it provides a quick approximation to the position of maxima and minima, whose more precise location can then be found readily from the trigonometrical expression if this is desired, when  $n$  is an integer. It may perhaps be wise to remark here that

experience shows that the width of the sheets must be increased enormously as  $\beta$  is diminished if a close approximation to the ideal

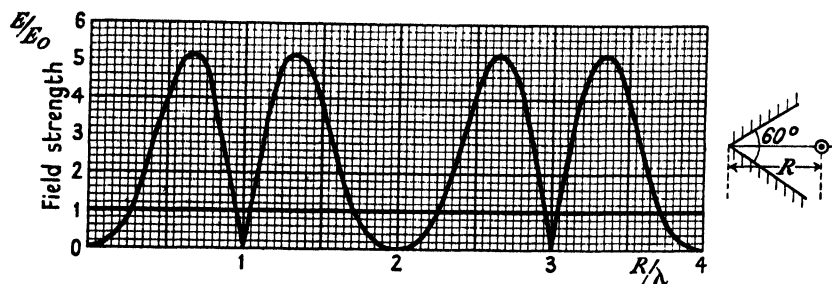


FIG. 3.11.

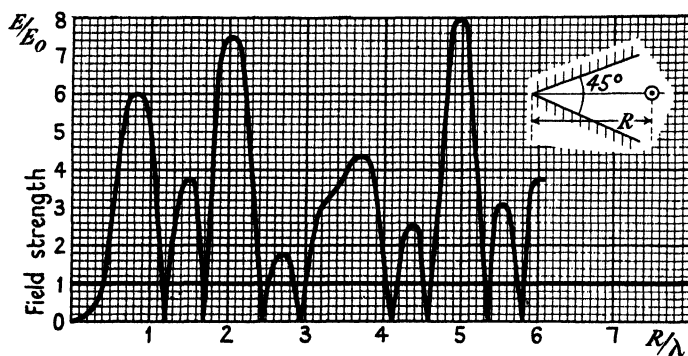


FIG. 3.12.

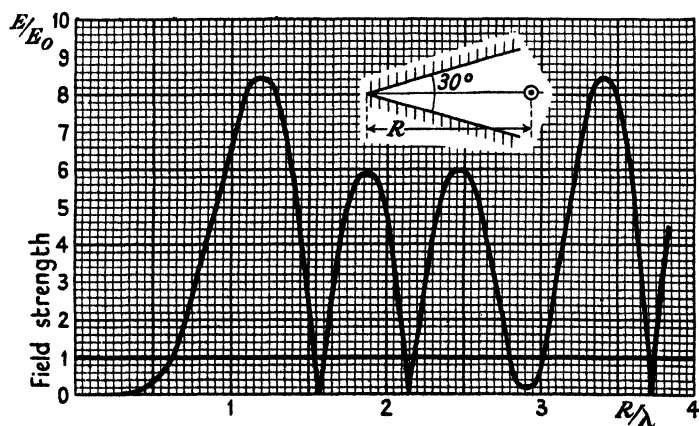


FIG. 3.13.

pattern is required. Unless the wavelength is only some 10 or 20 cm., the physical dimensions may well be intolerable for  $\beta$  less than, say,  $45^\circ$ , and hence it may well be that  $n$  larger than about 4 is of little

practical interest to many users. But a complete grip of the problem is much increased for everyone by considering the general case for  $n$  large, and we shall therefore make here a sub-section on the form of  $J_n(z)$ .

(a) *The general form of the Bessel function  $J_n(z)$*

Fig. 3.14 is a sketch of  $J_{16}(z)$  and is typical of the function  $J_n(z)$  provided  $n$  exceeds unity. It is characterized by a very leisurely rise

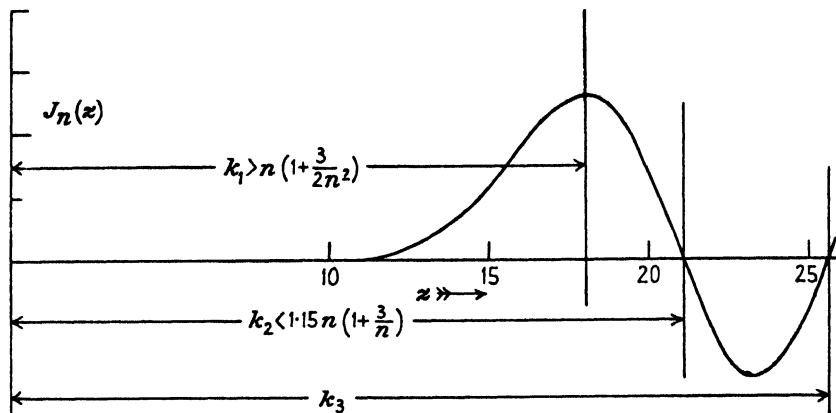


FIG. 3.14.

to its first maximum followed by a steep descent, through zero, to its first negative maximum: thereafter the function oscillates with an amplitude tending to vary as  $z^{-1}$  and with a period which rapidly tends to the value  $2\pi$  but never equals  $2\pi$  precisely. The general properties of this function have long been studied by mathematicians and are described fully in Chapters 8 and 15 of Professor G. N. Watson's *Theory of Bessel Functions*: the reader should be familiar with certain general properties which will now be quoted. First, it can be proved (see Watson, p. 486, 15.3) that, for all values of  $n$ ,  $J_n(z)$  and  $zJ'_n(z)$  are positive and increasing for all values of  $z$  less than  $n$ : hence, with reference to Fig. 3.14, the first maximum must occur at a value of  $z$  which is greater than  $n$ . Also it can be proved (*ibid.*, p. 487, 7) that the first zero occurs for a value  $j_n$  of  $z$  such that

$$j_n < \sqrt{\frac{1}{2}(n+1)(n+5)} \doteq 1.15n \left(1 + \frac{3}{n}\right), \text{ when } n \text{ is large;}$$

the empirical relation  $j_n \doteq 2.4 + 1.15n$  serves to locate approximately the first zero for positive values of  $n$  less than about 30. If  $j'_n$  denotes

the value of  $z$  which makes  $J'_n(z)$  zero for the first time, then it can be shown that

$$j'_n > \sqrt{\{n(n+3)\}} \doteq n\left(1 + \frac{3}{2n}\right), \quad \text{if } n \text{ is large;}$$

hence it follows that the first maximum occurs when  $z$  exceeds  $n$  and is less than  $1.15n$ , for  $n$  large: as  $n$  increases, the first maximum tends to occur more and more closely at  $z = n$ .

Again, it can be shown (*ibid.* (6)) that  $j''_n > \sqrt{\{n(n-1)\}}$  and  $< \sqrt{(n^2-1)}$ : hence the slope in Fig. 3.14 is a maximum very near indeed to  $z = n$ ; moreover, this proves that  $J'_n(z)$  is positive when  $z < n$ , thus showing there are no ripples on the curve as it rises towards its first maximum.

It can also be shown that  $Y_n(z)$  passes through zero for the first time when  $z$  has a value which lies between  $j'_n$  and  $j_n$ : the empirical relation  $Y_n = 0.89 + 1.1n$  serves to locate approximately the first zero of  $Y_n(z)$ .

It is also known (see *ibid.*, p. 746, Table VI) that  $n^{\frac{1}{2}}J_n(n) = 0.446$  to an accuracy closer than 0.25 per cent. for  $n > 3$  and that

$$n^{\frac{1}{2}}J'_n(n) \doteq 0.40;$$

also that  $Y_n(n) = \sqrt{3}J_n(n)$  and  $Y'_n(n) = \sqrt{3}J'_n(n)$  to the same order of accuracy.

The value of the first maximum is given by the approximate formula  $0.674885/n^{\frac{1}{2}}$ , which appears to be always slightly an over-estimate. Thus the ratio of the maximum of  $J_n(z)$  to  $J_n(n)$  is substantially equal to  $0.675/0.446 = 1.51$ : since this ratio is independent of  $n$ , it is clear that  $j_n$  must tend to the value  $n$  in the limit.

It is shown (*ibid.*, p. 441) that  $J_n^2(z) + Y_n^2(z)$  is a decreasing function of  $z$ , and it follows from the foregoing that

$$n^{\frac{1}{2}}\{J_n^2(n) + Y_n^2(n)\} = 2 \times 0.446;$$

hence it follows that  $n^{\frac{1}{2}}Y_n(j'_n) < 0.66$ . Also it is known that

$$J_n^2(z) + Y_n^2(z) < \frac{2}{\pi z \sqrt{\{1 - (n^2/z^2)\}}} \quad \text{and} \quad > \frac{2}{\pi z}, \quad \text{when } z > n,$$

an inequality which allows us to assess the rate at which successive maxima of  $J_n$  and  $Y_n$  tend to vary as  $z^{\frac{1}{2}}$ , since  $Y_n(z)$  is always very near zero when  $J_n(z)$  is a maximum and vice versa.

Also it can be shown (*ibid.*, p. 257) that  $J_n(xn)/J_n(n)$  is a non-increasing function of  $n$  for  $x < 1$ . Thus, consider the ratio  $J_n(0.9n)/J_n(n)$ : tables show this ratio equals 0.75, 0.60, 0.50, 0.40, and 0.27 when  $n = 5, 10, 15, 20$ , and 27 respectively and thus decreases as  $n$  increases. Accordingly, if a family of curves is plotted to an abscissa scale which varies

inversely as  $n$ , then the first maximum becomes relatively sharper as  $n$  increases.

(b) *Curve of forward field expressed in a Bessel series*

Having now a clear picture of the function  $J_n(k)$  we can foresee the general trend of the series  $J_n(k) + J_{3n}(k) + J_{5n}(k) + \dots$ . We now know that  $J_n(k)$  reaches its first maximum soon after  $k = n$  and that  $J_{3n}(n)$  is then extremely small; indeed, the second term in the series cannot be very important until  $k$  is approaching  $3n$ , save at those particular and intermediate values of  $k$  which make  $J_n(k) = 0$ . It is worth noting that when  $k = n$  we have  $2\pi R/\lambda = \pi/\beta$ , thus showing the circumferential width across the Vee is then equal to  $\frac{1}{2}\lambda$ . Hence the first maximum of forward field cannot occur till this circumferential width exceeds  $\frac{1}{2}\lambda$ : the limiting case of this general law is the well-known 'cut-off' property of a rectangular wave guide (when  $\beta = 0$  and  $n = \infty$ ) where the output is zero unless the width of the guide exceeds  $\frac{1}{2}\lambda$ .

The interval  $2nk$ , between  $k = n$  and  $k = 3n$ , embraces a number of wavelengths which increases with  $n$ , and hence the number of subsidiary maxima of forward field between the maximum near  $k = n$  and that near  $k = 3n$  increases as  $\beta$  decreases: this is another description of what we have called the 'heterodyne ripple effect' described by the trigonometrical form.

A numerical example will help to make clear the process of interpreting the Bessel series: thus take  $n = 6$  ( $\beta = 30^\circ$ ), for which the curve of forward field has been given already in Fig. 3.13. The ratio  $J_{18}(k)/J_6(k)$  must, in general, be small until  $k$  equals about 16, which corresponds to  $R/\lambda = 2.5$ ; hence up to about  $k = 16$  the curve of forward field must be substantially the function  $J_6(k)$ . The curves  $J_6(k)$  and  $J_{18}(k)$  are shown plotted in Fig. 3.15, and this shows clearly that only the first term of the series is significant up to, say,  $k = 15$ . It may be seen that the first maximum occurs at  $R/\lambda = 1.2$ , and this, of course, agrees with Fig. 3.13, which was plotted from the trigonometrical form. It is obvious from Fig. 3.15 that the forward field will be zero at  $k = 10$  and at  $k = 13.5$ , and close inspection will show that it scarcely falls to zero between  $k = 17$  and 20. Reference to Fig. 3.13 shows there is a minimum at  $R/\lambda = 2.9$  ( $k = 18.2$ ) whose value is just not zero. In the range of  $k$  between 20.3 and 23.2 both component terms are positive and must conspire to a grand maximum near  $k = 22$ : Fig. 3.13 shows there is a grand maximum, equal in value to the first, at  $R/\lambda = 3.4$  ( $k = 21.2$ ). Thus the whole structure of Fig. 3.13 is



made clear by a glance at Fig. 3.15 and could have been derived much more expeditiously from this figure: the correspondence would have been even more apparent if the second loop in Fig. 3.13 had been drawn below the axis.

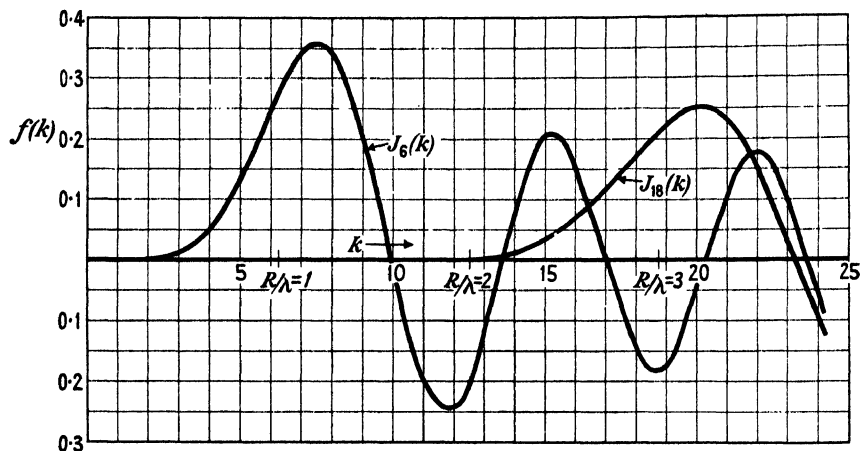


FIG. 3.15.

The Bessel description makes it quite obvious that minor maxima must occur between the first maximum and that maximum which is due largely to the first maximum of  $J_{3n}(k)$ : this behaviour could scarcely have been discerned from the trigonometrical form, typified by equation (3.15 *d*). The number of subsidiary maxima must increase with  $n$ ; thus if  $n = 20$  ( $\beta = 9^\circ$ ), the first maximum will occur near  $k = 24$  ( $R/\lambda = 3.8$ ), and the first maximum of  $J_{60}(k)$  near  $k = 66$  ( $R/\lambda = 10.5$ ); the interval is about  $7\lambda$ , and this is likely to embrace about a dozen subsidiary maxima.

It is hard to say which grand maximum will be the grandest peak: in Fig. 3.12 it is the third grand peak, while in Fig. 3.13 the first two grand peaks are equal in height. The height of the first peak should be given approximately by the formula  $4n \times 0.675/n^{\frac{1}{2}} = 2.7n^{\frac{1}{2}}$ : when  $n = 2, 3, 4$ , and  $6$  this yields a result which is too large by about 6 per cent. When  $n$  is very large and  $k$  approaches  $3n$  the curve of forward field may well be described as  $J_n(k)$  climbing up the comparatively broad hump of  $J_{3n}(k)$ , a description which is already appropriate even when  $n = 6$ , see Fig. 3.15. The larger  $n$  the more nearly will  $J_{3n}(k)$  be constant in a range  $\pi$  of the variable  $k$ , and thus the greater the chance that a positive maximum of  $J_n(k)$  will occur very near the crest of  $J_{3n}(k)$ : then the amplitude of  $J_n(k)$  will be of the order of  $3^{-\frac{1}{2}}$  of its

first maximum and the crest of  $J_{3n}(k)$  will be  $3^{-\frac{1}{2}}$  of the first maximum of  $J_n(k)$ . Accordingly, the second grand crest of  $E/E_0$  is likely to be approximately equal to

$$4n \left\{ \sqrt{\left( \frac{2}{3\pi n} \right)} + \frac{0.675}{(3n)^{\frac{1}{2}}} \right\} = 2.7n^{\frac{1}{2}} \times 0.7 \left( 1 + \frac{1}{n^{\frac{1}{2}}} \right).$$

According to this approximate estimate the second grand peak is likely to exceed the first unless  $n$  exceeds 64, but the ratio is only 1.25 even when  $n = 4$ . Though this formula may seem to be only of academic interest for exploring the limit when  $n$  is large, it is of use in practice because it is needful to assess the power gain when  $k$  is large and  $n$  equal to 8 or 10. Evaluation from the trigonometrical form is very laborious, and ordinary tables of Bessel functions do not go beyond  $k = 24$ . The experience exemplified by Fig. 3.12 gives the uneasy feeling that the grand peaks may go on growing until  $R/\lambda$  is much greater than 5, and therefore it is satisfactory to know how to estimate successive peaks without the necessity of precise evaluation. As an example of this process take  $n = 5$  and then the series is  $J_5(k) - J_{15}(k) + J_{25}(k) - \dots$ : the second zero of  $J_{15}(k)$  occurs at  $k = 24.4$  and is just beyond the ordinary tables. On plotting the two Bessel functions in the range up to  $k = 24$  it will be found that the first maximum of  $E/E_0$  occurs at  $k = 6.5$  and has the value 7.5; the first maximum of  $-J_{15}$  is almost coincident with the fourth maximum of  $J_5$ , and thus the second grand maximum is found to occur at  $k = 17$  ( $R/\lambda = 2.7$ ) and its value is  $E/E_0 = 9$ , thus being 1.2 times the first maximum; according to the approximate formula this ratio would be 1.23. The next grand peak will be caused by  $J_{25}(k)$  whose maximum cannot occur until  $k > 26.5$  and is probably near 27.5, and its value is  $0.675/25^{\frac{1}{2}} = 0.231$ . Since this is beyond the range of tables we must estimate the value of  $J_5 - J_{15}$  and do this by the asymptotic expression

$$J_n(k) \doteq \sqrt{\left( \frac{2}{\pi k} \right)} \cos\left(k - \frac{1}{4}\pi - \frac{1}{2}n\pi\right),$$

valid when  $k$  is large enough: assuming this requirement is satisfied it follows that

$$J_5 - J_{15} = \frac{1.596}{k} \sin\left(k - \frac{1}{4}\pi\right),$$

and this has maxima at  $k = 24.3, 27.4, 30.6$ , etc. The function can be plotted from tables up to  $k = 24$ , and if this is done it will be found to fit well with the asymptotic form. Moreover, we see from the above

that the positive maximum is sensibly coincident with the first maximum of  $J_{25}$  and a rough plot shows the grand peak must occur very near  $k = 28$  and that then  $E/E_0 = 20(0.23 + 0.30) = 10.6$ ; thus the third grand peak is possibly slightly the grandest. The general form having now been found, exact values could be found if necessary from the trigonometrical expression with comparatively little labour.

Turning now to obtuse-angled mirrors, curves of forward field for them are typified by Figs. 3.5 and 3.6. Obviously they are useless for producing highly directive beams, but they do find useful application when it is desired to produce a polar diagram which is substantially a circle with a sector cut out of it. The limiting case, when  $\beta = 360$  ( $n = \frac{1}{2}$ ), is useful in practice and has much theoretical interest. The Bessel series for  $N = \frac{1}{2}$  is

$$\frac{E}{\sqrt{2} E_0} = J_{\frac{1}{2}}(k) - J_{\frac{3}{2}}(k) - J_{\frac{5}{2}}(k) + J_{\frac{7}{2}}(k) + J_{\frac{9}{2}}(k) - \dots + j\{J_{\frac{3}{2}}(k) + J_{\frac{5}{2}}(k) - J_{\frac{7}{2}}(k) - J_{\frac{9}{2}}(k) + \dots\}. \quad (3.19)$$

These series were summed by Lömmel,<sup>†</sup> who showed that

$$J_{\frac{1}{2}}(k) - J_{\frac{3}{2}}(k) + J_{\frac{5}{2}}(k) - \dots = \frac{1}{\sqrt{2}} (P \cos k + Q \sin k)$$

and  $J_{\frac{3}{2}}(k) - J_{\frac{5}{2}}(k) + J_{\frac{7}{2}}(k) - \dots = \frac{1}{\sqrt{2}} (P \sin k - Q \cos k),$

where  $P = \frac{1}{2} \int_0^{2k} J_{\frac{1}{2}}(2k) d(2k)$  and  $Q = \frac{1}{2} \int_0^{2k} J_{\frac{3}{2}}(2k) d(2k).$

Now  $P$  and  $Q$ , known as Fresnel's integrals, have been tabulated (for example, see Watson, *Bessel Functions*, Table V, p. 744).

Hence 
$$\frac{E}{E_0} = P(\cos k - \sin k) + Q(\cos k + \sin k) + jP(\cos k + \sin k) + Q(\sin k - \cos k).$$

$$\therefore \frac{|E|}{|E_0|} = \sqrt{2(P^2 + Q^2)}^{\dagger},$$

and this is in a convenient form for evaluation from tables. Its structure is not yet apparent but may readily be disclosed, since we can approximate to the form of  $P$  and  $Q$  as follows. It is known that  $\int_0^{\infty} J_n(z) dz = 1$  for all values of  $n$  greater than  $-1$ . Now  $J_{\frac{1}{2}}(z) = \sqrt{(2/\pi z)} \sin z$  and thus, when  $z$  is large, each loop of the curve will differ in shape very

<sup>†</sup> See *Treatise on Bessel Functions*, Gray and Matthews, p. 210.

little from a sinusoid having the same maximum amplitude: using this approximation, it is simple to estimate the area under the curve  $J_{\frac{1}{2}}(z)$  from any, not too small, value of  $z$  to infinity. We will illustrate the process by estimating the area from  $z = 4$  to infinity: thus

$$\begin{aligned} \int_{4\pi}^{\infty} J_{\frac{1}{2}}(z) dz &\doteq 2 \sqrt{\frac{2}{\pi}} \left\{ \frac{1}{(\frac{9}{2}\pi)^{\frac{1}{2}}} - \frac{1}{(\frac{11}{2}\pi)^{\frac{1}{2}}} + \frac{1}{(\frac{13}{2}\pi)^{\frac{1}{2}}} - \dots \right\} \\ &= \frac{4}{\pi} \left( \frac{1}{9^{\frac{1}{2}}} - \frac{1}{11^{\frac{1}{2}}} + \frac{1}{13^{\frac{1}{2}}} - \dots \right) \\ &\doteq \frac{4}{\pi} \left( \frac{1}{9^{\frac{1}{2}}} + \frac{1}{13^{\frac{1}{2}}} + \frac{1}{17^{\frac{1}{2}}} + \dots \right) \\ &\doteq \frac{4}{\pi} \int_2^{\infty} \frac{dx}{(1+4x)^{\frac{3}{2}}} = \frac{2}{\pi} \left[ -\frac{1}{(1+4x)^{\frac{1}{2}}} \right]_2^{\infty} \doteq \frac{1}{\pi} \left[ -\frac{1}{x^{\frac{1}{2}}} \right]_2^{\infty}. \end{aligned}$$

Hence

$$\int_0^k J_{\frac{1}{2}}(z) dz \doteq 1 - \frac{1}{\pi \sqrt{(k/2\pi)}} \cos k = 1 - \sqrt{\left(\frac{2}{\pi k}\right)} \cos k = 1 - J_{-\frac{1}{2}}(k),$$

and similarly 
$$\int_0^k J_{-\frac{1}{2}}(z) dz \doteq 1 + J_{\frac{1}{2}}(k).$$

We may note here that the same process shows that

$$\int_0^k J_0(z) dz \doteq 1 - Y_0(k),$$

also that

$$\int_0^k J_1(z) dz \doteq 1 - J_0(k).$$

Accordingly,

$$\begin{aligned} \left| \frac{E}{E_0} \right| &\doteq \left\{ 1 + \frac{1}{2\pi k} - \frac{2}{\sqrt{(2\pi)k}} \cos(2k + \tfrac{1}{4}\pi) \right\}^{\frac{1}{2}} \\ &\doteq 1 - \frac{1}{\sqrt{(2\pi)k}} \cos(2k + \tfrac{1}{4}\pi), \quad \text{when } 2k \text{ is large.} \end{aligned}$$

This equation should represent approximately the curve shown in Fig. 3.5: both the equation and the curve show maxima and minima succeed each other at intervals of  $\frac{1}{2}\lambda$ , and this is in marked contrast with previous experience, where we have seen the distance from maximum to maximum tends to be  $\lambda$ . When  $k = \pi$  our approximation to  $P$  and  $Q$  gives  $E/E_0 = 0.86$ , whereas Fig. 3.5 shows the correct value is 0.82, suggesting that the approximation is closely correct so

long as  $R/\lambda$  exceeds about  $\frac{1}{2}$ . We note that  $|E|/|E_0|$  tends ultimately to unity and that the fluctuations of forward field will be less than 5 per cent. if  $R/\lambda > 9$ .

Fig. 3.6 suggests that when  $n = \frac{2}{3}$  the wavelength of the ripple is less than  $\lambda$  but greater than  $\frac{1}{2}\lambda$ : no sign of attenuation of amplitude appears in the range of  $k$  considered. When  $n = \frac{2}{3}$  the equation of the curve of forward field is, from (3.13 a),

$$\frac{E}{E_0} = \frac{8}{3} \left\{ \frac{\sqrt{3}}{2} (J_1 + J_5 + J_9 - J_{13} - \dots) + \frac{1}{2} j (J_3 - J_7 \dots) - (J_2 + J_6 + J_{10} + \dots) \right\}.$$

Now  $(J_2 + J_6 + J_{10} \dots) = \frac{1}{2}(1 - \cos k)$ , and thus fluctuates between zero and unity with wavelength  $\lambda$ . Accordingly the curve of forward field has one component which fluctuates periodically between  $8/3$  and zero, and thus it is possible the fluctuations depicted in Fig. 3.6 do not tend to die out when  $k$  is large. It is well to point out that these curves of forward field relate to a given constant *current* in the filament and not to a constant radiated power. In practical tests it is not easy to maintain the condition of constant current, and accordingly the position of maxima may not be found to agree with the ideal, for reasons which are not concerned with the limited area of the reflecting sheets but with the generator which supplies power to the aerial. For this reason the positions of zero field are more trustworthy points than maxima for comparing performance with the ideal.

### 3.6. Radiation resistance of a filament in a Vee reflector

Reflecting sheets find application in practice for restricting the radiation to a narrow sector of the equatorial plane. Almost all they can do could be done by a tall curtain array furnished with a 'reflecting curtain': they are not really an advance of possibilities inherent in the curtain arrays which have been in common use for twenty years and are to be seen in many places in this country, e.g. Rugby, Dorchester, Grimsby. But each member of a curtain must be fed by a cable and the current adjusted in both magnitude and phase: the cable system is complex, costly, and difficult to adjust. Those readers who have practical experience of aerials will agree that the main purpose of using a reflecting sheet is to avoid the necessity for many feeding cables and most will jump at the possibility, which the sheets provide, of escape from cables. Currents are induced in the screen automatically with the correct magnitude and phase: hence not only are the cables, as such, avoided but also the necessity for troublesome and nice

adjustment of them. A single in-line array combined with a reflector is the equivalent of many, perhaps 20 or 30, similar in-line arrays hung in curtain, and hence the necessary number of feeding cables is reduced by a factor of the order of 20. Since it is clear that a Vee reflector is used to avoid feeding cables, it is logical to expect to replace the long in-line array by a single half-wave aerial; then the cables are reduced to the irreducible minimum of one: and a single half-wave aerial can be used with excellent results. To avoid confusion, the study of a single half-wave aerial will be deferred till the next chapter. In the main, this chapter is dealing with general principles and is not clouded with discussing practical ways and means, which are referred to only in asides. We are still collecting our kit of general tools and gathering a background of informed horse-sense which later we shall use on practical problems: when that stage is reached we can make our practical guesses intelligently, a necessary but insufficient condition to justify calling a man an engineer or to warrant him practising his art. Speaking analytically, this chapter is restricted to two-dimensional problems: these are approximated to closely in practice by an in-line array.

If reflecting sheets are to be regarded only as an alternative to feeding cables, is there no overriding consideration which rules out one or other system entirely? If the wavelength is longer than about 10 or 15 m., sheets are impracticable because they cannot be made tall enough without providing masts of intolerable height. Windage is not an overwhelming factor because the continuous sheets can be replaced by curtain wires without appreciable detriment, provided always the wires are many wavelengths long. The writer suspects more could be done with screens than has been done so far, at wavelengths of the order of 15 m.

When the wavelength is less than, say, 40 cm., many cables become scarcely practicable, and when the wavelength is only a few centimetres many cables are impossible. The writer hazards the suggestion that a multiplicity of cables should be ruled out of consideration for fixed stations operating on a wavelength less than 3 m. and for mobile stations operating on a wavelength less than about 1.5 m.

After this preliminary we now reproduce a set of graphs showing radiation resistance as a function of  $R/\lambda$  for a wide range of the angle  $\beta$  between the sheets. They are calculated from equation (3.14) or by adding the contributions to  $E_p$  from the component images, for example, by (3.11 a), when these exist, whichever of the two equivalent methods happens to be the more convenient.

The resistances are reckoned relative to that of an isolated filament, and the value for it is 120 ohms per half-wave member of an in-line array. Fig. 3.16 relates to an aerial in the same plane as a semi-infinite sheet and it should be associated with the corresponding curve of forward field, which is given in Fig. 3.5. We note that the relative resistance is never far from unity, if  $R/\lambda$  exceeds 0.2, and oscillates

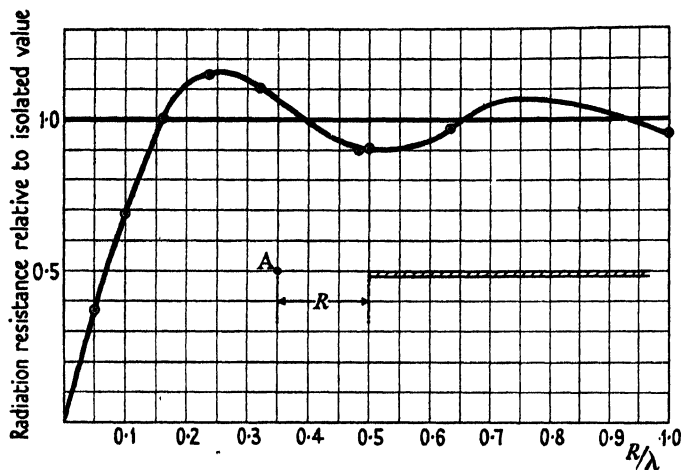


FIG. 3.16.

about this value with diminishing amplitude. The corresponding curve for a filament in front of a flat sheet has the equation  $1 - J_0(2k)$ , and thus oscillates with diminishing amplitude about the value unity: when  $R/\lambda$  exceeds about  $\frac{1}{4}$  this expression approximates to

$$1 - (\pi k)^{-\frac{1}{2}} \cos(2k - \frac{1}{4}\pi)$$

and thus is a maximum when  $R/\lambda = \frac{5}{16}, \frac{13}{16}, \frac{21}{16}$ , etc., and the maximum is near 1.1 when  $R/\lambda$  is of the order of 5. Fig. 3.17 is the corresponding curve for  $\beta = 120^\circ$ : once more the oscillations are of decreasing amplitude and successive maxima occur at intervals near  $\frac{1}{2}\lambda$ . Figs. 3.18-3.21 relate to  $\beta = 90^\circ, 72^\circ, 60^\circ$ , and  $45^\circ$  respectively. In all cases the amplitude of fluctuation decreases as  $R/\lambda$  increases, but it should be noticed that when  $\beta$  is less than  $90^\circ$  the initial fluctuations are very large; indeed, the resistance falls nearly to zero when  $R/\lambda = 1.2$  with  $\beta = 45^\circ$ . The reader should remember that the resistance per member of an in-line array can range between almost zero and some 400 ohms according to its distance from the apex of the Vee. Such changes will have a profound effect on the loading condition of the feeding cable, and it is essential to provide a suitable matching transformer between the said

cable and the aerial member. The said transformer must have a ratio capable of continuous adjustment if an appreciable range of  $R/\lambda$  is called for in operation or in initial adjustment of the polar diagram.

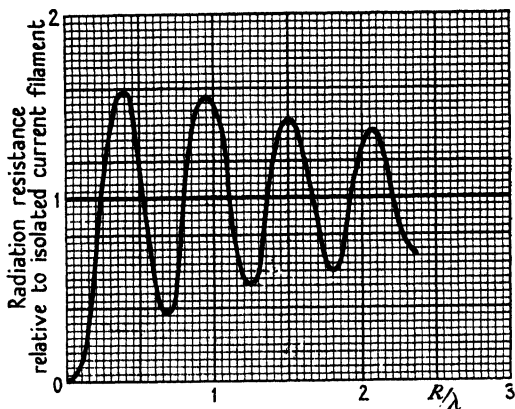
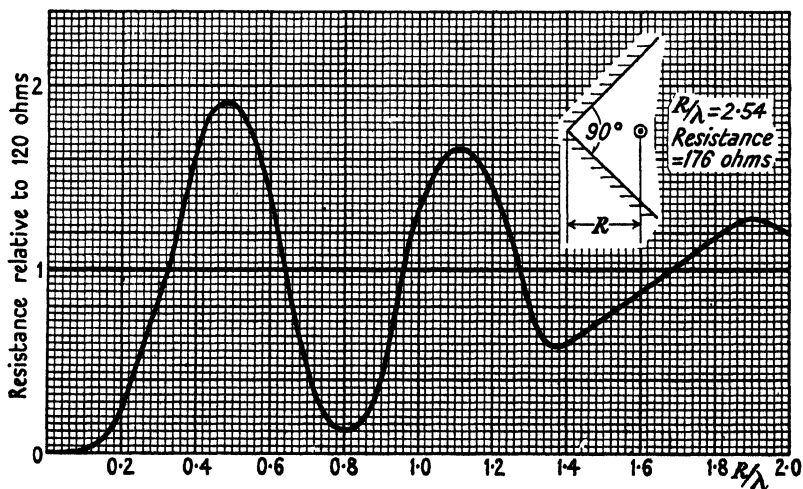
FIG. 3.17.  $\beta = 120^\circ$ .

FIG. 3.18.

The form of the resistance curve can be readily appreciated by a reasoned study of the Bessel expansion (3.14), namely,

$$\text{Relative radiation resistance} = 4n\{J_n(k)^2 + J_{3n}(k)^2 + \dots\}.$$

Every term of this is positive, and no more than one term is precisely zero for any value of  $k$ . It is inevitable the resistance cannot be negative, for this would denote an intake of power, but it is not otherwise obvious that



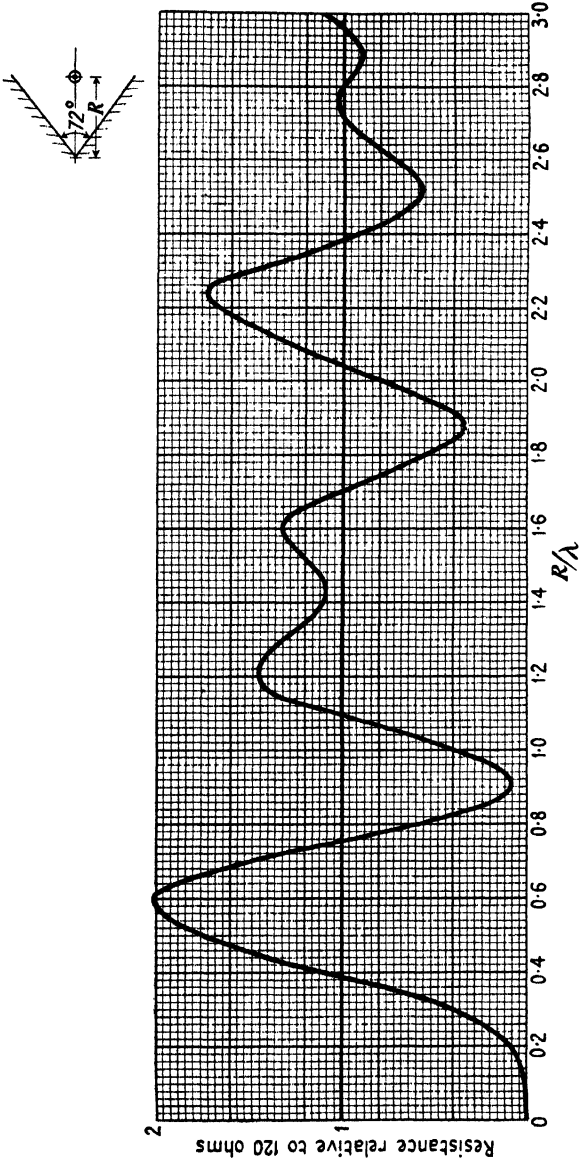


FIG. 3.19.

it cannot be zero: it may be very small, but it must be finite. At the first maximum of  $J_n(k)$  the contribution of the other terms is negligible, and

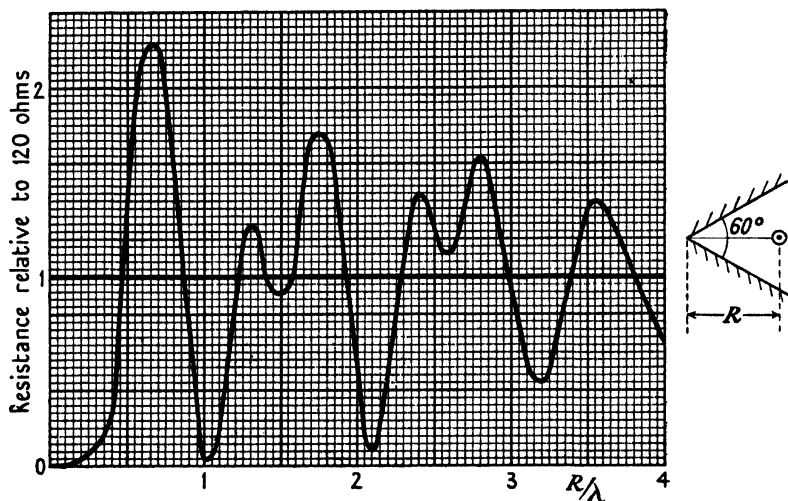


FIG. 3.20.

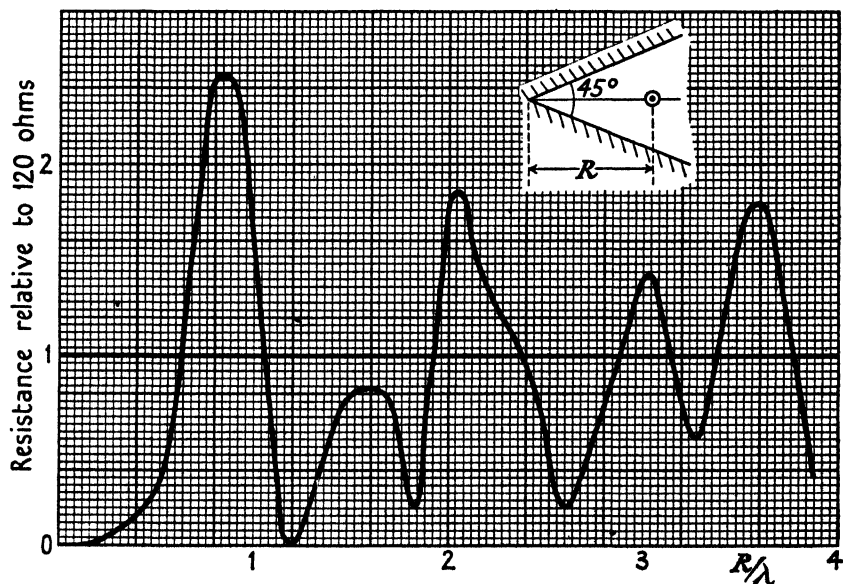


FIG. 3.21.

accordingly the first maximum value is given by the approximate formula  $4n \times (0.675/n^3)^2 = 1.8n^3$ : this formula over-estimates the ratio by about 16 per cent. for  $n = 2, 3$ , and 4. When  $\beta = 15^\circ$  the ratio is 4 and thus

the resistance is then 480 ohms per member. When  $n$  is large the resistance will fall periodically to very small values because  $J_{3n}(k)$  is then extremely small when  $J_n(k)$  is zero for the first time. Thus if  $n = 6$  ( $\beta = 30^\circ$ ),  $J_6(k) = 0$  when  $R/\lambda = 1.57$ , and then  $J_{18}(k) \div 10^{-3}$  and  $J_{30}(k) \div \frac{1.5}{10^{12}}$ : then the resistance per member is of the order of

$$\frac{24 \times 120}{10^6} = 2.9 \times 10^{-3} \text{ ohms.}$$

We saw in Chapter I that a tubular current has zero external field for certain radii. The corresponding condition can never occur precisely with a Vee but can be approached as closely as we please by the simple process of decreasing  $\beta$  and choosing  $R/\lambda$  correctly. This example should be arresting to those whose habitual tendency is to think in optical analogies. For it amounts to this: that a line source, however bright, can be made as near dark as we please by placing it suitably between two perfect mirrors. This result is not experienced in optics because every optical source is thousands of wavelengths in diameter and therefore cannot all be situated at a value of  $R/\lambda$  which makes for substantial extinction. But it is this reason alone which prevents us from experiencing this phenomenon, which to our gross scale optical experience seems absurd and impossible. This example should show the necessity of using optical parallels with due care and forethought: the parallel always exists and is valid if not used carelessly. The reader is warned against confusing the phenomenon just described with the much narrower one of zero forward field: this is only an example of the familiar experience of an extinction, by interference, on a particular bearing, and that bearing happens to be along the bisector of the Vee. In the interesting case we have just considered the field is very nearly zero in all directions. Conceivably this principle could be used for 'keying' a signal by the simple process of varying  $\beta$  or  $R/\lambda$  mechanically.

### 3.7. Power gain of long in-line array in a Vee reflector

Here the power gain will not be reckoned relative to a half-wave aerial and thus, in a sense, conflicts with the definition in § 2.10: it will be reckoned relative to an isolated in-line array. We consider only the 'forward power gain', since presumably this is the direction of principal interest and accordingly the forward gain is zero when  $R/\lambda$  is such as to make the forward field zero. For our purpose here, the gain is now the ratio of the square of the forward field to the relative resistance: it can be computed directly from Figs. 3.5–3.21. It follows from (3.16)

that so long as  $J_{3n}$ , etc., can be neglected, then the gain is independent of  $k$  and remains equal to  $4n$ , and this must certainly hold for  $k$  less than  $1.1n$ . This limiting value can be derived at once from Poynting's

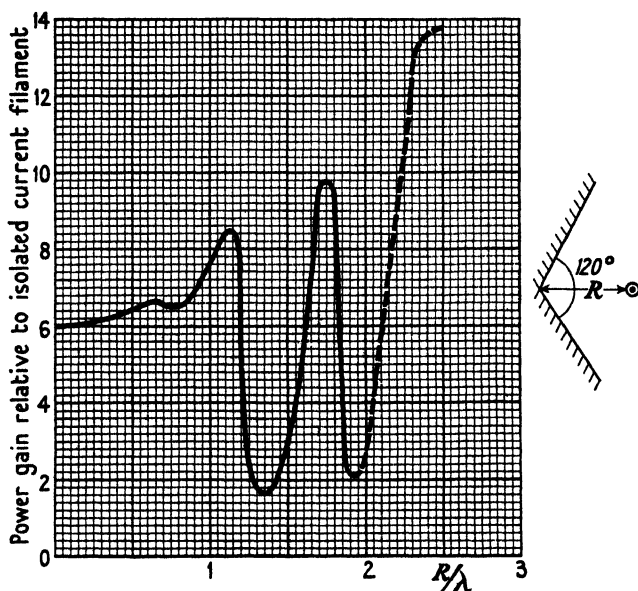


FIG. 3.22.

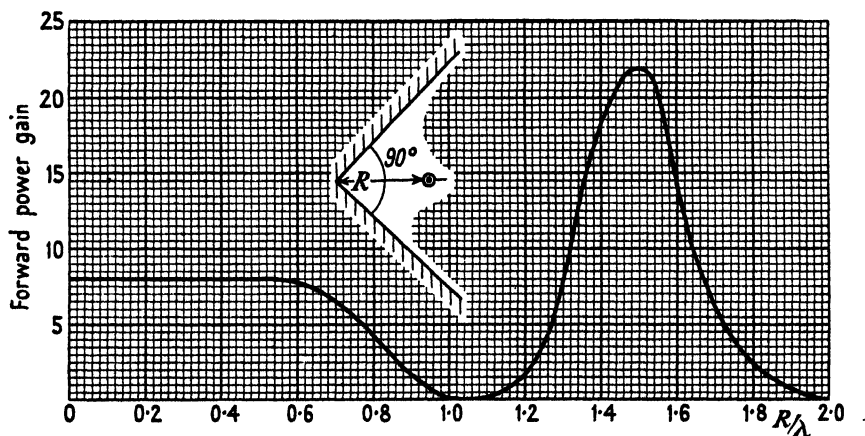


FIG. 3.23.

theorem: for the sheets restrict the radiation to a sector  $1/2n$  of the complete circle; moreover, in this sector the diffraction pattern is a sinusoid provided  $k$  is appreciably less than  $3n$ , and then the mean square field is half the square of the maximum and thus  $G = 4n$ .

Figs. 3.22–3.27 show  $G$  as a function of  $R/\lambda$  for  $\beta = 120^\circ, 90^\circ, 72^\circ, 60^\circ, 45^\circ$ , and  $30^\circ$  respectively. They show that  $G$  remains substantially constant until  $R/\lambda$  reaches the value for the first zero of forward field and then drops suddenly to zero. It is correct to say the forward gain falls to zero because the forward field is zero and yet the radiation

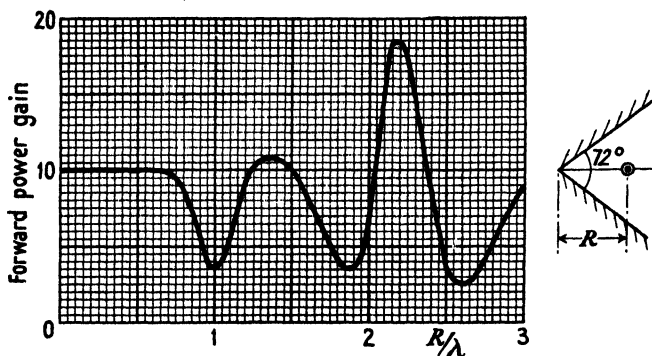


FIG. 3.24.

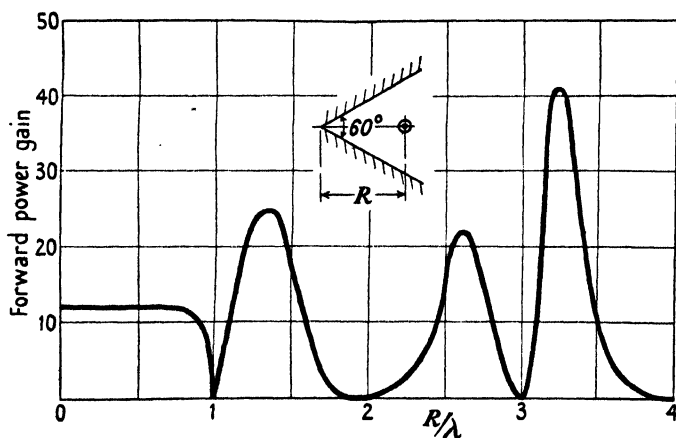


FIG. 3.25.

resistance is not then quite zero because  $J_{3n}$  is finite: though consideration of (3.16) will show that when  $n$  is large  $G$  must remain substantially equal to  $4n$  provided  $k$  does not exceed, say,  $2.5n$ . When  $n$  is very large the graph of  $G$  against  $R/\lambda$  must tend to become a horizontal line of height  $4n$ , interrupted with very steep crevasses at each station for zero forward field. This tendency is appearing in Fig. 3.27 and will become more pronounced as  $n$  increases. Hence when the angle  $\beta$  is very small, and the system is tending towards a wave guide, we may say that the gain is independent of  $k$  until  $k$  is verging on  $3n$ : a small

movement of the aerial may make a very large change in the radiation resistance but cannot alter the pattern or the gain. Thus in such circumstances the aerial may be situated anywhere (provided  $k < 3n$ ),

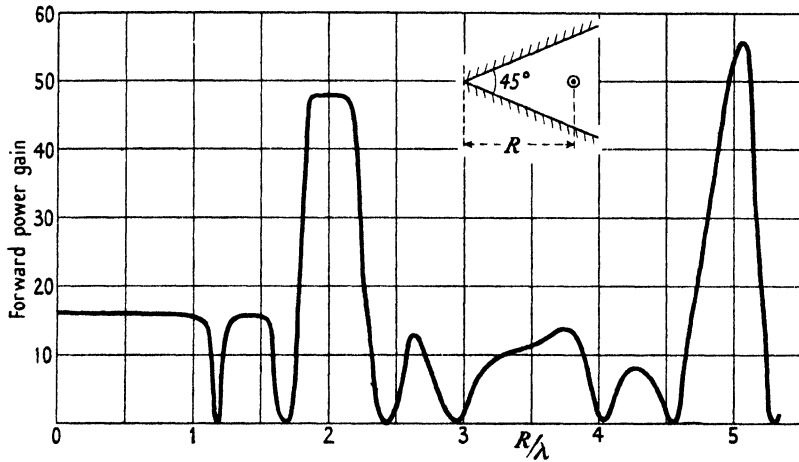


FIG. 3.26.

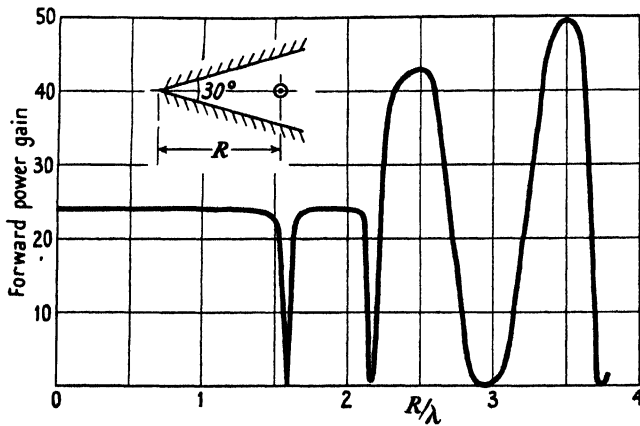


FIG. 3.27.

and the only purpose of adjusting its position is to match its resistance to the feeding cable. Consider now the range of  $\beta$  which is of more practical interest for mirrors, say  $\beta$  not less than  $45^\circ$ . When  $\beta = 45^\circ$  the aerial may be stationed anywhere within  $R/\lambda = 1$  or else should be near  $R/\lambda = 2$ , when the gain is 48. Then the gain of an  $N$ -member array would be  $29N$  and this is 580 when  $N = 20$ . Reference to

Fig. 3.12, etc., will show that the stations for grand optimum gain do not necessarily coincide precisely with the stations for maximum forward field. This is because, as may be seen in Fig. 3.21, the resistance is increasing in the range in which the forward field is increasing: this almost always occurs, and hence the curves of maximum forward field must not be used to determine the most favourable stations for the aerial. Figs. 3.22–3.27 show that the positions of optimum gain are often sharply defined, and thus the adjustment may be rather critical in practice: also they often occur when the space rate of change of resistance is large, and this involves violent changes in the condition of matching to the feeding cable. It will be necessary to examine Figs. 3.22–3.27 in closer detail when we come to discuss the relative merits of various constructions of practical aerials.

### 3.8. The shape of the diffraction pattern

Comparison of equations (3.15 *a–d*) with equations (2.2), (2.4), or (2.6) shows the patterns must have the general character of those illustrated by Figs. 2.2, 2.3, 2.4, etc., in that they evidently consist of a main beam and certain side lobes. Many particular cases are illustrated in Chapter X. Our purpose now is to examine the structure of these patterns and to learn to predict the shape before evaluation. We divide the Vee mirrors into two categories, those for which  $\beta$  is less than  $180^\circ$  and those for which it is between  $180^\circ$  and  $360^\circ$ : the analysis is completely general, but becomes a really powerful weapon only when  $\beta$  is not more than  $90^\circ$ . We reproduce here a few illustrative patterns for large values of  $\beta$ , but deem them outside our main discussion: they have many valuable practical applications, but not that of producing a sharp beam. We repeat here that the pattern for a filament is also the equatorial pattern of an in-line array, including a half-wave aerial. It is the most general equatorial pattern, and hence our discussion now is of much wider application than the previous portions of this chapter, which have related only to a long in-line array, except those portions which have been concerned with the pattern and forward field. Fig. 3.28 is the polar diagram for an aerial in the plane of a semi-infinite sheet and distant  $R/\lambda = 0.48$  from its edge: it is characterized by a sharp crevasse in the plane of the sheet. Fig. 3.29 is the polar diagram for an aerial distant  $0.79\lambda$  from the apex of an obtuse right-angled corner and is characterized by a  $90^\circ$  sector of zero field.

Figs. 3.30 and 3.31 show typical polar diagrams for  $\beta = 120^\circ$ .

Fig. 3.30 is for  $R/\lambda = 0.79$ , a 'station' which reference to Fig. 3.22 will show is still almost in the range where  $G = 4n$ . Fig. 3.31 is for  $R/\lambda = 2.38$ , which is near the station for grand optimum gain. Here the zero (in fact minimum) of the main beam occurs on a bearing of  $\pm 15^\circ$  and thus corresponds roughly with a curtain of 8 members

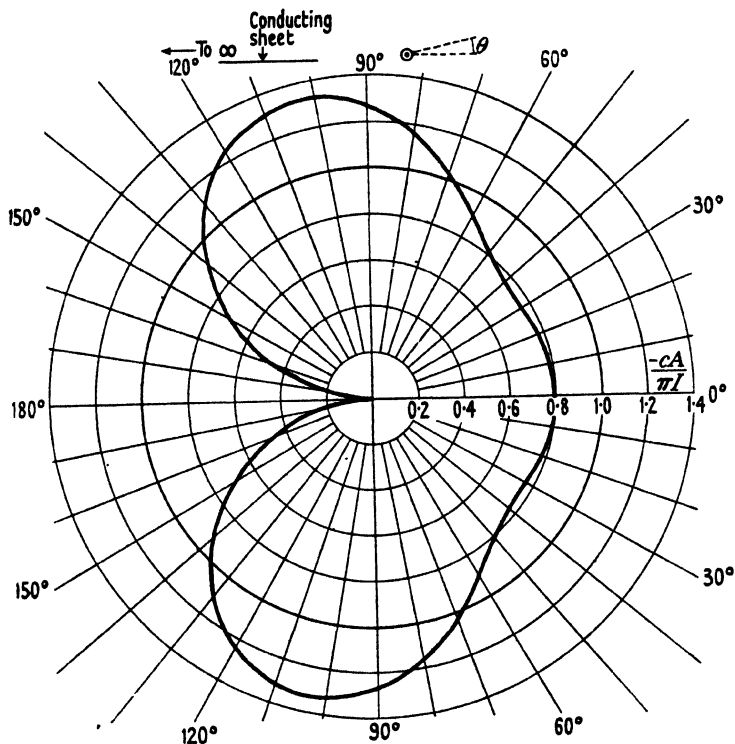


FIG. 3.28.  $R/\lambda = 0.48$ .

(width  $3.5\lambda$ ): however, it differs enormously from the curtain in that the side lobes are about 75 per cent. amplitude instead of the largest being 21 per cent. A sharp beam is always accompanied by large side lobes, because when  $R/\lambda$  becomes large the diagram tends to degenerate into a large number of sharp rays of approximately equal length. Let this suffice now for the discussion of the polar diagram of very wide angled mirrors.

In the following discussion it is implicit that  $\beta$  is less than  $90^\circ$ , though this restriction is not essential. The kernel of the whole process turns on expressing the pattern as a Fourier series, as in (3.17) and (3.15)



rather than in the form in (3.15*a-d*). To simplify things, in the beginning, we shall take  $n$  an integer and accordingly,

$$\frac{E}{E_0} = 4n(-1)^{in}\{J_n(k)\cos n\theta \pm J_{3n}(k)\cos 3n\theta + \\ + J_{5n}(k)\cos 5n\theta \pm J_{7n}(k)\cos 7n\theta + \dots\}, \quad (3.15)$$

negative signs going with  $n$  odd.

Since  $J_{3n}(k)$  is always positive and extremely small until  $k$  is approach-

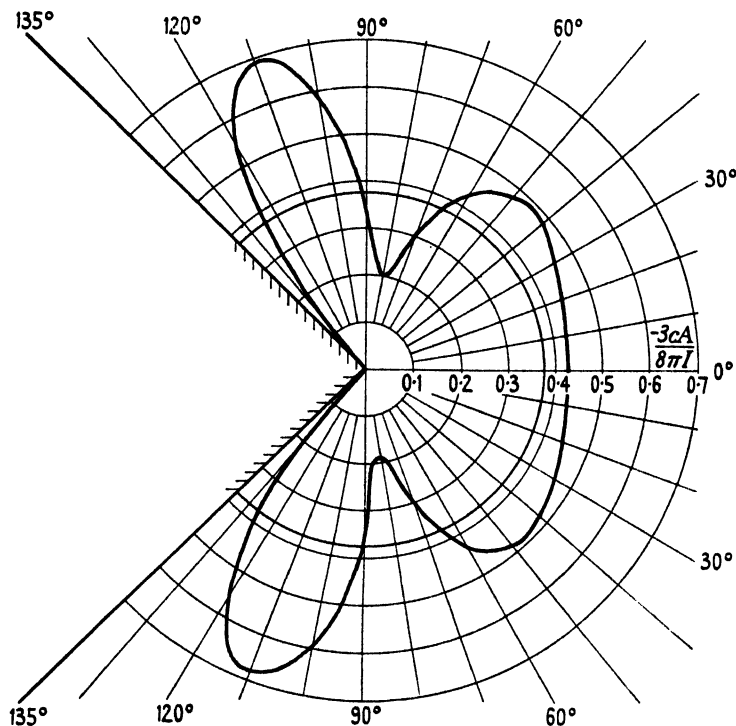
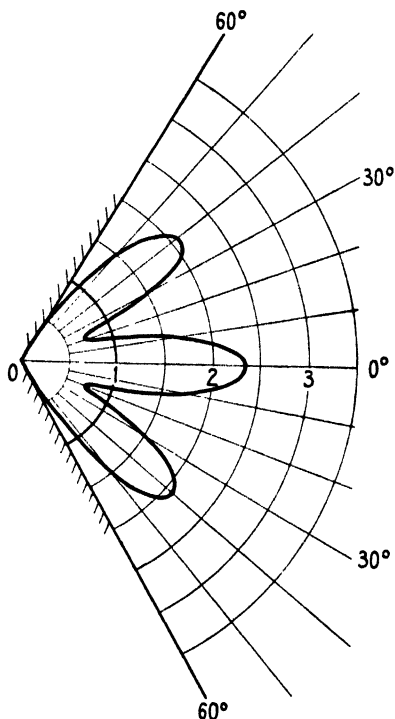
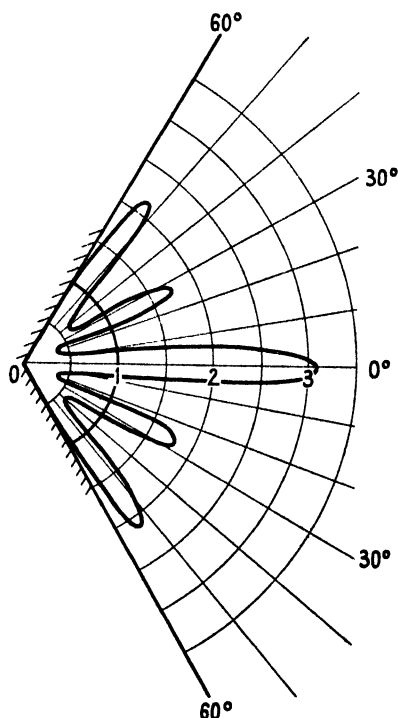


FIG. 3.29.  $R/\lambda = 0.79$ .

ing  $3n$ , (3.15) shows the pattern must differ insensibly from a simple sinusoid until the circumferential width across the Vee at the aerial is verging on  $\frac{3}{2}\lambda$ . It is true that in the interval between  $k = n$  and  $k = 3n$  there will have been approximately  $2n/\pi$  occasions on which  $J'_n(k)$  is zero and then the pattern is  $\cos 3n\theta$ ; but these are patterns of vanishingly small field strength and it is pendent to take account of them. A working rule, to memorize, is that the polar diagram cannot have any appreciable side lobes until the arcual width across the Vee, at the aerial, is verging on  $\frac{3}{2}\lambda$ . In such circumstances it is waste of time to evaluate patterns from equations like (3.15*c*) because the result cannot

be anything but a simple sinusoid. In the interval between  $k = 3n$  and  $5n$  (i.e. arcual width between  $\frac{3}{2}$  and  $\frac{5}{2}\lambda$ ) the pattern will consist of a sine curve and a third harmonic, and thus is the sum of two components typified by Fig. 3.32 (a) and (b). If the beam is to be sharpened by the third harmonic, then it must be disposed as in Fig. 3.32 (a), that is,  $J_{3n}$  and  $J_n$  must both be positive or both negative if  $n$  is even (see

FIG. 3.30.  $R/\lambda = 0.79$ .FIG. 3.31.  $R/\lambda = 2.38$ .

3.15). But  $J_{3n}$  is necessarily positive until  $k$  slightly exceeds  $3n$ ; whether or not  $J_n$  is positive in this region depends on  $n$ . Reference to tables will show that when  $n = 2, 3, 6$ , and  $7$ , then  $J_n(3n)$  is negative, whereas when  $n = 4, 5$ , and  $8$ ,  $J_n(3n)$  is positive. Accordingly if  $\beta = 60^\circ, 45^\circ, 25.6^\circ$ , or  $22.5^\circ$ , the main beam will tend to sharpen when the width across the Vee at the aerial is approaching  $\frac{3}{2}\lambda$ , but when  $\beta = 90^\circ, 36^\circ$ , and  $30^\circ$  it will tend to become more blunt. The amplitude of  $J_n(k)$  near  $k = 3n$  is approximately equal to  $\sqrt{(2/3n)}$  while  $J_{3n}(3n) = 0.44/(3n)^{\frac{1}{2}}$ , and hence then  $J_{3n}/J_n \doteq 0.7n^{1/6}$ : accordingly we are likely to be able to obtain a large third harmonic to sharpen the beam when the arcual width is approaching  $\frac{3}{2}\lambda$ . Fig. 3.33 is a useful guide for constructing

patterns approximating to a given shape: the curve in Fig. 3.33 (a) is the graph of the equation  $y = \cos x + 0.5 \cos 3x$  while 3.33 (b) exhibits  $y = \cos x + 0.6 \cos 3x$ : the first gives a side lobe of magnitude 6 per cent. and the second of 11 per cent. The angle in Fig. 3.33 is shown as  $\pm 90^\circ$ , but it will be understood that this is to be taken as  $\beta/2$ : the beam width at half-height in each figure is near  $30^\circ$ , and accordingly if we can obtain

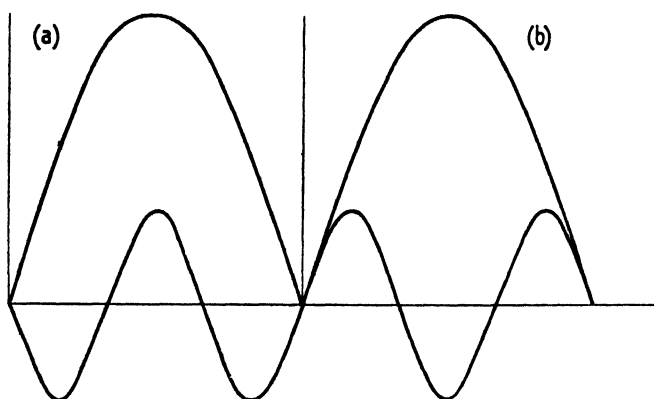


FIG. 3.32.

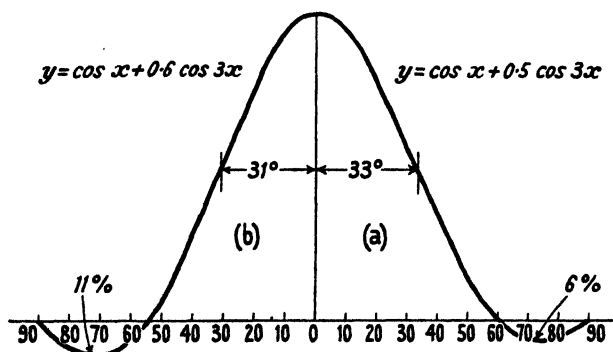


FIG. 3.33.

$J_{3n}/J_n \div \frac{1}{2}$ , the width of beam at half-height in field strength will be near  $\beta/3$ , say  $10^\circ$  if  $\beta = 30^\circ$ . As an example take  $\beta = 45^\circ$ , then  $J_{3n}/J_n$  is found to equal 1.05, 1.16, and 3.7 when  $k = 12, 13$ , and 14 respectively: accordingly the side lobes must be large though the main beam will be very sharp, and thus Fig. 3.33 cannot be approximated to in this range of  $k$  when  $\beta = 45^\circ$ . If  $\beta = 25.6^\circ$ , we find  $J_{3n}/J_n$  equals  $-0.58$ ,  $-0.6$ , and  $-1.5$  when  $k = 14, 20$ , and 21 respectively: thus the width of the beam, at half-height, will be near  $8.5^\circ$  if  $n = 7$  and  $R/\lambda \div 3.2$

(when the arcual width is  $1.42\lambda$  at the aerial); if this width is  $\frac{3}{2}\lambda$ , the side lobes will be large.

If the pattern  $y = \cos x + 0.5 \cos 3x - 0.06 \cos 5x$  can be constructed, the side lobes will be obliterated and there will be no appreciable field outside a bearing of  $\pm\beta/3$ : to attempt such a pattern the arcual width at the aerial must be approaching  $\frac{3}{2}\lambda$ .

So far we have used only the first rising portion of the curve of  $J_{3n}$ , but what of the region between  $k = 3n$  and, say,  $4.5n$ ? If  $k$  is large enough,  $J_n(k) \doteq \sqrt{(2/k)}\cos(k - \pi/4 - n\pi/2)$  and we must consider the relative phase of  $J_{3n}(k)$  and  $J_n(k)$  when  $k$  exceeds  $3n$ : the asymptotic expression shows that if  $n$  is divisible by 2 then the successive loops of  $J_{3n}$  and  $J_n$  will be nearly in phase with one another when  $k$  is large and will tend to vanish nearly simultaneously. But appeal to tables appears to show this condition does not arise till  $k$  is much larger than  $5n$ : thus it may be found that  $J_4$  and  $J_{12}$  are always of opposite sign in the range of  $k$  from 15 to 24, and accordingly throughout this range the third harmonic will increase the width of beam from a  $45^\circ$  mirror. If  $n = 5$ , then  $J_5$  and  $J_{15}$  are of unlike sign between  $k = 16$  and 22, and here the third harmonic will sharpen the beam (note,  $n$  is odd, see 3.15): when  $k = 19$ ,  $J_5 \doteq 0$  and when  $k = 20$ ,  $J_{15} \doteq 0$ , and thus it follows that near  $k = 19.6$  a pattern like Fig. 3.33 could result, and, moreover, then  $J_{25}$  can be made of the order of 6 per cent. Thus by nice adjustment of the position of the aerial it must be possible to produce a lobe-free beam entirely included with a total width of  $12^\circ$  if  $\beta = 36^\circ$ , but the adjustment will be critical. Reference to tables shows that if  $\beta = 30^\circ$ , then a very sharp beam with large lobes can be obtained if  $k = 22$  and a very perfect pattern if  $k = 23$ : further,  $J_{18}/J_6 = 0.38$ . In general a very careful choice of position can produce an almost lobe-free beam whose width at half-height is less than  $\beta/3$  provided  $\beta$  is less than about  $45^\circ$ .

We will close this section by an example to illustrate the use of the Fourier series to arrive rapidly at the shape of the polar diagram. Thus take  $\beta = 60^\circ$  (i.e.  $n = 3$ ) and  $k = 8$  (i.e.  $R/\lambda = 1.27$ ), which is substantially a station for maximum forward field, see Fig. 3.11. On substituting in (3.15) the appropriate values of  $J_n(8)$  we obtain

$$\frac{E}{E_0} = j \times 3.5 \left( \cos \theta + 0.434 \cos 3\theta - \frac{1}{10^4} \cos 5\theta \dots \right),$$

showing that only the first two terms are significant: these are sketched in Fig. 3.34. On reference to this figure it follows readily that when

$3\theta = 60^\circ$  the net ordinate is  $3.5(0.5 - 0.434) = +3.5 \times 0.066$ , showing that the field has not yet fallen quite to zero. When  $3\theta = 66^\circ$  the net ordinate is  $3.5(0.406 - 0.434 \times 0.951) = -3.5 \times 0.007$ , thus showing the bearing for zero field must be between  $20^\circ$  and  $22^\circ$ . Since the field is always zero when  $\theta$  exceeds  $30^\circ$ , it follows the maximum of the side lobe must occur near bearing  $\frac{1}{2}(30 + 22) = 26^\circ$ : at this bearing the net

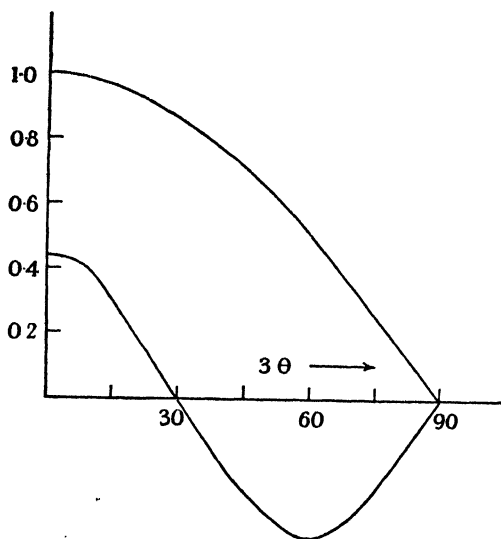


FIG. 3.34.

ordinate is  $3.5(0.21 - 0.43 \times 0.59) = 3.5 \times 0.044$ , showing that the maximum amplitude of the side lobe is near 3 per cent. This very simple and rapid computation shows the field is sensibly restricted to a central beam of total width  $43^\circ$  and inevitably will differ little from a simple sinusoid on a base of  $40^\circ$ . At  $\theta = 10^\circ$  the fractional height is  $1/1.434 = 0.698$ , and this is sensibly consistent with a sinusoid falling to zero at  $\theta = \pm 20^\circ$ : the total width at half-height of field strength is substantially equal to  $\frac{2}{3} \times 40 = 27^\circ$ . The process outlined in this example is vastly simpler than direct point-to-point computation from (3.15c), an equation which hides the form of the resulting graph.

### 3.9. Principle of improving the shape of the pattern by addition of a 'parasitic' aerial

There is a commonly accepted idea, doubtless based on optical treatment, that the 'direct rays from the aerial' ought to be obscured by a small reflector placed in front of it, the notion being that all the

energy should be directed into the main reflector before it emerges into free space. In our view this is but a crude description of a device which has useful applications in practice. In our view the subsidiary reflector is but an additional set of aerials, into which it is convenient to induce current rather than to supply them by separate cables. The parallel with the corresponding optical device is not very close because the subsidiary aerial is usually less than a wavelength from the source instead of being many thousands of  $\lambda$  distant. An example will serve to make clear our interpretation of the device, but we leave a detailed consideration until later. In practice the device has been used mainly with wide-angled mirrors, and for this reason we will take  $\beta = 90^\circ$  in our example. Tables show that when  $k = 3$ , then  $J_2 = 0.486$  and  $J_6 = 0.01$ ; and when  $k = 8.5$ ,  $J_2 = 0$  and  $J_6 = 0.3$ . Accordingly unit current at  $k = 3$  combined with a cophased current of magnitude about 0.75 at  $k = 8.5$  will together give a pattern near

$$y = \cos x + 0.46 \cos 3x.$$

Thus by the use of two aerials bearing currents suitably arranged in phase and magnitude it is possible to obtain a much narrower and more lobe-free beam than was possible to obtain from one aerial alone: the principle can be extended to obtain beams of any shape. It is a difficult device to carry into practice when the additional currents are induced, because it is difficult to obtain both the desired magnitude and phase: the desired phase is achieved by adjusting the length of the subsidiary aerial, since this controls the phase angle of its impedance. Consideration of a figure such as 3.33 shows that substantial advantage can accrue only if the subsidiary current is cophased or antiphased with the driven aerial. This example should suffice to give a rational description of the mechanism of a device which is commonly used, and will show experimenters, who were previously not conversant with it, the reason why an infinite variety of modifications of the pattern, mostly undesirable, can arise from the use of a 'parasite' aerial in a reflector.

### 3.10 Method of turning aside the main beam produced by a Vee reflector

To obtain a simple approach consider two reflecting sheets at right angles to one another and with the aerial not on the bisector, as described by Fig. 3.35, which shows the three image currents. Consideration will show the main beam is turned away from the bisector in a

sense opposite to  $\alpha$ . Appropriate use of equations (1.47) or (1.49) will show the general equation for the polar diagram is

$$\frac{E}{E_0} = 4n\{\epsilon^{j(n\pi/2)}J_n(k)\cos n\alpha\cos n\theta + \epsilon^{j(2n\pi/2)}J_{2n}(k)\sin 2n\alpha\sin 2n\theta + \epsilon^{j(3n\pi/2)}J_{3n}(k)\cos 3n\alpha\cos 3n\theta + \dots\}; \quad (3.20)$$

this reduces to (3.13 a) when  $\alpha = 0$ . Harmonics of even order have now

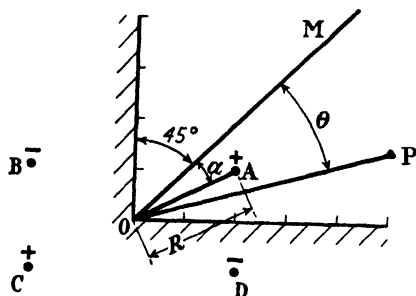


FIG. 3.35.

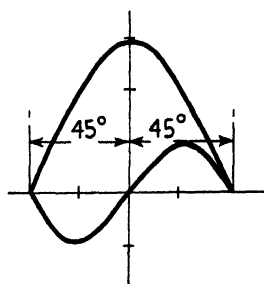


FIG. 3.36.

been introduced, and these make the polar diagram unsymmetrical about the bisector or, in other words, turn the main beam away from the bisector. We have seen that when  $k$  is not greater than about  $2n$  then  $J_{3n}/J_n$  is usually much less than unity and accordingly  $J_{4n}/J_n$  will be still more negligible: then the turning action will depend dominantly on  $J_{2n}$ , and thus the whole mechanism of the effect it is desired to produce is illustrated by Fig. 3.36. As an illustrative example take  $\beta = 90^\circ$  ( $n = 2$ ), then  $\sin 2\pi/2$ ,  $\sin 4\pi/2$ , etc., are zero and thus (3.20) reduces to

$$-\frac{E}{8E_0} = \{J_2(k)\cos 2\alpha\cos 2\theta - J_4(k)\sin 4\alpha\sin 4\theta + J_6(k)\cos 6\alpha\cos 6\theta - \dots\}.$$

If  $k = 3$ ,  $J_2 = 0.486$ ,  $J_4 = 0.132$ , and  $J_6 = 0.011$ , and thus

$$-\frac{E}{8E_0} \doteq \cos 2\alpha J_2(k) \left\{ \cos 2\theta - \frac{2J_4(k)}{J_2(k)} \sin 2\alpha \sin 4\theta \right\}. \quad (3.21)$$

This shows the effect of offsetting the aerial is to reduce the forward field in proportion to  $\cos 2\alpha$  and to introduce a sine second harmonic proportional to  $\sin 2\alpha$ . It should now be obvious from Fig. 3.36 that the main beam cannot be turned off centre by as much as  $22.5^\circ$  for any value of  $\alpha$ .

From (3.21),  $E/E_0$  is a maximum when

$$\sin 2\theta = \frac{1 - \sqrt{1 + 32x^2}}{8}, \quad \text{where } x \equiv \frac{2J_4(k)}{J_2(k)} \sin 2\alpha,$$

or

$$\theta \doteq x, \quad \text{when } \sin 2\alpha \ll 1.$$

Take  $\alpha = 22.5^\circ$ : then if  $k = 3$ ,  $x = 0.19$ , and accordingly it follows the maximum occurs when  $\theta = -9.5^\circ$ . When  $k = 3.6$  ( $R/\lambda = 0.55$ ) the

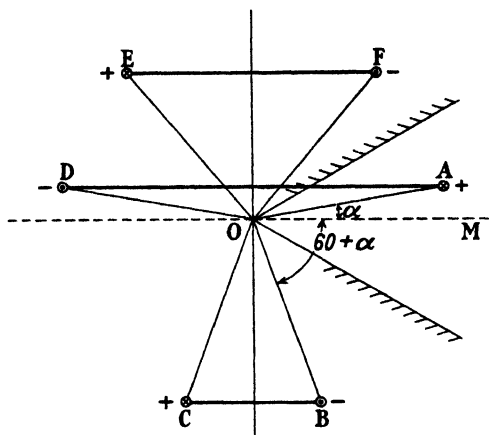


FIG. 3.37.

deflexion of the beam attains a very flat maximum of about  $14^\circ$  near where  $\alpha = 22^\circ$ : thus the beam cannot be turned through more than about  $12^\circ$  without producing a very large side lobe, which eventually becomes a symmetrical bifurcated beam when  $R/\lambda = 0.82$ , for all values of  $\alpha$ .

Details of a practical design will be left to a later chapter: meanwhile we will consider an important general principle. Fig. 3.37 shows the image system for sheets inclined to one another at  $60^\circ$ : careful consideration of this shows the polar diagram must be symmetrical about the bisector  $OM$  for all values of  $\alpha$ . It is helpful to consider the currents  $E$  with  $F$ ,  $D$  with  $A$ , and  $C$  with  $B$  as the sides of three separate rectangular coils whose planes are parallel: it should be obvious their resultant field must be symmetrical about the bisector plane  $OM$ , and accordingly it is impossible to turn the beam of a  $60^\circ$  reflector by offsetting the aerial. Diagrams of images, corresponding to Fig. 3.37, show the same surprising property obtains when  $n$  is an odd integer, which is when  $\beta = 60^\circ, 36^\circ, 25.7^\circ, 20^\circ$ , etc. Since the beam cannot be turned at all when  $\beta$  has one of these angles, it seems likely it cannot be turned much when  $\beta$  is less than about  $70^\circ$ : in other words, if it is



essential to turn the beam without turning the axis of the mirror, then it is essential to use a mirror of wide angle. Equation (3.20) shows that whenever  $n$  is an odd integer the even harmonics in the pattern are always in phase quadrature with the odd harmonics, and accordingly there can be no dissymmetry in the pattern of mean square field. The phase angle of the field changes from positive to negative as the bearing

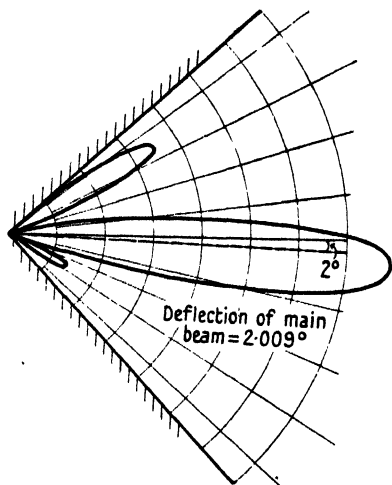


FIG. 3.38.

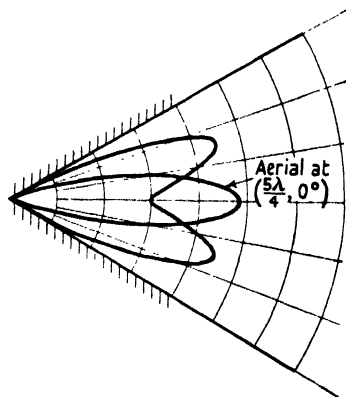


FIG. 3.39.

passes through that of the bisector, and it must be possible to utilize the said change of phase in a way which may be equivalent to that which would have been produced by turning the beam off centre. But the dissymmetry is purely one of phase and not of magnitude and cannot be discovered by a detector, such as a thermocouple, responding to mean square values. Numerical evaluation of (3.20) shows that the main beam is turned off centre for all values of  $\beta$  save those corresponding to  $n$  an odd integer, but that in fact the deflexion is insignificant when  $\beta$  is less than about  $75^\circ$ . Figs. 3.38 and 3.39 show the ideal pattern respectively for  $\beta = 90^\circ$ ,  $R/\lambda = \frac{3}{2}$ ,  $\alpha = 2^\circ$  and  $\beta = 60^\circ$ ,  $R/\lambda = \frac{5}{4}$  and  $\alpha = 10^\circ$ . In the second case the polar diagram remains symmetrical but has developed a dimple: in the first case the beam has been deflected by  $2.09^\circ$ , but at the expense of producing an enormous side lobe. This whole principle is a particular example of the general property (developed already in § 2.7) that the main beam is very hard to turn off centre, and may be said to be rigid, while the side lobes are always flexible and can be pushed readily from side to side.

If there are similar currents at  $\pm\alpha$  symmetry is restored, but the terms  $\cos n\alpha$ ,  $\cos 3n\alpha$ , etc., remain in (3.20). By suitable choice of  $\alpha$  any harmonic can be made zero for every value of  $k$ . In general the effect will be to make the pattern more nearly a perfect sinusoid than it would otherwise have been and thereby decrease the gain. On the other hand, a pair of offset aerials is a device which gives an extra degree of freedom for shaping the pattern, and very strange patterns can readily be produced by this means. For example, suppose  $\beta = 45^\circ$ ,  $\alpha = 7\frac{1}{2}^\circ$ , and  $R/\lambda = 3.8$ : then  $J_4(k) = 0$ , and consequently the term in  $\cos 4\theta$  is zero;  $\cos 12\alpha = 0$ , and thereby the term in  $\cos 12\theta$  is zero;  $J_{20}(24) = 0.162$  and  $J_{28}(24) = 0.022$ , and accordingly the pattern is five sensibly equal rays in a total bearing sector of  $45^\circ$ . A practical use for such a pattern is not apparent, but the example does illustrate a curious result which might conceivably arise accidentally and which would appear very surprising to those unpractised in the Fourier representation. If a single aerial on the bisector is replaced by a uniformly loaded arc of radius  $R$ , centred at the apex and subtending there an angle  $2\alpha$ , then the term  $\cos n\alpha$  in (3.20) will obviously be replaced by  $(\sin n\alpha)/n$ , etc. If the current loading is sinusoidal in the arc of aerials, then the diffraction pattern is a perfect sine curve for all values of  $k$ ; see also Chapter VI.

### 3.11. The diffraction pattern at a finite distance

The field at any distance  $r$  is given precisely by equation (3.13), which assumes the simpler form (3.15) when  $ar$  tends to infinity. We are studying these problems mainly to use the solutions as a guide in practical work and as a basis of comparison for polar diagrams which have been obtained experimentally from finite sheets. Therefore it is important to know what order of distance may be regarded as substantially infinite. The power available at very short wavelengths is likely to be very limited in practical testing, and thus the deflexion of the indicating galvanometer, actuated by a thermocouple, is commonly inadequate. Since the experimenter will commonly desire to reduce the distance between transmitter and receiver, he needs to know the shortest distance at which he may dare to work and yet obtain a pattern which differs insensibly from the ultimate limit. The guiding principle for deciding on the smallest safe distance is obvious on remembering that (3.15) is generalized from a set of images and was formed from the path difference between successive images and the observation point. In any specified case in practice it is an elementary

matter to decide whether the actual and the limiting path differences differ by a significant amount, bearing in mind that the largest path difference must be a small fraction of the range. Provided  $R/\lambda$  is not larger than about 4, then a range of about  $50\lambda$  is likely to be sufficient for most practical purposes. Thus Fig. 3.40 shows the ideal diffraction

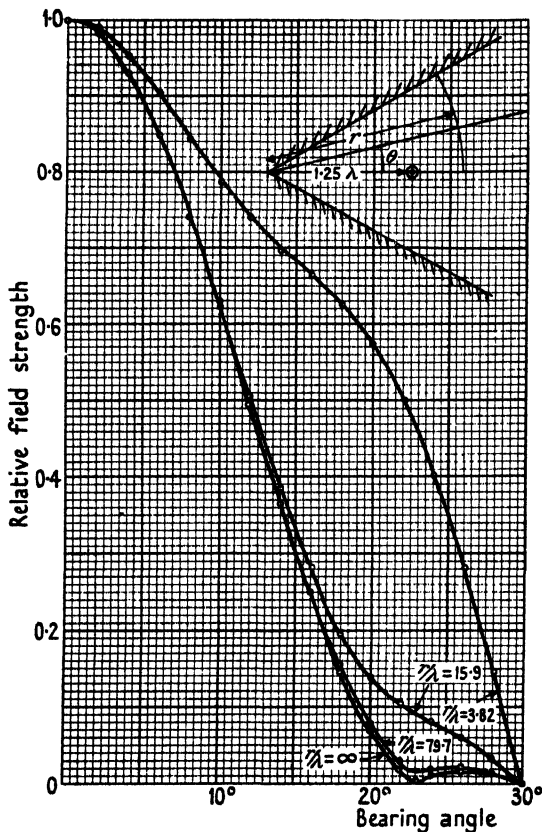


FIG. 3.40.

pattern at various ranges from the apex of a  $60^\circ$  Vee in which  $R/\lambda = \frac{5}{4}$  ( $k = 8$ ); the equation of the limiting pattern is  $0.291(\cos 3\theta + 0.43 \cos \theta)$ . This figure shows that when  $r/\lambda = 15.9$  the pattern is scarcely distinguishable from the limiting form for bearings up to  $15^\circ$  (i.e.  $\frac{1}{4}\beta$ ), and that when  $r/\lambda = 80$  the discrepancies are negligible everywhere. It does not seem necessary to labour this problem further by analysis: the informed experimenter should surely be capable of assessing the discrepancy in any particular case. Suffice it to say that experimental difficulties can often be mitigated enormously if the observers will

spend a few minutes assessing numerically the shortest range which is permissible.

### 3.12. Reciprocal properties of Vee mirrors

#### (a) *Two simple reciprocities*

Appropriate use of equation (1.49) shows that a current  $I \sin \theta$  situated at the point  $(R, \alpha)$  in Fig. 3.35 will produce a field at the point  $(r, \theta)$  given by the equation

$$\begin{aligned} \frac{cE}{4\pi nI} = & \{-J_n(ar) + jY_n(ar)\}J_n(k)\cos n\alpha \cos n\theta + \\ & + \{-J_{2n}(ar) + jY_{2n}(ar)\}J_{2n}(k)\sin 2n\alpha \sin 2n\theta + \\ & + \{-J_{3n}(ar) + jY_{3n}(ar)\}J_{3n}(k)\cos 3n\alpha \cos 3n\theta + \dots, \end{aligned} \quad (3.22)$$

where, as usual,  $a = p/c = 2\pi/\lambda$  and  $r > R$ . If  $R > r$ , then  $k$  and  $ar$  must be interchanged in (3.22). First consider the case where  $r > R$  so that  $P$  and  $A$  are situated as in Fig. 3.35, then (3.22) gives the field at  $P$  due to current  $I$  at  $A$ . But if the current filament had been situated at  $P$  and we required the field at  $A$ , we must use the form of (3.22) appropriate to a point closer to the apex than the current filament, and thus the variable coordinates are  $(R, \theta)$  with  $r > R$ ; accordingly (3.22) is correct as it stands, since  $\alpha$  and  $\theta$  are interchangeable. Accordingly, (3.22) shows that if unit current at any point  $A$  produces field  $E$  at any other point  $P$ , then unit current at  $P$  will produce field  $E$  at the point  $A$ : this is one important reciprocal property. It shows, for example, that the forward field test may be performed either by observing the field at a fixed and distant point, due to a transmitting aerial which is moved along the bisector, or by observing the field due to a fixed and distant transmitter at a receiving aerial which is moved along the bisector.

A second simple reciprocity is in respect of the angles  $\alpha$  and  $\theta$ . For (3.22) shows that if unit current at  $(R, \alpha)$  produces a field  $E$  at point  $(r, \theta)$ , then unit current at  $(r, \alpha)$  will produce field  $E$  at point  $(R, \theta)$ . Recognition of this property may find useful application in the testing of polar diagrams. In such a process it is usual to place the aerial on the bisector (i.e.  $\alpha = 0$ ) and to plot the field due to a distant aerial at  $P$ , as a function of  $\theta$ , by turning the whole reflector about an axis perpendicular to the plane of the paper. It is not essential to proceed in this way: the same result will be obtained (in the idealized conditions postulated) if the distant transmitter  $P$  is located with respect to the bisector so that  $\theta = 0$ : then instead of revolving the mirror, on a turntable, the aerial  $A$  may be moved on an arm of fixed radius  $R$  and the field plotted as a function of  $\alpha$ . Such a process would be practicable

even when the physical dimensions of the reflecting screens made it impracticable to turn the whole mirror about an axis. However, the reader should note we are discussing here a reciprocal property enjoyed by a certain idealized system in which the sheets extend to infinity and it may not hold for sheets of finite width. Thus, suppose  $P$  is a distant transmitting station on bearing  $\theta = \frac{1}{2}\beta$ : in ideal conditions it would produce zero field at  $A$ , but with sheets of finite width it will produce appreciable field at  $A$ , due to what optical parlance calls diffraction round the edge. But if  $A$  is placed in contact with the sheet, i.e.  $\alpha = \frac{1}{2}\beta$ , the field at  $A$  must be zero, and thus it must make some difference whether it is  $\alpha$  or  $\theta$  which equals  $\frac{1}{2}\beta$ . Also the reader should note that the reciprocity applies to field strength and not to the current which that field induces in a given aerial. If a distant transmitter at  $P$  induces a current in an aerial at  $A$  and this current is observed as a function of  $\alpha$ , it must not be overlooked that the radiation resistance of the aerial is a function of  $\alpha$ , and accordingly the induced current is not simply proportional to the inducing field.

(b) *Less simple reciprocities*

Suppose now that  $\theta = 0$  and  $\alpha$  is not zero: then we saw in § 3.10 that the aerial at  $A$  emits a main beam which is 'off centre' if  $\beta$  exceeds, say,  $70^\circ$ . In such circumstances an important parameter is always the forward field, i.e. the field on bearing  $\theta = 0$ . We note from (3.22) that the field at  $\theta = 0$  when  $\alpha = \alpha_1$ , is the same as the field when  $\alpha = 0$  and  $\theta = \alpha_1$ . Hence if the 'central diffraction pattern' is available, the field which it shows on bearing  $\pm\alpha_1$  will be the field on bearing zero when the aerial is offset an angle  $\pm\alpha_1$ : conscious recognition of this property will save much unnecessary computation in design work.

For a given value  $\alpha_1$  of  $\alpha$  there is a value  $\theta_1$  of  $\theta$  which makes  $E$  a maximum: a particular numerical case of this was solved in the last section; hence if  $\theta = \theta_1$ ,  $E$  will be a maximum when the aerial is set so as to make  $\alpha = \alpha_1$ . Accordingly tables could be derived for any given aerial showing  $\alpha_1$  for every value of  $\theta_1$ , and accordingly  $\theta_1$  could be deduced experimentally by observing the value of  $\alpha$  which made  $E$  a maximum. Here is a possibility of direction finding without the necessity of moving the mirror as a whole.

(c) *Reciprocity in power gain*

We have explored fully the stations a transmission aerial should have to make its forward power gain a maximum. The converse problem is to decide where a receiving aerial should be placed so that it shall

absorb the maximum amount of energy from the field incident on it. The word absorb is used here with deliberate intent and denotes a sink of energy and not mere re-radiation. We must suppose the filament is tuned in some manner, such as by the use of 'Franklin coils' or a plurality of cables feeding half-wave elements, so as to make the reactive component of its impedance zero: this is a pre-requisite for maximum dissipation of energy. Then it must pass the induced current through a resistance which is numerically equal to the radiation resistance: then only will the dissipation of energy be a true maximum. The radiation resistance, however, depends very much on the distance of the aerial from the apex (see Figs. 3.18–3.21), and thus the optimum loading resistance will also depend on this distance: accordingly it is not a constant and may well be far from 70 ohms. Moreover,  $E_r$ , the incident field at the aerial, also depends on  $k$ : accordingly both distance and loading position must be chosen so as to make  $E_r^2/R_r$  a maximum, both these quantities being functions of  $k$ . The reciprocal theorems show us that  $E$  will be the same function of  $k$  when the source is distant as the distant field was when the transmission aerial was close to the apex. Hence the condition for making  $E_r^2/R_r$  a maximum in reception is the same as that which makes the power gain a maximum in transmission. For example, the best possible reception with a  $60^\circ$  Vee (with unlimited sheets) will occur (see Fig. 3.25) when  $R/\lambda = 3.2$ , and to obtain the maximum dissipation the loading resistance (see Fig. 3.20) should be 0.44 of the isolated value, which is 53 ohms for a long in-line array. If the mirror angle is  $30^\circ$  the power gain is independent of  $k$  provided  $R/\lambda < 2$  (see Fig. 3.27), but for any given  $k$  within this range the power absorbed will not be a maximum unless the loading resistance is chosen appropriately to the value of  $R/\lambda$  in use, and this will fluctuate violently since it is proportional to  $J_0^2(k)$ . The loading resistance cannot in practice be inserted in the aerial itself but must necessarily be at the far end of a feeding cable: hence it must have that value which will 'look like' the radiation resistance from the aerial end of the cable. To minimize attenuation losses in the cable the loading resistance should equal the characteristic resistance of the cable, which often is 70 ohms. Hence when a  $30^\circ$  Vee is used at  $R/\lambda < 2$ , then  $R/\lambda$  should be chosen so that the radiation resistance is 70 ohms—that is, so that  $4nJ_n^2(k) = 70/120$ , which is when  $J_0(k) = \pm 0.156$ , and this occurs when  $k \doteq 5.4, 7.8, 10.8, 14$ . Fortunately these optima are blunt and thus the adjustment is not critical: thus suppose the loading resistance were 70 ohms in the previous

example of a  $60^\circ$  Vee instead of the correct value, 53 ohms. Then the power output would be  $(70+53)/(70+70) = 0.9$  of the optimum, a loss of about 0.5 dB, which is not significant. If the load resistance is 70 ohms, the power loss will be only of the order of 1.5 dB provided the radiation resistance is between 35 and 140 ohms. Figs. 3.19–3.21 show, however, that the radiation resistance may well vary between almost zero and 300 ohms, and thus it is not permissible to choose the aerial station at random even though it is in the range where the power gain is independent of  $R/\lambda$ . At very short wavelengths the best method of adjusting the receiver may well be to provide a 'distant operated' means of moving the aerial along the bisector of the Vee.

## IV

### HALF-WAVE AERIAL COMBINED WITH VEE REFLECTOR

#### 4.1. Introduction

IN the last chapter the aerial was a long filament, applicable in practice, with reservations, to a long in-line array. We now treat the problem of a single half-wave aerial, an important practical case because it involves only one feeding cable: it is a problem in three dimensions and thereby becomes much more complicated. Images can be found when  $n$  is an integer and then the problem is straightforward in all its aspects, and for most practical applications these particular cases suffice. In the last chapter we derived elegant general formulae in Fourier-Bessel expansions which were valid everywhere: formulae of the same general kind must exist for a doublet and Vee reflector, but they will not have the same elegance and simplicity because they have to be expressed as a series in  $P_n^m(\cos \phi)$ , where  $P_n$  is a Legendre polynomial and involves powers of  $\cos \phi$ : this renders them clumsy. Because it is bound to be clumsy we do not attempt to derive the general expression: to do so would but clutter many pages with dull analysis, difficult to evaluate numerically. By using reason, knowledge, and common sense we can pass round the obstruction without severe loss of generality.

#### 4.2. The radiation figure at a great distance

When the angle between the mirrors is  $180^\circ$ ,  $90^\circ$ ,  $60^\circ$ , etc., the field on any bearing  $\theta$  and angle of elevation  $\phi$  can be obtained by writing  $k \cos \phi$  for  $k$  in equations (3.15 *a-d*), and in addition multiplying their right-hand sides by the factor  $F_1 \times F_2$  defined in equations (2.8) and (2.9). If the source is a single doublet,  $F_2$  is unity and  $F_1 = \cos \phi$ ; if it is a single half-wave aerial, then  $F_2$  is unity and  $F_1$  is tabulated in Table 2.1; if it is an in-line array of  $N$  half-wave members, then  $F_1 \times F_2$  is defined by equation (2.9). Hence we have the field at any distant point for any system of aeriels combined with Vee mirrors provided only they are inclined at  $90^\circ$ ,  $60^\circ$ , etc.; generality is lacking only in respect of the mirror-angle  $\beta$ . In practice  $\beta$  is likely to be less than  $90^\circ$  and then the gaps between soluble angles are small and the lacunae have little practical significance. It so chances that the only cases which are really of interest and troublesome to do in three dimensions arise mainly in practice only in two dimensions, when the solution is simple.

When  $n$  is integral the equatorial pattern is given by (3.15 *a-d*) as



they stand, and these can be expanded in the Fourier series (3.15). It is scarcely open to doubt that (3.15) expresses the equatorial pattern for any angle  $\beta$  (including  $180^\circ$ ) when the source is a doublet or half-wave aerial or any collinear system at distance  $R$  from the apex: we can state that experiment shows it is valid for all values of  $n$  from  $\frac{1}{2}$  upward. Hence we know all about the equatorial pattern, and all that was said about the shape of the pattern in the last chapter holds good when the source is a half-wave aerial: §§ 3.8 and 3.9 have much wider application than was apparent in them.

Equation (3.15) is valid for expressing the forward field as a function of  $k$ , and so Figs. 3.5–3.13 are always valid provided it is remembered they apply only to the forward field in the equatorial plane. On bearing  $\theta = 0$  they will apply at any angle of elevation  $\phi$  provided we replace  $k$  by  $k \cos \phi$ . For example, consider Fig. 3.9, which shows the forward field for sheets at right angles. The forward field will be zero whenever  $(R/\lambda) \cos \phi = 1, 2, 3$ , etc. Hence the forward field will be zero at an angle of elevation of  $45^\circ$ , provided  $R/\lambda = \sqrt{2}, 2\sqrt{2}$ , etc. Also we note that, if  $R/\lambda = 1, 2$ , etc., then the forward field is not zero at a small angle of elevation. Accordingly stations for zero forward field in the equatorial plane now correspond to the condition where the beam is shot upwards. If the aerial is vertical and propagation is intended to proceed mainly by the Heaviside layer then, obviously, the aerial should be put at a station for zero forward field in the equatorial plane: then the beam will be turned upwards to the reflecting layer of ionosphere. We shall continue this study when we have discussed curves of radiation resistance and forward gain; such curves help enormously in understanding and forecasting the complete radiation figure.

### 4.3. Radiation resistance as a function of $k$

In this problem we suffer somewhat from not having a general equation corresponding to (3.14): we can deal only with  $\beta = 180^\circ, 90^\circ, 60^\circ$ , etc., and must calculate the radiation resistance by adding the inphase field, at the aerial, due to the current in itself and also due to the current in each image. We saw in equation (1.80) that we must take  $-cE_p/2a^2 = \frac{2}{3}X_0^2$  for an isolated half-wave aerial. Each image aerial is appreciably distant from the real aerial and this means the force at the real aerial due to the image will differ insensibly from what it would be if the image were a doublet of equal  $X_0$ : it is pedantic to make allowance for the images being half-wave aerials, in respect of the field they produce at the real aerial. Accordingly (1.69) may be

used to calculate the mutual forces, just as it was used in Chapter II to calculate the power gain of curtains; the process should be obvious and corresponds to that outlined just after equations (3.15*d*). Figs. 4.1–4.4 show radiation resistance as a function of  $R/\lambda$  for  $\beta = 180^\circ, 90^\circ, 60^\circ$ ,

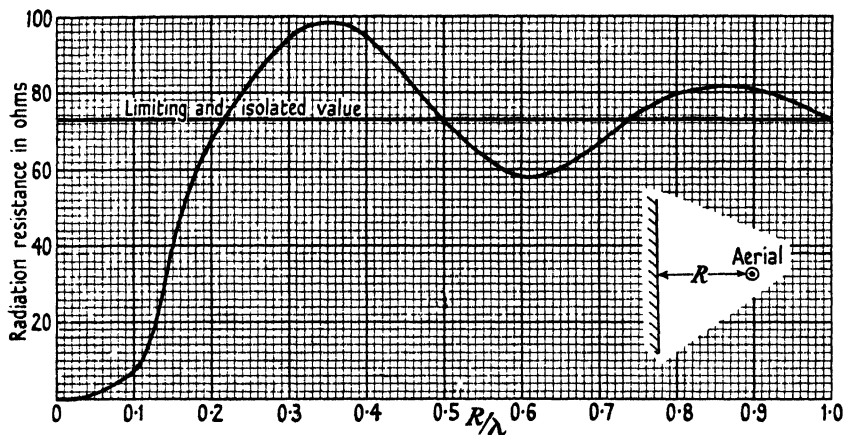


FIG. 4.1. Half-wave aerial in front of infinite sheet.

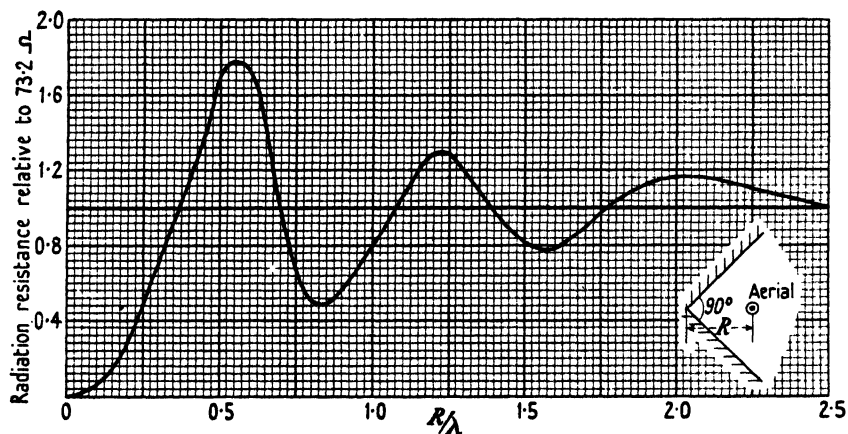


FIG. 4.2. Half-wave aerial in  $90^\circ$  corner.

$45^\circ$  respectively: naturally they are of the same general character as Figs. 3.18–3.21 and should be compared with them. For example, Figs. 3.20 and 4.3 (for  $\beta = 60^\circ$ ) correspond closely in general terms: the only outstanding difference is that the resistance does not fall to small values when the source is a half-wave aerial: this is because the radiation is always considerable at some angle of elevation even though it may be very small in the equatorial plane. It is to be presumed that Figs. 3.17 and 3.19 are a sound guide for the resistance of a half-wave

aerial in a mirror of angle  $120^\circ$  or  $72^\circ$  respectively, provided it is remembered the minima will be much larger than in these figures.

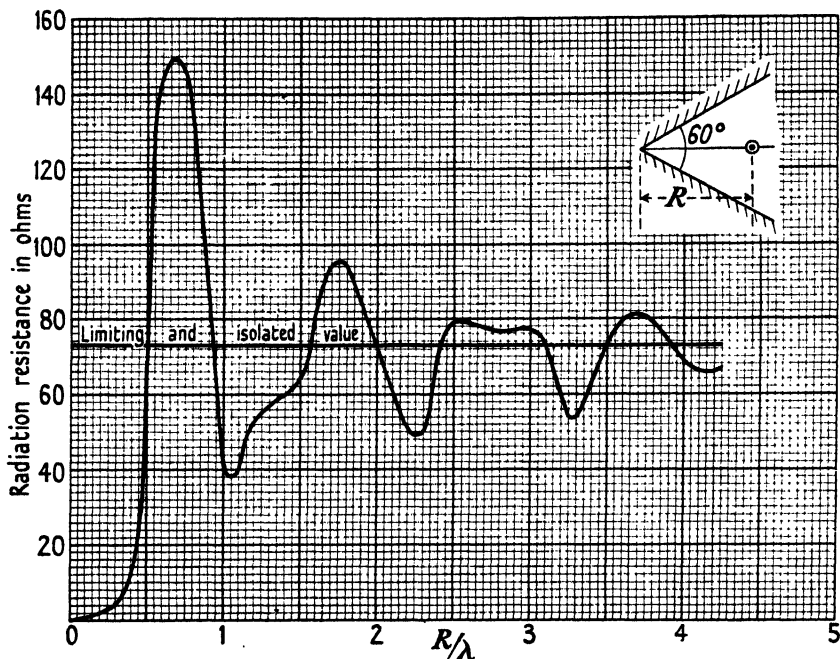


FIG. 4.3. Half-wave aerial in  $60^\circ$  corner.

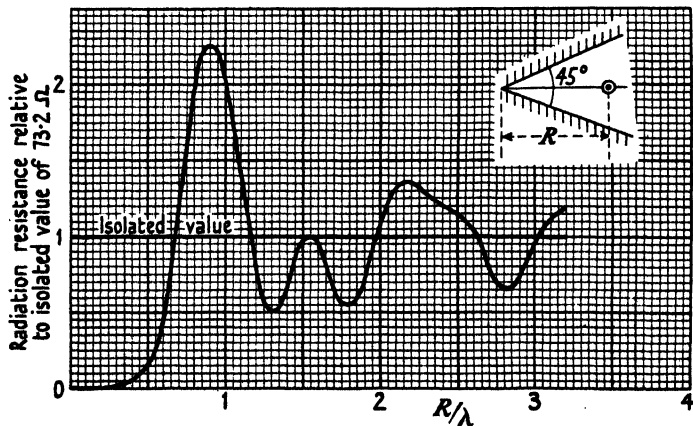


FIG. 4.4. Half-wave aerial in  $45^\circ$  corner.

When  $k$  is very small we can deduce  $E_P$  from the series expansion of equation (1.69) and thus find that the resistance, relative to the isolated value, is equal to  $\frac{1}{4}k^2$  when  $\beta = 180^\circ$  and  $\frac{8}{35}k^4$  when  $\beta = 90^\circ$ , and varies

as  $k^6$  when  $\beta = 60^\circ$ . We conclude that, when  $k$  is small, the relative resistance for  $\beta = \pi/n$  varies as  $k^{2n}$  for all values of  $n$ .

#### 4.4. Power gain as a function of $k$

Figs. 4.5 to 4.8 show the power gain as a function of  $k$  for  $\beta = 180^\circ$ ,  $90^\circ$ ,  $60^\circ$ , and  $45^\circ$ : they are naturally of the same character as Figs. 3.23,

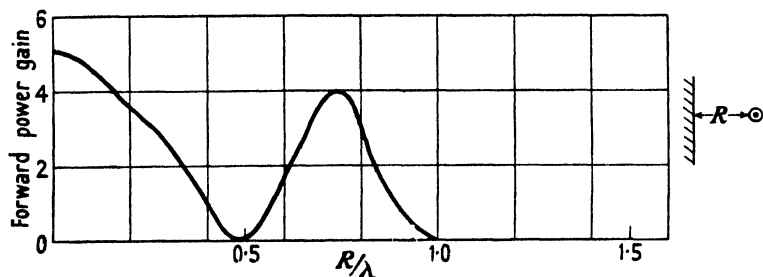


FIG. 4.5. Half-wave aerial in front of infinite sheet.

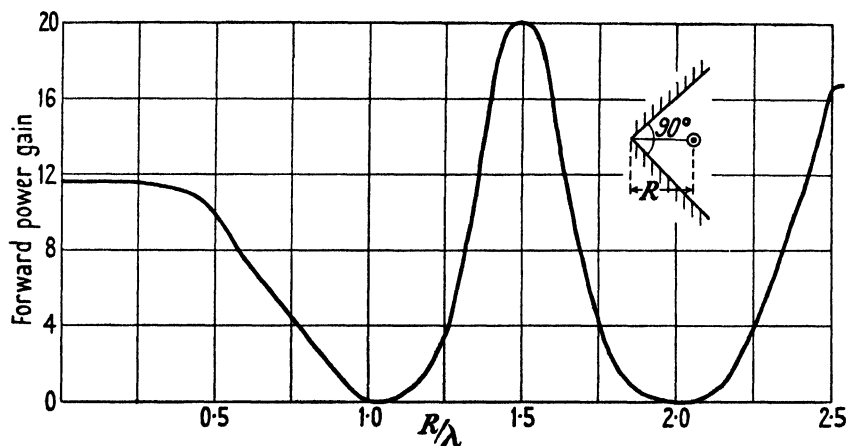


FIG. 4.6. Half-wave aerial in  $90^\circ$  corner.

3.25, and 3.26 and should be compared with them. But in making the comparison it should be recognized that Figs. 4.5–4.8 record power gain relative to a single isolated half-wave aerial, whereas Figs. 3.23, etc., record gain relative to a long isolated in-line array, which may itself have a very large power gain relative to a single half-wave aerial.

Figs. 3.23 and 4.6 correspond in showing that the aerial should be located at  $R/\lambda = \frac{3}{2}$  from the apex of a right-angled reflector; then the gain will be near 20.

There is general correspondence between Figs. 3.25 and 4.7 which relate to a  $60^\circ$  mirror. A long in-line array should be placed at  $R/\lambda = \frac{13}{4}$ ,

but Fig. 4.7 shows that the gain at  $R/\lambda = \frac{13}{4}$  for a single half-wave aerial is the same as at  $R/\lambda = \frac{5}{4}$ . At first sight this seems strange because the main beam must be much sharper when  $R/\lambda = \frac{13}{4}$  than it is when  $R/\lambda = \frac{5}{4}$ , and this suggests a higher power gain—a suggestion

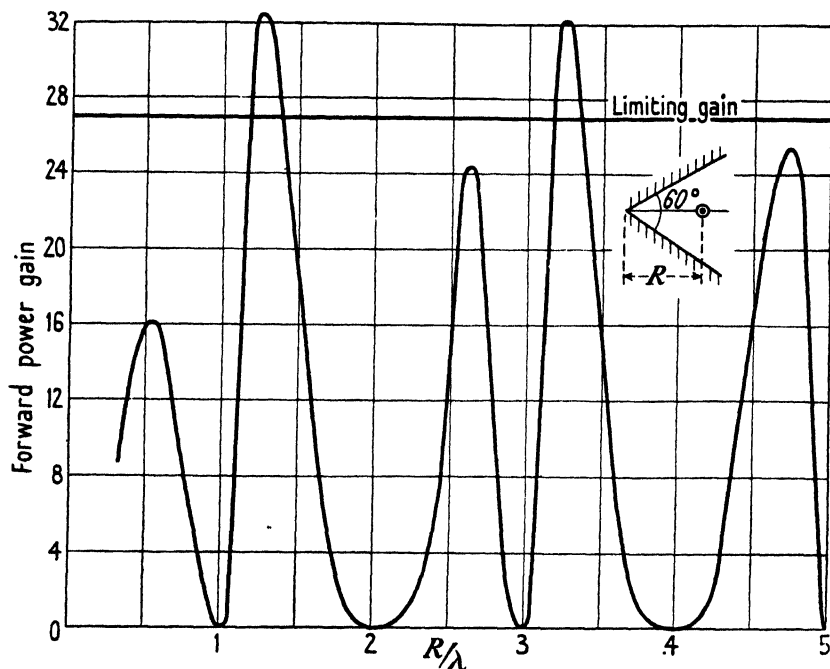


FIG. 4.7. Half-wave aerial in  $60^\circ$  corner.

which is borne out by Fig. 3.25. The diffraction pattern in the equatorial plane for  $R/\lambda = \frac{13}{4}$  is described in § 10.3(d) and reference there will show the main beam is very narrow and the side lobes are small—in fact a very attractive pattern. Why, then, is the power gain for a half-wave aerial no larger when  $R/\lambda = \frac{13}{4}$  than when  $R/\lambda = \frac{5}{4}$ , as would be suggested by the equatorial pattern which (as shown by Fig. 3.25) enhances the power gain in the ratio  $\frac{42}{25}$ ? The reason is that the half-wave aerial produces large beams whose maxima occur at substantial angles of elevation and thus are not disclosed appreciably in the equatorial pattern. Such large and subsidiary beams are vastly suppressed by an in-line array of several members. This discussion will be more clear when we have considered the solid figures of radiation, reproduced in the next section. Meanwhile the reader should learn to recognize what is disclosed by comparison of the family of Figs. 3.23, etc., with the family 4.5, etc. When corresponding stations show an advantage

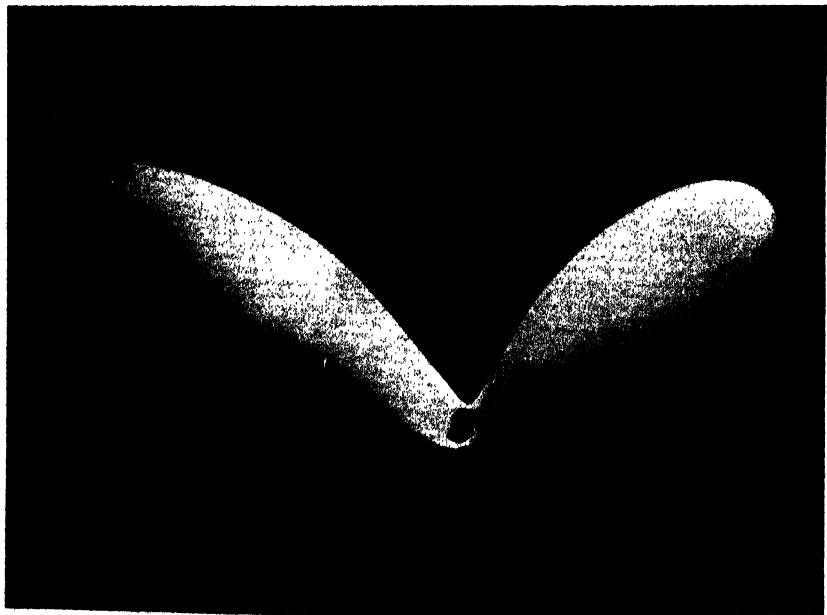


FIG. 4.9.  $R/\lambda = 1$ . Solid model of polar diagram of half-wave aerial distant  $\lambda$  from apex of  $60^\circ$  mirror. Field is strong only at high angles of elevation.

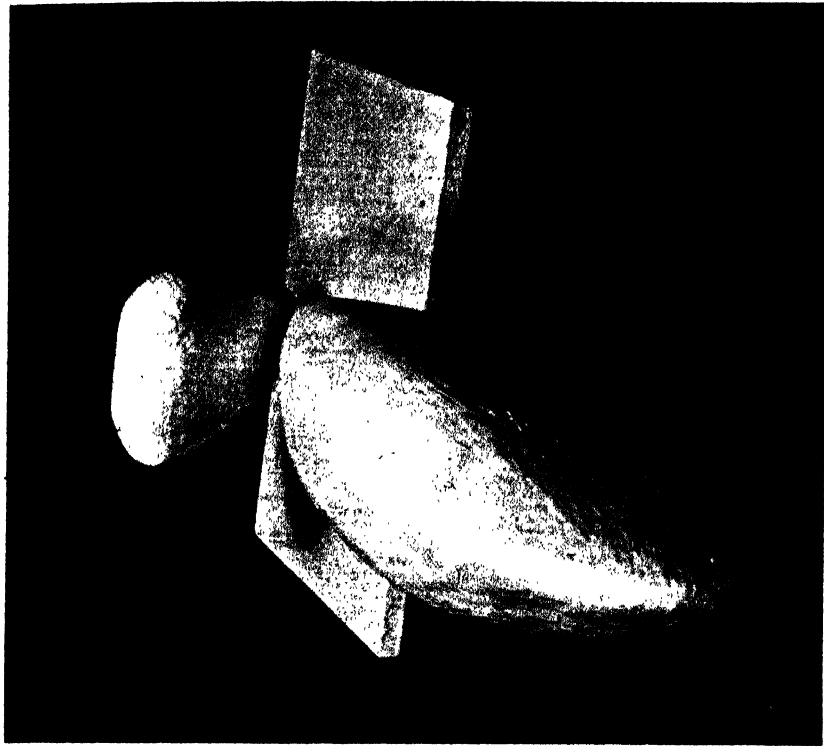


FIG. 4.10.  $R/\lambda = \frac{5}{4}$ . Solid model of polar diagram of half-wave aerial distant  $\frac{5}{4}\lambda$  from apex of  $60^\circ$  mirror. Forward gain 32.

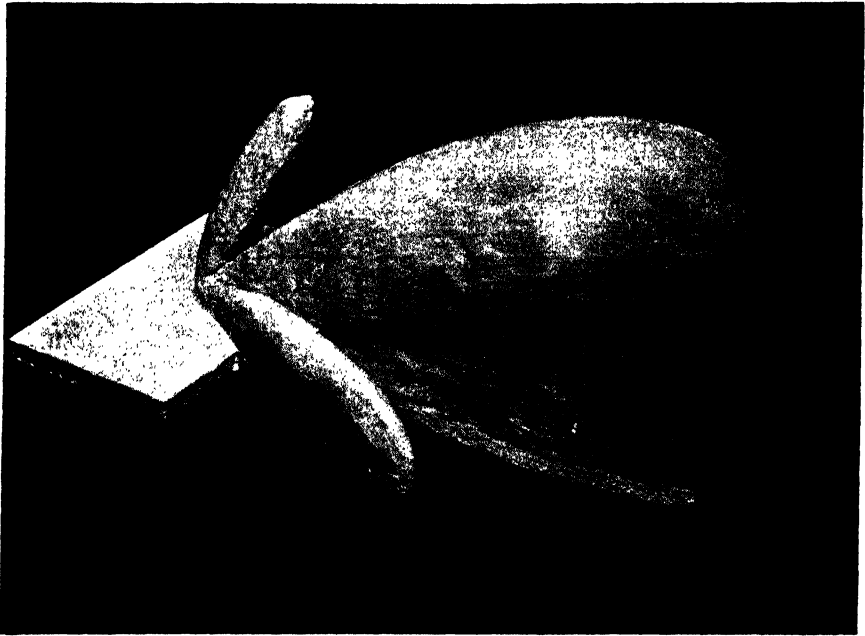


FIG. 4.11.  $R/\lambda = \frac{3}{2}$ . Solid model of polar diagram of half-wave aerial distant  $\frac{3}{2}\lambda$  from apex of  $60^\circ$  mirror. Forward gain 18. Note that field is not at its maximum in equatorial plane.



FIG. 4.12.  $R/\lambda = 3\frac{1}{4}$ . Solid model of polar diagram of half-wave aerial distant  $3\frac{1}{4}\lambda$  from apex of  $60^\circ$  mirror. Forward gain 32. Note large and sharp beams of radiation at high angles, not disclosed by pattern in equatorial plane.

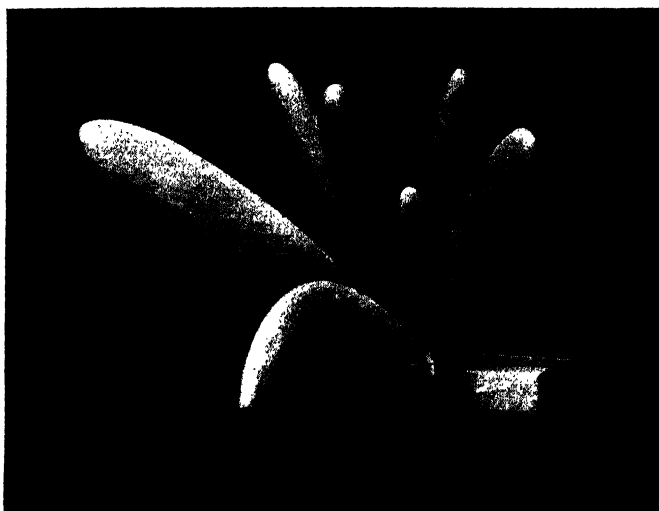


FIG. 4.13.  $R/\lambda = 3\frac{1}{4}$ . Different view of model in 4.12.

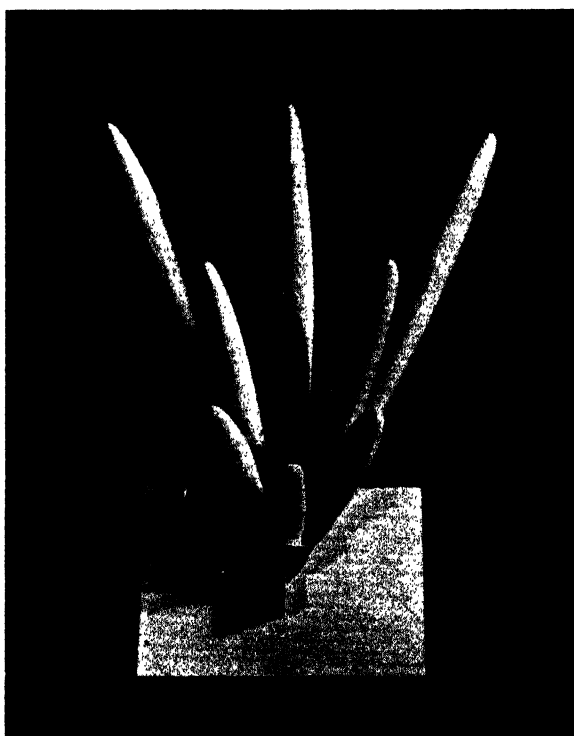


FIG. 4.14.  $R/\lambda = 3\frac{1}{4}$ . Another view of model in 4.12.



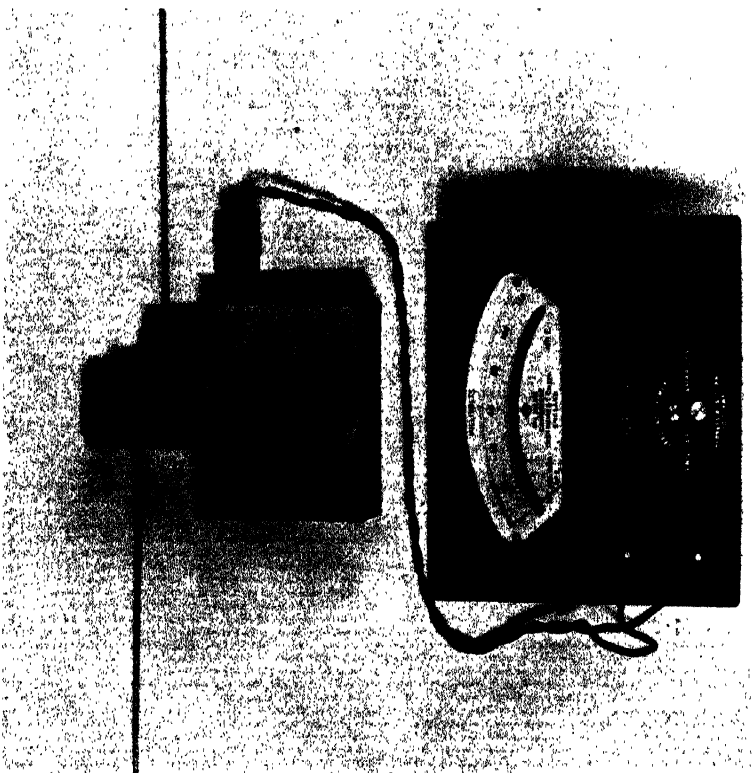


FIG. 9.1.

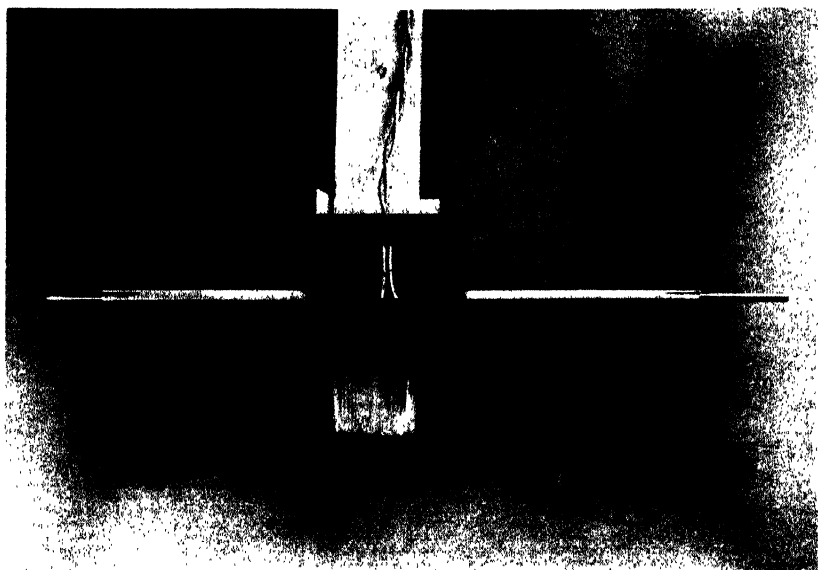


FIG. 9.2.

in the 3.23 family and not in the 4.5 family, then he should realize the outer station is undesirable with a single half-wave aerial because it is associated inevitably with large elevated beams which are not disclosed in the equatorial pattern.

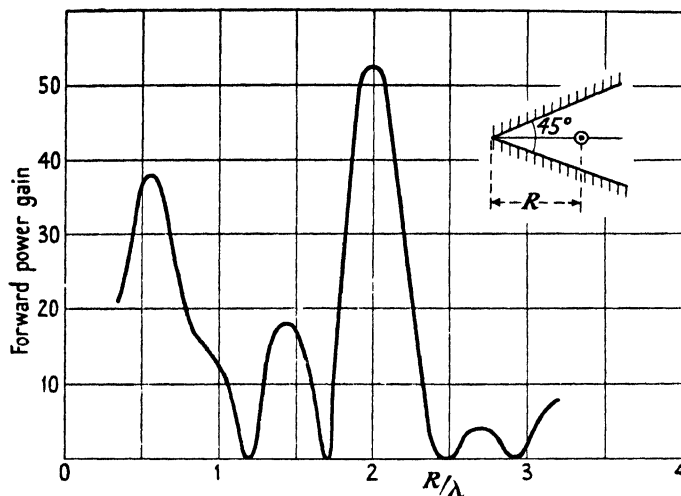


FIG. 4.8. Half-wave aerial in  $45^\circ$  corner.

Fig. 4.8 shows  $G = 52$  when  $R/\lambda = 2$  and  $\beta = 45^\circ$ , however, to attain this gain in practice it would be necessary to use very wide sheets and such would be tolerable only if  $\lambda$  is small.

#### 4.5. Some solid models of radiation figures

We have discussed in detail the shape of the equatorial pattern; but although we have given many formulae for the field on any bearing and angle of elevation, we have not done much evaluation from them. Provided the half-wave aerial is not too far from the apex of the Vee, then the patterns in the two principal planes are a sound guide to the field on any bearing and elevation. But when  $R/\lambda$  is large these two patterns give little guidance as to the field which would be experienced, shall we say, by an aeroplane flying anywhere. The general principle, which is not universally appreciated, can be illustrated well by the simple problem of a half-wave aerial parallel to an infinite flat sheet. Let the reader replace this system in his mind by the aerial and its image and remember that whenever the path difference from any point in space is  $\frac{1}{2}\lambda$  the field will be  $2E_0$ . Let the aerial and its image be separated a considerable distance, say  $40\lambda$ . Then consideration will show that an aeroplane could discover a very large number of points

in space from which the path difference would be  $\frac{1}{2}\lambda$  and an equal number from which this difference would be  $\lambda$ : at such points the field would be  $2E_0$  and zero respectively. Accordingly if a solid polar figure of radiation intensity were made it would be suggestive of a rolled-up hedgehog: the larger the distance of the half-wave aerial from the plane the greater the number of spikes and the sharper they would be. The same sort of thing must occur for a Vee reflector of any angle when the aerial is far away from the apex, though now the spikes will not all have equal length. It is desirable to look at this in another way: we have seen that when  $R/\lambda$  is large the radiation resistance must tend to the isolated value, and accordingly the output from a given current in the aerial then becomes independent of  $R/\lambda$ . It is obvious the width in the equatorial plane of the main beam must become narrower and narrower and this means, by Poynting's theorem, that less and less energy is radiated in it. Since the total radiated energy is constant the number of large narrow beams must increase with  $R/\lambda$ : if they do not appear in either of the two principal planes they must appear in some other plane, producing the effect we have compared to a hedgehog. It is instructive to think of this effect with light, where all radiators are likely to be millions of  $\lambda$  from the reflecting sheets, and to realize that what appears to be uniform light must be composed of millions of shafts with darkness between them. Because all real sources are vast in extent component shafts overlap and blur the effect: moreover, the life of an individual excited molecule is short.

The following figures are photographs of solid radiation figures relating to a half-wave aerial and a  $60^\circ$  mirror. In each of them the axis of the aerial is perpendicular to the table and the reader should think of the reflector standing on the table like a book standing up on edge, with its covers opened to  $60^\circ$ . In all save Fig. 4.9 the model shows only half the figure; there should be a similar 'mirror image' below the table-top. Fig. 4.9 is for the condition  $R/\lambda = 1$ : reference to Fig. 3.11 will show that the forward field is then zero; the equatorial pattern is found to consist of a pair of small and narrow lobes centred on about  $\pm 20^\circ$ . The beam, however, is a large one and directed up into the air (and, of course, also downwards) at an angle of elevation of about  $60^\circ$ . The black spot at the vertex of the model is intended to represent the mouth of a cave or cleft which ultimately narrows to a point: construction of the model made it impossible to hollow out this cave.

It is obvious from Fig. 4.9 that  $R/\lambda = 1$  is the proper station to use when communication is intended to be via the Heaviside layer. Fig.

4.10 relates to  $R/\lambda = \frac{1}{4}$ , which Fig. 4.7 shows is a station for maximum gain, and then  $G = 32$ . The pattern in the equatorial plane is lobe free and the straight sides of the main beam cut the bearing axis at  $\pm 19^\circ$ . In the other principal plane the field falls to zero at an angle of elevation of  $53^\circ$  and rises to a maximum at about  $75^\circ$ . The plate gives a very clear representation of the field and shows it is very small for elevations greater than about  $45^\circ$ , save in a narrow range centred on  $75^\circ$ . Fig. 4.11 is for  $R/\lambda = \frac{3}{2}$ : reference to Fig. 4.7 shows that now  $G = 18$ . The equatorial pattern shows the main beam has narrowed greatly and that two narrow but considerable side lobes have appeared. Reference to Fig. 3.25 will show that as  $R/\lambda$  increases from  $\frac{1}{4}$  to  $\frac{3}{2}$  the gain (reckoned on equatorial pattern) has fallen in the ratio  $\frac{17}{25} = 0.68$ . Why, then, has the gain for a half-wave aerial fallen in the ratio  $\frac{18}{32} = 0.56$ ? The answer is clear from Fig. 4.11 which shows the forward field increases with angle of elevation up to about  $30^\circ$  and that the main beam is narrowest in the equatorial plane. It is interesting to see the side lobes virtually vanish at an angle of elevation of about  $10^\circ$  and so would be perceived only by low-flying aircraft. Compare Fig. 4.10 and Fig. 4.11 as a system for searching for ships. It is true the main beam for  $R/\lambda = \frac{3}{2}$  is narrower than when  $R/\lambda = \frac{1}{4}$  and thus confers greater discrimination; but only at the price of a pair of large lobes which would be liable to give false bearings: the pattern for  $R/\lambda = \frac{3}{2}$  is not tolerable for searching for ships. If it is required to search for aeroplanes flying at an angle of elevation greater than about  $10^\circ$ , then the side lobes cannot give a false bearing because they do not persist above about  $\phi = 10^\circ$ . But above  $\phi = 10^\circ$  the main beam widens considerably and approaches that for  $R/\lambda = \frac{1}{4}$ , and thus there is little, if any, advantage in Fig. 4.11 over Fig. 4.10.

Now consider Figs. 4.12, 4.13, and 4.14, which relate to  $R/\lambda = \frac{13}{4}$ . Reference to Fig. 4.7 shows that now  $G = 32$ , as it did for  $R/\lambda = \frac{1}{4}$ , while Fig. 3.25 shows the gain on the equatorial pattern is 42 as compared with 25. Fig. 4.12 explains the discrepancy: the radiation figure has become a hedgehog. If the system is required for searching for ships, then  $R/\lambda = \frac{13}{4}$  is an excellent arrangement because the main beam in the equatorial plane is very sharp and the side lobes are comparatively small and very sharp. It is a good system for searching for ships and should find practical application: it is not necessary to stress its complete uselessness for searching for aeroplanes.

The practical designer of aerials should study these models long and studiously, for they are very instructive. They are capable of giving his imagination a power of insight and prediction which is of great

value: it can save many mistakes and a vast amount of laborious computation of patterns. There is one further point about Fig. 4.11 which is worth pointing out: when  $R/\lambda = 2$  the forward field is zero and the figure must once more approach that typified by Fig. 4.9; the tendency for this to occur is observable in Fig. 4.11 and is disclosed by the main beam being narrowest in the equatorial plane. The reader should have realized from § 3.8 that the smaller the angle of the mirror the larger must  $R/\lambda$  be before it is possible for a zero to occur in the vertical plane. Thus suppose  $\beta = 30^\circ$ , then the Fourier expression for the pattern is

$$\frac{E}{24E_0F_1} = J_6(k \cos \phi) \cos 6\theta + J_{18}(k \cos \phi) \cos 18\theta + \dots$$

Now  $J_{18}(k)$  is negligible till  $R/\lambda$  exceeds 2 and accordingly the field will be very near zero when  $J_6(k \cos \phi) = 0$ , and for this to be possible  $k \cos \phi \doteq 10$ , thus  $\phi \doteq 40^\circ$  if  $k = 13$ . It should also be noted that if the pattern in the equatorial plane is nearly a sinusoid then it will be much more nearly a sinusoid to an aeroplane flying at a given height and in a circle centred on the aerial.

Having now considered a single half-wave aerial and also an in-line array of infinite length, in a Vee reflector, the reader may wish for some guidance for intermediate cases of a few half-wave aerials in-line. They are very easily dealt with because, as we have seen in Chapter II, the pattern is always expressible as the product of three factors  $F_1 \times F_2 \times F_3$ , these factors having been defined in (2.8), (2.9), etc. The solid models shown in Figs. 4.9–4.14 give a three-dimensional exhibition of the product  $F_1 \times F_2$ . The factor  $F_3$  is merely that for  $N$  in-line members and is typified graphically by Fig. 2.2. It is most important to realize the three-dimensional pattern is the product of *independent* factors. Thus consider Figs. 4.12, 4.13, and 4.14, a hedgehog pattern which is useless in most practical applications. Suppose now there had been four half-wave aerials in line instead of one only. Then by (2.9) the field would be zero at an angle of elevation  $30^\circ$  on all bearings; just because there were four elements in line irrespective of their distance from the apex. The factor  $F_3$  would attain a maximum of value near 0.21, at an angle of elevation near  $60^\circ$ . Now 'operate with  $F_3$ ' on Figs. 4.12 and 4.13. Since the field at  $\phi = 30^\circ$  must be zero on all bearings, the two enormous upward pointing lobes must be suppressed almost completely. The large upward lobe in the forward direction must also be sensibly removed because its maximum is near  $\phi = 45^\circ$ .

There is a small back lobe centred at about  $\phi = 60^\circ$ ; this will be reduced to about 21 per cent. of its size in the Plate. With four in-line members all the lobes not in the equatorial plane will still show some amputated stumps, but not much can be left of them. The radiation figure must be reduced sensibly to the main forward beam shown in the plates. The radiation resistance of each member will be very near (see Fig. 3.20)  $0.44 \times 120 = 53$  ohms, and hence, from Fig. 3.11,

$$G \doteq \frac{(4 \times 5.2)^2 \times 73}{4 \times 53} = 150,$$

a fivefold increase on a single element. It is not surprising the increment should be as much as fivefold because five enormous beams have been suppressed almost completely. Had the  $60^\circ$  Vee been furnished with top and bottom cover plates, also extending to infinity and separated a distance  $\frac{1}{2}\lambda$ , the gain would be enormous and depend on the range: for in such circumstances the field strength would fall off as  $r^{-\frac{1}{2}}$  instead of as  $r^{-1}$  and the comparison has no meaning. But it seems possible that large cover plates of finite size may well increase enormously the gain obtainable from a single aerial.

#### 4.6. Half-wave aerial with axis perpendicular to the junction line of reflecting sheets

This disposition of the aerial with respect to the reflecting sheets is described by Fig. 4.15, which illustrates the particular case for  $\beta = 90^\circ$ . When  $\beta = 180^\circ, 90^\circ, 60^\circ, 45^\circ$ , etc., images can be found and the problem solved. Here, however, there is a marked difference of kind from the disposition in which the aerial was parallel to the sheets. Then the electric field was parallel to the sheet, having zero value at its surface. Now the electric field is perpendicular to the surface of the sheets and is not zero there. It is obvious from Fig. 4.15 that there is no net mutual action between the aerial and those two images which are perpendicular to it: mutual action arises only from the parallel image. Accordingly, for every value of  $R/\lambda$  the radiation resistance is the same as that of an aerial parallel to a flat sheet and also distant  $R$  from it. Likewise it is obvious the forward field in the equatorial plane is that of the aerial and its parallel image only, and hence cannot exceed twice that of an isolated aerial. Hence for

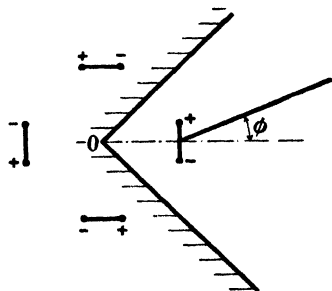


FIG. 4.15.

$\beta = 90^\circ$  and any given value of  $R/\lambda$  the forward power gain is the same as the forward gain of an aerial and flat sheet, and this cannot exceed 4. An observer in the equatorial plane would be unable to tell whether  $\beta$  was  $90^\circ$  or  $180^\circ$ , observers above the equatorial plane would perceive the difference. It is easy to show the equation of the pattern on bearing zero and angle of elevation  $\phi$  is

$$\frac{E}{2E_0} = \sin(k \cos \phi) \cos \phi + \sin(k \sin \phi) \sin \phi. \quad (4.1)$$

If  $R/\lambda = 1/\sqrt{2}$  or  $\sqrt{2}$ , then  $E = 0$  at  $\phi = 45^\circ$ ; hence in these special cases the field is zero at the sheet, and it is possible that then finite

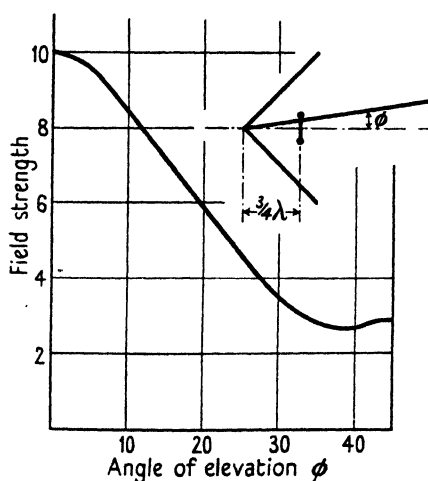


FIG. 4.16. Diffraction pattern.

sheets may produce an effect closer to the ideal than for any other value of  $R/\lambda$ .

There is a notion in common currency that the disposition of Fig. 4.15 is more favourable for suppressing side lobes than that in which the aerial is parallel to the sheets, the argument being that in Fig. 4.15 the lobes are operated on by the 'obliquity effect',  $\cos \phi$  or  $F_1$ .

When expanded in a Fourier series (4.1) becomes

$$\frac{E}{4E_0} = J_1(k) - (J_3 - J_5) \cos 4\phi - (J_7 - J_9) \cos 8\phi - \dots \quad (4.2)$$

This pattern for  $R/\lambda = \frac{3}{4}$  is shown in Fig. 4.16. It will be seen that the field is not zero when  $\phi = \pm 45^\circ$ , which is at the surface of the sheets. The disposition in Fig. 4.16 with  $\beta = 90^\circ$  is not of much practical

interest because  $G$  cannot exceed 4, whereas it can reach 20 if the aerial is parallel to the sheets and  $R/\lambda = \frac{3}{2}$  (see Fig. 4.6). The reason for the small gain follows readily from Poynting's theorem. According to the description of that theorem the gain will be large if the area on the circumscribing sphere is small where it is bathed by the radiation of high intensity, and this is in the equatorial plane. In the parallel disposition only one-quarter of the equatorial belt is so bathed, whereas in the perpendicular direction half of it is bathed. The writer is not aware of the perpendicular disposition having been used in Vees of small angle, and he leaves  $\beta = 60^\circ, 45^\circ$ , etc., as an exercise to the reader. In his opinion it is not a proper disposition for a half-wave aerial in a Vee: the Vee is used properly only when the aerial is parallel to the sheets.

#### 4.7. Frequency consciousness of aerials in Vee reflectors

It is sometimes desired to operate an aerial system over a band of wavelength which varies by some  $\pm 25$  per cent. from the mean. Then it is necessary to understand the effect which a change of wavelength will have on the equatorial pattern and the radiation resistance. First consider aerials parallel to the sheet. If  $R/\lambda$  is such that the width across the Vee at the aerial is less than  $\lambda$ , then, as we have emphasized, the equatorial pattern is sensibly a sine curve bounded by the sheets. Hence if  $R$  is such that the forward field does not fall to its first zero in the required range of  $\lambda$ , then that range of  $\lambda$  can have scarcely any effect on the equatorial pattern, in this respect the aerial is frequency unconscious. Suppose, for example,  $\beta = 30^\circ$ : we have given many numerical examples to show the pattern is always a sine curve until  $R/\lambda$  exceeds about 2.2. If then  $R/\lambda$  is less than 2.2 within the whole range of  $\lambda$ , the pattern is frequency unconscious, and no more need be said about the pattern. Reference to Figs. 4.2–4.4 will show that a small change of  $R/\lambda$  can cause a large change of radiation resistance, and therefore provision must be made for wide adjustment of the matching transformer between the aerial and the cable.

If  $\beta = 90^\circ$  and the aerial is in the perpendicular position, then the two principal patterns are likely to be very conscious of frequency, because the forward field goes through zero when  $R/\lambda$  goes through the values 0.5, 1, 1.5, etc., and thus a range of  $\pm 25$  per cent. in  $\lambda$  is bound to bring  $R/\lambda$  near one of these values. The whole problem of frequency consciousness should be straightforward to readers who have understood this and the previous two chapters.



### 4.8. Line doublets in Vee reflectors

The three-dimensional problem of a doublet in a Vee reflector is too cumbersome to justify solution, but the two-dimensional problem of a line doublet in a Vee is not unduly complex and is of practical interest, since we can use it to simulate a wide curtain array of half-wave elements. We will solve it in stages.

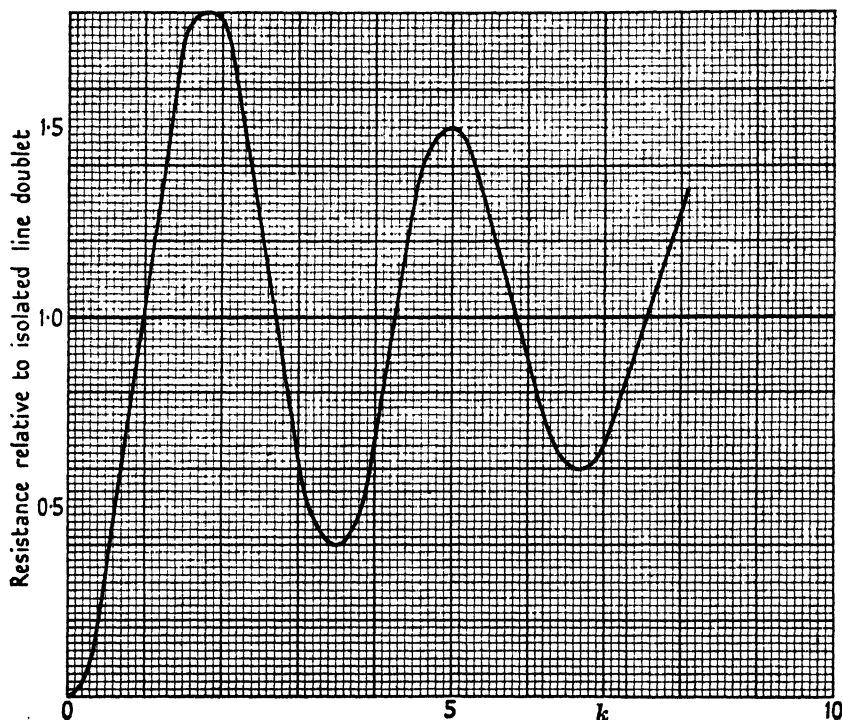


FIG. 4.17. Line doublet parallel to flat sheet.

(a) *Line doublet parallel to an infinite conducting sheet*

From (1.58) we have, for an isolated line doublet,

$$-\frac{cE_t}{a\pi Il} = \cos \phi \left[ \left\{ -\frac{J_1(ar)}{ar} + J_0(ar) \right\} - j \left\{ -\frac{Y_1(ar)}{ar} + Y_0(ar) \right\} \right]. \quad (1.58)$$

Let the doublet be parallel to the sheet and distant  $R$  from it. The inphase component of electric field at the doublet is then found to be

$$\begin{aligned} -\frac{cE_P}{a\pi Il} &= \frac{1}{2} - J(2k) + \frac{J_1(2k)}{2k} \\ &= \frac{3k^2}{4} \left( 1 - \frac{5}{18}k^2 \right), \quad \text{when } k \rightarrow 0. \end{aligned} \quad (4.3)$$

The forward field is  $2\sin k$  times that of an isolated line doublet, and so the power gain relative to an isolated line doublet is, when  $k$  tends to zero,

$$G = \frac{4 \sin^2 k \times \frac{1}{2}}{(\frac{3}{4}k^2)(1 - \frac{5}{18}k^2)} \div \frac{8}{3} \left(1 - \frac{k^2}{18}\right). \quad (4.4)$$

Figs. 4.17 and 4.18 show respectively the radiation resistance and forward power gain for a line doublet parallel to an infinite conducting

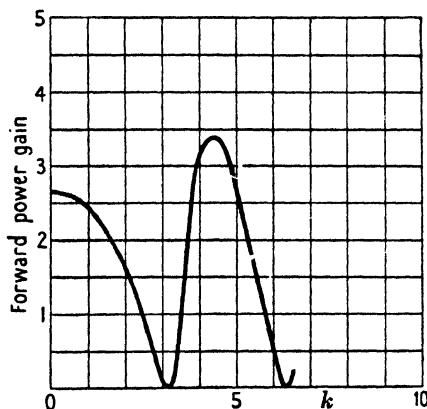


FIG. 4.18. Line doublet parallel to flat sheet.

sheet: the gain rises to a maximum of about 3.3 near  $R/\lambda = \frac{3}{4}$  and then the radiation resistance is about 20 per cent. greater than the isolated value. Doubtless this figure is substantially valid for a wide curtain of half-wave elements, and accordingly the resistance per member is, by § 2.16, about  $53 \times 1.2 = 64$  ohms, and the maximum gain would be near  $4.5N$ .

The complete solution of the fields can readily be obtained. In § 1.11 we saw that the vector potential of a line doublet was given by

$$-\frac{cA}{\pi I \delta l} = Y_0(ar) + J_0(ar)$$

and was everywhere parallel to the blade. Hence, by § 1.13, for two unlike and parallel doublets

$$-\frac{cA}{4\pi I \delta l} = \{Y_1(ar) + jJ_1(ar)\}J_1(k)\cos\theta + \{Y_3(ar) + jJ_3(ar)\}J_3(k)\cos 3\theta + \dots,$$

where the origin is midway between them and  $A$  is everywhere parallel to the two blades. The magnetic field is everywhere perpendicular to

the plane of the paper and  $H = \frac{1}{r} \frac{\partial A}{\partial \theta}$ , and accordingly

$$\frac{cH}{4a\pi I \delta l} = \frac{1}{ar} [\{Y_1(ar) + jJ_1(ar)\}J_1(k) \sin \theta + \{Y_3(ar) + jJ_3(ar)\}J_3(k) \sin 3\theta + \dots]. \quad (4.5)$$

(b) *Line doublet referred to any origin*

By proceeding as in § 1.12 we have, for two parallel like doublets,

$$\frac{cH}{2a\pi Il} = \{Y'_0(ar) + jJ'_0(ar)\}J_0(k) + 2\{Y'_2(ar) + jJ'_2(ar)\}J_2(k) \cos 2\theta + \dots$$

On superposing a like and an unlike pair of doublets we obtain the solution for a single line doublet referred to any origin in its equatorial plane. Addition will give  $H$  for any number of doublets placed at intervals round a circle of radius  $R$ , and from this the two components of electric field can be derived. Then if any radial planes exist in which  $E_r$  is zero a conducting sheet can be placed in such planes: we shall not develop a general solution here.

#### 4.9. An aerial in a rectangular wave guide

In § 1.20 we derived the main features of the solution for a long filament midway between two parallel conducting sheets. We now see this is the limiting case of a Vee reflector in which  $\beta = 0$  and  $k$  tends to infinity. It is usual to call such a system a rectangular wave guide and unusual to regard the wave guide as the limiting case of a Vee, though logical for us to do so here and to treat it purely as an aerial. In practice, sheets of finite width produce a pattern very near the ideal for infinite width; but the smaller  $\beta$  the wider must the sheets be. If  $\beta = 0$  no width of sheet suffices to produce a parallel beam; and Vee reflectors of very small angle have no practical interest as reflectors for an aerial. If the sides are parallel, then the pattern is improved by expanding the width near the open end. Then it is natural to regard the expanded part as the reflector and the parallel part as a pipe leading the energy flow to the ultimate reflector. It is a natural, practical, though not very logical description. It is a remarkable fact of practical experience that right-angled bends in the parallel portion make very little difference to the final result and this extraordinary property lends colour to the pipe conception. Thus the originating aerial need not be optically visible from the final Vee, or horn as it is commonly called. So far it has not been discovered how to treat the bends in analysis. We can, however, solve an aerial in a parallel rectangular pipe of

infinite length and we could now fill in more practical details of the solution which has been outlined in Chapter I.

If the width of the pipe is  $g$  then, as we have seen,  $g/\lambda$  must be at least  $\frac{1}{2}$ , or the inphase component of field is zero at the aerial, and accordingly its output is zero. When  $g/\lambda = \frac{1}{2}$ , then  $E_p$  is infinite, and accordingly it will in practice not be possible to get any current in the filament.

We will not develop the whole matter here but refer the reader for it to *Journal I.E.E.* 92 (1945), Part III, p. 8. Fig. 4 in it relates radiation resistance of the filament with  $g/\lambda$  and thus is a curve of the same general type as the series 3.17–3.21. Sections (4) and (5) of the same paper explain the process of obtaining the solution for a wave guide as the limit of the solution for a Vee reflector.

## THE SEMI-INFINITE SHEET: NETWORK REFLECTORS

### 5.1. Introduction

IN the last two chapters the reflecting sheets have extended to infinity. We are studying these problems only in the hope of applying their solutions to sheets which are only a few wavelengths wide, and therefore we badly need general guidance about the effect of finite width. Such guidance is given by putting  $n = \frac{1}{2}$  in the general expressions and thereby obtaining the solution for a semi-infinite sheet, or half-plane (see Fig. 3.4c). The reader may perhaps inquire why all such questions are not left to be answered by experiment: in the main they must be left to experiment, but it is a great help to have at least one precise analytical solution, since it will serve as a guide and save much blind experimentation and piling up of numerous experimental curves which can scarcely be interpreted. Analysis does show quantitatively the rate of approach to the limit, and such rate of approach is often very difficult to deduce by experiment. Not only do we need to know the performance in practice of a sheet of given width, but we also need to be able to estimate how much that performance would be improved by a given increment of width. The size of aerials is always largely governed by a variety of factors and expediciencies which are unrelated to its scientific and technical design: the technical designer needs always to be able to assess quickly the cost to the performance of having to make some surrender to the demands of constructional expediency. The solution of the half-plane is a valuable guide in this respect.

### 5.2. Long current filament in the presence of a half-plane

This solution is obtained by putting  $n = \frac{1}{2}$  in the equation leading to (3.20), and we have

$$\begin{aligned} \frac{cE}{2\pi aI} = & \{-J_1(ar) + jY_1(ar)\}J_1(k)\cos\frac{1}{2}\alpha\cos\frac{1}{2}\theta + \\ & + \{-J_1(ar) + jY_1(ar)\}J_1(k)\sin\alpha\sin\theta + \\ & + \{-J_1(ar) + jY_1(ar)\}J_1(k)\cos\frac{3}{2}\alpha\cos\frac{3}{2}\theta + \dots \quad (5.1) \end{aligned}$$

This describes the field at the point  $(r, \theta)$  due to a filament at the point  $(R, \alpha)$ , the origin being at the edge of the semi-infinite sheet. When  $ar$  tends to infinity this takes the form

$$\begin{aligned} -E/2E_0 = & \epsilon^{j\pi/4}J_1(k)\cos\frac{1}{2}\theta + \epsilon^{2j\pi/4}J_1(k)\sin\alpha\sin\theta + \\ & + \epsilon^{3j\pi/4}J_1(k)\cos\frac{3}{2}\theta + \epsilon^{4j\pi/4}J_2(k)\sin 2\alpha\sin 2\theta + \dots \quad (5.2) \end{aligned}$$

The main use here of (5.2) is to trace the change in the polar diagram as a filament, at a given distance from a sheet, approaches the edge. Thus suppose the distance from the sheet is  $\frac{1}{4}\lambda$  and that the filament

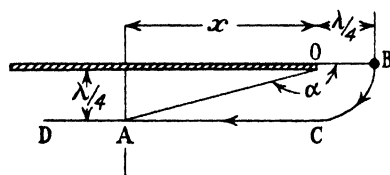


FIG. 5.1.

is moved in the manner indicated by Fig. 5.1, starting at  $B$ , round the semicircular arc  $BC$  and then along the line  $CD$ ,  $\alpha$  increasing from zero to  $\pi$  in the process. When  $x$  tends to infinity the equation of the

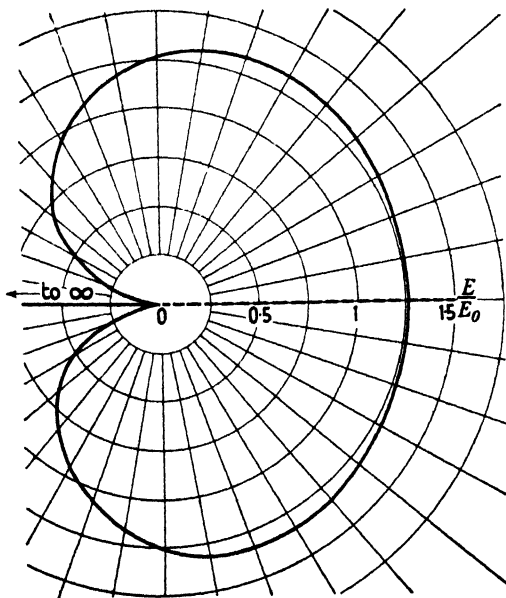


FIG. 5.2. Polar diagram for current filament distant  $\frac{1}{4}\lambda$  from edge of semi-infinite sheet and in plane of sheet.

diagram becomes  $E/2E_0 = \sin(\pi \cos \theta)$ , where  $\theta$  is measured from the normal. Equation (5.2) has been evaluated for  $\alpha = 0^\circ, 45^\circ$ , and  $90^\circ$  and also for  $x/\lambda = 0.407, 1.086$ , and  $2.215$ . To simplify computation, integral values of  $k$  have been used, and this leads to values of  $x/\lambda$  which are not integral: the values chosen for  $k$  correspond approximately with  $x/\lambda = \frac{1}{2}, 1$ , and  $2$ . Figs. 5.2-5.7 show the polar diagrams for these

positions and illustrate very beautifully the reflecting effect of a semi-infinite sheet. Fig. 5.8 superposes Fig. 5.6 on the diagram for  $x$  infinite:

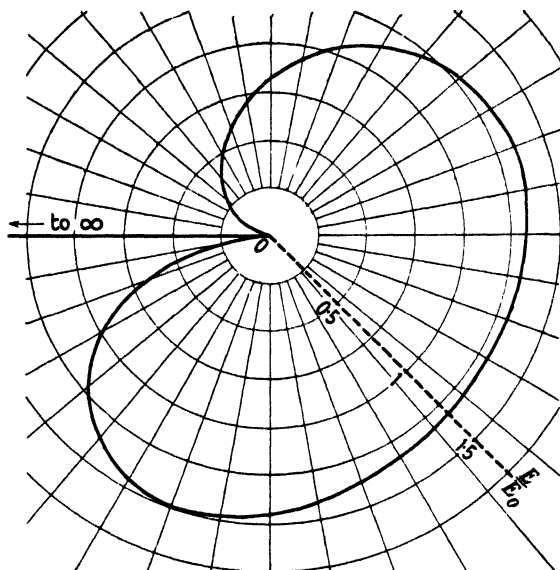


FIG. 5.3. Polar diagram for semi-infinite flat sheet, aerial at  $(\frac{1}{4}\lambda, 45^\circ)$

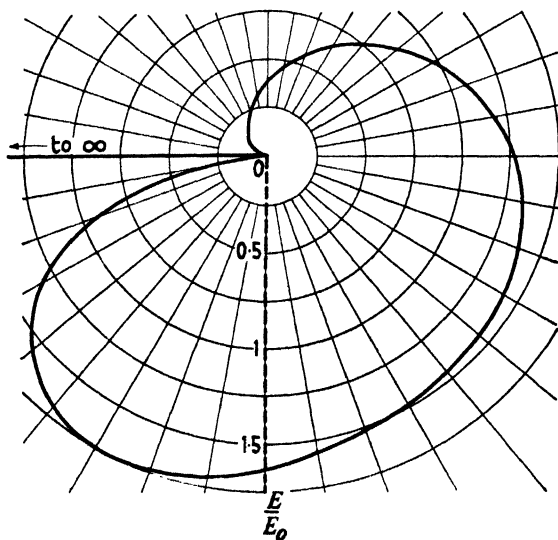


FIG. 5.4. Polar diagram for semi-infinite flat sheet, aerial at  $(\frac{1}{4}\lambda, 90^\circ)$ .

it may be seen that the left-hand halves of the two diagrams are indistinguishable and the right-hand halves differ only in that  $x = 1.09\lambda$

permits a small amount of diffraction round the edge of the sheet and also slightly sharpens the beam. The difference between Figs. 5.4 and 5.5 is very marked: that between Figs. 5.5 and 5.6 is not very marked.

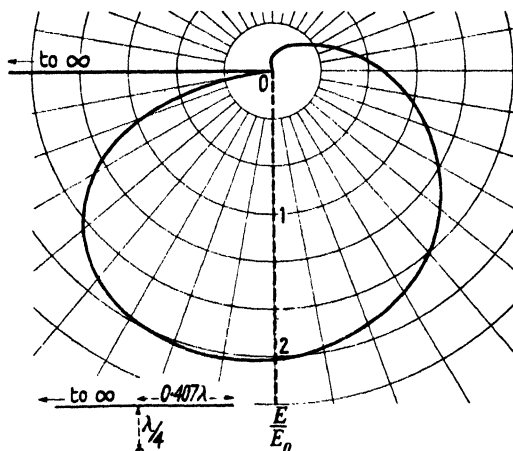


FIG. 5.5. Polar diagram for aerial distant  $\frac{1}{4}\lambda$  from semi-infinite flat sheet.

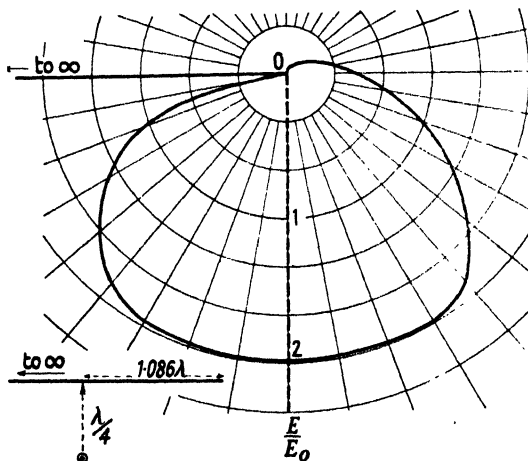


FIG. 5.6. Polar diagram for aerial distant  $\frac{1}{2}\lambda$  from semi-infinite flat sheet.

These three diagrams show it is enormously worth while to set back the aerial about  $\frac{1}{2}\lambda$  from the edge of the reflector, but thereafter the approach to the limit is very slow. It is very encouraging to find that when  $x/\lambda$  is even as small as  $\frac{1}{2}$  the pattern is not very different from that appropriate to an infinite sheet. Surely this tells us that sheets of very moderate width will give a performance approximating closely to the ideal limits we have studied in Chapters III and IV. We see



that increasing  $x/\lambda$  from  $\frac{1}{2}$  to 2.2 does not improve the performance very substantially: this shows the limit is not approached exponentially

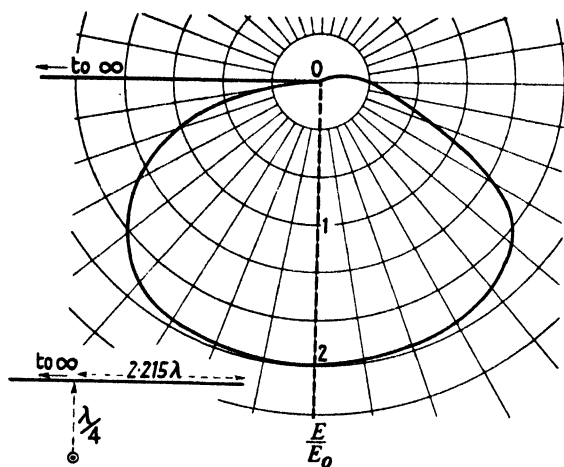


FIG. 5.7. Polar diagram for aerial distant  $\frac{1}{4}\lambda$  from semi-infinite flat sheet.

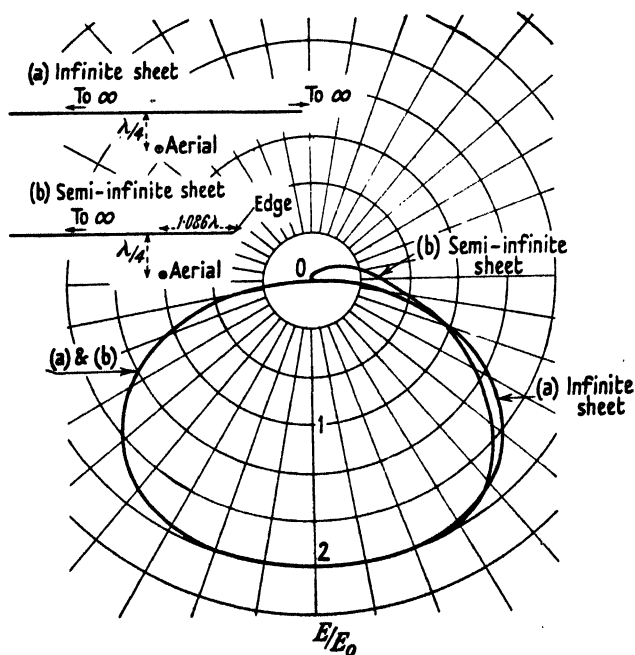


FIG. 5.8. Comparison of diffraction patterns of infinite and semi-infinite plane sheets: aerial distant  $\frac{1}{4}\lambda$  from sheets, and  $1.086\lambda$  from bounding edge in case of semi-infinite sheet.

and should tell the practical designer, without experiment, that an extravagant increase of width cannot be expected to reduce appreciably

a comparatively small diffraction round the edge. Fig. 5.9 shows the calculated diagram for a filament distant  $\frac{1}{10}\lambda$  from the sheet and with  $x/\lambda = 0.63$ : the left-hand half of this diagram differs insensibly from the limit and the two halves are not markedly dissimilar.

If the sheet were doubly infinite the field would be zero in its plane (i.e. on bearing  $\theta = 0$ ); when it is a half-plane the field on  $\theta = 0$  cannot

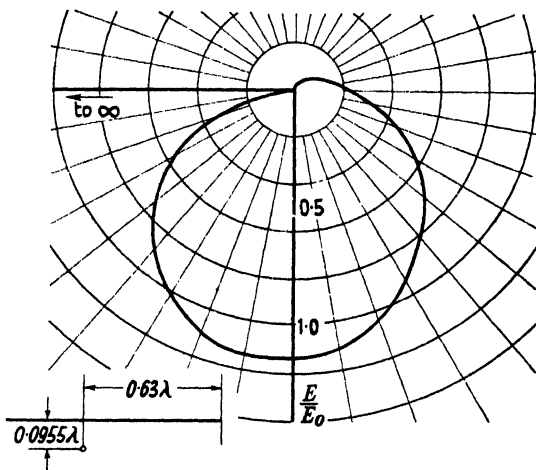


FIG. 5.9. Polar diagram for aerial distant  $\frac{1}{10}\lambda$  from semi-infinite flat sheet.

be zero because there must be some field behind the sheet. It may be found from Figs. 5.2–5.8 that the field on  $\theta = 0$  is expressed very closely by the empirical formula  $1.6|H_0(x/\lambda)|$ ; from this it would seem that  $x/\lambda$  must exceed 100 before the field at a distant point in the plane of the sheet is reduced to 5 per cent. of the field along the normal to the plane. This example illustrates forcibly the diminishing returns which must be expected to accrue from increasing the width of reflecting sheets.

For  $d/\lambda = \frac{1}{4}$ , the ‘front-to-back’ ratio is 24, 86, 156, and 200 when  $x/\lambda = 0.48, 1.09, 1.52$ , and  $2.22$  respectively. We conclude it is well worth while to make  $x/\lambda = 1$ , but scarcely worth while to make it exceed unity appreciably. If  $d$  is the shortest distance from the aerial to the sheet, we find that when  $x/d$  is constant and equal to  $\frac{5}{8}$  ( $\alpha = 143^\circ$ ) then the ‘back-to-front’ ratio is 0.195, 0.125, and 0.77 when  $d/\lambda = 0.048, 0.096$ , and  $0.25$  respectively: showing that, for a given configuration, the backward field increases as  $\lambda$  increases. In other words, it is more important that  $x/\lambda$  should be comparable with unity than that  $x/d$  should be large.

When  $d/\lambda = \frac{1}{4}$  and  $x$  is infinity the radiation resistance is

$$1 - J_0(\pi) = 1.304$$

relative to an isolated in-line array (i.e. 157  $\Omega$  per member). When  $\alpha = 0, 45^\circ$ , and  $90^\circ$  it may be found this ratio is 1.179, 1.198, and 1.242 respectively and when  $x/\lambda = 2.85$  it is 1.311. Thus it is clear the radiation resistance depends little on  $x/\lambda$  so long as this ratio exceeds zero. Mere inspection of Figs. 5.6–5.8 should show that the power gain differs little from the limiting value (3.06) so long as  $x/\lambda$  exceeds unity: indeed there may be some value of  $x/\lambda$  for which the gain slightly exceeds the ultimate limit. Computation shows that for  $d/\lambda = 0.1$  and  $x/\lambda = 0.13$  the resistance is 0.997 of what it would be if  $x$  were infinite. Equation (5.2) is very laborious to evaluate, but the series can be summed in certain special cases: thus the particular case  $\alpha = 0$  and  $\theta = 0$  was summed in § 3.5 (b); it is the forward field curve

$$\left| \frac{E}{E_0} \right| = \sqrt{2} (P^2 + Q^2)^{\frac{1}{2}},$$

the equation of the famous Cornu spiral, and where  $P$  and  $Q$  are Fresnel's integrals.

If  $\alpha = 0$  and  $\theta = \frac{1}{2}\pi$ , we have

$$\begin{aligned} -\frac{E}{E_0} &= [J_{\frac{1}{2}}(k) + J_{\frac{3}{2}} + J_{\frac{5}{2}} + \dots + j\{J_{\frac{1}{2}}(k) - J_{\frac{3}{2}}(k) + J_{\frac{5}{2}} - \dots\}] \quad (5.2a) \\ &= \frac{1}{2} \left[ \int_0^k J_{-\frac{1}{2}}(k) dk + \int_0^k J_{\frac{1}{2}}(k) dk + j \left\{ \int_0^k J_{-\frac{1}{2}}(k) dk - \int_0^k J_{\frac{1}{2}}(k) dk \right\} \right], \end{aligned}$$

since 
$$\int_0^z J_n(z) dz = 2(J_{n+1} + J_{n+3} + \dots).$$

$$\begin{aligned} \therefore \left| \frac{E}{E_0} \right| &= \frac{1}{\sqrt{2}} \left[ \left\{ \int_0^k J_{-\frac{1}{2}}(k) dk \right\}^2 + \left\{ \int_0^k J_{\frac{1}{2}}(k) dk \right\}^2 \right]^{\frac{1}{2}} \\ &\doteq \left\{ 1 + \frac{1}{\pi k} - \frac{2}{\sqrt{(\pi k)}} \cos(k + \tfrac{1}{4}\pi) \right\}^{\frac{1}{2}}, \quad \text{when } k \text{ is large.} \quad (5.2b) \end{aligned}$$

This is similar in form to the equation for the forward field, save that now the wavelength of the ripple is  $\lambda$  where previously it was  $\frac{1}{2}\lambda$ . It shows that when  $k$  is large the field on  $\theta = \pm \frac{1}{2}\pi$  tends to equal the forward field and that  $|E/E_0|$  tends to unity. Reference to Fig. 5.2 shows that when  $k = \frac{1}{2}\pi$  the forward field happens to equal that on  $\theta = \frac{1}{2}\pi$ , but that  $E/E_0 = 1.25$ . When  $k$  is very small, equations (5.2)

and (5.2*a*) show the forward field tends to be  $\sqrt{2}$  times the field on  $\theta = \pm \frac{1}{2}\pi$ . Exact evaluation shows this ratio is 0.70 and 0.74 when  $k = \frac{1}{2}$  and 1 respectively. The reciprocity theorem shows that we have also found an expression for the field on bearing zero for a filament at  $\alpha = \frac{1}{2}\pi$ : comparison of Figs. 5.2 and 5.4 shows the field on  $\theta = \frac{1}{2}\pi$  in Fig. 5.2 equals the field on  $\theta = 0$  in Fig. 5.4, and thus confirms this statement. We note, however, the field in the direction  $\frac{1}{2}\pi$  in Fig. 5.4 is much larger than the forward field in Fig. 5.2—because the sheet in Fig. 5.4 is much better able to reflect than when it is edge on, as in Fig. 5.2.

Now make  $\alpha = \frac{1}{2}\pi$  and  $\theta = \pm \frac{1}{2}\pi$ , thus giving the forward and backward field for a filament level with the edge of a semi-infinite sheet and at any distance from it. Now (5.2) becomes

$$-\frac{E}{2E_0} = \frac{1}{2\sqrt{2}} [J_1(k) - J_3 - J_5 + \dots + j\{J_3 + J_5 - J_7 - \dots\}] \pm j\{J_1(k) + J_3 + J_5 + \dots\}.$$

$$\therefore -\frac{E}{E_0} = \frac{1}{2} [P(\cos k - \sin k) + Q(\cos k + \sin k) + j\{P(\cos k + \sin k) + Q(\sin k - \cos k)\}] \pm j \sin k, \quad (5.2c)$$

where  $P \equiv \frac{1}{2} \int_0^{2k} J_{-1}(2k) d(2k)$ . It should be noted that the portion of this expression in square brackets is half the forward field for  $\alpha = 0$  and that the portion  $j \sin k$  is half the forward field for a doubly infinite sheet. Moreover, comparison of (5.2) and (3.22) shows the series involving  $J_1$  and  $J_3$  is the same as that which arises on putting  $n = 1$  in (3.22), for all values of  $\alpha$  and  $\theta$ : hence a component of the pattern for a semi-infinite sheet is always the pattern for a doubly infinite sheet. When  $2k$  is large,  $P = Q = \frac{1}{2}$  and then

$$-\frac{E}{E_0} = \frac{1}{2} \{\cos k + j(1 \pm 2)\sin k\} \quad \text{or} \quad \frac{|E|}{E_0} = \frac{1}{2}(1 + 8 \sin^2 k)^{\frac{1}{2}}. \quad (5.2d)$$

Hence the forward field fluctuates between  $\frac{3}{2}E_0$  and  $\frac{1}{2}E_0$  and the backward field equals  $\frac{1}{2}E_0$ . When  $k = \frac{1}{2}\pi$ , Fig. 5.4 shows the forward field is  $1.64E_0$ , whereas it would be  $2E_0$  for a doubly infinite sheet, and the front-to-back ratio is 4.1. It has been found that when  $k = 1$  the forward field is  $1.11E_0$  ( $1.68E_0$  for doubly infinite) and the front-to-back ratio 5.5: for  $k = \frac{1}{2}$  these magnitudes are  $0.7E_0$  ( $0.98E_0$  for doubly infinite) and 2.5 respectively. We have been calculating the field at infinity due to a current filament not far from the sheet: we should remember the

reciprocal theorem tells us the filament and observation point are interchangeable, but defer this aspect till Chapter VII.

### 5.3. Curtain array parallel to a half-plane

If the sheet is finite there will be some field on the side behind the aerial and hence there must be some field in the plane of the half-sheet whether or not field would exist on this bearing if the half-plane were

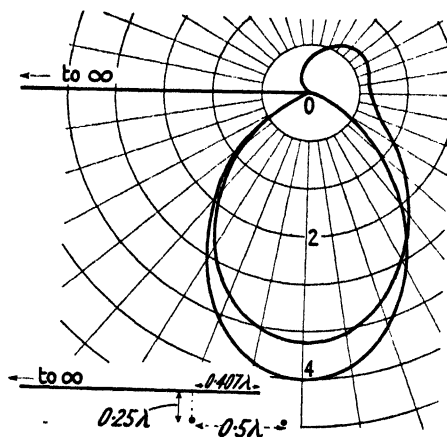


FIG. 5.10. Two aerials,  $0.5\lambda$  apart,  $0.25\lambda$  from semi-infinite plane sheet. (Overlapping bounding edge.)

absent. If a curtain with an even number of members has  $\frac{1}{2}\lambda$  spacing, the field in its plane is zero; but it cannot be zero in this plane if the curtain is parallel to a finite reflecting sheet. This feature is well illustrated in Fig. 5.10, which shows the pattern resulting from two parallel filaments  $\frac{1}{2}\lambda$  apart, parallel to and distant  $\frac{1}{4}\lambda$  from a half-plane disposed as shown in the inset diagram: the superposed symmetrical diagram shows the corresponding polar diagram for a doubly infinite sheet. The diffraction round the bounding edge is apparent, and the field in the plane of the bounded sheet is 0.24 of the forward field. In spite of the gross inadequacy of this reflector, in which one member is actually about  $0.1\lambda$  beyond the edge, the forward field is 0.86 of the ultimate limit. It is apparent that sheets of very moderate dimensions must produce a forward field nearly as great as the ideal upper limit, though they cannot be expected to make the diffracted field in the plane of the sheet very small. The pattern has been computed for two currents distant  $\frac{1}{4}\lambda$  from the sheet and situated at  $x/\lambda = 1.09$  and  $1.59$ : it was indistinguishable from the ideal in the range  $\theta = -90^\circ$  to  $\theta = +60^\circ$  from the normal. The fractional field in the plane of the sheet was

then only 2.5 per cent., showing that when the field would be zero in the absence of the sheet it would be very small provided the sheet projects about one wavelength beyond the current. This performance is markedly better than that of a single current at  $x/\lambda = 1.09$ , as exemplified in Fig. 5.6. If the sheet is doubly infinite it can be shown that the resistance of each of the two filaments is 1.33 times the

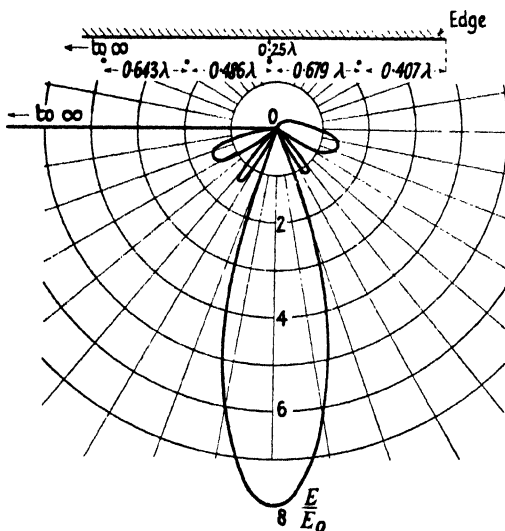


FIG. 5.11. Polar diagram of four-element curtain array near edge of semi-infinite flat sheet.

isolated value and thus it follows that the ideal gain is then 6. For the disposition shown in Fig. 5.10 the 'relative self-resistance' of the current nearest to and farthest from the edge is 1.231 and 1.228 respectively, while the 'mutual resistance' is +0.062, making the resultant values 1.293 and 1.290 respectively: it is instructive to note that a gross dissymmetry of position causes the two resistances to differ by less than 3 parts in a thousand. The forward field is 3.494 times that of a single current, and hence the forward gain is 4.90 as compared with the upper limit of 6.0.

Numerical results such as those leading to Figs. 5.5–5.7 can be added vectorially to give the polar diagram of four filaments at the stations used in these figures. The side spacings are  $0.679\lambda$ ,  $0.486\lambda$ , and  $0.643\lambda$  (mean  $0.603$ ) and  $x/\lambda = 0.407$  for the filament nearest the edge: these spacings are near  $0.5\lambda$ , the pitch commonly used in practice. The polar diagram for the system is shown in Fig. 5.11, while Fig. 5.12, plotted

as a diffraction pattern, compares it with the limiting form for a doubly infinite sheet. It may be seen that the bounding edge reduces slightly the amplitude of the two side lobes and increases slightly the bearing of their maxima: both results are experienced commonly in practice. It is as though the two lobes had slipped a little round the edge. When we come to examine experimental patterns we shall often

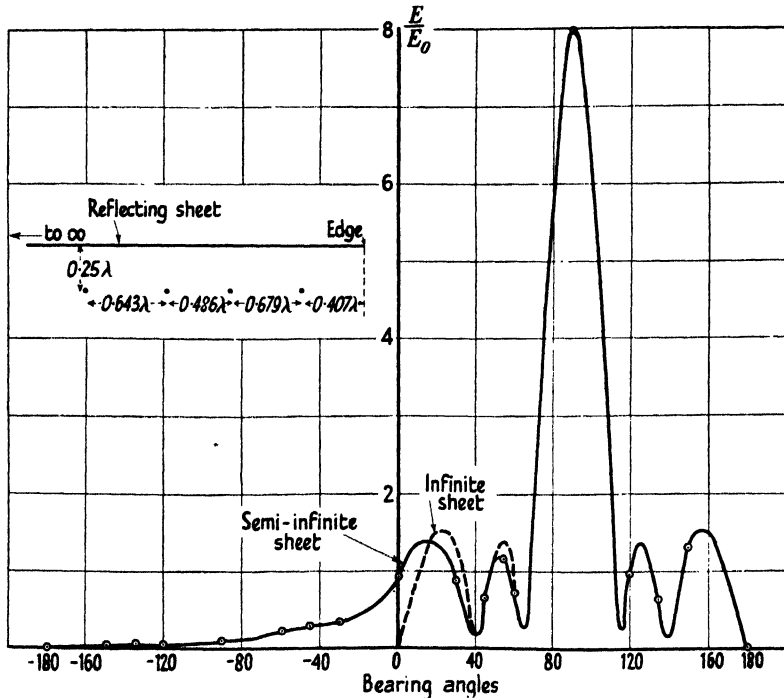


FIG. 5.12. Diffraction patterns of four-element array in front of infinite sheet or near edge of semi-infinite sheet.

speak of the outer lobes 'sliding round the edge'. The field in the plane of the sheet is 12.5 per cent. and the front-to-back ratio is found to be 96.

If the sheet were doubly infinite it may be found that the relative resistance of each of the outer pair is 1.02 and of each inner pair is 1.14; accordingly the gain would be 14.8 if all four currents are equal and cophased. Since gain is a measure of mean square field it is obvious from Fig. 5.12 that the gain with a half-plane cannot be appreciably less than the upper limit of 14.8. Accordingly there is good reason to hope that the ideal gains calculated in Chapters III and IV can be substantially realized in practice.

#### 5.4. Effect of bounding edge on the forward field

For a single filament situated so that  $x/\lambda = 1.8$  the forward field has been calculated for  $d/\lambda = 0.33, 0.63, 0.847, 1.018, 1.173$ , and  $1.312$ , and in each case it differed by no more than 1 per cent. from the value it would have had for a doubly infinite sheet. Thus it is concluded the forward field cannot be appreciably different from the ideal so long as the sheet is some  $4\lambda$  wide and  $d/\lambda$  is not much greater than  $\frac{3}{2}$ . Again, it can be found from Fig. 5.9 that, if  $x/\lambda = 0.63$  and  $d/\lambda = 0.1$ , then the forward field is only some 1 per cent. less than it would be for a doubly infinite sheet, and likewise from Fig. 5.5 when  $x/\lambda = 0.407$  and  $d/\lambda = \frac{1}{4}$ . It is thus to be expected that narrow sheets will not appreciably affect the curve of forward field so long as the distance of the aerial from the sheet is not much greater than its width. Accordingly, we may confidently expect to find that the stations for maximum and minimum forward field differ insensibly in practice from those calculated in Chapter III, provided always  $R/\lambda$  is not excessive compared with the width of the sheets.

#### 5.5. Density of current induced in each side of the sheet

It follows from (3.18) that the current density in the sheet at a distance  $r$  from the bounding edge is given by the equation

$$\frac{\lambda i}{I} = \frac{\pi}{2ar} \{A \pm B + j(C \pm D)\}, \quad (5.3)$$

where

$$A \equiv \sum_0^{\infty} (-1)^n (2n+1) Y_{\frac{2n+1}{2}}(ar) J_{\frac{2n+1}{2}}(k) \cos \frac{2n+1}{2} \alpha,$$

$$B \equiv 2 \sum_0^{\infty} (-1)^{n+1} n Y_n(ar) J_n(k) \sin n\alpha,$$

$$C \equiv \sum_1^{\infty} (-1)^n (2n+1) J_{\frac{2n+1}{2}}(ar) J_{\frac{2n+1}{2}}(k) \cos \frac{2n+1}{2} \alpha,$$

$$D \equiv 2 \sum_0^{\infty} (-1)^{n+1} n J_n(ar) J_n(k) \sin n\alpha.$$

For  $ar < k$ , interchange  $ar$  and  $k$  above. On the side of the sheet nearest the aerial we take  $A+B+j(C+D)$  and on the back side we take  $A-B+j(C-D)$ . The series denoted by  $B$  and  $D$  can be summed, and turn out to be half the current density which would exist if the sheet were doubly infinite. This shows that expression in the form  $A+B$ ,  $C+D$  has physical significance and that when the edge is infinitely remote  $A$  tends to  $B$  and  $C$  tends to  $D$ , so that the net current on the back is zero and on the front is  $2(B+jD)$ .



The study of these currents is worth while only in so far as they can be used to describe the radiation at a distant point. It is worth while to try to build up the pattern from the field of the current in the filament and the currents it induces in the sheet. The reader may interject that this has been done already without all the complexity of deriving the current, therefore why do it again? We do it because we must learn how to estimate the pattern which will result from Vee reflectors of finite width, a problem which cannot be solved analytically. If we can find the region here where the induced current is small we shall conclude that such portions of the half-plane could be removed without producing much effect in the portion of the sheet which remains: if we can find the effect on the pattern of omitting some portions of the induced current, we shall have made an approximation to the solution of a flat sheet of finite width. By now the reader should have learned that electric field at any point can be traced back to movement of electrons in conductors. If then the distribution of induced current is known, we shall calculate the pattern as the resultant field of the original filament of strength  $I$  together with the field due to induced filaments  $i \, dr$  distributed over both sides of the semi-infinite thin sheet. At any distance  $r$  from the bounding edge there is a current filament  $(A+B) \, dr$  on the front side and a filament  $(A-B) \, dr$  on the back side, the two filaments being separated by the negligible thickness of the sheet. Accordingly the net field, far off, must be that of a current filament  $(2A+2jC) \, dr$ ; in other words, the components  $B$  and  $D$  contribute no net effect to the field. Therefore it is only the components  $A$  and  $C$  which are of interest to us. When  $ar$  tends to zero we have

$$\frac{\lambda i}{I} = \frac{\pi}{2ar} J_1(ar) \cos \frac{1}{2}\alpha \{Y_1(k) + jJ_1(k)\},$$

since  $\frac{J_1(ar)}{ar}$ , etc., tend to zero,

$$\begin{aligned} &\doteq \sqrt{\left(\frac{\pi}{2ar}\right) \cos \frac{1}{2}\alpha \{Y_1(k) + jJ_1(k)\}}, \quad \text{when } ar \rightarrow 0. \\ \therefore \quad \frac{\lambda |i|}{I} &= \frac{\cos \frac{1}{2}\alpha}{\sqrt{(ark)}} \doteq \frac{d}{aR^{\frac{1}{2}}r^{\frac{1}{2}}}, \quad \text{when } \alpha \doteq \pi. \end{aligned}$$

Thus the density at the edge is always infinite but at a small finite distance from the edge decreases rapidly as  $R$  increases. The total current in a narrow strip of width  $b$  varies as  $b^{\frac{1}{2}}$  and thus is always finite. The infinity is of no practical importance and occurs only because the edge is sharp, in the mathematical sense. We shall see later

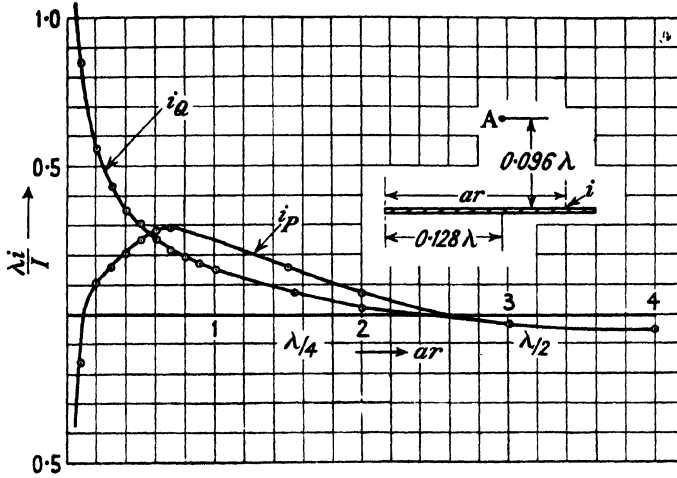


FIG. 5.13. Distribution of inphase and quadrature components of current induced in semi-infinite flat sheet by filament distant  $\frac{1}{10}\lambda$  from sheet and  $0.13\lambda$  from edge.

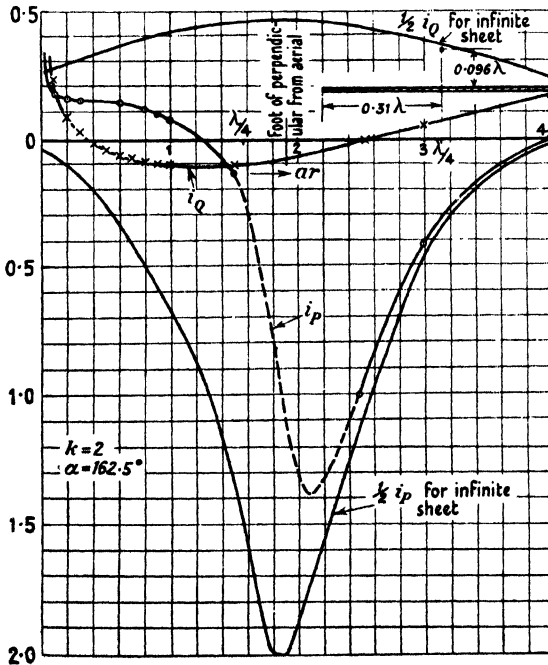


FIG. 5.14. Distribution of the two components of current induced in semi-infinite flat sheet by filament distant  $\frac{1}{10}\lambda$  from it and  $0.31\lambda$  from edge.

that the infinity does not occur if there is a very small cylinder at the edge, i.e. if the radius of curvature at the edge is finite, and so its appearance in the mathematics here is of no practical significance and we shall not discuss the matter further. Since both  $Y_{\frac{1}{2}}$  and  $J_{\frac{1}{2}}$  change sign periodically we note that the phase of each component of induced current at the edge changes periodically, with  $k$ , through  $180^\circ$ .

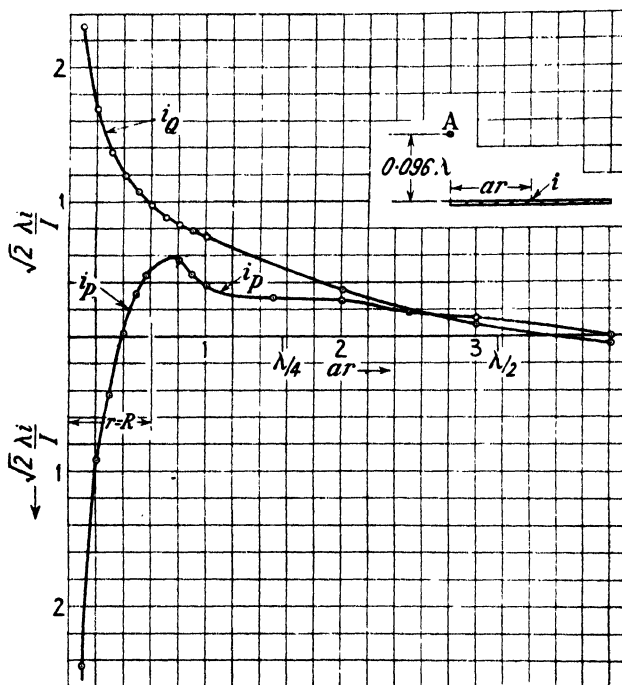


FIG. 5.15. Distribution of its two components of current induced in semi-infinite flat sheet by filament distant  $\frac{1}{10}\lambda$  from it and level with edge.

Fig. 5.13 shows the two components of induced current (due to terms  $A$  and  $C$  only) for the case where  $d/\lambda = 0.096$  and  $x/\lambda = 0.128$ . It should be noted that both are extremely small when  $r/\lambda$  exceeds, say, unity, and that  $i_P$  attains a maximum near the point closest to the aerial. This figure suggests that the currents induced in a sheet, say  $2\lambda$  wide, would differ little from those induced in the first  $2\lambda$  width of a half-plane, save that the induced current would rise sharply near the more distant edge. Fig. 5.14 shows the same pair of component densities for  $d/\lambda = 0.096$  and  $x/\lambda = 0.31$ , together with the two components for a doubly infinite sheet. On the near side of the sheet the two curves of  $i_P$  and  $i_Q$  are to be added, and on the far side

they are to be subtracted, to obtain the net resultant density. It may readily be seen that if this is done the resultant  $i_P$  on the near side will be a close approach to what would result in the doubly infinite sheet and on the far side it would be small save in the first  $\frac{1}{4}\lambda$  of width.

Close study of Fig. 5.14 will give a good idea of the general manner in which the net density must be distributed: we again emphasize, however, that the net density is of no interest in respect of the radiation, it is the components  $A$  and  $C$  alone which contribute to it. Fig. 5.15 shows the two components of induced density (due only to  $A$  and  $C$ ) for  $d/\lambda = 0.096$  and  $\alpha = 90^\circ$ : the density of both is extremely small at points more distant than about  $\frac{1}{2}\lambda$  from the edge.

### 5.6. Screening properties of a grid of parallel wires

We have been trying to assess the effect of using screens of finite width; groping a way from the idealized boundaries of analysis to the real boundaries of practice. Here then is the place to assess the result of replacing continuous sheets by wire netting, for it is often necessary to use rods or netting in order to reduce weight, windage, or obstruction of view. The analytical tools for dealing with grating reflectors were prepared in § 1.19, ready for their use here. We suppose a plane wave incident on an infinite flat grid of thin wires, parallel to the electric vector, and shall calculate the resultant field behind the grating. The incident field will induce currents, in the parallel wires of the grating, of such a value that the net field is just zero at the surface of each wire. The resultant field on the far side of the grating will depend on the magnitude and the phase of the induced current; these depend on the diameter of the wires and on the spacing between them. We saw in Chapter I that the field at each wire was given by the expression

$$\frac{cE}{a\pi I} = -\left\{1 + 2 \sum_1^{\infty} J_0(nag)\right\} + j\left\{Y_0(ab) + 2 \sum_1^{\infty} Y_0(nag)\right\},$$

where  $g$  is the distance between the centres of the thin wires of radius  $b$ . It follows from (1.66) that

$$\sum_1^{\infty} J_0(nag) = \frac{1}{ag} - \frac{1}{2} \quad \text{if } g/\lambda < 1, \quad \text{and then } \frac{cE_P}{a\pi I} = -\frac{2}{ag},$$

or  $cE_P = 2\pi(I/g)$ : this shows the inphase component of field at each wire is the same as the inphase component at the surface of a continuous sheet over which the concentrated currents were 'smeared' into a uniform density. Reference to (1.60) will remind the reader that the quadrature component of field at the surface of an infinite sheet is zero.

To obtain effective screening it is essential to simulate closely the effect of a continuous sheet, and hence it follows that the self-inductance, represented by the term  $Y_0(ab)$ , must be made nearly equal and opposite to the mutual inductance, represented by the term  $2 \sum_1^{\infty} Y_0(nag)$ . For a given grating of pitch  $g$ , this adjustment for approximate equality can be brought about only by correct choice of the wire radius  $b$ . Fig. 5.16

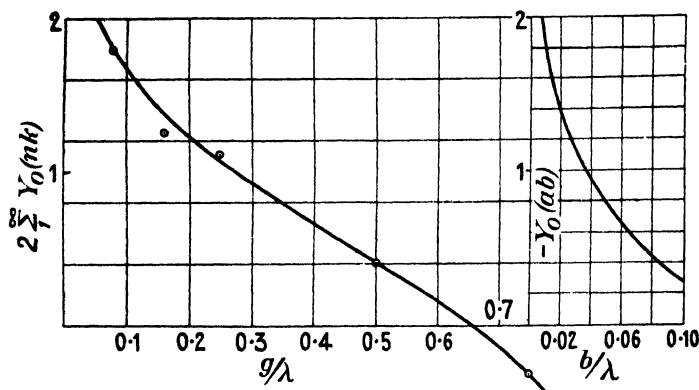


FIG. 5.16. Figure relating to infinite grating of wires.

has been prepared to assist in choosing this radius correctly: the left-hand curve shows the mutual term as a function of  $g/\lambda$  while the right-hand curve shows the self-inductance as a function of  $b/\lambda$ . As an example of its use take  $g/\lambda = \frac{1}{2}$ , then the left-hand curve shows the mutual term is 1.1 and the right-hand curve shows this will be neutralized if  $b/\lambda = 0.03$ . Similarly if  $g/\lambda = 0.45$ , then  $b/\lambda$  must be 0.07. Provided the radius is chosen correctly, then the impedance of the wires is purely resistive and the induced current will be in phase with the inducing field  $E$  and related to it by the equation  $cE = 2\pi I/g$ , provided  $g/\lambda < 1$ . In other words, the current per wire is equal, in magnitude and phase, to the current which would be induced in a width  $g$  of continuous sheet. In such circumstances the wave radiated by the grating will be equal in magnitude and opposite in phase to the incident field: this is the same as saying that the grating is a perfect screen. Though the grating is an open one, the result can be achieved by a proper choice of diameter and by no other means. In this solution, there are certain hidden approximations which need scrutiny: they arise from starting with the supposition that each wire is vanishingly thin and then choosing a precise diameter for it. We assume the

current density is uniform round the wire whereas there is sure to be some concentration on that half which is 'illuminated' by the incident wave: we have assumed the net incident field is constant all round the circumference and this is not precisely true. The error must be small provided we consider only cases in which  $b/\lambda$  is very small and  $b/g$  is small. The mutual force at the centre of the wire cannot differ appreciably from the value we have calculated (because  $b/g$  is small), but it may vary appreciably round the circumference. These refinements will become more clear in the next chapter: suffice it to say they are unlikely to be important so long as  $g/\lambda \succ \frac{1}{2}$ . Now suppose  $g/\lambda = \frac{1}{2}$  and  $b/\lambda = 0.06$ , then (see Fig. 5.16)

$$\frac{cE_Q}{a\pi I} = (-0.64 + 0.40) = -0.24 \quad \text{and} \quad -\frac{cE_P}{a\pi I} = \frac{2}{\pi} = 0.637.$$

Then the impedance of the wire is proportional to

$$\sqrt{(0.24^2 + 0.637^2)} = 0.637 \times 1.07$$

and its phase angle is  $\arctan 0.376 = 20.6^\circ$ . Accordingly the amplitude of the re-radiated wave will be 0.93 of the incident and it will be short of antiphase by  $20.6^\circ$ , and so the net amplitude on the far side will be near to  $0.97 \sin 20.6^\circ = 0.34$ . Thus, even if the spacing is as large as  $g/\lambda = \frac{1}{2}$  and the wires are only two-thirds of their correct diameter, the screening ratio still amounts to 0.64. It is rarely that the designer would be forced to make  $g/\lambda$  as large as  $\frac{1}{2}$ , and even  $g/\lambda = \frac{1}{4}$  may be considered large. Suppose  $g/\lambda = \frac{1}{4}$  and  $b/\lambda = 0.02$ , then reference to Fig. 5.16 will show the net quadrature field is about 0.30 while the inphase field is  $4/\pi$ , and so the phase angle of the impedance is  $13.3^\circ$  and the screening ratio is very near  $1 - \sin 13.3^\circ = 0.77$ . We have again chosen a radius which is only two-thirds of its correct value, and even so the screening ratio is 0.77.

It is apparent that even with a very open grid a screening ratio comparable with unity can certainly be obtained, provided the radius of the wire is reasonably close to that value which, according to Fig. 5.16, would give perfect screening. Now suppose  $g/\lambda = \frac{1}{8}$  and that  $b/\lambda = 0.01$ , instead of the correct value of 0.016, then from Fig. 5.16 the net  $E_Q$  is 0.25, while  $E_P = 8/\pi$ , and this leads to a screening ratio  $1 - \sin 5.5^\circ \doteq 0.9$ . It is not very helpful to give a general formula for the screening ratio, but a general statement of our results is as follows: If  $g/\lambda$  does not exceed  $\frac{1}{8}$  the screening ratio will exceed 0.9 if the radius of the wire is not less than 1 per cent. of a wavelength, which

is the same thing as saying that the screening ratio will certainly exceed 90 per cent. if the 'shadow ratio' of the grid is not less than 17 per cent. If  $g/\lambda$  is even as large as  $\frac{1}{2}$  it must be possible in practice to obtain a screening ratio of the order of 90 per cent. by choosing the diameter of the wire correctly, and when  $g/\lambda = \frac{1}{2}$  the 'shadow ratio' should be near 32 per cent. When the grating has been designed correctly there will exist a narrow range of frequency in which the screening ratio is almost perfect, the said range being centred on that at which the self and mutual inductance neutralize. The important point to remember is that the wires must not be extremely thin: the diameter of the wire in respect to the wavelength is just as important a factor as the ratio of gap to wavelength. The screening properties of the grating were examined by Sir Horace Lamb in the *Proceedings* of the London Mathematical Society in 1898 (vol. 29, p. 543), who points out that it had been set by Sir Joseph Larmor as a question in the Mathematical Tripos at Cambridge in 1894. Our solution is for a plane wave incident on the grating and we wish to use it as a guide for estimating the efficacy of the screens of a Vee reflector where the incident field is far from uniform: no doubt the simplified case is substantially applicable to the more complex one. In the Vee reflector there is always a concentration of induced current near the foot of the perpendiculars from the aerial on to the sheets. It is thus to be expected, and is confirmed by experiment, that a strip of sheet metal or gauze some  $\frac{1}{2}\lambda$  wide attached to the grating in the region of intense current density will much improve the overall performance of the netting, or the grid-like, sides of the Vee.

The more obvious application of the grating problem is to cases where screening is desired, but there are occasions when it is required to know how much undesired screening will be caused by some grating which is, so to speak, in the way of an aerial. Thus economy of masts and ground space often makes it necessary to erect aerial curtains in close proximity to one another and so disposed that one has to radiate through the other, 'firing through' as it is called in technical jargon. In such circumstances the curtain fired through commonly operates at a wavelength at least twice that of the curtain firing. Since the side spacing of a curtain is usually near  $\frac{1}{2}\lambda$ , the spacing of the curtain fired through will be  $\lambda$  or more with respect to the field incident on it. Since the wires of such curtains are tuned to the operating wavelength they will be wildly out of tune to the radiation fired through them. And in the circumstances we have in mind their radius is commonly extremely small, say  $b/\lambda$  of the order of  $10^{-4}$ . Therefore Fig. 5.16 shows that the mutual effect will

then always be negligible compared with the self-inductance effect and so the current induced in the obstructing curtain will depend almost entirely on the diameter of its curtain wires. It is a case where the screening is very small because the wires are extremely fine and not because the spacing is large compared with a wavelength. The method of estimating the current induced in any specific case will become more obvious after § 5.8, and the reader should then be able to deal with any particular application without further assistance.

### 5.7. Screening qualities of a squirrel cage of wires

Another estimate of the screening qualities of a grid can be made by studying the problem of a long current filament surrounded by a squirrel cage of  $n$  equally spaced thin wires each distant  $R$  from it. It follows readily from equation (1.49) and § 1.14 that, if each wire of a cage carries a current  $I$ , the inphase component of field at the surface of any one of the even number  $n$  of wires is expressed by the relation

$$-\frac{cE_P}{\pi a} = nI[J_0^2(k) + 2\{J_n^2(k) + J_{2n}^2(k) + J_{4n}^2(k) + \dots\}], \quad (5.4)$$

where  $k = 2\pi R/\lambda$ . The corresponding expression for  $E_Q$  is obtained by replacing  $J^2(k)$  by  $J(k)Y(k)$ . When  $n$  tends to infinity the right-hand side of (5.4) reduces to  $nI J_0^2(k)$ , the value appropriate to a tube carrying a uniformly distributed current  $nI$ . Here we realize that if  $R$  is such as to make  $J_0(k)$  zero, then  $E_P$  will be very small and the screening properties need close examination. There is also need to distinguish two cases. One where  $R/\lambda$  is notably less than unity and we are trying to estimate the effect of big holes in a structure which is desired to be a complete screen to some internal wire or piece of apparatus, and the other in which  $R/\lambda$  is fairly large and we are likening the cage to the open screen of a Vee reflector. In the first case  $J_0(k) = 0$  need not arise, in the second case it is very liable to arise. Suppose  $R/\lambda = 0.384$  so that  $J_0(k) = 0$  for the first time. Then evaluation from (5.4) gives the values collected in Table 5.1 below.

TABLE 5.1

$N$	2	3	4	6
$\frac{cE_P}{a\pi I}$	0.763	0.218	0.03	0.00015
$\frac{cE_P}{a\pi nI}$	0.381	0.073	0.0075	$2 \times 10^{-5}$



It follows from this that if the circumferential spacing is less than  $0.6\lambda$ , then  $E_P$  is less than 1 per cent. of the isolated value and the cage differs insensibly from the complete cylinder.

We will now suppose the circumferential distance between the wires is  $\lambda/10$  and evaluate  $E_P$  for various  $n$ , expressing it in terms of the limiting value for  $n$  infinite and  $nI = \text{constant}$ . The results of this computation are collected in Table 5.2, and they show that the approach

TABLE 5.2

$n$	$R/\lambda$	$k$	$nE_P/\infty E_P - 1$
4	0.064	0.4	$2.08 \times 10^{-8}$
6	0.096	0.6	$2.4 \times 10^{-12}$
8	0.128	0.8	$7.0 \times 10^{-16}$
10	0.160	1.0	$23 \times 10^{-20}$

to a continuous tube is extremely rapid for  $\frac{1}{10}\lambda$  spacing, irrespective of the radius of the cage. If the arcual spacing does not exceed  $\frac{1}{2}\lambda$ , then  $\frac{1}{2}n\lambda \succ 2\pi R$  and  $k$  does not exceed  $\frac{1}{2}n$ . We have seen that  $J_n(k)$  attains its first maximum when  $k$  is a little greater than  $n$  and the value of this maximum does not much exceed the maximum of  $J_0(k)$  in this region of  $k$ : thus  $J_{18}(k)$  attains its first maximum, of value 0.25, when  $k = 20$  and then  $J_0(20) = 0.17$ . Moreover  $J_{18}(10) = 1.5 \times 10^{-4}$ . Consideration of this will show that, so long as the spacing does not much exceed  $\frac{1}{2}\lambda$ , then  $\{J_n(k)/J_0(k)\}^2$  cannot exceed a few parts in  $10^6$ , so long as  $k$  is not very close to a value which makes  $J_0(k)$  zero. It is clear that, for spacings at least up to  $\frac{1}{2}\lambda$ , the inphase component of field differs insensibly from what it would be if the cage were replaced by a tube carrying the same total current. This corresponds precisely with the result of the analysis of a flat grating; provided we remember that with a tube (or cage) the actual value of  $E_P$  depends very much on the radius of the tube. As with a flat grating, the magnitude and phase of the induced currents will depend enormously on the radius of the individual wires of the cage. The possibility of infinite fields when the spacing is  $\lambda$  does not arise in a cage, because this spacing will never give perfect co-operation of phase from all contributing currents: it appeared in the analysis of the flat grid only because the width was infinite. The equation of the form of (5.4) is not suited for calculating  $E_Q$ , as its sum must converge logarithmically to infinity because it includes the self-inductance term which runs to infinity as the radius of the wire tends to zero. The difficulty cannot be avoided by using (1.49) to calculate the field at one wire due to the remaining  $(n-1)$  wires, as that series avoids

divergence at  $ar = k$  only because the terms are multiplied by  $\cos n\theta$ : an infinite series is unsuitable for calculating  $E_Q$  at a radius very near  $R$  and it is only there we are interested in  $E_Q$  in this particular problem. Accordingly we must calculate  $E_Q$  from the relation

$$\frac{E}{a\pi I} = \sum_2^n Y_0(a\rho),$$

where  $\rho$  is the typical chord from wire number 1 to any other wire. This has been done for an arcual spacing  $\frac{1}{16}\lambda$  and various  $n$ ; the results are collected in Table 5.3.

TABLE 5.3  
*Arcual spacing  $\frac{1}{16}\lambda$*

$n$	$R/\lambda$	$k$	$B$	$nJ_0(k)Y_0(k)$	$B - nJ_0Y_0$
4	0.064	0.4	-0.81	-2.34	+1.53
6	0.096	0.6	-0.21	-1.48	+1.27
8	0.128	0.8	+0.27	-0.615	+0.88
12	0.192	1.2	+3.87	+1.84	+2.03
16	0.256	1.6	+4.57	+3.07	+1.50
20	0.32	2.0	+3.8	+2.27	+1.53

In this table the column marked  $B$  shows the mutual term while the next column is proportional to  $E_Q$  for a tube of the same radius as the cage. Our main interest is in large cages, because we are thinking here about aerial reflectors. Accordingly, take  $n = 20$  in the table above: for this  $B - nJ_0(k)Y_0(k) = 1.53$ : reference to Fig. 5.16 shows this equals  $-Y_0(ab)$  for a wire in which  $b/\lambda = 0.016$ . Hence if the 20 cage wires have this radius, then  $E_Q$  at their surface will be the same as at the surface of a tube of the same radius. Such wires would be small compared with the spacing and with  $R$ , and so comply with the underlying approximations of the solution. We have seen that  $E_P$  always differs insensibly from the 'tube value': hence for  $n = 20$  and  $b/\lambda = 0.016$  the impedance of each wire will have twenty times the magnitude and the same phase angle as the impedance per unit length of a tube of the same radius as the cage. Accordingly such a cage must act as a perfect screen to a coaxial current filament, to the order of accuracy inherent in the approximate solutions. Now suppose wires for which  $b/\lambda = 0.016$  are used in a cage with  $n = 12$ , then  $E_Q$  is proportional to

$$2.03 - 1.53 = 0.5$$

and  $E_P$  is proportional to  $12J_0^2(1.2) = 5.4$ . The phase angle would then be  $5.3^\circ$  leading, whereas it would have led by  $18.7^\circ$  for a tube. It should

be clear from the last section that the screening ratio would be approximately equal to  $1 - \sin 13.4^\circ = 0.77$ . If the radius of the twelve wires had been such that  $b/\lambda = 0.008$ , then the screening ratio would have been very near unity. We may summarize these results as follows: If the arcual spacing is  $\frac{1}{10}\lambda$  and the shadow ratio near  $\frac{1}{5}$ , then the screening ratio is likely to be at least 80 per cent. for all cages whose diameter exceeds about  $\frac{1}{4}\lambda$ , and can always be made to differ insensibly from unity by nice choice of the radius of the cage wires.

Table 5.4 records a numerical example where the arcual spacing is  $\frac{1}{4}\lambda$ .

TABLE 5.4  
*Arcual spacing  $\frac{1}{4}\lambda$*

$n$	$R/\lambda$	$k$	$B$	$nJ_0Y_0$	$B - nJ_0Y_0$
6	0.24	1.5	+2.104	1.173	+0.931
8	0.32	2.0	+1.848	0.915	+0.933
10	0.40	2.5	+0.686	-0.241	+0.927

It shows that  $B - nJ_0Y_0$  is constant to 1 per cent. as  $n$  increases from 6 to 10: reference to Fig. 5.16 shows that  $E_Q$  will be zero if the wires are such that  $b/\lambda = 0.04$ , and then the screening ratio will be substantially unity; the shadow ratio is then 0.32. Reference to the last section will show that when  $g/\lambda = \frac{1}{4}$  the correct value of  $b/\lambda$  was 0.032. Thus it would appear to make little difference whether the grating is flat and of infinite width or a cage whose diameter is only of the order of one wavelength: we may feel confident that a grid reflector whose rods are parallel to the electric field will behave substantially as a continuous sheet provided the shadow ratio is of the order of one-fifth and the spacing not much more than  $\frac{1}{4}\lambda$ .

Note: For a more detailed treatment see *Journal I.E.E.* vol. 91, Part III, 1944, 14.

### 5.8. Three simple problems of rod reflectors

#### (a) *Aerial with one parallel rod as a reflector*

We saw in Chapter II that if two equal parallel currents in phase quadrature are separated by  $\frac{1}{4}\lambda$ , then the equatorial pattern is heart-shaped with zero field in one direction in the plane of the pair. We will now see if this can be achieved by placing a rod distant  $\frac{1}{4}\lambda$  from a long in-line array. Reference to tables will show that at this distance  $c|E|/a\pi I = 0.625$  lagging  $41^\circ$ . The 'parasite' rod must then have a diameter such that the phase angle of its impedance is  $90 - 41 = 49^\circ$ . At the surface of the rod  $E_Q/E_P = -Y_0(ab)$ , and hence in this case we

must choose  $b$  so that  $-Y_0(ab) = \tan 49^\circ = 1.15$  and thus (see Fig. 5.16)  $b/\lambda = 0.028$ . At the surface of this rod

$$\frac{c|E|}{a\pi I'} = (1^2 + 1.15^2)^{1/2} = 1.52;$$

hence the ratio of the induced to the inducing current is  $0.625/1.52 = 0.41$ . If the field in one direction is to be zero, the two currents must be in phase quadrature and also equal in magnitude, and so we find these essential conditions cannot be obtained when a long in-line array induces current in a thin rod distant  $\frac{1}{4}\lambda$  from it. If the radius of the 'parasite rod' is such that  $b/\lambda = 0.028$ , then the field in the plane of the two rods is proportional to  $(1+0.41)I$  in one direction and to  $(1-0.41)I$  in the other, the ratio of these two being 2.4. On bearing  $\pm 90^\circ$  the field would be proportional to  $(1^2 + 0.41^2)^{1/2}I = 1.09I$  and thus is  $1.09/1.41 = 0.77$  of the forward field, as compared with 0.71 for equal currents in quadrature. To obtain the power gain we must calculate the inphase field at the 'driven in-line array', and this arises from the current in itself and from the quadrature field there of the induced quadrature current in the parasite rod. Since  $Y_0(\pi/2) = 0.41$ , it follows that the inphase field at the driven in-line array is increased by the parasite in the ratio  $1 + 0.41 \times 0.41 = 1.168$  and therefore

$$G = \frac{(1.41)^2}{1.168} = 1.72.$$

Had the currents been equal and in phase quadrature the gain would have been 2, and hence the parasite does produce a reasonably close approximation to the best obtainable result and does it automatically and without the practical difficulty of driving both in-line arrays with currents of equal magnitude and quadrature phase. Note, however, that the performance we have estimated can be obtained only by correct choice of the radius of the parasite, and then only supposing that  $b/\lambda = 0.028$  is small enough not to strain unduly the approximation inherent in the solution. The exact solution for a parasite rod of any diameter is given in the next chapter. Note also that no system of tuning the parasite can improve the performance since it cannot make the induced current as large as the inducing current. We have obtained quadrature phase by adjusting the diameter of the rod. The phase could also be adjusted in practice by tuning methods, and it might happen that a slightly better performance would result from a larger induced current which was not truly in phase quadrature. Or, if we look at the problem from a slightly different aspect, we see that

the tuning adjustment which gives optimum gain or optimum ratio of forward to backward field is not likely to be very sharp.

(b) *Aerial and two parallel reflecting rods*

Now consider two parallel 'parasite' rods,  $\frac{1}{2}\lambda$  apart, placed symmetrically with respect to a long in-line array which is  $\frac{1}{4}\lambda$  from the plane through them; the driven aerial and the two parasite rods being thus at the corners of an isosceles triangle whose base is twice the perpendicular from apex on to base. In proposing this disposition we are thinking first of the idealized problem of an aerial  $\frac{1}{4}\lambda$  in front of an infinite sheet, then of the width of the sheet being reduced from infinity to  $\frac{1}{2}\lambda$ , then of this strip of sheet being replaced by two round rods at its bounding edges. In the presence of each other the radiation resistance of each of the two parasitic rods will exceed the isolated value by the factor  $\{1 + J_0(\pi)\} = 0.696$ , while the mutual reactance is proportional to  $Y_0(\pi) = +0.33$ . If their radius is such that  $b/\lambda = 0.03$ , then it follows from Fig. 5.16 that the reactance of each is proportional to  $-1.1 + 0.33 = -0.77$ , and hence the impedance of each is proportional to  $(0.77^2 + 0.696^2)^{\frac{1}{2}} = 1.04$  with lagging phase angle equal to  $\arctan 770/696 = 47.7^\circ$ . Each parasite rod is distant  $0.35\lambda$  from the driven in-line array and reference to tables will show that at their centres

$$-\frac{c|E|}{a\pi I} = 0.53 \sqrt{73^\circ}.$$

Accordingly the current induced in them will be  $0.53/1.04 = 0.51$  of the current in the driven array and leading it by  $102 - 47.7 = 54.3^\circ$ . To calculate the polar diagram of resultant field at a great distance we replace the two induced currents by a single current half-way between them and having an apparent strength  $2 \times 0.51 I \cos(\frac{1}{2}\pi \sin \theta)$  for a bearing at angle  $\theta$  from the normal: the phase of this single equivalent current always lags  $126^\circ$  on the 'driven' current  $I$ , distant  $\frac{1}{4}\lambda$  from it. In the forward direction the resultant field is the sum of a vector  $E_0$  and a vector  $1.02E_0$  lagging the first by  $-54.3 + 90 = 35.7^\circ$ : this sum is  $1.9E_0$ . In the backward direction the resultant field is the sum of a vector  $1.02E_0$  and a vector  $E_0$  lagging the first by  $144.3^\circ$ , and this sum is  $0.61E_0$ : hence the forward to backward ratio is 3.1. On bearing  $\pm 90^\circ$  the net field of the two induced currents is zero, because they are equal, cophased, and separated by  $\frac{1}{2}\lambda$ : hence the resultant field on these bearings is  $E_0$ , and this is 0.52 of the forward field.

We will now calculate the radiation resistance of the driven array. Each induced current is  $I_s = 0.31(1 + 1.39j)$ , and for separation  $0.35\lambda$

we have  $J_0(ar) = +0.110$  and  $Y_0(ar) = +0.52$ . Hence the field at the surface of the driven current is given by the formula

$$\begin{aligned}\frac{cE}{a\pi I} &= \{-1 + jY_0(ab)\} + 2 \times 0.31(1 + 1.39j)(-0.11 + 0.52j) \\ &= -1.52 + j\{Y_0(ab) + 0.226\},\end{aligned}$$

showing that the presence of the induced currents increases the radiation resistance in the ratio 1.52: the power gain is  $(1.9)^2/1.52 = 2.35$ . If the two rods were replaced by an infinite sheet, then we should have had

$$\frac{cE_P}{a\pi I} = -1 + J_0(\pi) = -1.35,$$

and the power gain would have been equal to  $(2)^2/1.35 = 2.96$ . Therefore the general performance with two thin rods is not vastly inferior to an aerial and infinite sheet. We have seen that the fractional field in the plane of the rods is 0.52 (contrasted with zero for an infinite sheet), and it would be instructive to compare this value with the fractional field in the plane of a semi-infinite sheet with an aerial  $\frac{1}{4}\lambda$  from the edge and  $\frac{1}{4}\lambda$  from the sheet. The appropriate value can be interpolated roughly from Figs. 5.4 and 5.5, which relate to  $x/\lambda$  zero and 0.41 respectively: in these the fractional field in the plane of the half-sheet is 0.78 and 0.42 respectively, suggesting it would be near 0.5 when  $x/\lambda = \frac{1}{4}$ .

In this numerical example we chose arbitrarily to make  $b/\lambda = 0.03$ : to assess the effect on the result of this arbitrary choice we will now take  $b/\lambda = 0.06$ , noting, however, that the approximation may be scarcely valid for so thick a rod. From Fig. 5.16 we now find the reactance is proportional to  $-0.63 + 0.33 = -0.30$ , and then it follows the impedance is proportional to 0.76 and its lagging phase angle is  $23.3^\circ$ : in this case  $I_2 = 0.7I_1$  and has a leading phase angle of

$$102 - 23.3 = 78.7^\circ.$$

The forward field is now found to be  $2.39E_0$  and the backward field is  $0.46E_0$ , giving a front-to-back ratio of 5.2. The fractional field at  $\theta = \pm 90^\circ$  is 0.42. The field at the surface of the driven current is now given by the formula

$$\begin{aligned}\frac{cE}{a\pi I} &= \{-1 + jY_0(ab)\} + 2(0.137 + 0.69j)(-0.11 + 0.52j) \\ &= -1.75 + j\{Y_0(ab) + 0.006\};\end{aligned}$$

hence the power gain is equal to  $(2.39)^2/1.75 = 3.3$ : the approximate solution has probably led to an over-estimate of the gain.

If the rods were thin wires tuned to resonance by suitably adjusted

Franklin coils the induced current would be  $(0.53/0.695)I = 0.761$  and would lead by  $102^\circ$ . Then the forward field would be  $2.51E_0$  and the backward field  $0.54E_0$ , giving a front-to-back ratio of 4.7. The fractional field on  $\theta = \pm 90^\circ$  would be 0.39. For the field at the surface of the driven current we now have

$$\frac{cE}{a\pi I} = \{-1 + jY_0(ab)\} + \frac{2(-0.11 + 0.52j)^2}{0.695} = -1.75 + j\{Y_0(ab) - 0.33\}.$$

It follows from this that the gain would be 3.6 and presumably this value could be obtained if the phasing coils were correctly adjusted.

The examples of the previous two sub-sections surely will inspire reasoned confidence in the expectation that finite sheets or even a few rods can produce results comparable with those appropriate to infinite sheets.

(c) *Aerial  $\frac{1}{4}\lambda$  in front of a three-rod grating*

The arrangement and notation is explained by Fig. 5.17. Let the rods of the grating be such that  $Y_0(ab) = 1$ , which is  $b/\lambda = 0.035$ . Let  $E_1$  and  $E_2$  be the fields at rods 1 and 2 respectively due to unit current in the aerial. Then substituting in (1.23) the values of  $J_0$  and  $Y_0$  appropriate to the relevant distances gives

$$\frac{cE_1}{a\pi} = 0.382 + 0.180j \quad \text{and} \quad \frac{cE_2}{a\pi} = -0.472 + 0.409j.$$

Let  $E'_1$  and  $E'_2$  be the field at rods 1 and 2 respectively due to the induced currents  $I_1$  and  $I_2$ , then

$$\begin{aligned} \frac{cE'_1}{a\pi} &= (-1-j)I_1 + (0.303 + 0.330j)I_2 + (0.22 + 0.23j)I_1 \\ &= -(0.780 + 1.23j)I_1 + (0.303 + 0.33j)I_2 \end{aligned}$$

$$\text{and} \quad \frac{cE'_2}{a\pi} = 2(0.303 + 0.330j)I_1 - (1+j)I_2.$$

The net field must be zero at the surface of the rods and therefore  $E_1 + E'_1 = 0$  and  $E_2 + E'_2 = 0$ . Using this condition we obtain two simultaneous equations for  $I_1$  and  $I_2$  and on solving them obtain  $I_1 = 0.38 + 0.2j$  and  $I_2 = (0.205 + 0.575j)$ , or  $|I_1| = 0.43$  and  $|I_2| = 0.61$ . It happens that the ratio of these two currents is almost exactly in the same ratio as the inducing field from the aerial; this is fortuitous, since the ratio depends on the value of  $b/\lambda$ .

Because the aerial is  $\frac{1}{4}\lambda$  in front of the grating it is only the quadrature

components of induced current which tend to make the backward field zero. Consideration will show that the forward field is

$$E_F = (1 + 2 \times 0.2 + 0.575) - (2 \times 0.38 + 0.205)j = (1.975 - 0.965j),$$

or  $|E_F| = 2.19$ , and the backward field is  $E_B = (0.025 + 0.965j)$ , or  $|E_B| = 0.966$ . In the plane of the grating we have

$$E_{\pi/2} = (1.205 + 0.575j) - 2(0.38 + 0.2j) = 0.445 + 0.175j,$$

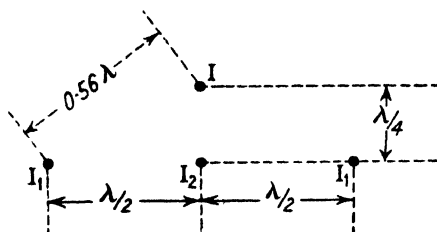


FIG. 5.17.

or  $|E_{\pi/2}| = 0.476$ . The field of the grating at the aerial follows readily from the values given already for  $E_1$  and  $E_2$ , and hence

$$\begin{aligned} \frac{cE}{a\pi} &= 2(0.382 + 0.180j)I_1 + (-0.472 + 0.409j)I_2 \\ &= -0.988 + 0.857j, \text{ on substituting for } I_1 \text{ and } I_2. \end{aligned}$$

The field at the surface of the aerial due to unit current in itself is  $cE/a\pi = -1 + jY(ab)$ : accordingly the net field at its surface is

$$\frac{cE}{a\pi} = -1.988 - 0.143j, \text{ if } b/\lambda = 0.035.$$

This shows that the presence of the grating doubles the radiation resistance, and so the forward power gain is  $(2.19)^2/1.988 = 2.42$ , as compared with 2.96 for an infinite and continuous reflecting sheet.

The results of the last three examples are summarized in Table 5.5.

TABLE 5.5

Number of rods.	1	2	3	sheet
Forward field	1.41	1.9	2.19	2
Front-to-back ratio	2.4	3.2	2.26	$\infty$
Power gain	1.72	2.35	2.42	2.96

The table demonstrates that a very simple reflecting screen produces a close approximation to the ideal limit in respect of forward field and of power gain but is not very effective in making the backward field very small: the polar diagram is bound to differ markedly from the ideal on bearings greater than about  $\pm 60^\circ$  from the normal to the screen.



The reader should not forget that the results collected in the table above are not completely general because they have depended on the arbitrary choice of  $b/\lambda$ : had  $b/\lambda$  been made very small indeed, then the effect of the reflector would have been negligible. But if  $b/\lambda$  is not less than about 0.04, then it is evidently a simple matter to produce a very effective screen from two or three rods. Analytical examples make it quite evident that sheets whose width is a wavelength or less will be very effective reflectors and that then the performance cannot be very sensitive to their geometrical shape, which is what the optician calls the 'figure' of the mirror.

(d) *Currents induced in a grid of three wires by an incident plane wave*

We will now calculate the currents induced in a grid of three wires by a plane wave incident along the normal, the electric vector being parallel to the wires. By symmetry, similar currents will be induced in the outside wires, namely, Nos. 1 and 3; but the currents induced in them need not necessarily be equal to the current induced in the middle wire. The induced currents must be such that the three together produce equal fields at the surface of each of the three wires and this field must be equal and opposite to the incident field  $E_0$ . Let each wire have a radius  $b$  and let the induced currents produce a field  $E_1$  at wires 1 and 3 and  $E_2$  at wire 2. Then

$$\frac{cE_1}{a\pi} = \{-1 + jY_0(ab)\}I_1 + \{-J_0(ad) + jY_0(ad)\}I_2 + \{-J_0(2ad) + jY_0(2ad)\}I_1$$

$$\text{and} \quad \frac{cE_2}{a\pi} = \{-1 + jY_0(ab)\}I_2 + 2\{-J_0(ad) + jY_0(ad)\}I_1.$$

Take  $d/\lambda = \frac{1}{2}$ , then

$$\begin{aligned} J_0(ad) &= -0.304, & Y_0(ad) &= 0.329, \\ J_0(2ad) &= +0.22, & Y_0(2ad) &= -0.23. \end{aligned}$$

First take  $b/\lambda = 0.035$  ( $Y_0(ab) = -1$ ); then on substituting in the above, making  $E_1 = E_2$  and solving, we obtain  $I_1/I_2 = 0.694(1 - 0.01j)$ , showing that the middle current is much the largest and all are sensibly cophased. On taking  $b/\lambda = 0.007$  ( $Y_0(ab) = -2$ ) and repeating we obtain  $I_1/I_2 = 0.78(1 + 0.052j)$ , showing that the middle current is again much the largest and that all are sensibly cophased. We note with interest that a fivefold increase of  $b$  reduces the ratio of  $I_2/I_1$  by only 10 per cent. and thus conclude the ratio is very insensitive to the radius of the wire.

For the larger wires we find  $cE_0/a\pi I_1 = 0.832(1 + 0.94j)$ , whereas for

a single wire we should have had  $cE_0/a\pi I_1 = (1+j)$ ; for the smaller wires  $cE_0/a\pi I_1 = 0.50(1+2.6j)$  as compared with  $(1+2j)$ . In the first case  $a\pi|I_1|/c = 0.88E_0$  and in the second case  $a\pi|I_1|/c = 0.716E_0$ ; this shows the magnitude of the currents is not very dependent on  $b$ . In short, the diameter of the wire has a large control on the phase of the induced current but small control on its magnitude or distribution between the three wires.

If the three-wire grid were replaced by an infinite sheet the induced density would be  $i = cE_0/4\pi$ . If we imagine the total current induced in the grid is smeared uniformly over the width, the average density would be  $i' = (2I_1 + I_2)/2d$ ; it may be found from the values above that  $|i'| = 0.97cE_0/4\pi$  for the larger wires and  $|i'| = 0.75cE_0/4\pi$  for the smaller wires. Both these values are reasonably close to the limit for a continuous sheet.

We may summarize these results as follows. All three currents will be sensibly cophased with one another, but will lag the incident field by an angle approximately equal to the impedance angle of a single isolated wire; the middle current will be about 1.35 times the outside currents and the average 'smeared density' will be near  $cE_0/4\pi$ .

It is important to realize that the middle current is considerably larger than the other two, because this will happen in a receiving curtain unless steps are taken to force equality. And again, the currents will not be equal in all three members of a transmitting array unless steps are taken to feed forcibly more current to the two outer members than to the middle member. This important practical point does not seem to be realized, and it appears to be assumed that similar feeding cables will feed similar currents to all three members. The uneven distribution will cause the pattern to differ appreciably from the assumed ideal, and it will reduce the power gain because it will increase the width of the main beam. To bring home this point we will calculate the power gain of a three-member curtain in which all three currents are cophased but the loading is 1:1.35:1.

For an outer wire we have

$$E_P = -1 + 1.35 \times 0.304 - 1 \times 0.22 = -0.81,$$

and for the middle wire,

$$E_P = -1 \times 1.35 - 2 \times -0.304 = -0.74.$$

The total work is

$$P = 2 \times 1^2 \times 0.81 + 1.35^2 \times 0.74 = 2.96$$

and the forward field is 3.35: this gives a power gain equal to

$$\frac{(3.35)^2}{2.96} = 3.75.$$

Had the loading been uniform we should have had  $P = 2.33$  and hence  $G = 3.86$ : the loss of gain is negligible.

This example is also instructive as a guide to the current induced in a flat strip of width  $\lambda$ , a problem which can be solved by the help of Mathieu functions, but the computation is not yet available. Presumably we shall expect a mean density near  $cE_0/4\pi$  with appreciable concentration towards the middle.

(e) *Currents induced in a grid of four wires by an incident plane wave*

From symmetry the current induced in wire no. 1 equals that induced in wire no. 4: likewise that induced in no. 2 equals that in no. 3.

Proceeding as in the last section and taking  $Y_0(ab) = -1$ , the solution gives  $I_1/I_2 = 0.87(1 - 0.017j)$ , again showing that all currents are substantially cophased with one another and that the two inner currents are larger than the outer currents. The ratio now is 1.15 as contrasted with 1.43 for the three wires, suggesting a rapid approach to the limiting case of infinite width. Now we find  $cE_0/a\pi I_1 = 0.725(1 + 0.97j)$  or  $a\pi|I_1|/c = 0.99$ : once more the phase angle of the current, relative to the incident field, is very nearly the same as the phase angle of the impedance of an isolated wire. The average 'smeared density' is  $i' = 2(I_1 + I_2)/3d$ , and it follows from the above that  $|i'| = 0.9cE_0/4\pi$ , and this is, again, close to the limiting value.

Now consider the power gain of a four-wire curtain bearing cophased currents with loading 1:1.15:1.15:1. The forward field is 4.3: the work from each of the outer wires is 0.72 and from each inner wire is 0.95, and then it follows the gain is 5.5. Had the loading been uniform the gain would have been 5.9.

### 5.9. Current induced in a thin rod placed perpendicular to the electric vector

In this problem two distinct component effects must be considered. Firstly, equal and opposite charges will be induced in the half-cylinders, separated by the diameter which is perpendicular to the electric field, and this produces a line doublet pointing along the field. Secondly, the incident field has a curl, and this will induce a current flowing round the surface of the rod; or according to the loose terminology commonly used in low-frequency technique, a circumferential current will be

induced by the magnetic field of the wave, which field is parallel to the rod. The appropriate equations for the line doublet are given in (1.58) and (1.59). The field along the axis of the line doublet and near to it is given by

$$\frac{cE_r}{a\pi I_1 l} = \left( -\frac{1}{2} + j\frac{2}{\pi} \times \frac{1}{a^2 r^2} \right). \quad (5.5)$$

The field of the current  $I$  flowing round the surface of the tube is given by (1.52), and accordingly the field at the surface of a tube of small radius  $b$  is

$$\frac{cE}{a\pi I_2} = -2\pi b \left( \frac{a^2 b^2}{4} + \frac{j}{\pi} \right). \quad (5.6)$$

Now approach the problem in a more elementary manner. If a cylinder of radius  $b$  is transverse to a static electric field  $E$ , it is well known† that a charge density  $Q \sin \phi$  is induced on the surface of the cylinder and such that  $2Q\pi = E$ ; moreover, the external field of this induced charge density is the same as that of a line doublet of moment  $M$  such that  $M = b^2 E/2$ . Accordingly the external electric field perpendicular to the rod and along the axis of the line doublet is  $2M/r^2 = (b^2/r^2)E$ . On writing  $I_1 = -jpQ$  in (5.5) we obtain  $E_r = (2M/r^2)(1 + j\frac{1}{4}\pi a^2 r^2)$ : the inphase component of this expression is the same as if the field were static and the quadrature term is relatively insignificant. This shows, as was natural to expect, that a field  $E \sin pt$ , incident perpendicular to the small rod, will induce a line doublet of moment  $b^2 E/2$ : therefore  $b^2 E/2 = I_1 l/p$ . The limiting form of (1.53) shows the internal magnetic field equals  $4\pi I_2$ , since  $H = E$  in the incident wave. We have now found the two components of current in terms of the incident electric field. Accordingly the re-radiated field at large distances is, from (1.58) and (1.52),

$$\frac{E_t}{E} = \frac{2\pi^3 b^2}{\lambda} (\cos \phi + \frac{1}{2}) \{-J_0(ar) + jY_0(ar)\}. \quad (5.7)$$

If the electric field had been parallel to the thin wire we should have had

$$\frac{E_t}{E} = \frac{1}{Y_0(ab)} \{-J_0(ar) + jY_0(ar)\}.$$

Accordingly the reflected fields on the two dispositions are in the ratio

$$\frac{3}{2} \times \frac{2\pi^3 b^2}{\lambda^2} Y_0(ab)$$

and this tends to the value  $\frac{3}{2}a^2 b^2 \log ab$  when  $ab$  is very small: when  $b/\lambda = 0.016$  the ratio is 0.035. Thus, as was to be expected, the scattering or reflecting effect of a thin wire is very much smaller when it is

† See, for example, Moullin, *Principles of Electromagnetism*, 206.

transverse to the field than when it is parallel to the field. It is interesting to note that the contribution to the scattered field arising from the circulating current (loop effect) is never less than half the contribution from the line-doublet effect.

### 5.10. Grating of thin wires perpendicular to the electric vector

Having just seen that a single transverse wire is very ineffective as a reflector, it is not worth while to develop a solution for an infinite grid corresponding to § 1.19 for a grid of wires parallel to the electric vector. It will suffice to indicate the steps of the process which would have to be gone through.

It is required to find the mutual effect due to a grid of similar and parallel line doublets separated a distance  $g$ . Then it follows from (1.59) that the inphase component of electric force at the centre of each line doublet and perpendicular to its infinite length is

$$-\frac{cE_P}{a\pi Il} = \frac{1}{2} + 2 \sum_1^{\infty} \frac{J_1(nag)}{nag}.$$

The sum of this series does not appear to be known, though it may possibly be derivable by means of a Fourier process corresponding to that used in § 1.19. Resort to tables of  $J_1$  shows that  $cE_P \div 2.04\pi(Il/g)$  when  $ag = 1$  and  $cE_P \div 2.04\pi(Il/g)$  when  $ag = 3$ . Thus it would seem, that for spacings up to about  $\frac{1}{2}\lambda$ ,  $E_P$  differs insensibly from what it would be in a continuous sheet if the current were 'smeared' uniformly across it: here there is correspondence with a grid which is parallel to the electric vector.

Close examination, which it is not worth while to reproduce in detail, shows that the mutual quadrature field from the grating cannot suffice to reduce very much the effective capacitance of each thin wire, and thus effective screening cannot be attained by nice choice of the diameter of the wires. The induced currents in each wire of the grid will not differ much from what they would have been if the wire had been isolated, and these were calculated in the last section.

### 5.11. Netting with square mesh of side $g$

Let the netting be placed perpendicularly to the direction of propagation of the incident wave: then every wire of the netting lies everywhere in the plane of the magnetic and electric vector but is not necessarily parallel to the electric vector. Let one set of wires be inclined at  $\phi$  to the electric vector and the other at  $(90^\circ - \phi)$ : then the field along one set is  $E \cos \phi$  and along the other is  $E \sin \phi$ . We shall assume the wires

so thin that the currents induced in them by the components of field perpendicular to their length are negligible: accordingly the only significant currents are those flowing along the length of the wires and the two perpendicular grids of current have no appreciable interaction. The field reflected by one set will be parallel to it and proportional to  $E \cos \phi$ ; and similarly for the other set, but proportional to  $E \sin \phi$ . Consideration will show that the vector sum is parallel to the incident field and proportional to  $E(\sin^2 \phi + \cos^2 \phi) = E$ . Hence, to the order of approximation we have used, the screening ratio of a square mesh does not depend on the inclination of the wires to the electric vector and is the same as a single grid of wires, of pitch  $g$ , parallel to the field. It seems probable that a hexagonal mesh is equivalent to a single grid of pitch  $\frac{1}{2}g$ .

## VI

### SOME PROBLEMS OF CYLINDERS

#### 6.1. Introduction

IN order to restrict the length of Chapter I we solved there only the two simplest problems of the cylinder, namely, a uniform current density flowing axially and a uniform current density flowing circumferentially; see §§ 1.8 and 1.15 respectively. These solutions must now be generalized to apply to any distribution, for only then can we find the resultant field of a long filament parallel to or transverse to a cylinder of any radius. Any distribution of axial or circumferential density can be expressed as a Fourier series, and hence the field of any given distribution of current can be found if we know the field due to a sinusoidal distribution of current density. We shall first consider currents which flow along the axis of the cylinder and with constant phase along its infinite length; accordingly we do not have to take account of electric charges and our problem is only a generalization of that solved in § 1.8. The effect of the inevitable charges which must accumulate at the very distant ends of the cylinder has been considered in § 1.7 and shown to be negligible. Charges must be present if current flows round the circumference, save only if the density is constant: consideration of circumferential flow is delayed until the end of this chapter.

#### 6.2. Field of a sinusoidal distribution of current density flowing along a cylinder

Let Fig. 6.1 represent the cross-section of a cylinder, of radius  $R$ , with current flowing perpendicular to the plane of the paper, alternating with frequency  $f = p/2\pi$  and distributed with density  $I_1 \cos \alpha$  round the circumference: thus if it is a positive maximum at  $A$  in Fig. 6.1 it is zero at  $B$  and  $B'$  and a negative maximum at  $A'$ . At any given instant of time current is flowing in the same sense over the whole of one half-circumference and in the opposite sense over the whole of the other half. Consider the field at a very distant point  $Q$  on bearing  $\theta$ . It is the sum of contributions from pairs of similarly placed and oppositely directed filaments, such as those typified by  $P$  and  $P'$  in Fig. 6.1. The vector diagram of field due to one such pair of unlike filaments is shown in Fig. 1.8 and the resultant is seen to be in phase quadrature with the field which would be due to an imaginary current  $I \sin pt$  at the centre of the cylinder. If unit current in either filament

alone would produce a field  $E_0$  at  $Q$ , then the two together produce a field  $2E_0 \sin \phi$ , where  $\phi = (2\pi R/\lambda) \cos(\alpha - \theta) \equiv k \cos(\alpha - \theta)$ . Accordingly

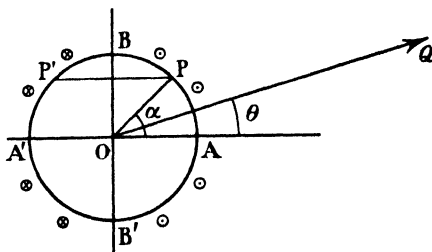


FIG. 6.1.

the resultant field at  $Q$ , due to all the filaments round the circumference, is given by

$$\begin{aligned}
 E &= 2E_0 I_1 \int_{-\pi/2}^{+\pi/2} \cos \alpha \sin \phi R d\alpha. \\
 \therefore \frac{E}{E_0} &= 2I_1 R \int_{-\pi/2}^{+\pi/2} \cos \alpha \sin \{k \cos(\alpha - \theta)\} d\alpha \\
 &= 4I_1 R \int_{-\pi/2}^{+\pi/2} \{J_1(k) \cos(\alpha - \theta) - J_3(k) \cos 3(\alpha - \theta) + \dots\} \cos \alpha d\alpha \\
 &= 4I_1 R \int_{-\pi/2}^{+\pi/2} \{J_1(k) (\cos \alpha \cos \theta + \sin \alpha \sin \theta) - J_3(k) \cos 3(\alpha - \theta) + \\
 &\quad + J_5(k) \cos 5(\alpha - \theta) - \dots\} \cos \alpha d\alpha \\
 &= 2\pi I_1 R J_1(k) \cos \theta.
 \end{aligned} \tag{6.1}$$

Hence, by (1.23),

$$\frac{cE}{a\pi I_1} = j 2\pi R J_1(k) \cos \theta \{-J_0(ar) + jY_0(ar)\}; \tag{6.1 a}$$

the factor  $j$  is required to show that the resultant field is (see Fig. 1.8) in leading phase quadrature with that of a current  $I \sin pt$  at the centre of the circle.

$$\text{Thus } \frac{cE}{a\pi I_1} = 2\pi R J_1(k) \cos \theta \{-Y_0(ar) - jJ_0(ar)\}. \tag{6.1 b}$$

When  $ar$  is very large  $Y_0(ar) \rightarrow J_1(ar)$  and  $J_0(ar) = -Y_1(ar)$  and then we may write (6.1 b) as

$$\frac{cE}{a\pi I_1} = 2\pi R J_1(k) \cos \theta \{-J_1(ar) + jY_1(ar)\}. \tag{6.2}$$



It follows from equation (1.43) that (6.2) is a solution of Maxwell's equations and thus must be valid everywhere, not only at infinity; it must hold for all values of  $r$  down to  $R$  and is the counterpart of (1.28). We must interchange  $ar$  and  $k$  for internal points and then it becomes

$$\frac{cE}{a\pi I_1} = 2\pi R\{-J_1(k) + jY_1(k)\}J_1(ar)\cos\theta. \quad (6.2a)$$

The field at the surface is

$$\frac{cE_R}{a\pi I} = 2\pi R\{-J_1(k) + jY_1(k)\}J_1(k)\cos\theta.$$

The radiation resistivity is  $a\pi/c \times 2\pi R J_1^2(k)$ ; this is zero when  $J_1(k) = 0$ , which occurs for the first time when  $R/\lambda = 0.61$ . The total output is

$$P = \int_0^{2\pi} iE_P R d\theta = \frac{a\pi}{c} J_1^2(k) \left( \frac{2\pi R I_1}{\sqrt{2}} \right)^2.$$

Reckoning in terms of the total mean square current round the circumference, the radiation resistance is thus seen to be  $30\pi^2 J_1^2(k)$  ohms per half wavelength.

Now consider a tube bearing an axially flowing current distributed as  $I_2 \cos 2\alpha$ : then if current is flowing upwards in two opposite quadrants it is flowing down in the other two. If these densities were concentrated at their points of maximum we should have the four current filaments which form the image system of a right-angled reflector. The field on bearing  $\theta = 0$  of such four filaments must be in antiphase with that of an imaginary positive filament at the centre, because the field of the negative pair is  $-2E_0$  while that of the positive pair is less than  $+2E_0$ , since they are not coincident. Applying this argument to the density  $I_2 \cos 2\alpha$  and proceeding as in (6.2), it follows that

$$\begin{aligned} \frac{cE}{a\pi I_2} &= j^2 2\pi R J_2(k) \cos 2\theta \{-J_0(ar) + jY_0(ar)\} \\ &= 2\pi R J_2(k) \{-J_2(ar) + jY_2(ar)\} \cos 2\theta, \end{aligned} \quad (6.3)$$

since  $J_0(ar) \rightarrow -J_2(ar)$ , when  $ar \rightarrow \infty$ .

Corresponding treatment of the densities  $I_3 \cos 3\alpha$ ,  $I_4 \cos 4\alpha$ , etc., shows that (6.3) can be generalized and gives

$$\frac{cE}{a\pi I_n} = 2\pi R J_n(k) \{-J_n(ar) + jY_n(ar)\} \cos n\theta \quad (6.4)$$

as the general expression for a current density  $I_n \cos n\theta$ : for internal points  $ar$  and  $k$  must be interchanged.

Note that the field is zero everywhere in the diametral planes passing through the points of zero current density and, accordingly, perfectly conducting and infinitely extended sheets may be placed in these planes. In other words, we have found the solution for a Vee reflector, of any angle, excited by a continuous arc of aerials at radius  $R$  and with current loading  $I_n \cos n\theta$ . We note with interest that the polar diagram is a sinusoid at any distance and thus side lobes are absent. It is an extension of the principle, developed in Chapter II, that the lobes of a flat array are reduced by concentrating the current in the middle portion: now we know how to make a lobe-free beam of any angular width. The forward field varies as  $J_n(k)$  and hence passes periodically through zero at intervals which tend ever closer to  $\frac{1}{2}\lambda$  as  $k$  increases. In this respect the curves of forward field resemble the families depicted in Figs. 3.9–3.13 for a single filament on the bisector of a Vee. Using the notation  $n\beta = \pi$  used in Chapter III, the total current in the ‘arc of aerials’ is  $I = 2I_n R/n$  and then the equation of the pattern may be written

$$\frac{E}{E_0} = \pi n J_n(k) \cos n\theta, \quad (6.5)$$

where  $E_0$  is the field which would obtain if the total current in the arc were concentrated in a filament and removed from the Vee. This shows there is one respect in which the present system differs markedly from that described by the family of curves Figs. 3.9–3.13. For in them the maxima of forward field, due to a given current, did not decrease as  $R$  increased, whilst here the said maxima tend to vary as  $R^{-1}$ . We found in Figs. 3.9, etc., that the forward field varied approximately as  $J_n(k)$  when  $k < n$ : now it varies precisely as  $J_n(k)$  for all values of  $k$ . It is easy to show that the power gain, relative to a single isolated filament carrying the same total current, is  $4n$  for all values of  $k$ . It follows at once from Poynting’s theorem that the gain must be independent of  $k$ ; because the output over the Poynting surface is proportional to the mean square field strength and this remains equal to one-half the square of the maximum since the pattern is always a sinusoid. This is also the reason why the gain tends to  $4n$  for a filament close to the apex of a Vee. When a Vee is excited by a sinusoidally loaded arc of aerials there are no stations for maximum gain, but the radiation resistance depends enormously on  $k$ , and falls periodically to zero. The fact that the gain can never exceed  $4n$  for a sinusoidally loaded arc

but can much exceed this value for a single filament may be compared with the reduction of gain which occurs when the loading of a curtain or in-line array is not uniform.

It should be noted that the external field is precisely zero everywhere (for  $r > R$ ) when  $J_n(k) = 0$ , a result which cannot occur when the current is concentrated into a single filament. It should also be noted that (3.13) can be written down at once, from (6.5), by expressing the concentrated loading as a Fourier series. It is instructive to consider the particular case when the length of the sinusoidally loaded arc is  $\frac{1}{2}\lambda$ : then  $k = n$  and (6.5) becomes

$$\frac{E}{E_0} = \pi n J_n(n) \cos n\theta = 0.446\pi n^{\frac{1}{2}} \cos n\theta;$$

see Chapter III (§ 3.5 (a)). This does not tend to zero as  $n$  tends to infinity, and hence the cut-off property of a truly parallel guide cannot be derived as a limiting case of the Vee: the reason is that unless the guide is truly parallel its width will exceed  $\frac{1}{2}\lambda$  after some distance from the apex.

The radiation resistance, reckoned in terms of the total current in the arc, is

$$30\pi^2 \times \frac{\pi^2 n J_n^2(k)}{4} \text{ ohms,}$$

per half wavelength of height. At the first maximum of  $J_n(k)$  this has the value

$$30\pi^2 \times \frac{\pi^2 n \left( \frac{0.675}{n^{\frac{1}{2}}} \right)^2}{4} = 30\pi^2 \times 1.12n^{\frac{1}{2}} \text{ ohms.}$$

Since the field behind the arc of current varies as  $J_n(ar)$ , there will be radii at which the field is zero provided  $k > 1.15n$ : accordingly a perfectly conducting sheet can be placed at such a radius without altering the field beyond the arc of current: then the apex of the Vee can be amputated. Hence by making  $n$  tend to infinity we have found the solution for a nearly parallel slot with an almost flat bottom, provided the width at the bottom of the slot exceeds  $0.525\lambda$ .†

Once it is realized that a sinusoidally loaded arc in a Vee reflector produces a sinusoidal beam without side lobes we have another degree of freedom in designing reflectors to produce a polar diagram of given shape. Thus a suitable combination of such an arc and a single filament can obliterate the  $\cos n\theta$  term and leave only the terms in  $\cos 3n\theta$ ,  $\cos 5n\theta$ , etc.

† For a fuller discussion of this limiting solution see *Journal I.E.E.*, Part III, 1945, 15.

The current density in the sides of the Vee is given by

$$\frac{i}{I_n} = \frac{\pi R n}{2r} J_n(k) \{Y_n(ar) + j J_n(ar)\}, \quad (6.6)$$

$$\text{or} \quad \frac{i}{I} = \frac{\pi n^2 J_n(k)}{4r} \{Y_n(ar) + j J_n(ar)\}, \quad (6.6a)$$

and in this form it resembles (3.18).

$$\begin{aligned} \therefore \frac{\lambda|i|}{I} &= 2n^2 J_n(k) \left( \frac{\pi}{2ar} \right)^{\frac{3}{2}}, \quad \text{if } ar > 2n, \text{ see p. 138,} \\ &= 0.35n^{\frac{1}{2}}, \quad \text{if } k = n \quad \text{and} \quad ar = 2k. \end{aligned}$$

Hence if the length of the loaded arc is  $\frac{1}{2}\lambda$ , then the induced density where the width is  $\lambda$  decreases very slowly as  $n$  increases. This probably means in practice that, as  $\beta$  decreases, the width of the sheets must be increased so as to maintain an aperture of given width.

### 6.3. Tube with sinusoidal distribution of axially flowing current density surrounded by a perfectly conducting tube

Let a current  ${}_1I_n \cos n\theta$  (with  $n$  an integer) be distributed round a tube of radius  $R_1$  and flow axially. Let a tube of radius  $R_2$  surround the first and carry a current  ${}_2I_n \cos n\theta$ . Then the field in the interspace is, by (6.4), given by

$$\begin{aligned} \frac{cE}{2a\pi^2 \cos n\theta} &= R_2 J_n(ar) \{-J_n(k_2) + jY_n(k_2)\} {}_2I_n + \\ &\quad + R_1 J_n(k_1) \{-J_n(ar) + jY_n(ar)\} {}_1I_n. \end{aligned}$$

If  ${}_2I_n$  is induced by  ${}_1I_n$  and if the surrounding tube is a perfect conductor, then  $E$  will be zero at  $ar = k_2$ , and this condition gives

$$\frac{{}_2I_n}{{}_1I_n} = -\frac{R_1 J_n(k_1)}{R_2 J_n(k_2)}.$$

Now  ${}_2I_n$  is a current density and the total current in any one band of like density is proportional to  ${}_2I_n R$ , and thus we have

$$\frac{\text{total outer current in a band}}{\text{total inner current in a band}} = -\frac{J_n(k_1)}{J_n(k_2)}. \quad (6.7)$$

Accordingly at the surface of the inner conductor we have

$$\frac{cE}{2a\pi^2 {}_1I_n} = -j \frac{R_1 J_n(k_1)}{J_n(k_2)} \{Y_n(k_2) J_n(k_1) - Y_n(k_1) J_n(k_2)\} \cos n\theta. \quad (6.8)$$

This equation shows the impedance of the inner tube is purely reactive,

as it must be since it is completely screened by the outer: and it is zero when

$$\frac{J_n(k_1)}{J_n(k_2)} = \frac{Y_n(k_1)}{Y_n(k_2)}. \quad (6.9)$$

If this condition is fulfilled, an axially flowing current will maintain itself without an applied voltage: in other words, it is a condition for a natural mode of oscillation.

The two tubes can be furnished with top and bottom covers at any distance apart, since the field is purely axial: then we obtain a closed chamber which is resonant whenever the frequency is such as to satisfy the condition (6.9). It is easy to show that if  $k_1^2 \gg n$ , this condition tends to become  $R_2 - R_1 = \frac{1}{2}\lambda$ .

We have presumed the current is constant in magnitude along the axis of the coaxial tubes. If it is distributed as  $\cos \pi y/g$ , then  $a$  in the previous equations must be replaced by  $a'$ , where  $a'^2 \equiv a^2 - b^2$  and  $b \equiv \pi/g$ ; compare § 1.9. If the distance between the cover plates of the closed resonant chamber is less than  $\frac{1}{2}\lambda$ , then the only possible distribution is constant along the axis. This means that the height of a resonant chamber ought always to be less than  $\frac{1}{2}\lambda$  in order to preclude modes in which the current density varies along the length. Provided the length is less than  $\frac{1}{2}\lambda$ , then the only possible modes with axial current are given by (6.9), where  $k_1 \equiv 2\pi R_1/\lambda$ .

We have now derived the whole and essential basis of the theory of resonant cylindrical chambers: we do not propose to study them further in this book on aerials, but it has been natural to include this section here so that the reader can continue the study if he desires.

#### 6.4. Current filament parallel to a metal cylinder

By means of equation (6.4) we can now determine the resultant field of a current filament parallel to a metal cylinder of any radius  $R$ , the origin of coordinates being at the centre of this cylinder. The field of a current filament, relative to an origin distant  $\lambda z/2\pi$  from it is given in equation (1.49) and described by Fig. 1.9: it is

$$\frac{cE}{a\pi I} = \{-J_0(ar) + jY_0(ar)\}J_0(z) + 2 \sum_{n=1}^{\infty} \{-J_n(ar) + jY_n(ar)\}J_n(z) \cos n\theta.$$

We propose to centre a cylinder at  $O$  in Fig. 1.9 (note: we now use  $R$  for the radius of the cylinder and make  $OB = \lambda z/2\pi$ ): the current filament at  $B$  will induce currents in the cylinder, the resultant field at  $(r, \theta)$  being due to the current  $I$  at  $B$ , together with the currents induced in the cylinder. The currents induced in the cylinder are determined

by the condition that the resultant field at its surface must be zero. Since (6.4) shows the field of a density  $I_n \cos n\alpha$  is everywhere proportional to  $\cos n\theta$ , the expression for the resultant field of  $I$  together with the induced density, expressed as a Fourier series, is found in a convenient form by adding (1.49) to a series whose terms are typified by (6.4). The magnitude of  $I_n$  being determined so as to make  $E$  zero at radius  $R$ . The general expression is

$$\frac{cE}{a\pi} = \{-J_0(ar) + jY_0(ar)\}\{IJ_0(z) + 2\pi RI_0 J_0(k)\} + \\ + 2 \sum_1^{\infty} \{-J_n(ar) + jY_n(ar)\}\{IJ_n(z) + \pi RI_n J_n(k)\} \cos n\theta$$

for  $ar > z$ . Inside or at the surface of the cylinder  $ar$  and  $z$  must be interchanged, also  $ar$  and  $k$ . At the surface  $E$  must be zero for all values of  $\theta$  and hence each term must be zero separately, and this gives

$$-\frac{I}{2\pi R} = \left[ \frac{-J_0(k) + jY_0(k)}{-J_0(z) + jY_0(z)} \right] I_0 = \frac{1}{2} \left[ \frac{-J_n(k) + jY_n(k)}{-J_n(z) + jY_n(z)} \right] I_n, \quad (6.10)$$

which leads to

$$-\frac{2\pi Ri}{I} = \frac{\{-J_0(z) + jY_0(z)\}}{\{-J_0(k) + jY_0(k)\}} + 2 \sum_1^{\infty} \frac{\{-J_n(z) + jY_n(z)\}}{\{-J_n(k) + jY_n(k)\}} \cos n\theta \quad (6.11)$$

for the general expression for the current density at any point of the surface: we shall write this in the form

$$-\frac{2\pi Ri}{I} = \frac{A_0 a_0 + B_0 b_0}{H_0^2} + 2 \sum_1^{\infty} \frac{A_n a_n + B_n b_n}{H_n^2} \cos n\theta + \\ + j \left\{ \frac{B_0 a_0 - A_0 b_0}{H_0^2} + 2 \sum_1^{\infty} \frac{B_n a_n - A_n b_n}{H_n^2} \cos n\theta \right\}, \quad (6.11 a)$$

where  $-J_n(z) \equiv A_n$ ,  $-J_n(k) \equiv a_n$ ,  $Y_n(z) \equiv B_n$ ,  $Y_n(k) \equiv b_n$ , and  $H_n^2 = J_n^2(k) + Y_n^2(k)$ . If the current is inside the cylinder it follows readily that

$$-\frac{I}{2\pi R} = \frac{J_0(k)}{J_0(z)} I_0 = \frac{1}{2} \frac{J_n(k)}{J_n(z)} I_n$$

and hence that

$$-\frac{2\pi Ri}{I} = \frac{J_0(z)}{J_0(k)} + 2 \sum_1^{\infty} \frac{J_n(z)}{J_n(k)} \cos n\theta. \quad (6.11 b)$$

Equation (6.11 b) shows that if  $R$  has a value which makes any one of the coefficients  $J_n(k) = 0$ , then the density  $I_n \cos n\alpha$  will run to infinity;

which shows that any order of resonance of a cylindrical chamber can be excited by an eccentric filament. It is important to note, however, that the exciting action for any mode is proportional to  $J_n(z)$ . Accordingly if it is necessary for some reason to use a chamber nearly large enough to be excited in the second mode, it will respond with great difficulty to that mode if the exciting wire is centred accurately: an understanding of this is important in the use of resonant chambers.

(a) *Numerical example of distribution of current density*

Equation (6.11) is very laborious to evaluate, but only by so doing is the general trend of its physical meaning disclosed. It is of great practical interest in two particular cases; when the current is so far away from the cylinder that the incident field is sensibly a plane wave, and when it is so close to the cylinder that the solution must be rapidly degenerating into that of a filament parallel to an infinite flat sheet. In approaching the second case we shall have an approximation to a filament in front of a flat sheet of finite width; this will occur when  $(z-k)/k$  is small and yet  $(z-k)/2\pi$  is not small. Since our concern is with the approach of a cylinder to an infinite plane, we will make the distance between the filament and cylinder near  $\frac{1}{4}\lambda$ , since this distance would be used in practice with a flat sheet. However, this requires that  $z-k = \frac{1}{2}\pi$  and this is troublesome in the use of tables: it will suffice to take  $z-k = 2$  which corresponds to the filament being distant  $0.32\lambda$  from the cylinder.

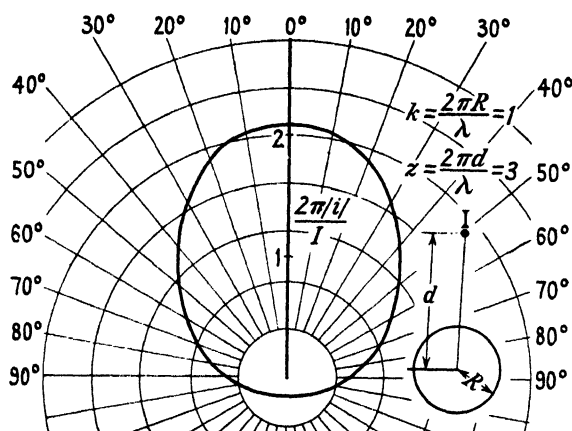
Familiar ideas of optics suggest the induced current density will be appreciable only on those portions of the cylinder which are 'visible' from the filament and, so to speak, illuminated by it. Here we need to distinguish two effects, namely, that the incident wave is not plane and the surface on which it falls is not plane. If the wave and the surface are plane the density is related to the field (see § 1.17) by the equation  $2\pi i/cE = 1$  and is in phase with it. If a filament is distant  $\lambda/2\pi$  from an infinite flat sheet it follows from (3.6) that  $2\pi i_0/cE = 1.052 \sqrt{12.5^\circ}$ , and this gives the limit (when the radius of the cylinder is infinite) for the current density at the 'bright spot' for the distance we have chosen. Evaluation from (6.10), for  $z-k = 2$ , gives the values collected in the following table for the 'bright spot' density and its phase lag with respect to the field incident there.

The table shows that the 'bright spot' density fluctuates, both in respect of magnitude and of phase, above and below its limiting value, but that the departures are small provided  $R/\lambda$  exceeds, say, 0.2.

TABLE 6.1

$R/\lambda$ . . . . .	0.158	0.475	0.795	1.58	$\infty$
$\lambda i/I$ . . . . .	2.10	1.83	1.90	1.97	1.84
Phase lag on field in degrees . . . . .	25.4	25.2	19.7	4.4	12.5

Fig. 6.2 shows a polar plot of  $\lambda|i|/I$  round a cylinder for which  $R/\lambda = 0.158$  ( $k = 1$ ) and shows that even in so small a cylinder the induced density is small over that portion of the cylinder which is in

FIG. 6.2. Mean square current density round cylinder of diameter  $0.32\lambda$ .

the optical shadow. Fig. 6.3 shows root mean square current density round cylinders for which  $k = \frac{1}{2}, 1, 3, 5$ , and 10: the short vertical stroke on each curve marks the angle at which the 'ray' from the aerial is tangential to the surface, thus  $35^\circ$  when  $k = 10$ . This figure demonstrates conclusively that the induced current in the dark area gets progressively less and less as  $R/\lambda$  increases. The labour of computing the current density is very great, but the obvious approach to a dark region suggests 'ray theory' may provide an approximate method of calculation. Accordingly we try the method of (3.6a) and compare the density with the equation  $2\pi|i|/c = |E| \cos \beta$ , where  $\beta$  is defined by the diagram inset in Fig. 6.3 and  $|E|$  is the field at distance  $AP = \rho$  from the current  $I$  at  $A$ . The inset graph compares the true density for  $k = 10$  with the density calculated by what we shall call 'ray theory'. There is a rough correspondence, but the agreement is not close. The agreement in respect of phase angle is quite hopeless: according to ray treatment  $i$  and  $E$  should always be cophased, whereas in this example  $i$  lags on  $E$  by  $4.4^\circ, 25^\circ$ , and  $44^\circ$  when  $\theta = 0^\circ, 10^\circ$ , and  $30^\circ$  respectively.



This and other experiences show the induced current is always finite at grazing incidence, whereas 'ray theory' requires it should then be zero and thus there must always be discrepancy: we shall see later the phase lag at grazing incidence appears to approach a limiting value of  $\frac{1}{2}\pi$ : in this numerical example it is  $\frac{1}{4}\pi$ .

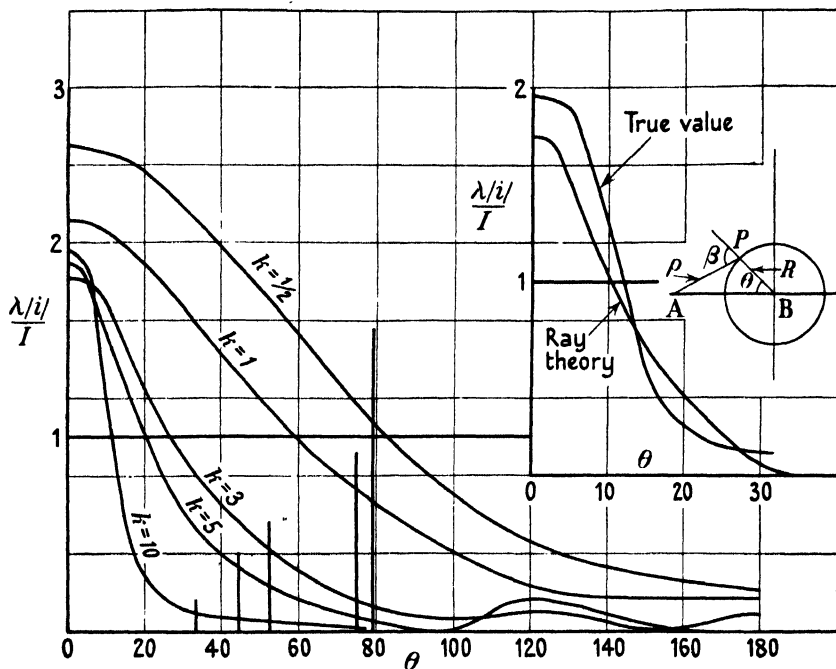


FIG. 6.3. Induced current density round circumference of cylinder for case where  $z-k=2$ : that is, aerial distant  $0.32\lambda$  from surface.

It is instructive to note that comparison of (6.11 *a*) and (6.11 *b*) shows that no single internal image current could induce the distribution of current that is induced by the external current and thus the cylinder cannot be replaced correctly by a single image. Note that (6.11) shows that no component of current density can become infinite if  $J_n(k) = 0$ , as it would do for an internal current.

(b) *The external field of the current in the presence of the cylinder*

By combination of (6.4) and (6.11) it follows the external field of the induced currents is

$$\begin{aligned}
 -\frac{cE}{\pi a I} = & \frac{\{-J_0(z) + jY_0(z)\}J_0(k)}{\{-J_0(k) + jY_0(k)\}} \{-J_0(ar) + jY_0(ar)\} + \\
 & + 2 \sum_{n=1}^{\infty} \frac{\{-J_n(z) + jY_n(z)\}J_n(k)}{\{-J_n(k) + jY_n(k)\}} \cos n\theta \{-J_n(ar) + jY_n(ar)\}. \quad (6.12)
 \end{aligned}$$

On making  $ar$  very large this becomes

$$-\frac{cE}{\pi a I} = \{-J_0(ar) + jY_0(ar)\} \left[ \frac{\{-J_0(z) + jY_0(z)\}J_0(k)}{\{-J_0(k) + jY_0(k)\}} + \right. \\ \left. + 2 \sum_1^{\infty} \frac{\{-J_n(z) + jY_n(z)\}J_n(k)}{\{-J_n(k) + jY_n(k)\}} \cos n\theta \right]. \quad (6.13)$$

Combination of (1.49), (6.4), and (6.11) gives the resultant external field as

$$\frac{cE}{\pi a I} = j \left[ \frac{\{J_0(z)Y_0(k) - J_0(k)Y_0(z)\}H_0(ar)}{H_0(k)} + \right. \\ \left. + 2 \sum_1^{\infty} \frac{\{J_n(z)Y_n(k) - J_n(k)Y_n(z)\}H_n(ar)}{H_n(k)} \cos n\theta \right], \quad (6.14)$$

where  $H_n(\ )$  stands for  $-J_n(\ ) + jY_n(\ )$ .

When  $ar$  tends to infinity this becomes

$$-\frac{cE}{\pi a I} = j\{-J_0(ar) + jY_0(ar)\} \left[ \frac{\{J_0(k)Y_0(z) - Y_0(k)J_0(z)\}J_0(z)}{\{-J_0(k) + jY_0(k)\}} + \right. \\ \left. + 2 \sum_1^{\infty} (j)^n \frac{\{J_n(k)Y_n(z) - Y_n(k)J_n(z)\}J_n(z)}{\{-J_n(k) + jY_n(k)\}} \cos n\theta \right]. \quad (6.15)$$

The diffraction pattern can be calculated from this for any  $k$  or  $z$ . It follows from (6.14) that the inphase component of field at the current is

$$-\frac{cE_P}{\pi a I} = \frac{\{J_0(k)Y_0(z) - Y_0(k)J_0(z)\}^2}{|H_0(k)|^2} + 2 \sum_1^{\infty} \frac{\{J_n(k)Y_n(z) - Y_n(k)J_n(z)\}^2}{|H_n(k)|^2} \quad (6.16)$$

and this gives the radiation resistance relative to an isolated filament.

### (c) Numerical examples of the external field and of the power gain

First we will continue the numerical example of a filament situated so that  $z-k=2$ . If the radius of the cylinder were infinite it would increase the forward field (see 3.15 a) in the ratio  $2 \sin 2 = 1.818$ . Fig. 6.4 shows forward field plotted as a function of  $R/\lambda$  up to  $k=10$ ; beyond that the labour of computation becomes prohibitive. It shows the forward field increases smoothly with  $R/\lambda$  and has reached 1.6 (the limit being 1.818) when  $R/\lambda = 7/4$ : when  $k=12$  the ratio is 1.69. The rate of approach to the limit is very slow: within the range  $k=2$  to 12 it can be expressed to an accuracy of 2 per cent., by the empirical relation

$E/E_0 = 1.818\{1 - 0.123(\lambda/R)^{\frac{1}{2}}\}$ , and according to this  $R/\lambda$  must exceed 16 before  $E/E_0$  is within 3 per cent. of its final limit. The lower curve in the same figure shows the 'back-to-front' ratio and this does approach zero rapidly: when  $k = 5$  it is about 2.5 per cent. and when  $k = 12$  it is less than 0.75 per cent.

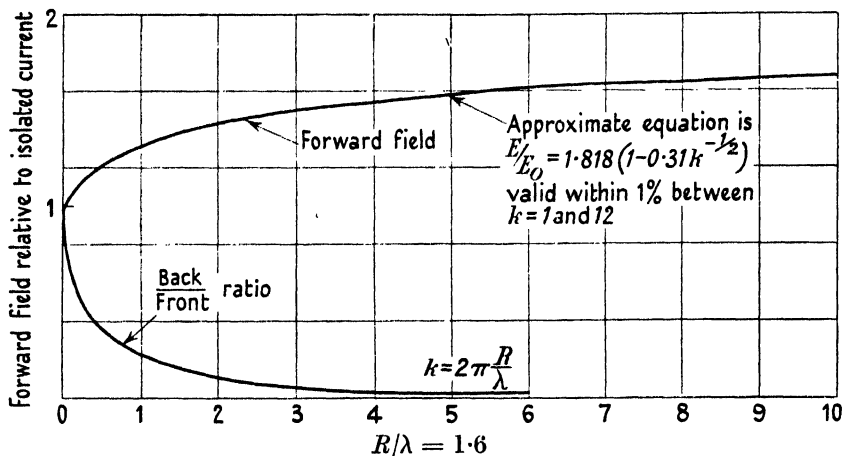


FIG. 6.4. Current distant  $0.32\lambda$  ( $z-k=2$ ) from surface of a cylinder. Curve of forward field and of back/front ratio as a function of  $R/\lambda$ .

The radiation resistance can be evaluated from (6.16). The limiting value, relative to an isolated current, is  $1 - J_0(4) = 1.3971$ , and accordingly the limiting gain is 2.36. Some representative values of relative resistance and gain are shown in Table 6.2 below.

TABLE 6.2

$R/\lambda$	0	0.032	0.08	0.16	0.32	0.47	0.8	1.6	$\infty$
Relative resistance	1	1.14	1.21	1.26	1.29	1.31	1.32	1.35	1.397
Gain	1	1.10	1.21	1.38	1.55	1.71	1.94	2.06	2.36

Table 6.2 shows the radiation resistance is more than 94 per cent. of the limit if  $R/\lambda$  exceeds 0.4, but then the approach to the limit is extremely slow. The empirical relation  $G = 2.36\{1 - 0.16(\lambda/R)^{\frac{1}{2}}\}$  is correct when  $R/\lambda = 0.8$  and 1.6: extrapolation from this shows  $R/\lambda$  must exceed 16 before the gain is within 4 per cent. of the final limit.

The diffraction pattern for  $k = 0, 2, 5, 7, 12$ , and infinity is shown in Fig. 6.5. It is interesting to note that the maximum near  $\theta = 37^\circ$  has appeared strongly even when  $R/\lambda$  is only 0.32. The field at  $\theta = 90^\circ$  is still not much less than unity even when  $R/\lambda = 1.9$  ( $k = 12$ ), and it is clear that  $R/\lambda$  must be very large before the field on this bearing

will fall to, say,  $\frac{1}{2}$ . If we are correct in presuming the gain is still only 0.96 of the limit when  $R/\lambda = 16$ , we must presume the field at  $\theta = 90^\circ$  is then still considerable because reference to Fig. 6.5 shows at once that the fractional contribution to the total output (by Poynting's theorem) is small in the arc  $90^\circ$  to  $180^\circ$ . Hence the field at  $\theta = 90^\circ$  may

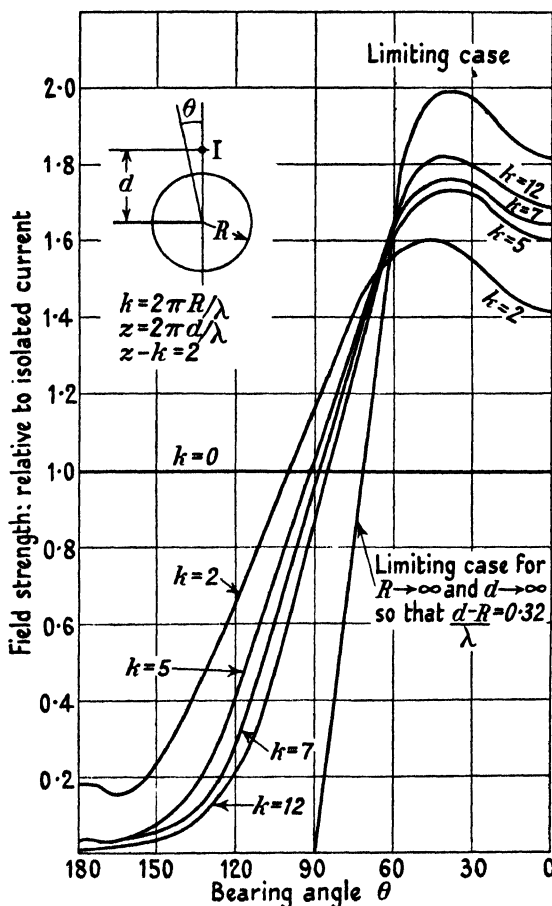


FIG. 6.5. Diffraction patterns for current parallel to cylinders of various radii.

well be still of the order of 0.2 when  $R/\lambda = 16$ . Thus it is clear that a cylinder of finite radius is comparatively ineffective in simulating an infinite sheet: up to, say,  $\theta = 70^\circ$  it will simulate an infinite sheet very closely even when  $R/\lambda = 1$ , but an enormous increase in size will make little reduction of field in the arc  $90^\circ$  to  $180^\circ$ . We may summarize the result as follows: If a cylinder is to be used as a reflector it had best be near one wavelength in radius: then the front-to-back ratio will

exceed 50 and the pattern between  $0^\circ$  and  $60^\circ$  will simulate closely that appropriate to an infinite sheet, but the gain will not exceed 2. Since the current density in the dark region is negligible, it seems fairly certain the cylinder could be replaced by a half-cylindrical shell without appreciable detriment.

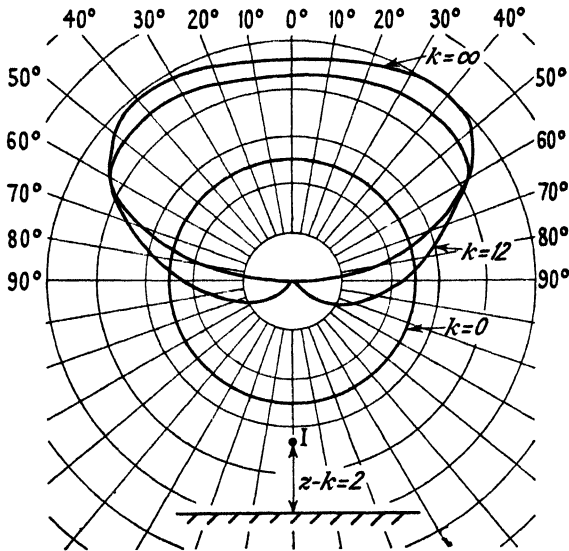


FIG. 6.6. Polar diagram for cylinder whose radius is  $1.9\lambda$  compared with that for a cylinder of zero radius and of infinite radius.

It is now instructive to compare these results with those arrived at in Chapter V for a semi-infinite sheet. Fig. 5.6 shows that when the semi-infinite sheet extends  $1.08\lambda$  beyond the filament, then the field in the plane of the sheet is 0.26 of the forward field, whereas for a cylinder where  $R/\lambda = 1$  it is 0.55 at  $\theta = 90^\circ$ . The flat sheet is thus seen to be relatively more effective, and this is to be expected. Fig. 5.6 is the pattern for a flat reflector limited in one sense, while Fig. 6.5 is the pattern for a round reflector, which is limited in both senses. Consideration of these two figures together suggests that a flat sheet reflector  $2\lambda$  in width should be competent to give a power gain near three and a relative field at  $\theta = 90^\circ$  of the order of 40 per cent. In short, a width  $2\lambda$  is about what should be used in practice.

Fig. 6.6 compares the polar diagram for  $R/\lambda = 1.9$  with that when  $R/\lambda$  is infinite or zero, and is a striking and reassuring comparison. The fair success, as reflectors, of comparatively small cylinders might be thought to be due mainly to the close proximity of the filament to

the cylinder; but within limits this is not true. To explore this effect a second numerical example has been evaluated for a filament whose distance is  $0.796\lambda$  ( $z-k=5$ ) from a cylinder whose radius is  $1.59\lambda$  ( $k=10$ ). Fig. 6.7 shows the distribution of current density for this example and compares it with that deduced from our 'ray theory'.

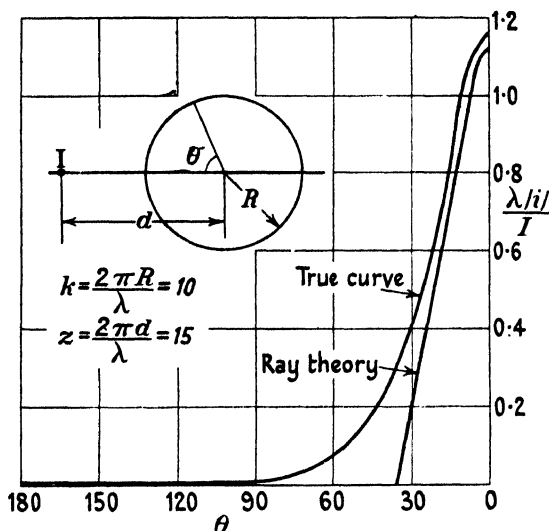


FIG. 6.7. R.M.S. current distribution round cylinder for  $k = 10$  and  $z = 15$ , i.e.  $R = 1.6\lambda$  and  $d - R = 0.8\lambda$ .

Here the ray theory is a successful approximation over  $20^\circ$  out of the  $30^\circ$  of illuminated arc, but the approximation must necessarily become bad when the glancing angle is approached. Fig. 6.8 shows the diffraction pattern and compares it with that appropriate to  $R/\lambda$  infinite. The two patterns bear a strong resemblance to one another and we may use the simile that the limiting pattern has slipped sideways. It is to be noted that the bearing of the minimum and the maximum has increased slightly, an effect which is commonly experienced in practice when comparing the experimental patterns from sheets of finite width with the ideal limiting patterns. We note once more that a comparatively small cylinder suffices to reproduce the salient features of the limiting pattern. These results, together with those of the last chapter, should reassure us that finite reflecting sheets will be found competent to reproduce very closely the outstanding features of an ideal pattern: evidently we shall not require to do more than make, from experience, an appropriate allowance for diffraction round the edges, or what an engineer would probably call a fringing effect.

## (d) Numerical example of the field quite close to the cylinder

Consider the inset diagram of Fig. 6.3: we wish to find the field at any point in the line through the centre  $B$  and perpendicular to  $AB$ . At the surface of the cylinder the field is necessarily zero: following

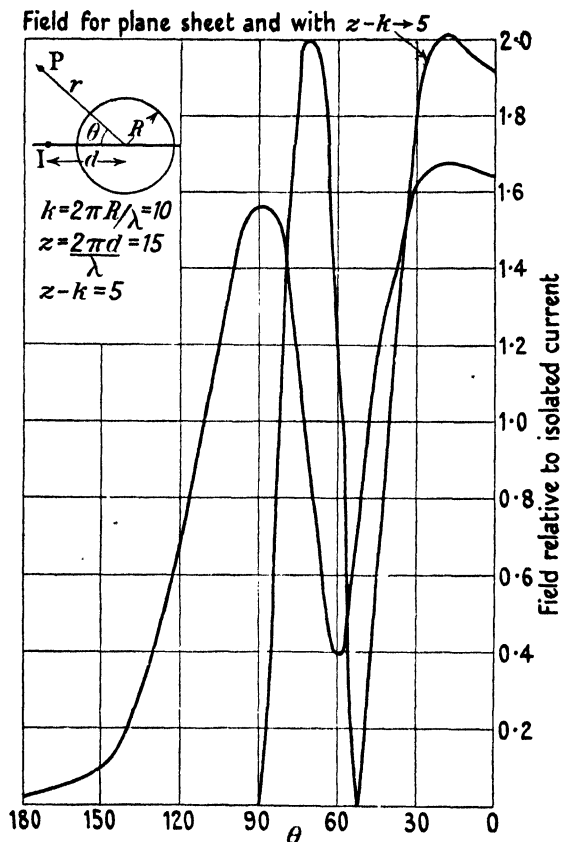


FIG. 6.8. Diffraction pattern for cylinder  $R/\lambda = 1.59$  and  $z-k = 5$ .

optical ideas it might be expected the field would remain almost zero until a point in this plane was reached from which the filament could be 'seen', using this word in its optical sense. Then the field would rise rapidly and pass through a maximum, since ultimately it must decrease in virtue of attenuation with increasing distance. The field at any point in this plane can be evaluated by putting  $\theta = \frac{1}{2}\pi$  in (6.14) provided  $ar > z$ : if  $ar < z$ , then  $z$  and  $ar$  must be interchanged. Fig. 6.9 shows the field in this plane due to a filament distant  $0.32\lambda$  from the surface of a cylinder of radius  $1.9\lambda$ . The filament cannot be 'seen' until a point

is reached in this plane distant  $1.86R$  from the surface, and this point is marked  $A$  in the figure. The graph in the figure shows the field has reached its maximum at a point much nearer the surface than the point  $A$  and that the maximum occurs very near the distance  $ar = z$ ; and from this distance the aerial cannot be 'seen'. At large distances the field varies as  $(ar)^{-\frac{1}{2}}$  and its absolute magnitude can be derived from (6.15). The dotted curve in Fig. 6.9 shows the asymptotic value for

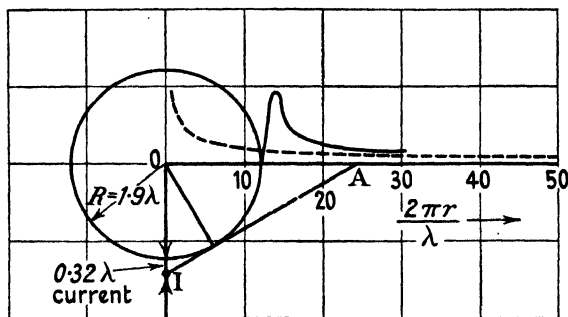


FIG. 6.9. Electric field close to cylinder and in diametral plane perpendicular to that containing the current.  $k = 2\pi R/\lambda = 12$ ,  $z = 2\pi d/\lambda = 10$ .

large distances, and it may be seen that the field approaches close to this limit even when  $ar$  is no larger than 30 (say  $r/\lambda = 5$ ): it is another example of the rapidity of approach to limiting values. Presumably the maximum typified in Fig. 6.9 will move away from the cylinder when  $R/\lambda$  becomes very large. But there is always a tendency for the field to be large at  $ar = z$ , for the series giving the quadrature component of field at  $\theta = 90$  and  $ar = z$  is the series for the quadrature component of the field at the filament with every odd term missing and with alternate terms of the remaining series having opposite signs. At the filament  $E_Q$  tends logarithmically to infinity. Hence, at  $\theta = \frac{1}{2}\pi$ ,  $E_Q$  is given by a convergent series which is the finite difference between two divergent series, and this difference may well be substantial. It is too laborious to pursue this much further, but it would seem the field in the shadow is much greater than the field, for  $\theta = 90^\circ$ , extrapolated back to this region. Thus the relative value of the distant field strength at  $90^\circ$  in the example recorded in Fig. 6.5 is approximately equal to  $1.68k^{-\frac{1}{2}} = 0.67(\lambda/R)^{-\frac{1}{2}}$ . According to this the field at distance  $r$  on bearing  $90^\circ$  is given approximately by

$$\frac{cE}{a\pi I} \doteq 2 \sqrt{\left(\frac{2}{\pi ar}\right)} \times \sqrt{\left(\frac{2.8}{aR}\right)} = \frac{2.7}{aR},$$

when  $r = R$ . According to this approximate formula the field on bearing



$\theta = 90^\circ$  is approximately equivalent to that of a current  $\frac{1}{2}(aR)^{-1}$  at the centre of the cylinder, and this may be regarded as giving an approximate lower limit for the field in much of the shadow region. Unfortunately the Bessel expression is very cumbersome to evaluate and this makes it very laborious to trace the approach to the conditions obtaining in optical experience. It would appear, however, that the radii must be very large before the 'optical path' treatment is approached closely.

(e) *Attempt to use the optical image treatment for estimating the forward field*

According to the treatment of geometrical optics the distance from the centre of the object and the image are related by the formula  $1/v + 1/u = 2/R$ . Hence if  $v = 14$  and  $R = 12$ , we find  $u = 21/2 = 10.5$ . For the example  $z = 14$  and  $k = 12$  we will place an image at  $u = 10.5$  and make it of such a strength that it neutralizes the field at the 'brightest spot' of the cylinder. Reference to tables shows that

$$|H_0(2)| = 0.557 \sqrt{66.3^\circ} \quad \text{and} \quad |H_0(1.5)| = 0.639 \sqrt{36.8^\circ}.$$

Accordingly the image current must be  $0.557/0.639 = 0.875$  times the current in the filament and lead it by  $150.5^\circ$ . Consideration shows the forward field is the sum of two vectors in the ratio 0.87 and inclined at  $29.5^\circ$ , and this equals 1.80, whereas Fig. 6.5 shows the forward field is then 1.7, and the field is 1.82 on a bearing of  $40^\circ$ . Thus the image treatment is seen to be approximately correct. Now treat the example of Fig. 6.8 in this manner: here we find  $u = \frac{15}{2}$  when  $z = 15$  and  $k = 10$ , and it follows from tables that the image current must be 0.718 of the filament current and leading it by  $71.2^\circ$ . The vector sum is found to be 1.71 where Fig. 6.8 shows it should be 1.64. Thus it seems the treatment by optical image gives the forward field very closely; but the image method cannot be expected to work well on other bearings, since the formula relates only to reflection from a small region of the cylinder near the bright spot. It does not seem possible to arrive at the position of the optical image by any but ray treatment.

### 6.5. Reciprocal properties with cylinders

Equation (6.14) gives the field at point  $(r, \theta)$  due to a current  $I$  at point  $(z, 0)$  in the presence of a cylinder of any radius  $k/2\pi$  provided  $ar > z$ . Equation (6.12) shows complete reciprocity in respect of the field of the induced current: thus, the field at  $(r, \theta)$  due to the current induced by a current  $I$  at  $(z, 0)$  is the same as the field at  $(z, 0)$  due to the currents induced by a current  $I$  at  $(r, \theta)$ . Hence the resultant field at  $(r, \theta)$  due to current  $I$  at  $(z, 0)$  is the same as the resultant field at

$(z, 0)$  due to a current  $I$  at  $(r, \theta)$ . This proves that the forward field test in reception will be the same as the forward field test in transmitting. Let the reactance of the filament be neutralized by tuning, as in a long in-line array: then the current which will flow in reception is directly proportional to the radiation resistance at the given position of the in-line array. The power absorbed will be a maximum when the loading resistance equals the radiation resistance at the given station of the filament. We have defined the power gain as the square of the relative forward field divided by the relative radiation resistance: when this quotient is a maximum we call the forward power gain a maximum. It follows from the reciprocal property described above that the power which can be absorbed in reception is a maximum when the aerial is at a station for maximum forward gain in transmission and in addition when the load resistance equals the radiation resistance for this station.

There is another interesting property, of a reciprocal character, which can be deduced from (6.16) which shows the power output due to the component density  $I_n \cos n\alpha$  is zero whenever  $k$  and  $z$  are related in such a way as to make

$$\frac{J_n(k)}{J_n(z)} = \frac{Y_n(k)}{Y_n(z)}$$

and, by (6.9) this is the condition for the  $n$ th order of resonance of a coaxial cylindrical chamber having radii  $z/2\pi$  and  $k/2\pi$ . Thus we see that an external current will induce a density  $I_n \cos n\alpha$ , where  $I_n$  is never zero or infinite even if  $k$  is such as to make  $J_n(k) = 0$ ; when  $J_n(k) = 0$  the external field of that component density is precisely zero: but if an external current is situated at a radius which satisfies (6.9), then the component density  $I_n \cos n\alpha$  makes no net contribution to the total power output. Equation (6.11) shows that when (6.9) is satisfied then the component  $I_n$  is exactly cophased with  $I$  and equal to

$$-\frac{J_n(z)}{J_n(k)} \frac{2I}{2\pi R}.$$

This cannot be zero or infinite because (6.9) cannot be satisfied if either  $J_0(z)$  or  $J_0(k)$  are zero.

## 6.6. Plane wave incident on a cylinder parallel to the electric vector

To obtain a solution for a plane wave incident on the cylinder and advancing from right to left we have only to put  $z$  infinite in (6.11) to

(6.14) and (1.49), remembering that now  $z > ar$ . In this range (1.49) becomes

$$\begin{aligned} \frac{cE}{a\pi I} &= J_0(ar)\{-J_0(z)+jY_0(z)\}+2\sum_{n=1}^{\infty} J_n(ar)\{-J_n(z)+jY_n(z)\}\cos n\theta \\ &= \{-J_0(z)+jY_0(z)\}\{J_0(ar)-2jJ_1(ar)\cos\theta-2J_2(ar)\cos 2\theta+ \\ &\quad +2jJ_3(ar)\cos 3\theta+2J_4(ar)\cos 4\theta-\dots\}, \end{aligned}$$

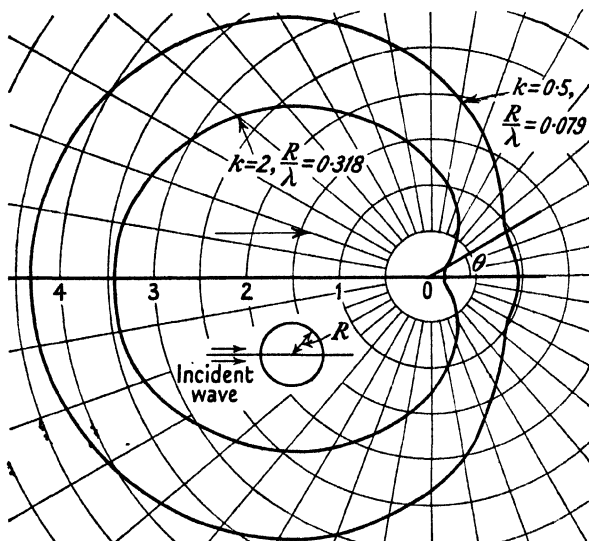


FIG. 6.10. R.M.S. current density round circumference of cylinder induced by plane wave.

when  $z \rightarrow \infty$  since then  $J_1 = Y_0$  and  $J_0 = -Y_1$ , etc. The incident field at the centre of the cylinder is

$$E_w = \frac{a\pi I}{c} \{-J_0(z)+jY_0(z)\}.$$

Accordingly (6.11) now becomes

$$\begin{aligned} -\frac{2\pi^2 ki}{cE_w} &= \frac{1}{-J_0(k)+jY_0(k)} - 2\left\{ \frac{\cos 2\theta}{-J_2(k)+jY_2(k)} - \frac{\cos 4\theta}{-J_4(k)+jY_4(k)} + \dots \right\} \\ &\quad - 2j\left\{ \frac{\cos \theta}{-J_1(k)+jY_1(k)} - \frac{\cos 3\theta}{-J_3(k)+jY_3(k)} + \dots \right\}, \quad (6.17) \end{aligned}$$

$$\begin{aligned} \text{or} \quad \frac{2\pi^2 ki}{cE_w} &= \left( \frac{J_0}{|H_0|^2} + \frac{2Y_1 \cos \theta}{|H_1|^2} - \frac{2J_2 \cos 2\theta}{|H_2|^2} - \frac{2Y_3 \cos 3\theta}{|H_3|^2} + \dots \right) + \\ &\quad + j\left( \frac{Y_0}{|H_0|^2} - \frac{2J_1 \cos \theta}{|H_1|^2} - \frac{2Y_2 \cos 2\theta}{|H_2|^2} + \frac{2J_3 \cos 3\theta}{|H_3|^2} + \dots \right), \quad (6.17a) \end{aligned}$$

where

$$|H_n|^2 \equiv J_n^2(k) + Y_n^2(k).$$

By means of this equation the two components of current density can be plotted as a function of  $\theta$ , but it is more instructive to plot  $|i|$ , the R.M.S. density: this has been done for  $R/\lambda = 0.079$  and  $0.318$  in Fig. 6.10, and these polar curves show the current at the 'bright spot' is very much greater than at the 'dark spot'. Fig. 6.11 shows  $|i|$  plotted

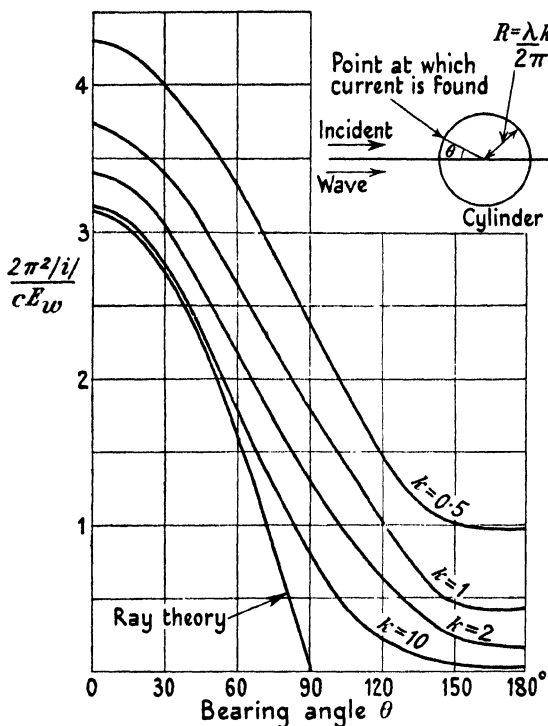


FIG. 6.11. Current distribution (R.M.S.) round cylinders of various radii, induced by plane wave.

against  $\theta$  in Cartesian coordinates for  $R/\lambda = 0.08, 0.16, 0.32$ , and  $1.6$ , together with a cosine curve for comparison, and shows the dark spot density tends rapidly to zero: when  $R/\lambda = 1.6$  ( $k = 10$ ) the dark spot density is only 1 per cent. of the bright spot density, and this is in accordance with the optical concept of illuminated area. The cosine curve shows the density calculated according to what we have called 'ray theory', and it may be seen that this is substantially correct over the first  $60^\circ$  of the  $90^\circ$  of illuminated arc when  $k = 10$ . Numerical evaluation shows there is strong tendency for the current induced at a given point on the cylinder to be in time phase with the field incident at that

point, and this is well illustrated by the results collected in Table 6.3 for  $R/\lambda = 1.6$  ( $k = 10$ ).

TABLE 6.3  
 $k = 10$

$\theta$	0	15	30	45	60	75	90
Phase lag relative to field	3.1	3.4	3.7	6.0	10.5	16.8	32.5

The discrepancy in both phase and magnitude at  $\theta = 90^\circ$  is large, presumably the magnitude of  $|i|$  falls slowly to zero when  $k$  tends to infinity, but it does not seem possible to deduce this from (6.17*a*); the phase discrepancy shows a strong tendency to tend rapidly to  $\frac{1}{2}\pi$  as is shown by Table 6.4.

TABLE 6.4  
*Magnitude and relative phase at  $\theta = 90^\circ$*

$k$	0	0.5	1	2	3	6	10	24
Magnitude relative to bright spot	1	0.54	0.47	0.38	0.32	0.26	0.23	0.17
Phase relative to incident field	90	42	39.5	35.3	35	33.5	32.5	31.6

Since Table 6.4 appears to show that the phase discrepancy tends rapidly to  $30^\circ$ , it may be that Table 6.3 is a fairly good guide to the phase discrepancy (as a function of  $\theta$ ) for large  $k$ , and accordingly that the discrepancy at  $\theta = 75^\circ$  tends to about  $15^\circ$ . We have now interpreted the cumbersome equation (6.17*a*) as showing that the current is nearly all on the illuminated side and follows ray theory closely over, say,  $\pm 60^\circ$  of arc. According to ray theory we should have  $2\pi i/cE = 1$  at the bright spot: when  $k = 5$  or  $10$  then  $2\pi i/cE = 1.08$  and  $1.01$  respectively, thus showing the rate of approach to the limit is very rapid.

When  $k$  tends to zero equation (6.17*a*) reduces to

$$\frac{2\pi^2 k |i|}{cE_w} \div \frac{1}{|H_0|^2} (1 + \pi k \cos \theta),$$

if  $2\pi k \ll 1$ , and this gives a ready means of assessing the size of rod at which the non-uniformity of current density becomes appreciable. It is, however, evident from Fig. 6.10 that the non-uniformity must be appreciable if  $R/\lambda$  exceeds, say,  $0.01$ : then the approximate formula above gives  $3/2$  for the ratio of the maximum to minimum density. It is perhaps surprising to find that the rod must be extremely small

before we may regard the induced density as uniform and calculable directly from (1.23), as was done in § 5.8*a*.

(a) *The external field of the currents induced in the cylinder*

This is obtained by making  $z$  tend to infinity in (6.12) and gives accordingly

$$-\frac{E}{E_w} = \frac{J_0(k)\{-J_0(ar)+jY_0(ar)\}}{\{-J_0(k)+jY_0(k)\}} - \frac{2J_2(k)\{-J_2(ar)+jY_2(ar)\}}{\{-J_2(k)+jY_2(k)\}} \cos 2\theta + \dots + \\ + 2j \left[ \frac{J_1(k)\{-J_1(ar)+jY_1(ar)\}}{\{-J_1(k)+jY_1(k)\}} \cos \theta - \frac{J_3(k)\{-J_3(ar)+jY_3(ar)\}}{\{-J_3(k)+jY_3(k)\}} \cos 3\theta + \dots \right]; \quad (6.18)$$

when  $ar \rightarrow \infty$  this becomes

$$-\frac{E}{E_w} = \{-J_0(ar)+jY_0(ar)\} \left[ \frac{J_0(k)}{\{-J_0(k)+jY_0(k)\}} - \frac{2J_1(k)\cos \theta}{\{-J_1(k)+jY_1(k)\}} + \right. \\ \left. + \frac{2J_2(k)\cos 2\theta}{\{-J_2(k)+jY_2(k)\}} - \dots \right], \quad (6.18a)$$

and this gives the diffraction pattern of the wave re-radiated or scattered by the cylinder. It is useful for estimating the echo which returns to the transmitter after the cessation of a transmission and is of interest in radiolocation. Figs. 6.12–6.13 show the polar diagram of re-radiated field for  $R/\lambda = 0.32$  and  $3.2$  respectively: they are characterized by a substantially constant mean square field in the bearing arc  $\pm 100^\circ$  together with an ever narrowing beam which provides the deep shadow. Fig. 6.14 exhibits the forward field and the backward field at any given distance as a function of  $k$ . The shadow field increases linearly with  $k$  according to the empirical formula  $0.8 + 1.03k$ , while the echoed field varies as  $k^{\frac{1}{2}}$  according to the empirical relation  $\frac{1}{2}\sqrt{(\pi k)}$ . It seems surprising to find the cumbersome expression (6.18*a*) describes only the simple linear and parabolic relations disclosed by the numerical evaluation recorded in Fig. 6.14, and a direct approach is not hard to find.

Thus consider Fig. 6.15 in which that half of the cylinder which is in shadow is shown shaded. Round the bright half the density is given approximately by the relation  $i = (cE_w \cos \alpha)/2\pi$  and round the dark half it is almost zero everywhere. We have seen that the density at a point such as  $B$  in Fig. 6.15 lags on the density at point  $A$  by an angle nearly corresponding to the path difference  $A'B$ . Now consider the field of these induced currents (flowing perpendicular to the plane of the paper) at a very distant point  $P$  in a direction parallel to  $OA$ . The component of field at  $P$  due to the density at  $B$  will lead on the component due to

the density at  $A$  by an angle corresponding to the path difference  $A'B$ ; but since the current at  $B$  lags on that at  $A$  by the same angle, it follows the components of field due to all the filaments of current will

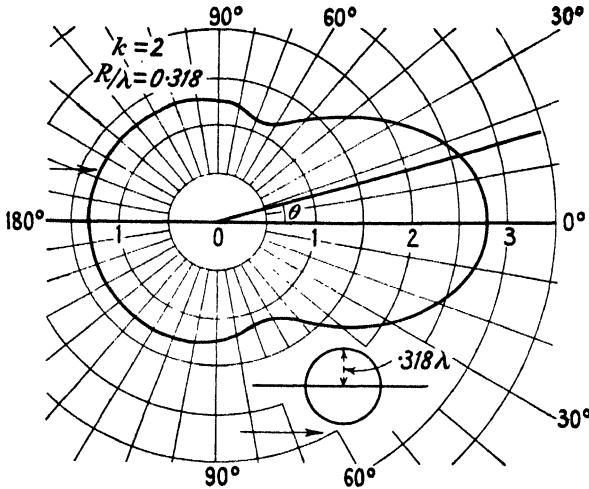


FIG. 6.12. Polar diagram of external field of induced current.  $k = 2$ ,  $R/\lambda = 0.318$ .

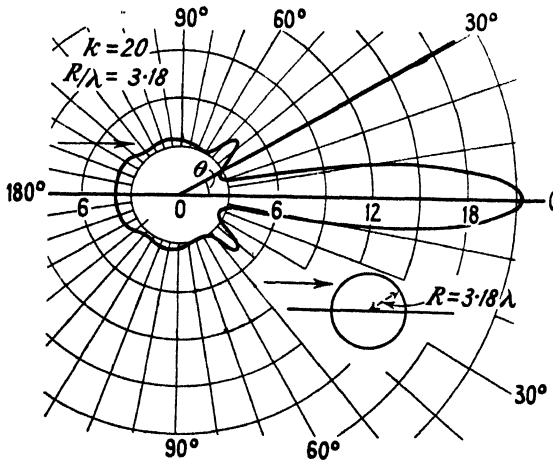


FIG. 6.13. Polar diagram of external field of current.  $k = 20$ ,  $R/\lambda = 3.18$ .

be cophased at a distant point  $P$ . It is as though all the current were in the plane  $AA'$ : since the density varies as  $\cos \alpha$  the total current is  $I' = cE_w/2\pi \times 2R$ . Hence the distant field in the direction  $AO$  is

$$E = \frac{a\pi I'}{c} \{-J_0(ar) + jY_0(ar)\} \quad \text{or} \quad \frac{E}{E_w} = aR \{-J_0(ar) + jY_0(ar)\},$$

whence  $|E|/|E_w| = k|H_0(ar)|$ , and this differs insensibly from the result disclosed by the straight line in Fig. 6.14. It must be an underestimate because it ignores the vanishingly small current on the dark half of the

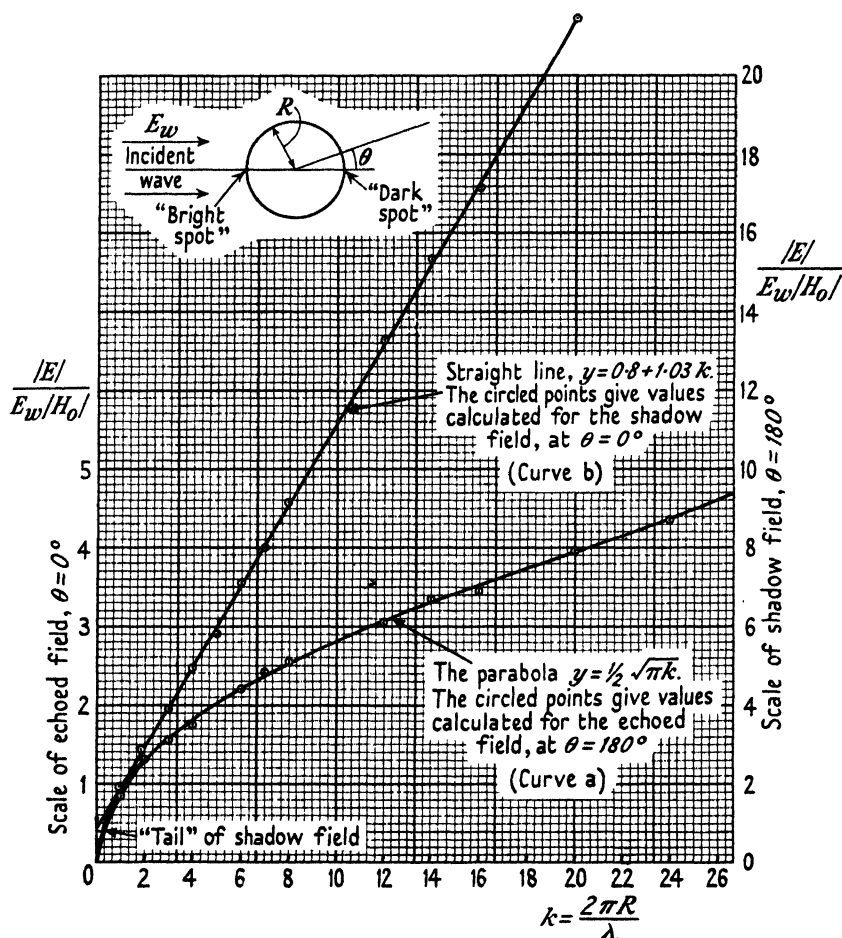


FIG. 6.14. External field (R.M.S.) at bearings  $0^\circ$  and  $180^\circ$ , due to current induced in cylinders of various radii, by the incidence of a plane electric wave.

cylinder and supposes that  $i$  varies precisely as  $\cos \alpha$  on the bright half and ignores the progressive discrepancy in phase which occurs as  $\alpha$  approaches  $90^\circ$ : it is instructive to note the underestimate is but 7 per cent. even when  $k$  is only 10. The 'shadow field' increases linearly with  $k$  because the total induced current increases linearly with  $k$  and all elements are effectively cophased in respect of the field they produce at a distant point. It should be noted that this property is independent



of the shape of the object provided the phase of the induced current is always sensibly that of the incident wave. We have ignored the discrepancy in the phase of the induced current, a discrepancy which tends to become  $30^\circ$  at  $C$  and  $C'$ : this will have small effect on  $|E|$  but will have a more noticeable effect on its phase. Thus, evaluation for (6.18a) shows the phase of the distant field lacks  $13^\circ$  and  $5.5^\circ$  from

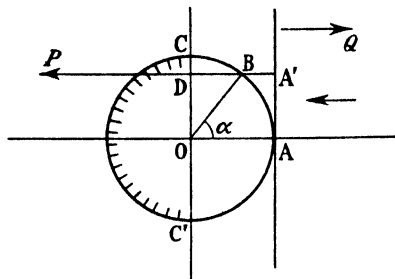


FIG. 6.15.

precise antiphase with the incident field there when  $k = 6$  or  $24$  respectively. These figures suggest the discrepancy from antiphase is approximately equal to  $10(\lambda/R)^{1/2}$  degrees of arc, and if this be true it will exceed  $1^\circ$  until  $R/\lambda$  exceeds  $100$ . This discrepancy of phase will give rise to a standing wave pattern in the region of deep shadow.

Now consider the 'echoed field' at a distant point  $Q$  in direction  $OA$  in Fig. 6.15. The effective path difference for filaments at  $B$  and  $A$  will be  $2A'B$ ; and thus the field is produced by a semicircle bearing a cosine distribution of induced current and the effective path difference being as though the radius were twice what it really is. The field at  $Q$  will have an inphase and a quadrature component, the second being given by (6.2a), on remembering the effective radius for path difference is  $2R$ . From this equation we have

$$\frac{cE_Q}{a\pi I_1} = \pi R J_1(2k) \times |H_0(ar)|, \quad \text{where } I_1 = \frac{cE_w}{2\pi}.$$

It can be shown the inphase component is given by

$$\frac{cE_P}{a\pi I_1} = 2R \left[ J_0(2k) - 2 \left\{ \frac{J_2(2k)}{1.3} + \frac{J_4(2k)}{3.5} + \dots \right\} \right] \times |H_0(ar)|.$$

When  $2k$  is very large  $J_0 = -J_2 = J_4$ , etc., and then

$$\begin{aligned} \frac{cE_P}{a\pi I_1 |H_0(ar)|} &\doteq 2R J_0(2k) \left\{ 1 + 2 \left( \frac{1}{3} - \frac{1}{15} + \frac{1}{35} \dots \right) \right\} \\ &\doteq 2R J_0(2k) \times 1.562 \doteq \pi R Y_0(2k) \doteq -\pi R Y_1(2k). \end{aligned}$$

Hence 
$$\frac{|cE|}{a\pi RI_1} = \pi |H_1(2k)| \times |H_0(ar)|,$$

whence

$$\frac{|E|}{|E_w|} = \frac{\pi k}{2} |H_1(2k)| \times |H_0(ar)| \doteq \frac{\pi k}{2} \sqrt{\left(\frac{1}{\pi k}\right)} H_0(ar), \quad \text{when } 2k \text{ is large} \\ = \frac{1}{2} \sqrt{(\pi k)} |H_0(ar)|, \quad (6.19)$$

and thus agrees precisely with the empirical relation found from Fig. 6.14. Evaluation of the approximate expression just given for  $E_P$  shows that if  $k$  exceeds 2 the expression in the curled brackets differs very little from  $\pi\sqrt{2}$  and hence we suspect  $E$  is given closely by the expression

$$\frac{E}{E_w} = \frac{\pi k}{2} \{-Y_1(2k) + jJ_1(2k)\} \times |H_0(ar)|, \quad (6.20)$$

and accordingly this will differ insensibly from the cumbersome expression (6.18a) at  $\theta = 0$ . It should be noted that  $E/E_w$  is unity when  $ar = k$ , provided  $k$  is large enough to replace  $H$  by its asymptotic form: moreover, it follows that in these circumstances the phase at  $ar = k$  is equal to  $k$ . Hence the approximate expression is correct in magnitude and phase at the surface of the cylinder provided  $k$  exceeds about 3, even though it was derived for application at large distances. Numerical evaluation from (6.18a) shows that  $E_P$  and  $E_Q$  differ insensibly from  $(\pi k/2)Y_1(2k)$  and  $(\pi k/2)J_1(2k)$  respectively provided  $k$  exceeds, say, 2. Thus  $E_Q$  should be zero, according to the approximate expression, when  $J_1(2k) = 0$ , which is when  $k = 1.91, 3.5$ , etc., whereas  $E_Q$  is in fact zero when  $k = 2.1, 3.5$ , etc.: and  $E_P$  should be zero when  $k = 1.09, 2.71, 4.3$ , etc., whereas  $E_P$  is zero when  $k = 1.5, 2.8, 4.3$ , etc. Hence the approximate expression (6.20) is correct at a large distance for  $k$  greater than, say, 2: strange to say, it seems to hold even down to  $ar = k$ .

No doubt the field on any bearing could be calculated from the approximate distribution of current, but to do so would be nearly as cumbersome as using (6.18a) and would not be very helpful, more especially since Figs. 6.12–6.13 have shown that the polar diagram is nearly a circle in the range of bearing  $\pm 110^\circ$ . The field at  $\theta = 90^\circ$  has been evaluated from (6.18a) and when plotted as a function of  $k$  is indistinguishable from the parabola  $y = (k/2)^{\frac{1}{2}}$  and thus is 81 per cent. of the field echoed along bearing zero.

According to geometrical optics the reflected rays appear to come from a focus half-way between the bright spot and the centre. Following the process used in § 6.4 (e), we attempt to replace the cylinder by an

equivalent current  $I'$  at this focus, determined in magnitude and phase so as to make the field zero at the bright spot: accordingly

$$\frac{cE_w(\cos k - j \sin k)}{a\pi I'} = \{-J_0(\tfrac{1}{2}k) + jY_0(\tfrac{1}{2}k)\},$$

and so 
$$\frac{|E|}{|E_w|} = \frac{|H_0(ar)|}{|H_0(\tfrac{1}{2}k)|} \doteq \tfrac{1}{2}\sqrt{(\pi k)}H_0(ar),$$

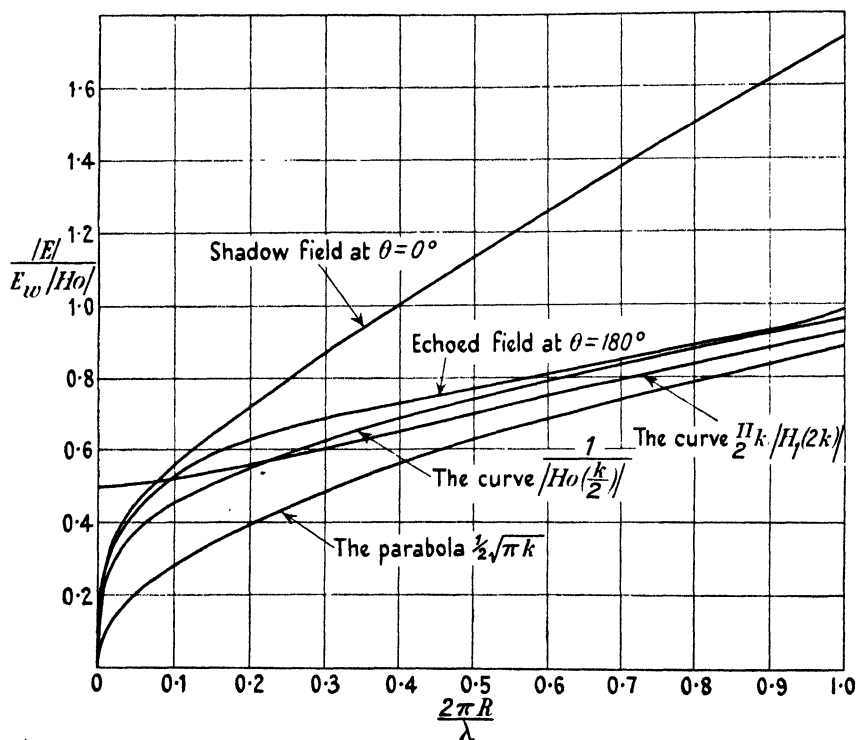


FIG. 6.16. External field at bearings  $0^\circ$  and  $180^\circ$ , due to currents induced in cylinders of various small radii.

since  $|H_0(\tfrac{1}{2}k)| = \sqrt{(4/\pi k)}$  when  $k$  is large. Thus by one approximate approach we have replaced the cylinder by an equivalent current at the centre of the cylinder and in the other treatment by an equivalent current at the optical focus.

Fig. 6.16 is an enlarged view of the foot of Fig. 6.14. It shows the echoed and shadow field differ noticeably when  $k$  exceeds say, 0.1 ( $R/\lambda = 0.016$ ). The lowest curve in the figure is the parabola  $\tfrac{1}{2}(\pi k)^{\frac{1}{2}}$ , the next above it is the echoed field calculated from the approximate expression (6.20). The curve between this and below the true value of the echoed field is that calculated by the focus treatment but using

the exact and not the approximate value of  $|H_0(\frac{1}{2}k)|$ . The focus treatment is the nearest approach and is substantially correct even down to  $R/\lambda = 0.016$ : either of the three approximate treatments is sensibly correct if  $R/\lambda$  exceeds about 0.1.

It is very difficult to understand why any one of the three approximate treatments should remain substantially correct even down to  $R/\lambda$  of the order of 0.1, for two of them are based on the supposition that current is almost zero round the dark half of the cylinder and Fig. 6.10 shows this condition has not nearly been attained when  $R/\lambda = 0.08$ . The third treatment, by the image method, would never have been thought of save for the guidance of geometrical optics and its physical significance is very obscure when  $k$  is small. It appears in analysis only if we happen to realize that

$$\frac{1}{2}k|H_1(2k)| \doteq \frac{1}{\pi|H_0(\frac{1}{2}k)|},$$

when  $k$  is large and we must then also recognize that this corresponds to a current at the optical focus.

The approximate expression (6.20) shows the echoed field is that of an equivalent current

$$I = \frac{ckE_w}{2a}\{-Y_0(2k) + jJ_0(2k)\}$$

at the centre of the cylinder: the phase of the said current being relative to the phase of the incident field at the centre. It follows from the properties of  $J_1(2k)$  that the phase of  $I$  is in advance of  $E_w$  at the centre by an angle  $\phi = 2k - \frac{1}{4}\pi$ , valid for  $k > 2$ . The distant field of a current filament is as though the disturbance originated at a distance  $\frac{1}{2}\lambda$  in advance of the filament (see § 1.7): hence, allowing for the advance in phase of the current, it follows that the phase of the echoed field is as though the disturbance originated from a point distant  $2R - \frac{1}{2}\lambda$  in front of the centre. The phase has been plotted for  $k = 1$  and the line is as though zero phase occurred at a distance  $0.204\lambda$  behind the centre: in this case  $2R - \frac{1}{2}\lambda = -0.182\lambda$  and thus there is substantial agreement. Accordingly the echoed field is equivalent to a current  $I = (cE_w/a)\sqrt{(R/2\lambda)}$  and its phase is as though the disturbance originated from a point  $2R - \frac{1}{2}\lambda$  in front of the centre. The foregoing discussion should be compared with that in §§ 6.4 (a)-(e).

## 6.7. The resultant field close to the cylinder

The incident and re-radiated field combine to form a complicated system of standing waves in the vicinity of the cylinder. It is useful

to assess the magnitude of the fluctuations of field which occur in the neighbourhood of the cylinder because this will give us an estimate of the disturbance caused by objects in the path of the wave: the fluctuations of field strength (standing wave pattern) which occur in the neighbourhood of trees, hedges, etc., is a familiar experience to those who have made propagation experiments at a wavelength of a few metres. It follows from the reciprocal theorem that the disturbance in the direction of propagation and towards the transmitter must be considerable. For if the distant field is observed when an aerial is moved progressively away from a metal cylinder, used deliberately as a reflector, we expect the forward field to be a maximum when the distance between the aerial and the surface of the cylinder is approximately an odd number of  $\frac{1}{2}\lambda$ : it is the forward field test we have quoted so often in Chapter III. The reciprocity theorem tells us that if we remove the aerial to infinity, then measure the resultant field near the cylinder, we shall encounter fluctuations corresponding precisely with those found in the forward field test.

First we will assess the rate at which the shadow behind the cylinder decreases with distance. We have seen, by means of Fig. 6.15, that the re-radiated field in this direction is always nearly in antiphase with the incident: since the echoed field varies as  $r^{-\frac{1}{2}}$ , and the incident field does not decrease with distance, the shadow must gradually fade away. But the reflected wave is not exactly in antiphase because we have seen the induced current density is never precisely cophased with the incident field, the discrepancy rising to  $30^\circ$  at the point of glancing incidence: thus the current that was ignored in Fig. 6.15 produces a quadrature component of reflected shadow field. Its magnitude must be small since the antiphase component, calculated via Fig. 6.15, agrees with the R.M.S. field evaluated laboriously from (6.18*a*) and recorded in Fig. 6.14. Computation from (6.18*a*) gives the values of  $E_P$  and  $E_Q$  recorded in Table 6.5 below.

TABLE 6.5

$k$	0.1	0.5	1	2	4	6	8	10	12	14	20	24
$E_P$	0.80	0.87	1.48	2.61	4.74	6.90	9.00	10.57	13.1	15.2	21.3	25.4
$E_Q$	-0.47	-0.72	-0.89	-1.08	-1.42	-1.59	-1.73	-1.87	-1.98	-2.1	-2.33	-2.50

It may be found that  $E_Q$  is given approximately by the empirical equation

$$-E_Q = \frac{1.7}{|H_0(k/20)|} \div 0.47k^{\frac{1}{2}},$$

and accordingly 
$$-\frac{E_Q}{E_P} \doteq 0.45k^{-1},$$

and hence 
$$-\frac{E}{E_w} \doteq 1.03k(1-j0.45k^{-1})\{-J_0(ar)+jY_0(ar)\}.$$

When  $k$  is large and  $ar$  is very large this can be expressed in terms of an equivalent current at the centre of the cylinder and thus the phase of the field corresponds to a starting-point  $\frac{1}{8}\lambda$  behind the centre. Accordingly the phase of the diminishing re-radiated wave tends to be  $45^\circ$  short of antiphase with the undiminishing incident wave. Consideration of Fig. 6.15 shows that that treatment could not give the phase, relative to the incident field, since the equivalent flat sheet could be situated anywhere between the centre and the bright spot. It then follows, from the expression for  $E_Q$ , that when  $ar$  is very large and  $k$  is large the resultant field is

$$\frac{|E|}{|E_w|} = \left(1 + \frac{2k^2}{\pi ar} - \frac{2k}{\sqrt{(\pi ar)}}\right)^{\frac{1}{2}} \doteq 1 - \frac{k}{\sqrt{(\pi ar)}},$$

and this suggests the mean square field will exceed  $\frac{2}{3}E_w$  if  $ar > 3k^2$ : this estimate describes the gradually diminishing shadow and ignores the ever decreasing superposed standing wave.

On bearing  $\theta = 90^\circ$ , computation from (6.18a) shows that

$$\frac{E}{E_w} \doteq 0.71\sqrt{k}\{\cos(112+85k)-j\sin(112+85k)\}\{-J_0(ar)+jY_0(ar)\},$$

where  $(112+85k)$  is in angular degrees. At the surface of the cylinder this gives  $-E/E_w = 0.56$ , whereas the correct value there is unity. Hence an empirical formula intended to apply only when  $ar$  is large is not grossly incorrect when  $ar = k$ , and this suggests the limiting expression will be nearly correct when  $ar$  is not much larger than  $k$ . The incident field has the same phase at all points in the plane  $\theta = 90^\circ$ , and hence the resultant field in this plane is obtained by adding unity to the right-hand side of the empirical equation above. On doing this we find

$$\frac{|E|}{|E_w|} \doteq 1 + 1.1 \sqrt{\frac{R}{r}} \cos(ar + \alpha),$$

showing that the fluctuation of R.M.S. field should be less than 10 per cent. when  $r/R$  exceeds 100.

In the direction of the distant transmitting station the resultant field is found, by (6.20), to be given by

$$\begin{aligned} \frac{E}{E_w} &\doteq e^{jar} + \frac{\pi k}{2} \{-Y_1(2k) + jJ_1(2k)\} \{-J_0(ar) + jY_0(ar)\} \\ &= e^{jar} - \sqrt{\left(\frac{R}{2r}\right)} e^{j(2k-ar)}, \quad \text{if } k \text{ is large;} \end{aligned}$$

and it is substantially correct even at  $ar = k$ .

$$\therefore \frac{|E|^2}{|E_w|^2} = 1 + \frac{R}{2r} - \sqrt{\left(\frac{2R}{r}\right)} \cos(2ar - 2k),$$

and according to this the fluctuations of R.M.S. field are about  $\pm 15$  per cent. when  $r \doteq 10R$  and about  $\pm 5$  per cent. when  $r \doteq 200R$ . Fig. 6.17

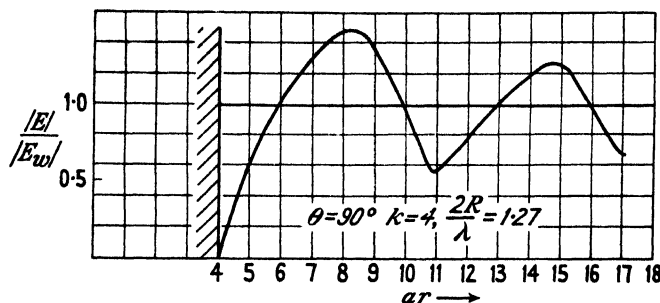


FIG. 6.17. Field strength in diametral plane perpendicular to direction of incident plane wave.

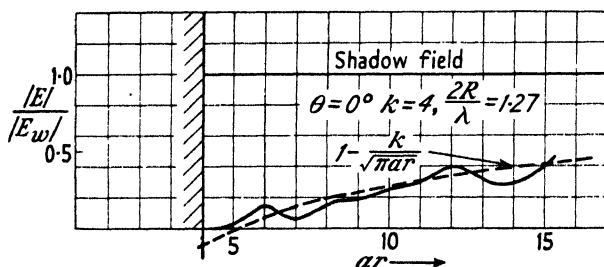


FIG. 6.18. Field strength in plane of deepest shadow.

shows the resultant field in the plane through the centre of a cylinder (for which  $2R/\lambda = 1.27$ ) and perpendicular to the direction of the incoming wave: here  $E/E_w$  never exceeds 1.5. When the cylinder is very large the first maximum will tend to equal 2 and the first minimum to be zero, and the fluctuations will tend rapidly to the value  $\pm 0.56\sqrt{(R/r)}$ , the minima being near a whole number of  $\lambda$  from the surface. Fig. 6.18 shows  $|E|/|E_w|$  in the direction of the deepest shadow for a cylinder for which  $2R/\lambda = 1.27$ : the dotted curve in the same figure is the plot of the approximate formula for the R.M.S. value of the resultant field. This approximates very closely to the correct value if the fluctuations are ignored. It is surprising this formula should approximate as closely as it does even when  $k$  is only 4, and suggests that the rough guess that the field will exceed two-thirds of the undisturbed value if  $r/R > 20R/\lambda$

is always closely correct. Thus it defines the extent of deep shadow very conveniently.

The results we have obtained are substantially correct for a very long cylinder. They will be applicable in practice when the cylinder is very long compared with a wavelength and at distances smaller than the length of the cylinder. If we are applying these formulae in practice to an object such as a tree, we must remember the re-radiated field will tend to fall off inversely as distance when this is comparable with the height of the tree and inversely as  $r^{-\frac{1}{2}}$  close up. Accordingly our formulae will grossly over-estimate the disturbance at distances greater than the height of the tree. An appeal to arithmetic shows the deep shadow is not likely to be very marked at distances greater than the height of a tree. It should be emphasized again that the shadow fades out only because the re-radiated field varies as  $r^{-\frac{1}{2}}$ , while the incident field (originating from a source at infinity) does not attenuate with distance. If the source is not very far away from the cylinder, as is the case when the cylinder is used deliberately as a reflector for an aerial, then both the incident and re-radiated field will attenuate with distance, at a rate which approaches ever nearer to equality, and then the deep shadow will tend to extend to infinity. The reader should also interpret this statement in terms of the reciprocity theorem.

By implication, we are mainly concerned here with objects for which  $R/\lambda$  is not very large. Suppose, however, that  $R = 1$  m. and  $\lambda = 0.1$  mm., so that  $R/\lambda = 10^4$ , then the deep shadow would persist to a distance of the order of 100 km. if the height of the cylinder were great compared with this distance (a practical absurdity). But the example serves to show that the deep shadow would persist for distances of the order of a mile or two from an object some 6 ft. in diameter and about a dozen feet high if  $\lambda$  were of the order of 0.1 mm. This example helps to explain the very wide extent of the shadow area which common experience shows us exists with waves of light.

## 6.8. The rate of working in re-radiation and the pressure of radiation

We have spent much effort in calculating the field strength echoed back to the source from a cylinder in the path of a wave. Poynting's theorem leads seductively to the idea that energy passes at the rate  $cE_{\theta}^2/4\pi$  across unit area perpendicular to the direction of propagation, though let it not be forgotten there is nothing to show that this amount of energy is associated with any particular unit area of wave-front.



Optical ideas of an obstructing barrier combined with Poynting's theorem lead some people to wish to relate the energy re-radiated with the area of wave front obstructed by the cylinder or other object. If the cylinder absorbed energy from the wave this would be a sound idea, but in our problem the cylinder is a perfect conductor and no energy is absorbed by it. We can calculate the work which would have to be done to maintain the currents which are induced by the incident field and this quantity is, in a sense, the re-radiated energy. But since it includes the strong field radiated in the shadow area it cannot be a very sensible measure of the energy reflected back towards the source, which is the implicit idea of the calculation. Before proceeding with the cylinder problem, consider first the very simple case of a plane wave incident on an infinite and perfectly conducting plane perpendicular to its direction of propagation. Equation (1.60) shows that if a uniform current density  $i$  flows in an infinite sheet, then there is an electric force opposing it given by  $-cE_P = 2\pi i$ . The electric field at the surface of the sheet must be zero, and accordingly  $E_P + E_w = 0$ , whence  $cE_w = 2\pi i$ . In the absence of the incident field, work at the rate  $E_P i = -cE_P^2/2\pi$  per unit area would be required to maintain the flow of  $i$ . And by Poynting's theorem the output of energy per unit area of sheet, reckoning the radiation in both directions, is  $2cE^2/4\pi$ ; thus, the two methods of estimating the work are in agreement. When the current density  $i$  is maintained by the incident field  $E_w$  it is perhaps natural to say that the incident field works at the rate  $E_w \times i = cE_w^2/2\pi$  per unit area. But this is twice the work which is supposed to be incoming from the incident field: on this reckoning the sheet appears to collect the energy from an area twice that of the wave-front. The energy is not dissipated and thus there is no contradiction of conservation of energy. In the presence of the reflecting sheet the field is zero on its far side and is a standing wave system on its near side. It is not correct to say the output of work from the sheet is the same as would be required to maintain the induced current in the absence of  $E_w$ : in the presence of  $E_w$  the output is zero. We will now make a similar calculation for the cylinder and evaluate  $P = R \int_0^{2\pi} e_w i d\theta$ , where  $i$  is given by (6.17a) and  $e_w$  is given by (1.49), which becomes

$$\frac{e_w}{E_w} = J_0(k) - 2J_2(k)\cos 2\theta + 2J_4(k)\cos 4\theta - \dots + \\ + 2j\{J_1(k)\cos \theta - J_3(k)\cos 3\theta + \dots\}.$$

To obtain the average rate of working the  $j$  term must be omitted from

the product. The terms involving  $Y$ 's and the products like  $J_1 J_3$  drop out in the process of integration and we obtain

$$P = \frac{2\lambda}{\pi} \frac{cE_w^2}{4\pi} \left( \frac{J_0^2}{H_0^2} + \frac{2J_1^2}{H_1^2} + \frac{2J_2^2}{H_2^2} + \dots \right).$$

The expression in the brackets has been evaluated in deriving the straight line in Fig. 6.14, for it is the inphase component of the shadow field at  $\theta = \pi$  in (6.18*a*) and indeed it is sensibly equal to the shadow field since we have seen, by the process described in Fig. 6.15, that the quadrature field is very small on this bearing. And we have found the shadow field is given by the empirical formula  $0.8 + 1.03k$ . Accordingly

$$P \doteq \frac{cE_w^2 R}{\pi} = \frac{cE_w^2}{4\pi} \times 4R,$$

and this is the power which Poynting's theorem suggests is crossing a strip of wave-front whose width is twice that of the obstructing cylinder. It is worth while to repeat this calculation according to the treatment described in Fig. 6.15. Then

$$P = \frac{cE_w^2 R}{2\pi} \int_{-\pi/2}^{+\pi/2} \cos \theta \, d\theta = \frac{cE_w^2 R}{\pi},$$

the same result as before.

It is instructive to make a similar calculation for the supposed output of work from the reflecting sheet in the system described by Fig. 3.2 and using the approximation for the induced current given in (3.6*a*). Then,

$$\begin{aligned} P &= 2 \int_0^\infty Ei \, dy \doteq \frac{c}{\pi} \int_0^\infty E^2 \sin \psi \, dy \\ &= \frac{2aI^2}{c} \int_0^\infty \frac{\sin \psi}{\rho} \, dy = \frac{2aI^2}{c} \int_0^\infty \frac{R}{R^2 + y^2} \, dy = \frac{\pi aI^2}{c}. \end{aligned}$$

This equals the output from the current in the absence of the reflecting sheet, whereas we should have expected the reflected energy to be half the total output of the isolated current. The calculations we have made do not represent the re-radiated energy but are merely a cumbersome way of stating that the field is zero in the deep shadow. The impulse to make the calculation has arisen only from optical concepts of energy in a wave-front and obstructing areas, concepts which are not helpful

when there is no sink of energy: we shall not labour the discussion further.

*Note.* The reader would be well advised here to consult an extremely clear treatment of 'The Absorption of Energy by a Wireless Aerial', by J. A. Ratcliffe, *Proc. Camb. Phil. Soc.* **27** (1931), 588.

The mechanical force on the cylinder (pressure of radiation) is

$$F = R \int_0^{2\pi} \frac{hi \, d\theta}{c},$$

where the induced density is  $i$ . Since  $e = h$  in the wave, the expression for  $F$  is the same as that just evaluated for  $P$  and hence it follows that  $F = RE_w^2/3000\pi$  dynes per unit length when  $E$  is reckoned in volts/cm. Langley's determination of the mean energy of sunlight is  $4.3 \times 10^{-5}$  ergs per cu. cm. and this corresponds to a field strength of 7 volts/cm. Hence, if sunlight were monochromatic and polarized with electric vector parallel to the axis of the cylinder, the pressure of radiation would be about 7 dynes per cm. of axial length on a cylinder 20 metres in diameter.

### 6.9. Field of currents flowing round the circumference of a cylinder

In § 2 of this chapter we derived the field of currents which flow axially: now we require corresponding expressions for currents which flow round the circumference. The simplest case, namely, a current whose density is constant round the circumference, was solved in § 1.15: we repeat here the expression for  $E$  and  $H$ , as follows:

$$E_T = \frac{2\pi k I_0}{c} \{-J_1(ar) + jY_1(ar)\}J_1(k) \quad (1.52)$$

$$\text{and} \quad H = \frac{2\pi^2 k I_0}{c} \{Y_0(ar) + jJ_0(ar)\}J_1(k), \quad (1.53)$$

$$\text{or} \quad = \frac{2\pi^2 k I_0}{c} \{Y_1(k) + jJ_1(k)\}J_0(ar)$$

for internal points.

Now consider a current density  $I_1 \cos \alpha$  flowing circumferentially as described by Fig. 6.19: in this, current is flowing in both half-cylinders towards  $B$  and away from  $B'$  and has its greatest density at points  $A$  and  $A'$ . Since the density diminishes to zero at  $B$  and  $B'$ , there must be electric charge distributed over the half-cylinder  $ABA'$  and also over

the half-cylinder  $AB'A'$ , the greatest density of charge being at  $B$  and at  $B'$ . In this problem the electric field will be due both to the retarded vector potential of the current and also to the retarded scalar potential of the charges, and it will have both a radial component  $E_r$  and a tangential component  $E_\theta$ . The magnetic field, however, is purely axial, and for this reason the magnetic is the easiest field to calculate initially: the two components of electric field are then to be derived from  $H$  by means of the circuital relations

$$\frac{dE_r}{dt} = -\frac{c}{r} \frac{\partial H}{\partial \theta} \quad \text{and} \quad \frac{dE_\theta}{dt} = c \frac{\partial H}{\partial r}.$$

Because the magnetic field has axial component only,  $H$  must satisfy Bessel's equation: accordingly for the general distribution  $I_n \cos n\alpha$  the solution must be of the form

$$\frac{cH}{I_n} = B\{Y_n(ar) + jJ_n(ar)\} \cos n\theta,$$

where  $B$  is a constant to be determined to suit the radius  $R$ .

Equation (1.53) shows that when  $n = 0$  then  $B = -2\pi^2 k J'_0(k)$ , and accordingly we shall guess that

$$-\frac{cH}{2\pi^2 k I_n} = J'_n(k) \{Y_n(ar) + jJ_n(ar)\} \cos n\theta, \quad \text{for } r > R \quad (6.21)$$

$$\text{or} \quad = J_n(ar) \{Y'_n(k) + jJ'_n(k)\} \cos n\theta, \quad \text{for } R > r \quad (6.21a)$$

and shall now show that (6.21) is possible. On putting  $ar = k$  and subtracting (6.21a) from (6.21) we find that  $H$  differs on the two sides of the boundary by an amount  $\delta H$  such that

$$\begin{aligned} \frac{\delta H}{2\pi^2 k} &= \{J'_n(k)Y_n(k) - Y'_n(k)J_n(k)\} \frac{I_n}{c} \cos n\theta \\ &= \frac{2}{\pi k} \frac{I_n}{c} \cos n\theta, \quad \text{by the Wronskian property.} \end{aligned}$$

Therefore  $\delta H = (4\pi I_n/c) \cos n\theta$ , and this is the value the curl of  $H$  must have round the conduction current density  $I_n \cos n\theta$ . Accordingly (6.21) is possible for the general solution and is correct.

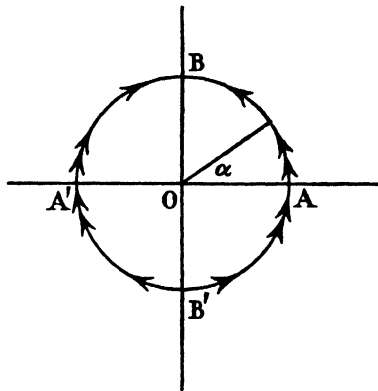


FIG. 6.19.

It then follows, from the circuital relations, that

$$-\frac{cE_r}{2\pi^2 k I_n} = \frac{nJ'_n(k)}{ar} \{-J_n(ar) + jY_n(ar)\} \sin n\theta \quad (6.22)$$

and 
$$\frac{cE_\theta}{2\pi^2 k I_n} = J'_n(k) \{-J'_n(ar) + jY'_n(ar)\} \cos n\theta. \quad (6.23)$$

Note that  $E_r$  is zero when  $n = 0$ , thus fulfilling the requirement of symmetry and agreeing with (1.52). These equations correspond to (6.4), which applies to a current flowing axially.

It should be noted that the external fields are all zero everywhere if  $J'_n(k) = 0$  and accordingly this is the resonance condition for a cylinder or chamber in which the current flows round the circumference: it corresponds to the resonance condition  $J_n(k) = 0$  for currents flowing axially. The smallest values of  $k$  which make  $J_n(k)$  and  $J'_n(k) = 0$  for  $n = 0$  to 4 are shown collected in Table 6.6.

TABLE 6.6

$n$	<i>Axial</i> current $J_n(k) = 0$	<i>Circumferential</i> current $J'_n(k) = 0$	<i>Ratio</i>
0	2.405	3.832	0.626
1	3.832	1.841	2.08
2	5.135	3.054	1.68
3	6.379	4.21	1.51
4	7.586	5.3	1.43
$n$ large	$1.15n$	$n$	1.15

We note that the first figure in the third column agrees with the second figure in the second column; this is because  $J'_0(k) = -J_1(k)$ . Hence the resonance frequency for an axial current  $I_1 \cos \alpha$  is the same as for a uniform current density flowing round the circumference of the tube. The first figure in the third column is out of sequence and this occurrence in such a series is somewhat surprising. It is, however, easy to understand why the lowest possible frequency must correspond to a current  $I_1 \cos \alpha$  flowing circumferentially. For consider the field at a very distant point in the direction  $AOA'$  in Fig. 6.19. It must be due dominantly to the line doublets concentrated near  $A$  and  $A'$ : this is partly because the current density is at its maximum at these points and partly because line doublets from other parts of the circumference are relatively ineffective owing to the obliquity of their direction. It is clear that the field will be very small when  $AA' = \frac{1}{2}\lambda$ , and hence the resonance frequency must be near that which corresponds to the diameter being half a wavelength: it follows from the table that

resonance occurs when  $2R/\lambda = 1.841/\pi = 0.585 = 0.5 \times 1.18$ . Similar consideration for an axially flowing current  $I_1 \cos \alpha$  (see Fig. 6.1) suggests  $2R/\lambda = 1$ : the true value is  $2R/\lambda = 3.832/\pi = 1.21$ .

### 6.10. Plane wave incident on a cylinder whose axis is perpendicular to the electric vector

If the amplitude of the undisturbed incident magnetic field is  $H$  and if the direction of propagation is from right to left, then its magnitude  $h$  at distance  $x$  from the centre of the cylinder is

$$\begin{aligned} \frac{h}{H} &= \sin p(t+x/c) \\ &= \cos ax + j \sin ax \\ &= \cos(ar \cos \theta) + j \sin(ar \cos \theta) \\ &= J_0(ar) - 2J_2(ar) \cos 2\theta + 2J_4(ar) \cos 4\theta - \dots + \\ &\quad + 2j\{J_1(ar) \cos \theta - J_3(ar) \cos 3\theta + \dots\}. \end{aligned}$$

If the density of current flowing round the circumference, as typified by Fig. 6.19, is

$$i = I_0 + I_1 \cos \theta + I_2 \cos 2\theta + \dots,$$

then the internal magnetic field is, by (6.21 a),

$$\frac{ch}{2\pi^2 k} = j[J_0(ar)H_0(k)I_0 + J_1(ar)H_1'(k)I_1 \cos \theta + \dots],$$

where  $H_n'(k) \equiv -J_n'(k) + jY_n'(k)$ .

The net internal magnetic field must be zero everywhere and therefore

$$\begin{aligned} \frac{cH}{2\pi^2 k} &= -jH_0'(k)I_0 = -\frac{1}{2}H_1'(k)I_1 = \frac{1}{2}jH_2'(k)I_2 = \frac{1}{2}H_3'(k)I_3 \\ &= -\frac{1}{2}jH_4'(k)I_4 = -\frac{1}{2}H_5'(k)I_5, \text{ etc.} \\ \therefore \frac{2\pi^2 ki}{cH} &= j\left\{\frac{1}{H_0'(k)} - \frac{2 \cos 2\theta}{H_2'(k)} + \frac{2 \cos 4\theta}{H_4'(k)} - \dots\right\} - \\ &\quad - 2\left\{\frac{\cos \theta}{H_1'(k)} - \frac{\cos 3\theta}{H_3'(k)} + \frac{\cos 5\theta}{H_5'(k)} - \dots\right\} \\ &= -\left(\frac{Y_0'}{|H_0'|^2} + \frac{2J_1' \cos \theta}{|H_1'|^2} - \frac{2Y_2' \cos 2\theta}{|H_2'|^2} - \frac{2J_3' \cos 3\theta}{|H_3'|^2} + \dots\right) + \\ &\quad + j\left(\frac{J_0'}{|H_0'|^2} - \frac{2Y_1' \cos \theta}{|H_1'|^2} - \frac{2J_2' \cos 2\theta}{|H_2'|^2} + \frac{2Y_3' \cos 3\theta}{|H_3'|^2} + \right. \\ &\quad \left. + \frac{2J_4' \cos 4\theta}{|H_4'|^2} - \frac{2Y_5' \cos 5\theta}{|H_5'|^2} - \frac{2J_6' \cos 6\theta}{|H_6'|^2} + \dots\right). \quad (6.24) \end{aligned}$$

The form of this equation resembles closely the form of (6.17 a).

As a numerical example we will take  $k = 2$  ( $R/\lambda = 0.32$ ): substitution of the appropriate value of  $J'_0$ , etc., gives

$$\begin{aligned} \frac{2\pi^2 k i}{cH} = & -(0.310 - 0.400 \cos \theta - 3.63 \cos 2\theta - 0.296 \cos 3\theta + \\ & + 0.455 \cos 4\theta + 6 \times 10^{-5} \cos 5\theta - 0.015 \cos 6\theta - \dots) - \\ & -j(1.67 + 3.5 \cos \theta + 1.44 \cos 2\theta - 0.95 \cos 3\theta - \\ & - 0.006 \cos 4\theta + 0.091 \cos 5\theta \dots). \end{aligned}$$

This equation gives  $2\pi|i|/cE = 1.08$  for the density at the 'bright spot' with a phase lag of  $7.3^\circ$  on the field incident there. Fig. 6.20 is the polar

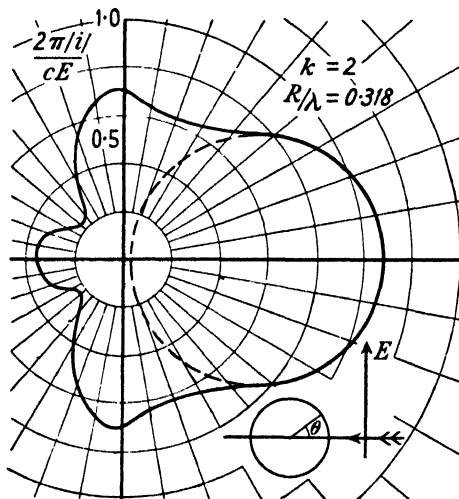


FIG. 6.20. Polar plot of current density round circumference of cylinder induced by plane wave whose electric vector is perpendicular to axis at cylinder.

plot of  $2\pi|i|/cE$  and shows that the induced density is much less on the dark than on the light half-cylinder. The phase of the induced density on the bright half is always within a few degrees of the incident field, the discrepancy being about  $3^\circ$  at  $\theta = 90^\circ$ .

If a wave is moving over a perfectly conducting sheet with its electric vector perpendicular and the magnetic vector parallel to the sheet, then the value of the induced density will be  $4\pi|i|/cE = 1$  and thus the density is half what it would be if the wave was moving perpendicular to the sheet. In our problem, the density at  $\theta = 90^\circ$  must surely approach the value given above in the limit when  $R/\lambda$  is very large. Reference to Fig. 6.20 will show that when  $\theta = 90^\circ$  then  $2\pi|i|/cE = 0.7$ , whereas we suggest the limiting value of this ratio would be 0.5: it

would seem there is a rapid approach to the limit. Fig. 6.21 shows the polar plot of  $2\pi|i|/cE$  based on this prediction, it being understood that the phase of  $i$  at any point follows the phase of the field at that point. If this figure is compared closely with Fig. 6.20 the resemblance is seen to be very striking. The labour of exact computation is very great,

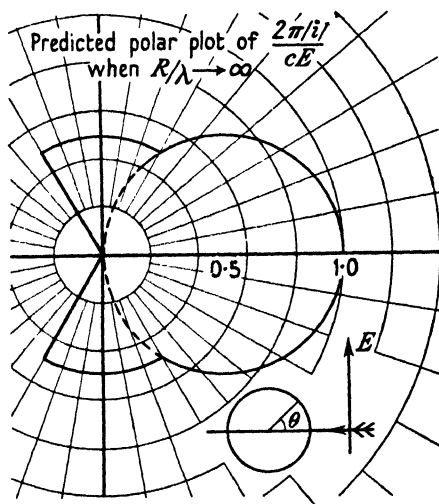


FIG. 6.21. Predicted polar plot of  $2\pi|i|/cE$  when  $(R/\lambda) \rightarrow \infty$ .

more especially as  $J'_n$ , etc., are not commonly tabulated, and accordingly it is not proposed to make further verification of the predicted current density.

### 6.11. The external field of the currents induced in the cylinder

By use of (6.23) and the values of  $I_n$  we obtain

$$\begin{aligned} \frac{E_\theta}{E} = & -2 \left[ \frac{J'_1(k)H'_1(ar)\cos\theta}{H'_1(k)} - \frac{J'_3(k)H'_3(ar)\cos 3\theta}{H'_3(k)} + \frac{J'_5(k)H'_5(ar)\cos 5\theta}{H'_5(k)} - \dots \right] \\ & + j \left[ \frac{J'_0(k)H'_0(ar)}{H'_0(k)} - \frac{2J'_2(k)H'_2(ar)\cos 2\theta}{H'_2(k)} + \frac{2J'_4(k)H'_4(ar)\cos 4\theta}{H'_4(k)} - \dots \right]. \end{aligned} \quad (6.25)$$

Now  $J'_n(z) = -\frac{n}{z}J_n(z) + J_{n-1}(z)$  and hence  $J'_n(z) \rightarrow J_{n-1}(z)$  when  $z \rightarrow \infty$ .

$$\therefore \frac{E_\theta}{E} = H_0(ar) \left[ \frac{J'_0(k)}{H'_0(k)} - \frac{2J'_1(k)\cos\theta}{H'_1(k)} + \frac{2J'_2(k)\cos 2\theta}{H'_2(k)} - \dots \right] \quad (6.26)$$

when  $ar \rightarrow \infty$ , and this gives the diffraction pattern of the wave re-radiated or scattered by a cylinder perpendicular to the electric vector.



Fig. 6.22 exhibits the scattered field for a cylinder in which

$$R/\lambda = 0.318 \quad (k = 2):$$

in this case the ratio of shadow to echoed field is 1.25. If we assume the echoed field varies as  $\sqrt{(\pi k)}$ , following the precedent of a cylinder

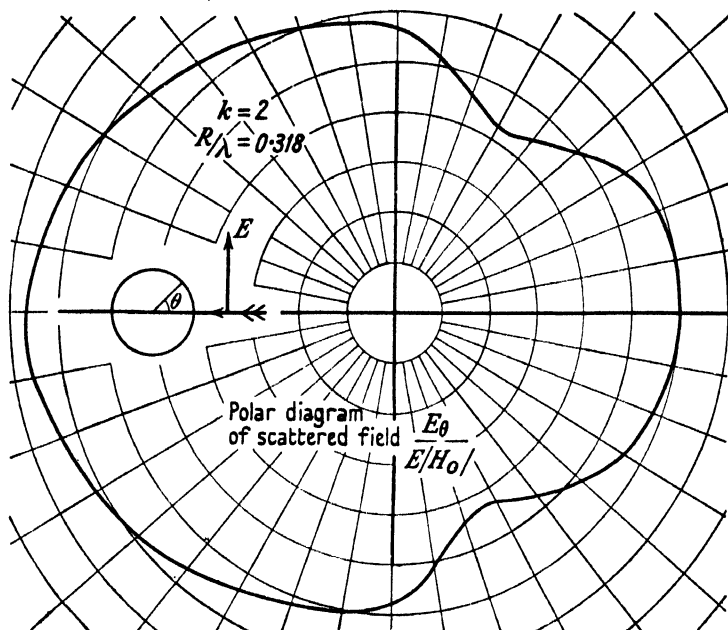


FIG. 6.22. Polar diagram of scattered field  $E_\theta/E|H_0|$ .

parallel to the electric vector, then  $E_\theta/E_w = 0.48\sqrt{(\pi k)}$  and this is in substantial agreement with the previous empirical formula

$$\frac{E}{E_w} = \frac{1}{2}\sqrt{(\pi k)}.$$

If we place a line doublet at the optical focus and adjust its strength to make the field zero at the bright spot, we obtain, by (1.58),

$$\frac{cE_w(\cos k + j \sin k)}{a\pi I'l} = \{J'(\tfrac{1}{2}k) - jY'(\tfrac{1}{2}k)\}.$$

$$\begin{aligned} \therefore \frac{|E_\theta|}{|E_w|} &= \frac{|H'_1(ar)|}{|H'_1(\tfrac{1}{2}k)|} \div \frac{|H_0(ar)|}{|H_0(\tfrac{1}{2}k)|}, \quad \text{when } \tfrac{1}{2}k \text{ is large,} \\ &\div \tfrac{1}{2}\sqrt{(\pi k)}|H_0(ar)|, \end{aligned}$$

and this agrees with the predicted value of the echoed field.

## VII

### FURTHER PROBLEMS OF CYLINDERS AND FLAT SHEETS

#### 7.1. Current filament parallel to and directly above a half-cylindrical boss rising out of an infinite plane; and the limiting case when the incident field is a plane wave

In § 6.4 the solution was obtained for a filament distant  $\lambda z/2\pi$  from the centre of a cylinder of radius  $R$ . If equal and opposite filaments are placed symmetrically with respect to the cylinder and on a diameter of it, then the electric field will be zero in the plane through the centre and perpendicular to that diameter: the field will not be disturbed if a perfectly conducting plane is placed in the plane of zero field, and then we have a filament placed symmetrically above a half-cylindrical protuberance rising out of an infinite plane. This system is of considerable practical interest since it simulates a horizontal aerial placed on the top of a rounded back or system of Downs. On adding to (6.14) the corresponding expression for the field of a current  $-I$  at  $(z\lambda/2\pi, \pi)$  we obtain

$$\frac{cE}{4a\pi I} = j \left[ \frac{\{J_1(z)Y_1(k) - J_1(k)Y_1(z)\}H_1(ar)\cos\theta}{H_1(k)} + \frac{\{J_3(z)Y_3(k) - J_3(k)Y_3(z)\}H_3(ar)\cos 3\theta}{H_3(k)} + \dots \right], \quad (7.1)$$

$$\text{where } H_n(k) \equiv -J_n(k) + jY_n(k),$$

$$= -\{-J_0(ar) + jY_0(ar)\} \left[ \frac{\{J_1(z)Y_1(k) - J_1(k)Y_1(z)\}}{H_1(k)} \cos\theta - \frac{\{J_3(z)Y_3(k) - J_3(k)Y_3(z)\}}{H_3(k)} \cos 3\theta + \dots \right] \quad (7.2)$$

when  $ar \rightarrow \infty$ , and this gives the diffraction pattern for any value of  $k$  and  $z$ .

It follows from (7.1) that the inphase field at the filament is

$$-\frac{cE_P}{4a\pi I} = \frac{\{J_1(z)Y_1(k) - J_1(k)Y_1(z)\}^2}{|H_1(k)|^2} + \frac{\{J_3(z)Y_3(k) - J_3(k)Y_3(z)\}^2}{|H_3(k)|^2}, \quad (7.3)$$

and this gives the radiation resistance relative to an isolated filament.

Unfortunately (7.2) is extremely tedious to evaluate when  $k$  is large, and hence it is difficult to use it to derive the pattern for a horizontal aerial on top of a high hill, such as the South Downs. But it is not the exact pattern which is needed so much as the trend of the pattern: will this tend to be that of an aerial at a height above an infinite plane equal to its height above the top of the hill, or at its height above the infinite

plane on which the hill stands? The purpose of the question we are now asking should become more clear if we make a digression. When we discussed in Chapter III the pattern due to an aerial parallel to an infinite plane we were thinking mainly of using the plane as a reflector to enhance the field in the direction of the normal to the plane, which in practice would be a sheet only a few  $\lambda$  in width. Now we are thinking

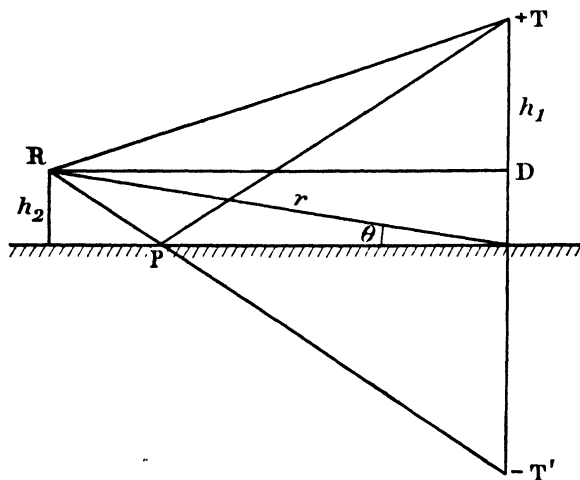


FIG. 7.1. Diagram to represent horizontal aerials  $T$  and  $R$  above a flat earth.

of a different aspect of the same analytical problem and have in mind a horizontal aerial transmitting, over a flat earth, to a distant receiving station near the ground, in contrast to a receiving station in an aeroplane flying high above the aerial. We are not now interested in the 'forward field' but in the field very close to the reflector, at whose surface the field is zero. Consider Fig. 7.1, which represents a transmitting aerial  $T$  parallel to the ground and at height  $h_1$  above it and a receiving aerial  $R$  at height  $h_2$ . Then

$$RT'^2 - RT^2 = DT'^2 - DT^2 = 4h_1 h_2.$$

$$\therefore RT' - RT = \frac{4h_1 h_2}{RT' + RT} \doteq \frac{2h_1 h_2}{r}.$$

If  $E_0$  is the field at  $R$  due to the current at  $T$ , then the resultant field at  $R$  due to the field of  $T$  and its image  $T'$  is (see (1.48))

$$\begin{aligned} \frac{E}{E_0} &= 2 \sin \left( \frac{2\pi}{\lambda} \frac{h_1 h_2}{r} \right) = 2 \sin \left( \frac{2\pi h_1}{\lambda} \sin \theta \right) \\ &\doteq \frac{4\pi h_1 h_2}{\lambda r}, \quad \text{when } \sin \theta \text{ is small.} \end{aligned} \quad (7.4)$$

Since  $E_0$  varies as  $1/r$  we find that  $E$  varies as  $h_1 h_2 / r^2$  for points close to the ground. In order to increase the field near the ground, due to a transmitter of given power, it is common practice to make  $h_1$  as large as possible by placing the transmitting aerial on top of a tower. We are asking the question, What will be the effect of placing the tower on top of a hill? Will the effective value of  $h_1$  be nearly equal to the height of the tower above the flat ground or the height of the tower above the summit of the large rounded hill? If we think of the problem in terms of geometrical optics we speak of the 'ray  $TP$  being reflected at  $P$  to  $R$ ' and on this view the hill below  $T$  is of no consequence if  $PT$  does not cut it. But the simple aerial at  $T$  does not produce a narrow ray  $TP$  and a narrow ray  $TR$  but fills the whole region with field. The field at  $R$  is due to the current at  $T$  together with all the currents induced in the flat ground and it is these which are equivalent in their effect to an image current at  $T'$ .

When the half-cylinder hill exists below  $T$  the field at  $R$  is not that due to  $T$  and  $T'$  but to  $T$  and  $T'$  together with the currents induced in the hill and its image. If the hill is high compared with  $h_2$ , no ray reflected from the hill (in the sense of simple geometrical optics) will reach  $R$  and then the presence of the hill is irrelevant according to elementary treatment. In all probability simple ray treatment is substantially correct, but it cannot be exact. The exact answer is contained in (7.2), but unfortunately this is very impracticable to evaluate when  $k$  is large. It seems, however, worth while to evaluate one numerical case and we will take  $k = 5$  ( $R/\lambda = 0.79$ ) and  $z = 7$  (i.e. the aerial  $1.112\lambda$  above the flat plane). The clearance between the aerial and the summit of this small hill is  $0.318\lambda$ . If the hill were removed the field would be zero at elevations of  $0^\circ$ ,  $26.8^\circ$ , and  $64.2^\circ$ : if the aerial was at a height  $0.318\lambda$  above the flat ground the field would be zero only along the ground. The pattern for a filament and complete cylinder ( $z = 7$ ,  $k = 5$ ) is shown in Fig. 6.5. We wish to compare the pattern derived from (7.2) with Fig. 6.5 and also with the equilobed pattern having zeros at elevation  $0^\circ$ ,  $26.8^\circ$ , and  $64.2^\circ$ .

On substituting the values of  $J_n(7)$ , etc., in (7.2) the equation of the pattern turns out to be

$$\begin{aligned}
 -\frac{E}{4E_0} = & (0.254 \cos \theta + 0.290 \cos 3\theta - 0.166 \cos 5\theta - 0.009 \cos 7\theta + \dots) + \\
 & + j(-0.114 \cos \theta + 0.116 \cos 3\theta + 0.288 \cos 5\theta - 0.216 \cos 7\theta + \\
 & + 0.058 \cos 9\theta - 0.0083 \cos 11\theta + \dots). \quad (7.5)
 \end{aligned}$$

The striking feature of this equation is the existence of the two quadrature components of field, the inphase component having been produced by the half-cylinder.

Curve (1) in Fig. 7.2 shows the pattern due to a filament at height  $1.1\lambda$  ( $z = 7$ ) above a flat plane, while curve (2) in the same figure shows

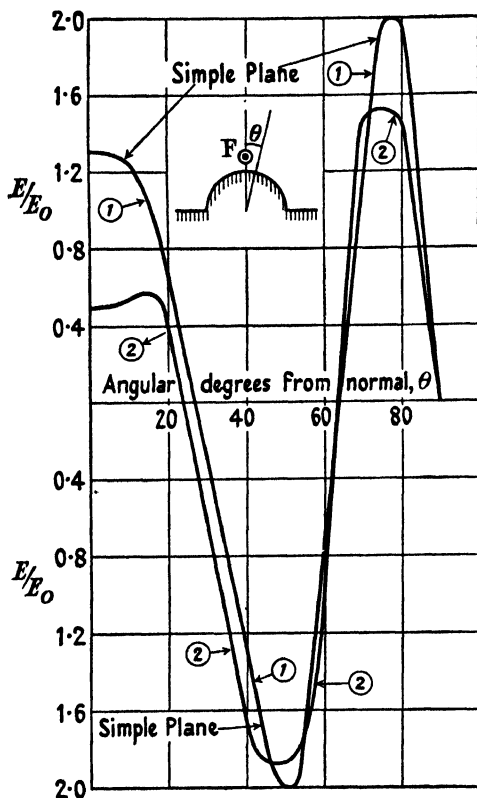


FIG. 7.2. Relating to the problem of a horizontal aerial erected on the top of a hill. Curve (1) is pattern for filament at height  $1.1\lambda$  above a flat plane: curve (2) is pattern of quadrature component of field of filament at height  $1.1\lambda$  above a flat plane having half-cylinder boss of radius  $0.79\lambda$  ( $k = 5$ ,  $z = 7$ ).

the quadrature component of equation (7.5). Comparison of these two curves shows that the pattern for quadrature component of field in our problem is a close approximation to the pattern which would obtain if the half-cylinder boss were absent: the bearings for zero and for maxima of field are changed but little by the presence of the boss, though the magnitude of the maximum near  $70^\circ$  is substantially reduced by it. The field strength along the normal ( $\theta = 0$ ) is considerably diminished

by the boss. Curve (1) in Fig. 7.3 shows the pattern for a filament at height  $0.32\lambda$  above a flat plane, while curve (2) in the same figure shows the antiphase component in equation (7.4): there is little correspondence between the two curves save that the 'forward field' of each is a minimum of the pattern.

Summarizing the results displayed in Figs. 7.2 and 7.3, we may say that the quadrature pattern is substantially the same as if the boss

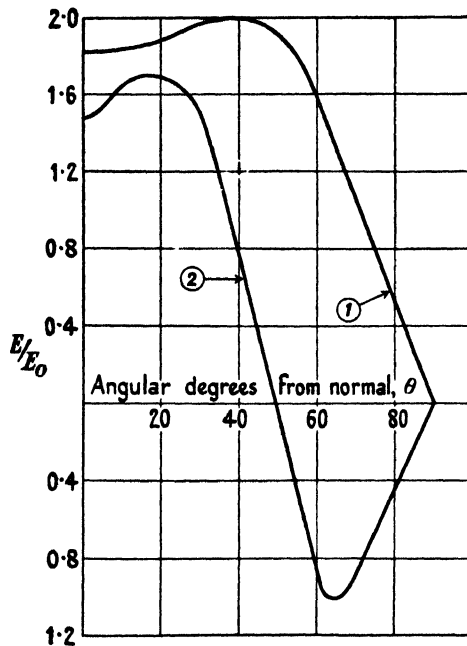


FIG. 7.3. Curve (1) is pattern for filament at height  $0.32\lambda$  above flat plane: curve (2) is pattern of antiphase component of field for filament  $0.32\lambda$  above crest of half-cylinder boss of radius  $0.79\lambda$  ( $k = 5$ ,  $z = 7$ ).

were absent, for  $\theta$  greater than  $20^\circ$ , but the boss produces an antiphase pattern which has little likeness to the pattern which would obtain if the radius of the hill were infinite.

Curve (2) in Fig. 7.4 exhibits the R.M.S. pattern for the system of our problem, while curve (1) is the R.M.S. pattern which would obtain if the boss were removed. Curve (2) shows that a minimum field occurs at the bearing where there would be zero field if the boss were absent, but we note that the magnitude at the minimum is half the maximum amplitude. The dimple at  $\theta = 25^\circ$  presumably represents the zero at  $\theta = 23^\circ$  in curve (1). The values of the maxima are reduced appreciably

by the boss, but the bearings at which they occur are not much changed by it. The point of great interest is that in the range of  $\theta$  from  $80^\circ$  to  $90^\circ$  the two curves are indistinguishable, thus demonstrating that the well-known formula  $E \propto (h_1 h_2 / r^2)$  is valid even when part of the height  $h_1$  is obtained by means of a hill. If the aerial is to be used for Radar service, then it is advantageous to obtain the total elevation by the help of a hill rather than by a single tower of height  $1.1\lambda$ , because the troublesome

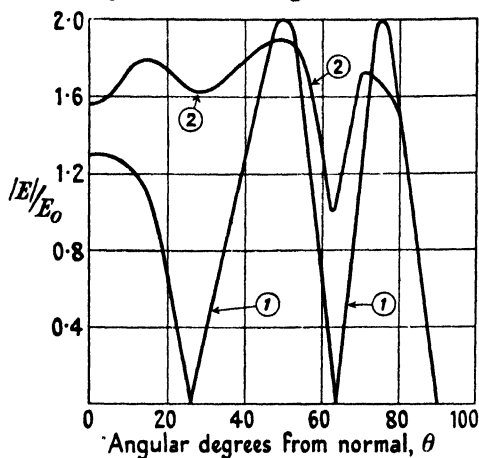


FIG. 7.4. Curve (1) is pattern for filament at height  $1.1\lambda$  above flat plane; curve (2) is pattern of R.M.S. field when a half-cylinder boss of radius  $0.79\lambda$  is below the filament ( $k = 5, z = 7$ ).

zero at  $\theta = 63^\circ$  is thereby removed: in other words, curve (2) is a more desirable pattern than curve (1) (both in Fig. 7.4) for observing the range of an aeroplane approaching the aerial. It is unfortunate the hill in our example is only  $0.79\lambda$  high, but the labour of evaluating (7.2) even for  $R = 2.5\lambda$  would be very great and thus we cannot change the scale of the picture very much. However, much communication is carried out by horizontally polarized waves at  $\lambda \doteq 20$  m. and then the hill in our example would be about 50 ft. high and thus is just worthy of the name hill.

It is, however, very instructive to notice, from Fig. 7.4, that the shape of the ground very near the aerial has an enormous effect on the pattern everywhere except in the range of  $\theta$  between  $80^\circ$  and  $90^\circ$  and this must mean that a vertical polar diagram is as much dependent on the flatness of the ground as it is on the phasing of the array. Experience very commonly shows a minimum where the ideal pattern should have a zero,<sup>†</sup> and this effect is almost certainly due to the shape

<sup>†</sup> See, for example, *Journal I.E.E.*, Part III, 1945, 70, Fig. 3.

of the ground rather than to losses in the ground or to mis-phasing in the array.

If  $ar < z$ , then (7.1) takes the form

$$\frac{cE}{4a\pi I} = j \left[ \frac{\{J_1(ar)Y_1(k) - J_1(k)Y_1(ar)\}}{H_1(k)} H_1(z) \cos \theta + \right. \\ \left. + \frac{\{J_3(ar)Y_3(k) - J_3(k)Y_3(ar)\}}{H_3(k)} H_3(z) \cos 3\theta + \dots \right] \quad (7.6)$$

and is obtained by interchanging  $ar$  and  $z$  in (7.1), and this gives the field in the region between the aerial and the cylinder. If  $z$  tends to infinity we have the solution for a plane wave incident normally on a flat sheet having a half-cylinder boss of radius  $R$  running parallel to the electric vector. When  $z \rightarrow \infty$ ,  $H_1 = -H_3 = H_5 = jH_0$ .

$$\therefore -\frac{E}{4E_0} = \frac{\{J_1(ar)Y_1(k) - J_1(k)Y_1(ar)\}}{H_1(k)} \cos \theta - \\ - \frac{\{J_3(ar)Y_3(k) - J_3(k)Y_3(ar)\}}{H_3(k)} \cos 3\theta + \dots, \quad (7.7)$$

where  $E_0$  is the field which would exist at the origin if the plane and its boss were removed. The standing wave pattern can be obtained from (7.7) and thus we now have a means of examining the disturbance caused by a round boss projecting from a flat reflector, when the boss is parallel to the electric vector. When  $k = 0$ , (7.7) reduces to

$$\frac{E}{4E_0} = \{jJ_1(ar) \cos \theta - J_3(ar) \cos 3\theta + J_5(ar) \cos 5\theta - \dots\} \\ = j \frac{1}{2} \sin(ar \cos \theta) \quad (\text{see McLachlan, p. 43, equation (15)}),$$

and this gives the standing wave pattern with  $E/E_0$  fluctuating between  $\pm 2$ . Equation (7.7) has been evaluated for  $k = 5$  ( $R = 0.79\lambda$ ) and the two components of field are shown in Fig. 7.5 and the R.M.S. field in Fig. 7.6, over a distance along the normal of about  $2\lambda$  in front of the boss. It is surprising the two components of  $E$  are so nearly in space quadrature in this range of  $ar$  since they must ultimately pass through zero together. Sufficient terms of the series have been taken to make the values valid to the accuracy of plotting: hence the phase of  $E_P$  and  $E_Q$  must change considerably in a further range of  $ar$  since, in Fig. 7.5, neither has yet attained closely the phase it must have when  $ar$  is very large, for then the zeros must occur when  $ar$  is an exact multiple of  $\pi$ . There seems little doubt that Fig. 7.6 is correct, even though its form is perhaps rather unexpected: it is interesting to note that the maxima



of  $|E|/E_0$  attain the value 2 at once: it is the minima which attain slowly their limiting value zero.

It is of interest to evaluate the current density induced on the cylinder and on the plane. The density on the cylinder follows at once from (6.11a) or (6.17a) by omitting the terms where  $n = 0, 2, 4$ , etc., and doubling the odd terms, and this shows at once that the density

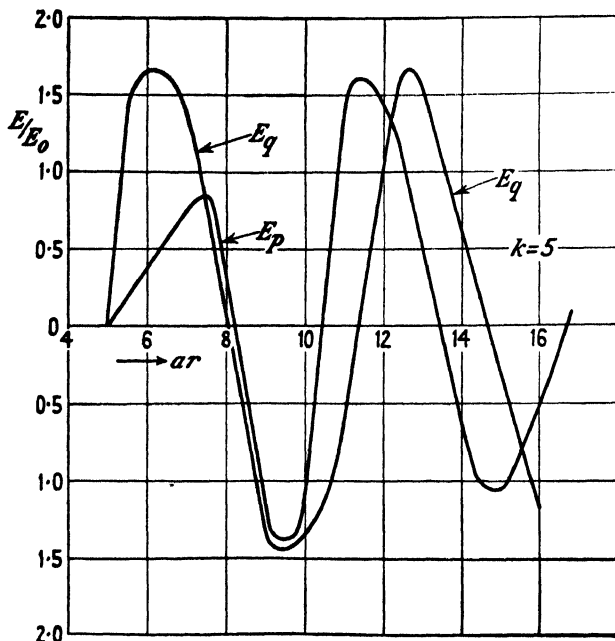


FIG. 7.5. Relating to problem of plane wave incident normally on a flat sheet having a half-cylinder boss of radius  $0.79\lambda$  ( $k = 5$ ).

is zero at the junction of the boss and the plane. Or the density can be deduced from (7.7) by the general relations

$$\frac{1}{c} \frac{dH_\theta}{dt} = \frac{\partial E}{\partial r} \quad \text{and} \quad \frac{1}{c} \frac{\partial H_\theta}{\partial t} = \frac{1}{r} \frac{\partial E}{\partial \theta} \quad \text{and} \quad cH = 4\pi i.$$

Whence the density on the plane is given by the equation

$$\frac{\pi i}{cE_0} = \frac{j}{ar} \left[ \frac{\{J_1(ar)Y_1(k) - J_1(k)Y_1(ar)\}}{H_1(k)} + \frac{3\{J_3(ar)Y_3(k) - J_3(k)Y_3(ar)\}}{H_3(k)} + \dots \right] \quad (7.8)$$

$$= \frac{1}{ar} \{J_1(ar) + 3J_3(ar) + 5J_5(ar) + \dots\}, \quad \text{if } k \rightarrow 0$$

$$= \frac{1}{2}, \quad \text{by a well-known series (see, for example, McLachlan, p. 51, Ex. 4),}$$

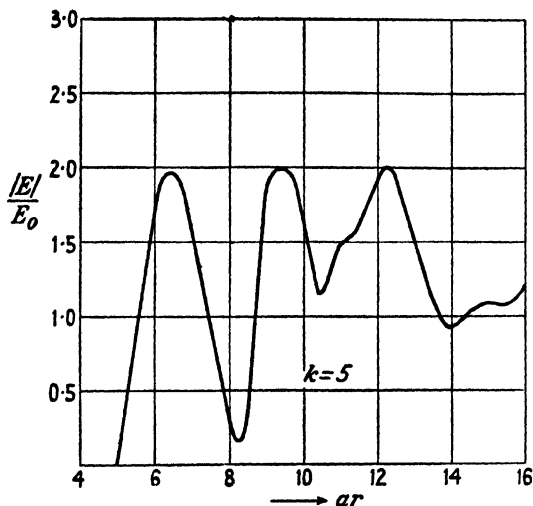


FIG. 7.6. Standing wave pattern along the normal to the plane through the centre of the boss of radius  $0.79\lambda$  ( $k = 5$ ).

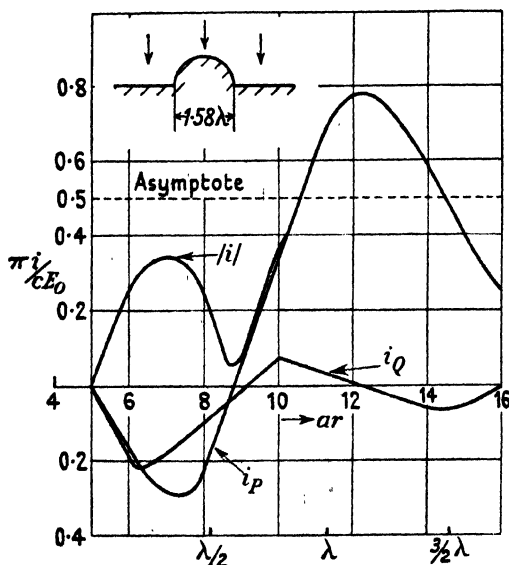


FIG. 7.7. Current density induced on plane which has a half-cylinder boss at diameter  $1.58\lambda$ ; plane wave and normal incidence.

and this is the well-known result, often used previously. When  $n \gg k$ , then  $J_n(k) \rightarrow 0$  (see Fig. 3.14) and accordingly the higher terms in (7.8) tend to the value they would have if  $k$  were zero. This shows that the

right-hand side of (7.8) must tend to the value  $\frac{1}{2}$  when  $ar \gg k$ , thus disclosing that the effect of the boss is local: our problem is to assess the range of  $ar$  in which this disturbance is appreciable.

Fig. 7.7 shows the two components of current density induced in the plane and also  $|i|$ , for the particular case  $k = 5$ . It shows that  $i_q$  is relatively very small and attenuates fairly rapidly with distance. It

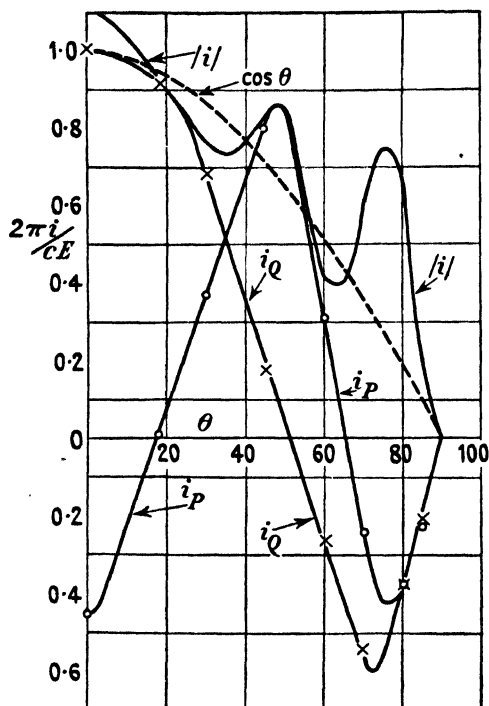


FIG. 7.8. Current density induced round the curve surface of the half cylinder of Fig. 7.7.

seems that  $|i|$  does not exceed  $8/5$  of the limiting value, but that the fluctuations are considerable up to a distance of several wavelengths from the protruding boss. This figure is very instructive for assessing the distance over which the disturbance persists of the uniform density which would obtain if the boss were absent: note that the induced density has a large antiphase component in the first  $\frac{1}{2}\lambda$  of distance.

The current density induced on the surface of the boss is shown in Fig. 7.8: at the 'bright spot'  $2\pi|i|/cE = 1.11$  and there it is  $31^\circ$  out of phase with  $E$ . According to what we have called 'simple ray theory' the curve of  $|i|$  would be a cosine curve of amplitude unity and this is the dotted curve in the figure. The true curve of  $|i|$  oscillates about

$\cos \theta$  with an amplitude which increases with  $\theta$ . The curves of  $i_P$  and  $i_Q$  show that the phase angle of the current tends very nearly to  $45^\circ$  when  $\theta$  tends to  $90^\circ$ : it will be remembered that when the plane is absent the phase of the induced current appears to tend to  $30^\circ$  at  $\theta = 90^\circ$ , the point of grazing incidence. It is clear that the simple ray theory is only very roughly correct in this problem and we remember that the Huyghens-Fresnel technique appears to demand that the current should have the phase and magnitude given by simple ray theory.

## 7.2. Current filament anywhere in the presence of an infinite plane having a half-cylindrical boss

We will now generalize the problem of the last section and allow the current filament to be anywhere (parallel to the boss) in contrast to being on the normal through the centre of the boss. The general problem is of practical interest because it discloses certain useful reciprocal properties and also because a particular case simulates a  $90^\circ$  Vee with limited sheets. If  $\theta$  in equation (6.14) is replaced by  $(\theta - \alpha)$  the field of a single filament is referred to a line at  $-\alpha$  to the normal through the filament: similarly if  $\theta$  is replaced by  $(\theta + \alpha)$  the zero line is shifted through  $+\alpha$ . If the two equations so formed are then subtracted we have the field at a point  $(ar, \theta)$  due to a filament at  $(z, \alpha)$  where the origin is at the centre of the boss and  $\theta$  and  $\alpha$  are angles of elevation above the plane. The equation is

$$-\frac{jcE}{4\pi aI} = \sum_1^{\infty} \frac{\{J_n(z)Y_n(k) - J_n(k)Y_n(z)\}}{H_n(k)} H_n(ar) \sin n\alpha \sin n\theta. \quad (7.9)$$

This reduces to (7.1) when  $\alpha = \frac{1}{2}\pi$  on remembering that  $\theta$  in (7.9) is  $(\frac{1}{2}\pi - \theta)$  of (7.1). If  $ar < z$ , then  $ar$  and  $z$  must be interchanged in (7.9). Accordingly it follows that if unit current at  $(z, \alpha)$  produces a field  $E$  at  $(ar, \theta)$ , then unit current at  $(ar, \theta)$  produces field  $E$  at  $(z, \alpha)$ ; thus there is perfect reciprocity. In particular it means that the vertical polar diagram can be obtained by measuring the field at a fixed receiving point, while  $\alpha$  is varied at the transmitter and  $z$  is kept constant. In practice it is often a simpler process to vary  $\alpha$  than to vary  $\theta$ , since to vary  $\theta$  demands either an aeroplane or movable kites. It also shows that in the approximate formula  $E/E_0 = (4\pi h_1 h_2)/\lambda r$  it does not matter whether the suffix 1 or 2 refers to the transmitter.

Since the wall of the cylinder meets the plane at  $90^\circ$  it seems likely that this region of the boundary can be used to simulate a  $90^\circ$  Vee reflector. We are everywhere looking for soluble problems which will

allow us to estimate how much the pattern due to sheets of finite width will differ from the ideal pattern, when the sheets extend to infinity. Here we have an approximation to a  $90^\circ$  Vee reflector made by one infinite sheet and a cylindrical boss. If we take  $k = 5$ ,  $z = 7$ , and  $\alpha = 14.6^\circ$ , the filament is situated at a point  $z' = 1.25$  from the junction of the plane and cylinder and at an elevation of  $45^\circ$  measured from this

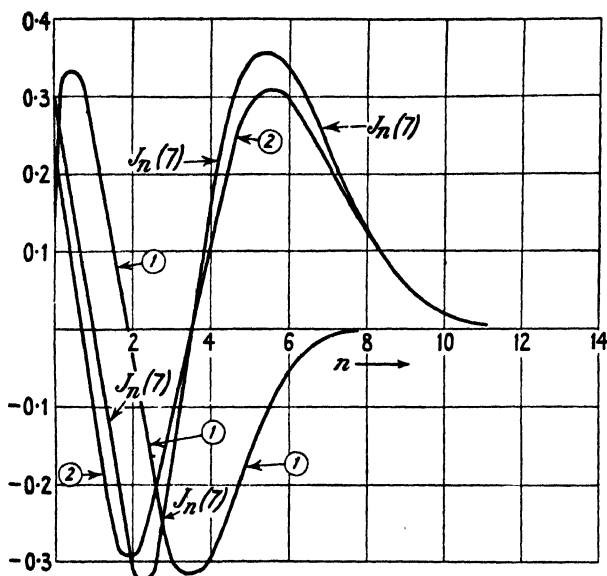


FIG. 7.9. Graphs of certain functions required in (7.10).

point. We propose to compare the pattern with the ideal pattern for a  $90^\circ$  Vee with the filament on the bisector and distant  $0.394\lambda$  from the apex. The ideal pattern for such a Vee is given by 3.15, and in this case is

$$\begin{aligned} -\frac{E}{8E_0} &= J_2(2.47)\cos 2\theta + J_6(2.47)\cos 6\theta \dots \\ &= 0.442 \cos 2\theta + 0.004 \cos 6\theta \dots \end{aligned}$$

When  $ar \rightarrow \infty$ , (7.9) takes the form

$$\begin{aligned} -\frac{E}{4E_0} &= (X_1 \sin \alpha \sin \theta - X_3 \sin 3\alpha \sin 3\theta + X_5 \sin 5\alpha \sin 5\theta \dots) + \\ &+ j(X_2 \sin 2\alpha \sin 2\theta - X_4 \sin 4\alpha \sin 4\theta + X_6 \sin 6\alpha \sin 6\theta - \dots), \quad (7.10) \end{aligned}$$

where

$$X_n \equiv \frac{\{J_n(z)Y_n(k) - J_n(k)Y_n(z)\}}{H_n(k)} \equiv \frac{x_n}{H_n(k)}.$$

On putting  $k = 0$ , equation (7.10) reduces to equation (3.20) with  $n = 1$ , as it should do.

Curve (1) in Fig. 7.9 shows

$$\frac{\{J_n(7)Y_n(5) - J_n(5)J_n(7)\}}{|H_n(5)|^2} J_n(5)$$

plotted as a function of  $n$  and is the real component of  $X_n$  in (7.10) for the case where  $z = 7$  and  $k = 5$ . Curve (2) in the same figure shows the imaginary component of  $X_n$ , this is readily seen to degenerate into

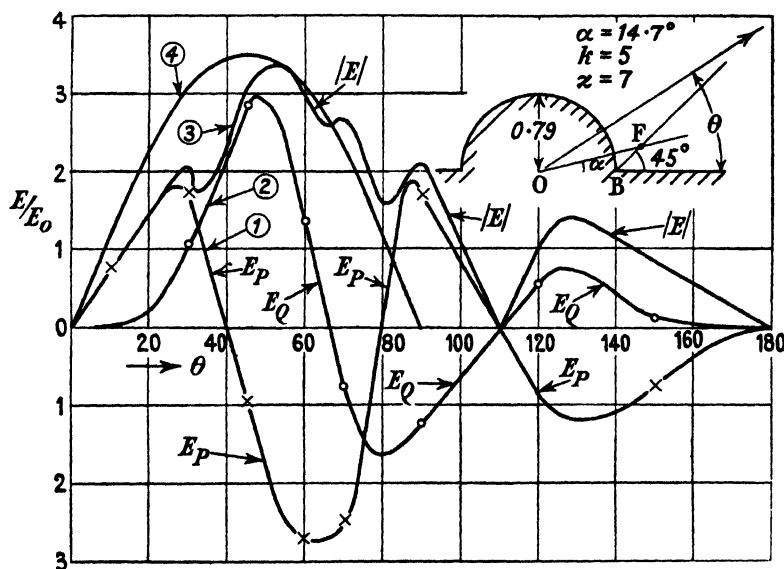


FIG. 7.10. Diffraction pattern due to filament and reflector system shown in inset diagram.

$J_n(7)$  when  $n$  is large. The figure also shows the plot of  $J_n(7)$ , and it may be seen that it is always a very good approximation to curve (2). A large amount of computation is required to derive Fig. 7.9, and therefore it is recorded here in case the reader should wish to solve other similar problems, using these values of  $z$  and  $k$ .

The inphase and quadrature components of field are shown by curves (1) and (2) in Fig. 7.10: curve (3) in the same figure shows  $|E|/E_0$  and curve (4) shows the ideal pattern for a  $90^\circ$  Vee with the filament on the bisector and at the same distance from the apex as the filament in our problem is from the point  $B$  in the diagram inset in Fig. 7.10. The purpose of this example is to compare curve (3) with the ideal curve (4). It may be seen that both have substantially the same maximum value, but in our problem this occurs at about  $54^\circ$  instead of at  $45^\circ$  in the ideal. The ideal falls to zero at  $\theta = 90^\circ$  and thereafter

$E$  is zero for it. The attempt to reach zero at  $\theta = 90^\circ$  is represented by the minimum at  $\theta = 80^\circ$  in curve (3). There is a big lobe with maximum at  $\theta = 130^\circ$ , and this results from the field refracted over the top of the cylinder. Seeing that the height of the cylinder is only  $0.79\lambda$ , it will surely be admitted that curve (3) is a surprisingly good approximation to curve (4) and therefore gives us sound reason for hoping that reflecting sheets of comparatively small size will suffice to produce patterns very similar to the ideal. The tremendous effect of this comparatively small cylinder is well illustrated by noting that the maximum value of  $E/E_0$  is 3.4, whereas it would be only  $2\sin(7\sin 14.7^\circ) = 1.96$  if the cylinder were removed, or 3.5 if the radius of the cylinder were infinite. It would be instructive to re-plot Fig. 7.10 for  $\alpha = 10^\circ$  (vice  $14.7^\circ$ ) to see if the maximum then occurred very near  $\theta = 45^\circ$ . It would also be instructive to derive the pattern for the arrangement shown by the diagram inset in Fig. 7.10 but with  $k$  and  $z$  equal to, say, 10 and 12, but this is left to an energetic reader; doubtless the result would be a much closer approximation to the ideal.

If  $ar < z$ , then  $ar$  and  $z$  must be interchanged in (7.9). When  $z \rightarrow \infty$  the equation for the field will be given by (7.10) provided that  $z$  is replaced by  $ar$  in it. If we then make  $\alpha$  tend to zero we shall have the field in the region of the cylinder when the source is a very distant filament close to the ground. Thus we can evaluate the shadow effect of a rounded hill, rising out of the plane, between a transmitter and receiver which are widely separated and both near the ground. Since  $\alpha$  tends to zero we must replace  $\sin n\alpha$  by  $2\pi nh/z$ , where  $h$  is the height of the transmitter at a large distance  $z\lambda/2\pi$ . We shall not give a numerical example of this problem but hope that some reader may do so.

### 7.3. Any Vee reflector with cylindrical back

Using the image process we can generalize (7.9) so as to apply to sheets inclined at an angle  $\beta = \pi/n$ : the general expression for the field is then found to be

$$\frac{cE}{4na\pi I} = j \left[ \frac{X_n(kz)}{H_n(k)} H_n(ar) \cos n\theta + \frac{X_{3n}(kz)H_{3n}(ar)}{H_{3n}(k)} \cos 3n\theta + \dots \right], \quad (7.11)$$

$$\therefore -\frac{E}{4nE_0} = \left\{ \frac{X_n(kz)}{H_n(k)} \cos n\theta - \frac{X_{3n}(kz)}{H_{3n}(k)} \cos 3n\theta \dots \right\} \quad \text{if } ar \rightarrow \infty. \quad (7.11a)$$

$$\text{Also we have} \quad -\frac{cE_P}{4na\pi I} = \frac{X_n^2(kz)}{|H_n(k)|^2} + \frac{X_{3n}^2(kz)}{|H_{3n}(k)|^2} + \dots \quad (7.12)$$

We can now study the effect of amputating the apex of the Vee, a device which is used in practice to reduce the size of the reflector. To fix ideas we will take as a numerical example  $\beta = 30^\circ$ , which is  $n = 6$ , and feel our way by exploring first the pattern for  $k = 0$ . Since the first maximum of  $J_n(z)$  occurs when  $z$  is just greater than  $n$ , the term  $J_{3n}(z)$  will not be appreciable until the aerial is at least  $2\lambda$  from the apex and till then the pattern will be a simple sinusoid. We will choose  $z = 16$  ( $R/\lambda = 2.55$ ), which Fig. 3.27 shows is a station for maximum forward gain. Reference to tables of  $J_n(z)$  shows that then  $E/E_0 = 4(\cos 6\theta + 0.4 \cos 18\theta)$ , a pattern which is  $12^\circ$  wide at half-height and having a 4 per cent. side lobe centred at  $\pm 13^\circ$ . We will now study the effect of providing curved backs of various radii. The parameter  $B \equiv J_6(16)Y_6(k) - J_6(k)Y_6(16) \doteq \frac{\sin(16-k)}{2\pi\sqrt{k}}$  is found to have the values shown in Table 7.1 below:

TABLE 7.1

$k$	4	6	8	9	10	11	12	13	14	15	16
100B	-25.5	-7.2	-3.5	+1.4	+4.6	+5.4	+2.2	-2.0	-4.4	-3.6	0

A plot of this shows  $B$  is zero when  $k = 8.7$  and  $12.5$ , and then the pattern consists only of the term in  $\cos 18\theta$  and is of little interest since it corresponds approximately to zero forward field: it occurs when the clearance between the aerial and the back is approximately  $\frac{1}{2}\lambda$  or  $\lambda$ , and in this respect the rounded back is then behaving as if it were an infinite plane. If  $k$  is less than 16 its effect on the term  $\cos 18\theta$  is negligible and it will remain  $-jJ_{18}(16)\cos 18\theta$ . The coefficient of  $\cos 6\theta$  has a real term (save when  $J_6(k) = 0$ ) which tends to deteriorate the resultant pattern, since the two components must be added vectorially. Now  $J_6(k) = 0$  when  $k = 9.9$  and  $13.4$ , and hence these give desirable radii for the back since this real term is then zero.

Reference to (7.11) will show that when  $J_n(k) = 0$  the coefficient of  $\cos n\theta$  is  $+jJ_n(z)$  and thus is precisely the same as if the back were absent. Thus it follows the radius of the back can be chosen so that its presence discloses itself in the pattern only to the second-order effect represented by the term  $\cos 18\theta$ : when  $k = 13.4$  this amounts to reducing this coefficient by about 3 per cent. of itself and adding a quadrature term whose fractional size is less than 1 per cent. It may thus be said that the back, even though large, need not affect the pattern. Accordingly we may amputate a length of at least  $2\lambda$  from the apex and



thereby decrease the physical size of the reflector very considerably. It is instructive to find analytically that this need have no effect on the ideal pattern, a result already known in practice from experiments with flat backs (see Chap. XII). The sagitta  $S$  of the round back is

$$\frac{S}{R} = (1 - \cos \frac{1}{2}\beta) \doteq \frac{\beta^2}{8} = 0.035, \quad \text{if } \beta = 30^\circ,$$

thus  $S = 0.07\lambda$  if  $R = 2\lambda$ , and so the back would be considered sensibly flat in optical practice. The correct procedure in practice would appear to be as follows:

Place the aerial at the station of maximum forward gain for a complete Vee: then amputate the apex at about  $0.4\lambda$  behind the aerial and close the opening with a flat back. Then find by experiment the precise position at which the aerial gives the sharpest pattern. A more exact method is to amputate the vertex at a radius which makes  $J_n(k) = 0$  and then proceed as above. The main effect of a flat back is to cause the stations for zero forward field to occur at distances which are multiples of  $\frac{1}{2}\lambda$  from it, but the positions of these stations will merge into those for the complete Vee when the distance between the aerial and the back becomes large.

Reference to equation (3.18) shows the current density behind the aerial has a first term which varies as  $|H_n(k)|J_n(ar)$  and this tends to be small when  $ar < k$ . Hence, in amputating the vertex we are amputating a portion which carries comparatively little current, and thus its removal would not be expected to affect the pattern very appreciably. The region of large current density in the sheets (beyond the aerial) persists further as the angle of the Vee decreases, and then relatively wider sheets must evidently be required to reproduce a close approximation to the ideal pattern. This result is familiar in practice (the reason for it is now obvious) and is particularly exemplified by the pattern which is observed from a rectangular wave guide (the limiting case of a Vee) which has not been furnished with a flared exit.

Remembering that the vector potential  $A$  is related to  $E$  by the equation  $E = -jaA$  and that  $4\pi i = H = -\partial A/\partial r$  it follows from (7.11) that the current density at the 'bright spot' of the back is

$$\frac{i}{I} = \frac{2\pi n}{\lambda} \left[ \frac{B\{-J'_n(k) + jY'_n(k)\}}{\{-J_n(k) + jY_n(k)\}} + \dots \right] = -\frac{12\pi}{\lambda} \times \frac{4.4}{100} \times \frac{(-0.185 + 0.082j)}{(-0.082 - 0.209j)},$$

when  $n = 6, \quad k = 14, \quad z = 16.$

$$\therefore \frac{|i|}{I} = \frac{48\pi}{100\lambda} \sqrt{89^\circ}.$$

At  $ar = 2$  the field incident from the aerial is  $cE/a\pi I = 0.557 \overline{60^\circ}$ , hence  $2\pi i/E = 0.86$ . Accordingly the 'bright spot' density is given to a fair approximation by simple ray theory. The density on the back at the point where it joins a side of the Vee must be approached as a limit (because there we cannot take  $\partial A/\partial r$  without penetrating the boundary), but it seems certain that  $i$  must be zero at this point.

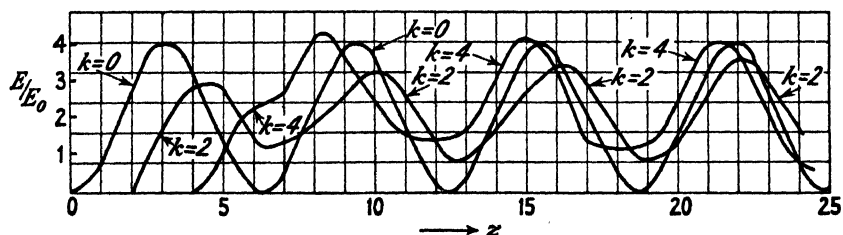


FIG. 7.11. Some curves of forward field for a  $90^\circ$  reflector having a convex back.

We will now explore the effect of a curved back on a mirror of wide angle: this is a step towards the analysis of a shallow parabola, a form used extensively in practice. Fig. 7.11 shows the curves of forward field for a  $90^\circ$  Vee having a curved back of radius  $R/\lambda = 0, 0.32, \text{ and } 0.64$  respectively. It shows that the back prevents the field from falling to zero, because it produces a quadrature term: when  $z$  is large the three curves tend to coincide and the effect of the back becomes insignificant. When  $k = 9$  the forward field reaches its grand optimum, of value 22. Then the equation of the pattern is

$$\frac{E}{8E_0} = 0.145(\cos 2\theta + 1.40 \cos 6\theta + 0.86 \cos 10\theta + 0.03 \cos 14\theta),$$

and then the main beam is  $20^\circ$  wide at half-height and the side lobes are small. We will now suppose there is a curved back such that  $k = 4$ . Then evaluation of the radiation resistance shows that its relative value is 1.17 when  $z = 8$ , 0.95 when  $z = 9$ , and 0.5 when  $z = 10$ . Consideration of these values, in relation to Fig. 7.11, suggests the gain is a maximum near  $z = 8$ . Computation shows that then the pattern is

$$\frac{E}{E_0} = 0.7\{(1 + 1.7j)\cos 2\theta + 3.9 \cos 6\theta + 0.7 \cos 10\theta + 0.01 \cos 14\theta\}.$$

This is plotted in Fig. 7.12, which shows also, for comparison, the pattern for a  $90^\circ$  Vee without curved back and with the aerial at  $\frac{3}{2}\lambda$  from the apex. It may be seen that the back of radius  $0.64\lambda$  does not alter the width of the beam at half-height, but it does increase the side lobes:

the quadrature term in the field prevents the R.M.S. field from passing through zero. The forward field is  $4.1E_0$  and hence

$$G = \frac{(4.1)^2}{1.17} = 14.3,$$

which is the same value as for  $k = 0$  and  $z = 8.7$ . Evaluation shows the gain is a maximum when  $z = 8$  and equals 12.5 when  $z = 10$ . Clearly the main effect of the back is to increase the lobes without

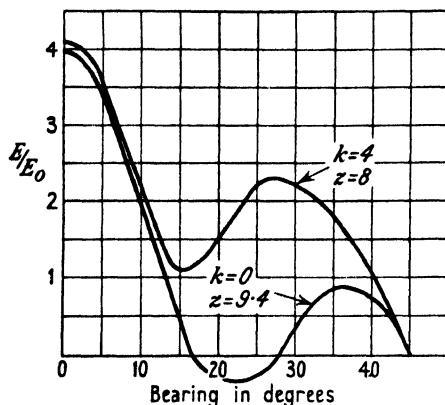


FIG. 7.12. Diffraction pattern for a  $90^\circ$  reflector with convex back ( $k = 4$ ,  $z = 8$ ).

appreciable increase in the width of the main beam. Evaluation shows that when  $k = 2$  the grand optimum gain is 18 and occurs when  $z = 9.3$ : if  $z$  does not exceed 5, then the gain is substantially constant and equal to 8, and thus shows the effect on the pattern must be negligible. Hence if the aerial is close to the apex then some of the apex can be amputated without detriment; but when the aerial is some  $\frac{3}{2}\lambda$  from the apex then a curved back will increase the side lobes and thus offset the advantage of some saving of space. It is, however, very striking to find that a *convex* back to the mirror does not have a violent effect; this might not be obvious by an approach from geometrical optics. If the radius of the back is very large we might be inclined to think the pattern would approach that for an infinite flat sheet. On the other hand, the field must be constrained, by the sides, to an arc of  $\pm 45^\circ$ , and this consideration suggests the pattern tends to become a sinoid. On the other hand, if the radius of the back is large the aerial must be very distant from the apex, and this we associate with a 'porcupine' pattern of very fine lobes. Thus there are conflicting tendencies to a single sinoid or to a porcupine. Accordingly we presume a round back

of large radius will tend to reduce the side lobes which otherwise would have existed. It thus seems conceivable that a back of large radius may be capable of producing a pattern having a very sharp main beam and comparatively small side lobes, or at any rate to group the porcupine lobes under a reasonably sharp envelope: a concept and mechanism we shall meet again when discussing the parabola.

#### 7.4. Filament anywhere in a Vee reflector with cylindrical back

In the last section the filament was on the bisector of the Vee: now we shall generalize the analysis so as to apply to a filament which is not on the bisector and we do this because it leads to a solution which is of great practical interest.

The equation for the pattern can be inferred at once from equation (3.20) since the form of (7.9) and (7.12) show that the curved back is described completely by replacing the  $J_n$ ,  $J_{2n}$ , etc., in (3.20) by the expression denoted by the symbol  $X$  in (7.10).

For the problems we have in mind now, there are to be a pair of similar and cophased filaments disposed symmetrically on each side of the bisector: accordingly the terms involving  $\sin \alpha$  in (3.20) vanish, and the equation of the resulting pattern is

$$-\frac{jE}{8nE_0} = \{\epsilon^{jn\pi/2} X_n \cos n\alpha \cos n\theta + \epsilon^{j(3n\pi/2)} X_{3n} \cos 3n\alpha \cos 3n\theta + \dots\}. \quad (7.13)$$

It is a common device in practice to use two or more Vee reflectors side by side and with axes parallel, thus forming an array of Vees: it is considered that any one aerial is almost completely screened by its own Vee (from the other aerials in their own Vees) and hence that each aerial and Vee will perform substantially as if the other Vees did not exist. Such an arrangement cannot be examined analytically because we cannot deal with reflecting sheets of finite width, and the width must necessarily be finite if two are to be placed side by side. But it seems likely that an approximate solution of the double Vee problem can be obtained by using a round back to simulate the middle portion of the **W** formed by a pair of Vees, side by side. Since the sides of the Vee in our solution are necessarily radii of the round back, the only **W** which we can attempt to simulate is one whose angles are  $90^\circ$ . Accordingly  $n$  must have the value 2 in (7.13), which then becomes

$$\frac{jE}{16E_0} = \left[ \frac{J_2(z)Y_2(k) - J_2(k)Y_2(z)}{H_2(k)} \cos 2\alpha \cos 2\theta + X_6 \cos 6\alpha \cos 6\theta + \dots \right].$$

The disposition we have in mind is described by the inset diagram in Fig. 7.13, in which the dotted tangents meeting at  $C$  would be the apex of the  $W$  which we are simulating by the arc  $DGE$ : the pair of similar filaments are represented by  $F_1$  and  $F_2$ . As a numerical example we shall take  $k = 7$  and  $z = 8$ , and this makes  $\alpha = 38.2^\circ$ ,  $DF_1 = 1.33$ , and

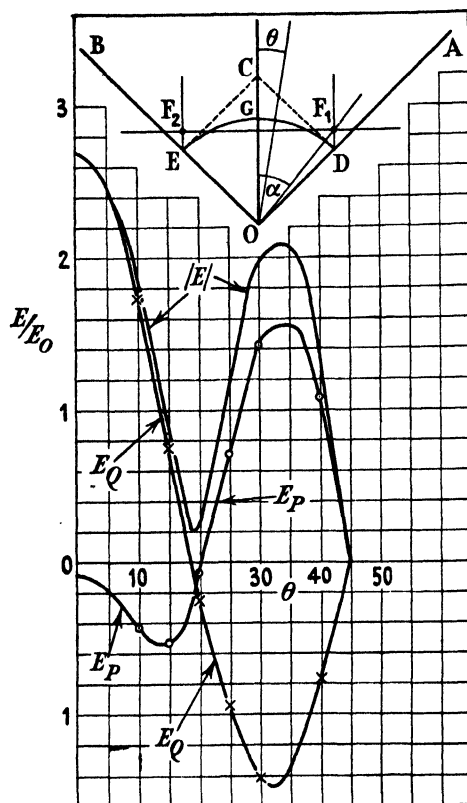


FIG. 7.13. Relating to the problem of two  $90^\circ$  reflectors, side by side.

$F_1 F_2 = 9.9$ : it should be noted that  $F_1$  and  $F_2$  are not visible from one another in the optical sense. The ideal pattern for the  $90^\circ$  Vee  $ADC$  is a simple sinusoid within the bearings  $\pm 45^\circ$ . If the two filaments were alone in space their field would be given by the equation

$$\frac{E}{2E_0} = \cos\left(\frac{9.9}{2} \sin \theta\right)$$

and this is zero when  $\theta = 18.5^\circ$  and  $72^\circ$ . We wish to see if the pattern approximates to the form  $\cos(4.95 \sin \theta) \cos 2\theta$ , and this is zero when  $\theta = 18.5^\circ$  and  $45^\circ$  and has a side lobe whose maximum is at  $\theta = 39.4^\circ$ ,

with fractional value 0.19. Fig. 7.13 shows the two components of field, and also  $|E|$ , appropriate to the circular back of this numerical example. It may be seen that  $|E|$  falls to a sharp minimum at  $\theta = 19^\circ$  and thus agrees closely with our expectation that  $|E|$  would pass through zero at  $\theta = 18.5^\circ$ : the side lobe has a maximum of 76 per cent. and occurs when  $\theta = 33^\circ$  as compared with our expectation of 19 per cent. at  $\theta = 39.4^\circ$ . Thus our expectation has been fulfilled in the main, save that the side lobe is four times too big. We must now consider whether the discrepancy would probably tend to disappear as the radius of the circular back increased or whether the back is ineffective. The answer to this question is probably supplied by Fig. 7.14, which shows the ideal pattern for  $z = 8, k = 0$ , and  $\alpha = 38.2^\circ$ . If this be compared with the curve for  $|E|$  in Fig. 7.13 it will be seen that the curved back has decreased the forward field from 3.06 to 2.70 but it also has vastly decreased the amplitude of the side lobe. The value of  $E/E_0$  in the forward direction is 1.53 for a single  $90^\circ$  Vee when  $k = 1.33$ : hence our concept of the behaviour of two such Vees side by side would give a

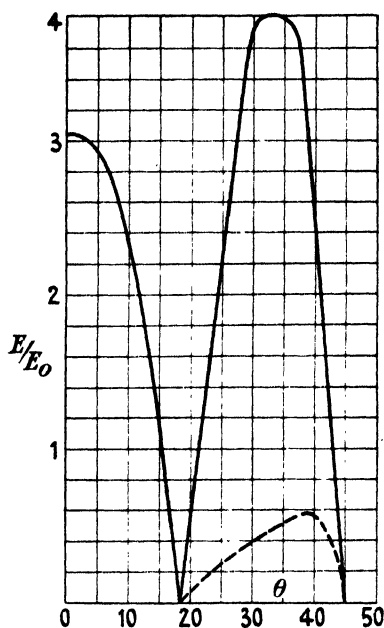


FIG. 7.14. A certain diffraction pattern for comparison with 7.13.

forward field of 3.06 and this happens to agree precisely with the forward field in Fig. 7.14, but is greater than the forward field for the circular back when  $k = 7$ . The dotted side lobe in Fig. 7.14 is the curve  $3.06 \cos(4.95 \sin \theta) \cos 2\theta$ , the main beam of this curve being indistinguishable from the main beam drawn in this figure. Comparing Figs. 7.13 and 7.14 it does seem reasonable to suppose that increasing the radius of the curved back would tend to make the curve of  $|E|$  differ insensibly from the curve  $3.06 \cos(4.95 \sin \theta) \cos 2\theta$  and thus that our concept of the behaviour of two similar Vees, side by side, was substantially correct.

The length of the dotted sides  $EC$  and  $DC$  in the inset diagram in Fig. 7.13 is only  $1.12\lambda$ , and we may surely expect that the ideal pattern which would result from them would be a closer approach to what we

expect than the ideal pattern which does result from the circular back. Accordingly this example again gives us good reason to hope that sheets whose width is only a very few wavelengths will produce a pattern which is a close approximation to the ideal.

Fig. 7.14 is very instructive in showing that the bearing for zero field is precisely the bearing at which this would occur if the Vee were removed and the two aerials left free in space. It shows there is a strong tendency for the pattern to be the product of the pattern due to the two aerials in free space and the pattern due to one aerial in the Vee. This principle should be useful in predicting an approximate pattern without the labour of complete evaluation.

Reference to (7.3) and (7.9) will show that at each filament

$$-\frac{cE_P}{16a\pi I} = \frac{\{J_2(z)Y_2(k) - J_2(k)Y_2(z)\}^2}{|H_2(k)|^2} \cos^2 2\alpha + \dots$$

Substituting in this expression for  $z = 8$  and  $k = 7$  gives

$$-\frac{cE_P}{a\pi I} = 0.364.$$

With a simple  $90^\circ$  Vee and  $k = 1.33$  we have

$$-\frac{cE_P}{a\pi I} = 4\{J_2^2(1.33) + J_6^2(1.33)\dots\} = 0.29$$

and this shows the resistance of each filament in the round-backed **W** is 1.25 times as great as if it were similarly situated in a true Vee. Since the forward field (see Fig. 7.13) is 2.7, it follows that

$$G = \frac{(2.7)^2}{2 \times 0.364} = 10.$$

The ideal gain for the simple  $90^\circ$  Vee is 8 (see Fig. 3.23), and thus this round-backed **W** improves the gain in the ratio  $10/8 = 1.25$ ; in the limit this ratio would be 2.

### 7.5. The density of current induced at the apex of the Vee

In Chapter V we found that the induced current had an infinite density at the edge of a half-plane: we dismissed this infinity as being without practical significance because we said it arose only because the edge was sharp: now we can furnish this edge with a cylinder of any radius and examine what effect this has on the induced density. To do this we require an expression for the field at a radius which is less than

$z/2\pi$ , and this is obtained by interchanging  $ar$  and  $z$  in (7.11), thus giving

$$\begin{aligned}\frac{cE}{4na\pi I} &= j \left[ \frac{\{J_n(ar)Y_n(k) - J_n(k)Y_n(ar)\}}{H_n(k)} H_n(z) \cos n\theta + \dots \right] \\ &\equiv j \left[ \frac{X_n(ar)H_n(z)}{H_n(k)} \cos n\theta + \frac{X_{3n}(ar)H_{3n}(z)}{H_{3n}(k)} \cos 3n\theta + \dots \right].\end{aligned}\quad (7.14)$$

The vector potential  $A$  is obtained from the relation  $E = -jaA$ , then the tangential and radial components of magnetic field are given from the relations

$$H_\theta = \frac{\partial A}{\partial r} \quad \text{and} \quad H_r = \frac{1}{r} \frac{\partial A}{\partial \theta}.$$

We note that  $\partial A / \partial \theta = 0$  for all values of  $\theta$  at  $ar = k$ , showing, as it should do, that no magnetic field penetrates the cylinder. We have

$$\frac{cH_\theta}{4\pi nI} = a \left[ \frac{\{J'_n(ar)Y_n(k) - J_n(k)Y'_n(ar)\}}{H_n(k)} H_n(z) \cos n\theta + \dots \right].$$

If  $i$  is the current density on the surface of the cylinder, then  $4\pi i = cH_\theta$ ,

$$\therefore \frac{i}{nI} = a \left[ \frac{\{J'_n(k)Y_n(k) - J_n(k)Y'_n(k)\}}{H_n(k)} H_n(z) \cos n\theta + \dots \right].$$

But

$$J_n Y'_n - J'_n Y_n = -\frac{2}{\pi k},$$

$$\therefore \frac{i}{nI} = \frac{2a}{\pi k} \left[ \frac{H_n(z)}{H_n(k)} \cos n\theta + \frac{H_{3n}(z)}{H_{3n}(k)} \cos 3n\theta + \dots \right], \quad (7.15)$$

a result which might well have been guessed from (6.11 b),

$$\begin{aligned}&\doteq \frac{2a}{\pi k} \frac{\{Y_n(z) + jJ_n(z)\}}{Y_n(k)} \cos n\theta, \quad \text{if } k \rightarrow 0. \\ \therefore \frac{|i|}{nI} &= \frac{2an}{k} J_n(k) |H_n(z)| \cos n\theta, \quad \text{since } J_n Y_n \rightarrow -\frac{1}{n\pi}, \\ &= \frac{an(\frac{1}{2}k)^{n-1} |H_n(z)|}{\Gamma(n+1)}, \quad \text{when } k \rightarrow 0, \\ &= \frac{2}{\sqrt{(kz)}}, \quad \text{when } n = \frac{1}{2}.\end{aligned}$$

Hence even in the extreme case of  $n = \frac{1}{2}$  the current density at the edge is never infinite so long as this edge has a round nosing of finite radius. If the edge is truly sharp the magnetic field at it must have two directions, and this is impossible unless that field is zero: the magnetic field is not zero if  $\beta$  is  $180^\circ$  or more. Once the round nose is



provided the direction of the magnetic field becomes unique at all points round it. At the point where the cylinder meets the sheet the induced density is zero both on the sheet and on the cylinder, and this is another example showing that the density is always zero at the apex of an angle which is just less than  $180^\circ$ . We have now disposed of the necessity for an infinite density at an obtuse angle and may guess that in all circumstances the density at a point of small curvature tends to be inversely proportional to the square root of that curvature.

### 7.6. Method of producing a non-reflecting chamber

If an aerial is enclosed within a chamber having perfectly conducting walls, the output of energy is zero and the internal field is disposed in a system of standing waves. If the walls have finite conductivity, energy will be dissipated in them: at once the idea suggests itself that it may be possible to arrange their conductivity so as to absorb just that amount of energy which would be crossing the boundary if the physical barrier did not exist. Then it would seem the existence of the barrier would not be perceptible from the aerial and the field inside it would be as though the aerial were in free space. We will put this idea in a manner which will appeal to transmission engineers: if a concentric cable is terminated with the characteristic resistance the reflection is said to be zero, and it is said to be as though the cable extended to infinity: is there any characteristic resistance for the walls of a chamber which will produce the same effect? Since energy can be dissipated only by the flow of current, and since current in the walls must produce a field inside the chamber, it seems impossible to prevent a standing wave system from being set up. This argument is inescapable and applies also to a cable. Close examination shows it is possible to prevent all reflection if the chamber has a double wall. The outer must have perfect conductivity and the inner must be a thin sheet of high-resistance material: both the resistivity and the distance between the shell and the outer wall must be chosen correctly. We will now work out a particular problem and discuss its physical interpretation later. Let a current filament be surrounded coaxially by a perfectly conducting tube of radius  $R_3$  and also by a very thin cylindrical shell of radius  $R_2$ , less than  $R_3$ , of resistivity  $\rho$ . By (1.27) the field of an axial current  $I$  distributed uniformly round a tube of radius  $R$  is

$$\frac{cE}{\pi r I} = J_0(k)\{-J_0(ar) + jY_0(ar)\}, \quad \text{for } r > R: \quad (1.27)$$

for  $R > r$ ,  $ar$  and  $k$  must be interchanged. Let a current  $I_1$  on the

common axis induce currents  $I_2$  and  $I_3$  in the shell and the outer wall respectively. Then the general expression for the field at radius  $R_2$  is

$$\begin{aligned} \frac{cE_2}{a\pi} &= [\{-J_0(k_3) + jY_0(k_3)\}I_3 + \{-J_0(k_2) + jY_0(k_2)\}I_2]J_0(k_2) + \\ &\quad + \{-J_0(k_2) + jY_0(k_2)\}I_1 \\ &= -\{J_0(k_3)I_3 + J_0(k_2)I_2 + I_1\}J_0(k_2) + \\ &\quad + j\{Y_0(k_3)J_0(k_2)I_3 + Y_0(k_2)J_0(k_2)I_2 + Y_0(k_2)I_1\}. \quad (7.16) \end{aligned}$$

The field outside  $R_3$  is

$$\frac{cE}{a\pi} = \{J_0(k_3)I_3 + J_0(k_2)I_2 + I_1\}\{-J_0(ar) + jY_0(ar)\}.$$

Since the tube of radius  $R_3$  is a perfect conductor it follows that the field must be zero everywhere for  $r > R$  and accordingly

$$J_0(k_3)I_3 + J_0(k_2)I_2 + I_1 = 0.$$

Substituting this condition in (7.16) gives

$$\frac{cE_2}{a\pi} = -j \frac{X_0(k_2 k_3)}{J_0(k_3)} \{J_0(k_2)I_2 + I_1\}, \quad (7.17)$$

where  $X_0(k_2 k_3) \equiv J_0(k_2)Y_0(k_3) - J_0(k_3)Y_0(k_2)$ .

But 
$$E_2 = \frac{\rho}{t} \frac{I_2}{2\pi R_2}, \quad \therefore \frac{cE_2}{a\pi} = \frac{c\rho}{t} \frac{I_2}{2\pi^2 k_2} \equiv \frac{I_2}{Z}.$$

Then substitution in (7.17) gives

$$\begin{aligned} \frac{I_2}{I_1} &= -\frac{jX_0(k_2 k_3)Z}{J_0(k_3) + jX_0(k_2 k_3)ZJ_0(k_2)}, \\ \frac{I_3}{I_1} &= -\frac{1}{J_0(k_3) + jX_0(k_2 k_3)ZJ_0(k_2)}, \\ \therefore \frac{I_3}{I_2} &= -\frac{j}{X_0(k_2 k_3)Z} \equiv -j\alpha. \quad (7.18) \end{aligned}$$

Now both  $X_0$  and  $Z$  are essentially real quantities, hence (7.18) shows that  $I_3$  and  $I_2$  are in phase quadrature with one another for all values of  $R_3/R_2$  and of  $\rho$ .

The field inside the tube of radius  $R_2$ , due to the induced currents  $I_2$  and  $I_3$ , is

$$\begin{aligned} \frac{cE}{a\pi} &= [\{-J_0(k_2) + jY_0(k_2)\}I_2 + \{-J_0(k_3) + jY_0(k_3)\}I_3]J_0(ar) \\ &= [-J_0(k_2) + \alpha Y_0(k_3) + j\{Y_0(k_2) + \alpha J_0(k_3)\}]J_0(ar)I_2, \quad \text{by (7.18).} \end{aligned}$$

We wish to arrange that this field shall be zero for all values of  $r$  less than  $R_2$ : if this is to be so, then it is essential that

$$-J_0(k_2) + \alpha Y_0(k_2) = 0 \quad \text{and} \quad Y_0(k_2) + \alpha J_0(k_2) = 0.$$

$$\therefore J_0(k_2)J_0(k_3) + Y_0(k_2)Y_0(k_3) = 0 \quad (7.19)$$

and 
$$\alpha = \frac{J_0(k_2)}{Y_0(k_3)}. \quad (7.20)$$

The condition (7.19) is independent of  $\alpha$  and thus is independent of  $\rho$ : it is a purely geometrical condition. If  $k_2$  is large it reduces to  $\cos(k_3 - k_2) = 0$ , or  $(R_3 - R_2)/\lambda = \frac{1}{4}, \frac{3}{4}, \frac{5}{4}$ , etc., and no solution is possible unless  $k_3$  exceeds 0.894.

Combining (7.17) and (7.18) gives

$$\frac{c}{2\pi^2 k_2} \frac{\rho}{t} = J_0^2(k_2) + Y_0^2(k_2) \quad (7.21)$$

$$\doteq \frac{2}{\pi k_2}, \quad \text{if } k_2 \text{ is not small,}$$

then 
$$\rho/t = \frac{4\pi}{c} = 120\pi, \quad \text{in ohm units.} \quad (7.21 a)$$

We have now found both the spacing and the resistivity which will make the field inside  $R_2$  precisely the same as it would be if both tubes were removed. A non-reflecting chamber then results for the particular frequency which makes  $(R_3 - R_2)/\lambda = \frac{1}{4}$ , etc., and then it is precisely as though the central rod were in free space. This solution does not demand the central current should be a filament: if it is a tube of radius  $R$ , then it is necessary only to replace  $I_1$  above by  $J_0(k_1)I_1$ .

If  $R_2$  happens to be such that either  $J_0(k_2)$  or  $Y_0(k_2)$  is zero, then it follows, from (7.19), that  $R_3$  must be such as to make  $Y_0(k_3)$  or  $J_0(k_3)$  zero respectively, since  $J_0(k_2)$  and  $Y_0(k_2)$  cannot both be zero simultaneously: if  $k_2$  is large, this condition obviously approaches  $(R_3 - R_2)/\lambda = \frac{1}{4}$ . If  $Y_0(k_2)$  is zero for the first time, then reference to tables will show that  $k_3 - k_2 = 1.511$ , whereas  $\frac{1}{2}\pi = 1.571$ : hence the clearance is then 4 per cent. less than  $\frac{1}{4}\lambda$ . If  $J_0(k_2)$  is zero for the first time, then  $R_3 - R_2$  is 1.3 per cent. less than  $\frac{1}{4}\lambda$ . These examples show the limiting clearance is approached very quickly and has sensibly been attained even when  $R_2/\lambda$  is only of the order of 0.14.

On making use of (7.19) and (7.20) it follows that

$$\frac{I_3}{I_1} = -\frac{1}{J_0(k_3) + jY_0(k_3)},$$

and hence

$$\frac{|I_3|}{|I_1|} = \left(\frac{\pi k_3}{2}\right)^{\frac{1}{2}}.$$

$$\begin{aligned}
 \text{Also } \frac{I_3}{I_2} &= j \frac{Y_0(k_2)}{J_0(k_3)} \doteq j \frac{\sin(k_2 - \frac{1}{4}\pi)}{\cos(k_3 - \frac{1}{4}\pi)} \left( \frac{k_3}{k_2} \right)^{\frac{1}{2}} \\
 &= j \frac{\sin(k_2 - \frac{1}{4}\pi)}{\cos(\frac{1}{2}\pi + k_2 - \frac{1}{4}\pi)} \left( \frac{k_2 + \frac{1}{2}\pi}{k_2} \right)^{\frac{1}{2}}, \quad \text{since } k_3 - k_2 = \frac{1}{2}\pi, \\
 &= -j \left( 1 + \frac{\lambda}{4R_2} \right)^{\frac{1}{2}}, \tag{7.22}
 \end{aligned}$$

showing that the two induced currents tend to become equal in magnitude when  $R_2/\lambda$  is large.

If the field everywhere within the resistive tube is to be the same as the 'isolated field' of  $I_1$ , then the dissipation must equal the square of this field divided by the resistance of the tube: accordingly

$$P = \frac{a^2 \pi^2 I_1^2 |H_0(k_2)|^2}{c^2} \frac{2\pi R_2 t}{\rho} = \frac{2\pi^2 k_2 t |H_0(k_2)|^2}{\rho} \frac{a\pi I^2}{c^2}, \quad \text{by (7.16).}$$

This gives an interpretation of the physical meaning of (7.16), for it is obvious that  $k_2 |H_0(k_2)|^2/\rho$  must be constant if the dissipation is to be independent of  $R_2$ . The product  $k_2 |H_0(k_2)|^2$  equals 0.33, 0.54, 0.59, 0.62, 0.64 when  $k_2$  equals 0.1, 0.5, 1.0, 2.0 and infinity respectively: thus showing that  $\rho/t$  differs little from  $120\pi$  ohms† if  $R_2/\lambda$  exceeds 0.16 (i.e.  $k_2 = 1$ ); it must have the value  $62\pi$  ohms if  $R_2/\lambda = 0.016$ .

By Poynting's theorem the outflow of power is at the rate of  $EH/4\pi$  per unit area. If this power is to be dissipated in a thin shell and the field at the shell is to remain equal to  $E$ , then it follows that

$$\rho/t = \frac{4\pi E}{H}.$$

When  $E = H/c$ , as in a plane wave, we have  $\rho/t = 4\pi/c$ .

The mechanism of the whole problem is exposed by proceeding to the limit of  $R_2$  tending to infinity. If a plane wave is incident on a perfectly conducting sheet it induces a current density  $i = cE/2\pi$ ; if the sheet has an ohmic resistivity such that  $\rho/t = 4\pi/c$ , then the current induced will be half as much as if the resistivity were zero. This means that the screening ratio of the said resistive sheet is one-half: the net field behind it is half the incident field and the sheet re-radiates forward a wave of half the intensity of the incident waves. If a perfectly

† *Note.* If current flows radially through an annular disk of thickness  $t$  and having external and internal radius  $a$  and  $b$  respectively, then it is easy to show that the resistance of the disk is  $(\rho/2\pi t)\log(a/b)$ . If such a disk is used as the termination of a coaxial cable, then it follows that the resistance of the disk will equal the characteristic resistance of the cable when  $\rho/t = 120\pi$ , a result which is independent of  $a/b$ .

conducting plane is placed behind and parallel to the resistive sheet it will re-radiate a wave whose intensity is half the original undisturbed wave. Accordingly in front of the resistive sheet there will be two re-radiated waves of equal intensity, each half the intensity of the original incident wave: one is originated by the current induced in the resistive sheet and the other by the current induced in the perfectly conducting sheet which is behind the resistive sheet. These two re-radiated waves, of equal intensity, will cancel each other precisely if they are exactly in antiphase with one another: consideration will show this will occur if the space between the two sheets is  $\frac{1}{4}\lambda$ ,  $\frac{3}{4}\lambda$ , etc. We have now found the simple and obvious description of the whole effect analysed completely for a cylindrical wave. We now understand why the spacing is never precisely equal to  $\frac{1}{4}\lambda$  and why  $\rho/t$  is never precisely equal to  $4\pi/c$ : these discrepancies are due entirely to the cylindrical character of the wave. It is interesting to find that the effect of the cylindrical wave-front is negligible when its radius of curvature exceeds about  $0.15\lambda$ .

The field between  $R_3$  and  $R_2$  is given by the equation

$$\frac{cE}{a\pi I_1} = - \frac{\{J_0(k_2)J_0(ar) + Y_0(k_2)Y_0(ar)\} \{-J_0(k_2) + jY_0(k_2)\}}{|H_0(k_2)|^2} \quad (7.23)$$

$$\text{or} \quad \frac{c|E|}{a\pi I_1} \doteq \sqrt{\left(\frac{2}{\pi ar}\right)} \cos \frac{2\pi}{\lambda}(r - R_2), \quad \text{if } k_2 \text{ is large;} \quad (7.24)$$

thus the field in the interspace differs insensibly from a quarter of a sinusoid when the spacing is  $\frac{1}{4}\lambda$ .

We have now found the principle to be used in the construction of a room in which short-wave aerials can be tested as though they were in free space: also we see how to construct a device for absorbing the power radiated by an aerial without disturbing the impedance of the aerial. In the second application the thin resistive shell will be a tube whose diameter is not vastly greater than the diameter of the rod which forms the aerial: the output can be deduced from the temperature rise of the shell or by measuring the interspace field with a monitor aerial.†

It is essential to the theory of operation that  $t/\lambda$  shall be very small and also that  $\rho$  shall be so large that the current induced in the shell will have sensibly a constant density through its thickness. If the shell were of copper it may be calculated that the thickness would have to be  $0.44 \times 10^{-8}$  cm. in order that  $\rho/t$  should equal  $120\pi$  ohms: this is meaningless since it is less than molecular dimensions. If  $t = 0.1$  mm., then  $\rho = 3.8 \Omega$  per cm. cube; this is more than  $2 \times 10^6$  times the resistivity

† See *British Patents*, No: 585,460 and 587,616.

of copper, one-tenth the resistivity of a 3 per cent. NaCl solution, and one-thousandth part of the resistivity of 'tap water'. The effective depth of penetration in a conductor is given by  $d = (1/2\pi)\sqrt{(\rho/f)}$ , where  $\rho$  must be expressed in E.M., C.G.S. units: if  $\rho = 3.8$  ohm units it follows from this that  $d = 0.1$  mm. when  $f = 10^{12}$ , which is when  $\lambda = 0.3$  mm. Accordingly the depth of penetration need not be considered even when  $\lambda$  is only of the order of 1 cm. Experience shows that paper sheets impregnated with colloidal graphite can readily be made to have a resistance near  $120\pi$  ohms for a strip of unit width and length: and that the resistance of such paper is sensibly constant from point to point and not much dependent on age if it is protected from moisture.

Before leaving this problem it is instructive to find the ratio of  $I_3/I_2$  when the interspace between the shell and perfectly conducting wall is very small, for this will correspond to a badly conducting skin on the surface of the perfectly conducting wall. It follows from (7.18) that

$$\begin{aligned}\frac{I_3}{I_2} &= \frac{j}{\sqrt{(4/\pi^2 k_2 k_3) \sin(k_3 - k_2) Z}}, \quad \text{when } k_2 \text{ is large} \\ &= -\frac{j\pi k_3}{2atZ}, \quad \text{when } k_3 \doteq k_2 \\ &= -\frac{jcp}{4\pi at^2} = -\frac{jx}{2\pi} \frac{\lambda}{t}, \quad \text{where } \frac{\rho}{t} \equiv x \frac{4\pi}{c}.\end{aligned}$$

Hence if  $x$  is of the order of unity,  $I_3/I_2 \gg 1$  since  $t/\lambda$  is very small, thus showing that relatively very little current will flow in the badly conducting skin.

We can now consider the particular case where  $J_0(k_3) = 0$ , the resonance condition for the surrounding chamber. Then  $I_3$  would be infinite if the inner shell were absent, and the solution would break down because we have ignored the resistivity of the walls. It now follows from p. 289 that  $I_2/I_1 = -1/J_0(k_2)$  for all values of  $\rho$ , and hence  $I_2/I_1 \gg 1$  since  $k_3 - k_2$  is very small and  $J_0(k_3)$  is zero. Then there will be a very large current (relative to  $I_1$ ) in the thin shell and a vastly larger quadrature current in the perfectly conducting wall just behind it. It means that a small but finite resistivity in the wall will force the current to penetrate deeper than might have been expected, and change its phase very rapidly, if the frequency is just verging on resonance. It is obvious that something of this character must occur, because current at the radius which makes  $J_0(k_3) = 0$  has no external field, however large this current may be, and thus cannot screen  $I_1$ . In order to screen  $I_1$  the induced current must penetrate to a radius slightly greater than that

for which  $J_0(k_3) = 0$  in order that it shall have an external field to neutralize externally the field due to  $I_1$ .

At  $\lambda = 10$  cm.,  $\rho'/d$  for copper is  $14.3 \text{ m}\Omega$ , whereas  $\rho/t$  for the absorbing screen has to be  $120\pi$  ohms and these values are in the ratio  $2.6 \times 10^4$ : if we take  $\lambda/t = 600$  and  $x = 1$ , then the current in the copper is 100 times the current in the contiguous high-resistance layer and then the energy loss in this layer would be 2.6 times as much as in the copper. Though the current in the layer is very small, it would produce a substantial loss unless  $x \gg 1$  or  $\lambda/t$  is very small indeed: it would have an ill effect as a lining for a resonant chamber or a wave guide. If the layer were of manganin the penetration depth would be about 0.01 mm. at  $\lambda = 10$  cm., so that it would be impossible to make it so thin that the density was substantially constant through it. This means that a surface layer of metal is bound to carry almost all the induced current and effectively screen a copper backing behind it.

We now understand completely the theory and action of what opticians call a 'black screen' and realize it must consist of two screens separated by  $\frac{1}{2}\lambda$ . The discussion of black screens in *Theory of Huygens' Principle*, Baker and Copson (pp. 98, 117, and 152) suggests this essential feature was not understood by Kottler, Voigt, Kirchhoff, and others.

It is appropriate to discuss briefly here another problem which bears a superficial similarity to the black screen but in reality is very different. It is the reflection from the boundary of a plane face of dielectric, and the particular technical application we have in mind is the device, developed largely by Miss Blodget, of depositing a transparent  $\frac{1}{4}\lambda$  layer on the lenses of binoculars or the glass fronts of instruments. We can present this device in a manner familiar to engineers by using the terminology and ideas of propagation through a coaxial cable. In such, the propagation is by an electric field which is purely radial and normal to the inner and outer conductors. If an infinite length of cable is joined to a source through a finite length of a different cable, the input impedance will not be that of an infinite length because the discontinuity at the junction will set up a standing wave system: reflection is said to occur at the boundary. Suppose both lengths have inner and outer conductors of the same diameter, but that the infinite length has a dielectric of constant  $K$  while the finite length has a dielectric of constant unity. Then the characteristic impedance of the infinite length will be  $K^{-1/2}$  of that of the finite length. If the two lengths are joined through a piece of a third cable it is possible to 'match' one piece to the other provided the third cable has a length of  $\frac{1}{4}\lambda$ : let  $Z_0$  be the characteristic

impedance of this link. Then if it is loaded by a resistance  $R_2$ , it will 'look like' a resistance  $R_1$ , such that  $R_1 R_2 = Z_0^2$ . Here we wish to 'step up'  $R_2$  to  $R_1$  in the ratio  $K^{\frac{1}{2}}$  and thus must make  $Z_0 K^{\frac{1}{2}} = Z'_0$ , where  $Z'_0$  is the characteristic impedance of the air core cable. If the conductors are uniform throughout, then the  $\frac{1}{4}\lambda$  link must have a dielectric constant  $K'$  such that  $K' = K^{\frac{1}{2}}$ : transferring this to refractive indices gives  $\mu' = \mu^{\frac{1}{2}}$ . As a numerical example take  $Z'_0 = 70$  ohms and  $K = 2$ , then the characteristic impedance of the infinite length of cable will be 49.5 ohms, whence  $Z_0$  must be 59 ohms, and this requires that

$$K' = \left(\frac{70}{59}\right)^2 = 1.4.$$

If the dielectric of the infinite length is glass having refractive index 1.5, then the refractive index of the  $\frac{1}{4}\lambda$  surface layer must be 1.23. If the inner radius of the cable tends to infinity, the propagation of a plane wave is approached and then we have reached, by familiar means, the solution to which the Blodget device applies. It is not a 'black screen' but a screen which permits a sudden change of medium to have no effect on the propagation: a double boundary is always needed to smooth over the transition from one medium to another, whether the second medium is a dielectric or a perfect conductor.

### 7.7. Extension of sections 7.3 and 7.6 to include rectangular wave guides and their correct termination

In Chapter III all the general equations were developed for a filament in a Vee reflector. Though these solutions are complete only when the sides of the Vee extend to infinity we have derived the solutions in the expectation and hope that they will be approximately correct for sheets of finite width. This has in general involved the further implication that  $\beta$ , the angle of the Vee, is not very small. But if  $\beta$  tends to zero we might expect our solutions to degenerate into the classic solutions for a rectangular wave guide: it is instructive to look at this limit, both for its analytical value and also to remind the reader that wave guides are a particular case of an aerial with reflecting screens. The general equation for the inphase component of field at the aerial (when on the bisector) is given by (3.14), which we repeat here

$$-\frac{cE_P}{a\pi I} = 4n\{J_n^2(k) + J_{3n}^2(k) + J_{5n}^2(k) + \dots\}. \quad (3.14)$$

Since each term of the infinite series is essentially positive and since not more than one term can be precisely zero for any given value of  $k$ , it



follows that the output of the aerial can never be zero for any value of  $n$ : regarding this from the point of view of Chapter III this is not surprising. But it is well known that the output of any generator in a parallel and rectangular wave guide is precisely zero if the width of the guide is less than  $\frac{1}{2}\lambda$ . Hence if (3.14) is to degenerate into the solution of a parallel wave guide when  $n$  tends to infinity (that is,  $\beta$  tends to zero), then we should expect to find  $E_P$  remained zero until  $k$  exceeded some definite numerical value and it is clear from (3.14) that this is not so. Suppose the circumferential width of the guide at the aerial is  $\frac{1}{2}\lambda$ , then  $\frac{1}{2}\lambda = R\beta = R\pi/n$  or  $k = n$  and accordingly

$$-\frac{cE_P}{a\pi I} = 4n\{J_n^2(n) + J_{3n}^2(n) + J_{5n}^2(n) + \dots\}.$$

Reference to § 3.5(a) and Fig. 3.14 will show that each  $J$  in this series must be positive and that every term is less than the preceding term, and that the first term is vastly the greatest when  $n$  is very large. Accordingly,  $-cE_P/a\pi I \doteq 4 \times 0.446^2 n^4$  and this tends to infinity with  $n$ . If the width across the guide, at the aerial, is just less than  $\frac{1}{2}\lambda$  the output will be finite, though extremely small. Thus it seems the complete cut-off property disappears if the sides lack parallelism by any amount, however small. Is this apparent discrepancy of behaviour due to the fact that the width across the guide will exceed  $\frac{1}{2}\lambda$  at a sufficient distance from the apex, or is it due to the tapered closure of the guide at the apex and behind the aerial? We can remove this second possible cause by putting a curved metal back behind the aerial and amputating the portion between the said back and the apex, then we shall have a conductor near the bottom of a slot whose sides are radial and very nearly parallel. The general equations for this arrangement are given in (7.11) and (7.12), but are very cumbersome because we have chosen a filament as the source. Since we are investigating a basic principle it is not necessary to choose that particular source which happens to look, superficially, most like a source which would be used in practice. The cumbersomeness disappears if the filament is replaced by a sheet bearing a current density which varies sinusoidally across it, and indeed we then obtain the most general solution, since any source can be built up from it by the use of a Fourier series. If an axially flowing current density  $I_n \cos n\alpha$  is distributed round a cylinder of radius  $R$ , then we have shown in (6.4) that

$$\frac{cE}{a\pi I_n} = 2\pi R J_n(k) \{-J_n(ar) + jY_n(ar)\} \cos n\theta, \quad (6.4)$$

and this gives the field in a Vee which is excited by a current sheet bearing a sinusoidal loading. It is convenient to write the maximum density  $I_n$  in terms of the total current  $I$  in the arc, the two being related by the relation  $I = 2I_n R/n$ . Accordingly

$$\frac{cE}{a\pi^2 I} = nJ_n(k)\{-J_n(ar) + jY_n(ar)\}\cos n\theta \quad (7.25)$$

if  $R > r$  in (7.25), then  $ar$  and  $k$  must be interchanged. If the current bearing arc has radius  $R_2$  and if there is a perfectly conducting sheet of radius  $R_1$  behind it, then the equation for the current  $I_1$  induced in this arc is

$$\{-J_n(k_1) + jY_n(k_1)\}I_1 + \{-J_n(k_2) + jY_n(k_2)\}I_2 = 0.$$

It follows readily from this that, for  $r > R_2$ ,

$$\begin{aligned} \frac{cE}{a\pi^2 I_2} &= n \frac{\{Y_n(k_1)J_n(k_2) - J_n(k_1)Y_n(k_2)\}}{Y_n(k_1) + jJ_n(k_1)} \{-J_n(ar) + jY_n(ar)\}\cos n\theta. \\ \therefore -\frac{cE_P}{a\pi I} &= n \frac{\{Y_n(k_1)J_n(k_2) - J_n(k_1)Y_n(k_2)\}^2}{|H_n(k_1)|^2} \cos n\theta \\ &\doteq \frac{n\{\sqrt{3}J_n(k_2) + Y_n(k_2)\}^2}{4} \cos \theta, \quad \text{if } k_1 = n. \end{aligned} \quad (7.26)$$

This expression is zero only for the special values of  $k_2$  which make  $Y_n(k_2) = -\sqrt{3}J_n(k_2)$ . Now  $Y_n(z)$  is negative when  $z$  is very small and passes through zero for the first time when  $J_n(z)$  is still positive; hence  $E_P$  cannot be zero for the first time until  $k_2$  exceeds the value which first makes  $J_n(z) = 0$ , and accordingly  $k_2$  must exceed  $1.15n$  when  $n$  is very large. ( $E_P = 0$  for  $n = 10$  when  $k = 15.2$ ,  $J_{10}$  having passed through zero near  $z = 14.4$ .) The value of  $z$  which makes  $Y_n(z)$  zero for the first time seems to approach  $n$  continuously. Hence when  $Y_n(k_2) = 0$  the value of  $E_P$  must be about three-quarters of what it would be if the round back were removed, and thus will vary as  $n^{\frac{1}{2}}$ . Hence it seems the complete 'cut-off' property of a parallel guide is absent if the sides lack parallelism by any amount, however small. The output falls to zero when the distance between the exciting sheet and the reflecting back has a certain critical value, and there is a corresponding adjustment for a guide whose sides are truly parallel.

If  $z$  is appreciably less than  $n$ , then  $Y_n^2(z) \gg J_n^2(z)$ : accordingly, if  $k_2 = n$ ,

$$-\frac{cE_P}{a\pi^2 I_2} = 0.2n^{\frac{1}{2}} \left\{ 1 + \frac{J_n(k_1)}{Y_n(k_2)} \sqrt{3} \right\}^2.$$

If  $n = 30$ , then  $J_{30}(20)/Y_{30}(20) = -10^{-5}$ : hence we conclude that the back closing the Vee has a negligible effect on  $E_P$  until  $k_1$  is verging on  $n$ .

Thus we conclude the absence of complete 'cut off' is due entirely to the fact that the width across the guide will gradually exceed  $\frac{1}{2}\lambda$  at a great distance from the exciting current even when  $n$  tends to infinity. This suggests the classic solution for a parallel guide may be so sensitive to the exact form of the bounding walls as to make it slightly unreliable in practice.

We will now generalize the problem of the non-reflecting cylindrical chamber so as to apply to a Vee-shaped chamber: when  $n$  becomes large this amounts to investigating the correct termination for a slightly tapered wave guide. We shall suppose the Vee is excited by a sinusoidally loaded current sheet of radius  $R$  carrying a total current  $I_1$ , that it has a thin resistive sheet of radius  $R_2$  and a perfectly conducting sheet of radius  $R_3$ , the total induced currents being  $I_2$  and  $I_3$  respectively. Then proceeding as in (7.16), etc., we find that the three equations (7.18) are unchanged provided only that  $J_0$  is replaced by  $J_n$ : thus

$$\frac{I_3}{I_1} = -\frac{1}{J_n(k_3) + jX_n Z J_n(k_2)} \quad (7.27)$$

and 
$$\frac{I_3}{I_2} = -\frac{j}{X_n Z}.$$

The equation corresponding to (7.19) is now

$$J_n(k_2) J_n(k_3) + Y_n(k_2) Y_n(k_3) = 0. \quad (7.28)$$

If  $k_3 < n$ , then both  $Y_n(k_2)$  and  $Y_n(k_3)$  are negative and both the  $J$ 's are positive, and hence (7.25) cannot have a solution for  $k_3 < n$ : hence if the field between the resistive sheet and the source is to be the same as if the Vee extended to infinity, then the circumferential width across the closed end of the Vee must exceed  $\frac{1}{2}\lambda$  for all values of  $n$ . If

$$J_n(k_3) = 0$$

for the first time, then  $Y_n(k_2)$  must also be zero: accordingly then

$$\frac{R_3 - R_2}{\lambda} = \frac{0.15n}{2\pi},$$

when  $n$  is very large. If  $n = 1$  we find that

$$\frac{R_3 - R_2}{\lambda} = 0.34 \quad \text{when} \quad k_3 = 2.2 \quad (Y_1 \text{ is zero when } k_3 = 2.18)$$

and 
$$\frac{R_3 - R_2}{\lambda} = 0.254 \quad \text{when} \quad k_3 = 3.8 \quad (\text{which is when } J_1 \text{ is zero}).$$

If  $n = 16$  ( $\beta = 12.3^\circ$ ) we find  $Y_{16}(z)$  is zero for the first time when

$z = 17.5$  and for the second time when  $z = 23.5$ , and  $J_{16}(z)$  is zero when  $z = 21.1$ , and therefore

$$\frac{R_3 - R_2}{\lambda} = 0.57 \quad \text{when} \quad k_2 = 17.5:$$

according to these two examples the limiting formula above always underestimates the clearance.

We are now able to understand the whole problem of the wave guide much more completely than before the start of this section. A generator in a parallel guide will have no output whatsoever if the width is less than  $\frac{1}{2}\lambda$ , and in such circumstances the field in the guide has a constant phase throughout its infinite length and the magnitude decreases continuously with distance from the source. If the width of a parallel guide exceeds  $\frac{1}{2}\lambda$ , then a generator in it has an output of power: if the generator is a sinusoidally loaded current sheet, then the mean square field is independent of the distance from it, but the phase changes periodically with a wavelength which is greater than  $c/n$ . Since the field does not attenuate with distance it is completely misleading to forget that the length of the guide must be infinite, and it is useless to suppose the solution is applicable to a long finite length of resistanceless guide. If the guide is a Vee, no matter how small its angle, any generator will have an output no matter where it is situated (save the special stations corresponding to  $J_n(k) = 0$ ): it is not necessary the width of the guide at the generator should exceed  $\frac{1}{2}\lambda$ , though the output will be very small indeed if that width is appreciably less than  $\frac{1}{2}\lambda$ . In all circumstances the field in the guide will change its phase continuously with distance, and the magnitude will decrease approximately as the inverse square root of the distance from the apex. What matters is not that the width of a guide should be nowhere less than  $\frac{1}{2}\lambda$  but that it should not be less than  $\frac{1}{2}\lambda$  everywhere. But since our solutions apply accurately only to a guide whose length really is infinite, they can be related to reality only by some device which will make a finite length of guide behave as though its length were infinite. This device is a black screen termination consisting of a resistive film combined with a perfect conductor correctly spaced behind it. Equation (7.28) shows this device is impossible unless the greatest width of the guide slightly exceeds  $\frac{1}{2}\lambda$ . Hence the wave guide analysis cannot be applied accurately to any realizable problem unless there is a width slightly greater than  $\frac{1}{2}\lambda$ , and presumably this is the full interpretation of what the 'cut-off' property hints at. If the infinite Vee guide has a conducting back between the

sinusoidally loaded generator sheet and the apex, then (7.22) and (7.23) show that the field is the same as if the back were removed and the generator current suitably adjusted in magnitude and phase. Hence our solution applies to a finite length of Vee guide closed at each end by concentric arcs and having within it a resistive film. If  $n$  is very large the difference in width between the two ends can be made as small as we please provided only that the greater exceeds  $\frac{1}{2}\lambda$ . Approach in this way would be instructive in showing whether or not the solution for parallel sides is sensitive to perfect parallelism. It would be interesting to analyse the case where there is a resistive film between the generator and the conductive back which closes off the apex of the Vee and to see if this can be made black. If so we could have a black screen at each end of a finite length of Vee guide and so, on making  $n$  infinite, approach the solution for a sinusoidally loaded generator in a doubly infinite parallel guide. It is worth remarking that perfect termination can be obtained only if the generator is a sinusoidally loaded arc, and this is true whether the guide is a Vee or has parallel sides.

#### FURTHER PROBLEMS OF HALF-PLANES

##### 7.8. Plane wave incident on a half-plane having a cylinder at its bounding edge

Consider a current filament in the same plane as a half-plane which is bounded by a cylinder. If the distance between the filament and the centre of the cylinder tends to infinity, then we have a plane wave incident on a cylinder which is parallel to the electric vector, the cylinder having an infinitely extended fin which is parallel to the direction of propagation. Thus we can examine the effect of adding the said fin to the problem solved in § 6.6. We shall derive now the current density induced round the cylinder. The general expression is given in (7.15), but now we must make  $n = \frac{1}{2}$  and make  $z$  tend to infinity. When  $z \rightarrow \infty$ ,  $J_{\frac{1}{2}}(z) = -J_{\frac{1}{2}}(z) = J_{\frac{3}{2}}(z)$  and  $Y_{\frac{1}{2}}(z) = J_{\frac{1}{2}}(z)$ , etc.: hence (7.15) becomes

$$\frac{i}{I} = \frac{a}{\pi k} H_{\frac{1}{2}}(z) \left[ \left\{ \frac{\cos \theta/2}{H_{\frac{1}{2}}(k)} - \frac{\cos 5\theta/2}{H_{\frac{3}{2}}(k)} + \frac{\cos 9\theta/2}{H_{\frac{5}{2}}(k)} - \dots \right\} + \right. \\ \left. + j \left\{ \frac{\cos 3\theta/2}{H_{\frac{1}{2}}(k)} - \frac{\cos 7\theta/2}{H_{\frac{3}{2}}(k)} + \frac{\cos 11\theta/2}{H_{\frac{5}{2}}(k)} - \dots \right\} \right].$$

But

$$H_{\frac{1}{2}}(z) = \frac{\sqrt{2}}{1-j} H_0(z) = \frac{1+j}{\sqrt{2}} \frac{cE_0}{a\pi I},$$

where  $E$  is the field which would exist at  $ar = 0$  if the cylinder and half-plane were absent.

$$\therefore \frac{\sqrt{2} \pi^2 k i}{c E_0} = (1+j) \left[ \left\{ \frac{J_{\frac{1}{2}}(k) \cos \theta/2}{|H_{\frac{1}{2}}(k)|^2} - \frac{Y_{\frac{1}{2}}(k) \cos 3\theta/2}{|H_{\frac{1}{2}}(k)|^2} - \frac{J_{\frac{1}{2}}(k) \cos 5\theta/2}{|H_{\frac{1}{2}}(k)|^2} + \frac{Y_{\frac{1}{2}}(k) \cos 7\theta/2}{|H_{\frac{1}{2}}(k)|^2} + \frac{J_{\frac{1}{2}}(k) \cos 9\theta/2}{|H_{\frac{1}{2}}(k)|^2} - \dots \right\} + \right. \\ \left. + j \left\{ \frac{Y_{\frac{1}{2}}(k) \cos \theta/2}{|H_{\frac{1}{2}}(k)|^2} + \frac{J_{\frac{1}{2}}(k) \cos 3\theta/2}{|H_{\frac{1}{2}}(k)|^2} - \frac{Y_{\frac{1}{2}}(k) \cos 5\theta/2}{|H_{\frac{1}{2}}(k)|^2} - \frac{J_{\frac{1}{2}}(k) \cos 7\theta/2}{|H_{\frac{1}{2}}(k)|^2} + \frac{Y_{\frac{1}{2}}(k) \cos 9\theta/2}{|H_{\frac{1}{2}}(k)|^2} + \dots \right\} \right], \quad (7.29)$$

and this is the equation corresponding to (6.17 *a*) for the problem where the fin is absent.

Evaluation of this equation for  $k = 2$  gives  $2\pi i/cE = 1.07 \sqrt{11}^\circ$  and  $0.41 \sqrt{35.5}^\circ$  at  $\theta = 0$  and  $90^\circ$  respectively: reference to Fig. 6.11 and Table 6.4 will show these values are indistinguishable from those obtained for the simple cylinder without a fin: thus showing, as would be expected, that the fin has no appreciable effect on the current distribution round the 'bright' semicircle, though it must make the density precisely zero at the 'dark spot'. We are aware that when  $n$  is not an integer the Bessel solutions are multi-valued and in that sense seem dubious for numerical use. Therefore it is instructive and encouraging to note that numerical evaluation for a case where  $n = \frac{1}{2}$  does not show appreciable discrepancy from a very similar problem for which  $n = 0$ .

### 7.9. Current induced in a half-plane when the coplanar current filament is very distant

We are repeatedly feeling our way towards calculating the induced density by a 'ray theory' in the hope of finding approximate solutions for problems which are not soluble formally. In the problem of the long cylinder parallel to the electric field the ray theory worked well save near the points of grazing incidence, where we found a limiting phase lag near  $30^\circ$  even when the cylinder had a fin. The half-plane excited by a very distant coplanar filament gives an example of a plane wave at grazing incidence on a conductor: hence the exploration of this problem is useful in the general search. Having just examined the density induced round a cylinder at the bounding edge it will suffice now to find the density induced on the two sides of a sheet terminating in a sharp edge. We revert to (5.3) and note the terms  $B$  and  $D$  are zero since the filament is coplanar ( $\alpha = 0$ ). When  $k \rightarrow \infty$ ,

$$J_{\frac{1}{2}}(k) = -J_{\frac{3}{2}}(k) = J_{\frac{5}{2}}(k) \dots \quad \text{and} \quad Y_{\frac{1}{2}}(k) = J_{\frac{1}{2}}(k).$$

The general expression is

$$\frac{\lambda i}{I} = j \frac{2\pi n^2}{ar} \{H_n(k)J_n(ar) + 3H_{3n}(k)J_{3n}(ar) + \dots\}.$$

When  $n = \frac{1}{2}$  and  $k \rightarrow \infty$ , this becomes

$$\begin{aligned} \frac{\lambda i}{I} &= \frac{\pi}{2ar} [-\{Y_{\frac{1}{2}}(k) + jJ_{\frac{1}{2}}(k)\}\{J_{\frac{1}{2}}(ar) - 5J_{\frac{3}{2}}(ar) + 9J_{\frac{5}{2}}(ar) - \dots\} + \\ &\quad + \{J_{\frac{1}{2}}(k) - jY_{\frac{1}{2}}(k)\}\{3J_{\frac{3}{2}}(ar) - 7J_{\frac{5}{2}}(ar) + 11J_{\frac{7}{2}}(ar) - \dots\}] \quad (7.30) \\ &= -\frac{1}{2}\pi \{-J_{\frac{1}{2}}(k) + jY_{\frac{1}{2}}(k)\}\{J_{\frac{1}{2}}(ar) + jJ_{-\frac{1}{2}}(ar)\}, \\ &\quad \text{since } \frac{2n}{z} J_n(z) = J_{n+1}(z) + J_{n-1}(z), \\ &= -\frac{1}{2}\pi \sqrt{\left(\frac{4}{\pi^2 k ar}\right)} \{\cos(ar+k) + j \sin(ar+k)\}. \end{aligned}$$

This shows that  $|i|$  varies as  $(ar)^{-\frac{1}{2}}$  and differs in phase by  $\frac{1}{4}\pi$  from the local field which would exist if the sheet were absent. The density on each side of the sheet at  $\lambda$  from its edge is  $1/2\pi$  of what it would have been if the sheet had been doubly infinite and the field incident normally on it: at  $4\lambda$  from the edge it is half this amount, and so on.

When the filament is close to a doubly infinite plane we have seen that  $i$  varies as  $r^{-\frac{1}{2}}$  as grazing incidence is approached, whereas here  $i$  varies as  $r^{-\frac{1}{2}}$  where now  $r$  is the distance from the bounding edge of the half-plane. The reason why the current density decreases so much more rapidly in the first case is because there is an intense concentration of current just below the filament, thereby producing zero force all along the plane. When there is a bounding edge the field of the induced current will decrease, with distance from the edge, much more rapidly than the decrease of field from the very distant coplanar filament. Accordingly the induced current in the half-plane must persist appropriately to make up for the said decrease of the field due to it: the appropriate law turns out to be  $i$  varies as  $r^{-\frac{1}{2}}$ . In a sense it is correct to say that induced current exists only because there is a bounding edge. This example would perhaps have been more complete if we had situated the filament on a bearing at  $\alpha$  to the plane of the half-plane and arranged  $\alpha$  so that as  $k$  goes to infinity  $\alpha k/2\pi = \frac{1}{4}\lambda$ , and then we should have had direct comparison with a doubly infinite plane excited by a filament distant  $\frac{1}{4}\lambda$  from it. But to have included this refinement would have complicated the analysis unduly.

When a plane wave was incident on a cylinder of radius such that  $R/\lambda = 24/2\pi$  we found the current density at the point of grazing incidence was  $1.07/2\pi \times cE/2\pi$ , and perhaps this shows the limit for a

cylinder is  $1/2\pi$ ; which, according to ray theory, is as though the wave were incident at  $\arcsin 1/2\pi = 9.2^\circ$ .

### 7.10. Current density induced in a half-plane when a plane wave is incident normally on it

This example is of great interest because it shows the rate at which the disturbance caused by an edge fades away with distance from the edge when incidence is normal. We must now put  $\alpha = \frac{1}{2}\pi$  in equation (5.2): then terms involving  $J_1$ ,  $J_3$ ,  $J_5$ , etc., appear in the analysis and may be thought of as representing the attempt to establish the conditions obtaining on a doubly infinite plane.

Taking first the series denoted by  $B$  and  $D$  in (5.3) and writing  $ar \equiv z$ , we have

$$\begin{aligned}\frac{\lambda i}{I} &= \frac{\pi}{z} j \{ H_1(k) J_1(z) - 3 H_3(k) J_3(z) + 5 H_5(k) J_5(z) - \dots \} \\ &= \frac{\pi j H_1(k)}{z} \{ J_1(z) + 3 J_3(z) + 5 J_5(z) + \dots \}, \\ &\qquad\qquad\qquad \text{since } J_1 = -J_3, \text{ etc. when } k \rightarrow \infty.\end{aligned}$$

Now  $\sin(z \sin \theta) = 2\{J_1(z) \sin \theta + J_3(z) \sin 3\theta + \dots\}$ ;

hence, on differentiating,

$$z \cos(z \sin \theta) \cos \theta = 2\{J_1(z) \cos \theta + 3J_3(z) \cos 3\theta + \dots\}.$$

$$\therefore z = 2\{J_1(z) + 3J_3(z) + \dots\}, \quad \text{on putting } \theta = 0. \quad (7.31)$$

Accordingly

$$\frac{\lambda i}{I} = \frac{1}{2}\pi \{Y_1(k) + jJ_1(k)\} = \frac{1}{2}\pi \{-J_0(k) + jY_0(k)\}, \quad \text{when } k \rightarrow \infty;$$

whence  $cE = 4\pi i$ , where  $E$  is the incident field of the plane wave. Accordingly this turns out to be half the current which would exist if the sheet were doubly infinite and agrees with the general statement following (5.3). The terms denoted by  $A$  and  $C$  give

$$\begin{aligned}\frac{\lambda i}{I} &= \frac{\pi}{2\sqrt{2}z} [ \{Y_{\frac{1}{2}}(k) + jJ_{\frac{1}{2}}(k)\} J_{\frac{1}{2}}(z) + 3\{Y_{\frac{3}{2}}(k) + jJ_{\frac{3}{2}}(k)\} J_{\frac{3}{2}}(z) - \\ &\qquad\qquad\qquad - 5\{Y_{\frac{5}{2}}(k) + jJ_{\frac{5}{2}}(k)\} J_{\frac{5}{2}}(z) - \dots + ] \\ &= \frac{\pi}{2\sqrt{2}z} [ \{Y_{\frac{1}{2}}(k) + jJ_{\frac{1}{2}}(k)\} \{J_{\frac{1}{2}}(z) + 5J_{\frac{3}{2}}(z) + 9J_{\frac{5}{2}}(z) + \dots\} + \\ &\qquad\qquad\qquad + \{Y_{\frac{3}{2}}(k) + jJ_{\frac{3}{2}}(k)\} \{3J_{\frac{1}{2}}(z) + 7J_{\frac{3}{2}}(z) + 11J_{\frac{5}{2}}(z) + \dots\} ] \quad \text{when } k \rightarrow \infty \\ &= \frac{\pi}{2\sqrt{2}} \left[ \{Y_{\frac{1}{2}}(k) + jJ_{\frac{1}{2}}(k)\} \left\{ J_{-\frac{1}{2}}(z) + \int_0^z J_{\frac{1}{2}}(z) dz \right\} + \right. \\ &\qquad\qquad\qquad \left. + \{-J_{\frac{1}{2}}(k) + jY_{\frac{1}{2}}(k)\} \left\{ -J_{\frac{1}{2}}(z) + \int_0^z J_{-\frac{1}{2}}(z) dz \right\} \right] \quad (7.32)\end{aligned}$$



by use of the recurrence formula  $2nJ_n(z) = z\{J_{n+1}(z) + J_{n-1}(z)\}$

$$\equiv \frac{\pi}{2\sqrt{2}} \{Y_{\frac{1}{2}}(k) + jJ_{\frac{1}{2}}(k)\} \times (F + jG).$$

It has been shown previously that

$$\int_0^z J_{\frac{1}{2}}(z) dz \doteq 1 - J_{\frac{1}{2}}(z)$$

and also a corresponding approximate expression for the other integral: hence it follows that both  $F$  and  $G$  tend to unity when  $z$  is large. Some values of  $F$  and  $G$  are shown collected in Table 7.2 below.

TABLE 7.2

$z$	0.2	0.5	1.0	1.5	2.0	3	4	5	6
$F$	1.79	1.16	0.926	0.870	0.891	0.967	1.02	1.03	1.01
$G$	0.351	0.560	0.772	0.918	0.894	1.06	1.08	0.999	0.978

This table shows that both  $F$  and  $G$  differ very little from unity if  $z$  exceeds, say, 3, and then

$$\begin{aligned} \frac{\lambda i}{I} &\doteq \frac{\pi}{2\sqrt{2}} \{Y_{\frac{1}{2}}(k) + jJ_{\frac{1}{2}}(k)\} (1 + j) \\ &= \frac{\pi}{2\sqrt{2}} [Y_{\frac{1}{2}}(k) - J_{\frac{1}{2}}(k) + j\{J_{\frac{1}{2}}(k) + Y_{\frac{1}{2}}(k)\}] \\ &= \frac{\pi}{2\sqrt{2}} \sqrt{\left(\frac{2}{\pi k}\right)} \{-\cos k - \sin k + j(\sin k - \cos k)\} \\ &= \frac{1}{2}\pi \sqrt{\left(\frac{2}{\pi k}\right)} \{-\cos(k - \tfrac{1}{4}\pi) + j\sin(k - \tfrac{1}{4}\pi)\} \\ &= \frac{1}{2}\pi \{-J_0(k) + jY_0(k)\}, \end{aligned}$$

whence  $cE = 4\pi i$ , where  $E$  is the field incident on the sheet.

We have now shown that the terms  $B$  and  $D$  in (5.3) give a uniform density  $cE = 4\pi i$  at all points of the semi-infinite sheet, right up to the edge, and that the terms  $A$  and  $C$  in (5.3) give a density which differs insensibly from the same magnitude if  $z$  exceeds, say, 3. On the 'bright side' of the sheet the two densities are to be added and on the dark side subtracted; hence the resultant density is nearly zero on the dark side and nearly given by  $cE = 2\pi i$  all over the bright side.

Since  $J_0(k)$  tends to  $\sqrt{(2/\pi k)}\cos(k - \frac{1}{4}\pi)$  and  $-Y_{-\frac{1}{2}}(k) = \sqrt{(2/\pi k)}\cos k$  it follows that  $\{Y_{\frac{1}{2}}(k) + jJ_{\frac{1}{2}}(k)\}$  is a vector whose modulus is proportional

to the incident field but whose phase lags the field by  $\frac{1}{4}\pi$ : when  $F = G$  the current density leads  $\frac{1}{4}\pi$  on  $H_z(k)$  and then is in phase with the incident field. The following table shows  $(F^2 + G^2)^{1/2}/\sqrt{2}$ ,  $\arctan G/F$ , and also  $\frac{1}{4}\pi - \arctan G/F$ , which is the angle by which the density lags on the incident field.

TABLE 7.3

$z$	0	0.2	0.5	1.0	1.5	2	3	4	5	6
Arctan $G/F$	45	11	25.7	39.8	43.4	45	47.8	46.6	44.2	44.2
Lag on field	45	34	19.3	5.2	1.6	0	-2.8	-1.6	0.8	0.8
$(F^2 + G^2)^{1/2}/\sqrt{2}$	$\infty$	1.29	0.91	0.85	0.92	0.92	1.00	1.04	1.00	0.99

This table shows that the component of density represented by the terms  $A$  and  $C$  of (5.3) is sensibly in phase with the field at all points more distant from the edge than, say,  $r/\lambda = 0.2$  ( $z = 1.25$ ). By means

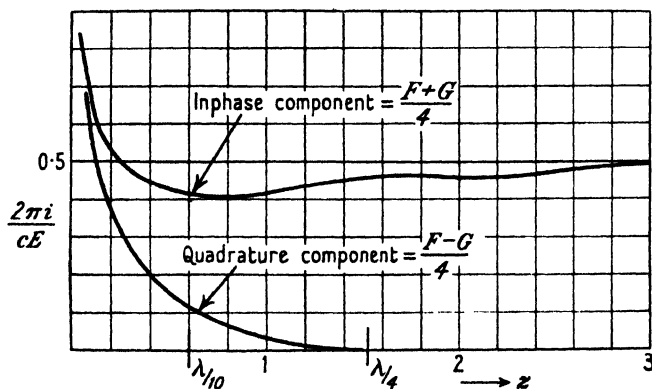


FIG. 7.15. Components of current density induced near edge of a half-plane by a plane wave incident normally on it.

of the same table, the  $A$  and  $C$  component can readily be divided into a component which is in time phase with the incident field and another component which is in time quadrature thereto. This has been done and the result is shown plotted in Fig. 7.15: both these components run to infinity at the edge because the edge is sharp; the infinity would be removed by slight rounding. But even with a sharp edge neither component of density exceeds the ultimate limiting value so long as  $r/\lambda$  exceeds  $\frac{1}{10}$ : the quadrature component has become negligible permanently if  $r/\lambda$  exceeds  $\frac{1}{4}$ . It may be seen that the edge effect has sensibly died out if  $r/\lambda$  exceeds  $\frac{1}{4}$  and is never very substantial if  $r/\lambda > \frac{1}{10}$ . The net inphase density on the 'bright side' is obtained by adding  $\frac{1}{2}$  to each ordinate in Fig. 7.15: on the dark side by subtracting  $\frac{1}{2}$ .

Proceeding in this manner the curve of R.M.S. density on each side can be obtained and these densities are shown plotted in Fig. 7.16; reference to it shows the R.M.S. density on the bright side is substantially constant so long as  $r/\lambda > \frac{1}{20}$ . The net current density on the bright side is everywhere nearly in phase with the incident field, the lag angle being

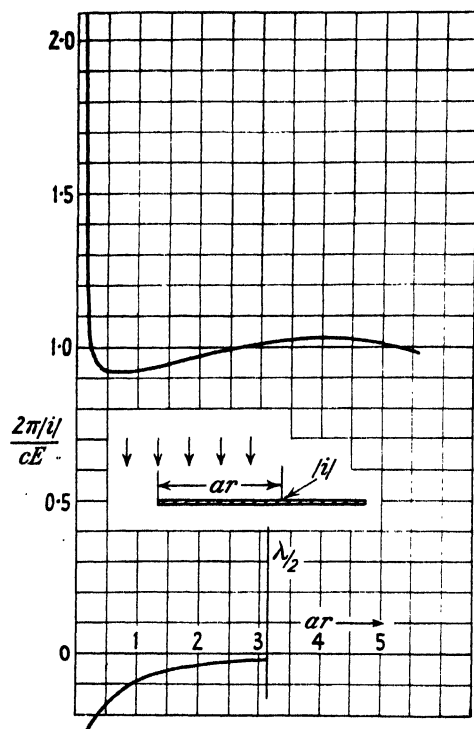


FIG. 7.16. Density of R.M.S. current induced on bright and on dark side of a half-plane by a plane wave incident normally.

$19^\circ$  when  $z = 0.2$  and  $45^\circ$  when  $z = 0$ . It is surely instructive and perhaps surprising to find that the edge disturbs the current density appreciably over a range which is only of the order of  $\frac{1}{10}\lambda$ . We have repeatedly used a current filament to simulate a long in-line array and have argued that if a very long wire were placed parallel to the electric vector of a wave then there would be little trace of standing waves on the wire, the current being sensibly constant in magnitude and phase along most of the length: how long the wire would need to be to approach closely to this condition is not known. The discovery that the disturbance due to the edge is negligible at distances greater than  $\frac{1}{10}\lambda$  from the edge suggests that, if the problem of a semi-infinite

wire could be solved, the current would be found sensibly uniform in magnitude and phase at distances greater than  $\frac{1}{4}\lambda$  from its end, and within this range it would be nearly a quarter of a sinusoid. We should obtain a more reliable guide if we could solve the problem of a line doublet anywhere in a Vee of any angle; but the unwieldiness due to expressing  $H_1(z)$  from an origin not on the doublet makes this solution impracticable.

At the edge the density lags  $\frac{1}{4}\pi$  on the local field, but this lag falls rapidly to zero with increase of  $ar$ . Hence if a wave is incident normally on a sheet of finite, but very great width, the R.M.S. induced current will be very nearly constant across the whole width; but it will have an appreciable quadrature component very near the edges. This is suggestive in respect of the currents induced in a wide panel of a beam array. The terms  $B$  and  $D$ , in (5.3), in the current distribution reverse their sense on opposite sides of the very thin sheet and hence their net effect on the re-radiation is negligible: the re-radiation comes entirely from the current represented by the terms  $A$  and  $C$ , since they do not reverse their sense on opposite sides. Hence the total effective current for re-radiation is the contribution from  $A$  and  $C$  on each side: the terms  $A$  and  $C$  yield a distribution which is substantially constant in magnitude and phase and equal to  $cE/4\pi$ . Hence the total effective re-radiating current is substantially constant and equal to  $cE/2\pi$ . Hence the work done in re-radiation is  $cE^2/2\pi$  per unit area of sheet and this is twice the energy per unit area of wave-front. This is another example of the apparently general principle that an obstacle re-radiates twice the power supposed to be associated with the area of wave-front it obstructs.

### 7.11. Resultant field due to a plane wave incident normally on a half-plane

We will now explore the field of a plane wave which is disturbed by normal incidence on a half-plane: to use optical parlance, we will examine the diffraction due to a straight edge. Here the source is a current filament at infinity, thus simulating a plane wave. Exploration must be restricted to a radius much smaller than the distance to the filament, for otherwise the incident field cannot be likened to a plane wave; but the radius of exploration may be very large compared with the wavelength. Equation (5.2) gives the field at an infinite distance, on bearing  $\theta$ , due to a current filament at  $(k, \alpha)$ : by the reciprocal theorem the same equation gives the field at  $(k, \alpha)$  due to a current

filament on bearing  $\theta$  at infinity. In our problem here we must put  $\alpha = \frac{1}{2}\pi$  in (5.2) and this gives

$$\begin{aligned} -\frac{E}{E_0} = & \{J_{\frac{1}{2}}(ar)\cos\frac{1}{2}\theta + J_{\frac{3}{2}}(ar)\cos\frac{3}{2}\theta + J_{\frac{5}{2}}(ar)\cos\frac{5}{2}\theta + \dots\} + \\ & + j\{J_{\frac{1}{2}}(ar)\cos\frac{1}{2}\theta - J_{\frac{3}{2}}(ar)\cos\frac{3}{2}\theta + J_{\frac{5}{2}}(ar)\cos\frac{5}{2}\theta - \dots\} + \\ & + j2\{J_1(ar)\sin\theta + J_3(ar)\sin 3\theta + \dots\}. \quad (7.33) \end{aligned}$$

This series can be summed only when  $\theta = \pm\frac{1}{2}\pi$  and when  $\theta = 0$ : this has been done already in (5.2*a*), etc. When  $\theta = 0$  we have (see (5.2*b*))

$$\frac{E}{E_0} = \frac{1}{\sqrt{2}} \left[ \left\{ \int_0^{ar} J_{-\frac{1}{2}}(z) dz \right\}^2 + \left\{ \int_0^{ar} J_{\frac{1}{2}}(z) dz \right\}^2 \right]^{\frac{1}{2}}.$$

It has been shown, at the end of § 3.5, that

$$\int_0^{ar} J_{\frac{1}{2}}(z) dz \doteq 1 - J_{-\frac{1}{2}}(ar)$$

and this led to the approximate expression (5.2*b*),

$$\frac{E}{E_0} \doteq \left\{ 1 + \frac{1}{\pi ar} - \frac{2}{\sqrt{(\pi ar)}} \cos(ar + \tfrac{1}{4}\pi) \right\}^{\frac{1}{2}},$$

which shows that the ripple will be less than 8 per cent. if  $r/\lambda$  exceeds 8 and thereafter the field will be almost undisturbed by the barrier: resort to tables shows that  $E/E_0 = 0.935$  when  $ar = 50$ . Fig. 7.17 shows the diffraction pattern in the plane of the sharp edge and in the first wavelength of distance from it: the first maximum of R.M.S. field exceeds the undisturbed value by 35 per cent. It is instructive to derive the limiting expression more directly in terms of the current induced in the sheet, which we have seen differs very little from a uniform density equal to that which would be induced in a doubly infinite sheet.

For our purposes here, in a book of this character, it does not suffice to calculate the field appropriate to the specified boundary because we want to apply the solution to practical cases where the real boundary cannot comply precisely with that described by the idealized sharp edge. In our view the field is due entirely to the currents induced in the boundary, and accordingly ought to have been calculated explicitly from the induced current rather than from the general equation for the field which includes the current only indirectly and by implication. Accord-

† *Note.* These Fresnel integrals are tabulated, up to  $z = 50$ , on p. 744 of Watson's *Bessel Functions*.

ingly we will calculate the field, in the plane of the edge, which would result from the simplest approximation to the induced current, and this approximation is to assume the induced current is constant right up to the edge and has the value  $i = cE_0/2\pi$ , where  $E_0$  is the field which the undisturbed plane wave would have in the plane of the metal sheet.

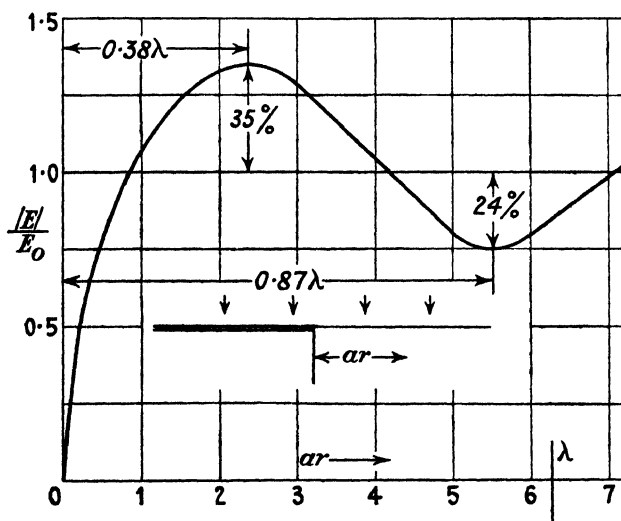


FIG. 7.17. Standing wave pattern near edge of semi-infinite sheet and in its plane, due to a plane wave incident normally.

Thus, with reference to Fig. 7.18, we require the field at  $P$  due to a uniform density  $i$  on one side of the half-plane  $OA$ , whose edge  $O$  is distant  $r$  from  $P$ . On dividing the half-plane into filaments of width  $dy$ , the field at  $P$  is given by the expression

$$\frac{cE}{a\pi i} = - \int_r^\infty J_0(ay) dy + j \int_r^\infty Y_0(ay) dy.$$

It is easy to show, by the process used in § 3.5 (b), that

$$\int_0^z J_0(z) dz \doteq 1 - \sqrt{\left(\frac{2}{\pi z}\right)} \sin\left(z - \frac{1}{4}\pi\right) \doteq 1 - Y_0(z),$$

and similarly that  $\int_0^z Y_0(z) dz \doteq -J_0(z)$ .

Hence 
$$\frac{2E}{E_0} = Y_0(ar) - jJ_0(ar)$$

and thus is characteristic of a concentrated current located at the edge: adding this to the undisturbed field at  $P$  gives

$$\begin{aligned}\frac{E}{E_0} &= 1 + \frac{1}{2}Y_0(ar) + j\frac{1}{2}J_0(ar). \\ \therefore \frac{|E|}{E_0} &= \sqrt{\{1 + \frac{1}{4}|H_0(ar)|^2 + Y_0(ar)\}} \\ &\doteq \left\{1 + \frac{1}{2\pi ar} - \sqrt{\left(\frac{2}{\pi ar}\right)\cos(ar + \frac{1}{4}\pi)}\right\}^{\frac{1}{2}}. \quad (7.34)\end{aligned}$$

This is of the same form as the correct expression, given by (5.2*b*), but the amplitude of the fluctuation is only  $1/\sqrt{2}$  of what it ought to be.

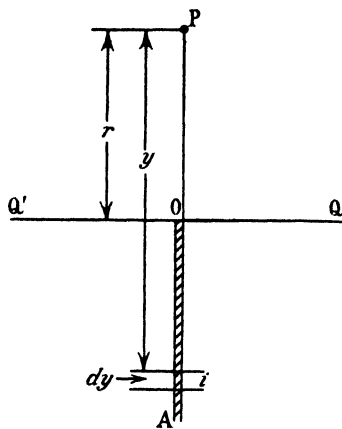


FIG. 7.18.

This discrepancy must be due to the disturbance of the induced density which in fact occurs near the edge, and accordingly the precise magnitude of the discrepancy must depend on the exact shape of the edge. Nevertheless, since we are hoping to be able to calculate fields from an assumed and approximate induced density, it is necessary to track down more completely the cause of the discrepancy in this calculable 'test case'.

Substituting in (5.2*a*) the approximate expression for the integrals gives

$$\begin{aligned}\frac{E}{E_0} &= \frac{1}{2}[2 + J_1(ar) - J_{-1}(ar) + j\{J_1(ar) + J_{-1}(ar)\}] \quad (7.35) \\ &= \frac{1}{2}\left[2 + \sqrt{2}\sqrt{\left(\frac{2}{\pi ar}\right)}\{\sin(ar + \frac{1}{4}\pi) + j\cos(ar - \frac{1}{4}\pi)\}\right] \\ &= \left[1 + \frac{1}{\sqrt{2}}\{Y_0(ar) + jJ_0(ar)\}\right].\end{aligned}$$

Comparison of the structure of this expression with the expression leading to (7.34) shows that the current which really is induced in the sheet produces a field which is  $\sqrt{2}$  times as great as the field due to a uniform density. Reference to Fig. 7.15 suggests the main cause of discrepancy is probably due to ignoring the quadrature component of induced current: its magnitude, using our previous notation, is

$$\frac{F-G}{4}.$$

When  $ar \ll 1$ , then

$$\frac{F-G}{4} \doteq \frac{1}{4}\sqrt{(2/\pi)}\{(ar)^{-\frac{1}{2}} + \frac{2}{3}(ar)^{\frac{1}{2}} - (ar)^{\frac{3}{2}}\}.$$

$$\therefore \frac{2\pi}{cE} \int i_Q dr = \frac{1}{4a} \sqrt{\left(\frac{2}{\pi}\right)} \{2(ar)^{\frac{1}{2}} + \frac{4}{15}(ar)^{\frac{3}{2}} - \frac{2}{3}(ar)^{\frac{5}{2}}\};$$

using this expression, combined with graphical integration from Fig. 7.15, the total estimated quadrature current is given by

$$\frac{2\pi}{cE} \int_0^\infty i_Q dr = \frac{0.29}{a}.$$

If all this current be supposed concentrated at the edge then its field at  $P$  will be  $0.145E_0\{Y_0(ar) + jJ_0(ar)\}$ . Accordingly the total field at  $P$  in phase with the incident field and due to the current in the sheet should have been reckoned as  $(0.5 + 0.145)E_0Y_0(ar) = 0.645E_0Y_0(ar)$ , and this is a much closer approximation to the correct value, which is  $0.705E_0Y_0(ar)$ .

This investigation suffices to show it is essential to take account of the disturbance of the induced density by the edge; we note, however, that the positions of the maxima and minima will be calculated correctly even when the edge effect is ignored.

We will now assess the effect of finite curvature at the edge. When the edge is furnished with a rod of radius  $\lambda k/2\pi$ , then the term which was  $J_1(ar)$  in (7.33) will become

$$\frac{J_1(ar)Y_1(k) - J_1(k)Y_1(ar)}{Y_1(k) + jJ_1(k)},$$

and there will be corresponding expressions for all other terms. When  $k \ll 1$  this tends to become  $J_1(ar) + \tan k J_{-\frac{1}{2}}(ar)$ . We will take account of the rod at the edge only in the first term of (7.33), so that where we



had  $J_{\frac{1}{2}}(ar)$  we shall now have  $J_{\frac{1}{2}}(ar) + \tan k J_{-\frac{1}{2}}(ar)$  and there will not be any other change. Accordingly (5.2b) becomes

$$\begin{aligned} \frac{|E|}{E_0} &= \frac{1}{\sqrt{2}} \left[ \left\{ \int J_{-\frac{1}{2}} \right\}^2 + \left\{ \int J_{\frac{1}{2}} \right\}^2 + \tan^2 k J_{-\frac{1}{2}}^2(ar) + \right. \\ &\quad \left. + 2 \tan k J_{-\frac{1}{2}}(ar) \int J_{-\frac{1}{2}}(ar) dr \right]^{\frac{1}{2}} \\ &\doteq \left\{ 1 + \frac{1}{\pi ar} - \frac{2}{\sqrt{(\pi ar)}} \cos(ar + \tfrac{1}{4}\pi) + k \sqrt{\left(\frac{2}{\pi ar}\right) \cos ar} + \frac{k}{\pi ar} \sin 2ar \right\}^{\frac{1}{2}} \end{aligned} \quad (7.36)$$

if  $k \ll 1$ , and thus the finite curvature is seen to introduce a double-frequency term which varies as  $k/r$  and it modifies slightly the size and phase of the main ripple: the approximate size of the main ripple is now  $(1 - \frac{1}{2}k)/\sqrt{(\pi ar)}$ . This new estimate is probably substantially valid for a radius of curvature up to about  $\frac{1}{20}\lambda$ ; then the fractional amplitude of the ripple will be reduced by about 15 per cent. When the disturbance of density at the edge was ignored we found a ripple proportional to  $\frac{1}{2}$ , whereas it ought to be proportional to  $1/\sqrt{2}$ , an underestimate of 40 per cent. When the shape of the edge is not known precisely, save that it is not sharp, then it seems not unlikely the best method of estimating the field is to assume the current density is uniform right up to the edge. At any rate we now know the extreme limits of uncertainty.

Now consider the field along the line  $QQ'$  in Fig. 7.18; when  $\theta = \frac{1}{2}\pi$

$$\frac{E}{E_0} = \frac{1}{\sqrt{2}} [ \{ J_{\frac{1}{2}} - J_{\frac{3}{2}} + J_{\frac{5}{2}} - J_{\frac{7}{2}} + \dots \} + j \{ J_{\frac{1}{2}} + J_{\frac{3}{2}} - J_{\frac{5}{2}} - \dots \} \pm j \sin ar ].$$

This series has been summed already in (5.2c): provided  $ar$  is large enough to write  $\int J_{\frac{1}{2}}(2ar) d(2ar) = 1$ , we have seen, in (5.2d), that

$$\frac{|E|}{E_0} = \frac{1}{2}(1 + 8 \sin^2 ar)^{\frac{1}{2}}, \quad \text{for } \theta = \frac{1}{2}\pi, \quad \text{and} \quad \frac{|E|}{E_0} = \frac{1}{2} \quad \text{when } \theta = -\frac{1}{2}\pi.$$

The interpretation of this result is obvious on consideration of Fig. 7.18. For the field at  $Q$  and  $Q'$ , due to the currents induced in the sheet, must be half the field due to a doubly infinite sheet together with a current of order  $-jcE/(a\pi/2)$  concentrated at the edge of the sheet. Thus it is a field whose modulus is  $\frac{1}{2}E$  together with a field whose modulus is  $E/\sqrt{(\pi ar)}$  and whose phase is  $\frac{1}{4}\pi$  behind the field  $\frac{1}{2}E$ . Combining the field of the induced currents with that of the incident wave we obtain a resultant which fluctuates between  $(1 + \frac{1}{2})$  and  $(1 - \frac{1}{2})$  on the 'bright side' of the sheet and remains everywhere equal to  $\frac{1}{2}E$  on the dark side.

Hence on the edge of the geometrical shadow there is, in the limit, no diffraction pattern. To obtain the field at comparatively small  $ar$  and on  $\theta = -\frac{1}{2}\pi$  it is necessary to evaluate from (5.2c), though use of the reciprocal theorem allows us to make use of some values which have been derived already in producing figures such as 5.4. For example, that figure showed a filament  $\frac{1}{4}\lambda$  from the plane of a sheet and level

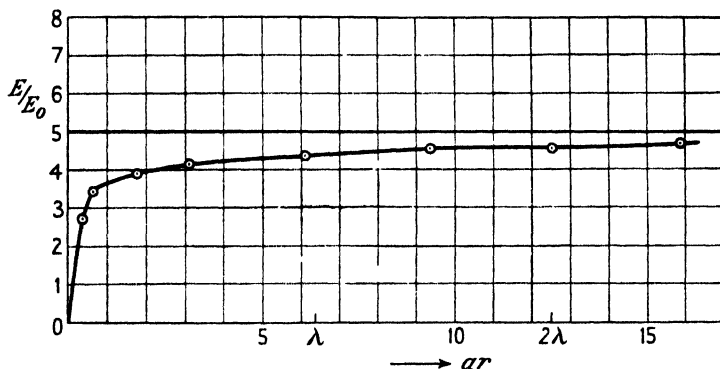


FIG. 7.19. Plane wave incident normally on semi-infinite sheet: curve showing re-radiated field along line of geometrical shadow.

with the edge produced a field  $0.39E_0$  at a very distant point on bearing  $-\frac{1}{2}\pi$ : hence this will be the field at  $\frac{1}{4}\lambda$  from the sheet and level with the edge due to a very distant filament at  $+\frac{1}{2}\pi$ . Whenever  $k = \pi, 2\pi$ , etc., we see that

$$\frac{|E|}{E_0} = \frac{1}{\sqrt{2}} (P^2 + Q^2)^{\frac{1}{2}},$$

and we have recently seen that this equals 0.467 when  $2ar = 50$ : thus the ripples will sensibly have died out when  $r/\lambda$  exceeds about 4. Fig. 7.19 shows  $E/E_0$  in the range  $r/\lambda$  up to 2.5: it appears that the field increases steadily up to its limiting value  $\frac{1}{2}$  without ever exceeding this value, and no ripple is discernible.

When  $\theta = \frac{1}{2}\pi$ ,

$$\begin{aligned} \frac{\sqrt{2}}{E_0} \frac{\partial E}{\partial \theta} &= \left\{ \frac{1}{2} J_{\frac{1}{2}}(ar) + \frac{3}{2} J_{\frac{3}{2}} - \frac{5}{2} J_{\frac{5}{2}} - \dots \right\} + j \left\{ \frac{1}{2} J_{\frac{1}{2}}(ar) - \frac{3}{2} J_{\frac{3}{2}} - \frac{5}{2} J_{\frac{5}{2}} \right\} \\ &= \frac{1}{2} ar \left[ \{ J_{\frac{1}{2}}(ar) + J_{\frac{3}{2}}(ar) \} + j \{ J_{-\frac{1}{2}}(ar) - J_{-\frac{3}{2}}(ar) \} \right] \end{aligned}$$

since  $2nJ_n(z) = z\{J_{n+1} + J_{n-1}\}$ .

$$\therefore \frac{1}{E_0} \left| \frac{\partial E}{\partial \theta} \right| = \sqrt{\left( \frac{ar}{\pi} \right)}, \quad \text{at } \theta = \pm \frac{1}{2}\pi,$$

and thus increases continuously with distance from the edge. At  $\theta = 0$ ,

$$-\frac{1}{E_0} \frac{\partial E}{\partial \theta} = j \frac{\partial}{\partial \theta} \{\sin(ar \sin \theta)\} = jar.$$

Algebraic expressions have now been found for  $E$  and  $\partial E/\partial \theta$  at  $\pm \frac{1}{2}\pi$ , and thus it is possible to sketch the general form of the distribution curve of mean-square field at any distance from the edge: the idea will be assisted by reference to Fig. 5.4, which is such a curve for the distance  $\frac{1}{4}\lambda$ . If the reader will refer to this figure and remember that  $E/E_0$  is constant and equal to  $\frac{1}{2}$  at  $\theta = -\frac{1}{2}\pi$  while  $\partial E/\partial \theta$  varies as  $r^{\frac{1}{2}}$ , he will realize this means that the field just inside the region of optical shadow decreases as  $r$  increases.

At a small distance  $y$  on either side of the line of shadow

$$\frac{E}{E_0} = \frac{1}{2} \left( 1 \pm \frac{2ay}{\sqrt{(2\pi ar)}} \right).$$

When this problem is discussed in books on optics it is commonly said the edge shines as if self-luminous and that the diffracted light appears to come from the edge: it is instructive to examine what these statements mean in terms of the mechanism and of the apparatus we are thinking of here. The eye is a highly directive receiving aerial and perceives not only  $E$  but  $\partial E/\partial \theta$ : it performs 'direction finding' in the sense used in radio communications. Imagine that a small loop receiver, on bearings  $\theta = 0$  and  $-\frac{1}{2}\pi$ , is used to examine the 'direction' of the incoming field. To do this it is perhaps simplest to derive  $H$  the magnetic field and then to find the direction of the resultant  $H$ . Thus

$$\frac{\partial E}{\partial r} = \frac{1}{c} \frac{\partial H_\theta}{\partial t} = -jaH_\theta \quad \text{and} \quad \frac{1}{r} \frac{\partial E}{\partial \theta} = -jaH_r.$$

When  $\theta = 0$ ,

$$\begin{aligned} -\frac{1}{aE_0} \frac{\partial E}{\partial r} &= \{J'_1(ar) + J'_3 + \dots\} + j\{J'_1(ar) - J'_3 + \dots\} \\ &= \frac{1}{2}\{J_{-1}(ar) + J_1\} + \frac{1}{2}j\{J_{-1}(ar) - J_1\}, \end{aligned}$$

since  $2J'_n = J_{n-1} - J_{n+1}$  and  $\frac{1}{E_0} \frac{\partial E}{\partial \theta} = jar$ .

Hence  $H_r = -E_0$  and

$$H_\theta = \frac{E_0}{\sqrt{(2\pi ar)}} \{\cos(ar + \tfrac{1}{4}\pi) - j \sin(ar + \tfrac{1}{4}\pi)\}.$$

Hence if a small coil is placed on bearing  $\theta = 0$  and with its plane at an angle  $\beta$  to the plane of the sheet, the flux  $\phi$  through it is

$$\frac{\phi}{E} = \left\{ \frac{\cos(ar + \frac{1}{4}\pi)}{\sqrt{(2\pi ar)}} \cos \beta - \sin \beta \right\} - \left\{ \frac{j \sin(ar + \frac{1}{4}\pi)}{\sqrt{(\pi ar)}} \cos \beta \right\}.$$

This can be zero only if  $\sin(ar + \frac{1}{4}\pi)$  is zero: then  $\phi$  will be zero when  $\beta \doteq (2\pi ar)^{-1}$ . At distances not greater than about  $\frac{1}{2}\lambda$  the field would appear to come from the edge, but at large distances the apparent direction would not be far from the source: at a distance of  $4.5\lambda$  the apparent bearing would be incorrect by about  $5^\circ$ . One effect of the edge will be to blur the minimum of the direction-finding coil. When  $\theta = \frac{1}{2}\pi$  we have seen that  $(1/r)(\partial E/\partial \theta)$  varies as  $r^{-1}$ , thus showing that  $H_r$  decreases continuously, whereas  $E$ , and thus  $H_\theta$ , rapidly approach  $\frac{1}{2}E_0$ . Accordingly the apparent bearing of the source would rapidly approach the true bearing as  $r$  increases.

The field might be explored by an observer moving continuously on a given bearing or on a path parallel to or perpendicular to the sheet. The field at various points along a path parallel to the sheet and distant  $\frac{1}{4}\lambda$  from it are given (by use of the reciprocal theorem) by the values of front-to-back ratio recorded in § 5.3. They are arranged more conveniently for this purpose in Table 7.4 below, where intensities are expressed relative to the value when the distant aerial is just 'visible'.

TABLE 7.4

*Path parallel to sheet and distant  $\frac{1}{4}\lambda$  from it*

Distance from edge	0	0.48 $\lambda$	1.09 $\lambda$	1.57 $\lambda$	2.22 $\lambda$
Relative intensity	1	0.17	0.046	0.025	0.02

The table shows that the shadow develops very rapidly with distance from the edge, for a path only  $\frac{1}{4}\lambda$  behind the sheet: there is no sudden discontinuity in crossing the line of geometrical shadow and no diffraction pattern effect along this path.

Though our solution in an infinite series of Bessels is exact, it is impracticable to evaluate it when  $ar$  exceeds, say, 2, and we are driven to use approximate methods for calculating the fields at large distances. This is comparatively simple to do since we now know the current induced in the semi-infinite sheet. Let  $OA$  in Fig. 7.20 represent the semi-infinite sheet: we wish to calculate the resultant field at a point  $P$  distant  $x$  behind the plane of the sheet and distant  $b$  in front or behind the plane of the geometrical shadow. We require the field radiated by



path  $PP'$  distant  $b$  behind the plane of the sheet, as shown in Fig. 7.21. We must evaluate the field at  $P$  due to a uniform density  $i = cE_0/2\pi$  in the half-plane  $OA$ . It will be equal to the field at  $P$  due to a semi-infinite sheet  $BA$  less the field of the portion  $BO$  of width  $x$ . The field of  $BA$  is  $\frac{1}{2}E$ . To simplify the evaluation of the field due to  $BO$  we shall suppose  $b \gg x$ : then the field at  $P$  of elementary filaments of current at  $B$  and at  $O$  will be sensibly equal in magnitude, though these may differ considerably in phase. For a typical element at  $R$  we have

$$PR - PB \doteq y^2/2b.$$

Hence the phase-angle  $\phi$  of an elementary filament at  $R$ , relative to one at  $B$ , is

$$\phi = \pi y^2/\lambda b.$$

Let an element of unit width at  $B$  produce a field  $\delta E$  at  $P$ , then

$$\frac{c \delta E}{a\pi} \equiv i\{-J_0(ab) + jY_0(ab)\},$$

whence

$$\delta E = \frac{aE_0}{2}\{-J_0(ab) + jY_0(ab)\}.$$

Then an element of unit width at  $R$  will produce at  $P$  a field whose inphase component, relative to an element at  $B$ , is  $\delta E \cos \phi$  and quadrature component is  $\delta E \sin \phi$ . Hence the field at  $P$  due to the current in the whole strip of width  $x$  is

$$\begin{aligned} E_P &= \delta E \int_0^x \cos \phi \, dy = \delta E \int_0^x \cos \frac{\pi y^2}{\lambda b} \, dy \\ &= \frac{\delta E}{2} \sqrt{\left(\frac{b\lambda}{2}\right)} \int_0^{\pi x^2/\lambda b} \sqrt{\left(\frac{2}{\pi\phi}\right)} \cos \phi \, d\phi \\ &= \frac{\delta E}{2} \sqrt{\left(\frac{b\lambda}{2}\right)} \int_0^{\pi x^2/\lambda b} J_{-\frac{1}{2}}(\phi) \, d\phi. \end{aligned}$$

Similarly

$$E_Q = \frac{\delta E}{2} \sqrt{\left(\frac{b\lambda}{2}\right)} \int_0^{\pi x^2/\lambda b} J_{\frac{1}{2}}(\phi) \, d\phi,$$

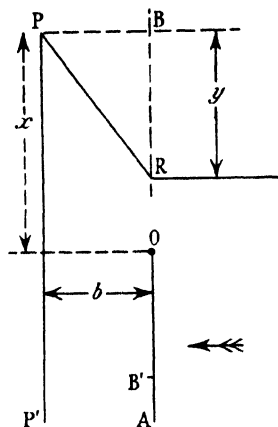


FIG. 7.21.

$$\begin{aligned} \therefore E &= \frac{aE_0}{4} \sqrt{\left(\frac{b\lambda}{2}\right)} \left\{ \int_0^{\phi_1} J_{-\frac{1}{2}}(\phi) d\phi - j \int_0^{\phi_1} J_{\frac{1}{2}}(\phi) d\phi \right\} \{-J_0(ab) + jY_0(ab)\} \\ &= \frac{1}{4}\sqrt{2} \left\{ \int J_{-\frac{1}{2}} - j \int J_{\frac{1}{2}} \right\} \{-\cos(ab - \frac{1}{4}\pi) + j \sin(ab - \frac{1}{4}\pi)\}. \quad (7.37) \end{aligned}$$

In deriving this expression it has been stated explicitly that  $x/b \ll 1$ : nevertheless if  $\frac{1}{2}ax$  is large it is possible for  $ax^2/2b$  to be large and then  $\int J_{\frac{1}{2}} \doteq 1$ . In such circumstances

$$\begin{aligned} E &= -\frac{1}{4}\sqrt{2}(1-j)\{\cos(ab - \frac{1}{4}\pi) - j \sin(ab - \frac{1}{4}\pi)\} \\ &= -\frac{1}{2}(\cos ab - j \sin ab). \quad (7.38) \end{aligned}$$

This is independent of  $x$  and equal to half the field of a doubly infinite plane. This result was to be expected and shows the field of a uniformly loaded strip approximates to that of an infinite sheet provided the half-width is many wavelengths and the point of observation not too distant. If  $B$  in Fig. 7.21 is above  $O$ , the field at  $P$  of the current in  $OA$  is the field of  $BA$  less the field of  $BO$ : we have just seen this difference will tend to zero and then the net field at  $P$  is that of the incident wave alone. If  $B$  is below  $O$  in Fig. 7.21, then the field of  $OA$  will tend to become  $\frac{1}{2}E + \frac{1}{2}E$ : then the net field at  $P$  due to the incident wave and due to the current in the sheet will tend to zero and the shadow will be complete.

Denote  $\int J_{-\frac{1}{2}}$  and  $\int J_{\frac{1}{2}}$  by  $P$  and  $Q$  respectively. Then (7.37) shows the field of the strip  $BO$  is represented by a vector which lags

$$\theta = \arctan \frac{Q}{P}$$

on a vector which leads the incident field by  $\frac{1}{4}\pi$ . Hence this vector leads the phase of the incident wave by an angle  $\phi = \frac{1}{4}\pi - \theta$ . The component of field due to the strip  $BO$  which is in phase with the incident wave at  $P$  is thus given by

$$\frac{E_P}{E} = \frac{\sqrt{2}}{4} \sqrt{(P^2 + Q^2)} \cos \phi = \frac{\sqrt{2}}{4} \sqrt{\frac{(P^2 + Q^2)}{2}} (\cos \theta + \sin \theta) = \frac{P + Q}{4}.$$

Similarly 
$$\frac{E_Q}{E} = \frac{P - Q}{4}.$$

Hence the field at  $P$  due to the current in the half-plane  $OA$  is

$$\frac{E'}{E} = \left(\frac{1}{2} - \frac{P + Q}{4}\right) + j \frac{P - Q}{4}.$$

Hence the net resultant field at  $P$  due to the incident wave together with the field of the currents in the half-plane  $OA$  is

$$\frac{E''}{E} = 1 - \left(\frac{1}{2} - \frac{P+Q}{4}\right) + j\frac{P-Q}{4} = \frac{1}{2} + \frac{P+Q}{4} + j\frac{P-Q}{4}. \quad (7.39)$$

If  $B$  in Fig. 7.21 is below  $O$ , then the field of the strip  $B'O$  must be added to that of the half-plane  $B'O$  and then the resultant field at  $P$  will be given by

$$\frac{E'''}{E} = \frac{1}{2} - \frac{P+Q}{4} + j\frac{P-Q}{4}. \quad (7.40)$$

$$\therefore \frac{|E'''|^2}{E^2} = \left(\frac{1}{2} \pm \frac{P+Q}{4}\right)^2 + \left(\frac{P-Q}{4}\right)^2 = \frac{(1 \pm P)^2 + (1 \pm Q)^2}{8}. \quad (7.41)$$

Now  $P \doteq 1 + J_+(\phi_1)$  and  $Q \doteq 1 - J_-(\phi_1)$ .

Hence in the shadow region

$$\frac{|E'''|^2}{E^2} = \frac{J_+^2(\phi_1) + J_-^2(\phi_1)}{8} = \frac{1}{4\pi\phi_1} = \frac{\lambda b}{4\pi^2 x^2} \equiv \frac{1}{4\pi\zeta^2}. \quad (7.42)$$

Hence to this order of approximation there are no maxima or minima of mean square field in the shadow region. Fig. 7.22 shows the fractional field as a function of  $x\sqrt{(\pi/\lambda b)}$  both in the shadow and in the light region. It may be seen that the curve falls continuously to zero in the shadow region and oscillates in the bright region. In the shadow, the curve becomes asymptotic to  $|E|/E_0 = 1/(2\sqrt{\pi}\zeta)$  as given by (7.42) and is sensibly indistinguishable from this asymptote when  $\zeta$  exceeds, say, 2: the oscillations lie under an envelope which is the same hyperbola plotted to the origin (0.1). In the shadow  $|E|/E_0$  is less than 0.01 if  $\zeta$  exceeds 28: similarly the fractional amplitude of oscillations is less than 1 per cent. when  $\zeta > 28$ . The first maximum of  $|E|/E_0$  occurs when  $\zeta = 1.52$  and the first minimum when  $\zeta = 2.40$ : hence the distance from the edge of the geometrical shadow to the first maximum is  $\frac{2}{3}$  times the distance between the first maximum and the first minimum and very nearly equal to the distance between the first two maxima. At the first maximum  $OP - PB \doteq 0.48\lambda$  (see Fig. 7.21); at the second maximum this extreme path difference is near  $0.96\lambda$ . A general expression is  $x_{\max} = \sqrt{\{b\lambda(2n-1)\}}$  and  $x_{\min} = \sqrt{\{b\lambda 2n\}}$ , where  $n$  is any integer (excluding zero): for the first maximum and minimum more correct values at  $x_{\max} = 0.86\sqrt{b\lambda}$  and  $x_{\min} = 1.83\sqrt{b\lambda}$ .

It might have been expected the maxima and minima would occur when the field due to the currents in the sheet was precisely in phase or in antiphase with the incident field: our interpretation of (7.37)



shows this occurs when  $\theta = \frac{1}{4}\pi$ , which is when  $Q = P$ . This occurs when  $\zeta^2 = 2.49, 5.52, 8.7, 11.7$ , etc., or  $\zeta = 1.57, 2.35, 2.96$ , etc., and thus does not coincide precisely with the maxima and minima of R.M.S. field. Moreover, coincidence of phase will occur both in the shadow region and in the bright region, and from this point of view a diffraction

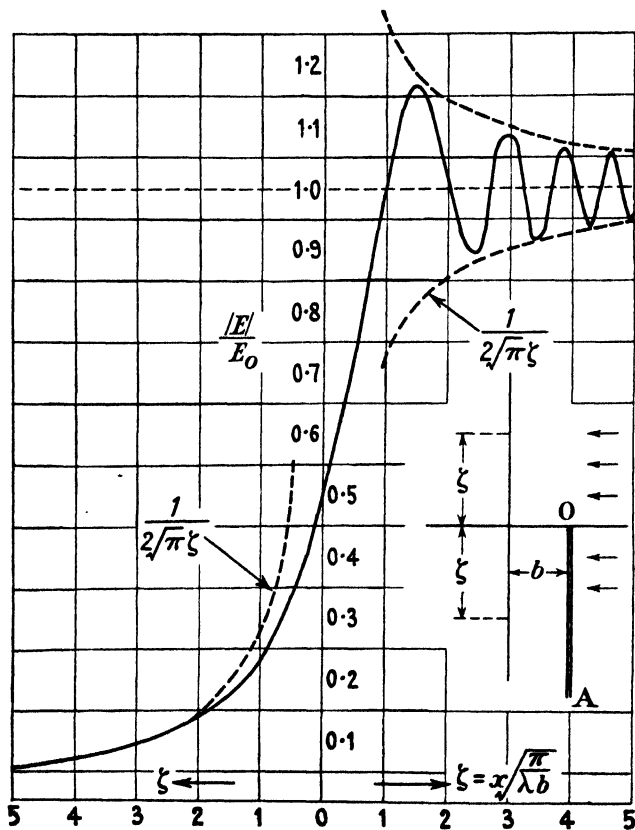


FIG. 7.22. Diffraction pattern for sharp edge.

pattern might be expected to occur in both regions, but it does not occur in the dark region. There are similarly placed stations in both regions at which the *phase* of the field would be unaltered if the screen were removed. It just happens the functions  $P$  and  $Q$  are such that (7.41) is oscillatory when  $P$  and  $Q$  are positive, and non-oscillatory when they are negative: the absence or otherwise of oscillation does not appear susceptible of any simple physical description. Commonly we associate a diffraction pattern with two vectors which are periodically in phase or in antiphase: here we have two vectors whose phase

never differs by more than a few degrees and whose proximate coincidence may denote either a maximum or a minimum.

This problem has been studied and examined in optics for more than a century. If a reasonably sharp edge is caused to throw a shadow on an opaque screen parallel to itself, one or more bright lines, parallel to the edge of the shadow, may be observed. These bright lines are presumably the successive maxima in Fig. 7.22. Since the response of the eye is approximately proportional to the logarithm of the intensity (Weber-Fechner law), the eye is able to be aware of a small fractional increase and therefore the crests of the maxima stand out as bright lines even though their fractional increase is not large. The eye associates the edge with the boundary of the dark shadow: this boundary must start at the place where the intensity is at the limit of vision. Accordingly the distance between the apparent edge and the first bright line must be much larger than  $1.52\zeta$  and can have no definite value. In radio-frequency measurements we are equipped with two distinct measuring instruments, the eye and the ammeter. Thus the intensity in the shadow region can be measured since we know, by eye, where the edge of the geometrical shadow lies. It should be recognized that the intensity in the shadow region falls off only as the inverse distance from the edge and accordingly field will be perceptible at very large distances behind the edge. No doubt this accounts for the comparative absence of sharp shadow encountered in most propagation experiments. Since the observed optical effects are not markedly dependent on the sharpness or straightness of the edge, we conclude that physical undulations, even if many  $\lambda$  high, do not affect the performance appreciably.

Equation (7.42) is valid only when  $b \gg x$  and when  $b/\lambda$  is large. It would be of interest to know its order of approximation when  $b/\lambda$  is not large. This can be assessed from Table 7.4 which refers to  $b/\lambda = \frac{1}{4}$ . Comparison of the values recorded in it with those deduced from Fig. 7.22 show that when  $b/\lambda = \frac{1}{4}$  then  $E/E_0$  at a given value of  $\zeta$  is about one-third of what it would be if  $b/\lambda$  is large. Thus it is concluded that (7.42) is substantially valid even when  $b$  is only a few wavelengths.

## 7.12. Plane wave incident normally on an infinite sheet in which there is a parallel-sided aperture

A formal solution of this problem has been obtained by Morse and Rubenstein,<sup>†</sup> and their very interesting paper on 'Diffraction of Waves by Ribbons and Strips' should be consulted. They obtained a general

<sup>†</sup> See *Phys. Rev.* **54** (1938), 895; McLachlan, *Theory of Mathieu Functions*, p. 360.

solution in Mathieu functions and have performed the necessary evaluation to obtain some diffraction patterns. Their problem is a wave incident on a strip of finite width, and this can be converted to apply to an aperture in an infinite plane. Unfortunately for us here they have not completed their solution to the point of evaluating the density of induced current across the width of the strip: we should like to know how much the two bounding edges cause the density to depart from the value  $i = cE/2\pi$ . The labour of completing this part of their solution is too great to undertake now and the writer hopes that some industrious reader will be stimulated to complete the task and thereby render complete § 7.10. The writer must rest content with pointing out where this much needed solution exists, waiting for a lengthy and painstaking use to be made of it. However, pending this having been done, it seems worth while to attempt a very rough approximate solution for a narrow aperture parallel to the electric vector. First of all we will make the simplification which, in effect, is made in the classical treatment of this problem by the methods of physical optics and assume that the induced density is uniform right up to the edges of the parallel-sided gap of width  $g$ . We will then find the field due to this density at any point on the surface of either half-plane. Clearly this must equal the field which would obtain if the gap did not exist less the field due to a uniformly loaded strip of width  $g$ . Hence it follows readily from (1.46) that at a point on either half-plane, distant  $r$  from the midline of the aperture,

$$\frac{cE}{2\pi i} = 1 - \{J_0(ar) + jY_0(ar)\} \int_0^{k_1} J_0(k) dk - 2\{-J_2(ar) + jY_2(ar)\} \int_0^{k_1} J_2(k) dk + \dots$$

where  $k_1 = 2\pi g/2\lambda$ . If we now situate a like pair of filaments of strength  $I$ , separated a distance  $2R$ , symmetrically in the plane of the aperture, their field will be

$$\frac{cE}{2\pi aI} = \{-J_0(ar) + jY_0(ar)\}J_0(k') + 2\{-J_2(ar) + jY_2(ar)\}J_2(k') \dots,$$

where  $k' = 2\pi R/\lambda$ . In order to make the field of this pair of filaments tend to zero at large distances in their plane we will purposely make  $2R = \frac{1}{2}\lambda$ : then  $J_0(k') = 0.472$ ,  $J_2(k') = 0.24$ , and  $J_4(k') = 0.012$ . If it

is now possible to find  $k_1$  so that  $-0.472a = iI \int_0^{k_1} J_0(k) dk$  and also

$-0.24aI = i \int_0^{k_1} J_2(k) dk$ , then the net field across the sheets will be very

nearly constant. This is fulfilled very closely when  $k' = 3$  and then  $\int_0^3 J_0(k) dk = 1.386$  and then  $2I = 5.90\lambda i/2\pi$ . The total current which would have been induced in the strip where the aperture is (if the aperture had been absent) is  $6\lambda i/2\pi$ ; accordingly the net external field behind the aperture will be sensibly that of a concentrated current  $0.1\lambda i/2\pi = 0.1cE/2\pi a$ . Hence in this case it would seem that the width of the equivalent aperture is about  $\frac{1}{60}$  of its actual width. What we have done is to find a pair of currents in the aperture which will cause the density induced in the planes, by them and the incident wave, to be substantially constant right up to the bounding edges. These currents ought to have been situated at the edges instead of inside the aperture, but the neutralization of the  $J_2$  term could not then have been attained. If we are satisfied to neutralize only the term involving  $J_0$ ,

then 
$$-J_0(k_1)I = \frac{i}{a} \int_0^{k_1} J_0(k) dk:$$

if only the second term in the expansion of  $J_0(k_1)$  is retained then it follows that

$$-(2I - gi) = \frac{gi k^2}{6}.$$

It would appear from this that the effective width of a very narrow aperture is  $k_1^2/6 = 1.6(g/\lambda)^2$ ; this is a rough estimate which is not expected to hold if  $g/\lambda > \frac{1}{4}$ . This approach, rough as it is, serves to show that the field which 'passes through' a very narrow aperture is reduced enormously by the concentration of current which must occur at its edges. Only numerical appeal to the Morse and Rubenstein analysis can show whether these rough estimates are reasonably correct. It should be noticed that the external field must be very nearly that of a concentrated current filament in the aperture and hence must have sensibly the same strength on all bearings. A very narrow aperture cannot produce a narrow beam of field: this can occur only for an aperture whose width is many  $\lambda$ .

## VIII

### THE SINGLE ISOLATED AERIAL

#### 8.1. The electric doublet and the thin linear aerial

THE equations for the field of an electric doublet were developed in § 1.21 but were not then explored further than was necessary to arrive at equation (1.82) (for the output of a half-wave aerial), which was required for immediate use. Since any distribution of current can be built up from the appropriate distribution of doublets, the field of any distribution can thus be found by superposition: thus the field due to any current distribution can be found by the help of equations (1.69), (1.70), and (1.74). But we are still left with the grave problem of discovering what distribution is possible on a conductor of specified shape. In this book we have made repeated use of the concept of a current filament, without inquiring much how such a filament would be produced, knowing that, ideally, it could be produced by a multiplicity of separately-fed short dipoles. Given such a filament, we have found the distribution of filaments induced in Vee reflectors and cylinders.

Our problem now is to find the field due to an aerial consisting of a single long straight thin wire. Reality confronts us at once on the question of how the current is to be produced in the wire. We may seek simplicity by supposing it is induced by an incident field whose electric vector is parallel to the wire. To bring the analysis within bounds which may conceivably be possible we know the wire must be replaced by a surface of revolution, such as an ellipsoid: such a departure from the geometrical form of a uniform wire is not likely to be of much practical significance. The problem is soluble in terms of Mathieu functions, and it has been done.† The solution is very troublesome to disentangle, but it has solved analytically the reflection from an ellipsoid and in particular from a long wire. But this is not the problem of a receiving aerial, in the ordinary sense of these words, because in such the current must be led through an auxiliary impedance associated with the recording gear. The insertion of the said impedance, be it direct or through a transmission line, must necessarily introduce a discontinuity in the ellipsoid, and the said discontinuity must invalidate the analysis by an amount whose relative importance cannot be assessed with certainty. Thus the attempted simplification of inducing the

† See, for example, Page and Adams, *Phys. Rev.* **53** (1938), 819.

current by an incident field fails, and leads back to the equivalent of the transmitting aerial having current fed to it by a generator. Clearly the precise problem is outside the scope of analysis and also of generalized description.

Until recently investigators have had to be content to evaluate the fields due to assigned distributions, choosing such distributions as seemed to them reasonably appropriate; but of recent years E. Hallen, C. J. Bouwkamp, R. King, and C. Harrison and others have derived distributions which they believe are closely appropriate to the idealized aerial they postulate.

It is not proposed to develop fully the analysis of the linear aerial in this book and in the main we shall be content with evaluating the fields due to assigned distributions of current: not only does this suffice for most practical purposes, but it is an extremely valuable way of perceiving the mechanism which has to be described by more complete solutions.

A doublet is an infinitesimal element and therefore must not be approached within a distance comparable with its length, and this length can be shrunk indefinitely; accordingly the force at the doublet itself is meaningless and moreover must tend to infinity when  $r$  is put equal to zero in the equation for its field. It is convenient to express the field as a component  $E_P$  which is in phase with the current and a component  $E_Q$  in quadrature thereto. Equation (1.79) shows that  $E_P$  is finite when  $r$  is zero and thus, strange to say, we can go right up to the doublet itself in respect of this term: it is the component of force which describes the output of work from the doublet, and this is the reason why it remains finite at the origin. Equation (1.23) exhibited the same property for a current filament, which is an infinitely long collinear distribution of doublets. Since we know the value of  $E_P$  AT a doublet there is no serious difficulty in evaluating  $E_P$  at any point on the axis of any finite collinear distribution of cophased doublets. The expression for this is given in (1.80).†

Fig. 8.1 exhibits the variation of  $E_P$  along the axis of a doublet and also along the axis of a sinusoidal distribution of cophased doublets of total length  $\frac{1}{2}\lambda$ . Remembering that  $X_0 \equiv \int i \, dl$ , this figure shows that

† A more extended form of this expression will be found in equation (13 a) on p. 545 of *Journal I.E.E.*, vol. 78 (1936) and should be referred to if more terms are required. The particular case where the length of the aerial is  $\frac{1}{2}\lambda$  is of outstanding importance: moreover, experience has shown that then the distribution is substantially a sinusoid and therefore it is appropriate to evaluate the field of a sinusoidal distribution.

the axial distribution of  $E_P$  is scarcely dependent on whether a given number of metre amperes is distributed sinusoidally along a length  $\frac{1}{2}\lambda$  or concentrated into a doublet at the middle of this length. This discovery is very important since it shows that the mutual field between

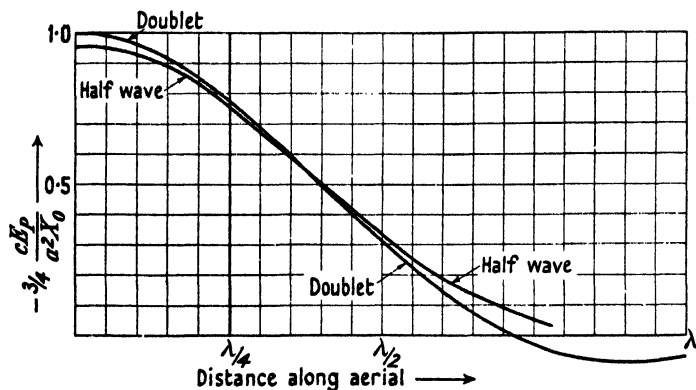


FIG. 8.1. Distribution of inphase component of electric force along the axis of a doublet and of a half-wave aerial.

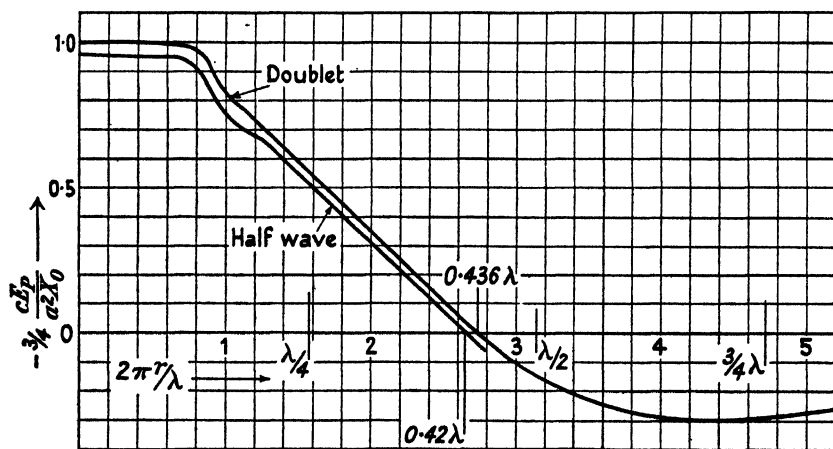


FIG. 8.2. Distribution of inphase component of electric force in the equatorial plane of a doublet and of a half-wave aerial.

any two members of an in-line array is insensibly dependent on the distribution along any typical member, and accordingly that it is permissible to regard each member as a doublet in so far as mutual action is concerned: this simplifies computation enormously. Fig. 8.2 shows the distribution of  $E_P$  in the equatorial plane for such a half-wave distribution and for a doublet of equal strength: again the two curves

of  $E_P$  differ insensibly. Thus the mutual action, in respect of  $E_P$ , of two parallel half-wave elements must be sensibly the same as that between two parallel doublets. Fig. 8.3 shows the distribution of the vertical component of  $E_P$ , due to a doublet, along a line parallel to its axis and distant either  $\frac{1}{8}\lambda$  or  $\frac{1}{4}\lambda$  from it. Curve 2 of this figure shows that  $E_P$  is substantially constant throughout the distance  $\pm\frac{1}{4}\lambda$  from the equatorial

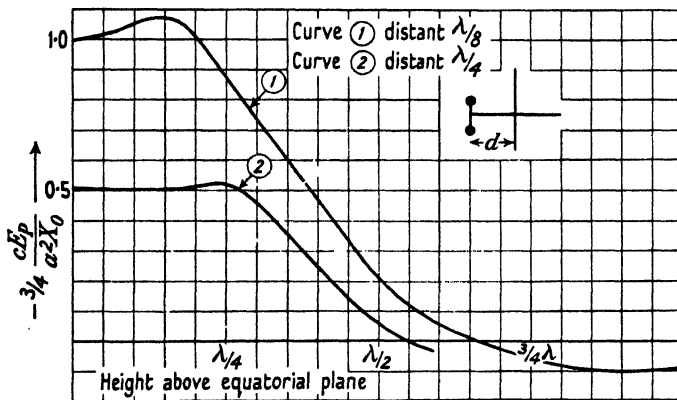


FIG. 8.3. Distribution of inphase component of electric force along a line parallel to the axis of a doublet: curve (1) distant  $\frac{1}{8}\lambda$  from axis, curve (2) distant  $\frac{1}{4}\lambda$  from axis.

plane in a line distant only  $\frac{1}{4}\lambda$  from the doublet. Accordingly, close consideration will show that  $E_P$  must be substantially constant along a line parallel to a half-wave aerial and not closer than, say,  $\frac{1}{4}\lambda$  to it. Recognition of this fact simplifies enormously the calculation of the mutual interaction between parallel half-wave elements of an array: the reader should now be able to satisfy himself that only a small second-order difference can result in the output by allowing, very laboriously, for the small variation of mutual field along the length of half-wave elements. Recognition of points such as these we have just made permits much analysis to be stripped of extremely cumbersome trappings, trappings which obscure the vital points of the problem and yield an answer whose apparent accuracy far exceeds that to which the real problem can be stated.

Fig. 8.4 shows the distribution of  $E_Q$  along lines parallel to a doublet and at various distances from it and is useful for estimating the mutual reactance between parallel aerials: a reactance which affects the condition for resonance. Fig. 8.5 shows the distribution of  $E_Q$  in the equatorial plane of a doublet and also of a half-wave aerial, the curve



for the half-wave aerial having been obtained by laborious computation from the component dipoles making up the sinusoidal distribution. This figure shows that at distances exceeding about  $\frac{3}{8}\lambda$  the half-wave aerial is scarcely distinguishable from an equivalent dipole at its middle point; but for distances closer than  $\frac{1}{4}\lambda$  the sinusoidal distribution has

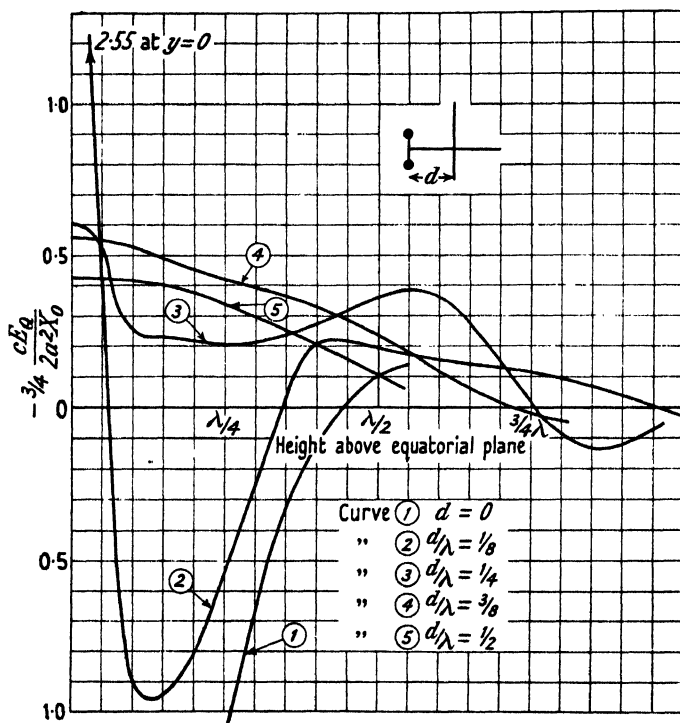


FIG. 8.4. Distribution of quadrature component of electric force parallel to axis of a doublet and at various distances from it.

a profound effect, as would be expected. It is impracticable to evaluate  $E_Q$  in the region where  $x < \frac{1}{8}\lambda$ , but it certainly passes through zero near this point. It is instructive to compare the distribution of  $E_P$  and  $E_Q$  in the equatorial plane of a half-wave aerial, as shown in Figs. 8.2 and 8.5 with the corresponding distribution of  $E_P$  and  $E_Q$  for a current filament, as shown in Fig. 1.5. For the half-wave aerial  $E_P$  passes through zero when  $x/\lambda = 0.42$ , whereas this occurs for the current filament when  $x/\lambda = 0.38$ : at the middle of the half-wave aerial

$$-\frac{cE_P}{2a^2} = \frac{\lambda I}{\pi^2}, \quad \text{whence} \quad -\frac{cE_P}{a\pi I} = \left(\frac{1}{2}\pi\right)^2 = 0.405,$$

as compared with the value unity when the loop current  $I$  persists throughout the filament. For the half-wave aerial  $E_Q$  passes through zero when  $2\pi x/\lambda \doteq 0.8$  and when  $2\pi x/\lambda = 4.5$ : for the current filament this occurs when  $2\pi x/\lambda = 0.89$  and  $3.96$ . Thus the equatorial field of a half-wave aerial is a close approach to that of a filament.

If an aerial  $\frac{1}{2}\lambda$  long, bearing a cophased sinusoidal distribution of

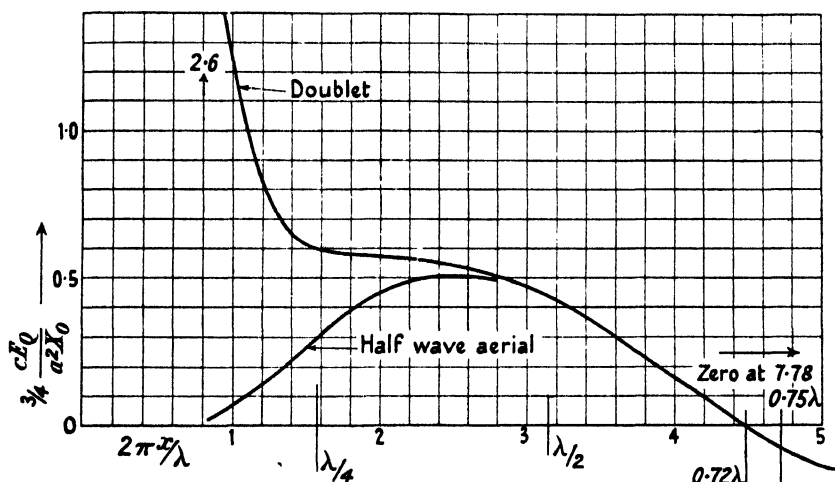


FIG. 8.5. Distribution of quadrature component of electric force in equatorial plane of a doublet and of a half-wave aerial.

current, is resonant, then  $E_Q$  must be zero everywhere along the wire. It seems probable from Fig. 8.5 that  $E_Q$  is not zero at the wire but has the sense of an inductive reactance. It is certain from Fig. 8.5 that  $E_Q$  along a doublet is capacitive in sense. Hence it seems likely that  $E_Q$  will have zero value at the midpoint of an aerial when its length is somewhat less than  $\frac{1}{2}\lambda$ : thus this figure suggests the known fact that the resonant length is slightly less than  $\frac{1}{2}\lambda$ .

## 8.2. Radiation resistance of a linear aerial

The total output of a linear aerial is given with complete generality (equation 1.80) provided only that the current is cophased throughout its length. The output can be expressed in terms of an equivalent resistance measured from any point in the aerial. It has been usual to postulate that the current distribution is part of a sinusoid, having zero value at the extreme tips. One of the earliest and classic examples of such evaluations was made by B. van der Pol in 1917,<sup>†</sup> who used the

<sup>†</sup> *Proc. Phys. Soc.* **29** (1917), 269.

Poynting method. In a sense his results were very general in that he implied the existence of a capacitance roof since he did not insist that the current was zero at the tips, but he ignored radiation from the roof; but of this later. In 1924 Stuart Ballantine† used the Poynting method to calculate the radiation resistance of a sinusoidal distribution of current along a straight line whose total length did not much exceed  $\frac{3}{2}\lambda$ .

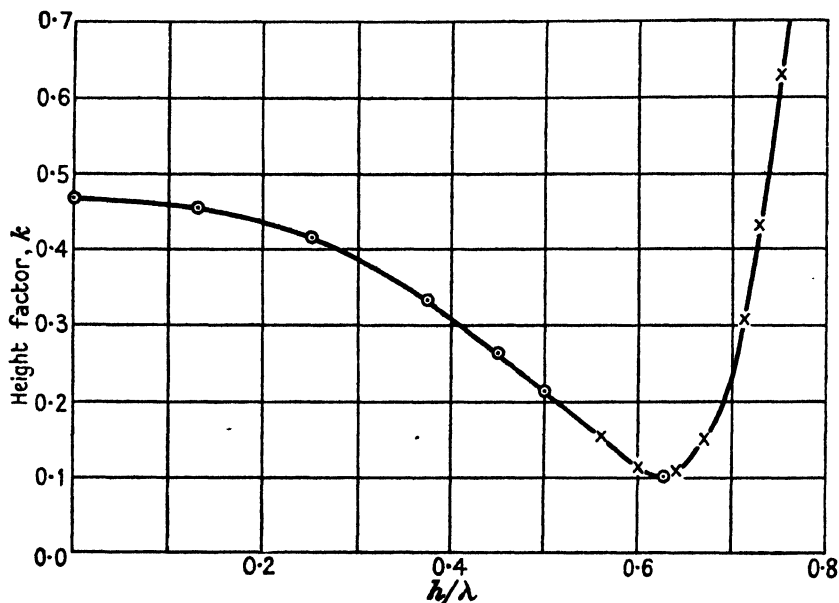


FIG. 8.6. Power-gain as a function of height of linear aerial.

The writer repeated these calculations, by the method of evaluating  $E_P$ , and in effect they are recorded in Fig. 8.6 which displays them in terms of a 'height factor', which is equal to 0.61 divided by the power gain. The figure shows that the gain reaches a maximum value of 2.05 when the total length is  $1.24\lambda$ ; when the total length is  $1.46\lambda$  the gain is unity. These values are important in relation to 'broadcast' aerials intended to give a direct ray service (i.e. without assistance from the Heaviside layer), and then they apply to a vertical tower standing on but insulated from the ground. The tower which will be most economical of power for a given field strength in the equatorial plane will have a height of  $0.62\lambda$  above the ground: the 'gain' of such a tower will be twice that of a tower whose height is  $\frac{1}{4}\lambda$  above the ground. The saving of power is due to the relative reduction of high-angle radiation, and the mechanism

† *Proc. I.R.E.* 12 (1924), 386.

by which this occurs should be obvious from consideration of the factor  $F_1$  of Chapter II. The reduction of high-angle radiation also reduces the interference which the station causes at distances where the transmission has been assisted by the Heaviside layer. Since the current at the foot of a tower  $0.62\lambda$  high is small the radiation resistance measured from this point is necessarily large; if the current distribution is sinusoidal it is about 110 ohms. The precise value depends enormously on the current distribution, and experience in any given application may well show that the resistance differs substantially from this value; but the power gain will differ very little from 2 since the gain is insensitive to the precise distribution. In general the aerial will be fed through a cable whose characteristic resistance is of the order of 50 ohms; in order to prevent the development of unduly high voltages along the cable some transforming device is required to match the high resistance of the aerial to the lower impedance line. This may be a double-wound transformer, or it may be the equivalent of an auto transformer and consist of tapping the feeding cable to a point on the tower at a considerable distance above its grounded end; such a device is often called shunt excitation.

If the current distribution is cophased and truly sinusoidal, then the radiation resistance referred to the middle point of a thin isolated wire has the values given in the table below.

TABLE 8.1

$h/\lambda$	$\frac{1}{2}$	$\frac{3}{4}$	0.9	1.0
Resistance in ohms	73.14	107	212	198.4

If the aerial stands perpendicular to a flat and perfectly conducting earth, then the values of both  $h/\lambda$  and of resistance, in the table above, should be halved.

For a given number of 'metre-amperes', or in other words, a given field strength in the equatorial plane, the output is substantially independent of the form of the current distribution. This fact must not lead to the erroneous idea that radiation resistance is independent of distribution. The radiation resistance is defined as the quotient of power output and the square of the current at a given point: for a given output this quotient will depend enormously on the magnitude of the current at the measuring point and this magnitude does depend on the shape of the distribution curve of given area. Thus if the distribution curve is a triangle, then the current at the middle point of the aerial is  $4/\pi$

times the current at that point for a sinusoid of the same area; accordingly the radiation resistance of a wire  $\frac{1}{2}\lambda$  long would then be

$$\left(\frac{\pi}{4}\right)^2 \times 73.14 = 45 \text{ ohms.}$$

For the very small effect of the distribution curve on the output see the end of § 1.22. Although 73.14 ohms is a well-known and classic value for the radiation resistance of an isolated half-wave aerial, the writer suspects it may not always be fulfilled in practice because it is so intimately related to a distribution which is precisely sinusoidal. The numerical relation between equatorial field and power output rests on a very firm basis and is almost inexorable, but the numerical values of the radiation resistance of real aerials are much less certain.

If the cophased distribution of current is spread uniformly round a tube of radius  $r_a$ , then equation (1.80 *a*) becomes†

$$\frac{cP}{4a^2} = \frac{2}{3} X_0^2 \left[ 1 - \frac{a^2}{5} \left( \frac{X_2}{X_0} + 2r_a^2 \right) + \dots \right].$$

If the length of the tube is  $\frac{1}{2}\lambda$  and the distribution is a sine curve the expression for  $P$  becomes

$$\frac{cP}{4a^2} = 0.6097 X_0^2 \left[ 1 - 16.2 \frac{r_a^2}{\lambda^2} \left( 1 - 6.35 \frac{r_a^2}{\lambda^2} + 22.2 \frac{r_a^4}{\lambda^4} + \dots \right) \right].$$

According to this the output will be reduced by less than 4 per cent. so long as the radius does not exceed  $\frac{1}{20}\lambda$ : the radiation resistance is 60 ohms when  $r_a/\lambda = \frac{1}{8}$ .

### 8.3. The resonant length and the $Q$ of a half-wave aerial

If a thin rod is parallel to the electric vector of a field there is some length at which the induced current will be a maximum and this can properly be called the resonant length: it is not far from  $\frac{1}{2}\lambda$ . The exact length is not of much practical interest because such a system does not provide for making use of the induced current. To make use of the current the rod must be broken to insert a resistance either directly or at the end of a cable. Once this is done a P.D. must exist between the faces of the broken end, and the precise frequency of resonance must depend on the shape and area of the said ends. Thus the practical problem has ceased to be a universal one and we are no longer considering the resonance of an aerial, *per se*, but of a particular aerial with its particular inevitable attachments. For this reason the search for a precise

† For further terms of this series see *Journ. I.E.E.* 88, Part 3 (1941), p. 53, equation (15).

mathematical solution seems somewhat pedagogic: the same remark applies to finding precisely the current distribution.

Consider the problem of a thin uniform rod, of length near  $\frac{1}{2}\lambda$  parallel to the electric field. Fig. 8.1 shows that a sinusoidal distribution of current does not produce a constant value of  $E_P$  along the rod, and consideration will show that this cannot result from any distribution even vaguely resembling a sinusoid. The current induced by the field must produce a uniform electric field all along the rod, equal and opposite to the inducing field. Hence it follows the field cannot induce a current which is cophased along the length: any attempt at a solution must provide for two current distributions in time quadrature. Thus it certainly is impossible for the current to be cophased in the reception problem, and probably this is also true of the transmission problem, though it does not seem possible to prove it by a reciprocal theorem. In order that current shall flow in a transmitting aerial there must be an electric field in phase with it. At any point, such field will be provided dominantly by a surface charge of electricity in phase with that current, and so demands two current distributions in time quadrature: it is not obviously necessary that the 'back e.m.f.' of radiation should be constant along the length. Our expressions for output are correct and general for a cophased current distribution; but if there are two quadrature distributions, the quadrature field of the quadrature distribution will do work on the inphase component of current and vice versa; thus there is mutual work between the two distributions and thus (1.80a) will not be correct for one distribution in the presence of the other. An expression corresponding to (1.80a) can be found for  $E_Q$ , the quadrature component of field due to any cophased distribution: it is given in § 15, equation 43, of *Journ. I.E.E.*, loc. cit. Evaluation from it shows that  $E_Q$  is not zero at every point of a rod of length  $\frac{1}{2}\lambda$  carrying a cophased sinoidal distribution of current: there is everywhere a small residue whose sense is such as to give the aerial an inductive reactance. This suggests that the resonant length is less than  $\frac{1}{2}\lambda$ . It is difficult to discuss this problem quantitatively without reproducing a mass of computation which is not sufficiently sound in principle to justify permanent record. In deriving a series expression for  $E_Q$  corresponding to equation (1.80) for  $E_P$  one series arises from delayed vector potential and a second series arises from delayed scalar potential of charges: in each of these two series the terms alternate in sign, and the first term in each is the expression which would result if the vector or scalar potential had been evaluated

without retardation. Since in each case the second term is negative, this shows that the effective capacitance increases and inductance decreases with a small increase of frequency above zero. Accordingly it is logical to regard the second term in the contribution to  $E_Q$  which arises from the vector potential as an inductive effect.† And accordingly to regard the ‘inductive field’ at any point along the aerial as consisting of the 1st, 3rd, 5th, etc., terms of the contribution to  $E_Q$  arising from  $[A]$  together with the 2nd, 4th, etc., terms arising from  $[dV/dx]$ . With this convention it can be shown that on a wire of radius  $r_a$  and length  $\frac{1}{2}\lambda$ , bearing a sinoidal distribution of cophased current, the quantity  $-cE_Q/2a$  has the values  $(\log \lambda/2r_a - 0.06)$ ,  $1/\sqrt{2}\{\log(\lambda/2r_a) + 0.6\}$ , and 1.6 at the middle point, at the two quarter points, and at the two tips respectively. Equation (1.23) shows that at the surface of a filament

$$-\frac{cE_Q}{2a} = -\frac{1}{2}\pi Y_0(ar_a) = -\left(\log \frac{\pi r_a}{\lambda} + \gamma\right) = \left(\log \frac{\lambda}{2r_a} - 1.05\right).$$

Comparison shows the expressions we have just given for  $E_Q$  are approximately equal to the reactance of an infinite filament multiplied by the current at the point considered, save at the tips where the current is zero and  $E_Q$  is not zero. To a first approximation the wire behaves as though it had a constant inductance per unit length. To find the apparent input reactance  $X$  we must evaluate  $\int E_Q i dx$  and divide it by  $I^2$ . Using the value of  $E_Q$  we have found, for the mid-point tips and quarter points, we estimate that  $X = 30\pi\{\log(\lambda/2r_a) + 0.32\}$  ohms. Since the radiation resistance is 73 ohms this gives

$$Q = 1.3\left(\log \frac{\lambda}{2r_a} + 0.32\right),$$

whence  $Q = 12.6$ ,  $9.4$ , or  $6.4$  according as  $\lambda/2r_a = 10^4$ ,  $10^3$ , or  $10^2$ . If a similar calculation is performed for a triangular (vice sinoidal) distribution of current it will be found that  $Q = 1.39\{\log(\lambda/2r_a) + 0.39\}$ , giving  $Q = 13.4$ ,  $10.2$ , or  $6.9$  according as  $\lambda/2r_a = 10^4$ ,  $10^3$ , or  $10^2$ . This shows the calculation is insensitive to the shape of the current distribution, and thus it seems the  $Q$  of a half-wave aerial must be near 6.5 if its diameter is about 2 per cent. of its length. The  $Q$  is very small compared with the values commonly met with in concentrated circuits: thus the tuning should be very blunt and this accords with common experience. The phase angle is likely to be about  $45^\circ$  if the frequency is  $7\frac{1}{2}$  per cent. off tune.

† For a fuller discussion of this principle see *Radio Frequency Measurements*, p. 27, and *Principles of Electromagnetism*, p. 268.

When the total length is  $\frac{1}{2}\lambda$ , then evaluation has shown that  $E_Q$  is not zero at the middle of the aerial but has there a residue approximately equal to  $E_P$  and has the sense corresponding to inductive reactance. Hence the phase angle should then be near  $45^\circ$  lagging and, as we have just seen, this corresponds to a frequency about 7 per cent. off tune. Hence we suggest the natural wavelength of a straight thin isolated rod is about 7 per cent. more than twice its physical length. In the early days of the century H. M. Macdonald attempted to calculate the natural wavelength of a rod and estimated it at 2.53 times the physical length. Experimental work by R. M. Wilmotte† suggests the ratio 2.1, our estimate is 2.14. This ratio must depend slightly on the ratio of length to diameter and on the shape of the rod near its tips. Resonance will necessarily be very blunt, therefore the precise length for resonance is of little practical importance or scientific interest.

We have seen the current distribution cannot be cophased throughout the length. Divide the distribution into two components, one in phase with the current at the mid-point of the length and one in quadrature thereto. Then, by definition, the second distribution will have zero value at the middle point; and zero value at each tip, by physical necessity. It may be likened to the dominant distribution on a whole wave aerial but compressed into half a wavelength. Its presence will have most effect on the R.M.S. distribution of current near the quarter points of the length, hence there is *prima facie* reason for supposing the R.M.S. distribution will be rather fuller than a sinusoid and more nearly conforming to a parabola. If the aerial is transmitting, then we may regard this second, and comparatively small, distribution as producing (by means of its own  $E_Q$ ) the distribution of  $E_P$  demanded by the output from the first distribution. On this supposition the writer computes that the fractional value of the quadrature component is 36 per cent. Then the R.M.S. current at various points along the length would be as shown in the table below, the third row of which shows the value the current would have if it were everywhere cophased and distributed sinusoidally.

TABLE 8.2

Distance from middle point	0	$\frac{1}{4}$	$\frac{1}{2}$	$\frac{3}{4}$	1
Relative magnitude of current	1	0.92	0.80	0.59	0
$\cos y$	1	0.87	0.71	0.5	0

† See *Journ. I.E.E.* 46 (1928), 617.



Consideration by Poynting's theorem shows that the total output of power will be the same as the sum of the powers which would be radiated if each component existed alone (compare also § 2.22, p. 117), though the output of one component will be enhanced while the other is reduced by the simultaneous existence of the two. Since we know the output depends dominantly on  $X_0$ , and little on its shape, we thus see the total output will be  $1 + (0.36)^2 = 1.13$  times what it would be if the quadrature component did not exist. We have also reason to expect that resonance occurs when the length is about 7 per cent. less than  $\frac{1}{2}\lambda$ , and this would make the resistance about 14 per cent. less than 73 ohms. Thus it seems likely the radiation resistance at resonance is very near 73 ohms, notwithstanding that the resonant length is appreciably less than  $\frac{1}{2}\lambda$ .

This problem should be investigated more thoroughly by combination of experiment and analysis. This has not yet been done, partly from lack of precise understanding of the factors involved and partly from lack of development of experimental technique. The writer thinks it could be done in the following manner. A straight thin tube some inch or so in diameter should be supported vertically by the least practicable amount of stays. It must be supported just clear of a copper gauze mat whose side is at least 12 ft. Then the impedance between the foot of the tube and the mat must be measured as a function of wavelength over a range of about  $\pm 20$  per cent. from four times the length of the tube. The inevitable leads between the 'aerial terminals' and the measuring gear provide a 'transformer action' which cannot be allowed for with certainty: therefore  $\lambda$  must be long enough to make the effect negligible. The writer has had considerable experience in this matter and considers it is impracticable for  $\lambda$  to be less than 3 m. if the measurements are to be independent of the short, but inevitable, connecting leads: he would advise the rod should not be shorter than one metre. Suppose it has this length and that the magnitude and phase angle of the impedance is measured over a range of some  $\pm 20$  per cent. from 4 m. The distribution of mean square current along the rod must then be explored by measuring the current induced in a small loop placed close to the rod and at various stations along it. The distribution curve, obtained in this manner, will certainly not differ much from half a sinusoid and the whole purpose of the experiment is to assess the discrepancy. It follows, after reduction, from (1.80 a) that if the distribution is fuller than a sine curve the radiation resistance must exceed 73 ohms when the length of the rod is  $\frac{1}{2}\lambda$ . It is essential

to correlate measured values of resistance with observed distribution curves. If the bona fides of the measurement is upheld by finding that the resistance does depend on the distribution curve in the general manner in which it must depend on it, then it should be possible, on close consideration, to estimate approximately the phase distribution. If these tests are performed with rods of length say, 1, 2, or 3 metres, it ought to be possible to cross-check the measurements, if they are valid. This should suffice to outline the procedure, an essential feature of which is correlation of radiation resistance and current distribution.

#### 8.4. Brief survey of refined analytical solution

A very recondite solution for a straight cylindrical wire was published by E. Hallen in the *Nora Acta Uppsala*, in 1938: by means of an integral equation he derived an expression for the current distribution appropriate to the cylindrical conductor. He defined a parameter  $\Omega \equiv 2 \log(2l/r_a)$ , where  $2l$  and  $2r_a$  are the length and diameter of the wire respectively. We have arrived at this parameter in the last section, in the form  $\log \lambda/2r_a$  for the case where  $2l = \frac{1}{2}\lambda$ . Hallen derived the various parameters of the aerial in a series of inverse powers of  $\Omega$ . Hallen's work has been continued, extended, and more fully evaluated by C. J. Bouwkamp,<sup>†</sup> whose results are well summarized by the following table, taken from his paper, and which relate to an aerial in the conditions when the reactive component of its impedance is zero.

TABLE 8.3

$2l/r_a$	.	.	.	150	1800	22000	
$\Omega$	.	.	.	10	15	20	
$4l/\lambda$	.	.	.	0.944	0.964	0.976	$\frac{1}{2}\lambda$ aerial
$(\lambda - 4l)/\lambda$	.	.	.	5.6%	3.6%	2.4%	
Resistance in ohms				60.4	67.7	70.5	

$2l/\lambda$	.	.	.	0.87	0.928	0.948	} $\lambda$ aerial
$(\lambda - 2l)/\lambda$	.	.	.	13%	7.2%	5.2%	
Resistance in ohms				1150	2900	5500	

According to our rough estimate the resonant length of an aerial in which  $2l/r_a = 100$  was 7 per cent. less than half the wavelength; this is in reasonable accord with Bouwkamp's value of 5.6 per cent. for an aerial in which  $2l/r_a = 150$ . It is interesting to note that, according to the table, the 'end correction' is as much as 2.4 per cent. even when the ratio of length to diameter is  $11 \times 10^3$ . On the supposition of a

<sup>†</sup> *Physica*, 9, no. 7 (July 1942).

cophased sinusoidal distribution of current the radiation resistance is given by the expression  $R = 120k \tan^2(\pi l/\lambda)$ , where  $k$  is given by Fig. 8.6. According to this the resistance would be 64, 66.2, and 70.5 ohms when  $\Omega$  had the three values for which Bouwkamp calculates the resistance as 60.4, 67.7, and 70.5 ohms respectively. Following the arguments used in the last section, we should expect the resistance to exceed 64 ohms when  $4l/\lambda = 0.944$  because there is necessarily an output of work from the quadrature component of current. Therefore it is surprising that Bouwkamp's value (60.4 ohms) is less than 64 ohms, since we should have expected to find it greater than 64 ohms. It is to be regretted that Bouwkamp did not record a plot of the current distribution for  $\Omega = 10$ . Bouwkamp† refutes the statement by L. V. King‡ that the radiation resistance of an aerial is not the same when receiving as when transmitting. For very many years the present writer has recorded his expectation of the property stated categorically by L. V. King, and even now he suggests it would be well to regard this question as *sub judice*.

Ronald King and C. W. Harrison have extended Hallen's analysis to derive the distribution of current along a symmetrical centre-driven antenna,§ and they give many figures showing the distribution of the two components of current along aerials whose total length ranges between  $\frac{1}{2}\lambda$  and  $\frac{3}{2}\lambda$  and having  $\Omega = 10, 30$ , and  $\infty$ . It is difficult to discover their estimate of the resonant length, but according to their Fig. 21 the resistance is 57 ohms when  $4l/\lambda = 0.944$  and  $\Omega = 10$  and this is even less than Bouwkamp's value.

It does seem probable that the resistance at resonance of an isolated half-wave aerial is less than 73 ohms. However, the problem is not of much importance in practice, for the following reason. It is only when  $\lambda$  is less than, say, 4 m., that a simple unsupported rod is practicable, and in this range of  $\lambda$  a plurality of aerials is almost certain to be used. At long wavelengths, say  $\lambda > 50$  m., an isolated aerial is likely to be a tapered lattice-work tower and not a simple cylinder.

### 8.5. Aerials with a large capacitance roof

When it is impracticable to erect a mast as high as  $\frac{1}{4}\lambda$  it is common to spread a capacitance of large area between a succession of masts and to connect it to the ground through a 'down lead'. Then the current along the down lead is likely to be substantially constant in magnitude and phase. The currents in the roof do not contribute much to the

† Loc. cit., p. 622.

§ *Proc. Inst. Rad. Eng.* 31 (1943), 549.

‡ *Phil. Trans. Roy. Soc.* 1937, 381.

output because  $E_P$  along them tends to be neutralized by the oppositely directed image currents in the ground. The radiation resistance of an aerial with a flat L-shaped roof was calculated by G. W. Pierce.† It was also calculated by a different process by the present writer,‡ who generalized it for roofs in the form of a T or a cross. These general equations permit any particular case to be solved by appropriate evaluation from them. The currents in the roof do not contribute to the field strength in the equatorial plane and thus are useless for a direct ray service: but they do mean the output is greater than if they did not exist since they may enhance the field strength at high angles of elevation. Such increment of output can be much reduced by folding the roof wires back on themselves: the net effect of the roof wires will then be neutralized more completely than it would have been by the comparatively distant image currents, in the ground, of the unfolded wires. When the roof wires are folded it is likely their total length will need to exceed what it would be if they were not folded, and this effect will tend to introduce some 'diminishing returns' from the folding process. Folded roof aerials have been used with advantage in high-power broadcasting stations where it was impracticable to use a mast higher than, say,  $\frac{1}{8}\lambda$ . Full details of the relevant calculations and power gain values will be found in § 11 of the paper in the *Journ. I.E.E.* referred to already; also the calculation of the radiation resistance of an aerial in the form of an inverted cone, a disposition of historic interest since it is reminiscent of the famous Marconi transatlantic aerial erected in the early years of the century at Poldhu, Cornwall. It does not seem necessary to develop the analyses of roofed aerials in detail here: they all approximate closely to a doublet whose semi-height is the length of the uplead. The next approximations have been worked out fully and the appropriate references have been given. A point of great practical importance in all that work is to show that if  $X_0$  can be determined by an absolute measure of the field strength at a comparatively nearby point in the equatorial plane, then the total output of power is known with great certainty and precision. Thus it follows that an acceptance test of guaranteed output should be based on a measurement of field strength rather than of input current to the aerial. The input current is more difficult to measure in absolute terms (the writer is here thinking of wavelengths not less than, say, 300 m.) than the field strength and is not a direct measure of the output of power.

† See *Electric Oscillators and Electric Waves*, p. 434.

‡ See *Journ. I.E.E.*, loc. cit., Table 2 and equations (29-32).

### 8.6. Inductance and capacitance per unit length of an aerial

Many *ad hoc* attempts have been made in the past to analyse the performance of an aerial in terms of the equations of a transmission line. The transmission line is a two-dimensional problem, and the solution is specified to be such that the electric field has no component parallel to the conductors. In such circumstances two parameters emerge which happen to be the capacitance and the inductance per unit length of a line of infinite length carrying a static charge or steady current. The solution for a finite length is not obtainable save for the particular terminal condition of a conducting sheet perpendicular to the axis of the twin cable. The length of an aerial is not infinite, and it is obvious the field has a component parallel to the axis, hence the solution for the cable is not applicable and little more need be said.

Our rough analysis of the  $Q$  of a half-wave aerial showed that neither  $E_P$  nor  $E_Q$  was proportional to the current at the point considered, and this showed the parameters are not constants per unit length. Lengthy explanation cannot describe more clearly than has been done already why the line treatment is invalid and inapplicable, and it is senseless to develop a cumbersome analysis attempting to estimate the degree of approximation. An aerial is a distributed system whose input impedance can be inductive or capacitive. Various networks can be postulated which will simulate its input impedance approximately, but such have no important significance. The ladder network or cable must have characteristics which correspond in a rough-and-ready manner with an aerial, and if it is helpful to use them as a rough model, by all means let this be done, provided always the real aerial is not then compelled to possess by supposition, or faulty argument, parameters it does not possess. If a cable is used to provide a technique for rough calculation let its poor claim to such use be recognized. This is not to say that many technical articles which use the line equations for aerials are not very useful guides to the engineer seeking rough quantitative description: they do not help him appreciably to understand why the aerial behaves in the manner he finds it behaves.

## EXPERIMENTAL SECTION

### IX

#### GENERAL EXPERIMENTAL METHODS AND EQUIPMENT

**9.1.** In the previous chapters we have studied very thoroughly the behaviour of certain typical aerial systems which have been idealized, for the purpose of analysis, in ways which are unlikely to conflict severely with realizable aeriels. Thus we start by knowing a great deal about the way real aeriels will behave and our measurements will be directed to exploring the discrepancy between the behaviour of real and of idealized aeriels. This statement may perhaps sound as if the purpose of our measurements was purely academic and pedagogic, but that is far from being so. Our purpose is to explore the behaviour of a real aerial with all possible economy of effort, and that effort is economized to an enormous extent if we consistently set out to explore the discrepancy between the real and the idealized performances. If we work in that way it means we have thought out very carefully what we want to measure and we know, within comparatively narrow limits, what we ought to find. It is the antithesis of the procedure which starts off by hoping to recognize generalized behaviour if only sufficient experimental data are available. Every unused experimental result is a waste of time which usually could have been avoided by more forethought: but often the evil is not limited to a mere waste of time because the unused experiment may confuse the issue. It is the essence of a systematic and scientific approach that we should use experiment to provide the detail which we have been unable to calculate. Experiment should be required only for the final engineering adjustment of the aeriels which are to be built or have already been built. So much is known and understood about aeriels that the bulk of the development work can be, and should be, done on paper.

The first thing is to define the range of wavelength we intend to use: this range is from 10 to 100 cm., and on rare occasions, from 3 to 300 cm. The problem is both simpler and more restricted in the range 3 to 30 m. and then scarcely needs detailed description. The first essential tool is a valve generator: if the wavelength exceeds, say, 30 cm., then a pair of suitable triode valves can be used in 'push-pull'. If the wavelength is less than about 30 cm. it will be necessary to use a magnetron or clystron tube. Considerations of flexibility, reasonable portability, and expense usually impose severe restrictions on the output, and this is

likely to be less than 10 watts. Field work is usually hampered at some stage by lack of power, and therefore the experimenter should provide himself with as powerful a generator as he can obtain. The next essential is a wavemeter which is both light and easy to operate. The work has to be carried out in the field, often in cold, drizzle, and high wind, and therefore it is essential that all instruments shall be very easy to handle: otherwise they just would not be used. There are few occasions when it is important to know the wavelength closer than about  $\pm 2$  per cent., accordingly the wavemeter should have the simple character suited to such an order of accuracy. Avoid multirange wavemeters: provide several instruments each with a spectrum width of only about  $\pm 10$  per cent. and let each be direct reading on a circular dial. Down to about  $\lambda = 80$  cm. a combination of variable air condenser and suitable inductance is satisfactory. An instrument of this character having a range from 200 to 240 Mc/s is shown in Fig. 9.1, and this illustration serves to describe the general class of instrument which is suitable and which we have in mind. Beware of robbing the laboratory of some high-grade instrument suited for indoor use: such desecration will not be justified because the tool will not be suitable. An essential key to the great art of measurement is to provide instruments suited to each particular application: good work will not necessarily be done by providing the most refined instrument available. If good field work is to be done on aerials, then the experimenter must have the wit and energy to provide himself with tools suitable for the purpose. A small effort of common sense and a considerable effort of simple construction must not be avoided by the lazy process of indenting for the 'best that money can buy': such efforts very often are avoided and in consequence many have suffered misery and exasperation for months.

In the range of wavelength from 10 to 50 cm. some form of coaxial tube resonator is convenient and suitable, the wavelength being measured directly on a centimetre scale. A chamber consisting of two coaxial cylinders closed by flat metal disks at each end resonates when the length is  $\frac{1}{2}\lambda$ ; 'a trombone construction' based on this principle is essentially sound. If the chamber is open at one end, resonance occurs when the length of the inner cylinder is about  $\frac{1}{4}\lambda$ ; in practice this construction works very well, though it is a little less sound in technical principle than the first: the clearance between the two cylinders should be a small fraction of  $\lambda$ . Because the trombone has a linear scale one instrument will cover adequately the range 10 to 50 cm. In the range round 5 cm. a resonant cavity type of meter is likely to be most suitable.

The resonance condition of all three types is best indicated by means of a crystal detector and pivoted galvanometer, thereby avoiding the need for any power supply: now that reliable crystal detectors are obtainable commercially in the form of a replaceable capsule, there is no longer reason to be disinclined to use crystals.

The next requirement is a turn-table on which the aerial and reflector can be mounted. Its construction is a simple mechanical problem and need not be considered in detail here. It should be a wooden structure, and unless it is made very robustly it will be the cause of endless trouble and waste of time. The table-top should be some 5 or 6 ft. in diameter and strong enough to bear a couple of people standing on it. The underside should be provided with cupboards which are reasonably weatherproof and the generator can be housed in them.

The reciprocity theorems, developed in earlier chapters, show that the same polar diagram will be obtained if the aerial which is to be revolved on the turn-table is used as a transmitter or as a receiver. The writer has always used it as the transmitter. It is often desirable, even necessary, to change the position of the transmitter or the receiver relative to surrounding objects, such as trees, hedges, buildings, etc., which inevitably border all testing sites. The turn-table is a fixture on a concrete base and cannot be moved: the transmitter will involve a feeding-point from some A.C. supply and this is not readily moved about the site. Hence there is something to be said for combining the immovable and the difficult-to-move accessories: in other words, to use the revolving aerial as a transmitter and the fixed aerial as receiver. For convenience of writing we shall suppose this régime is adopted and then the receiver will mean the fixed aerial. The receiving aerial must be fitted with a thermocouple (or equivalent device) with leads connecting it to a galvanometer situated at the transmitting turn-table. Measurements will almost always be hampered by some lack of sensitivity, and therefore we must improve the power gain of the receiving aerial by furnishing it with some form of reflector. But increased sensitivity is not the only reason why the receiving aerial must be fitted with a reasonably directive reflector. The reflector is required to help shield the receiving aerial from fields re-radiated by objects, on the site, which are excited unintentionally by the transmitter. The illumination of such objects varies as the transmitter is revolved on its turn-table, and hence any field they reflect into the receiver is not a constant but is a function of the variable bearing of the turn-table: the more directive the receiving system the better, in every way. A Vee



reflector, of angle about  $60^\circ$ , is suitable for the receiver; the appropriate dimensions will depend on the wavelength, and the reader will be able to choose them when he has read the next chapter. Because occasions are bound to arise when it is desired to move the receiver to some other place on the site, it is wise to make the receiving reflector as light and portable as possible, consistent with its size, which is determined mainly by the wavelength. It must carry an aerial, about half a wavelength long, and the position of this aerial should be adjustable on the bisector of the Vee. The aerial proper must consist of two metal rods joined together by a sensitive thermocouple. To obtain the best sensitivity the aerial should be tuned and the couple should have a resistance equal to the radiation resistance of the aerial, when at a station of maximum gain for the Vee reflector in which it is to be used. But the true optimum is very blunt and usually the experimenter is justified in ignoring refinements and in using the most sensitive couple available to him. Vacuum couples are available having a heater whose resistance is 120 ohms and such that a current of 4 mA through them produces a steady current of  $240\ \mu\text{A}$  in a unipivot of resistance 10 ohms: such a couple is suitable for our purpose. The best position in the Vee for a given aerial and couple must be located by experiment: the optimum will be found to be very blunt. It is sensible to construct the aerial of two pieces of copper tube (say, about  $\frac{5}{16}$  in. diameter) which penetrate into a bakelite block to support them: the said block forming a box to contain and protect the thermocouple. Tubes are used for the aerial in order that they may be furnished with extension rods which telescope into them: thereby providing a means of tuning and of making one aerial suitable for a wavelength range of nearly two to one. If the ends of the tube are slit axially by a fine saw cut, some 2 cm. long, an adequate friction grip is provided for the extension rods. Fig. 9.2 is a photograph of such an aerial-cum-couple assembly and should serve to show the reader the character of apparatus we have in mind. It was made for measurements at  $\lambda = 125$  cm. but is serviceable down to about  $\lambda = 70$  cm. Experience will teach the reader that tuning is very blunt, and he will soon learn to regard the measuring aerial as a tool which does not require regular and nice adjustment. The measuring aerial should be robustly made and must be readily detachable from its reflector. Experimenters should be well drilled in the discipline of removing it every night from the reflector and on every occasion when work ceases for an hour or two: it should be the responsibility of one man to demount it and return it to the office every night. Then it will

never be left long exposed to inclement weather nor have to survive crashing with the reflector in a gale of wind. In the writer's experience much better service results from the use of a removable aerial in a light, even a flimsy, reflector than from an aerial built into a robust reflector. It may be tempting to build the whole apparatus in a form resembling what would be used in operational practice, on the plea that such aerials stand up satisfactorily to continuous exposure. They do, but they are also under continuous care and maintenance, and their fixings are gale-proof. As we shall sometimes need to move the receiver about the site its fixings will not be gale-proof, and if a collapse occurs a heavy reflector is likely to receive serious damage, whereas flimsy screens receive surprisingly little damage when capsized by the wind. If the undamaged aerial is carried out to the receiving reflector, then it is fairly certain work can always be started after only a few moments' delay and thus the blessing of security of operation is achieved: then we shall almost certainly be able to make use of an hour or two of fine weather, even after an interlude of some weeks.

Of the field apparatus, it is only the turn-table itself which demands robust construction, and much time will be wasted if it is not made properly.

All will wish to use a unipivot galvanometer with the thermocouple, but occasions are bound to arise when lack of power renders its sensitivity inadequate. Mirror galvanometers such as the 'Cambridge Spot Galvo' are amazingly robust and manageable for field work, and are vastly more sensitive than a unipivot: the lamp can be energized from the supply feeding the turn-table, but will require a small portable transformer to step down to 4 V (a 230-V supply to the lamp should not be tolerated or allowed on a galvanometer used in the field: danger from shock is serious in these conditions of use). Usually it is necessary to place the galvanometer in a box, to screen it from the wind. The use of a sensitive galvanometer is a simple and cheap way of enhancing the sensitivity of measurement. Workers are strongly advised to seek to improve the galvanometer as the first means of improving the overall sensitivity: they will find it is the easiest and cheapest thing to improve first. The galvanometer must be provided with a resistance box giving it a 1, 2, 5 range: this needs attention in construction because it must inevitably be associated with long leads, which have appreciable resistance, and users must be on the look-out to see these leads are not changed inadvertently.

Power is severely limited, and accordingly the distance between

transmitter and receiver should be as short as is consistent with obtaining the limiting form of the polar diagram. It is therefore important to understand clearly how to assess this shortest permissible distance. First refer to Fig. 3.40 which depicts the ideal pattern at various distances from the apex of a  $60^\circ$  Vee: it suggests that a distance of some  $60\lambda$  may be regarded as substantially infinite. The deciding factor is that the path difference between the various images and the receiver must be substantially the same as if the receiver were at infinity. It is a simple matter to assess the degree of approximation in any given case. It is a good working rule that the receiver should not be closer than  $50\lambda$  and seldom need be farther than  $100\lambda$  from the transmitter: it is very common to find much greater distances in use, and in general this denotes a lack of understanding of the problem.

A reader who has had no previous experience and is about to start on aerial measurements will be looking for direct guidance about the power he will require. If  $\lambda$  does not exceed one metre, then the available range of small transmitting valves is small and there will not be much choice in the generator, and the input to it will be about 30 W. Short-wave generators are inconvenient and inflexible things, and it will be difficult to get more than about 5 W into the transmitting aerial. With the class of generator that he is almost bound to be using the experimenter should obtain adequate results from a 100-ohm couple and single aerial (with reflector) at distances of some 60 or  $70\lambda$ , provided a 'spot galvanometer' is used. This dictum should give him confidence to make a start and begin to get his own personal experience, which he must gain for himself. He must learn to adjust the generator so as to get out of it all it can give, must satisfy himself that the long leads from the thermocouple to the galvanometer have not got so high a resistance as to be a dominating factor controlling the sensitivity of the galvanometer, and that the galvanometer has a coil of suitable resistance. If the galvanometer deflexions are still inadequate and it is unwise to reduce the distance between transmitter and receiver, then the problem of improving the gain of the receiving aerial must be faced; we shall suppose it is fitted with a Vee reflector. If the sides of the Vee are as large as can be tolerated (or as large as they need be for the wavelength), then a rough but systematic study must be made of the effect of moving the receiving aerial along the bisector when the angle of the Vee is, say,  $45^\circ$ ,  $60^\circ$ , and  $90^\circ$ : by such means an optimum will be found. If this will not suffice, then he may have to face the complication of

using several collinear half-wave aërials in the reflector. Then the thermocouple, hitherto placed at the middle of the single aerial, must be replaced by a coaxial cable and all such cables joined in parallel, through a suitable junction box, finally feeding current into a common thermocouple. If any real benefit is to be obtained this will involve an attempt to match the load to the line. The writer has used a receiver which had eight collinear half-wave aërials in parallel, feeding a couple. He was provided with the complete outfit and did not construct it: it served its purpose and that was all that mattered. But he is sceptical whether its behaviour was in fact much better than could have been obtained from a single aerial and a large Vee. He strongly advises against the use of more than one aerial until the experimenter is well versed in the art.

Field work is essentially more exacting than work in the comfort of a laboratory, and therefore simplicity of apparatus is an essential requisite of successful and reliable work. If improvement by a factor of about two will suffice, then some extra attention to generator and galvanometer will probably surmount the difficulty. If a much larger gain is required, then the design of the whole receiving aerial will require close consideration, and such a major problem will be better understood when the ensuing chapters have been read: our concern now is to get the reader started on experimental work.

The degree of sensitivity in respect of length of aerial and of its position can be assessed, in a general manner, from the following example. The receiving aerial was that shown in Fig. 9.2; its length was adjustable and the heater (of the thermocouple) had a resistance of 110 ohms. It was associated with a 90° reflector (whose screens were 5 ft. high and 5 ft. wide) and could be moved along the bisector: the wavelength was 128 cm. (i.e. about 4 ft.). The following table records the reading of the galvanometer at five positions of the aerial and for five lengths of aerial.

TABLE 9.1

<i>Length of aerial</i>	<i>Distance of aerial from apex in cm.</i>				
	80	70	60	50	40
	<i>Deflection of galvanometer</i>				
63 cm. . .	13.3	13.3	11.2	8.3	5.7
59 . . .	12.2	12.0	11.7	10.5	7.2
55 . . .	11.4	12.1	12.8	10.9	7.6
51 . . .	8.5	10.3	10.8	10.6	6.7
47 . . .	7.0	8.1	8.6	6.7	5.2

When the length of the aerial is  $\frac{1}{2}\lambda$  (63 cm.) the galvanometer deflexion passes through a blunt maximum when the aerial is about 75 cm. from the apex: when the length is 55 cm. (or less) the blunt optimum occurs when the distance is near 60 cm. As a first guess we might expect the aerial ought to be  $\frac{1}{2}\lambda$  long (for then it will be tuned) and ought to be about  $\frac{1}{2}\lambda$  from the apex of a station for maximum gain. Suppose we choose  $R = 60$  cm. ( $R/\lambda = 0.47$ ): then experiments with this aerial and couple showed the current is greatest when the length of the aerial is 55 cm. ( $0.43\lambda$ ) and is then 1.14 times as great as when the length was  $0.5\lambda$ . On the other hand, if we choose  $R = 70$  cm. ( $R/\lambda = 0.54$ ), then the current is greatest when the length is  $\frac{1}{2}\lambda$ . What really matters is to recognize that the adjustment for optimum is very blunt indeed: provided the aerial is about  $\frac{1}{2}\lambda$  long and about  $\frac{1}{2}\lambda$  from the apex, then nice adjustment cannot do more than make a slight increase of deflexion; in practice this means that nice adjustment is not worth while.

Reference to Fig. 4.2 shows the radiation resistance is 125 ohms when  $R/\lambda = \frac{1}{2}$ , and thus we find that the resistance of the heater then in use happens to be very near the optimum value.

An alternative arrangement is to replace the thermocouple by a tuned circuit, across which is connected a diode valve (such as B.T.H. D1). It was found that the sensitivity of a particular assembly of this kind was 1.5 times that of the couple, when using the same galvanometer for either system and in circumstances when the response of the diode was proportional to the square of the voltage.

The inexperienced worker is very liable to think that it is no easy undertaking to measure the polar diagram of an aerial and reflector at wavelengths less than one metre: but if so he is wrong, for it is a very simple process. It is very easy to get frightened by observing that the galvanometer reading fluctuates wildly when he moves about in front of the aerial, and to suppose his observations will be dependent on all kinds of random circumstances. Ordinary gauze screens are very perfect reflectors, and provided he will keep behind them his presence will have no effect, because he is perfectly screened by the reflector. Aerials may suitably be described as very good-tempered things having great powers of ignoring imperfect apparatus. After a lifetime of experience on high-frequency measurements the writer knows of none so easy to make as on aerials in the range of wavelength between 50 and 100 cm.: almost all the familiar troubles of high-frequency measurements seem to be absent. He regards the testing of aerials in much the same light

as he regards the testing of a dynamo: it is extremely simple provided you understand what you are doing and what you are trying to find out.

The novice is almost sure to expect that reliable results cannot be obtained unless he can use a clear, open, and level site, and the more his mind dwells on geometrical optics the more pessimistic he will become. Because we are testing highly directional aërials and using a highly directional receiver there is very little trouble from the site. If we are testing an aerial which is almost omni-directional, then, and only then, is the site important. The writer has had long experience of working in a large level open field, and he has also done even more work in the midst of the Trafford Park works of Messrs. Metropolitan Vickers Electric Co., Ltd., at Manchester: he did not find that work in the factory was more difficult than work in the open fields. If the reader will have the courage to use the flat roof of a building he will be well repaid by saving hours of time travelling to and from a distant field, remote from his workshop and laboratory.

It is not necessary to write more about a very simple process: let the reader gather his own personal skill and experience.

## 9.2. The monitor aerial

In the last section we were thinking mainly of the apparatus for plotting polar diagrams, and then the only requirement of the receiving aerial was that it should give as much response as possible to a given field strength: our concern was with relative and not with absolute values. But there are occasions when it is desired to use an aerial to make an absolute measure of a field strength or to make measurements which shall be relatively correct over a very long period of time. Thus it may be required to make an absolute measure of the power radiated by an aerial or at any rate to compare the powers radiated from it from day to day or week to week. At long wavelengths this second requirement would be met by an aerial ammeter; but a straightforward ammeter is not practicable at the wavelengths and powers we have in mind, for reasons which should be obvious to the reader but will not be detailed here. It is common practice to use a small aerial, close to the main aerial, as the equivalent of an ammeter: such an aerial is often called a 'monitor aerial' and the output is said to be monitored by it.

An early exponent of the use of a monitor aerial was Dr. J. S. McPetrie,<sup>†</sup> who developed it as a means of making an absolute measure

<sup>†</sup> See *Wireless Engineer*, 16 (1939), 342.

of field strength and therefrom inferred the power output of the aerial which was being monitored. The small current induced in the monitor aerial is measured by a fine wire thermocouple: since the heater wire of the thermocouple is very thin, the frequency error of the instrument can be made negligible. The monitor aerial plays a part equivalent to the ammeter-transformer of low-frequency practice, and our problem now is to calculate the equivalent of the transformation ratio.

(a) *The impedance of a short thin aerial*

The diameter of the monitor aerial will be supposed very small compared with  $\lambda$  and then the field will be sensibly cophased and constant all over its cross-section: the field is supposed to be constant along the length of the monitor. First we suppose the field is static and we attempt to calculate the total charge on each half of the monitor. If an ellipsoid of revolution is placed with its long axis parallel to a uniform field, then there will be positive charge over the whole of one half and negative over the whole of the other. It is well known that the charge on the surface of a cross-section slice of given thickness varies directly as the distance of that slice from the centre of the ellipsoid. If  $Q$  is the total charge on one half and  $E$  the intensity of the uniform field in which the ellipsoid is situated, then it is known that†

$$\frac{Q}{E} = \frac{\pi b^2}{N}, \quad (9.1)$$

where 
$$N = \frac{4}{3} \frac{b^2}{a^2} \left( 1 + \frac{3}{5} e^2 + \frac{3}{7} e^4 + \frac{3}{9} e^6 + \dots \right), \quad (9.2)$$

in which 
$$e^2 \equiv 1 - \frac{b^2}{a^2}.$$

When  $a \gg b$ , then 
$$N \doteq 4\pi \frac{b^2}{a^2} \left( \log \frac{2a}{b} - 1 \right). \quad (9.3)$$

If  $E$  fluctuates harmonically and very slowly, then  $Q$  will alternate, and thus an alternating current  $I$  will flow across the equatorial plane and its value will be  $I = pQ$ , and thus

$$I = \frac{p\pi b^2 E}{N} = \frac{p\pi b^2 (2aE)}{2Na} = \frac{p\pi b^2 V}{2Na}, \quad (9.4)$$

where  $V$  is the voltage from end to end of the ellipsoid. Thus the

† See, for example, *Magnetic Induction in Iron*, Sir J. A. Ewing, p. 25.

quantity  $\pi b^2/2Na \equiv C$  is the effective capacitance of the system. When  $a/b \gg 1$ , then

$$C \doteq \frac{a}{8\{\log(a/b) - 0.3\}}, \quad (9.5)$$

and

$$Z = \frac{1}{pC} = \frac{2Na}{\pi b^2 p} = \frac{30Na}{\pi^2 b^2} \text{ ohms} \quad (9.6)$$

$$= \frac{120}{\pi a} \left( \log \frac{a}{b} - 0.3 \right) \text{ ohms, when } \frac{a}{b} \gg 1.$$

It will be seen shortly that a very desirable length for a monitor aerial is  $\frac{1}{4}\lambda$ , which corresponds to  $a = \frac{1}{8}\lambda$ . Some values of  $Z$ , for various values of  $a/b$ , are shown collected in Table 9.2 below for a monitor whose length  $l$  is equal to  $\frac{1}{4}\lambda$ : it follows from (9.5) that the impedance is inversely proportional to the length, and accordingly if this length is less than  $\frac{1}{4}\lambda$  then the values in Table 9.2 must be increased in the appropriate proportion.

TABLE 9.2

$a/b$	1	2	4	10	30	100	500	1,000
$Z$ ohms	102	205	256	610	960	1,300	1,800	2,000

Since the diameter,  $2b$ , is likely to be of the order of 1 per cent. of the length  $l$ , it follows from this table that the impedance of a monitor of length  $\frac{1}{4}\lambda$  is likely to be between 1,000 and 1,500 ohms, and in such circumstances  $I \doteq \lambda E/4000$ : in general for a monitor of length  $l$ ,  $I \doteq El^2/250\lambda$ . This expression ignores the reduction of effective impedance due to the inductive impedance of the monitor, an effect which must become very important as resonance is approached. Rather than attempting to estimate this inductive effect we shall appeal to experiment, which shows that inductance is only just becoming appreciable when  $l = \frac{1}{4}\lambda$ .

A complete solution of this problem will be found in *Currents in Aerials and High Frequency Networks*, F. B. Pidduck (Clarendon Press), p. 36, § 13. Pidduck evaluates the case where the length is verging on  $\frac{1}{2}\lambda$  and also the case where  $l \ll \lambda$ . In the second case his equation (80) gives the expression  $I = El^2/380\lambda$  for a wire in which  $a/b = 500$ . In such circumstances Table 9.2 shows that  $Z = 1,800$  ohms and thus we should have given  $I = El^2/450\lambda$ . Thus there is a discrepancy of 18 per cent. between our approach from an elongated ellipsoid and Pidduck's evaluation for a cylindrical wire: it is perhaps to be expected that the



current induced in a long cylinder would be greater than in a long ellipsoid. McPetrie (loc. cit.) proposes the formula

$$I = \frac{Ea}{Z_0} \tan \frac{2\pi a}{\lambda},$$

where, he says, ' $Z_0$  represents the characteristic impedance of the aerial and is in the neighbourhood of 500 ohms'. If  $a/\lambda \ll 1$ , McPetrie's formula becomes  $I = 2\pi Ea^2/500\lambda = Fl^2/320\lambda$  and thus corresponds with an ellipsoid in which  $a/b = 100$ : the three methods of approach give reasonably concordant results. There is not much sense in arguing too closely about these results because the current must be measured by a thermocouple placed at the mid-point of the length and this involves cutting the aerial into two halves and thereby making it less like an ellipsoid or long cylinder. It is true that the ohmic resistance of the couple will be small compared with the impedance of the aerial and thus it will, *per se*, reduce the current by a negligible amount, but it does not necessarily follow that cutting the aerial into two portions will have a negligible effect on its reactance. Presumably it is a cardinal feature of McPetrie's concept of a monitor aerial that the resistance of the measuring instrument plays a negligible part in the total impedance, and this will obtain if the monitor is short.

We will now describe some experiments which were designed to investigate the dependence of the induced current on the length and on the diameter of a monitor aerial, which was placed parallel to an electric field of constant intensity. The monitor aerial consisted of two equal lengths of brass rod connected by a thermojunction whose heater had a resistance of 15 ohms and whose sensitivity was such that a current of 65 mA through it produced an e.m.f. of 24 mV in the couple, the response obeying a square law. The thermocouple was housed in a bakelite block which served to support a pair of tapped sockets into which the two pieces of rod were screwed. The measurements were made at, or near, a wavelength of 125 cm. The said bakelite block was 7.5 cm. long in the direction of the aerial, 5 cm. wide, and 4 cm. thick: the block had a diamond-shaped profile so as to reduce the volume of dielectric as much as was compatible with mechanical strength and fulfilment of its functions. The aerial rods were pieces of brass wire which were  $\frac{1}{16}$ ,  $\frac{1}{8}$ ,  $\frac{1}{4}$ , or  $\frac{3}{8}$  in. diameter. The source of field was a half-wave aerial which was distant  $\frac{1}{2}\lambda$  from the apex of a  $90^\circ$  reflector: the monitor was placed on the bisector of the  $90^\circ$  Vee and was distant  $\frac{1}{2}\lambda$  from the half-wave aerial, and thus it was distant  $\lambda$  from

the apex of the Vee. Throughout the duration of these experiments the field strength was observed and recorded at a very distant point, thereby monitoring the output of the half-wave aerial and disclosing any temporal changes in the field incident on the monitor aerial, whose characteristics were being studied. The procedure was as follows: The response of the thermocouple was recorded when the tip-to-tip length of the monitor aerial of given diameter was 34 cm. (i.e.  $0.274\lambda$ ). The two rods were then unscrewed from the bakelite block and each of them was reduced in length by 1 cm. They were then screwed once more into the bakelite block and the new response of the thermocouple was observed, having previously ascertained that the field at the distant point had its correct and standard value. The process of shortening was repeated, centimetre by centimetre, nine times: then the tip-to-tip length of the monitor had been reduced to 18 cm. (i.e.  $0.145\lambda$ ) of which the central length of 7.5 cm. was occupied by the bakelite block, which housed the thermocouple. This series of measurements was performed on each diameter of rod, and there were four of them.

The results are recorded in Fig. 9.3 in which the square root of the induced current is plotted against the tip-to-tip length of the monitor: each of the four curves in this figure relates to a rod of given diameter; it may be seen that each curve is asymptotic to a straight line through the origin. According to our simple analysis  $I^{\frac{1}{2}}$  should vary as  $l$ , when  $l/\lambda$  is very small. Fig. 9.3 shows that this relationship is substantially valid even up to  $l/\lambda = \frac{1}{4}$ : with the rod of largest diameter the current is then 16 per cent. greater than if  $I$  had continued to vary as  $l^2$ , and with the smallest diameter the increment of current is then 5 per cent. The experiments recorded in Fig. 9.3 show that increasing the diameter increases the induced current: a sixfold increase of diameter increases the current in the ratio 1.44. Taking a general view of these experiments, they may be said to show that the current is very insensitive to the diameter, and this is in accordance with Table 9.2, and increases as the square of the length up to a value of  $l/\lambda$  which is nearly equal to  $\frac{1}{4}$ . It is to be expected that the current should tend to increase more rapidly than  $l^2$  because of the increasing importance of the inductive reactance, an effect which is ignored in (9.5). In the experiments described here it is likely that a substantial fraction of this inductive effect is concentrated in the fine wire of the heater of the thermocouple. It should also be noted that (9.4) and (9.6) predict that  $I$  should increase less rapidly than  $l^2$  because the factor  $N$  increases as  $a/b$  increases: but Table 9.2 shows that  $N$  changes very slowly with  $a/b$

and hence this effect should not be important in the range covered by Fig. 9.3, since in it the range of  $a/b$  is only from 18 to 200. If the monitor could be represented correctly by an ellipsoid, then

$$I\{\log(a/b) - 0.3\}$$

would be constant when  $a$  is constant and  $b$  is variable. We can use Fig. 9.3 to examine whether this formula is substantially correct: we

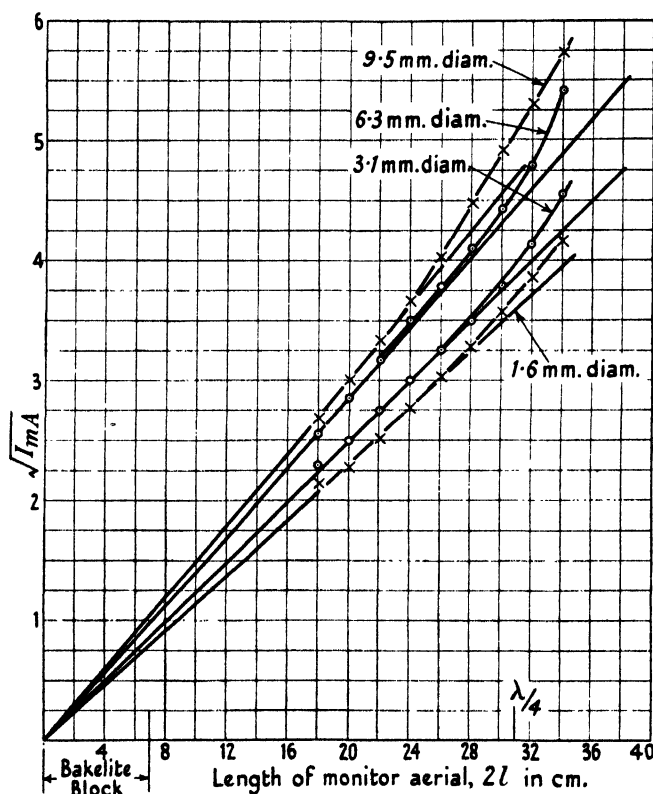


FIG. 9.3. Curves showing relation between induced current and length of monitor aerial and its dependence on the diameter of the aerial rod.

will choose  $l = 30$  cm. and use the values of  $I^{\dagger}$  given by the straight lines, thus removing the effect attributed to inductive reactance. The results of the analysis are collected in Table 9.3 below, and they show that  $I$  does vary with  $b$  in a manner very similar to that appropriate to an ellipsoid.

The last column records an attempt to find an empirical formula which represents the observed results more closely.

TABLE 9.3

$b$ (mm.)	$I$ (mA)	$a/b$	$\log(a/b) - 0.3$	$I\{\log(a/b) - 0.3\}$	$I\{\log(a/b) - 1\}$
4.75	21	32	3.15	66	51
3.15	18.5	48	3.55	66	52
1.55	14	94	4.25	60	50
0.8	12	187	4.95	60	51

These experiments cannot serve to find the absolute value of the impedance of a monitor. But they do serve to show that we need have no anxiety about the inductive impedance (even when a thermocouple is in series with the monitor) so long as  $l/\lambda$  is just less than  $\frac{1}{4}$ : in general we shall desire to make the monitor as long as we dare to do and hence we are now likely to make its length verging on  $\frac{1}{4}\lambda$ . We see that the current increases very slowly with the diameter and in substantially the manner we expect, and it appears that a suitable value for the ratio of length to diameter is about 100. Having regard to the general accordance of the ellipsoid approach, McPetrie's approach, and Pidduck's approach, it seems likely that  $I \doteq EI/1300$  for a monitor whose length is  $\frac{1}{4}\lambda$  and whose diameter is 1 per cent. of its length. It seems likely that this formula is correct to closer than 10 per cent. If  $\lambda$  is measured in centimetres, then the formula becomes

$$E_{\text{volts/cm.}} = \frac{5.2}{\lambda_{\text{cm.}}} I_{\text{mA}},$$

since it applies to a monitor whose length is  $\frac{1}{4}\lambda$ .

Fig. 9.4 shows the relation between induced current and length of a monitor (diameter 3.2 mm.,  $\lambda = 125$  cm.) in the range of length between about  $\frac{1}{4}\lambda$  and  $\frac{1}{2}\lambda$ . The current passes through its maximum when  $l/\lambda = 0.45$ : thus resonance occurs at a length which is substantially less than  $\frac{1}{2}\lambda$ , and this is probably due to the concentrated inductance of the thermocouple heater, situated at the middle of the length. The current at resonance will depend appreciably on the resistance of the said heater: in this experiment the said resistance was 15 ohms and the radiation resistance was presumably in the neighbourhood of 70 ohms. It should be noticed that the resonance is very blunt: the current being greater than half the resonance value so long as the length is within  $\pm 12$  per cent. of the resonant length. This is in general accordance with the small values of  $Q$  that we estimated in Chapter VIII. Fig. 9.4 does not merit close analysis because it relates to a monitor which has a particular thermocouple in it and we should expect the curve to be

altered appreciably if the couple were replaced by another couple of different construction: it is, however, of considerable practical interest since it portrays the behaviour of an aerial which is loaded with a concentrated resistance at its middle point. It is, however, instructive to compare Fig. 9.4 with Fig. 13 on p. 40 of Pidduck (*loc. cit.*) which shows  $I^2$  as a function of  $l$  for a rod whose length is 500 diameters,

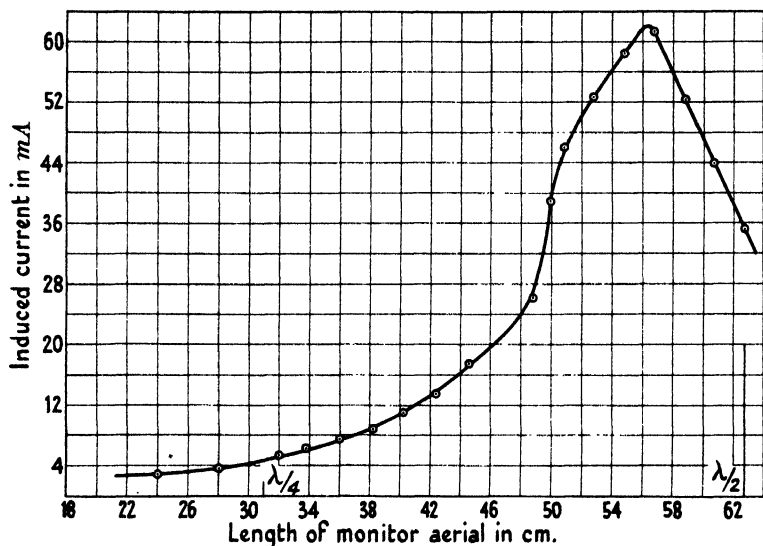


FIG. 9.4. Monitor aerial, made of  $\frac{1}{8}$ " diameter rod, in constant field strength at  $\lambda = 125$  cm.: dependence of induced current on length of aerial.

both when the rod is a perfect conductor and also when it has a resistance of  $50\Omega$  at its middle point.

We have been studying the design of a monitor aerial for use in circumstances when it is required to infer the value of the incident electric field from the measured value of the induced current. But the reader should guard against the false impression that every aerial used for measurement purposes ought to comply with the conditions we have laid down. Thus in the first section of this chapter we discussed in outline the receiving system required for testing the performance of an array or a reflector. Then the absolute value of the field strength is not required, only the relative values on various bearings from the axis of the transmitting array. In such measurements it is permissible to use a measuring aerial much longer than  $\frac{1}{4}\lambda$  and in general to make use of a close approach to resonance. Thus reference to Fig. 9.4 will show there is a sixteen-fold increase of induced current as the length is

increased from  $\frac{1}{4}\lambda$  to resonance, and this means an increase of sensitivity of enormous practical value.

A thermocouple must be used when absolute measurements are required, but when only relative values are needed it may be convenient to replace the couple by a diode. Then one method, which has been used by the writer, is to replace the thermocouple by a carbon rod resistor ( $\frac{1}{2}$  W type) having a resistance of about 60  $\Omega$ . The P.D. developed across this resistor is applied to a small diode tube (such as B.T.H. D1) having a suitable load resistance and smoothing condenser. It is of course necessary to make a relative calibration (at low frequency) of the scale of the indicating instrument-diode combination. By appropriate choice of the load resistance the response can be made substantially linear, and usually this is more convenient than the square law of the couple. For a given galvanometer, the response from a D1 diode, used in the way described, is about the same as the response from a thermojunction having a heater of resistance about 50  $\Omega$ . Alternatively, the diode may be replaced by a capsule-type crystal rectifier (such as were developed about 1942). But here a word of warning is required: such crystals may give a response which increases more rapidly than  $v^2$  and it can be troublesome to obtain a substantially linear response from them for voltages which are less than about 0.5 V. The certainty that the response of a couple will vary as the square of the heater current is a great insurance against misleading blunders in aerial measurements. If the reader uses some form of rectifier, then he must always be on the watch to make certain that he knows the manner in which the galvanometer deflexion varies with the current induced in the aerial, and never forget that very unexpected results may possibly be due more to an unrecognized behaviour of the rectifier than to an unexpected behaviour of the aerial system that is being tested.

A readily portable short monitor, complete with self-contained thermal ammeter, is an instrument commonly associated with aerial testing: usually it is meant to be held in the hand and presented to one aerial after another. Such a tool makes a valid instrument for ascertaining that successive members of an array are alive, but it can very easily give a very false impression of the current in successive members. For this purpose it is important to replace the aerial by a small loop: the reasons why this is necessary will be explained in a later chapter. Though the writer has long appreciated the necessity of using a loop rather than an aerial, in certain circumstances, he has not had practical experience of doing so and accordingly cannot give advice, based on

experience, about their appropriate construction. When absolute values of field strength are required he feels sure that an aerial must be used and not a loop. This is because it will be virtually impossible to remove what the common parlance of direction-finding has long termed the 'aerial-effect' of a loop.

### 9.3. Monitor aerial used to explore the equatorial field of a half-wave aerial

This seems to be the most appropriate place in the book to record the investigation of the field in the vicinity of a half-wave aerial: it serves both as an example of the use of a monitor aerial and also as the experimental counterpart of some of the analysis contained in Chapter VIII. We wish to observe the field in the equatorial plane of a half-wave aerial: since the field is a function of the angle of elevation, the monitor aerial ought to be short in order that the variation along it of the vertical component of field shall be small. Such variation, however, can be significant only when the monitor is very close to the half-wave aerial. Consideration of Figs. 8.3 and 8.4 will show that the vertical component of field must be substantially constant over a distance  $\pm \frac{1}{3}\lambda$  from the equatorial plane so long as the radial distance in the equatorial plane exceeds, say,  $\frac{1}{3}\lambda$ . Accordingly it should be permissible to use a monitor whose total length is verging on  $\frac{1}{4}\lambda$ , the limit for which its impedance can be estimated with reasonable accuracy.

The electric field in the equatorial plane of a doublet is well known and is given by equation (9.7) below

$$\frac{c|E|}{2a^2X_0} = \frac{1}{ar} \sqrt{\left(1 - \frac{1}{a^2r^2} + \frac{1}{a^4r^4}\right)}, \quad (9.7)$$

where  $a \equiv 2\pi/\lambda$  and  $2X_0$  is the area under the current distribution curve. When  $r/\lambda = 0.15$  the value of the radical is unity, and when  $r/\lambda = 0.25$  and  $0.5$  its value is  $0.89$  and  $0.95$  respectively. Hence if  $r/\lambda$  exceeds  $\frac{1}{4}$  we may consider, without sensible error, that the field varies inversely as the distance from the mid-point of the doublet. Close consideration of Figs. 8.2 and 8.5 will show that the field in the equatorial plane of a half-wave aerial is scarcely distinguishable from the field of a doublet, having the same value of  $X_0$ , provided  $r/\lambda$  exceeds about  $\frac{1}{4}$ . Within the range of  $r/\lambda = \frac{1}{4}$  the field must depend appreciably on the precise degree of approach to resonance.

In the experiments to be described now a monitor aerial  $\frac{1}{4}\lambda$  long was used to measure the field of an isolated half-wave aerial operating at a wavelength of 125 cm. The monitor was parallel to the half-wave

aerial and the equatorial plane of the monitor coincided with the equatorial plane of the half-wave aerial. The current induced in the monitor was observed as the distance between the axis of the monitor and the half-wave aerial was increased from 10 to 210 cm. (i.e. from  $0.08\lambda$  to  $1.72\lambda$ ). If the transmitting aerial was a doublet, then (9.7) shows that  $E \times ar$  tends to be constant when  $r/\lambda$  exceeds about  $\frac{1}{2}$ :

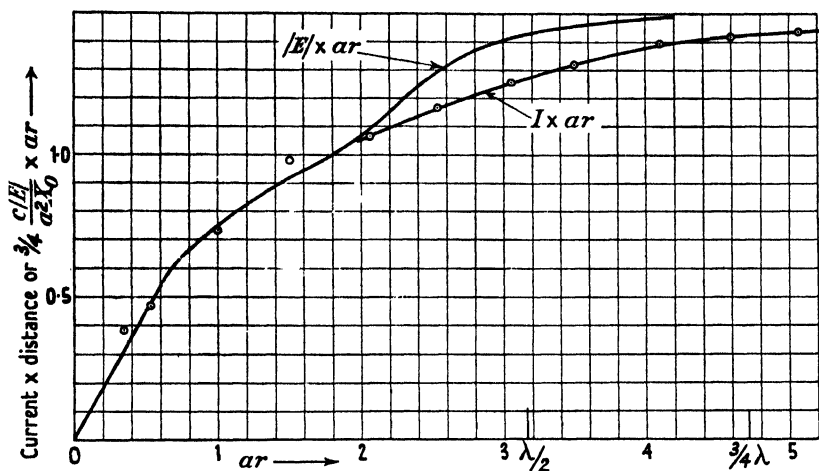


FIG. 9.5. Exploration of field in equatorial plane of a half-wave aerial.

accordingly the product of the current induced in the monitor and the distance of the monitor from the half-wave aerial should tend to become constant; experiment showed it did become constant when  $r/\lambda$  exceeded  $\frac{1}{2}$ . Clearly the best way of analysing these results is to present the product  $I \times r$  as a function of  $r$ . The relation between  $r$  and the product  $E \times r$  for a half-wave aerial can be deduced by vector addition of Figs. 8.2 and 8.5, always remembering that the values of  $E_Q$  in Fig. 8.5 are somewhat uncertain, for a half-wave aerial, when  $r/\lambda$  is less than, say, 0.2: however,  $E_P$  is then large and constant and  $E_Q$  should be relatively small, and hence  $E$  should be dominated by  $E_P$ , which is known with considerable certainty. The upper curve in Fig. 9.5 shows  $E \times ar$  deduced in this manner: the lower curve (having observation points marked) in the same figure shows the observed values of  $I \times ar$  and plotted to a scale such that the observed limiting value of this product (viz.  $I_{m\Delta} \times r_{cm.} = 900$ ) is taken as 1.5. The two curves are in reasonably close agreement, the only notable discrepancy being near  $ar/\lambda = \frac{1}{2}$ , the region where  $E_P$  is negligible. This test was repeated at a frequency of 230 and 248 Mc/s but no significant changes were



observable. The substantial agreement between the two curves in Fig. 9.5 suggests that a monitor of length  $\frac{1}{4}\lambda$  will give a valid measure of  $|E|$  even when it is as close as  $\frac{1}{10}\lambda$  to the half-wave aerial. Since the relation between  $E_P$  and  $ar$  is known with considerable certainty for a half-wave aerial (see Fig. 8.2), it should be possible to deduce the relation between  $E_Q$  and  $ar$  from the observed relation between  $E$  and  $ar$ .

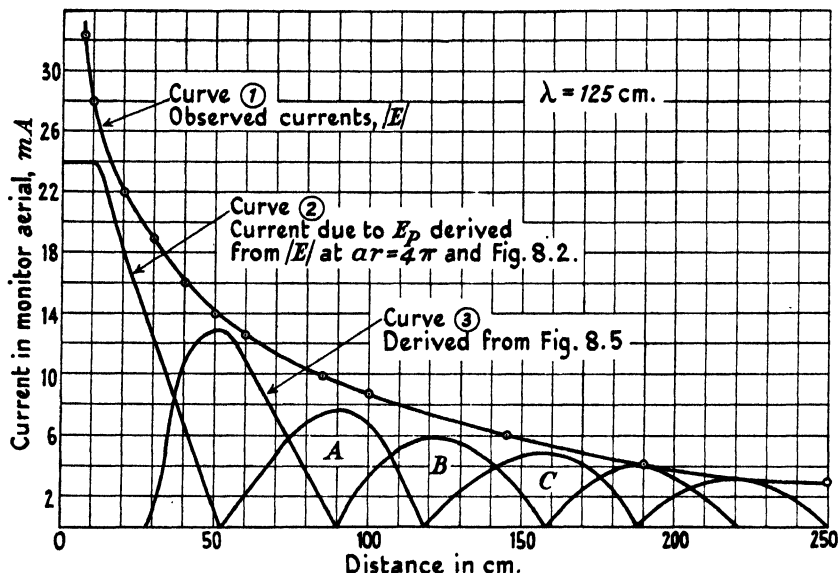


FIG. 9.6. Analysis of the two components of field in equatorial phase of a half-wave aerial.

Thus curve (1) in Fig. 9.6 is the observed relation between distance and the current induced in a monitor aerial of length  $\frac{1}{4}\lambda$  which was excited by a half-wave aerial operating at  $\lambda = 125$  cm. At  $ar = 2$  the current induced in the monitor was 3.0 mA, and at this distance (9.7) gives

$$\frac{cE}{2a^2X_0} = \frac{1}{4\pi};$$

at  $ar = 0$  we have, see Fig. 8.2,

$$\frac{cE_P}{2a^2X_0} = \frac{2}{3} \times 0.96.$$

Accordingly at  $ar = 0$  the current induced in the monitor aerial due to  $E_P$  alone should be  $\frac{2}{3} \times 0.96 \times 4\pi \times 3 = 24$  mA, since the current induced by  $|E|$  was found to be 3.0 mA at  $ar = 2$ . According to this method of computation, curve (2) in Fig. 9.6 represents the monitor current

which would be induced if  $E_P$  alone were acting: in other words, curve (2) represents  $E_P$  to the same scale that curve (1) represents  $|E|$ . Curve (3) in Fig. 9.6 represents  $E_Q$  to the same scale and it is derived from Fig. 8.5. For correct agreement the maxima of the loops of curves (2) and (3) should be on curve (1), but in fact they lie beneath it. In the range of the graph the observed currents cover a range of 10 to 1 and this means a range of 100 to 1 in galvanometer deflexion. Even though a good range multiplier was used, it is improbable that the monitor currents were precisely in the ratio 10 to 1 when  $r$  was increased from 9 to 250 cm. Since it is certain that  $E_Q$  must pass through zero at a distance near 90 cm. ( $ar = 4.5$ ), it would have been better (though less illustrative of the principle of the analysis) to have taken  $r = 90$  cm. as the fiducial point rather than  $r = 250$  cm. If  $r = 90$  cm. is taken as the fiducial point, then the ordinate scale of curves (2) and (3) must be increased in the ratio  $9.5/7.5 = 1.27$ . If this is done it will be found that the crests  $A$ ,  $B$ , and  $C$  lie on curve (1) and that at  $r = 20$  cm.  $i_P$  should be 23 mA, when in fact the measured value of  $|i|$  was 22 mA. But such change of scale would make  $i_Q = 16$  mA when  $r = 50$  cm., whereas the observed value of  $|i|$  was only 13.5 mA. Close consideration of these results will show that the greatest value estimated for  $E_Q$ , for a half-wave aerial, in Fig. 8.5 must be about 18 per cent. too large and that  $E_Q$  must pass through zero near  $r/\lambda = \frac{1}{4}$ . The measurements were repeated at  $\lambda = 130$  cm. and showed that  $E_Q$  very near the aerial (i.e. closer than 12 cm.) was relatively much larger than when  $\lambda = 125$  cm., thus showing that 125 cm. was closer than 130 cm. to the natural wavelength of this particular aerial.

Since the distribution of  $E_P$  is known with very considerable certainty, it must be possible to use this method effectively for exploring the distribution of  $E_Q$  near a half-wave aerial, since the point at which  $E_P$  attains its first maximum must be a reliable fiducial point for determining the curve corresponding to curve (2) in Fig. 9.6. A systematic exploration of the dependence on frequency of the distribution of  $E_Q$  would reveal valuable information about the performance of a linear aerial near its first resonant frequency.

These experiments can be used to give a very rough check of the absolute calibration of a monitor aerial. Thus in one measurement the current in the monitor aerial ( $\frac{1}{4}\lambda$  long and 3.1 mm. diameter) was found to be 7.4 mA when the monitor was distant  $\frac{1}{2}\lambda$  from the aerial. Reference to the appropriate curve in Fig. 9.3 suggests that the inductance effect increases the current by about 6 per cent. when  $l/\lambda = \frac{1}{4}$ : accordingly

we will reckon the induced current as 7 mA instead of its recorded value of 7.4 mA. Taking the impedance of the monitor aerial as 1300  $\Omega$  (see Table 9.2,  $a/b = 100$ ), we have  $(|E| \times 31)/1300 = 7/1000$ , whence  $|E| = 29$  V/m. We have, from (9.7)  $E = (120\pi X_0/\lambda r)$  V/m., where  $X_0$  is in metre amperes,  $\lambda$  and  $r$  are in metres. Hence, taking  $|E| = 29$  V/m. we find that in this experiment  $X_0 = 0.06$  metre amperes. The output of an isolated aerial is given by the equation  $P = (480\pi^2 k X_0^2)/\lambda^2$  watts, where  $k$  is a factor depending on the length of the aerial and the distribution of current along it. For a doublet  $k = 0.666$ , for a half-wave aerial with sinusoidal distribution  $k = 0.6095$ , and for a half-wave aerial with triangular distribution of current  $k = 0.616$ . Hence we may take  $k = 0.61$  with great confidence; whence  $P = 2900(X_0/\lambda)^2 = 6.6$  W, when  $X_0 = 0.06$  and  $\lambda = 1.25$ . It was known from the input to the valve generator that the output was 5 W if the efficiency was 25 per cent. or 10 W if the efficiency was 50 per cent. Hence the power output deduced from the monitor aerial has a value which is known, for quite other reasons, to be substantially correct. We can approach the matter in a way which is slightly different. If the distribution of  $X_0$  is sinusoidal and if the length of the aerial is  $\frac{1}{2}\lambda$ , then the relation between the equatorial field at  $r/\lambda = \frac{1}{2}$  and the current  $I_A$  at the mid-point of the aerial is  $|E| = 120I_A/\lambda$ . For the monitor aerial (of length  $\frac{1}{4}\lambda$ ) we have  $|E|\frac{1}{4}\lambda = 1300I_m$ , whence  $I_m/I_A = 3/130$ . Since  $I_m = 7$  mA, this gives  $I_A = 0.3$  A, whence  $P = 73 \times (0.3)^2 = 6.6$  W. It should be realized that the two methods need not have agreed precisely, because  $I_m$  gives a value of  $X_0$  and a given value of  $X_0$  need not necessarily be associated with a radiation resistance of 73  $\Omega$ .

Having regard to the known input to the valve generator it is probably correct to say that the field incident on the monitor was 29 V/m. within  $\pm 10$  per cent., and hence that these limits probably contain the uncertainty with respect to the precise value of the impedance of this monitor and the frequency error of the thermocouple used with it.

## X

### TESTS OF VEE REFLECTORS

#### 10.1. Preliminary

WE presume the reader is equipped with a turn-table, a generator, and a receiver and has made sufficient preliminary experiments to give him the feel of the work. We set out to discuss the performance of Vee reflectors excited by a single half-wave aerial, and our purpose is to discover how nearly the polar diagram resulting from sheets of given size approximates to the ideal limit for infinite planes. In the tests about to be described the sheets were made of fine-meshed copper gauze mounted on a wooden framework: in a later chapter we describe the effect of replacing the gauze by wire netting or expanded metal sheet. At present we are concerned only with the effect of the finite size of perfectly reflecting sheets; we shall not confuse the issue by discussing here the effect of using finite sheets of imperfectly reflecting material. The performances which can readily be compared with the ideal are the forward field and the equatorial pattern: patterns in other planes are very difficult and troublesome to obtain. The reader is to imagine a Vee reflector set up on the turn-table and used as a transmitter: the single half-wave aerial, fed by concentric cable, must be movable along a wooden lath bisecting the Vee. It is wise to make the supporting laths very light and to supplement their inherent lack of rigidity by strings attached to the corners of the screen.

#### 10.2. Forward field tests

The ideal curves of forward field are depicted in Figs. 3.5–3.13, and we wish to discover by experiment how nearly these are simulated when the screens have specified dimensions. We remind the reader that Figs. 3.5–3.13 relate to a constant current in the aerial and that the radiation resistance of the aerial depends enormously on its distance from the apex. It is very well known that the output of a valve generator, fed by a given voltage on the anodes, depends greatly on the resistance with which it is loaded and that the maximum output can be obtained in a given load only by coupling it through the equivalent of a transformer whose ratio can be adjusted to the optimum condition. In our experiments the aerial is to be moved continuously along the bisector of the Vee and in this process its radiation resistance will vary widely, and so it is inevitable the power input to the aerial will vary widely and in a somewhat haphazard manner. It is not practicable to

readjust the generator to maximum output at each setting of the aerial: the labour of doing so would be prohibitive and unendurable, and at best the means of doing so scarcely exist since the small generators we have in mind are extremely inflexible tools. And lastly, the means of measuring the input power to the aerial are still inadequate, underdeveloped, and cumbersome. The only practicable course is to leave the generator alone when the aerial is moved. Consequently it is unlikely the power input is constant, since the radiation resistance is certainly varying over a wide range. Probably the changes of current could be measured by a loop monitor aerial, such as is outlined in the last chapter: the writer has never done so and the procedure would scarcely justify the labour. However, all this is merely to point out that the experimental curves of forward field cannot be expected to agree exactly with the ideal curves depicted in Figs. 3.5–3.13 because this series relates to a *constant* current in the aerial and it is most unlikely this condition will obtain in the experiments. Ideally there should be stations at which the forward field is zero, no matter how large the current in the aerial, and reference to figures such as 3.18–3.21 will show the resistance then is finite. Hence at these stations the current fed into the aerial by the generator should be finite, and ideally the forward field should then be zero: accordingly it would seem the stations for zero forward field should in practice be more reliable points for comparison than the stations for maximum forward field, since these last may well be vitiated, not by the finite size of reflector, but by the completely independent factor that the current in the aerial may happen to be larger when it is near a station of maximum forward field than when it is precisely at such a station.

Before tabulating experimental results it is well to consider the general effect of finite size. If the aerial is very far in front of the aperture of the Vee, it is obvious the Vee cannot have much effect on the forward field: if any effect is detectable the fluctuations must be small and the field cannot possibly fall to zero. Hence an effect of finite size must be to convert zeros into minima when the aerial is far in front of the aperture: unless the plane of the aperture is well in front of the first station for zero forward field we must expect to discover a minimum and not a zero.

The writer has made a very comprehensive set of forward field tests using Vee reflectors whose angles were  $360^\circ$ ,  $270^\circ$ ,  $180^\circ$ ,  $120^\circ$ ,  $90^\circ$ ,  $72^\circ$ ,  $60^\circ$ , and  $45^\circ$ : he has used screens of various sizes and employed both 125 and 50 cm. wavelengths. Experience has shown him that so long

as the size of the sheets is what may be called sensible and reasonable, then the maxima and minima of forward field occur very near the ideal stations. Integrated experience shows the discrepancies are very small and therefore the forward field test is an unsuitable one for disclosing the discrepancy between any given reflector and the ideal. This discovery is of great practical importance and value, and the reader should now register in his mind that he may use the calculated values with great confidence. He should, however, demand to see for himself the evidence supporting this sweeping statement. The writer has fourteen tables before him which all support the statement so strongly that it is obviously redundant to reproduce them all and he must attempt to select the most instructive samples. The first relates to a test at  $\lambda = 50$  cm. of a flat reflecting sheet  $3.6\lambda$  wide and  $1.5\lambda$  high (i.e. 6 ft.  $\times$  2½ ft.): in this simple case the first maximum should occur when the aerial is distant  $\frac{1}{4}\lambda$  (i.e. 12.5 cm. = 4.9 in.) from the sheet and the second when it is  $\frac{3}{4}\lambda$ . The results of the test are recorded in Table 10.1.

TABLE 10.1

*Flat sheet  $3.6\lambda$  wide and  $1.5\lambda$  high, at  $\lambda = 50$  cm.*

Measured distance, in.	3.2	9.5	13.9	19.5
Ideal distance . . .	4.9	9.8	14.7	19.6
Discrepancy, in. . .	-1.7	-0.3	-0.8	-0.1

The scope of this test includes two stations for zero forward field; at each of these the field appeared to pass through zero and not merely fall to a minimum. It may be seen that at both stations for zero field the discrepancy of position is insignificant. Hence we find experimentally that a sheet of half-width  $1.8\lambda$  suffices to produce zero forward field for an aerial distant  $\lambda$  from the plane: it is encouraging to find that a sheet so modest in size will do this. The discrepancy for the two maxima is appreciable but, from what has been said previously, there is no particular necessity to ascribe this to the finite size of the sheet. Table 10.2 relates to a test, also at  $\lambda = 50$  cm., using a  $120^\circ$  Vee each of whose sheets was  $3.6\lambda$  wide and  $1.5\lambda$  high. It follows from these dimensions that the aerial was in front of the aperture plane when its distance from the apex exceeded  $1.8\lambda$  (i.e. 36 in.).

TABLE 10.2

*Mirror angle  $120^\circ$ , sheets  $3.6\lambda \times 1.5\lambda$ , at  $\lambda = 50$  cm.*

Measured distances, in.	8	13.5	19.5	26	33	40	47	53.5	59.5
Ideal distance . . .	8.6	12.2	19	25.5	32.5	..	..	..	..
Discrepancy, in. . .	-0.6	+1.3	+0.5	+0.5	+0.5	..	..	..	..

The ideal distances are derived from Fig. 3.7: further points are very laborious to evaluate, but the complete wavelength of the oscillation appears to be  $0.7\lambda$  and this corresponds here to an interval of 7 in. between succeeding maxima and minima. The table shows this interval is in fact very close to 7 in., and thus it appears that the discrepancies are negligible even when the aerial is distant some  $3\lambda$  from the apex, and then is far in front of the plane of the aperture. It is clear that sheets of very modest dimensions have sufficed to reproduce closely the ideal forward field characteristic.

The next test, also at  $\lambda = 50$  cm., was made on a right-angled corner reflector and is recorded in Table 10.3.

TABLE 10.3

*Mirror Angle  $90^\circ$ , sheets  $3.6\lambda \times 1.5\lambda$ , at  $\lambda = 50$  cm.*

Measured distance, in..	..	20.5	30	42	49.5
Ideal distance .	9.8	19.6	29.5	39.4	49
Discrepancy, in. .	..	+0.9	+0.5	+2.6	+0.5

Here the first maxima could not be examined because the 'impedance thimble' on the aerial cable fouled the apex. There is only one serious discrepancy: it is the second station for zero field, the complete curve (which had an observation point at every inch of distance) had a kink on it in this neighbourhood. When the test was repeated using sheets  $9\frac{3}{4}$  ft. wide (vice 6 ft.) the kink was still apparent though smaller in size, and thus its existence was presumed to be a function of the size of the sheet. Moreover, the field did not fall to zero at 20.5 and 42 in. as it should do, but passed through a minimum, which was some 20 per cent. of the maximum. Evidently the effect of finite area was being encountered, but it should be noted that the main effect is to convert a zero into a minimum without much change of position.

A forward field test ( $\lambda = 50$  cm.) from a reflector whose sheets were  $6\lambda$  wide and  $1.5\lambda$  high inclined at  $72^\circ$  (i.e.  $N = 5/2$ ) showed negligible discrepancies in the first six stations: at the seventh and eighth stations the measured distance was 2 in. more than the ideal. Reference to Fig. 3.13 will show the eighth station occurs at  $R/\lambda = 3.55$  and accordingly  $R = 70$  in. in this test, and at this station the discrepancy was 2 in., which is  $0.1\lambda$ . The subsidiary humps near  $R/\lambda = 1.5$  and  $2.8$  in Fig. 3.13 appeared in the experimental curve: in short, the forward field test for sheets  $6\lambda$  wide inclined at  $72^\circ$  differed insensibly from the ideal for values of  $R/\lambda$  up to 3.5.

A forward field test ( $\lambda = 50$  cm.) from sheets  $3.6\lambda$  wide inclined at  $60^\circ$  showed a negligible discrepancy in the position of the first four stations: the third maximum and fourth zero (see Fig. 3.11) each occurred 2 in. farther out than the ideal; the fourth maximum was correct, but the fifth minimum occurred 8 in. (i.e.  $0.4\lambda$ ) short of the ideal position. This test was then repeated with sheets  $6\lambda$  wide: such increase of width moved only the station for the fifth minimum, which then was short by only 4 in.: it did, however, increase the magnitude of the third and fourth maxima, relative to the first and second, without changing their positions.

A forward field test ( $\lambda = 50$  cm.) from sheets  $3.6\lambda$  wide inclined at  $45^\circ$  showed the discrepancies for the first eight stations (see Fig. 3.12) were within about  $\pm 1$  in. and no appreciable change resulted from increasing the width of the sheet to  $6\lambda$ .

These results are troublesome to digest and we suggest the following rough summary: Sheets  $3.6\lambda$  wide and  $1.5\lambda$  high inclined at any angle between  $45^\circ$  and  $180^\circ$  will reproduce the first six or seven stations of maxima or minima with a discrepancy less than  $\frac{1}{10}\lambda$ ; wider sheets increase the relative magnitude of 'far out' maxima.

In Tables 10.4 to 10.6 we record some forward field tests with screens  $2\lambda$  wide and  $1.5\lambda$  high (vice  $3.6\lambda \times 1.5\lambda$  previously) which were made at  $\lambda = 125$  cm. (vice 50 cm. previously).

TABLE 10.4

*Mirror angle  $90^\circ$ , sheets  $2\lambda \times 1.5\lambda$  ( $\lambda = 125$  cm.)*

Measured distance, cm.	65	120	130	140	189	230
Ideal distance . .	62.5	125	..	..	187.5	250
Discrepancy, cm. .	+2.5	-5	..	..	+1.5	-20

In this test a subsidiary maximum (about 33 per cent. in field strength) occurred at  $R = 130$  cm. (its existence may have been due partly to change of output of the valve generator). The second legitimate station for zero field should occur when  $R = 250$  cm. and then the aerial would be  $0.6\lambda$  in front of the plane of the aperture: this station was represented by a minimum (about 30 per cent. in field strength) and occurred 20 cm. ( $0.16\lambda$ ) short of the ideal distance. A similar test with sheets  $\frac{5}{2}\lambda \times \frac{3}{2}\lambda$  showed the first maximum occurred at 40 and the first minimum at 108 cm., the subsidiary maximum was still present and occurred at 120 cm., the second legitimate maximum occurred at 180 cm. Evidently reducing the width of sheet from  $2\lambda$  to  $\frac{5}{2}\lambda$  has had a noticeable effect.



TABLE 10.5

*Mirror angle 60°, sheets  $2\lambda \times 1.5\lambda$  ( $\lambda = 125$  cm.)*

Measured distance, cm.	70	130	150	160	170	210
Ideal distance . . .	81.5	125	..	163	..	250
Discrepancy, cm. . .	-11.5	+5	..	-3	..	-40

Here the second hump of the forward field curve had a small dimple on its crest and this occurred at  $R = 160$  cm., which is where the single maximum should occur in the ideal (the dimple may have been due to the valve generator). When the test was made with sheets  $\frac{5}{4}\lambda$  wide the first minimum occurred at 125 cm. and the first maximum at 150 cm.; the dimple was not present.

TABLE 10.6

*Mirror angle 45°, sheets  $2\lambda \times 1.5\lambda$  ( $\lambda = 125$  cm.)*

Measured distance, cm. .	80	150	193	230
Ideal distance . . .	100	150	188	210
Discrepancy, cm. . .	-20	0	+5	+20

When the width of the sheet was  $\frac{5}{4}\lambda$  these discrepancies became 0, -6, -18, and 0 cm. respectively.

We learn from these tests, at  $\lambda = 125$  cm., that sheets only  $\frac{5}{4}\lambda$  wide suffice to produce a fair approximation to the forward field test. Were it not for the analytical probing in previous chapters it would surely have been amazing to find that sheets a mere wavelength or so wide could suffice to produce a recognizable approach to the ideal: our practical experience is extremely encouraging in showing that analysis of idealized problems is of great help in practical design. We now suggest the following rough summary: provided the reflecting sheets are about  $2\lambda$  wide, then the stations for maximum and minimum forward field will occur within about  $\pm \frac{1}{20}\lambda$  of the ideal distances, at any rate so long as the aerial is not much in front of the aperture plane. When the reader has gained experience for himself he will have complete confidence that the forward field test will always agree very closely with the ideal: he will not seek to relate closely the small discrepancies with the size of the sheets but will be content to check the positions of the stations experimentally in each individual case when the aerial and reflector have been made according to the design he has based closely on ideal values.

*Note.* For some further information about forward field tests see *Journal I.E.E.*, Part III (1945), 'Theory and performance of corner reflectors for aerials', § 6.

### 10.3. The equatorial pattern

#### (a) *General survey*

If the reflecting sheets extended to infinity, then the field would remain zero on all bearings greater than  $\pm\frac{1}{2}\beta$ : this condition cannot obtain when the sheets have a finite area, for inevitably there will be some diffraction round their edges. In our experimental study we require to observe the magnitude of the said diffraction and also the magnitude and bearing of the various side lobes. It is the writer's experience, and probably the experience of everyone, that the observed diffraction pattern is never perfectly symmetrical: this phenomenon may cause undue worry to the inexperienced. When the experimenter first meets this effect he may well be inclined to attribute it to small imperfections in the mechanical construction of the reflector, such as the aerial being slightly to one side of the bisector or the gauze sheets not truly flat. Reference to § 3.10 will remind the reader that a very small displacement of the aerial from the bisector has a very small effect on turning the main beam but does produce considerable dissymmetry of the side lobes and thus seems to offer a rational explanation of the effect. However, we must remind him further that when  $\beta = 60^\circ, 36^\circ$ , and  $25.6^\circ$ , etc., the mean square pattern is bound to be symmetrical, and hence there are certain particular cases where a slight and accidental offset of the aerial cannot be invoked to explain dissymmetries in the experimental pattern. The writer has not found that  $60^\circ$  mirrors give perfectly symmetrical patterns: he is convinced that the observed dissymmetries of the lobes is not due primarily to a very small 'offset' of the aerial. The figure of the good optical mirrors is said to be correct to within  $\pm\frac{1}{20}\lambda$ . Hence if the sheets are flat within about  $\pm 1$  in. for  $\lambda = 50$  cm., then they rival the best optical practice: thus it does not seem likely that a slight waviness in the gauze sheets is important. Experience shows it is not important, for a large bulge (2 or 3 in. deep) does not produce a detectable effect on the side lobes. The writer is convinced the observed dissymmetries are not produced by imperfections in the mirror itself. He thinks they must be due to reflections and interference by objects, such as trees, hedges, etc., on the site itself. It must be possible to settle this question by comparing the patterns observed when the receiver is placed successively at various points on an arc of given radius. If the side lobes depend slightly on the location of the receiver in the testing site, then the discrepancies must be due to neighbouring objects. The writer has not had an opportunity to make this experiment, but it ought to be

carried out thoroughly and systematically and the result of the tests published.

When such dissymmetries are observed in tests of a multi-element curtain or in-line array it is common to blame the feeding cables and to set about the laborious process of shortening this one or lengthening that one a trifle: those who have had the misfortune to do this operation know how troublesome it is to do and how unconvincing are the results.

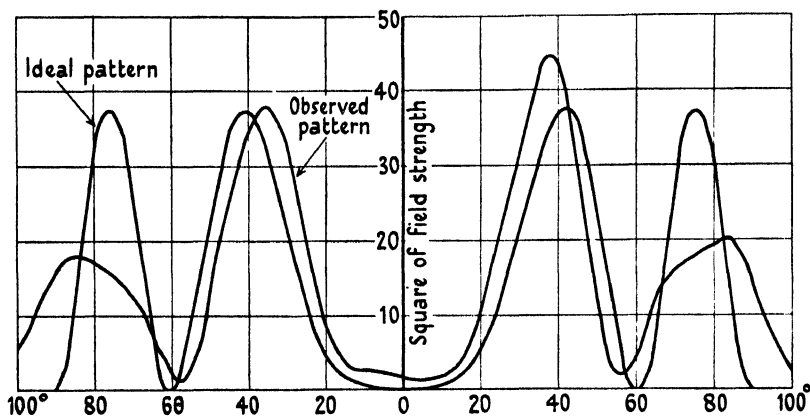


FIG. 10.1. Ideal diffraction pattern for aerial distant  $\lambda$  from plane of infinite flat sheet and observed pattern for an aerial distant  $\lambda$  from a sheet  $3.6\lambda$  in width,  $f = 600$  Mc/s, width of sheet 6 ft.

If it is a fact, as the writer suspects, that the fault may be due to the site and not to the cables, then more harm than good is being done by the process. The reader will readily understand that when observing a lobe on a bearing of, say,  $+60^\circ$  the main beam may be illuminating strongly some neighbouring object and reflections from it may fall on the receiver: when the transmitter is turned to bearing  $-60^\circ$  the main beam illuminates a different locality and hence any re-radiation effects will not be the same as they were on bearing  $+60^\circ$ . At present we must accept this small disability which accompanies experimental work, and expect to find it.

Before working systematically through the family of Vee reflectors we will choose a pair of experimental patterns which contain a wealth of detail and offer them to the reader as evidence to show that sheets only a few wavelengths wide do suffice to reproduce a striking similarity to the ideal limit. Thus Fig. 10.1 shows the ideal pattern for an aerial distant  $\lambda$  from an infinite flat sheet and the observed pattern resulting from an aerial distant  $\lambda$  from the plane of a sheet  $3.6\lambda$  wide: the test

was made at  $\lambda = 50$  cm. First note that the experimental pattern is not symmetrical, the right-hand lobes being higher than the left-hand lobes: this is a typical example of the effect we believe is due to the site and not to the reflector *per se*. Both the first maxima and both the first minima occur at bearings which are  $4^\circ$  less than the ideal: note

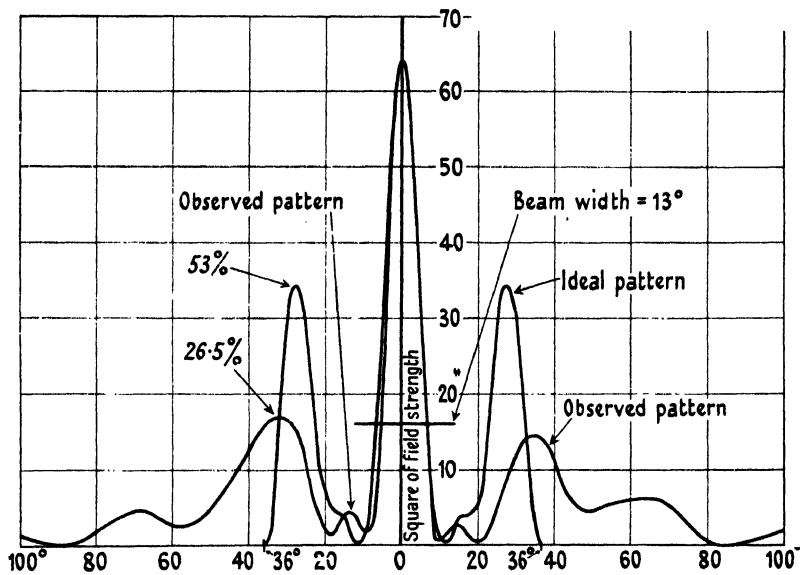


FIG. 10.2. Ideal pattern for  $72^\circ$  corner reflector,  $k = 14$ . Observed pattern for  $75^\circ$  corner reflector with sheets  $9\frac{1}{2}$  ft. wide:  $f = 600$  Mc/s and  $R = 44$  in.

these two minima do not fall quite to zero, nor does the forward field. In the ideal pattern the field must be zero behind the sheet, but we note the observed pattern shows the field is not zero on bearings greater than  $\pm 90^\circ$ : this is the diffraction round the edge of the sheet, of which we have spoken and which we have calculated analytically for a half-plane. We note the two outside maxima are much too small and occur on a bearing which is about  $10^\circ$  too large: it is somewhat as though these lobes had slid over the edge, a metaphor which will often be used. Though this particular pattern is not likely to be of practical use, it is surely very interesting and encouraging in demonstrating that a sheet less than  $4\lambda$  wide can produce so much of the detail of the ideal pattern. The flat sheet reflector will be explored fully in the next chapter.

Fig. 10.2 shows the ideal pattern for a  $72^\circ$  Vee when  $R/\lambda = 2.2$ , which reference to Fig. 3.10 will show is a station for maximum forward field. It also shows the observed pattern obtained from sheets  $6\lambda$  wide inclined at  $75^\circ$ . We note once again that the two big lobes have 'slid

over the edge' but their maxima occur on a bearing not much greater than the ideal: again the observed pattern is not truly symmetrical. Note that the ideal pattern is tending to form a subsidiary maximum at  $16^\circ$  and that this appears in the observed pattern as a pimple at  $15^\circ$ . The observed main beam is indistinguishable from the ideal and is  $13^\circ$  wide at half height (in field strength). Again we find that comparatively small sheets have produced a pattern which 'attempts to

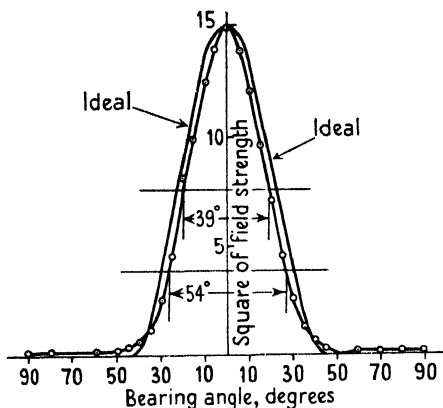


FIG. 10.3. Ideal and observed patterns.  $\beta = 90^\circ$ ,  $R/\lambda = 0.53$ ,  $k = 3.3$ . Sheets  $\frac{1}{2}\lambda$  wide and  $\frac{3}{4}\lambda$  high.

copy' the ideal very closely and may be said to fail in the attempt only because the outside lobes are bound to 'slide over the edge'. It is particularly important to note that the main beam is reproduced faithfully, and if that is our main purpose and desire, then the performance can be predicted from the ideal calculation alone; we shall see this is true in general. Moreover, we find the side lobes are smaller than the ideal and since side lobes are objectionable we realize that finite sheets produce a pattern which can have features more desirable than has the ideal; the discrepancies between the actual and the ideal tend to mitigate those features of the ideal pattern which would be undesirable in practical applications. We trust these two figures have sufficed to persuade the reader that the performance of Vee reflectors can be predicted very closely from the calculations appropriate to infinite sheets: the practising engineer is called on to do little more than make an intelligent estimate for the diffraction round the edge.

#### (b) Pattern at the first station

The family of curves in Figs. 3.22–3.27 has shown that for each angle of the Vee there are a succession of stations at which the forward gain

is a maximum, and accordingly it is the pattern appropriate to these stations which is of outstanding practical interest: we shall limit our experiments to them. Reference to § 3.8 will remind the reader that the ideal pattern must be indistinguishable from a simple sinusoid provided the length of arc across the Vee at the aerial is less than about  $\frac{3}{4}\lambda$ : at this limit the aerial is always farther from the apex than the first station for maximum gain. Accordingly, at the first station for maximum gain the ideal pattern must be a simple sinusoid and it will suffice to record these experiments in tabular form: however, to make this method quite clear we include Fig. 10.3, which compares graphically a certain observed pattern with the ideal sine curve. We will now record the patterns produced by sheets of various sizes when the aerial is at the first station for maximum gain: the wavelength in these experiments was 125 cm.

TABLE 10.7

*Mirror angle 90°,  $R/\lambda = 0.52$*

	Width for $\frac{1}{2}$ -power	Width for $\frac{1}{4}$ -power	Fractional power at 45°
Ideal	45°	60°	0
Screens $2\lambda \times \frac{3}{2}\lambda$ .	33°	48°	3%
Screens $\frac{3}{2}\lambda \times \frac{3}{2}\lambda$ .	38°	55°	3%
Screens $\frac{3}{4}\lambda \times \frac{3}{4}\lambda$ .	38°	56°	5%

This table shows the beam is considerably narrower than the ideal, an experience which is often encountered. If the width of sheet was progressively increased indefinitely, the width of beam at half-power would increase asymptotically to 45°; accordingly there must be a minimum width of beam and the table shows this minimum occurs when the width of sheet is near  $2\lambda$ . It is of great interest to note that when the width of sheet is decreased from  $2\lambda$  to  $\frac{3}{4}\lambda$  then the diffraction round the edge, at  $\theta = 45^\circ$ , increases only from 3 to 5 per cent.: in this respect the extra width is scarcely justified. This is in accordance with the analytical prediction arrived at in § 5.2, where it was found that the field in the plane of the half-sheet fell rapidly to a small value and thereafter could be decreased appreciably only by an extravagant increase in the width of sheet. Table 10.7 shows that for a 90° mirror it is unnecessary to use sheets wider than  $2\lambda$  and scarcely worth while to make them wider than  $\frac{3}{4}\lambda$ : this is a very satisfactory and surely somewhat amazing discovery of great use for settling the dimensions for a practical design.

TABLE 10.8  
*Mirror angle 60°,  $R/\lambda = 0.52$*

	Width for $\frac{1}{2}$ -power	Width for $\frac{1}{4}$ -power	% power at 30°	% power at 45°
Ideal	30°	40°	0	0
Screens $2\lambda \times \frac{3}{2}\lambda$	36°	49°	14	1
Screens $\frac{3}{2}\lambda \times \frac{3}{2}\lambda$	55°	78°	42	14

This table shows that sheets  $2\lambda$  wide do not suffice to produce a beam as narrow as the ideal. In fact comparison with Table 10.7 shows that closing the angle from 90° to 60° has widened the beam slightly: if the sheets are  $\frac{3}{2}\lambda$  wide, this widening effect is very marked.

TABLE 10.9  
*Mirror angle 45°,  $R/\lambda = 0.6$*

	Width for $\frac{1}{2}$ -power	Width for $\frac{1}{4}$ -power	% power at 22.5°	% power at 45°
Ideal	22.5°	30°	0	0
Screens $2\lambda \times \frac{3}{2}\lambda$	44°	62°	32	3
Screens $\frac{3}{2}\lambda \times \frac{3}{2}\lambda$	68°	95°	80	36

This table shows that sheets  $2\lambda$  wide do not produce a beam as narrow as the ideal for 45° mirrors. In fact decreasing the mirror angle from 90° to 45° has produced a progressive increase in the width of the beam and without appreciable change in the fractional power on bearing 45°. Hence if sheets  $2\lambda$  wide can be tolerated in a given application, then it is best to incline them at 90°. On the other hand, if a beam width of about 44°, at half-height, suffices for a particular application, then it can be obtained by an aperture of  $\frac{3}{2}\lambda$  by using sheets  $2\lambda$  wide inclined at 45° or by an aperture  $2.1\lambda$  wide by using sheets  $\frac{3}{2}\lambda$  wide inclined at 90°. The first alternative will usually be preferable because the first mirror will be more compact than the second: even though the beam is much wider than the ideal for a 45° mirror, it is the same as the ideal width for a 90° mirror and the reflector is less bulky than if its angle had been 90°.

Fig. 10.4 shows the ideal pattern for a 45° mirror with  $R/\lambda = 0.8$  and also the pattern which was produced by sheets  $6\lambda$  wide. The observed pattern is much narrower than the ideal (19° as compared with 31° at half-height in field strength) and the side lobes are only of the order of 3 per cent. in power. It is an attractive pattern for practical use and this example is of considerable value. When the

width of the sheet was reduced from  $6\lambda$  to  $3.6\lambda$  the main beam was very slightly wider than the ideal and was accompanied by side lobes about 12 per cent. in power. Comparing these results with Table 10.9 shows that sheets  $2\lambda$  wide are much too narrow, sheets  $3.6\lambda$  wide just reproduce the ideal beam, sheets  $6\lambda$  wide produce a beam whose width

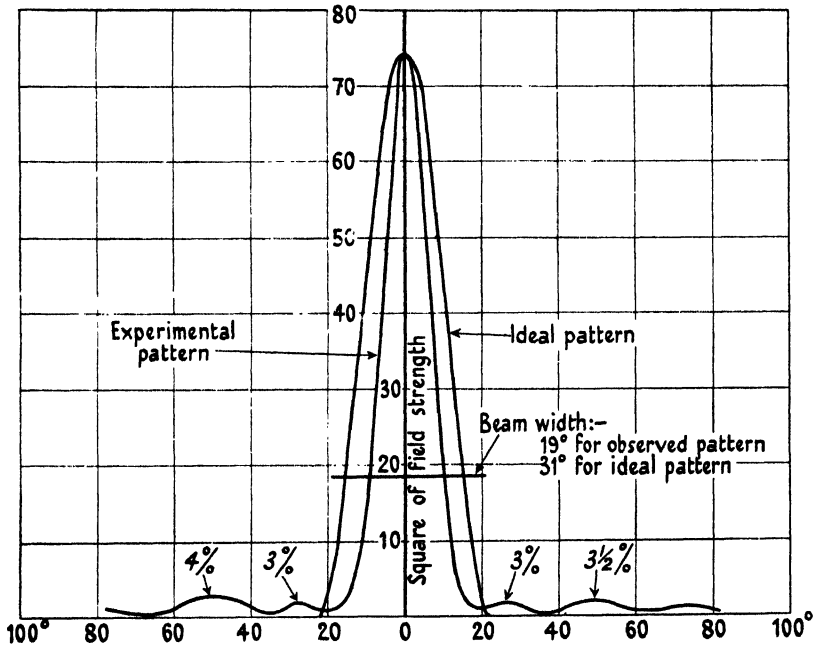


FIG. 10.4.  $45^\circ$  corner reflector. Sheets  $9\frac{1}{2}$  ft. wide,  $f = 600$  Mc/s  
 $R = 16$  in.  $= 0.81\lambda$ .

is two-thirds of the ideal: a gross increase in the width of sheet must therefore increase the width of beam appreciably while reducing the 'diffraction round the edge' by a very small amount. Thus there is an optimum width which is about  $6\lambda$  for  $\beta = 45^\circ$ .

These three tables provide the engineer with all the information required for designing a Vee mirror to be operated at the first station for maximum gain.

### (c) Pattern at the second station

The second station for maximum gain occurs when  $R/\lambda$  is of the order of  $\frac{3}{2}$ : the exact value depends on  $\beta$  and can be found by reference to Figs. 3.22–3.27. We will now include  $\beta = 120^\circ$  because such a Vee provides a useful introduction to the parabola and is a first approximation to it. It is instructive to give a general consideration to the shape



of the ideal pattern. If the reflector is a flat sheet, then the polar diagram is a set of equal rays, two more being added for each additional  $\frac{1}{2}\lambda$  of distance between aerial and sheet. Imagine now the flat reflector is hinged in the middle and that we study the change of pattern while  $\beta$  is being decreased from  $180^\circ$ : when  $\beta = 120^\circ$  the hinged sheets are still very open and the polar diagram must be reminiscent of that for a

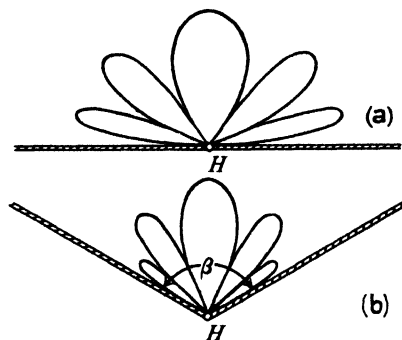


FIG. 10.5.

flat sheet. We shall expect to find that closing the angle of the Vee from  $180^\circ$  to  $120^\circ$  has the effect of crowding the substantially equal rays of a polar diagram into a smaller total arc of bearing: this is a very powerful method for predicting roughly the diagram of mirrors of large angle. All patterns can of course be evaluated by means of the Fourier series with Bessel coefficients, but the process is rather cumbersome when  $n$  lies between 1 and 2. When  $R/\lambda = 0.79$  ( $k = 5$ ) and  $\beta = 120^\circ$  the ideal polar diagram is found to consist of three nearly equal petals: the forward field is given by  $E/E_0 = 2.34$ , while the maximum of a petal is  $E/E_0 = 2.1$ , centred on bearing  $\pm 40^\circ$ : the R.M.S. field falls to a minimum value  $E/E_0 = 0.75$  at  $\theta = \pm 20^\circ$ . Had the sheet been flat and  $R/\lambda = \frac{3}{4}$ , then the polar diagram would have consisted of three petals of equal length centred at  $\theta = 0$  and  $\pm 70^\circ$  with zero field at  $\theta = \pm 48^\circ$ . If this diagram is compressed into an arc of  $120^\circ$  it corresponds very closely with the true pattern for  $\beta = 120^\circ$ . It is very helpful to imagine a rubber bag under air pressure having the same shape as the polar figure; then to imagine the effect of squeezing this bag between two boards meeting in a V: the diagram in Fig. 10.5 may help the reader to understand the imaginary apparatus we have in mind.

This very figurative description, by means of a model, often helps to give simple approximate answers to the questions which assistants are apt to raise during the discomforts of field work. But there

is another approach, more suited to the office, which allows us to predict the general form of a polar diagram without the labour of evaluation. When the forward field falls to zero the output does not also fall to zero and this means that the main beam has shrunk to zero and that two side lobes have appeared. At the second station for zero forward field there will be four side lobes, etc. Speaking generally, the angular width of the main beam and side lobes is roughly equal. As the angle of the Vee decreases, the distance of the aerial from the apex at the first station of zero forward field increases (the circumferential width across the Vee being then somewhat greater than  $\frac{1}{2}\lambda$ ). It now follows that as the angle of the Vee is decreased the ideal pattern must remain substantially constant, when plotted to a scale which maintains its total angular width constant and equal to  $\beta$ , provided  $R/\lambda$  is increased by an amount appropriate to the decrease of  $\beta$ : and in the range of  $\beta$  between  $180^\circ$  and  $90^\circ$  this increase of  $R/\lambda$  will not be very marked. The description by means of a rubber bag squeezed between boards is only a visual interpretation of the more systematic argument we have just given. It is really beside the point to prepare a figure in which the diffraction patterns (for a given  $k$ ) for, say,  $\beta = 180^\circ$ ,  $120^\circ$ , and  $90^\circ$  are plotted to a common base and then to comment on their agreement or disagreement. Given an appropriate adjustment of  $k$  they must be substantially similar. The general correspondence is apparent from the following example.

The stations for maximum forward gain of a half-wave aerial in a  $120^\circ$  Vee cannot be calculated and their positions must be guessed from the known stations appropriate to a long current filament, as shown in Fig. 3.22:  $R/\lambda = 1.75$  is one such station and we will choose this to correspond with the second station for  $\beta = 120^\circ$  (possibly it ought to be considered the third station). Fig. 10.6 shows the ideal polar diagram for this station: it is found that  $E/E_0 = 2.4$  for the main beam,  $E/E_0 = 1.35$  for the lobe centred on  $\theta = 20^\circ$ , and  $E/E_0 = 2.1$  for the lobe centred on  $50^\circ$ . For a flat sheet and  $R/\lambda = 1.75$  we should have had five equal rays with  $E/E_0 = 2$ : imagine squeezing them into an arc of  $120^\circ$  and compare the result with the true diagram. Fig. 10.7 also shows the observed pattern which was produced by sheets  $3.6\lambda$  wide and  $1.5\lambda$  high, with dimensions according to the inset diagram: again we note the observed pattern is not truly symmetrical.

The main beam is scarcely distinguishable from the ideal and is about  $13^\circ$  wide at half-height in power. The lobes centred on  $\theta = 20^\circ$  appear in the experimental figure but are much smaller than the ideal.

The ideal lobes centred in  $\theta = 52^\circ$  have 'slid over the edge' and are centred on  $\theta = 60^\circ$ . We see that these sheets reproduced the ideal main beam and 'attempted' to reproduce the whole pattern. The pattern

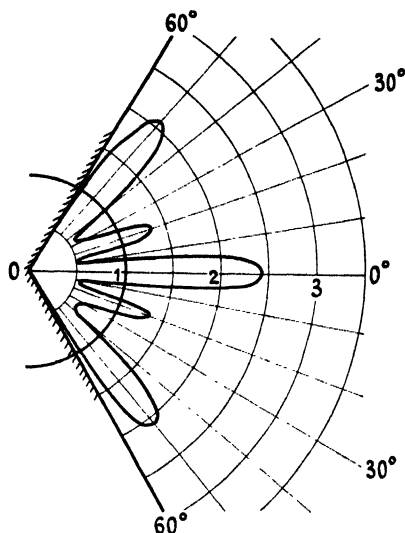


FIG. 10.6. Ideal polar diagram for  $120^\circ$  corner reflector, filament distant  $1.75\lambda$  from apex,  $k = 11$ .

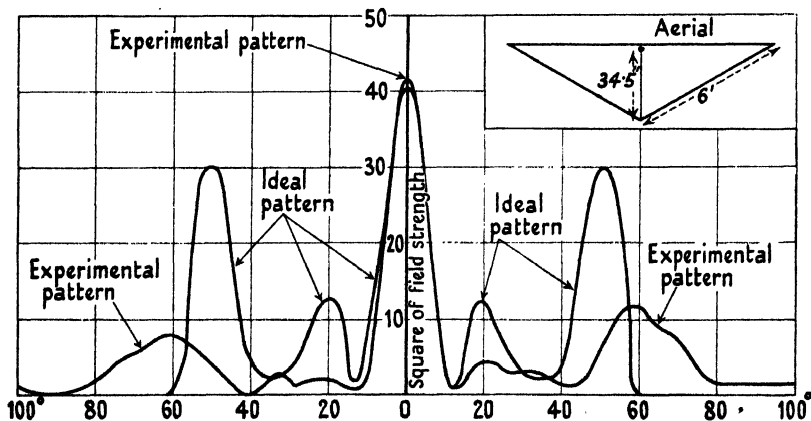


FIG. 10.7.  $120^\circ$  corner reflector,  $k = 11$ .  $\lambda = 50$  cm. = 1.63 ft.

they did produce is more tolerable for practical purposes than the ideal: the good features of the ideal are unimpaired, the undesirable features are diminished, at the price of a certain amount of diffraction round the edges. When  $N$  is a fraction the Fourier treatment involves the mathematical difficulty that the field is multivalued (in the Riemann sense) and hence it is not quite certain it represents the problem to

which we have applied it; when  $N$  is an integer images can be found and the series is not multivalued. The correspondence between the observed and the ideal patterns in Fig. 10.7 must surely show the ideal pattern predicted from the Fourier series is the correct solution or at least very near it. Fig. 10.8 compares the experimental with the ideal pattern at  $k = 5$ : the correspondence is so close that it leaves no

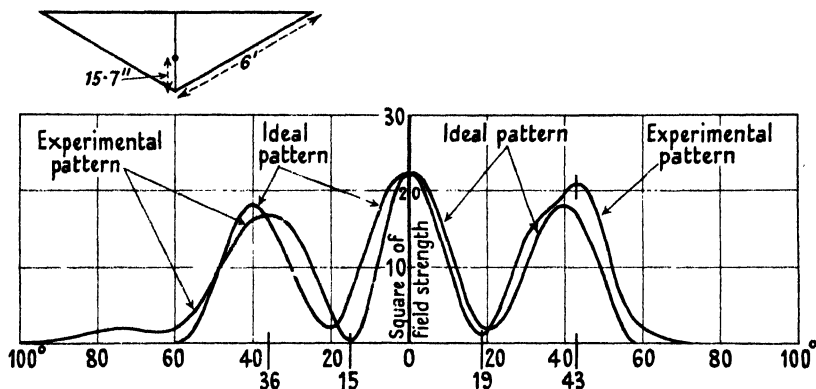


FIG. 10.8.  $120^\circ$  corner reflector;  $k = 5$ ,  $R/\lambda = 0.79$ .  $\lambda = 50$  cm. = 1.63 ft.

reasonable room for doubt that the Fourier series is valid for all values of  $N$ . We have now produced a main beam only  $13^\circ$  wide, accompanied by lobes which, though large, may not be intolerable, and, moreover, a main beam which we can predict beforehand.

We will now examine fully the  $90^\circ$  reflector with the aerial at the second station. Fig. 10.9 shows the ideal pattern for  $R/\lambda = \frac{3}{2}$  and also the pattern obtained experimentally from sheets  $6\lambda$  wide by  $\frac{3}{2}\lambda$  high. It shows that the observed main beam is scarcely distinguishable from the ideal, save to the extent that it is  $1.5^\circ$  narrower at half-height (in field strength). The very small lobe, centred on  $\theta = 22^\circ$  in the ideal, appears magnified in the experimental pattern, while the lobe which should be centred on  $\theta = 36^\circ$  has 'slid over the edge' completely. This experiment was repeated with sheets  $3.6\lambda$  wide, but the result was not distinguishable from that shown in Fig. 10.9 for sheets  $6\lambda$  wide. Thus we conclude that sheets  $3.6\lambda$  wide suffice for the  $90^\circ$  reflector and that any practicable increase of width will have no sensible effect. Comparison of Figs. 10.7 and 10.9 shows that decreasing the angle from  $120^\circ$  to  $90^\circ$  has made a small improvement in the main beam but has decreased the lobes considerably: thus it is better to use these sheets inclined at  $90^\circ$  and to do so will also reduce the aperture and general bulk of the reflector.

Table 10.10 records the observed pattern produced by sheets  $2\lambda \times \frac{3}{2}\lambda$ ; the measurement was made at a wavelength of 125 cm.

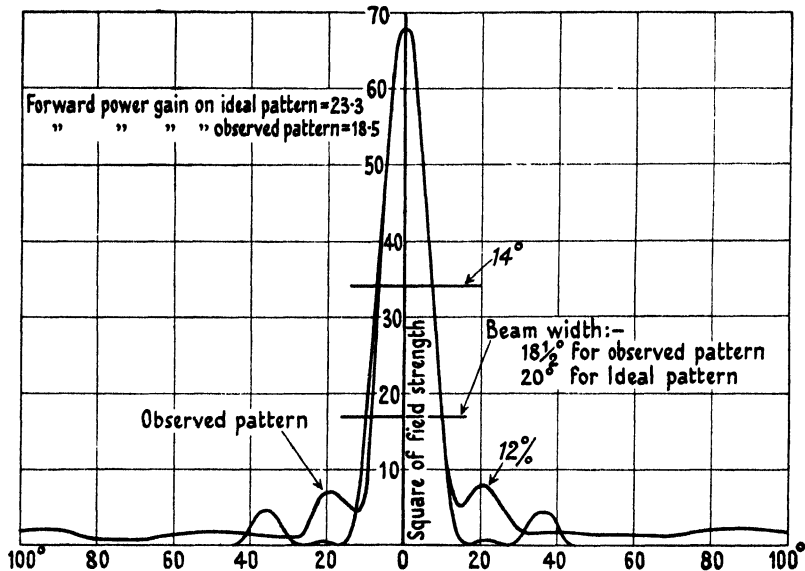


FIG. 10.9. 90° corner reflector,  $R/\lambda = \frac{3}{2}$ .  $\lambda = 50$  cm. = 1.63 ft., sheets  $9\frac{1}{2}$  ft. wide.

Table 10.10 shows that the main beam produced by sheets  $2\lambda$  wide is appreciably wider than the ideal and that on bearings between 20° and 100° there is a general background of the order of 10 per cent. in power. Sheets  $2\lambda$  wide are still well worth while for the second station: interpolation between this result and Fig. 10.9 suggests the sheets should be about 2.5 to  $3\lambda$  wide for use with the second station in a 90° reflector.

TABLE 10.10

*Mirror angle 90°,  $R/\lambda = \frac{3}{2}$ , sheets  $2\lambda \times \frac{3}{2}\lambda$*

	Width at $\frac{1}{2}$ -power	Width at $\frac{1}{4}$ -power	% power at 38°	% power at 60°	% power at 90°
Ideal	14.5°	20°	8	0	0
Observed	18.5°	25°	7	10	4

A representative pattern near the second station for a 75° mirror has been shown already in Fig. 10.2. Once more the observed and ideal main beams are scarcely distinguishable and are 13° wide at half-power: the observed side lobes are very large, though much smaller than the ideal.

The ideal gain of a 60° mirror attains its second maximum, value 32,

when  $R/\lambda = \frac{5}{4}$ . Then the first zero occurs when  $\theta = 23^\circ$ , though the straight sides of the main beam cut the bearing axis at  $19^\circ$ : the side lobe between  $23^\circ$  and  $30^\circ$  of bearing has a maximum which is much less than 1 per cent. in power and thus the ideal pattern is effectively a lobe-free beam of width  $19^\circ$  at half-height, in field strength. The observed pattern produced by sheets  $3.6\lambda$  wide is shown in Fig. 10.10:

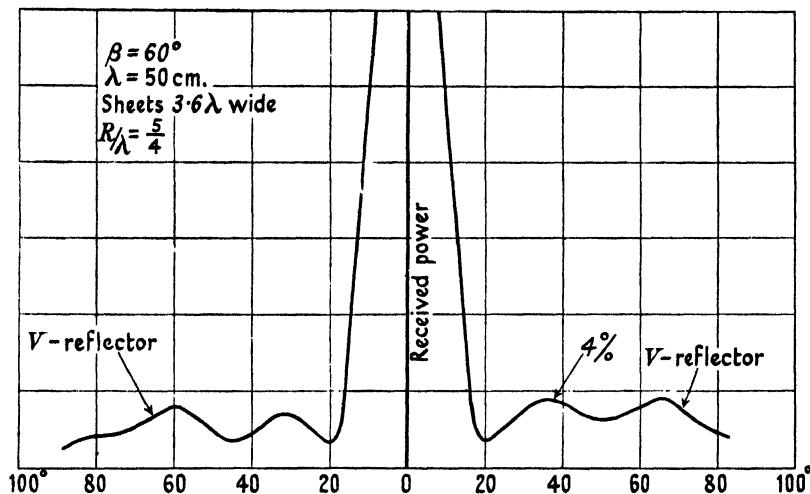


FIG. 10.10.  $60^\circ$  corner reflector,  $R/\lambda = \frac{5}{4}$ .  $\lambda = 50$  cm. = 1.63 ft., width of sheets  $3.6\lambda$ .

the straight sides of the main beam cut the bearing axis at  $19^\circ$  and this coincides with the ideal: there is diffraction round the edge amounting to about 4 per cent. in power on bearings between  $30^\circ$  and  $80^\circ$ . This is about the best practicable Vee reflector for wavelengths round 50 cm. Table 10.11 records the pattern observed from sheets  $2\lambda \times \frac{3}{2}\lambda$  and  $\beta = 60^\circ$ , the wavelength being 125 cm.

TABLE 10.11

*Mirror angle  $60^\circ$ ,  $R/\lambda = \frac{5}{4}$ , sheets  $2\lambda \times \frac{3}{2}\lambda$*

	Width at $\frac{1}{2}$ -power	Width at $\frac{1}{4}$ -power	% power at $30^\circ$	% power at $50^\circ$	% power at $70^\circ$
Ideal	$12^\circ$	$19^\circ$	0	0	0
Observed	$29^\circ$	$41^\circ$	14	10	2.5

It shows that sheets  $2\lambda$  wide do not suffice to produce the ideal main beam, and comparison with Table 10.10 shows the main is much broader than when the sheets were inclined at  $90^\circ$ . Thus we find that if the second station is to be employed with sheets  $2\lambda$  wide, then the

mirror angle should be  $90^\circ$ , but if sheets  $3.6\lambda$  wide can be tolerated they should be inclined at  $60^\circ$  and will then produce the ideal main beam.

It is appropriate here to make a comparison between the  $60^\circ$  mirror and an equivalent curtain array. We have stated that the straight sides of the ideal beam cut the bearing axis at  $\pm 19^\circ$  and hence, by (2.3), the main beam is equivalent to that of a curtain array having 6 members spaced  $\frac{1}{2}\lambda$  apart: such a main beam being accompanied by the well-known series of lobes which start with an amplitude of 20 per cent. in field (i.e. 4 per cent. in power). It has been found that sheets  $3.6\lambda$  wide reproduce the ideal main beam, but that it is accompanied by lobes centred on  $36^\circ$  and  $66^\circ$  each about 4 per cent. in power: thus such sheets happen to be a very close equivalent of a 6-member curtain in front of a large flat reflector. Thus by using the  $60^\circ$  Vee the pattern obtained from a single aerial and cable is equivalent to that from six aeriels and six cables, in a curtain. The aperture of this particular Vee reflector is  $3.6\lambda$ , the width of the 6-member curtain is  $2.5\lambda$ , and the reflecting sheet behind it would need to be at least  $3.6\lambda$  wide. Thus for equal width the Vee reflector gives an equivalent performance with five less cables: we have said in Chapter III that sheet reflectors are really a device for saving a plurality of feeding cables and here we are able to make a direct comparison. If the sheets are increased in width, the side-lobe field will be reduced at a very slow rate, the main beam being unaffected.

Let it be pointed out here that the width of the beam, for a given  $R/\lambda$ , does not depend on the aperture of the mirror and the whole of our treatment shows the beam width depends only on  $\beta$  and  $R/\lambda$ : there is, however, a common misconception, based on optics, that the width of beam is proportional to the aperture of mirror.

The second station for  $\beta = 45^\circ$  is when  $R/\lambda = 2$  and then the ideal gain is about 53. We remember that the pattern cannot depart appreciably from a sinusoid until the arcual width, across the Vee, at the aerial exceeds about  $\frac{3}{2}\lambda$ . When  $R/\lambda = 2$  and  $\beta = 45^\circ$  the width is  $1.57\lambda$ , and thus we are just within the range when the third harmonic in the pattern is becoming appreciable. Fig. 10.11 shows the ideal pattern: its width at  $\frac{1}{4}$ -power is  $26^\circ$  as compared with  $30^\circ$  for a sinusoid. The same figure shows the pattern produced by sheets  $6\lambda$  wide: the observed main beam is much narrower than the ideal, but now the rudimentary side lobes have swollen into formidable realities. When the sheets were reduced in width from 6 to  $3.6\lambda$  the main beam was scarcely affected, but then it was accompanied by enormous side lobes centred on  $\pm 30^\circ$ . If the second station is to be used with  $\beta = 45^\circ$  we conclude the sheets

ought to be about  $7$  or  $8\lambda$  wide, in order to curb the lobes: it is to be expected the main beam will be narrower than the ideal.

At  $\beta = 45^\circ$  we have reached the limit of practicability for a wavelength of  $50$  cm.; for sheets  $10$  ft. wide scarcely suffice at the second station because they permit lobes of the order of  $30$  per cent. in field

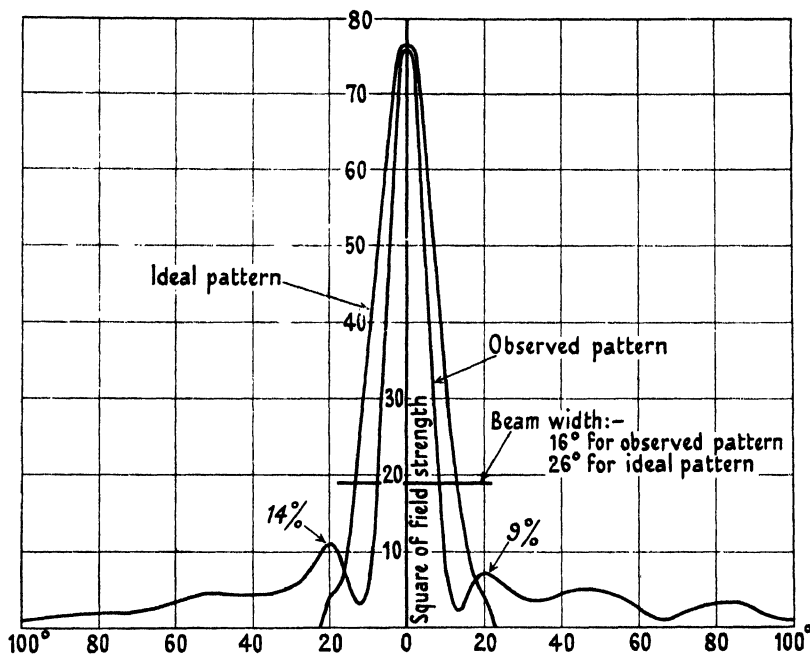


FIG. 10.11.  $45^\circ$  corner reflector,  $R/\lambda = 2$ .  $\lambda = 50$  cm. =  $1.63$  ft., sheets  $9\frac{1}{2}$  ft. wide.

strength. A width much in excess of  $10$  ft. is scarcely tolerable or practicable. Further consideration of § 3.8 will show that when  $\beta$  is less than about  $45^\circ$  then  $R/\lambda$  must be large before we can hope to obtain an ideal pattern appreciably sharper than the simple sinusoid, and accordingly the necessary width of sheet must increase very rapidly as  $\beta$  diminishes. In fact, if  $\beta$  is  $45^\circ$  or less it is probably best to use the first station, and then we can hope for a beam of width less than  $\frac{2}{3}\beta$  only in so far as finite sheets often produce a beam narrower than the ideal.

#### (d) Patterns for the third station

The reader will now realize the third station can be contemplated only for mirrors of comparatively wide angle and then the main beam is likely to be accompanied by very large lobes. Fig. 10.12 shows the ideal pattern for  $\beta = 90^\circ$  and  $R/\lambda = \frac{1}{2}$  and also the observed pattern



produced by sheets  $6\lambda$  wide. The figure is interesting chiefly in demonstrating the way in which comparatively narrow sheets 'make a brave attempt' to reproduce the ideal patterns, but in general they cannot achieve the legitimate side lobes in full strength. This particular mirror achieves a main beam only  $11^\circ$  wide, but the side lobes are enormous, even though they are moderate compared with the ideal.

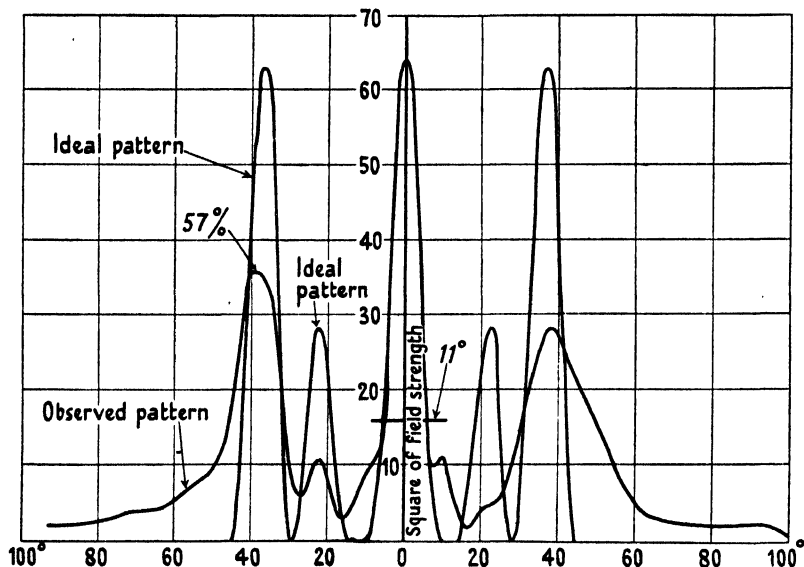


FIG. 10.12.  $90^\circ$  corner reflector,  $R/\lambda = \frac{5}{2}$ .  $\lambda = 50$  cm. = 1.63 ft., sheets  $9\frac{1}{2}$  ft. wide.

The ideal equatorial pattern for  $\beta = 60^\circ$  and  $R/\lambda = 3\frac{1}{2}$  is attractive in having a main beam only  $10^\circ$  wide at half-height accompanied by very narrow 25 per cent. lobes centred on  $\pm 18^\circ$ . The complete polar figure is reproduced in Figs. 4.12–4.14. Suffice it to say now, however, that sheets  $6\lambda$  wide produce a main beam wider than the ideal and accompanied by a pair of vast lobes: the third station for  $\beta = 60^\circ$  cannot be used unless sheets at least  $10\lambda$  wide can be tolerated.

It is important to remember that these observed equatorial patterns have been produced by a half-wave aerial. Now reference to Figs. 4.12–4.14 will remind the reader forcibly that the ideal polar figure of a half-wave aerial may contain large beams which do not disclose themselves in the equatorial pattern. It may well be that the discrepancy between the observed and the ideal side lobes in the equatorial pattern is due as much to lack of height as to lack of width in the sheets. Thus, the large side lobes observed in the experiment just recorded may possibly be due to the large upward tilted beams (in Figs. 4.12–4.14)

having, so to speak, fallen down towards the equator; and they have done so because the height of the screens was inadequate. A full investigation would require the polar diagram at various angles of elevation and these are very troublesome to obtain. It must not be forgotten that the half-wave aerial is apt to produce sharp beams of high-angle radiation when  $R/\lambda$  is large and these may ruin the suitability of the aerial as a searching device. They will not be disclosed in the equatorial pattern and accordingly this pattern may be very misleading.

## PERFORMANCE OF HALF-WAVE AERIAL AND FLAT SHEET: PERFORMANCE OF NETWORK REFLECTORS

THIS chapter is the experimental counterpart of Chapter V, where we analysed the problem of a filament parallel to a half-plane and did so mainly for the purpose of assessing the diffraction round edges. Now we examine experimentally the pattern due to a half-wave aerial associated with a flat sheet of finite size.

### 11.1. Aerial opposite the middle of a rectangular sheet

We have anticipated this problem by including Fig. 10.1 in the last chapter, for the reasons stated there. It compares the ideal pattern with that obtained from a half-wave aerial distant  $\lambda$  from the plane of a sheet  $3.6\lambda$  wide: however, this particular pattern is not likely to have practical application since the pattern of greatest practical importance is the single lobe which obtains when  $r/\lambda = \frac{1}{4}$ .

Fig. 11.1 records certain measurements at a wavelength of 125 cm. (i.e. 4 ft.). A half-wave aerial was placed 31.25 cm. ( $\frac{1}{4}\lambda$ ) in front of the plane of sheets 5 ft. ( $\frac{5}{4}\lambda$ ) high and the polar diagram was observed when the width of the sheet was  $\frac{1}{2}\lambda$  and also when the width was  $3\lambda$ : these two diagrams and also the ideal diagram are reproduced in Fig. 11.1: in it the left-hand curve is the diagram produced by a sheet  $\frac{1}{2}\lambda$  wide and the right-hand curve that produced by a sheet  $3\lambda$  wide. When the width is  $3\lambda$  the field is not a maximum on bearing zero, and this shows that the aerial is too far from the sheet to produce a diagram corresponding to the ideal for  $R/\lambda = \frac{1}{4}$ . The back-to-front ratio is 0.1 and 0.3 for the wide and narrow sheets respectively and the fractional fields on  $\theta = 90^\circ$  is 0.1 and 0.45: the calculated values of the back-to-front ratio for a corresponding half-plane are 0.06 and 0.1, and for the field at  $\theta = 90^\circ$  are 0.2 and 0.4 respectively. In both curves in Fig. 11.1 the field rises to a maximum at  $\theta = 180^\circ$ : reference to Figs. 5.6–5.9 shows that a half-plane does not tend to form a lobe at  $\theta = 180^\circ$ , since the field decreases continuously as  $\theta$  increases.

The two diagrams recorded in Fig. 11.1 were observed over the range  $0^\circ$ – $360^\circ$  and were, as usual, not quite symmetrical: the values recorded for any bearing  $\theta$  are the mean of the values observed on bearings  $\pm\theta$ . Since the gain tends to be nearly constant when  $R/\lambda$  is less than  $\frac{1}{4}$ , it seems natural to attempt to economize width by making  $R/\lambda$  small. The polar diagram appropriate to a single aerial and flat

sheet is not likely to be used in practice unless the wavelength is several metres. Or, put it this way, if  $\lambda$  is several metres, then an array or reflector system is necessarily bulky: if the station is a mobile one, then the problem may well be to endow it with some degree of directivity by using the smallest possible reflector. Presuming that there is a crippling restriction on absolute dimensions, then our best chance is to

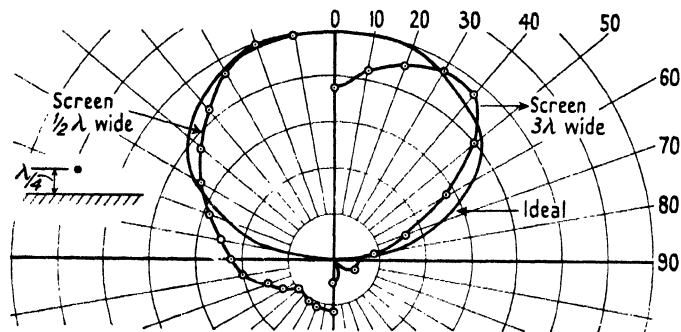


FIG. 11.1. Polar diagrams for half-wave aerial distant  $\frac{1}{4}\lambda$  from a flat metal sheet.

use a flat sheet near the aerial, and it remains to discover by experiment the narrowest sheet which will be worth while to use. Having such possible circumstances in mind the following experiments were made with a half-wave aerial distant only  $\lambda/10$  and  $\lambda/20$  from the sheet. Measurements were made at a wavelength of 120 cm.; the screens were  $1.6\lambda$  high and their total width was either  $\frac{1}{4}$ ,  $\frac{1}{2}$ , or  $\frac{5}{4}\lambda$ . The experimental results are shown collected in Table 11.1 below.

TABLE 11.1  
*Flat sheet of height  $1.6\lambda$*

Total width of screen	Front/Back ratio		% field strength in plane of sheet	
	$d/\lambda = \frac{1}{10}$	$d/\lambda = \frac{1}{20}$	$d/\lambda = \frac{1}{10}$	$d/\lambda = \frac{1}{20}$
$\frac{5}{4}\lambda$	3.2	4.0	30	32
$\frac{1}{2}\lambda$	7.5	7.5	36	32
$\frac{1}{4}\lambda$	2.5	2.5	52	52

We note first that the performance with  $d/\lambda = \frac{1}{10}$  is substantially the same as when  $d/\lambda = \frac{1}{20}$ ; also that the diffraction round the edge, as measured by the field strength in the plane of the sheet (which ideally should be zero), decreases very slowly with increasing width, and this is in accordance with the analytical predictions in Chapter V. It appears from the series of Figs. 5.4–5.7 that when  $d/\lambda = \frac{1}{4}$  and the sheet

is semi-infinite, that the fractional field in the plane of the sheet is 50 per cent. when  $x/\lambda = \frac{1}{2}$ , 35 per cent. when  $x/\lambda = 1$ , and 21 per cent. when  $x/\lambda = 2$ . Our experimental equipment does not approximate to a half-plane, but applying that notation to them the largest value of  $x/\lambda$  is  $\frac{5}{8}$  and then the field in the plane of the sheet would be 60 per cent. if  $d/\lambda = \frac{1}{4}$ . Experiment shows it is about 30 per cent. for a sheet only

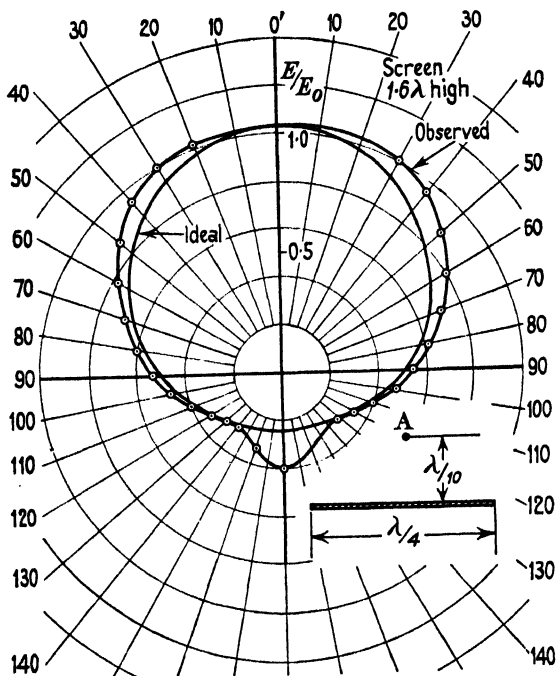


FIG. 11.2. Polar diagram of aerial and a flat sheet.

$\frac{5}{8}\lambda$  total width, and thus turns out to be less than our analysis might have led us to predict. As a very rough guess we might assume the diffraction round each edge of a sheet  $\frac{1}{4}\lambda$  wide is the same as that round the edge of a half-plane where  $x/\lambda = \frac{1}{8}$ : on this basis we can construct a hypothetical diagram and term it the ideal. The pattern has been worked out for an aerial distant  $d/\lambda = \frac{1}{10}$  and situated so that  $x/\lambda = \frac{1}{8}$  ( $\alpha = 143^\circ$ ), and Fig. 11.2 compares the experimental polar diagram for  $d/\lambda = \frac{1}{10}$  and a sheet  $\frac{1}{4}\lambda$  wide with the said ideal. The agreement is reasonably close in the range of bearing from zero to  $\pm 140^\circ$ . However, the observed front-to-back ratio is only 2.5 to 1, whereas our rough estimate gives 4 to 1. It is interesting to note from Table 11.1 that the front-to-back ratio does not increase continuously with the width of

the sheet. The field in the plane of a semi-infinite sheet has been worked out for the case where  $d/\lambda = \frac{1}{10}$  and  $x/\lambda = 0.63$  ( $\alpha = 171.5$ ) and turns out to be 21 per cent. The first row of Table 11.1 shows this ratio was found to be 30 per cent. for each edge of a sheet of total width  $1.25\lambda$ . Thus it seems the single edge is only a very rough guide to a double edge.

It is, however, clear that a sheet  $\frac{1}{2}\lambda$  wide provides quite an effective reflector, while Fig. 11.2 shows that a sheet only  $\frac{1}{4}\lambda$  wide confers a very substantial benefit. It is probably safe to interpolate that a sheet  $2\lambda$  wide would produce as near an approach to the ideal as would be worth while or practicable to attempt. We shall see later that such sheets may be constructed from widely spaced rods or very open netting: thus a sheet  $\frac{1}{4}\lambda$  wide need not offer much wind resistance and thus may be a very practicable device for mobile stations using a wavelength of some 5 metres. Much the same results could be obtained from a single tuned rod, often called a parasite. Then it is necessary to choose adroitly both the distance between the aerial and the rod and also the tuning of the rod. Use of the narrow sheet obviates both these difficulties and in this respect is the preferable arrangement. The ultimate decision is likely to turn on the height of sheet which can be tolerated: the height can probably be less than  $1.6\lambda$  without detriment to the pattern. If  $\lambda$  is less than 4 m. it will probably be best to use a narrow sheet, and if  $\lambda$  exceeds 6 m. best to use a tuned parasite.

## 11.2. Aerial in the plane of the sheet

If the aerial is in the plane of the sheet the polar diagram is substantially a circle with a sharp crevasse in the plane of the sheet: such a system has valuable properties for rough direction-finding since there is no ambiguity of sense. Incoming signals from all bearings will produce about the same signal strength: on hearing a signal the observer turns the sheet (with the aerial attached to it) about a vertical axis until silence occurs. He then knows the signal is coming in on that bearing of the sheet and is in the sense away from the aerial. Having this application in mind we must now explore the sharpness of the bottom of the crevasse which is produced by a sheet of practicable dimensions. Once more we are faced by the practical requirement of keeping the reflecting sheets small: accordingly we shall experiment with an aerial close to the edge of the flat sheet. First consider the shape of the ideal crevasse: to do this we have to evaluate equation (5.2) near  $\theta = \pi$  and with  $\alpha = 0$ . Denote by  $\phi$  the bearing from the plane

of the sheet (i.e.  $\phi = 180^\circ - \theta$ ), then it follows from (5.2) that when  $k$  is very small

$$\frac{E}{E_0} = 2J_1(k) \sin \frac{1}{2}\phi.$$

Also, when  $k$  is very small the power output is equal to

$$\frac{120\pi^2}{\lambda} J_1^2(k) I^2$$

and, moreover,  $E_0$  is always proportional to  $I$ : hence for a given power output  $E_0 J_1(k)$  is constant, and accordingly the field on a given bearing in the crevasse is then independent of  $k$ . Hence, provided  $k$  can be reckoned as small and the input power is constant, the crevasse should be independent of the distance between the aerial and the edge of the sheet: evaluation shows this approximation is valid up to about  $R/\lambda = 0.2$ . For *constant power* the ideal crevasse is twice as steep when  $R/\lambda = \frac{1}{2}$  as when  $R/\lambda = 0.1$  and three times as steep when  $R/\lambda = 1$ . But to take advantage in practice of this improvement will involve the use of a much wider sheet. In § 2.1 we saw that two equal currents can produce a polar diagram with a crevasse falling to zero field, provided they are phased appropriately to their separation. It can readily be shown that when this condition is fulfilled then

$$\frac{E}{2E_0} = \sin(\frac{1}{2}k \sin^2 \frac{1}{2}\phi) \div \frac{1}{2}k \sin^2 \frac{1}{2}\phi$$

and thus the ideal crevasse has a round bottom. The ideal crevasse for the half-plane has a sharp bottom and is therefore more suited inherently to the purpose we have in mind here, if it is attainable in practice.

Fig. 11.3 shows the ideal pattern for  $R/\lambda = \frac{1}{10}$  and the observed patterns produced by various sheets whose widths covered a range of 5 to 1. The effect on the observed pattern of this fivefold increase of width is not very striking, and hence we conclude it is not worth while to use a sheet wider than  $\frac{5}{2}\lambda$  and scarcely necessary to make it wider than  $\frac{1}{2}\lambda$ . The effect was then studied of varying the height of a screen whose width was  $\frac{1}{2}\lambda$ . Then it appeared the sharpness of the crevasse was very dependent on the height of the screen: reduction of height tends to produce a pimple at the bottom of the crevasse, this said pimple having become enormous when the height neared  $\frac{1}{2}\lambda$ . Figures such as 5.13 and 5.15 show the current density induced in the screen is concentrated mainly in a strip, whose width is of the order of  $R$ , at the leading edge: therefore it is important to provide high conductivity in this strip. Experiment showed the shape of the crevasse

could be improved considerably by placing a strip of sheet brass (width about  $R = \frac{1}{10}\lambda$ ) on the leading edge of a screen made from steel wire gauze having a  $\frac{1}{8}$ -in. mesh. Fig. 11.4 records various attempts to produce a steep-sided crevasse. Curve *A* is the pattern due to a screen, of steel gauze,  $\frac{3}{4}\lambda$  square. Curve *B* is the pattern which resulted when the conductivity of the leading strip of this screen was improved by

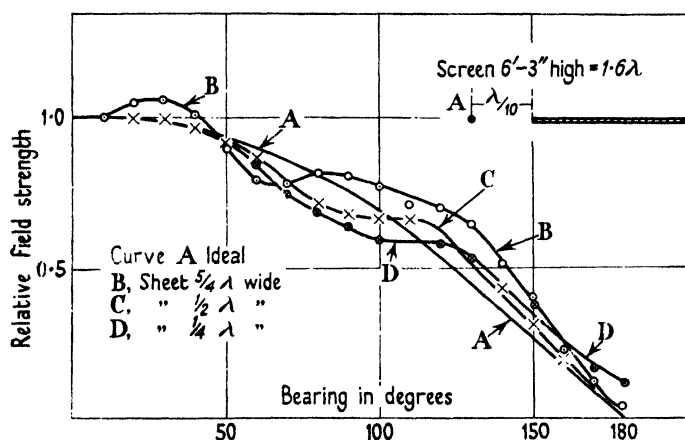


FIG. 11.3. Diffraction patterns for aerial in plane of a flat sheet.

clipping to its surface a brass strip 1 ft. wide: the improvement is very marked and the reason for the effect well understood. A similar strip was then placed towards the trailing edge: the effect of this is recorded by curve *C* and is small, as was to be expected. Curves *D* and *E* show the effect of adding roof-plates, as described in the inset diagram. Such roof-plates steepen the sides of the crevasse but give it a flat floor. An enormous amount of experimentation was made in the attempt to sharpen the crevasse: for example, by fitting a narrow T-strip on the leading edge and by forming the screen from a wedge of small angle, etc., but all to no avail. The really important factor is that the leading portion of the screen should be a continuous strip of brass sheet: probably this is the only example where the conductivity of a reflector matters appreciably. Further improvement can come only from increasing the size of the screen, height appearing to matter more than width. The total width of the flat bottom of the crevasse need not be more than  $10^\circ$ , but it is extremely difficult to reduce this width below  $5^\circ$ .

Those whose experience has been mainly with rod aerials may expect to find critical effects when the height of a narrow screen is  $\frac{1}{2}\lambda$ ,  $\frac{3}{4}\lambda$ , etc. Such tuning effects, however, do not occur to any noticeable extent.



Thus the pattern due to a screen 2 ft. wide and 4 ft. high was observed at 230, 240, and 250 Mc/s: no significant difference occurred in this range of frequency, which was centred on a wavelength of 4 ft. A sheet 2 ft. wide and 2 ft. high was tested over this range of frequency: the

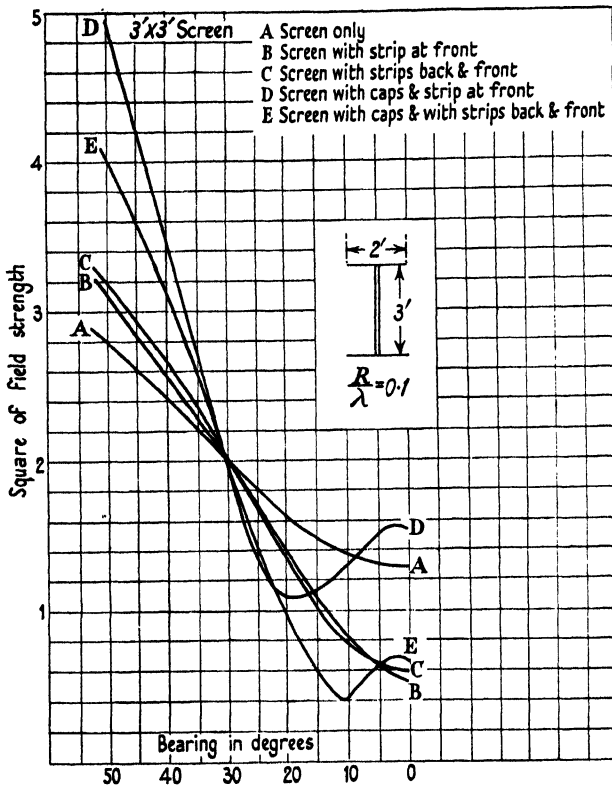


FIG. 11.4. Relating to aerial in plane of a flat sheet.

pattern has a large pimple in the middle of the crevasse and this pimple decreased continuously as the frequency increased; since the decrease was continuous, the effect was not one of resonance.

### 11.3. Aerial level with edge of sheet ( $\alpha = 90^\circ$ )

An ideal pattern for this disposition is shown in Fig. 5.4. If there is an aerial on each side of the sheet and if this pair is energized alternately, the beam will wave from side to side: this might find practical application. Fig. 11.5 shows the ideal polar diagram for an aerial level with the edge and distant  $\frac{1}{10}\lambda$  from it. Also the observed diagrams which resulted from sheets  $\frac{5}{4}\lambda$ ,  $\frac{1}{2}\lambda$ , and  $\frac{1}{4}\lambda$  wide: the diagram

is markedly unsymmetrical even when the sheet is only  $\frac{1}{4}\lambda$  wide. This figure is generally instructive, but does not call for detailed comment. When the width of the sheet was  $\frac{1}{2}\lambda$  the diagram was found to be sensibly independent of the height of the sheet so long as it was not less than  $\frac{3}{4}\lambda$ .

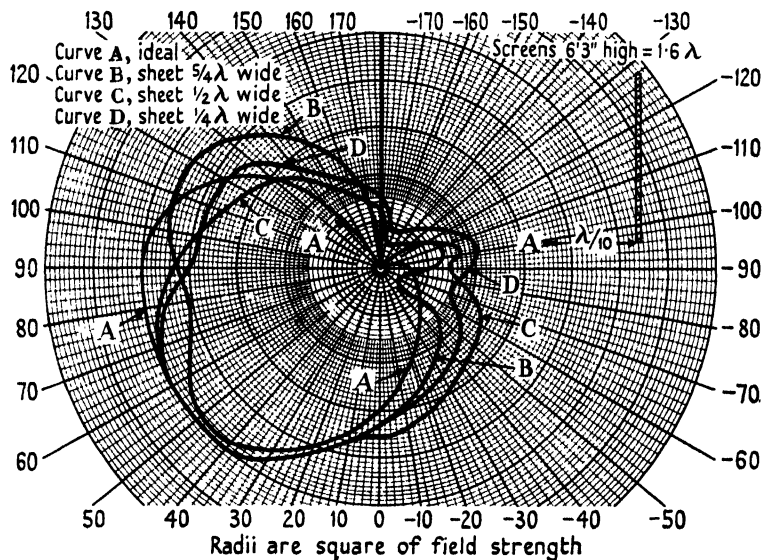


FIG. 11.5. Polar diagrams for aerial level with edge of a flat sheet.

#### 11.4. Continuous sheets compared with sheets of netting

In §§ 5.6 and 5.7 it was found that a grid of rods will reflect almost as well as a continuous sheet, provided the rods themselves are not extremely thin: the diameter of the rods is as important a factor as the spacing between them. It was stated there that the screening ratio should exceed 90 per cent. provided the 'shadow ratio' of the grid was not less than 17 per cent. and the spacing not much in excess of  $\frac{1}{3}\lambda$ : and that screening ratios near unity can be obtained even when the spacing is near  $\frac{1}{2}\lambda$  provided the diameter of the rods is chosen correctly, by means of Fig. 5.16.

There would be no particular interest in checking our formulae by experiment: they serve their purpose by pointing out the mechanism of the process and they provide a general scale of sizes. We conclude from them that screening should be sensibly perfect if the spacing does not exceed about  $\frac{1}{2}\lambda$ : let us consider what this means in actual dimensions. If  $\lambda = 125$  cm., then  $\frac{1}{2}\lambda$  equals 6 in.; hence if  $\lambda$  exceeds about

1 metre, then a 6-in. mesh is virtually equivalent to a continuous sheet, provided of course the wire itself is not too fine. If  $\lambda = 10$  cm., then we may expect a  $\frac{1}{2}$ -in. mesh to be equivalent to a continuous sheet: we now have a general scale in mind. Our purpose here will be served by giving a few comparisons of the performance of continuous and of netting sheets of given size.

A  $90^\circ$  Vee was constructed by stretching fine mesh copper gauze on two wooden frames of side 5 ft. The equatorial pattern was observed at a wavelength of 125 cm. with the aerial set at  $R/\lambda = 0.53$ . Then the gauze was removed and replaced by expanded metal having a 2 in.  $\times$  1 in. diamond mesh. Careful comparison of the patterns obtained from these two coverings showed that if there was any discrepancy, then it was less than the errors of measurement and these were small: no difference could be detected in the width of the beam at half- or at quarter-height (in power) or in the fractional power on bearing  $\pm 45^\circ$ . Thus it was concluded that a diamond mesh  $\frac{1}{48}\lambda \times \frac{1}{24}\lambda$  was indistinguishable, as a reflector, from a continuous sheet: in the light of our analysis it would have been very surprising if any difference of performance could be detected. A comparison was also made between expanded metal (1 in.  $\times$  2 in. diamond mesh) spot-welded to a  $\frac{1}{2}$  in.  $\times$   $\frac{1}{2}$  in. iron frame 5 ft. wide and  $6\frac{1}{4}$  ft. high and S.W.G. 20 wire netting with  $1\frac{1}{4}$  in.  $\times$   $1\frac{1}{4}$  in. mesh, stretched on wooden frames of similar size. The said wire netting (on wooden screens) produced a pattern which was just measurably wider than that produced by the expanded metal (on iron frame) for bearings up to  $\pm 40^\circ$ : for bearing angles larger than  $40^\circ$  the two patterns were not distinguishable. Here the comparison is mainly to assess the effect of reducing considerably the diameter of the wires of the grid. The experiment shows we may regard  $1\frac{1}{4}$  in.  $\times$   $1\frac{1}{4}$  in. wire netting as the equivalent of a continuous surface for wavelengths of 125 cm. and over. This experiment has established a point of great practical value, for experimenters will experience vastly less trouble from wind and weather if they use wire netting on their screens rather than a continuous sheet or copper gauze: its use reduces by a whole order the general difficulties attendant on aerial research. Also the engineer must learn confidence in using netting for permanent aerials, thereby reducing weight and windage enormously. High-quality netting of S.W.G. 16 steel wire is obtainable commercially and it requires very few supporting ribs.

The next example relates to the use of a grid such as we have typified in analysis. Two square gratings of parallel rods were made by welding

the ends of 5-ft. lengths of  $\frac{5}{8}$ -in. diameter brass tube, pitched 5 in. centre to centre, to a small channel bar: the two gratings were then joined together with planes at right angles, thus forming a structure which could not fail to be likened to half of a child's play-pen. It was used as a  $90^\circ$  Vee reflector at a wavelength of 125 cm.: the gratings then being  $\frac{5}{4}\lambda \times \frac{5}{4}\lambda$  with rods parallel to the half-wave aerial, which was mounted in the bisector at  $R/\lambda = 0.52$ . The width of the observed pattern was  $42^\circ$  and  $60^\circ$  at half- and quarter-height in power respectively, and the fractional power on  $45^\circ$  was 3 per cent. Corresponding figures for copper gauze screens (also 5 ft.  $\times$  5 ft.) were  $38^\circ$ ,  $56^\circ$ , and 5 per cent., thus showing the rods produced a beam  $4^\circ$  wider than that produced by continuous sheets, the diffraction round the back being scarcely changed. Here there was an extremely open and light structure functioning almost as well as continuous sheets of similar dimensions. Here the pitch of the grating is  $\frac{5}{16} = 0.104\lambda$ , and reference to Fig. 5.16 will show the correct radius for the rods is  $0.013\lambda$ : in fact their diameter was  $\frac{5}{16}$  in. which was  $0.0065\lambda$ , and thus they were known to be too thin for perfect reflection of a plane wave.

The writer has not had an opportunity to make an accurate comparison, but he has strong reasons for believing that a mesh of about  $\frac{1}{2}$  in. formed with S.W.G. 16 wire or expanded metal is sensibly the equivalent of a continuous sheet when used in reflectors for a wavelength of 10 cm.

We will now examine the performance of a comb of rods about  $\frac{1}{2}\lambda$  long: we have in mind structures corresponding to those illustrated in the paper by A. W. Nagy in the *Proc. Inst. Radio Engineers*,† and more especially the right-angled corner illustrated in the paper by J. D. Krauss in the same journal.‡ Krauss had a wooden set square with arms  $2.3\lambda$  long and pushed through them a large number of thin parallel rods  $0.94\lambda$  high. His paper gives some small-scale reproductions of the polar diagram which resulted from an aerial distant about  $\frac{1}{2}\lambda$  from the apex of the so-formed Vee: they appear to be a close approach to the ideal.

The writer has made a systematic examination of comb reflectors of the type used by Krauss. He used a light wooden right-angled set square with arms 4 ft. long and pierced them with holes pitched 4 in. apart. Through the said holes were pushed 23 steel rods, each  $\frac{5}{16}$  in. diameter and 2 ft. long, thus forming a right-angled corner comb reflector. Tests were made at or near a wavelength of 125 cm. (i.e. 4 ft.),

† Vol. 24 (1936), 233.

‡ Vol. 28 (1940), 513.

and thus the comb approximated to a pair of sheets  $\lambda$  wide and  $\frac{1}{2}\lambda$  high at right angles to one another, the shadow ratio of the so-formed grating being  $\frac{5}{8} = 0.08$  and the pitch  $\frac{1}{2}\lambda$ . Bearing in mind the rooted faith which many radio engineers have in the virtues of a rod which happens to be  $\frac{1}{2}\lambda$  long, it was desirable to examine the frequency consciousness of this reflector, since its rods were 2 ft. long and this is near  $\frac{1}{2}\lambda$ . Thus there was a twofold object in this experiment: (a) to compare the performance of the comb with that of a pair of gauze sheets 4 ft. wide and 2 ft. high; (b) to see if there is some wavelength, near 4 ft., at which a resonance effect is apparent. A half-wave aerial was placed on the bisector and 73 cm. (about  $0.6\lambda$ ) distant from the apex. A sheet of fine copper gauze, 2 ft. wide, was folded round the outside of the comb and supported by it, thereby backing the comb by a continuous sheet. The equatorial pattern resulting from this arrangement was observed: the gauze sheet having been removed from the comb the pattern was observed once more: the results are recorded in Table 11.2 below.

TABLE 11.2

	Width at half-height in power			Width at quarter-height in power			Power on bearing $45^\circ$			Back-to-front ratio, in power		
	$45^\circ$			$60^\circ$			0			0		
Ideal . . . .												
Mc/s . . . .	200	220	240	200	220	240	200	220	240	200	220	240
Gauze sheet on comb	$46^\circ$	$46^\circ$	$42^\circ$	$67^\circ$	$69^\circ$	$63^\circ$	8%	10%	8%	5%	< 1%	2%
Bare comb . . .	$51^\circ$	$54^\circ$	$47^\circ$	$73^\circ$	$81^\circ$	$70^\circ$	12%	19%	12%	7%	3%	2%

On the whole the beam tends to become slightly narrower as the frequency rises; presumably this is mainly because the sheets become relatively larger as the wavelength decreases, the total range of  $\lambda$  being 20 per cent. The pattern produced by the comb is always a little wider than that produced by gauze sheets: this is to be expected, but it is instructive to note that the removal of 92 per cent. of the reflecting area increases the width at half-power by only 10 per cent. This emphasizes once more that sheets may be reduced to 'a mere spider's web' without reducing their reflecting properties appreciably, provided the pitch of the web is only a small fraction of  $\lambda$ .

To examine the frequency effect more thoroughly than is described in Table 11.2 the rods of the comb were all cut to a length of 65.25 cm., which is  $\frac{1}{2}\lambda$  when the frequency is 230 Mc/s. The pattern was then observed in the frequency range 210–250 Mc/s, which is centred on the

frequency at which the rods are  $\frac{1}{2}\lambda$  long. The tests are recorded in Table 11.3.

TABLE 11.3

*Comb aerial reflector, arms 4 ft. wide, rods 65.25 cm. long,  
aerial 73 cm. from apex of right angle*

<i>Frequency</i>	<i>Width at half-height in power</i>	<i>Width at quarter-height in power</i>	<i>Power on bearing of 45°</i>	<i>Back-to-front ratio, in power</i>
Mc/s				
210	47°	67°	8%	10%
220	44°	67°	13%	5%
230	53°	75°	15%	8%
240	47°	70°	12%	3%
250	48°	70°	10%	1%

Table 11.3 shows that the beam width and the diffraction round the edge passes through a blunt maximum when the frequency is 230 Mc/s and thus there is a trace of a resonance effect: the effect, however, is deleterious to the performance of the reflector. Presumably the blunt resonance dictates the phase of the current induced in the rods and constrains it to be other than it would be in a large continuous sheet. At any rate we have found that the resonance effect is blunt, unimportant, and on the whole to be avoided. If the reader thinks over this problem and this experiment in the light of various sections of Chapter II he will realize the effective resistance and impedance of any given rod will depend on its position in the comb and also on the relative current in other rods. Hence all the rods will not be resonant simultaneously, and any resonance condition inferred from the observed pattern can only be a general average. A simple and sharp resonance effect is not to be expected: experiment shows that such as does occur is deleterious. Accordingly the informed designer will specify rods which are slightly longer than  $\frac{1}{2}\lambda$  and will not call for close tolerance of manufacture.

The previous chapter has shown us that sheets a few  $\lambda$  wide may be expected to produce patterns closely resembling the ideal: now we know that even these comparatively small sheets can be replaced by rods or wide-mesh netting without appreciable detriment to the performance of the reflector.

### 11.5. Half-wave aerial and two coplanar untuned parasite rods

In § 5.8 we solved some simple and typical examples involving parasite rods parallel to a current filament. Now consider two rods, each of radius  $b$ , distant  $R_2$  from one another and coplanar with a current filament which is distant  $R_1$  from the closest rod, distant

$R_3 = R_1 + R_2$  from the farther rod: denote the current filament by the letter  $A$  and the rods by  $B$  and  $C$  respectively. The self-impedance of each of the rods  $B$  and  $C$  is given by the equation

$$Z = -\frac{\pi a}{c} \{-J_0(ab) + jY_0(ab)\}.$$

Denote the electric field at  $B$  due to current  $I_A$  at  $A$  and current  $I_C$  at  $C$  by  $E_B$ : then

$$\frac{cE_B}{\pi a} = \{-J_0(k_1) + jY_0(k_1)\}I_A + \{-J_0(k_2) + jY_0(k_2)\}I_C = \frac{c}{\pi a} ZI_B.$$

On writing down the corresponding equation for  $E_C$  we obtain the relations

$$H_0(k_1)I_A - ZI_B + H_0(k_2)I_C = 0,$$

$$H_0(k_3)I_A + H_0(k_2)I_B - ZI_C = 0.$$

These give  $I_B$  and  $I_C$  in magnitude and phase relative to  $I_A$ . Let  $R_1 = \frac{1}{10}\lambda$ ,  $R_2 = \frac{1}{4}\lambda$ , and  $r = 0.0076\lambda$ . Then numerical evaluation gives

$$\frac{I_B}{I_A} = -0.46 \angle 47.5^\circ \quad \text{and} \quad \frac{I_C}{I_A} = 0.12 \angle 49.7^\circ.$$

It now follows the field at  $A$  due to  $I_2$  and  $I_3$  is given by

$$E = -\frac{c}{\pi a} (0.406 + 0.168j),$$

and hence the radiation resistance of filament  $A$ , in the presence of the parasite, is 0.594 of what it would be if isolated. The process of deriving the polar diagram is straightforward: it is shown in Fig. 11.6. The forward field is  $1.11E_0$  and it follows the gain  $= 1.22/0.59 = 2$ : the front-to-back ratio is 2.5. The curve on the left-hand side of the same figure, distinguished by observation points every  $10^\circ$ , is the observed diagram due to a half-wave aerial and two  $\frac{3}{4}$ -in. diameter rods (open circuited at each end)  $\frac{3}{8}\lambda$  high. The distance between the two rods was  $\frac{1}{4}\lambda$  and the coplanar half-wave aerial was distant  $0.1\lambda$  and  $0.35\lambda$  from them; the wavelength was 125 cm. and consequently the radius of the rods was then  $0.0076\lambda$ : thus the configuration of aerial and rods corresponds with that postulated in the ideal diagram of Fig. 11.6. The correspondence between the observed and ideal patterns is really very close when it is remembered we have used a two-dimensional problem to simulate one in three dimensions: no doubt the approximation has been assisted here by the smallness of the distances  $R_1$  and  $R_2$ .

When the two  $\frac{3}{4}$ -in. diameter rods were replaced by two pieces of  $\frac{3}{4}$  in.  $\times$   $\frac{3}{4}$  in. brass angle, joined electrically at top and bottom by a 12-in.

length of the same angle, the observed pattern differed from that shown in Fig. 11.6 by little more than the limits of experimental error. Now the metal bridge pieces across the ends, forming a closed frame 6 ft.  $\times$  1 ft., might be expected to disturb the impedance of the rods considerably; yet the effect on the diagram was not significant. Thus we infer that tuning effects in parasitic rods which are much longer

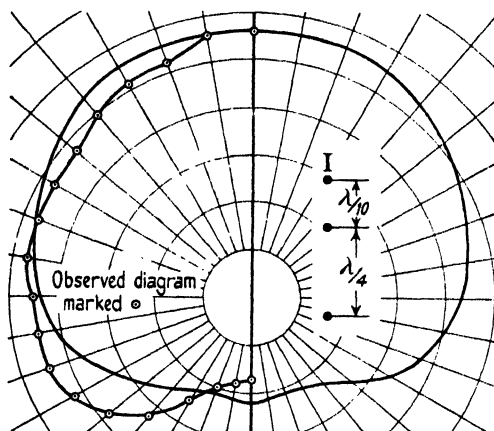


FIG. 11.6. Polar diagram due to an aerial coplanar with a pair of untuned rods.

than the driving aerial are not important and that their effective impedance does not depend much on the shape of their cross-section. Moreover, the effect, on the pattern, of screwing to the said angle frame a copper sheet 12 in. wide and 6 ft. high was also insignificant, thus demonstrating even more forcibly that the shaping of a reflector of this character is not important. Analysis of the half-plane has shown that in it the current density is dominantly concentrated in a narrow strip near the leading edge and always rises rapidly near a bounding edge. Hence, if we had started by using a sheet in this problem, our analytical experience would have taught us to expect the induced current would be concentrated near the edges, and this would have suggested the narrow sheet must be behaving very like two parallel rods: this supposition is borne out by these experiments.

The close agreement between the ideal and observed patterns in Fig. 11.6 may possibly be fortuitous in this particular experiment; provided it is not accidental it would seem the two-dimensional method is a very powerful tool for predicting the pattern due to an aerial combined with two or three parasites. Everyone knows from experience that the pattern due to a single parasite is vastly dependent on the



tuning of the parasite when it is near  $\frac{1}{2}\lambda$  long. Accordingly we warn the reader that our remarks here apply only to parasite rods which are much longer than the driving aerial and considerably longer than  $\frac{1}{2}\lambda$ . To complete this experiment fully it would be very instructive to measure the distribution of current along the parasites, and probably this could be done by the use of a loop monitor such as is described in Chapter IX. Since the rods are three times as high as the aerial, they might be expected to produce three times as much field per ampere in them. Yet the ideal diagram of the two-dimensional problem is derived on the supposition that unit current in either of the three rods is equally effective in producing field at a distance. The more closely we consider this particular problem the more surprising it becomes that the ideal and observed patterns should agree closely. Systematic experiment would inevitably disclose the mechanism of the agreement and such a straightforward research is well worth doing. We would remark here that the agreement between the ideal and the observed patterns for Vee reflectors is not surprising in the same sense. For whether the source is an infinite filament, half-wave aerial, or doublet, an image system can be used when  $n$  is an integer, and thus our ideal patterns have not supposed a two-dimensional problem when  $n$  is an integer. They have supposed a two-dimensional problem when  $n$  is not an integer (i.e.  $\beta = 360^\circ, 120^\circ, 72^\circ$ , etc.), but even then experiment has upheld the approximation. Even so, we have not derived the ideal pattern by calculating the field due to infinitely long current filaments distributed over the sheets and a half-wave aerial at the source. But in comparing the observed and ideal patterns in Fig. 11.6 we are tacitly assuming the rods and the aerial are the same height, when they are not. Either the current induced in the rods attenuates very rapidly with height or else it changes sense and forms negative loops such that the net metre amperes are closely equivalent to a half-wave aerial: the second of these two effects is probably the more important.

## XII

### TURNING THE BEAM OFF CENTRE: USE OF VEE REFLECTORS SIDE BY SIDE: TROUGH REFLECTORS

#### 12.1. Further analysis of turning the beam off centre

THE general principles of this problem were developed in § 3.10 and the general equation describing it is (3.20). The reader should remind himself of certain important properties discovered there. Firstly, that when  $\beta = 60^\circ, 36^\circ, 25.7^\circ, 20^\circ$ , etc., the pattern *cannot* be made unsymmetrical by placing the aerial to one side of the bisector of the Vee, and secondly, that the amount of dissymmetry which can be produced is negligible if  $\beta$  is less than about  $75^\circ$ ; thirdly, that offsetting the aerial has relatively much more effect on the side lobes than on the main beam. It is for the third reason that it is a practical proposition to turn the beam, by offsetting the aerial, only when the aerial is near the first station for maximum gain. On considering these three factors together it emerges that a  $90^\circ$  Vee with  $R/\lambda$  near  $\frac{1}{2}$  is the case of much the most practical importance, and accordingly it alone need be considered fully.

We saw in Fig. 3.36 that the turning action is due to the existence of a second harmonic term in the Fourier expansion of the equatorial pattern. When  $n \geq 2$  and  $R/\lambda = \frac{1}{2}$  the third harmonic and higher terms are negligible. With this simplification we derived, from (3.21), an equation for the angle through which the maximum of the main beam is turned away from the bisector by an aerial which is offset an angle  $\alpha$  from the bisector. The equation is

$$\sin 2\theta = \frac{1 - \sqrt{1 + 32x^2}}{8x},$$

where

$$x \equiv \frac{2J_4(k)}{J_2(k)} \sin 2\alpha.$$

A glance at Fig. 3.36 shows that when  $J_2(k) = 0$  the pattern becomes a symmetrical bifurcated beam with the two maxima on bearings  $\pm 22.5^\circ$ . Only in this limiting condition can the beam be turned through an angle as much as  $22.5^\circ$ ; and moreover it is obvious that if it is turned through more than about  $16^\circ$  a large side lobe must be produced. We need to be familiar with the effect of increasing  $\alpha$  when  $R/\lambda$  is constant and also of increasing  $R/\lambda$  when  $\alpha$  is constant. When  $\alpha = 0$  the forward gain is a maximum when  $R/\lambda = \frac{1}{2}$ , and hence we may expect to give  $k$  some value between 3 and about 3.5: reference to tables shows that

$J_2(k) = 0$  when  $k = 5.03$  (i.e.  $R/\lambda = 0.81$ ), and this sets an absolute upper limit on  $k$ . When  $k = 3$  we found in Chapter III that the maximum of the beam occurs at  $\theta = -9.5^\circ$  when  $\alpha = 22.5^\circ$ . When  $k = 3.5$  it may be found that the maximum occurs at  $-\theta = \alpha$  for  $\alpha$  less than  $13^\circ$  and that  $\theta$  attains a blunt maximum of  $14.5^\circ$  near  $\alpha = 22.5^\circ$ .

In designing for a practical application we presumably require to turn the beam as much as possible and to do so without also producing a large side lobe. There are two independent variables,  $\alpha$  and  $R/\lambda$ , which can be chosen at will to suit our purpose best. Our starting-point is the recognition that  $\theta_{\max}$  is roughly proportional to  $-\alpha$ , but cannot exceed  $22.5^\circ$ ; we want  $\theta_{\max}$  as large as possible. The writer has examined this problem numerically in great detail: he considers the proper procedure is always to make  $\alpha$  near  $22.5^\circ$  and then to choose  $R/\lambda$  to suit the particular requirements which are desired. Accordingly we adopt the simple rule that the aerial should slide along a rod which approximately bisects the angle between the bisector of the Vee and one of the reflecting sheets: this angle is not critical and therefore it shows lack of understanding to specify it to a close tolerance in the drawings. It will now be realized why  $\alpha$  was chosen as  $22.5^\circ$  in the numerical example following Fig. 3.36: the ideal pattern for  $\alpha = 22.5^\circ$ ,  $k = 3.5$  is shown in Fig. 12.1. We now examine the manner in which the pattern will change as  $R/\lambda$  increases from a very small value, with  $\alpha$  constant and equal to  $22.5^\circ$ ; when  $k$  is very small,  $\theta_{\max}$  will be very small, since then  $J_4(k)/J_2(k) = k^2/48$ ; when  $k = 3$  we have found that  $\theta_{\max} = 9.5^\circ$ ; when  $k = 3.5$ , Fig. 12.1 shows that  $\theta_{\max} = 14^\circ$ , then there is an  $8^\circ$  side lobe; when  $k = 5.03$ ,  $J_2(k) = 0$  and consequently

$$\theta_{\max} = 22.5^\circ$$

and the pattern is a symmetrical bifurcated beam. Hence by adjusting  $R/\lambda$  we have a considerable control of  $\theta_{\max}$  and an enormous control over the relative magnitude of the field strength on bearing  $\theta = 0$ . The ratio of field on  $\theta = 0$  to field on  $\theta = \theta_{\max}$  will be called the 'field ratio'. The desire to turn the beam away from the bisector will, in practice, usually be associated with the intention of sweeping it periodically first to one side and then to the other, such process being performed continuously and independently of any rotation which the whole Vee may be given on a turn-table. Then the current induced by an incoming signal will be the same with the aerial at  $\pm\alpha$  only when the whole Vee is turned so as to make its bisector point along the

direction of the said incoming signal. By the aid of this subterfuge and device the said direction can be discovered more precisely than if its determination depended only on estimating the bearing of the maximum of a rather blunt beam. It will, however, be realized that the operative field strength is that on bearing  $\theta = 0$  and not at  $\theta_{\max}$ : accordingly the field ratio is a parameter of great practical importance

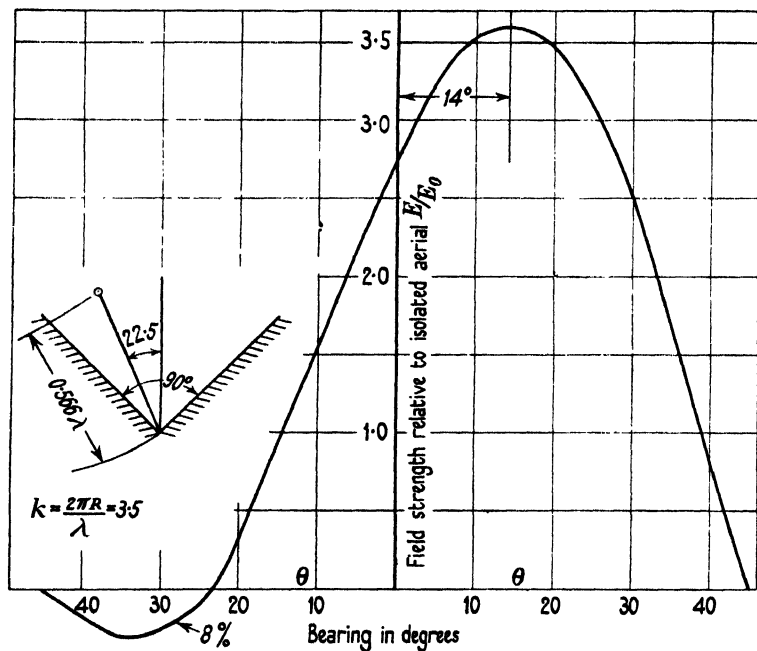


FIG. 12.1. Ideal  $90^\circ$  reflector, aerial not on bisector.

and must be under control. Labour can be saved in evaluating this ratio if the following two points are kept in mind. First, for given values of  $\alpha$  and  $k$  we have an equation to determine  $\theta_{\max}$  and hence  $E_{\max}$  can be evaluated directly by substitution in (3.21). Secondly, (3.21) shows that  $\alpha$  and  $\theta$  are interchangeable, hence the field on  $\theta = 0$  for some given  $\alpha$ , say  $\alpha_1$ , is the same as the field on  $\theta = \alpha_1$  when  $\alpha = 0$ .

Fig. 12.2 shows the observed patterns (at  $\lambda = 125$  cm.), produced by screens  $\frac{1}{2}\lambda$  wide and  $\frac{3}{4}\lambda$  high, when  $R/\lambda = 0.53$  ( $k = 3.3$ ) for  $\alpha = 0$  and  $\alpha = \pm 22.5^\circ$ . The equation for  $\theta_{\max}$  shows that ideally the maximum should occur at  $\pm 15.8^\circ$ , whereas in fact it occurs in this reflector at  $\pm 12^\circ$ , thus showing that sheets  $\frac{1}{2}\lambda$  wide do not suffice to turn the beam through an angle quite as large as the ideal. This figure shows the observed 'field ratio' is  $\sqrt{(11.2/15)} = 0.865$ : the ideal value being 0.71.

When  $R/\lambda$  was increased from 0.53 to 0.59 (i.e.  $R$  from 66 to 74 cm. in these tests, in which  $\lambda$  was 125 cm.) it was found that the beam was turned through  $\pm 16^\circ$  with a field ratio of 0.76, as compared with the ideal values  $17.1^\circ$  and 0.65. Fig. 12.3 shows the observed patterns from these sheets when  $R/\lambda = 0.67, 0.75$ , and 0.84. We note, as predicted, that the field ratio decreases as  $R/\lambda$  increases, and clearly it has here

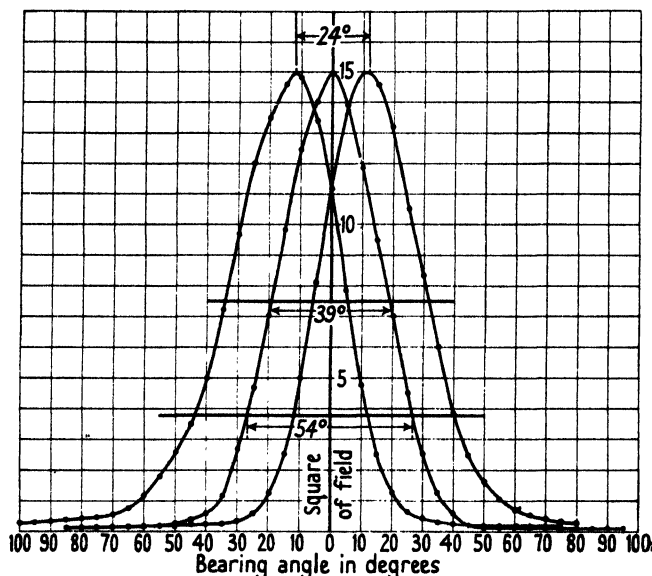


FIG. 12.2. Observed diffraction patterns corresponding with 12.1.

passed through zero for some value of  $R/\lambda$  between 0.75 and 0.84: the ideal value for this occurrence is  $R/\lambda = 0.81$ .

Figs. 12.2 and 12.3 together demonstrate that the ideal analysis is a very close guide to the behaviour of quite small sheets and serves to predict their performance very closely. Those who have perseverance and industry to understand this description will find they can predict and handle these aerials with complete confidence and success. Indeed, after this discussion, prediction and design are scarcely called for. It will suffice to build the reflector with sheets some  $\frac{3}{4}\lambda$  wide, arrange that  $\alpha$  shall be about  $22^\circ$  and that  $R/\lambda$  is adjustable between about 0.5 and 0.6: when the aerial system has been built the precise value of  $R/\lambda$ , which suits the given requirements most closely, must be found by experiment. The total separation of the two peaks in curve (3) of Fig. 12.3 appears to be  $50^\circ$ , whereas ideally this separation should be  $45^\circ$  when  $R/\lambda = 0.81$ : the writer thinks it is possible for finite sheets

to turn the beam through a little more than  $22.5^\circ$  when  $\alpha$  exceeds  $22.5^\circ$ , but this caveat is of little practical importance.

If the beam is to be turned from side to side periodically it will not be done by oscillating the aerial mechanically through  $\pm\alpha$ , but by providing one aerial at  $+\alpha$  and another aerial at  $-\alpha$  and switching the power to one or the other. Hence, in practice, we must consider the

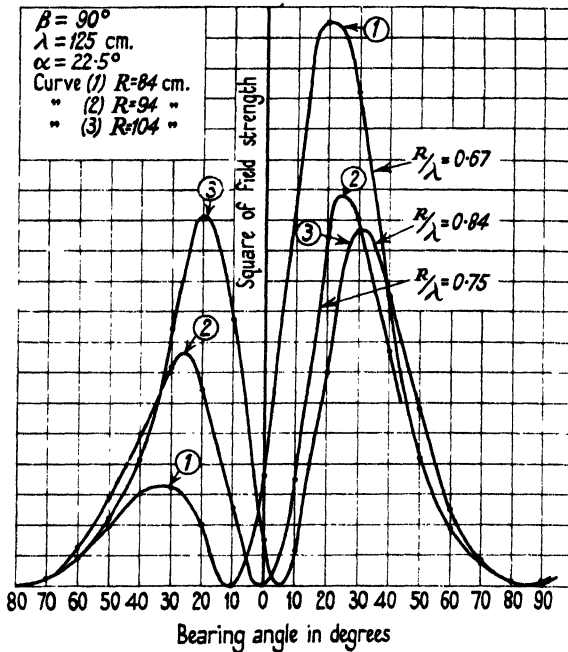


FIG. 12.3. Observed diffraction patterns for  $90^\circ$  mirror.

pattern produced when there is a driven aerial at  $+\alpha$  and a 'parasite' aerial at  $-\alpha$ . If the current induced in the parasite is equal and opposite to that in the driven aerial, then consideration will show the pattern must be a symmetrical bifurcated beam. If the two currents are equal and cophased, then the pattern must be symmetrical about the bisector. Accordingly it is obvious the disturbance due to the idle or parasite aerial must depend very much on the phase as well as on the magnitude of the current induced in it: its presence can increase or decrease the 'field ratio' according as the induced current is nearly anti- or nearly co-phased. The experimental patterns shown in Fig. 12.4 are reproduced to illustrate this effect: curve (1) records the pattern when the idle aerial was a thin rod  $\frac{1}{2}\lambda$  long and curve (2) when the idle aerial was a rod  $\frac{1}{2}\lambda$  long interrupted by a small air gap in the

middle of its length. When the idle aerial was absent the beam was turned through  $16^\circ$  and the square of the field ratio was  $(0.76)^2 = 0.55$ . Accordingly we presume that for curve (2) the induced current had a large antiphased component, whereas for curve (1) it had a strong quadrature component. In practice the idle aerial will be a replica of the driven aerial and will have a length of feeding cable attached to it:

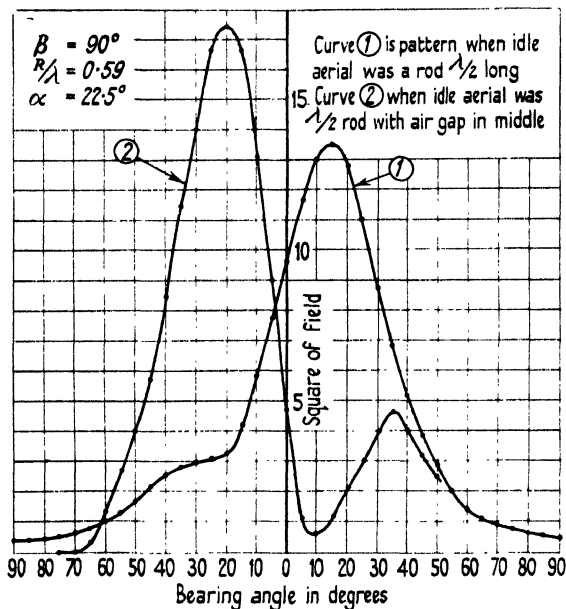


FIG. 12.4. Observed diffraction patterns for  $90^\circ$  mirror.

the termination of the said cable will provide a means of controlling (within limits) the magnitude and phase of the current induced in the parasite. Thus it was found that when the parasite was a replica of the driven aerial and was attached to 230 cm. of coaxial polystyrene cable (equiv. length near  $2.6\lambda$ ), then the pattern was equivalent to that produced by a single aerial at  $R/\lambda = 0.52$ , whereas in fact  $R/\lambda$  was equal to 0.59.

The ideal values of radiation resistance can be evaluated by adding  $E_P$  due to the four images, in the manner often used in Chapters II and III. With  $R/\lambda = 0.566$  ( $k = 3.5$ ) it may be found that the radiation resistance is 128, 120, 90, or 44 ohms according as  $\alpha = 0^\circ, 10^\circ, 20^\circ$ , or  $30^\circ$ . Thus if  $\alpha = 22.5^\circ$ , we may expect the resistance to be near 70 ohms when  $R/\lambda$  lies between 0.5 and 0.6. Reference to Fig. 12.1 shows the width of the base of the main beam is about  $70^\circ$  and this is likely to mean that the power gain, reckoned on bearing  $\theta_{\max}$  will be

greater than if  $\alpha = 0$ . Computation shows that when  $R/\lambda = 0.566$  this maximum gain equals 8.5, 9.5, and 11.5 according as  $\alpha = 0^\circ$ ,  $10^\circ$ , or  $20^\circ$ : the forward gain passes through the minimum value 6 when  $\alpha = 20^\circ$  and attains 8.5 when  $\alpha = 27^\circ$ .

Fig. 12.5 shows the ideal pattern for  $\beta = 90^\circ$ ,  $R/\lambda = 1.6$ , and  $\alpha = 5^\circ$ : it is characterized by an enormous side lobe, centred on  $32^\circ$ , whose

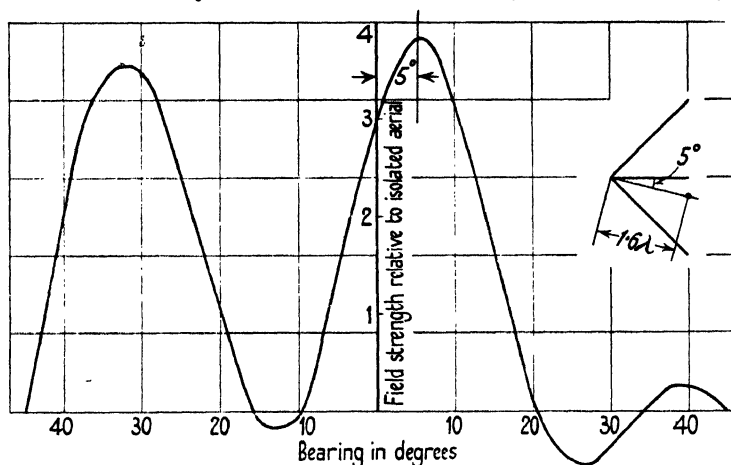


FIG. 12.5. Ideal diffraction pattern for  $90^\circ$  mirror, with  $R/\lambda = 1.6$  and  $\alpha = 5^\circ$ .

presence would make the pattern intolerable. Thus we find it is not practicable to use the second station when it is desired to turn the beam from side to side. However, it should be noticed that a small dissymmetry of the aerial has now produced an enormous dissymmetry of the side lobes, showing that perfect symmetry of the lobes is very dependent on perfect symmetry of the system. This suggests that some of the lack of symmetry which is almost always observed in experimental patterns may perhaps be due in part to small mechanical imperfections in the system: though the writer has always found that when local irregularities are produced (say, by bulging the sheets), they do not appear to alter the pattern. However, the reader must not forget that the centre line of the *main* beam is not sensitive to  $\alpha$ : if the reflector is made with reasonable accuracy the main beam will always be found to be on centre.

The observed pattern depicted in Fig. 12.6 is reproduced to demonstrate that when  $\beta = 60^\circ$  the pattern must always remain symmetrical for all values of  $\alpha$ : the mechanism of this property was explained in § 3.10. In the experiment recorded in Fig. 12.6  $R/\lambda$  was  $\frac{1}{2}$  and  $\alpha$  was  $15^\circ$ , yet the pattern remains perfectly symmetrical, as predicted. It should,



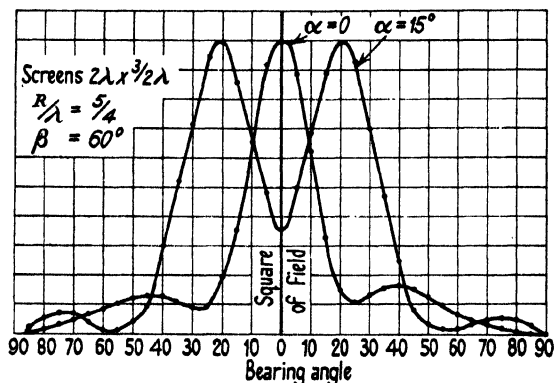


FIG. 12.6. Demonstration that 60° mirror always produces a symmetrical diffraction pattern.

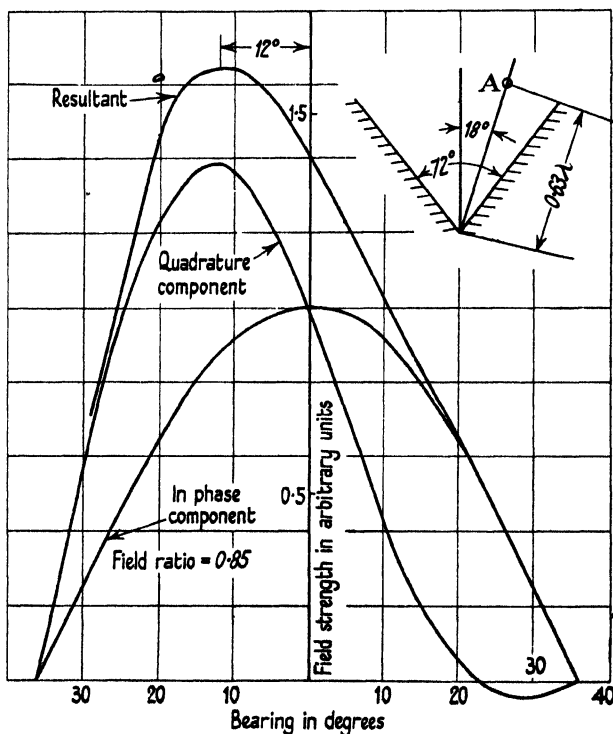


FIG. 12.7. Ideal 72° reflector, aerial not on bisector.

however, be remembered that there is a dissymmetry in the phase of the field. If  $\alpha$  is oscillated periodically, the received field strength will be subject to a phase modulation on all bearings save  $\theta = 0$ . Hence if

aural reception is used, it should still be possible to use a  $60^\circ$  mirror in a 'beam splitting' system and thereby make use of the larger power gain which obtains for this angle than for  $\beta = 90^\circ$ : but if the signal is displayed on a cathode-ray tube the system will, and must, fail completely.

If  $n$  is a fraction, say  $\frac{5}{2}$ , then the pattern is the vector sum of two quadrature components. Close study of equation (3.21) will show that it is only one of these components which becomes unsymmetrical when  $\alpha$  is not zero, and accordingly the net angle turned through by the main beam is less than it would be if the symmetrical component were absent. The ideal pattern for  $n = \frac{5}{2}$  ( $\beta = 72^\circ$ ) has been evaluated for  $R/\lambda = 0.63$  and  $\alpha = 18^\circ$  and is reproduced in Fig. 12.7: the main beam is turned through  $12^\circ$  and the field ratio is 0.86. This figure serves to substantiate the rather sweeping statement that when it is required to turn the beam from side to side then the angle of the mirror must not be appreciably less than  $90^\circ$ .

## 12.2. Pair of Vee reflectors side by side

Experience has shown that sheets a few wavelengths wide produce a close approximation to the ideal pattern, appropriate to infinite sheets: hence it seems probable that if two Vee reflectors are set side by side, forming a W, then the pattern due to an aerial in one Vee will be very nearly the same as if the other Vee were removed, and consequently if each leg of the W has an aerial in it the resultant pattern will be substantially the vector sum of the two component patterns. Thus, refer to the left-hand inset diagram in Fig. 12.8, which represents a W of angle  $\beta$  with aeriels denoted by  $A$ , separated a distance  $d$ . Let the pattern for one leg alone be observed experimentally and denote it by  $E = f(\theta)$ . Then if both aeriels carry equal and cophased current, it seems reasonable to expect the resultant pattern will be expressed by the equation

$${}_PE = 2f(\theta)\cos\left(\frac{\pi d}{\lambda}\sin\theta\right),$$

and if the currents are equal but in phase quadrature by the equation

$${}_QE = 2f(\theta)\cos\left(\frac{\pi d}{\lambda}\sin\theta + \frac{1}{2}\pi\right).$$

Since this problem is not soluble analytically, our surmise can be tested only by experiment. If the surmise is correct, then  $E$  will be zero when  $\sin\theta = \lambda/2d$ , no matter what the value of  $f(\theta)$  on this bearing. Hence the pattern resulting from equal cophased currents in a W

should be much narrower than for a single Vee, provided that  $d/\lambda$  is considerable. Thus if the reflecting sheets are  $2\lambda$  wide, then  $d = 4 \sin \frac{1}{2}\beta$ , and accordingly the field should be zero when the bearing is such that  $\sin \theta = 1/(8 \sin \frac{1}{2}\beta)$ : thus  $\theta = 14.5^\circ$  if  $\beta = 60^\circ$ . The power gain should be larger than for a single Vee alone and it should be possible to construct a curtain array of Vee reflectors. A plurality of Vees have been

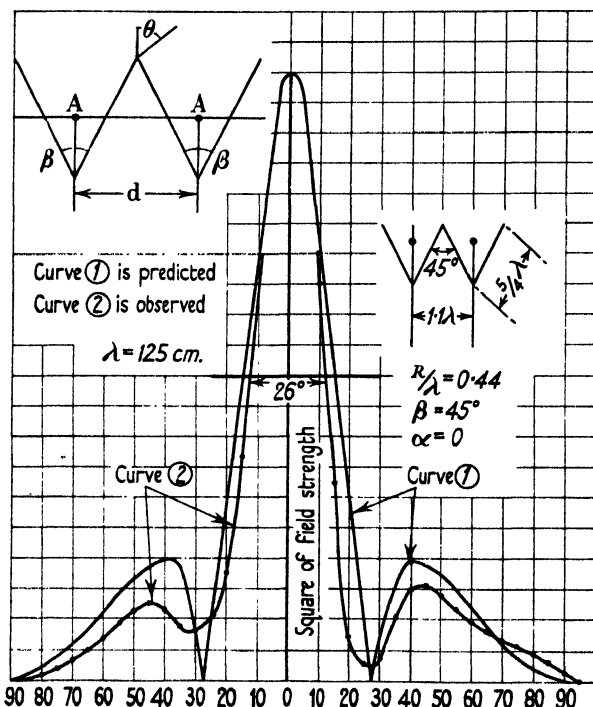


FIG. 12.8. Diffraction pattern for a pair of  $45^\circ$  reflectors, side by side.

illustrated in several technical papers but without systematic discussion of their action. J. D. Krauss† draws a diagram of a W but does not comment on it. We have seen pairs of Yagi aerials in operation and also one leg of a W used as transmitter and the other as receiver. There has been a rough and instinctive appreciation of the action, but we have not met a systematic experimental analysis. We will first dispose of something which may enter the reader's mind and appear paradoxical.

We are proceeding in the expectation that an aerial in one leg of the W is screened from the aerial in the other leg to a degree such that the mutual interaction is insignificant, and hence the radiation resistance is the same as if only one Vee were present. In calculating power gain

† *Proc. I.R.E.* **28** (1940) 513.

we have always had to evaluate radiation resistance and the impression may have grown up that this resistance must be less than the isolated value if the gain exceeds unity: this is not necessary, and consideration should show the reader that if the interaction is negligible then the gain is equal to the number of members; it is thus to be expected the gain of a W is nearly twice that of a Vee.

To assess the general validity of the treatment just outlined experiments were made at  $\lambda = 125$  cm. A pair of  $45^\circ$  Vees each consisting of two gauze sheets 5 ft. wide by  $6\frac{1}{4}$  ft. high (i.e.  $\frac{5}{4}\lambda \times \frac{3}{2}\lambda$ ) were mounted side by side on a turn-table: each had a half-wave aerial on its bisector distant 55 cm. ( $R/\lambda = 0.44$ ) from its apex. The pattern due to one aerial alone was observed and found to be slightly unsymmetrical, 'diffraction round the edge' being less on the side to which the other Vee was attached: the width at half-power was  $(35^\circ + 23^\circ) = 58^\circ$  and the power at  $\theta = 22.5^\circ$  was 43 per cent. and 76 per cent. The measured separation between the two aerials was 138 cm., and accordingly  $d/\lambda = 1.1$ . Since the pattern from each single Vee of the W structure was somewhat unsymmetrical, a hypothetical pattern was constructed which was the mean of the patterns due to one Vee alone: its width at half- and quarter-power was  $60^\circ$  and  $93^\circ$  respectively. The ordinates of this said mean pattern were multiplied by  $\cos(1.1\pi \sin \theta)$  and the result is depicted in curve (1) of Fig. 12.8: it passes through zero at  $\theta = \pm 27.1^\circ$  and is  $30^\circ$  wide at half-power. The two similar aerials were fed simultaneously through two ostensibly similar cables branching from a two-way junction box, fed by a single cable from the valve generator: it was hoped the currents in the two aerials would be equal and cophased. The pattern which then resulted is recorded by curve (2) in Fig. 12.8. The observed pattern is seen to be a very close approach to the predicted pattern, and thus proves that the resultant pattern is substantially the vector sum of the two isolated components: the experiment has thus demonstrated what it was designed to prove and further demonstration of this important principle is not essential. It will, however, be noted that the observed pattern is not truly symmetrical and this proves the currents were not truly cophased. Fig. 12.9 shows the result of multiplying the ordinates of the said mean pattern by  $\cos(1.1\pi \sin \theta + \frac{1}{4}\pi)$  and is what should result from equal currents in phase quadrature.

Figs. 12.10 and 12.11 show the pattern observed when first one and then the other feeding cable was lengthened by a link whose electrical length purported to be  $\frac{1}{2}\lambda$ . Such insertion should increase the phase

difference between the currents (a difference intended to be zero but which in fact was not zero) by  $90^\circ$ . Ideally these should have resulted in Fig. 12.9 and its mirror image: in fact the two patterns are very different, because the phase difference was not zero initially and thus the phase difference became more than  $90^\circ$  in one case and less in the other. Fig. 12.10 is a close approximation to Fig. 12.9, whereas

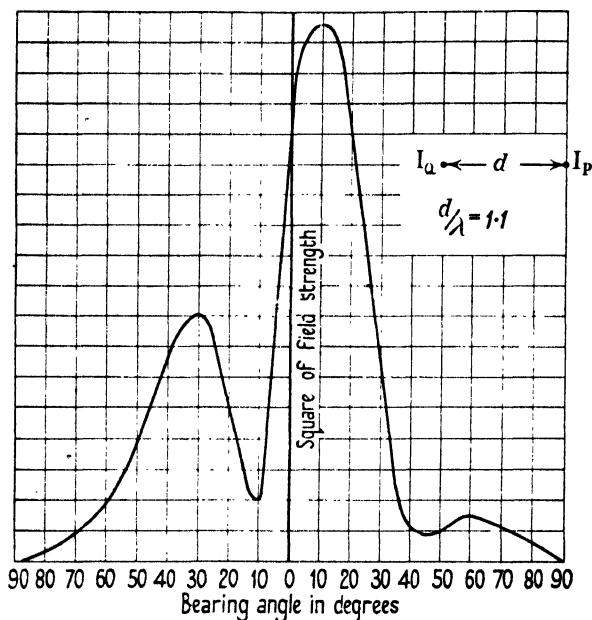


FIG. 12.9. A predicted diffraction pattern for a pair of  $45^\circ$  reflectors, side by side.

Fig. 12.11 shows the two currents must have been substantially in antiphase after inserting the link in the lead to that aerial which was lagging initially. This group of figures, taken collectively, affords very complete proof of the vector addition of the two component patterns and establishes a principle which will find many applications. Also the experiment, *per se*, provides a desirable aerial system in which the beam can be swung from side to side. Thus, compare Figs. 12.10 and 12.2: the single right-angled reflector produced a beam  $39^\circ$  wide at half-height capable of being turned  $\pm 22^\circ$  off centre in the limiting case: the W produces a beam only  $26^\circ$  wide at half-height and capable of being turned through  $\pm 22^\circ$  in the limit. In the first case the aperture was  $1.76\lambda$  and in the second the total aperture was  $2.2\lambda$ , the increment of width being 25 per cent. Now compare the system with a 5-member curtain having side spacing  $\frac{1}{2}\lambda$ : for such, the first zero is at  $\pm 24^\circ$  and

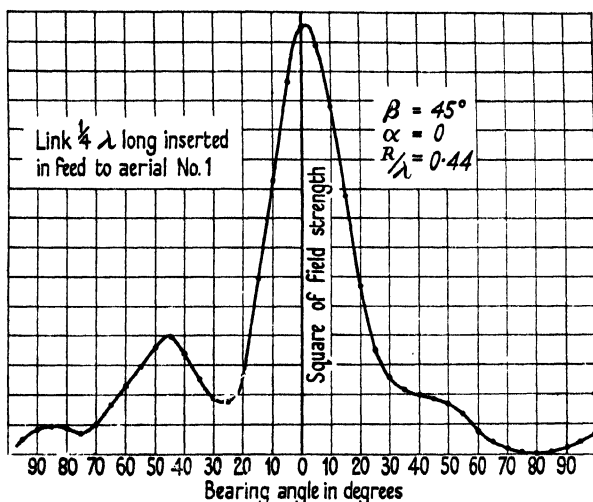


FIG. 12.10. An observed diffraction pattern for a pair of  $45^\circ$  reflectors, side by side.

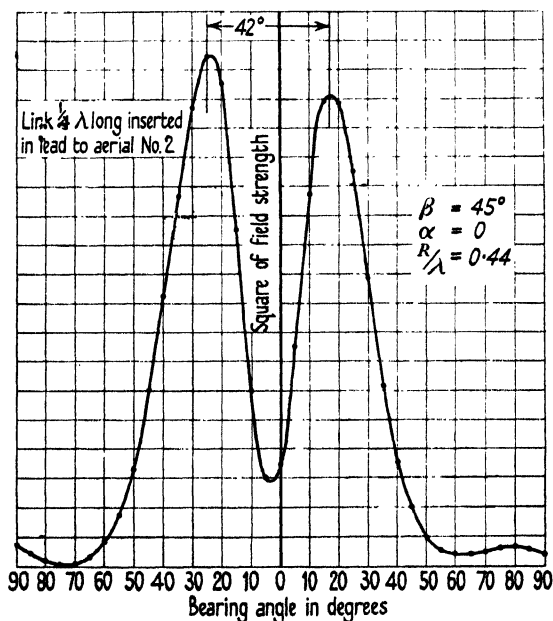


FIG. 12.11. An observed diffraction pattern for a pair of  $45^\circ$  reflectors, side by side.

the first side lobe 4 per cent. in power. Fig. 12.8 shows the minima occur at about  $\pm 25^\circ$  and the lobe is 12.5 per cent. in power. The two patterns are thus seen to be very comparable; the curtain requires five

feeding cables and the W only two. Clearly a curtain of Vee aerials is a very practicable device for producing a narrow beam by means of only a few feeding cables.

An attempt at a mathematical analysis of two Vees, side by side, was made in § 7.4 and it was intended as an introduction to the series of experiments we have just described. That analytical approach was possible only for a W whose angles were  $90^\circ$  and thus the solution is not directly comparable with the experimental results which have just been recorded.†

However, it is worth while to compare Fig. 12.8 with Fig. 7.13 and with the dotted curve in Fig. 7.14. First of all it should be pointed out that curve (1) of Fig. 12.8 differs in kind from that in Fig. 7.14 in that it is an experimental curve (for the  $45^\circ$  Vee which was used) whose ordinates have been multiplied by  $\cos(1.17\pi \sin \theta)$ , whereas the dotted curve in Fig. 7.14 is an ideal pattern for a  $90^\circ$  Vee whose ordinates have been multiplied by  $\cos(1.56\pi \sin \theta)$ : this explanation accounts for the side lobes in curve (1) of Fig. 12.8. Curve (2) of Fig. 12.8 shows that the field strength does not pass through zero at  $\theta = \pm 28.5^\circ$  but falls only to a minimum value which occurs near this bearing. Reference to the curve of  $|E|$  in Fig. 7.13 shows that the field strength does not pass through zero at  $\theta = \pm 18^\circ$  but falls only to a minimum which occurs near this bearing. The reason for this minimum is apparent from the curves of  $E_P$  and  $E_Q$  in the same figure, since it will be seen that these do not pass through zero simultaneously. Thus it would seem that the observed minima recorded in curve (2) of Fig. 12.8 are characteristic of the use of a W and need not be attributed to the finite area of the reflecting sheets. The width at quarter-power of the observed beam in curve (2) of Fig. 12.8 is  $34^\circ$ , whereas the corresponding width in Fig. 7.13 is  $26^\circ$  for the  $90^\circ$  W. Hence in this respect the performance of the given  $45^\circ$  W was less desirable than the predicted performance of a certain idealized W of angle  $90^\circ$ . It is very likely that the performance obtainable from four given sheets would be very insensitive to the angle of the W which they formed, provided this angle lay between about  $90^\circ$  and  $45^\circ$ . Indeed, this is likely to be so, quite apart from the effects of diffraction round the edges of the sheets,

† Although the writer had long realized the problem could be approached in the way this is done in Chapter VII, he had not evaluated the solution at the time when an urgent practical application demanded that the experiments recorded in Figs. 12.8 and 12.10 should be made. For that application it was clear that a  $45^\circ$  W would give a more desirable performance than a  $90^\circ$  W and time was not available to test both these W reflectors. He has not had an opportunity to test a  $90^\circ$  W since evaluating the solution recorded in Fig. 7.13: it would be interesting to make this comparison.

because closing the W will reduce the separation between the two aerials and thus tend to counteract the benefit of the sharper Vee. If experiment bears out this prediction, then the final choice of the W to be used in a given application can be determined by consideration of available floor space for the complete reflector. It would be instructive to make this simple *ad hoc* research and to record it for the guidance of practical designs.

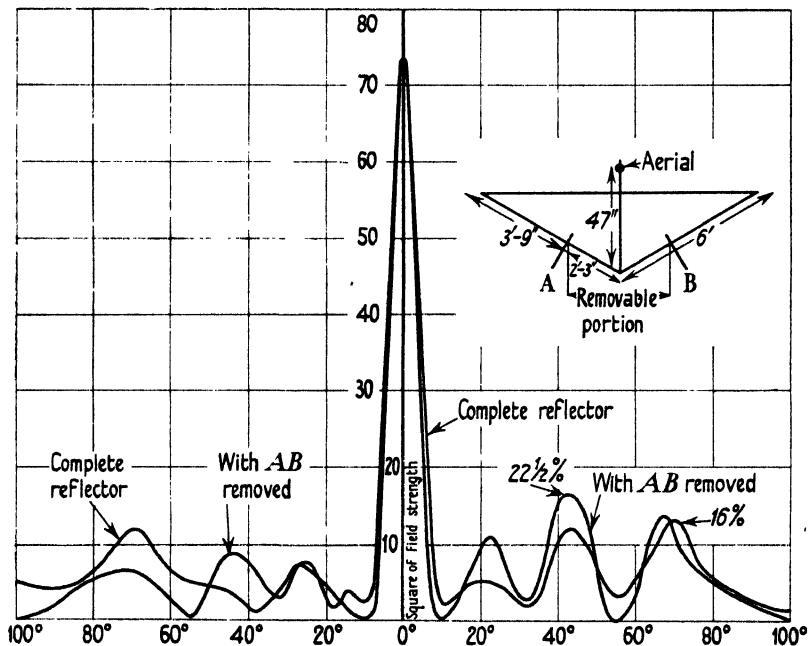


FIG. 12.12. Diffraction pattern for 120° trough reflector,  $\lambda = 50$  cm.,  $R = 47$  in.

### 12.3. Trough-shaped reflectors

In optical practice we are familiar with mirrors which are shaped accurately to curved surfaces, parabolas, spheres, etc., whereas in radio work we obtain good performance from flat mirrors forming a Vee. The problem can be solved analytically for flat surfaces but not for parabolic surfaces. By now the reader should understand Vee mirrors very thoroughly and it is probable that the more he thinks about them the more obscure and surprising will the optical behaviour of a parabola appear to be. In attempting to find a mental bridge between the behaviour of a Vee and a parabola it is natural to try to associate various parts of the pattern with various parts of the reflecting surface, and to try experimentally the effect of local changes of shape in the



Vee. With this purpose in mind the writer explored the effect of amputating the apex of a Vee, closing the opening by a flat sheet parallel to the aperture plane: thus forming a mirror whose plan view was a regular trapezium or, more simply, a trough. Thus, refer to the inset diagram in Fig. 12.12 which shows, in plan view, a  $120^\circ$  Vee reflector whose sides were 6 ft. wide: they were made by combining a sheet  $3\frac{3}{4}$  ft. wide with a sheet  $2\frac{1}{4}$  ft. wide. If the two smaller sheets are removed and some other sheet placed across  $AB$ , we have what will now be termed a trough. In this particular structure the width of the floor of the trough was 0.37 of the width of the aperture. Measurements were made at  $\lambda = 50$  cm. (20 in.). Had the Vee been complete and infinite in extent then reference to Fig. 3.8 will show the forward field would be a maximum when the aerial was distant 33.5, 47, and 59 in. from the apex. In the initial experiment the floor of the trough was left open and then the front-to-back ratio was found to have the values shown in the table below.

TABLE 12.1

Distance of aerial from apex .	33.5 in.	47 in.	59 in.
Back-to-front power . . . .	0.3	0.13	0.16
Back-to-front field strength .	0.55	0.36	0.4

It is instructive to note that the backward field is only of the order of half the forward field even when the hole is  $2.3\lambda$  wide.

The bottom of the trough was closed by a flat sheet and the forward field was observed as a function of the distance  $D$  of the aerial from the said flat bottom. Reference to the said inset diagram will show that the apex of the Vee was 13.5 in.  $\equiv h$  behind the said floor. It is instructive to compare the value of  $(h+D)$  at a station for maximum or minimum forward field with the corresponding distance  $R$  observed for the complete Vee, and for this purpose the table below has been compiled.

TABLE 12.2

*Forward field test;  $120^\circ$  trough,  $h = 13.5$  in.*

$D$ observed, inches .	15	19	25	30	35.5	43	48
$(D+h) = R'$ . . . .	28.5	32.5	38	43	49	56	61
$R$ observed for Vee .	19.5	26	33	40	47	53.5	59

When  $D = 15, 25, 35.5$  in., etc., the forward field was a maximum. This table shows that the flat floor pushes forward the stations for maxima and minima, and by an amount which decreases as  $D$  increases:

thus when  $D = 25$  in. then  $R' - R = 5$  in., and when  $D = 48$  in.  $= 2.4\lambda$  then  $R' - R = 2$  in.  $= 0.1\lambda$ . The largest peak of forward field occurred with the trough when  $D = 35.5$  in. and for the complete Vee when  $R = 47$  in.

Fig. 12.12 shows superposed the observed pattern, at these stations, which resulted from the complete Vee and also from the trough. It may be seen that the amputation has had no significant effect on the main beam but has had a small effect on the side lobes. As usual, the side lobes are not symmetrical, and therefore very close comparison of them in the two figures has little meaning. On the whole it is fair to say that the effect of converting the Vee into a trough is scarcely noticeable and is certainly negligible for practical purposes.

It is very striking to discover that so drastic a change of shape, or of the figure as the optician would call it, has had scarcely any effect on the pattern. From the purely practical point of view it shows, once more, that it displays a lack of understanding to demand close tolerances in the construction of mirrors: and it discourages us from expecting to find outstanding virtues in a parabolic shape. Moreover, it gives us leave to reduce the depth of the mirror and thereby save an appreciable amount of floor space. The writer has done much systematic measurement of the effect of converting a Vee into a trough. He finds the effect on the main beam is always negligible and the effect on the lobes is usually small; sometimes they are decreased and sometimes increased by the trough shape. Recognition of the comparative unimportance of the shape of the back of the mirror is an important principle to have established since it will assist us in approximating to solutions of cases which cannot be dealt with analytically. The other aspect is the purely practical one of how much floor space can be saved by using a trough and here the reader will look for direct guidance. If  $\beta = 90^\circ$ , then  $R/\lambda$  should be  $\frac{3}{2}$ : if  $R/\lambda = \frac{3}{2}$ , then large lobes are bound to accompany the sharp main beam. Accordingly we presume that  $R/\lambda = \frac{3}{2}$  is the only station of real interest, and for this it is permissible to amputate a depth of from 1 to  $1\frac{1}{4}\lambda$ . If  $\beta = 60^\circ$  we ought to make  $R/\lambda = \frac{5}{4}$  and then it will be permissible to amputate a depth  $\lambda$ . Thus we realize the depth which may be amputated cannot be very large, though it is certainly worth while for wavelengths greater than about 50 cm.

Fig. 12.13 shows the pattern observed from a  $45^\circ$  trough described by the inset diagram, at  $\lambda = 50$  cm. The aerial was distant 5.5 in. from the flat back and was then at a station of maximum forward field:

the amputated depth was 42 in., and hence the aerial was then 47.5 in. from the apex, whereas the maximum occurred when the aerial was 40 in. from the apex of the complete Vee. This figure should be compared with Fig. 10.11, which relates to the corresponding station for the aerial: the two observed patterns are scarcely distinguishable and thus the amputation has not had an appreciable effect. The aerial

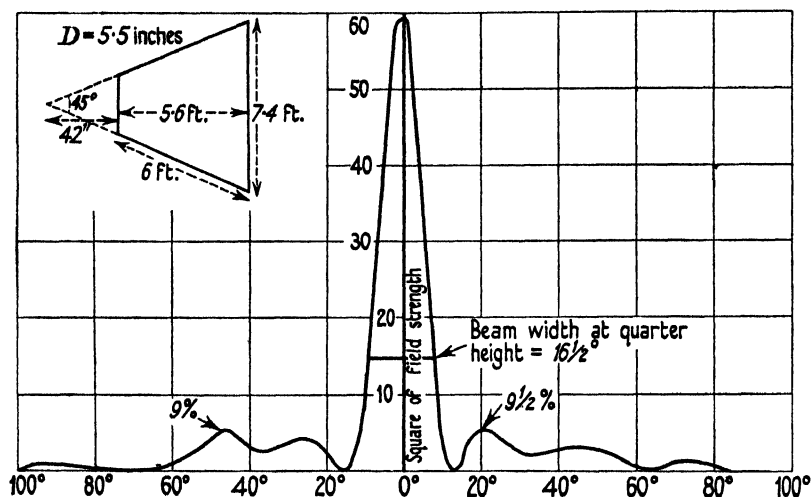


FIG. 12.13. Diffraction pattern for 45° trough reflector,  $\lambda = 50$  cm.

ought to be situated at  $R/\lambda = 2$  in the ideal Vee and then the gain is 53: thus we suggest that a depth of nearly  $2\lambda$  can and should be removed from the apex of a 45° mirror. Fig. 12.13 is an attractive pattern for practical application. A pair of such troughs side by side, operated as described in § 12.2, would produce a very sharp and substantially lobe-free beam. We have in it the basis for a practical design which is well worth remembering.

If the aerial is to be near the first station of maximum forward field, then it is so close to the apex that not much can be amputated and it will be scarcely worth while to adopt trough shape to save space. Nevertheless, for the sake of completeness, we now record some tests of troughs formed by amputating less than one wavelength from the apex of a Vee.

Two gauze-covered square sheets each measuring 5 ft. by 5 ft. were hinged to a sheet 5 ft. by 2 ft.; at one extreme this formed a flat sheet 12 ft. wide by 5 ft. high and at the other extreme a rectangular trough 2 ft. wide and 5 ft. deep. It may be calculated from this that when the slanting sides of the symmetrical trough were inclined to one another

at  $90^\circ$ ,  $78^\circ$ ,  $60^\circ$ ,  $45^\circ$ , and  $30^\circ$ , then the slant sides of the complete Vee would have been 6.4, 6.6, 7, 7.6, and 8.8 ft. respectively. Measurements were made at  $\lambda = 125$  cm. (4 ft.), and hence the said slant side ranged from 1.6 to  $2.2\lambda$ . We remember the ideal pattern for a Vee differs insensibly from a simple sinusoid until the length of arc across the Vee at the aerial is appreciably in excess of  $\frac{1}{2}\lambda$ : in this range the gain is almost independent of  $R/\lambda$  and thus the aerial does not need to be stationed with precision. The curve of forward field from the trough was observed for various values of  $\beta$  between  $90^\circ$  and  $30^\circ$ , and the position of the aerial for the first maximum did not appear to be appreciably different from what it would have been if the reflector had been a Vee instead of a trough: moreover, the first station for zero forward field was advanced by not more than 20 cm., which here is  $\frac{1}{3}\lambda$ . Accordingly the existence of the flat bottom to the trough may be ignored in choosing the position of the aerial. Or we may well put it this way: make the bottom of the trough about  $\frac{1}{2}\lambda$  wide and then situate the aerial as near the bottom as it is convenient to do. In the tests recorded below the aerial was situated at the observed station for maximum forward field and this was always about 25 cm. from the flat floor: it is, however, quite certain that the observed and recorded patterns are not sensitive to the aerial station. The outstanding features of the observed patterns are recorded in the table below.

TABLE 12.3

$\beta$	Slant height of equiv. 'Vee'	Aperture	Width at half- power	Width at quarter- power	Power on $\theta = \frac{1}{2}\beta$	Power on $\theta = 45^\circ$
	ft.	ft.				
$90^\circ$	6.4	9	$36^\circ$	$51^\circ$	3.5%	3.5%
$78^\circ$	6.6	8.3	$38^\circ$	$53^\circ$	5.5%	3.5%
$60^\circ$	7.0	7	$39^\circ$	$54^\circ$	18.0%	2.5%
$45^\circ$	7.6	5.8	$47^\circ$	$68^\circ$	50.0%	7.0%
$30^\circ$	8.8	3.6	$59^\circ$	$81^\circ$	83.0%	14.0%

The figures in the last four columns show that the pattern is almost independent of  $\beta$  in the range  $90^\circ$  to  $60^\circ$ , hence  $60^\circ$  is the best angle for practical purposes since it makes the least bulky reflector.

We have recorded elsewhere that sheets 8 ft. wide inclined at  $60^\circ$  produced a beam whose width at half- and quarter-power was  $36^\circ$  and  $49^\circ$  respectively with 14 per cent. power at  $\theta = \frac{1}{2}\beta$  and 1 per cent. at  $\theta = 45^\circ$ . Had the Vee been amputated to a trough the sheets here would have been 7 ft. wide: the discrepancy between the trough

pattern and the Vee pattern for 8 ft. sheets is not more than is reasonable to attribute to a difference of 1 ft. in width. Hence it seems reasonable to state that the trough shape, *per se*, did not affect the pattern. We have also recorded elsewhere that sheets 8 ft. wide inclined at  $45^\circ$  produced a pattern described, in the same notation, by  $44^\circ$ ,  $62^\circ$ , 32 and 3 per cent.: the trough resulted from the amputation

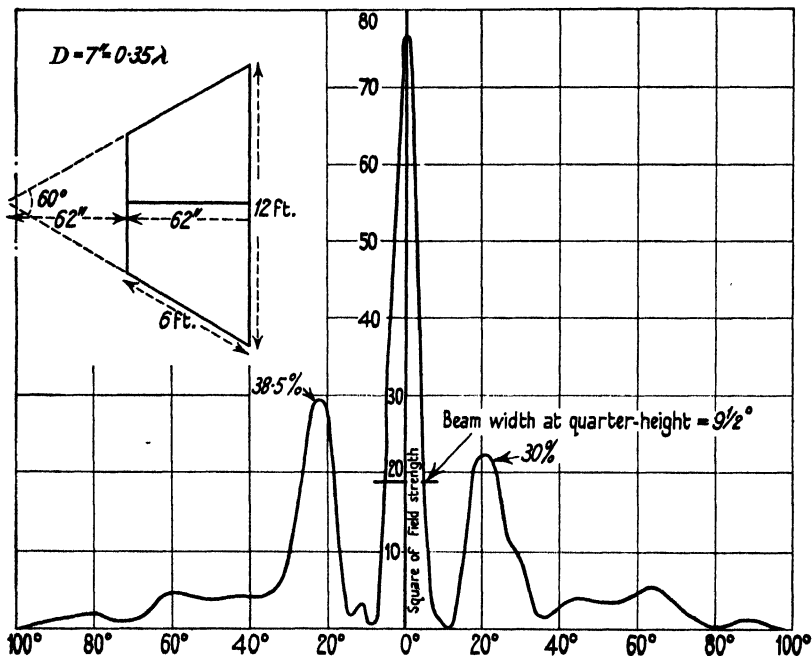


FIG. 12.14. Diffraction pattern for  $60^\circ$  trough reflector.  $\lambda = 50$  cm.,  $D = 7$  in.

of a Vee whose sheets would have been 7.6 ft. wide and its pattern is described by  $47^\circ$ ,  $68^\circ$ , 50 and 7 per cent.; here, then, there are signs that the trough shape has deteriorated the pattern slightly. However, reference to the table shows that, with these sheets,  $\beta$  ought not to be as small as  $45^\circ$  and hence this reflector was not of practical interest. We will close with the following dictum. Provided the sheets are wide enough to make advantageous use of some given angle  $\beta$ , then the Vee can be converted into a trough, whose floor width is about  $\frac{1}{2}\lambda$ , without appreciable effect on the pattern.

Fig. 12.14 shows the observed pattern (at  $\lambda = 50$  cm.) due to the  $60^\circ$  trough described in the inset diagram. It was taken at a station of maximum forward field which occurred when  $D = 7$  in. and this makes  $R' = D + h = 69$  in.: for the complete and ideal Vee this

distance would have been 66 in. The ideal pattern passes through zero at  $8^\circ$  and  $12^\circ$  and  $23^\circ$  and has a side lobe, of amplitude 14 per cent. in power, centred on  $18^\circ$  (see Figs. 4.12–4.14). It may be seen that the main beam and neighbouring very small lobes of the ideal pattern for the Vee are reproduced faithfully, but the large lobe is much too big and its bearing about  $4^\circ$  larger than it ought to be. The pattern for

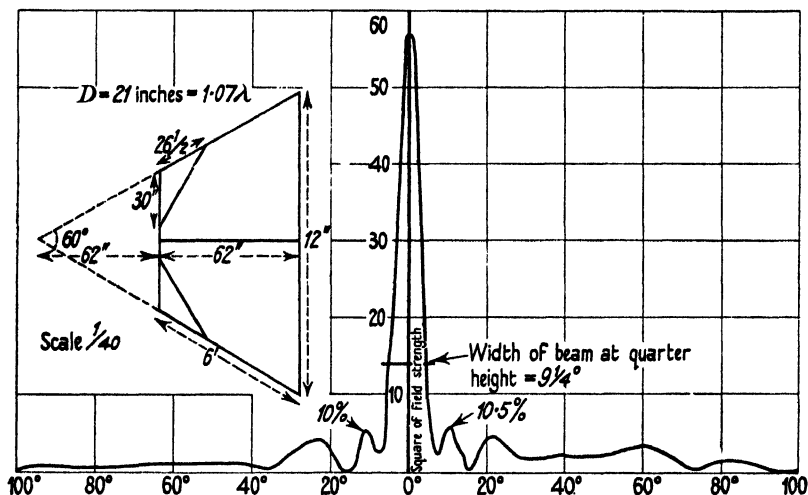


FIG. 12.15. Diffraction pattern for a modified  $60^\circ$  trough reflector.  $\lambda = 50$  cm.,  $D = 21$  in.

the complete Vee had larger lobes (they were 68 per cent. in power and were centred on  $\pm 25^\circ$ ) and it exhibited more diffraction round the edge and a much larger 'back-to-front ratio'. Hence, on the whole, the flat back has made the pattern approach more nearly to the ideal for the Vee. Fig. 12.15 shows the pattern which was observed when certain small sheets were placed across the angles of the trough, in the way described by the inset diagram. Comparison of Figs. 12.14 and 12.15 shows that these sheets across the angles have had an enormous effect in decreasing the side lobes, without appreciably altering the main beam. Save for the diffracted field on bearings greater than  $30^\circ$ , this pattern is now an extremely close approach to the ideal pattern for a  $60^\circ$  Vee with  $R/\lambda = 3.25$ . Here we meet a case where the shaping of the back of the mirror has been advantageous: we shall not discuss it further now.

The reader ought now to turn back to section 4 of Chapter VII and refresh his memory of the analytical discussion of the effect of a convex back to the Vee. An inevitable effect of such a back is to produce two

component patterns which are in phase quadrature with one another, and this means that the field cannot pass through zero on any bearing but will fall only to a minimum at certain bearings. Figs. 12.12–12.15 do not show that minima (in contrast to true zeros) are a conspicuous feature of the patterns resulting from flat-backed troughs. This effect was conspicuous in the pattern of a certain  $72^\circ$  trough ( $n = \frac{5}{2}$ ), but it must be remembered that minima are also characteristic of a complete Vee when  $n$  is not an integer. With the evidence before us there is no more reason to attribute the minima to the flat back, *per se*, than to the particular angle of the Vee. The minima, due to the curved back, are well typified in the ideal pattern shown in Fig. 7.11. The discussion in Chapter VII showed that if the radius of the back is chosen so as to make  $J_n(k) = 0$ , then the back is not likely to have much effect on the pattern provided the aerial is not much farther away from the apex than the second station for maximum forward field. But this does not say that, in this range of  $z$ , no back will disturb the pattern much, but it surely helps us to a general understanding of why flat backs often do not disturb the pattern very much.

The equatorial pattern for  $\beta = 60^\circ$  and  $R/\lambda = 3\frac{1}{2}$  is very attractive (it has been defined earlier on page 384), and it is tempting to examine whether this very desirable pattern is inevitably ruined by a curved back. After close consideration the writer has realized that it would involve prohibitive labour to settle this question definitely and for these reasons. If the aerial is about  $3\frac{1}{2}\lambda$  from the apex there will be six lobes and the main beam. From the argument of § 10.3 (c) and Figs. 4.13 and 4.14 we realize there is a strong tendency for all seven of these petals to have nearly the same length. But a particular value of  $R/\lambda$  may exist at which the main beam is vastly longer than the other petals, and such a case occurs for  $\beta = 60^\circ$  when  $R/\lambda = 3\frac{1}{2}$ . When there is a curved back there are two independent variables,  $k$  and  $z$ . For making the comparison we are looking for we should presumably choose  $z$  so that  $z/2\pi \doteq 3\frac{1}{2}$  and must then derive the patterns for various values of  $k$  round about  $k/2\pi = 3$ . If each of these patterns has very large lobes we have proved only that for the given value of  $z$  there is no value of  $k$  which gives substantially the same pattern as obtains when  $R/\lambda = 3\frac{1}{2}$  and  $k = 0$ . It would be necessary to repeat the process for various values of  $z$  and a vast amount of labour would be involved before the question could be answered with certainty. The labour is not justified. The analysis of the curved back, given in Chapter VII, is of immense value in showing that a convex

back need not (and indeed seldom can) have the general effect which would be suggested by geometrical optics. This helps us a good deal to understand the general reasons why a flat back often does not disturb the pattern much. It is tempting to use the ideal pattern for a curved back as the ideal pattern with which to compare the observed patterns from a flat back trough, for then we could assess the effect due to the back of the mirror being flat instead of convex. But unfortunately this is not practicable because we cannot decide on the proper and appropriate values to choose for  $k$  and  $z$ ; and it is likely the ideal pattern may be very sensitive to the precise values of these two parameters. We must leave the problem in a qualitative stage and not press it to a quantitative stage.

In comparing the size of the side lobes which are produced by a given Vee or trough we must be careful not to overlook the fact that the exciting aerial is a half-wave aerial and not an infinite filament. If the screens were unlimited in extent this would not matter, but when the height of the screens is comparatively small it is possible that it does matter.

#### 12.4. Analysis of a $45^\circ$ Vee with circular back

After giving these experimental results for troughs it seems appropriate to examine the current density in a Vee with a circular back. We will take  $\beta = 45^\circ$  (i.e.  $n = 4$ ) and  $k = 4$ . Then the sagitta of the arc is  $s = R(1 - \cos 22.5^\circ) = 0.076R$ , whence  $s/\lambda = 0.048$  when  $k = 4$ : accordingly the back is flat within 5 per cent. of a wavelength. We will take  $z = 7$  and then the aerial is distant  $0.48\lambda$  from the back; accordingly the forward field would be almost zero if the back were flat and infinitely extended. The density of current induced in the curved back is given by (7.15), and hence we have

$$\begin{aligned}\frac{\lambda i}{I} &= 4 \left[ \frac{H_4(7)}{H_4(4)} \cos 4\theta + \frac{H_{12}(7)}{H_{12}(4)} \cos 12\theta + \dots \right] \\ &= 4 \left[ (0.58 + 0.019j) \cos 4\theta + \frac{2.4}{10} j \cos 12\theta - \dots \right].\end{aligned}$$

And this shows the distribution is sensibly a simple sinusoid and cophased with  $I$ : if the flat back had been an infinite plane, then the 'bright spot' density would have been given by the expression

$$\frac{\lambda i}{I} = (1 + 1.05j),$$

thus showing that both the magnitude and phase of the 'bright spot'



density is modified profoundly by the sides of the Vee. The density induced in the sides of the Vee is given by the expression

$$\frac{\lambda i}{I} = \frac{32\pi}{ar} \left[ \frac{X_4(ar, k)H_4(z)}{H_4(k)} - \frac{3X_{12}(ar, k)H_{12}(z)}{H_{12}(k)} + \dots \right].$$

Fig. 12.16(a) shows the two components of induced density for  $\beta = 45^\circ$ ,  $k = 0$ , and  $z = 7$ , while Fig. 12.16(b) shows these two com-

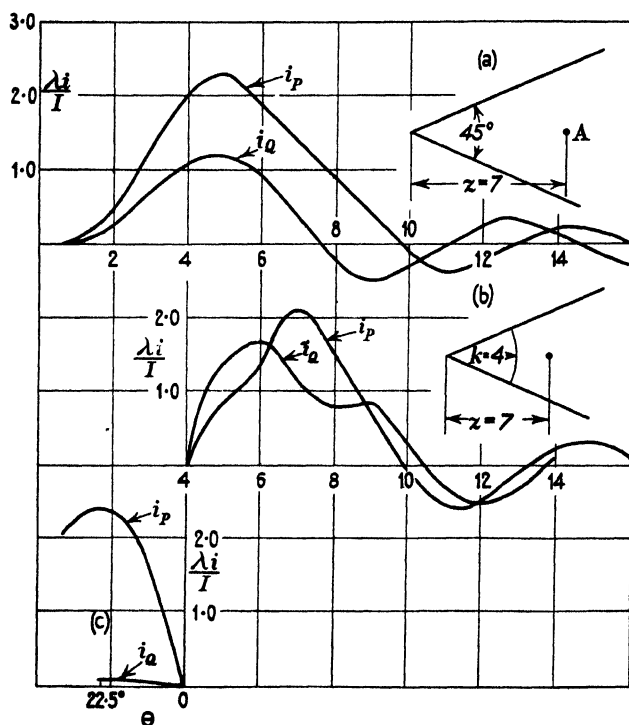


FIG. 12.16. Distribution of induced current in  $45^\circ$  reflectors.

ponents when  $k = 4$ : comparison of these two figures is instructive and shows that the main effect of the presence of the back is to force the current in curve (a) down to zero at  $k = 4$ . Fig. 12.16(c) shows the distribution of current round the curved back whose total width is  $\frac{1}{2}\lambda$ .

When  $k = 0$  and  $z = 7$  the equation for the pattern is

$$\frac{E}{16E_0} = 0.1578 \cos 4\theta + 0.0026 \cos 12\theta,$$

and when  $k = 4$  it is

$$\frac{E}{16E_0} = (0.14 - 0.25j) \cos 4\theta + 0.0026 \cos 12\theta.$$

The presence of the back has an insensible effect on the third harmonic term in the pattern and in both cases the pattern differs insensibly from a simple sinusoid. The back makes a large change in the phase of the field and increases its R.M.S. value in the ratio 1.8. A curved back can do no more than modify the relative values of the Fourier components of the pattern and give them phase angles relative to one another. It is no use looking for a mechanism which will produce a very blunt beam, such as geometrical optics might suggest would be produced by the convex back.

### 12.5. Vee reflectors used to curb the side lobes of curtain arrays

It seems appropriate to place this section here because it can be helpful in feeling our way towards analysing the behaviour of a parabola.

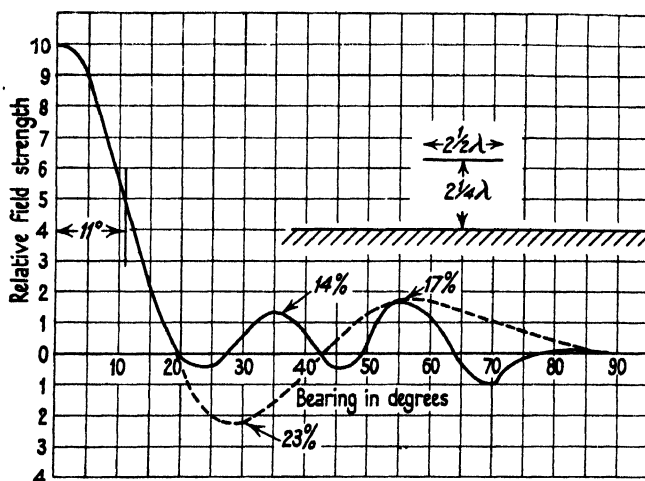


FIG. 12.17. Diffraction pattern for a 6-member curtain array whose plane is  $2\frac{1}{4}\lambda$  in front of an infinite reflecting sheet.

The dotted curve in Fig. 12.17 shows the pattern for a curtain having six equal and cophased currents spaced  $\frac{1}{2}\lambda$  apart: it is characterized by large side lobes centred on  $\theta = 28^\circ$  and  $58^\circ$ . Such a curtain would usually be provided with a flat sheet reflector, so as to restrict the radiation to one direction along the normal. Consideration will show that the side lobes can be modified considerably if the distance between the curtain and the reflecting sheet is chosen suitably. The curtain may be replaced by a single equivalent current at the middle point of its width, the strength of this equivalent current depending on the bearing angle in the manner required to give the pattern for the curtain alone.

The pattern of the curtain in the presence of the screen can be

calculated from this equivalent current and its mirror image behind the screen. If the distance between the curtain and the screen is chosen so as to make the field, of the equivalent current and its image, zero when  $\theta$  is near  $28^\circ$ , then the large side lobe will be much reduced. The equation for the resultant field is

$$E = 2E' \sin\left(\frac{2\pi d}{\lambda} \cos \theta\right),$$

where  $d$  is the distance between the planes of the curtain and the reflector and  $E'$  is the field of the curtain alone on bearing  $\theta$ : thus the field is seen to be the product of two independent factors. The values of  $\theta$  at which the second factor is zero are shown collected in Table 12.4 for various values of  $d/\lambda$ .

TABLE 12.4

$d/\lambda$	$\theta$							
5/4	37	66	90					
7/4	31.2	55.3	73.5	90				
9/4	27	49	64	77.5	90			
13/4	22.6	39.6	52.5	62.6	72	81	85.5	90

This table shows that when  $d/\lambda = \frac{13}{4}$  the field is zero when  $\theta = 22.6^\circ$  and  $39.6^\circ$ ; accordingly it must be a maximum when  $\theta$  is near  $31^\circ$ . But the maximum of the first side lobe of a 6-member curtain occurs when  $\theta = 28^\circ$ , the field passing through zero when  $\theta = 19^\circ$  and  $42^\circ$ . Hence, if  $d/\lambda = \frac{13}{4}$ , the first two zeros of the second factor are very near the first two zeros of the first factor and thus the side lobe of the curtain will not be appreciably reduced by the reflector. But if  $d/\lambda = \frac{9}{4}$  the table shows the reflector makes the field zero when  $\theta = 27^\circ$  and this is almost the bearing for the maximum of the side lobe. Fig. 12.17 shows the pattern for a 6-member curtain distant  $2\frac{1}{4}\lambda$  from an infinite reflecting sheet: the dotted curve in the same figure shows the pattern for the curtain alone. In the presence of the reflector there are now seven bearings on which the field is zero, whereas there were only three such bearings for the curtain alone. For many purposes the reflector (if spaced at  $2\frac{1}{4}\lambda$ ) has improved the pattern considerably.

If a curtain array is combined with a  $90^\circ$  Vee, then the field will be zero on bearings greater than  $45^\circ$  and thus the Vee removes the outer side lobes. The equatorial pattern for a single aerial in a  $90^\circ$  Vee is given in equation (3.15 *b*) and is

$$\frac{E}{2E_0} = \cos(k \cos \theta) - \cos(k \sin \theta), \quad (3.15 \ b)$$

the phase of the field being as though the single aerial were at the apex of the Vee. It is helpful to look at the structure of (3.15*b*) in a way we have not done explicitly before. The second factor in it is the same as the first factor save that it is plotted from the origin ( $\theta + \frac{1}{2}\pi$ ). Hence to obtain the curve  $\cos(k \cos \theta) - \cos(k \sin \theta)$  we have only to plot, on transparent paper, the simple curve  $\cos(k \cos \theta)$  in the range of  $\theta$  from  $0^\circ$  to  $90^\circ$ , then fold it about the ordinate at  $45^\circ$ , and subtract the two

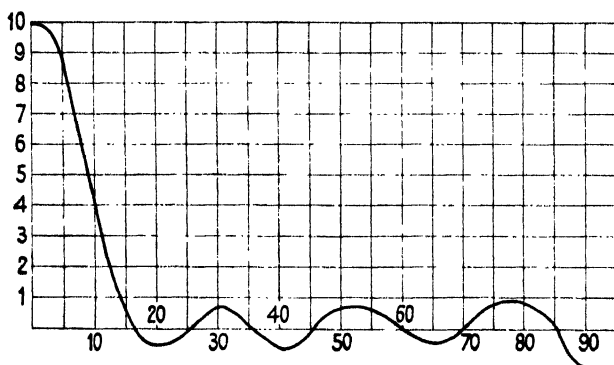


FIG. 12.18. Diffraction pattern for two parallel 7-member curtain arrays separated a distance  $5\lambda$ .

halves which have now become superposed. The reason for this should be obvious from consideration of the images. Thus, the two positive currents are in one line with the origin and separated a distance  $2R$ , and their resultant field is  $2E_0 \cos(k \cos \theta)$ . The pattern due to the two negative images must be the same shape as that due to the two positive currents, but its axis is turned through  $90^\circ$ .

Fig. 12.18 shows the ideal pattern for two parallel 7-member curtains separated by  $5\lambda$ : the zeros at  $16.5$ ,  $34.8$ , and  $59.5$  are due to the curtain having 7 members and the two intermediate zeros are due to the two curtains being  $5\lambda$  apart.

If the right-hand half of Fig. 12.18 is pivoted round the point  $\theta = 45^\circ$  and turned clockwise through  $180^\circ$  and the two superposed patterns are then added, the result will give the pattern for a 7-member curtain distant  $2\frac{1}{2}\lambda$  from the apex of a  $90^\circ$  Vee. This is shown in Fig. 12.19: the dotted curve in this figure shows the pattern for the 7-member curtain in isolation. The largest side lobe has a fractional amplitude of 9 per cent. and is centred on  $\theta = 40^\circ$ : in practice much of this would 'slide over the edge' of the finite reflecting sheets. Thus the pattern would be a substantially lobe-free beam whose width at half-height is  $16^\circ$ .

These examples suffice to show how the lobes of a curtain can be curbed enormously by the use of a wide-angle Vee. If the middle members of the curtain carry a relatively larger current, then the lobes will be still further reduced. We remind the reader that if the curtain is not flat but is an arc of radius  $R$  (stretching right across the Vee) and carrying a sinusoidal distribution of current, then the pattern is a true

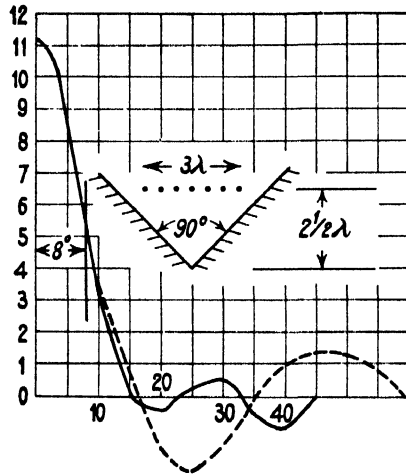


FIG. 12.19. Diffraction pattern for 7-member curtain in a 90° reflector.

sinusoid for all values of  $R$ . Thus, in general, the width of the main beam will tend to be increased if the curtain is convex to the aperture. Consideration will show that a concave curtain must produce the same pattern as an equivalent curtain in the plane of the bisector: the loading and spacing of the said equivalent curtain being a function of the curvature.

## XIII

### PARABOLIC REFLECTORS

#### 13.1. Introduction

CONSIDER the problem of a long current filament which is parallel to the generators of a parabolic cylinder, is inside it, and on the axis of a parabola which is a cross-section. The current filament will induce currents in the metal of the parabolic cylinder and they will flow along the generators. The electric field at any point will be the resultant of the field due to the original current filament and the component fields due to all the filaments induced in the metal cylinder, whose shape is a parabola. It is a two-dimensional problem, and it has to satisfy the condition that the electric field is zero at all points on the metal wall. The problem is reminiscent of the problem of a filament between two flat metal sheets and the solution of this has occupied a large portion of this book. But the analytical solution for the parabola is not forthcoming. Since two intersecting straight lines are the asymptotes of a hyperbola it might be expected that the solution for flat sheets would indicate the solution for a hyperbolic cylinder, but it does not do so: hence we do not get even the lead of a hyperbola to help us towards a parabola. In writing this we recollect that the solution for flat sheets is, analytically speaking, unsatisfactory when images do not exist: experience has shown that the solution is very valuable and is reliable when applied to reflectors used in practice, but this good fortune does not remove the analytical trouble. Having regard to the analytical trouble (of multiple values) which arises with flat sheets and the analytical impasse which arises with a hyperbola and a parabola, the writer is inclined to suspect that no completely satisfactory solution exists for infinitely extended reflectors. He suspects that a correct solution would include the parabola, the hyperbola, and all flat sheets. Perhaps it is a fortunate accident that the solution for flat sheets is analytically correct when images can be found, and this means that the form of the general solution happens to simplify itself enormously in these particular cases. It may be that the general solution is not of the form  $F(r) \times \phi(\theta)$ , but that it just happens to degenerate into this form in the image cases. This would mean that the analytical form of the solution is extremely sensitive to the exact form of the boundary, but that the numerical value of the solution is not unduly sensitive to that form. From a practical point of view we get on very well indeed by

using a solution which is not all it should be and perhaps the step between flat sheets and a parabola may be less than it seems to be.

The experiences recorded in the last chapter show that, in general, 'trough reflectors' behave very much as though the apex of the Vee had not been amputated; accordingly the analysis for the Vee is substantially valid for a trough. This must lead to the expectation that the behaviour of a parabolic cylinder will be very similar to that of a flat-sided trough: accordingly we shall set out with the expectation of finding that the forward field passes through a succession of maxima and minima as the distance is varied between the aerial and the vertex of the parabola.

But when the problem is approached in this way the reader will surely inquire why a parabola should be used in preference to a trough or a Vee, since to do so strays farther outside the range of analytical guidance and moreover requires the reflector to be built to a shape which is much more difficult to construct than a Vee or a trough. Now a parabola is defined as the locus of a point which moves so as to be equidistant from a given line and a given point: the said given point has long been called the focus, and this is the Latin word for a fire and for a hearth. This will recall to the reader his 'schoolboy' knowledge of parabolic mirrors and the enormous importance of putting the source of light at the focus of the parabola. It explains why we think of using parabolic reflectors for aerials: we do so with the expectation of finding a focus.

The approach we have taken may seem forced and pedantic, but it has been taken very deliberately to bring home the contrast between our experience with aerials and our experience with, say, the headlights of a motor-car. This contrast has long been very apparent to the writer and it led him, in 1941, to conduct the series of experiments which will now be discussed.

### 13.2. Experiments with parabolic cylinders

The experiments to be described now were made at a wavelength of 50 cm. and they were deliberately schemed so as to make the approach to the investigation follow the procedure used with Vee reflectors. In other words, they were made in the expectation that the behaviour of parabolic reflectors would be substantially similar to that of Vee or trough reflectors, but in the hope that it would prove to be dissimilar to a Vee and akin to that of the parabolic mirrors used for optical purposes. Three frames, each of height  $2\frac{1}{2}$  ft., were made in wood and

shaped to a parabola: fine-meshed copper gauze was nailed to these wooden frames, thus forming a cylinder whose length was  $2\frac{1}{2}$  ft. and whose cross-section was a parabola. All wooden parts were on the convex side of the gauze and thus the reflector presented a smooth metal surface to the exciting aerial. Each of the three frames had an aperture of 12 ft., but the depth between the aperture plane and the vertex of the parabola was not common: these depths were 5, 4, and 3 ft. respectively for the cylinders, which will in future be designated *A*, *B*, and *C*. The wooden frames were extremely well made and the width conformed to parabolic shape within  $\pm\frac{1}{2}$  in. at any distance from the vertex: since the wavelength was near 20 in., this means that the 'figure' of the mirrors was correct to within  $\pm 2.5$  per cent. of  $\lambda$  and thus was more perfect than the best optical practice. It follows from the stated dimensions that the focal lengths of the cylinders *A*, *B*, and *C* were 21.5, 27, and 36 in. respectively. When the wavelength was 50 cm. the aperture of each was  $7.5\lambda$  and the height of each was  $1.5\lambda$ ; the focal lengths being  $1.1\lambda$ ,  $1.35\lambda$ , and  $1.82\lambda$  respectively. By tearing strips of gauze off the wooden frame it was possible to investigate the effect of a progressive decrease of the aperture of a parabola of given focal length: this process was carried out on cylinder *A* and on that one only.

The wooden frame was mounted on a wooden turn-table and placed so that the axis of the parabolic cylinder was vertical. The aerial was a half-wave dipole which could be moved along a light wooden bar which pointed along the axis of a parabolic section. The axis of the aerial was vertical and thus the electric field was perpendicular to the ground.

The receiving aerial was distant  $100\lambda$  from the axis of the turn-table and it consisted of an in-line array of eight half-wave aerials connected to a thermocouple: the said in-line array was parallel to the axis of a small reflecting cylinder (which, incidentally, was shaped to a parabola) which served both to improve the 'gain' and to shield the receiver from spurious fields radiated by surrounding objects.

#### (a) *Forward-field tests*

Having taken a few diffraction patterns to discover which bearing of the turn-table corresponded to the centre line of the main beam pointing directly at the receiver, the table was set at this bearing and the response of the receiver was plotted as a function of the distance between the aerial and the vertex of the parabolic cylinder—thus



performing a test corresponding to what has been termed the forward-field test for Vee reflectors.

The curves of forward field which were observed for the three cylinders are reproduced in Fig. 13.1. In each case they disclose stations of maximum, minimum, and zero forward field and so follow the precedent of Vee reflectors, as we were very inclined to expect. Any

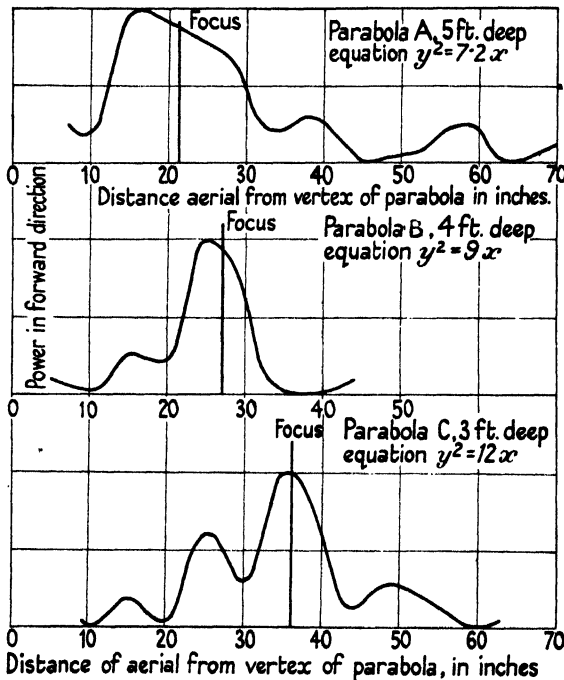


Fig. 13.1. Curves of forward field for parabolic cylinders.

station of maximum forward field has properties akin to what we mean by using the word focus: but there is only one point which is the geometrical focus of a parabola, and optical experience might lead us to suppose that a parabolic reflector would have only one station for maximum forward field, and this would be at the focus of the parabola. The forward field curve for parabola *A* in Fig. 13.1 has three stations exhibiting focal properties and none of them is at the focus of the parabola. Parabola *C* has four stations for maximum forward field and one of them is very nearly at the focus of the parabola: does the coincidence of the grand maximum of forward field with the focus in this case disclose a special virtue of parabolic shape or is the coincidence accidental? The answer to this question is given in Fig. 13.2, which

relates to parabola *A* when successive strips of gauze were torn off it, so as to leave a metal cylinder having the apertures stated on the curves in the figure. The focus was in the plane of the aperture in curve (b) in Fig. 13.2 and also in the lowest curve in Fig. 13.1, and accordingly these two cylinders then have a certain correspondence.

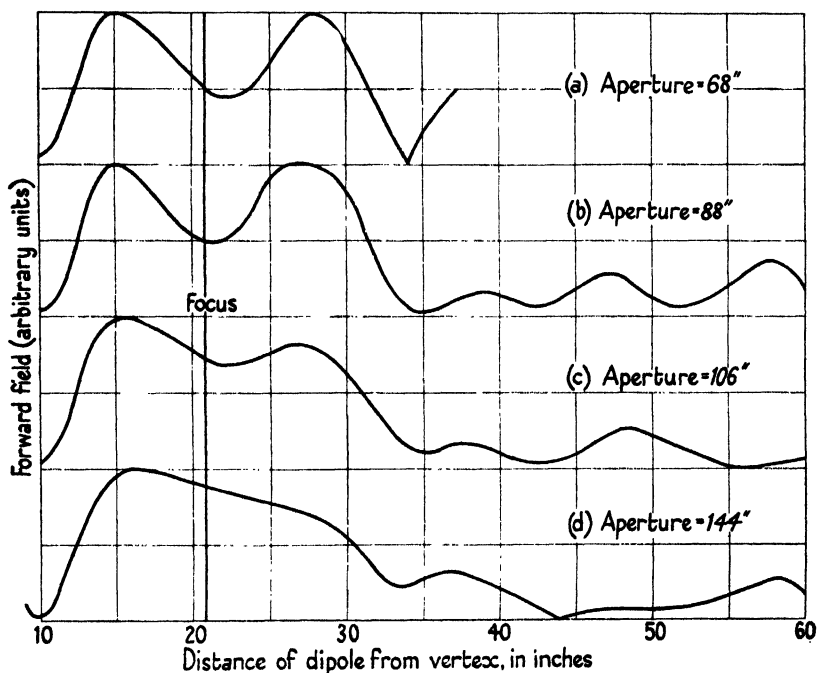


FIG. 13.2. Curves of forward field for parabolic cylinders.

with one another; but the curves of forward field show no correspondence. Every curve in the two figures shows a zero of forward field when the aerial is near  $\frac{1}{2}\lambda$  from the vertex and in this respect the parabola is then acting as though it were a flat sheet. The collective evidence of the two figures shows that the forward field has no strong tendency to be a maximum when the aerial is at the focus of the parabola and also shows that parabolic reflectors have a succession of stations for maximum forward field. Surely these curves suffice to show that the optical properties of parabolic mirrors have not begun to appear in the reflectors used here? What is this discrepancy due to? Presumably it is only a matter of scale, and consideration will show that the discrepancy of scale is immense. The spectrum of visible light is contained within the range of wavelength from, say,  $7 \times 10^{-5}$  to

$4 \times 10^{-5}$  cm., and hence an aperture of 7 cm. is more than  $10^5$  wavelengths: in our experiments the aperture is  $7.2\lambda$ . Moreover, in optics the most perfect point-source will have a diameter which is several thousands of  $\lambda$ , whereas here that diameter is about 1 per cent. of  $\lambda$ . In optics there is no possibility of exploring the focus within a small fraction of  $\lambda$ , but only within a small fraction of the focal length. Apart from mere discrepancy of scale the optical problem and the radio problem are not the same, and it is not essential to demand exactly similar behaviour. It is difficult to believe that a vast parabolic reflector would exhibit optical behaviour when excited by a single radio aerials, though it would doubtless do so if it were excited by a vast swarm of aerials which were grouped in the neighbourhood of the focus. The optical description of the parabolic mirror in terms of constancy of path length is seductively simple. But if we approach the problem only with our experience of aerials, it is very hard to understand the undoubted importance in optics of the focus of a parabola.

*(b) Relation between aperture and width of main beam*

In the period 1940–1 there was a general belief that the width of the main beam, from a parabola, was strictly in the inverse proportion to the aperture. It is now widely realized that that belief is a fallacy, but doubtless the fallacy will tend to linger, more especially as things do conspire so as to make the rule roughly correct. Our knowledge and understanding of Vee reflectors makes us associate the width of the beam with the distance of the aerial from the apex. We know very definitely that the width of beam does not depend only on the aperture since a small axial displacement of the aerial, in a reflector of given aperture, may cause the central beam to disappear. Moreover, it is known that the main beam produced by a given Vee may well be appreciably narrower than the ideal and then an increase in the aperture may cause an increase in the width of the beam. In short, with Vee reflectors the aperture does not enter into the problem so long as the aerial is not much in front of its plane. Why then should it be supposed that the aperture of a parabola is important?

If the reflector is parabolic, then there is only one station for the aerial which has logical significance and that is the focus. If the aerial is not at the focus, then there is no reason for using a parabolic shape: it is a mere fancy shape if the aerial is not at the focus, and we can scarcely expect to make any interesting generalizations from experiments on

parabolic mirrors which are used in a way not directly appropriate to this shape. Consideration of Figs. 13.1 and 13.2 is almost sufficient to show that parabolic shape cannot have any very special meaning when the focal length is only of the order of a couple of wavelengths. Nevertheless a study was made of the relationship between width of beam and aperture when the aerial was at the focus. A close study was made of the width of the beam as the position of the aerial was changed slightly in the close neighbourhood of the focus: denoting the distance between the aerial and the vertex by  $d$ , the focal length by  $F$ , we shall study the width  $2\theta$ , of the main beam, as  $d/F$  passes through the value unity, hoping to find (if parabolic shape has any virtue) that  $2\theta$  is a minimum when  $d/F = 1$ . The width of the beam is defined here from the bearing  $\theta_1$  at which the field is zero or a minimum for the first time: the sensitivity of the galvanometer and the shape of the patterns was such that it is believed that  $\theta_1$  could be determined within limits which certainly did not exceed  $\pm 0.5^\circ$ . The wooden frame  $A$ , for which  $F/\lambda = 1.1$ , was used when the amount of copper gauze on it gave a parabola whose aperture was  $7.3\lambda$  or  $5.8\lambda$  or  $4.6\lambda$  or  $3.5\lambda$  (see also Fig. 13.2). The results of these experiments are collected in Table 13.1.

TABLE 13.1

*Cylinder A. Focal length 21.5 in.*

$d/F$	Aperture $7.3\lambda$					Aperture $5.8\lambda$			
	0.93	0.96	1.0	1.07	1.11	0.93	0.98	1.02	1.07
$2\theta_1$	17	16	15.5	14	14	23	20	18	17
$d/F$	Aperture $4.6\lambda$					Aperture $3.5\lambda$			
	0.93	0.96	1.02	1.07		0.93	1.02	1.12	
$2\theta_1$	27	24	21	21.5		28	24	21	

The table shows that in all four cases  $\theta_1$  is changing continuously as  $d/F$  passes through unity; thus establishing that the focus is not a station for minimum width of beam: thus the beam does not 'focus' particularly well when the aerial is at the focus, proving that the focus here is not a point of outstanding peculiarity or virtue.

A plane current sheet of width  $b$ , bearing a uniform and cophased current loading has a beam width defined by the equation  $\sin \theta_1 = \lambda/b$ , and presumably the belief in the importance of the aperture is associated with this formula. Table 13.2 shows the values of  $\theta_1$  observed for the parabolas and the corresponding values of  $\arcsin \lambda/b$  for the pattern

obtained when  $d/F = 1$ , the precise value of  $\lambda$  having been found to be 49.3 cm.

TABLE 13.2

$\theta_1$ . . .	7.75	9.25	11	12.5
$\arcsin \lambda/b$ .	7.7	9.9	12.8	16.6

The agreement happens to be within the limits of experimental error for the two larger apertures but is widely outside these limits for the two smaller apertures. Thus the width of beam does not vary inversely as the aperture for a parabola of given focal length.

It seemed worth while to study what effect a small change of  $\lambda$  had on the pattern obtained when  $d/F = 1$ ; this experiment is recorded in Table 13.3.

TABLE 13.3

*Cylinder A. Focal length 21.5 in. = 54.5 cm.*

$d/F$ . . . . .	Aperture $4.6\lambda$			Aperture $3.5\lambda$		
	0.93	1.02	1.12	0.93	1.02	1.12
$2\theta_1$ for $\lambda = 49.3$ cm. .	27	21	22	28	24	21
$2\theta_1$ for $\lambda = 53.5$ cm. .	28	24	20	32	28	20

When  $d/F = 1$  an increase of 8 per cent. in  $\lambda$  has increased  $\theta_1$  by 16 per cent. in both apertures, thus showing again that  $\theta_1$  is not equal to  $\lambda/b$ . The condition of  $F = \lambda$  is very nearly attained when  $\lambda = 53.5$  cm., and Table 13.3 shows that no peculiar result occurs when  $d = F = \lambda$ .

Table 13.4 records a similar test for cylinder *B*.

TABLE 13.4

*Cylinder B.  $F = 27$  in. =  $1.35\lambda$ , aperture  $7.2\lambda$*

$d/F$	0.92	0.96	1.0	1.04	1.08
$2\theta_1$	22.75	23.75	24.5	25.25	27.5

Thus Table 13.4 shows that  $2\theta_1$  is changing continuously as  $d/F$  passes through the value unity: here, however,  $2\theta_1$  is increasing with  $d/F$  whereas it was decreasing with  $d/F$  in cylinder *A*. Since the aperture was  $7.2\lambda$  it follows that  $2 \arcsin \lambda/b = 15.4^\circ$ , whereas  $2\theta_1 = 24.5^\circ$  when  $d/F = 1$ . The measurements were repeated for various values of  $\lambda$  between 55.1 and 48.7 cm. and showed that  $2\theta_1$  decreased as  $\lambda$  increased and was  $20.5^\circ$  when  $\lambda = 55.1$  cm.

TABLE 13.5

*Cylinder C.  $F = 36$  in.  $= 1.8\lambda$ , aperture  $7.2\lambda$ , and in focal plane*

$d/F$	0.86	0.92	0.99	1.08	1.14
$2\theta_1$	14	17	21	15	13

Here  $2\theta_1$  passes through a blunt maximum when  $d/F$  is near unity and then is about 40 per cent. greater than  $2\lambda/b$ : here the focus of the parabola has the converse of a focusing property. At  $d/F = 1$  it was found that  $2\theta_1$  decreased continuously as  $\lambda$  was increased from 46 cm. to 53 cm. It is relevant to compare Table 13.5 with that part of Table 13.1 which relates to an aperture of  $4.6\lambda$ , because each relates to a parabola in which the aperture was in the focal plane: in Table 13.1,  $F/\lambda = 1.1$  and in Table 13.5,  $F/\lambda = 1.8$ . In both cases  $2\theta_1$  is near  $22^\circ$ , although the apertures are in the ratio 1.56: this shows that the beam width does not bear a simple relation to the aperture even for parabolas having apertures in the focal plane. The width of the focal planes was 7.2, 9, and 12 ft. in cylinders *A*, *B*, and *C* respectively, whereas  $2\theta_1$  was equal to  $15.5^\circ$ ,  $24.5^\circ$ , and  $21^\circ$  respectively at  $d/F = 1$ : this shows that the width of the focal plane is not the determining factor and that was already apparent since an increase of  $\lambda$  may either increase or decrease  $2\theta_1$ . These systematic tests have failed to discover that the focus of a parabola has any outstanding property.

(c) *Attempt to turn the beam by offsetting the aerial*

This experiment was performed on cylinder *A* when it had an aperture of 12 ft. The half-wave aerial was placed at the focus and the turn-table was moved until the response of the receiver was at its maximum: the aerial was then offset from the focus and the table turned until the response became a maximum again. It was found that offsetting the aerial  $3\frac{1}{2}$  in. from the focus (i.e.  $\alpha = 10^\circ$  in our notation) turned the beam through  $4^\circ$  in the opposite sense and increased its width from  $15^\circ$  to  $35^\circ$ . Hence the main beam produced by a parabolic reflector is difficult to turn away from the axis and has what we have previously called the rigidity which is associated with the main beam produced by a curtain array or a Vee reflector.

(d) *The complete diffraction pattern for  $d/F = 1$*

The curves of forward field, Figs. 13.1 and 13.2, make it evident that a great variety of patterns can be obtained from a parabolic reflector. But for the purpose of this discussion there is only one pattern of general interest and it is the pattern when the aerial is at the focus.

For a given parabolic reflector there may well be patterns which are more desirable for practical use, but our purpose here is to discover why reflectors should be made parabolic.

Fig. 13.3 shows the diffraction pattern resulting from cylinder *C* (12×3 ft.) when the aerial was at the focus and  $\lambda = 49.3$  cm.: since our main interest is in the side lobes, the peak of the main beam has not

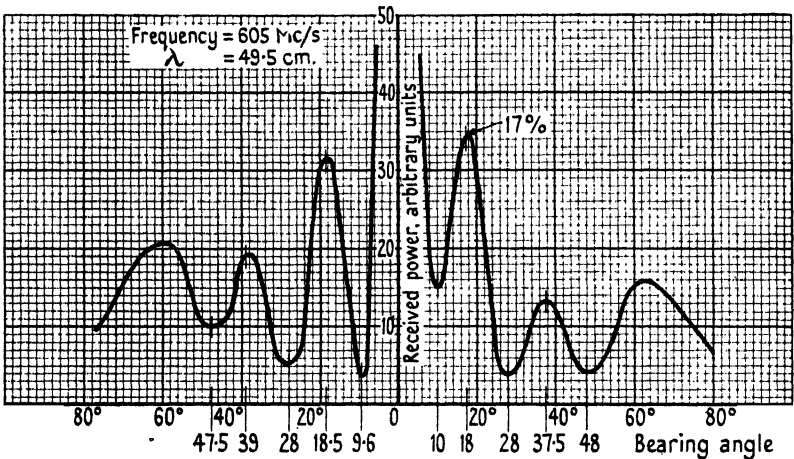


FIG. 13.3. Diffraction pattern for parabolic cylinder: aerial at focus and  $F = 1.86\lambda$ .

been included in the figure. This pattern exhibits dissymmetries of the kind with which we are already familiar. The aerial was found to be at the middle of the aperture within less than  $\frac{1}{2}$  in. in 12 ft. (i.e.  $\alpha < 0.08^\circ$ ). Though the values of the maxima and the minima differ considerably on the two sides of the main beam, yet it should be noticed that the bearings of the maxima and minima are symmetrical within about one degree.

The pattern was recorded at five frequencies between 650 and 561 Mc/s and the observed angles of maxima and minima are recorded in Table 13.6.

TABLE 13.6

*Cylinder C (12×3 ft.), aerial at focus*

$f$ Mc/s	$f/\lambda$	$\theta_1$	$\theta_2$	$\theta_3$	$\theta_4$	$\theta_5$	$\theta_6$
650	2.0	14	22	30	41	50	60
625	1.92	11.5	19	28	38	48	61
605	1.86	9.75	18	28	39	47	61
575	1.76	9	16	26	36	47	61
561	1.72	8	14.5	25	33	46	60

This table shows that it is only  $\theta_1$  and  $\theta_2$  which are appreciably dependent on the frequency: it also emphasizes, once more, that the width of the main beam is not proportional to the number of wave-

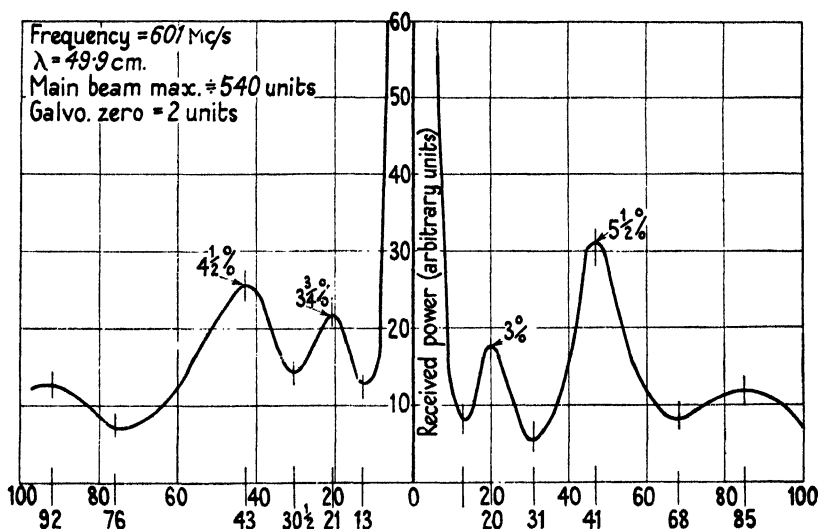


FIG. 13.4. Diffraction pattern for parabolic cylinder: aerial at focus and  $F = 1.35\lambda$ .

lengths in the aperture, since here the width of the beam increases with the frequency. Fig. 13.4 shows the pattern due to cylinder *B* ( $12 \times 4$  ft.) when the aerial was at the focus and  $\lambda = 49.9$  cm. ( $f = 601$

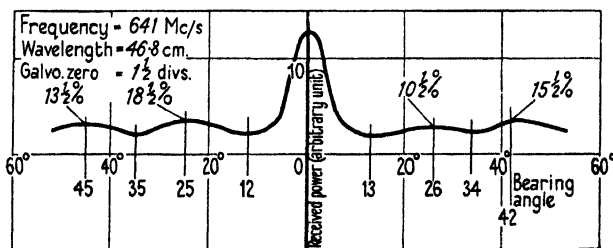


FIG. 13.5. Diffraction pattern for parabolic cylinder *B*.

Mc/s): it is a more desirable pattern than Fig. 13.3 since it has smaller side lobes, but the two do not differ much in general character. Figs. 13.5 and 13.6 show the pattern for cylinder *B* when  $f = 641$  and  $544$  Mc/s respectively. Once more the bearings for maxima and minima do not depend much on frequency, but the general level of the side lobes is least when  $f$  is near 600 Mc/s. The last four figures show that parabolic shape has no marked superiority over a Vee or a trough,



either in respect of width of beam or size of side lobes. Indeed, the whole behaviour seems to correspond very closely with that of a trough.

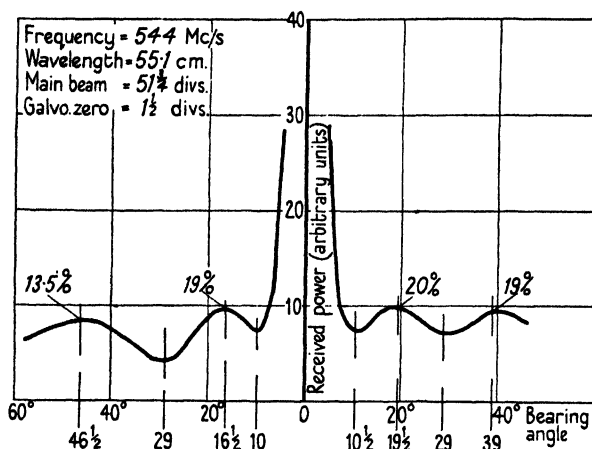


FIG. 13.6. Diffraction pattern for parabolic cylinder *B*.

### 13.3. Comparison of parabola with a Vee

Cylinder *C* is possibly of special interest because it has the focus in the plane of the aperture, and this is a very common disposition. The latus rectum of a parabola subtends an angle of  $128^\circ$  at the vertex and hence it would be of interest to compare the performance of cylinder *C* with a Vee of angle  $128^\circ$  and aperture 12 ft.: this would show the effect of bulging the flat sides of the Vee into the parabolic form. It would also be desirable to compare the observed with the ideal patterns for such a Vee, but the ideal pattern for a  $128^\circ$  Vee would be troublesome to compute since it would entail values of  $J_{1.4}$ , etc. It was felt that  $\beta = 120^\circ$  involving  $J_1$ , etc., was a sufficiently close approximation for our purpose. Flat sheets 6 ft. wide were available, and these gave an aperture 10.4 ft. wide when set at  $120^\circ$  to one another. We are thus about to compare a parabola 3 ft. deep and 12 ft. wide with a Vee 3 ft. deep and 10.4 ft. wide. We know that the pattern for the Vee should be specified as a function of the distance between the aerial and the vertex. Hence it is natural to compare the patterns when the aerial is the same distance from the vertex of the parabola as it is from the apex of the Vee, though it does not necessarily follow that these are the patterns which ought to be compared. Figs. 13.7, 13.8, and 13.9 show the superposed patterns for the parabola and the  $120^\circ$  Vee when the distance of the aerial from the apex (or vertex) was 25, 34, and 47 in. respectively. A glance at Figs. 13.7 and 13.9 shows that a profound

effect on the pattern is produced if the straight sides of the reflector are strained and curved to parabolic form. First consider Fig. 13.7. The patterns for this Vee have been compared, in § 10.3 (c), with the

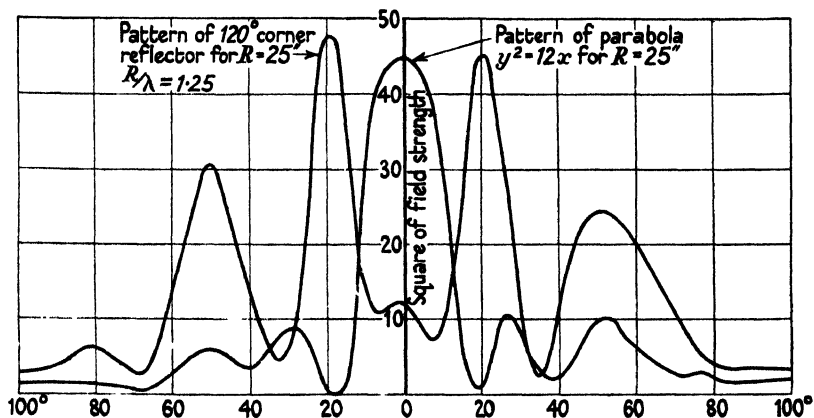


Fig. 13.7. Diffraction patterns for parabolic cylinder and for 120° corner reflector.

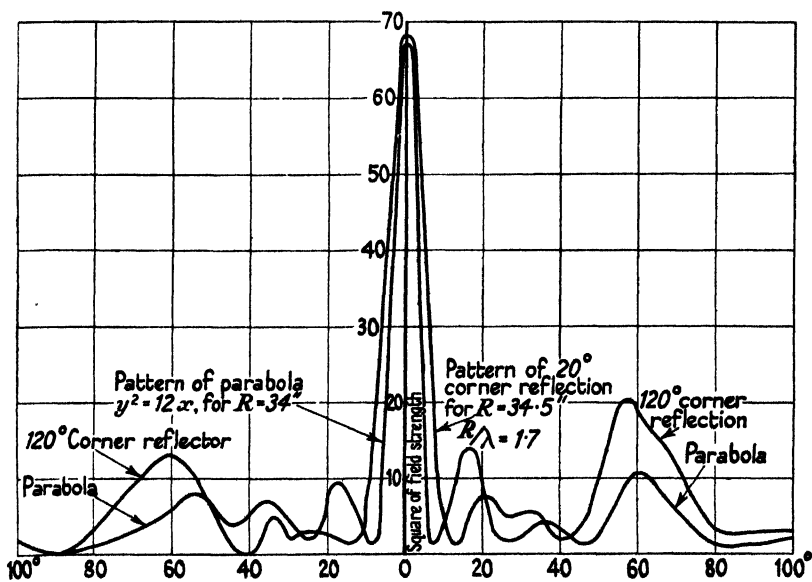


Fig. 13.8. Diffraction patterns for parabolic cylinder and for 120° corner reflector.

ideal and found to be closely in agreement with them. The pattern in Fig. 13.7 is for the station  $R/\lambda = \frac{1}{2}$  and the station for minimum forward field occurs at  $R/\lambda = 1.65$ . The central beam is almost non-existent and has been replaced by a wide bifurcated beam: all this is thoroughly characteristic of an aerial very near a station for minimum

forward field. On the other hand, reference to the lowest curve in Fig. 13.1 will show that  $R = 25$  in. is a station for maximum forward field for this parabola, and the pattern for the parabola in Fig. 13.7 has the characteristics which we associate with an aerial near a station of maximum forward field in a Vee. Hence with our experience and understanding of a Vee it is natural for us to associate the contrast

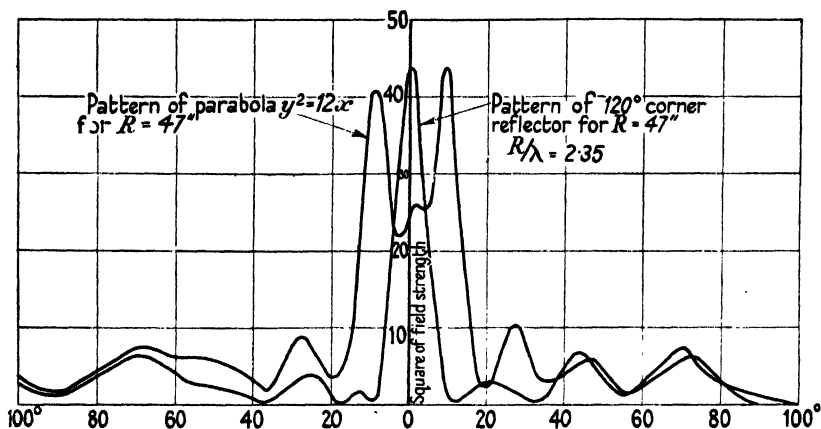


FIG. 13.9. Diffraction patterns for parabolic cylinder and for  $120^\circ$  corner reflector.

between the two patterns in Fig. 13.7 more with the position of the aerial relative to a station of maximum forward field than with very special properties of the parabolic shape of the reflecting surface. Extrapolation from Fig. 3.8 shows that  $R/\lambda = 2.3$  is a station for maximum forward field for a  $120^\circ$  Vee: at  $\lambda = 50$  cm. this will occur at  $R = 47$  in., whereas reference to the lowest curve in Fig. 13.1 shows that  $R = 44$  in. is a station of minimum forward field for this parabola. Hence if  $R$  is increased from 25 to 47 in., we should expect that the pattern for the parabola would have a form typified by the pattern for the Vee in Fig. 13.7 and the pattern for the Vee would be typified by the pattern for the parabola in Fig. 13.7, save only that the central beam had become narrower (because of the increase of  $R/\lambda$ ). Reference to Fig. 13.9 shows that these predictions from general principles are fulfilled completely. Thus, if we had never heard of the optical properties of a parabolic mirror but had worked out the properties of a Vee and had experimented with a Vee and had also experimented with a trough and then been confronted with a parabola, we should have found the behaviour of a parabola completely understandable and should never have suspected the remarkable properties which parabolic mirrors have in optics.

Now consider Fig. 13.8 which relates to  $R = 34$  in., which is near a station for maximum forward field both for the Vee and for the parabola and, incidentally, is very near that very special point, the focus of the parabola. The patterns for the parabola and the Vee do not differ in any marked degree, save only that the central beam from the parabola is about two-thirds the width of the central beam from the Vee. Here the aerial is virtually at that station which is of peculiar interest in the parabola, and hence that pattern in Fig. 13.8 should properly be termed the true and proper pattern intrinsic to this reflector. Yet it is just this very pattern which is changed least if the parabolic sides are drawn taut into the chords from the vertex to the ends of the latus rectum. It is just when the aerial is at the focus that this gross change of figure makes scarcely any difference to the pattern. Surely this establishes that what we are observing is not a focus in the optical sense?

Reference to Table 13.5 shows that the width of the central beam passes through a maximum near  $d/F = 1$ , and hence it is unlikely that patterns for Vee and parabola, near  $R = 34$  in., could be found which would agree more closely than the two which are exhibited in Fig. 13.8.

Table 13.5 was drawn up to dispose of the fallacy that the width of the beam is equal to the ratio of the wavelength to the aperture; and it did so largely by showing that the width was not only very sensitive to  $d/F$  but was a maximum and not a minimum when  $d/F = 1$ . Now we can understand why it passes through a maximum as  $d$  increases from 31 to 41 in. This follows from Fig. 13.1, which shows that the forward field is a minimum when  $d = 30$  and when  $d = 44$  in.: at these values of  $d$  the central beam will either have disappeared and been replaced by a bifurcated beam or shrunk to a small pimple at the bottom of a trough in the bifurcated beam. Such a pimple is seen to exist in Fig. 13.9, but happens there to be slightly unsymmetrical: it also appears in the pattern for the Vee recorded in Fig. 13.7. Hence it is in accordance with the observed curves of forward field that the width of the beam should be a maximum, in this parabola, when the aerial is at the focus: this is, however, completely contrary to any idea of an optical focus or of the width of beam depending on the aperture.

It must be conceded that, as shown by Fig. 13.8, the parabola produces a pattern which is slightly more desirable for practical use than the pattern for the Vee, but it does not follow that this is due necessarily to parabolic shape: it may be that a small increase in the width of the flat sheets would have brought the two patterns into very

close agreement, though it has to be granted that the main beam was indistinguishable from the ideal.

So far we have been comparing the patterns corresponding to similar distances between the aerial and the vertex or the apex and the discussion has shown that this is not a proper basis of comparison at stations of maximum forward field. But if, for the moment, we regard

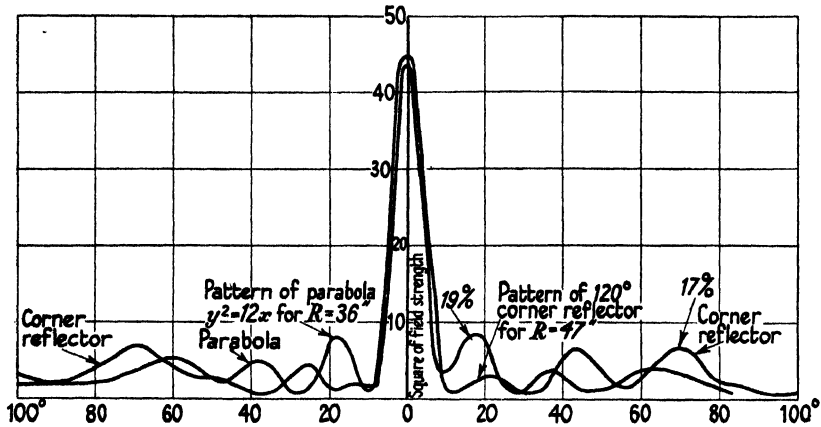


FIG. 13.10. Diffraction patterns for parabolic cylinder and for  $120^\circ$  corner reflector.

a parabola as akin to a Vee whose apex has been amputated, then it follows that the  $n$ th station for maximum forward field of the parabola may well correspond to the  $(n+1)$ th or  $(n+2)$ th, etc., maximum station for the Vee. Hence it is surely more reasonable to seek to find a pattern, at a maximum station, for the Vee which coincides substantially with the pattern from that maximum station most nearly coinciding with the focus of the parabola. This has been done in Fig. 13.10 which shows, superposed, the focal pattern of the parabola (cylinder  $C$ ) and the observed pattern for the Vee at  $R = 47$  in. ( $R/\lambda = 2.35$ ). Now the two main beams are scarcely distinguishable and, from a practical point of view, there is not much to choose between the two sets of side lobes: hence it is submitted that a  $120^\circ$  Vee can produce the same main beam and substantially similar side lobes as the parabola with the aerial at the focus.

It is interesting to compare the positions of the maxima and minima of forward field which were observed for the Vee with those observed for the parabola (Fig. 13.1) when  $47-36 = 11$  in. has been added to their distance from the vertex. The comparison is shown in Table 13.7.

It may be seen that the last five stations are sensibly coincident; moreover, the grandest maximum for the Vee occurred when  $R = 47$  in.

and the grandest maximum for the parabola when  $d = 36$  in. Thus there is good reason for associating the maximum at 36 in. for the parabola with that at 47 in. for the Vee; and when this is done the two patterns are found to be sensibly identical. In fact the performance of the parabola can be predicted completely from the ideal performance of a  $120^\circ$  Vee.

TABLE 13.7

$R$ for Vee . . .	14 min.	19 max.	26	33 max.	40	47 min.	54	59 max.
$(R+11)$ for Parabola	..	28	30	36	41	47	54	60

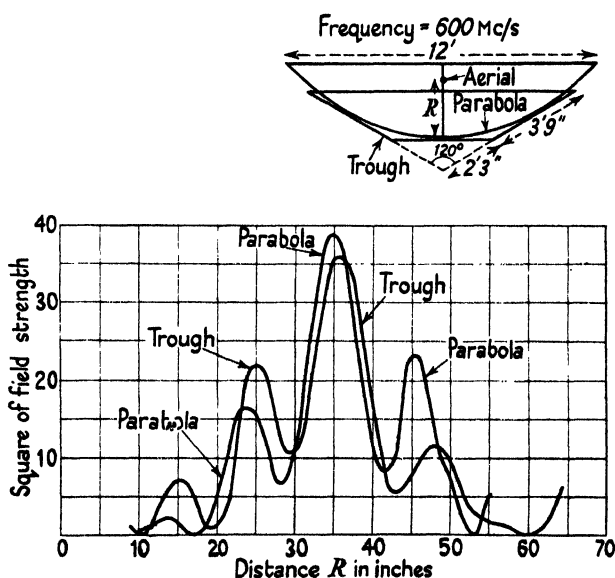


FIG. 13.11. Curves of forward field for a certain parabolic cylinder and for a certain  $120^\circ$  trough reflector.

Two gauze sheets of width 3.75 ft. were available: from these a trough was constructed with sloping sides inclined at  $120^\circ$  and with an aperture of 10.4 ft.: thus it was as though the first  $2\frac{1}{4}$  ft. of the slant side of the previous Vee had been removed and a flat sheet placed across the hole left by the amputation. The distance between the bottom of the trough and the apex of the complete Vee was thus equal to 13.5 in. The inset diagram in Fig. 13.11 compares the cross-section of the trough with the cross-section of the parabola (cylinder  $C$ ). Fig. 13.11 records the forward field test for the trough and also for the parabola, the abscissa being the distance between the aerial and the

floor of the trough or the vertex of the parabola. The two curves are strikingly similar and show that the two reflectors are substantially identical in respect of forward field.

Fig. 13.12 shows, superposed, the pattern for the trough when the aerial was distant 34.5 in. from its flat floor and the pattern for the parabola when the aerial was distant 39 in. from its vertex. It was

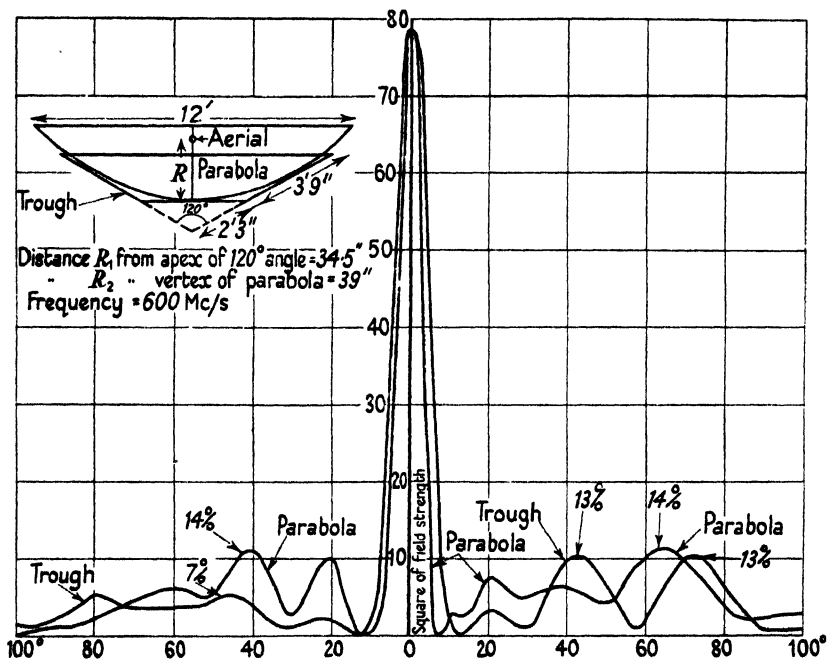


FIG. 13.12. Diffraction pattern for a certain parabolic cylinder and for a certain trough reflector.

found that the pattern from the parabola at  $d = 39$  in. was slightly better than that obtaining when  $d = 36$  in.; and hence that pattern was recorded in Fig. 13.12 so as to credit the parabola with its most favourable performance. The difference between the two patterns is not very significant, and it is clear that the trough and the parabola are almost equivalent. There is here no special virtue in the parabolic shape: in the main it is merely a device for reducing the depth of the Vee, for a given aperture, and is surely no more than a very complicated method of amputating the apex. In short, we find that the pattern is not very sensitive to the shape (opticians would call it the figure) of the reflector and that the analysis of the Vee can be used as a close guide to the performance of a reflector whose shape approximates only roughly to a Vee. One would suppose from this that the analysis ought

to be very tolerant of the exact shape of the boundary; whereas in fact the analysis seems to be very sensitive to the boundary in so much as the solution is multivalued unless  $\beta$  is precisely a proper fraction of  $\pi$ .

### 13.4. Use of parasitic aerial with reflector

When a single aerial is used to excite a parabolic reflector, then the practice is almost universal of placing an unfed half-wave aerial in front of that aerial which is being fed with current by a generator. It is commonly said that the parasite serves to reflect those rays, from the driven aerial, which would otherwise pass directly out of the aperture and turn them back into the parabolic mirror; so that they emerge again as a substantially parallel beam. The use of a parasite follows a long-established practice in optics in which a small reflector is placed in front of the source in order to intercept the rays of light which would otherwise emerge without reflection by the parabolic mirror.

The habit of using some form of reflector in front of the source was established in the early applications of aerials and parabolic reflectors. Thus it was used in the micro-ray link established in January 1934 between Lympne in England and St. Inglevert in France, on a wavelength of 17.4 cm. In that application the auxiliary reflector was a hemisphere and has been described by McPherson and Ullrich.† They appear to have been satisfied that their parabolic reflectors were behaving as they would do in optics and they describe the auxiliary reflector in terms of the Gouy effect. They also rely on an analysis due to R. Darbord‡ which seems to depend on ideas of reflection of rays from the parabolic surface and which leads to the conclusion that the aperture should be in the focal plane.

Having regard to the previous sections of this chapter we can hardly accept the notion that a parasitic aerial reflects back those rays which would emerge through the aperture without reflection by the parabola. We should naturally describe the effect of the parasite aerial on the pattern in terms of the superposition of the patterns due to the simultaneous action of two aerials at different distances from the apex of a Vee. Such an arrangement was discussed analytically in § 3.9, where it was shown that a second aerial can be used to modify the shape of the pattern and to control the side lobes. And it seems probable that this is a satisfactory and complete explanation of the benefits which are known to accrue from the use of a parasite aerial with a parabolic

† See *Journal I.E.E.* 78 (1936), 636.

‡ See *Le Journal de Physique*, 7 (1932), 105.



reflector. It may be that the familiar optical description may turn out to be only another way of saying the same thing, but if this be so, then the bridge between the two methods of description is not clear at present. The optical way seems to the writer to be little more than a rough qualitative guide, in contrast to our way which is systematic and quantitative.

The writer has made a few experiments on the use of a parasite aerial. But his interpretation of its action emphasizes the number of independent variables involved and this has an inhibiting effect on *ad hoc* experimentation. If our description is correct and complete, then it must be recognized that the component pattern due to the parasite aerial will depend on its distance from the vertex and it can well be at a station for which its forward field is very small. The resultant of the two component patterns will depend on both the phase and the magnitude of the current induced in the parasite. At a given station the said phase and magnitude will be sensitive to the length of the parasite. Again, the use of a parabola is justified only if the source is at its focus: if there are to be two aerials they cannot both be at the focus, and hence one at least of them cannot be using the parabola properly. To explore the effect of the parasite systematically, patterns should be observed for all distances between aerial and parasite, for all lengths of parasite, and for all stations of the aerial: a formidable task indeed. The writer's experience is restricted to a parasite distant  $\frac{1}{2}\lambda$  in front of the aerial, which was at the focus of parabola *C*. When the length of the parasite was  $0.6\lambda$  it was found that the side lobes were reduced to about one-third their amplitude (in power) without any measurable change in the bearings of their maxima or minima and without change of their inherent dissymmetries. When the length of the parasite was  $0.4\lambda$  the side lobes were increased in power, without change of bearing, and the values of the minima were increased relatively to the maxima. Reference to the lowest curve in Fig. 13.1 shows that an aerial  $\frac{1}{2}\lambda$  in front of the focus would be near a station of minimum forward field and hence its pattern would have side lobes which were relatively large. Thus it is in a position where it is competent to have a large effect on the lobes in the resultant pattern: the pattern due to the driven aerial alone appears in Fig. 13.10. If the two patterns are substantially in antiphase, then it may well be that the lobes would be reduced considerably by the parasite. If the two patterns are substantially in phase quadrature, then the result is likely to be an increase in the general level of side-lobe field. In changing the length of the parasite from  $0.6\lambda$  to  $0.4\lambda$  there

would be a considerable change in the phase of the current induced in it. The observed results seem to be roughly in accordance with what was to be expected.

### 13.5. Parabola excited by means of a wave guide

Much has been written in this book about the field of a current in a thin aerial, usually accompanied by a reflector, but not much has been said about the method of supplying the current to the said aerial. In principle this is obvious and is often, and commonly, done by dividing the aerial into two portions and attaching them to the conductors of a twin or a coaxial cable, which cable is supported in a line perpendicular to the aerial and passes out through a hole in the back of the reflector. So long as the diameter of the cable is small compared with  $\frac{1}{4}\lambda$ , then the currents induced in its metal sheath will be small and they will not affect the pattern appreciably. But if the wavelength is not more than 10 cm., the diameter of the cable cannot be much less than  $\frac{1}{4}\lambda$  and then its presence in the reflector will be important. In such circumstances it is common to give up the conventional form of cable and proceed in a different manner. We will approach the problem in a manner which may seem a little pedantic to those who are accustomed to use and construct wave guides in much the same spirit that they would use water pipes: but even if it is pedantic it is also instructive. We are used to the performance of an aerial which is near the apex of a Vee, and know that the pattern will always be a simple sinusoid so long as the width across the Vee at the aerial does not much exceed  $\frac{1}{2}\lambda$ . Accordingly currents induced in the sheath of a cable cannot disturb the pattern so long as the aerial itself is at a width not much greater than  $\frac{1}{2}\lambda$ . But in such circumstances the width of the central beam of the pattern depends only on the angles of the Vee. Hence the beam can be made narrow only by making  $\beta$  small and we know that this will involve immensely wide sheets. We may feel sure that the diffraction round the edge of the sheets will be inhibited by furnishing these edges with wing sheets: by appropriate choice of the size and Vee angle of these wing sheets we may well expect to obtain a pattern which is a close approximation to the ideal for the narrow Vee in which the aerial proper is located. It is then but an unimportant step to make the sides of the Vee parallel, and this is commonly called a wave guide.

But when the side sheets are parallel, i.e.  $\beta = 0$ , it is certain that wing sheets at their ends cannot reduce the width of the beam to zero. The aerial in the guide will induce currents in its parallel walls and the

distribution of this induced current is readily calculable when the parallel walls extend to infinity. In practice they cannot extend to infinity; in the apparatus we are picturing here they end in wing sheets forming a Vee. The current induced in the parallel walls will inevitably persist along the wing sheets and the radiated field must depend mainly on that current which does persist in the wing sheets. Inevitably the current in the wing sheets will have a distribution which is characterized by a phase which changes with an approximately constant wavelength, and thus it is surely very likely that the equatorial pattern will be very akin to that produced by a Vee excited by a single aerial not far from the apex. In other words, we shall expect a pattern which is substantially a sinusoid contained within the angle  $\beta'$ , where  $\beta'$  is the angle of the Vee formed by the wing plates.

The imaginary experimental apparatus we have just postulated is very akin to that used by Barrow and Lewis.<sup>†</sup> They worked at  $\lambda = 50$  cm. and used a wave guide 50 cm. wide and 15 cm. high and about 2.4 m. long. Its end was furnished with wing plates  $4\lambda$  wide and they were hinged so that they could be set to form a Vee of any angle between zero and  $90^\circ$ . The wing sheets were furnished with a top and bottom cover sheet of width 1.43 m. Apart from putting the aerial near the end of a wave guide, their experiments are very like those described in Chapter X. There the sheets forming the Vee were  $3.6\lambda$  wide by  $1.5\lambda$  high and without cover plates, whereas the sheets used by Barrow were  $4\lambda$  wide by  $0.3\lambda$  high and had cover plates. Fig. 4 of Barrow's paper shows the polar diagrams which were recorded (at a distance of  $60\lambda$ ) when  $\beta = 0^\circ, 10^\circ, 20^\circ, 30^\circ, \dots, 90^\circ$ . Provided  $\beta$  did not exceed  $60^\circ$  there were no side lobes and this accords with our expectation: but there was a very considerable field in the backward direction and this is in marked contrast to our experience with sheets which were  $1.5\lambda$  high. Barrow (*loc. cit.*, Fig. 5) gives a curve in which area of unit circle/area of pattern is plotted as a function of  $\beta$ : this ratio is what we have called the gain in § 3.7, where it was shown that its value is  $4\pi$  when the aerial is not far from the apex. Barrow found the gain had the value 5 when  $\beta = 0^\circ$  and when  $\beta = 90^\circ$  and that it passed through the blunt maximum, of value 16, near  $\beta = 55^\circ$ . Our ideal gain for  $\beta = 60^\circ$  is 12, whereas Barrow found the value 15: thus he also found that the observed pattern can be narrower than the ideal. When  $\beta = 30^\circ$  he found the gain was 11, whereas the ideal is 24: we should say that this showed that sheets of width  $4\lambda$  were insufficient

<sup>†</sup> See *Proc. I.R.E.* 27 (1939), 41.

to produce the ideal pattern when  $\beta = 30^\circ$ , and this accords with our experience.

Barrow's paper should be consulted, but it does not seem necessary to discuss it further here. It has been cited to uphold our prediction that if the aerial is situated in a wave guide, projecting backwards from the apex, then the pattern is likely to be akin to that appropriate to an aerial not far from the apex of the Vee. The long feeding cable for the aerial has been replaced by the wave guide and this often has practical advantages when the power is so great that the insulation of the cable is liable to be punctured by the high voltage. The main point of our argument is that the current induced in the walls of the guide will persist along the wing plates and the pattern could be calculated completely if this distribution were known. Experience with an aerial has shown us that the pattern is insensitive to the shape of the reflecting surface (be it Vee, trough, or parabola), and we should confidently expect to find the same result in an apparatus similar to that used by Barrow and Lewis.

However, a system conforming in general type to that used by Barrow is not one in common use when a wave guide is used to excite a reflector. Both according to our interpretation and to Barrow's result the pattern is not likely to differ very markedly from a sine curve included within the angle  $\beta$ . If a very narrow beam is required, while maintaining  $\beta$  at a value which is not very small, then something must be done to correspond to moving the aerial a long way from the apex of the Vee. In other words, the wave guide must be pushed through the apex of the Vee until it protrudes a distance corresponding to an aerial at  $2\pi R/\lambda \equiv k$ , where  $k > n$ . It will scarcely suffice to push the pipe through the apex because then the current inside the guide will not be situated favourably for inducing currents in the sides of the Vee. It will be necessary to fit small wing plates to the guide so that they can carry the current which will induce currents in the Vee: the wing plates must be short if the pattern is not to conform mainly to the subsidiary Vee formed by them. The writer has little doubt that the system just described would work, but he has not tried it. The common device is to place a flat plate across the mouth of the guide and at a distance of the order of  $\lambda$  from its end. It is commonly said that the purpose of this plate is to reflect the direct radiation from the mouth of the guide back on to the mirror. However, we should say that the plate is placed in front of the guide in order to have currents induced in it, thereby forming a current sheet whose width is of the order of  $\lambda$ . The

said current sheet then takes the place of the single aerial fed by a cable: the guide is used as a device to produce current in a comparatively narrow sheet, but nevertheless one whose width suffices to help appreciably the formation of a narrow beam from the reflector. The clearance between the end of the guide and the flat sheet requires nice adjustment, by experiment, because the distance has to be such as to favour a large current being induced in it and to suit the transmission of power through the guide, and to be such that the guide does not unduly screen, from the reflector, the current induced in the sheet, etc. The adjustment of distance corresponds roughly with the adjustments which would have to be made to several cables feeding a narrow curtain array which was placed in a Vee.

In the writer's opinion this description is applicable to a parabola in which the guide protrudes through the vertex and has a metal plate across its orifice. If the paraboloid is about 2 m. in diameter and its focus is in the plane of the aperture, then the plate across the orifice of the guide will be about  $5\lambda$  distant from the vertex if  $\lambda = 10$  cm. This would correspond to  $R \doteq 10\lambda$  for a Vee, and that is  $k = 60$ . Inevitably the main beam will then be extremely narrow, and in general it would be expected to be accompanied by a family of large and narrow side lobes. Whether parabolic shape has peculiar properties in diminishing side lobes for very large values of  $k$  we are unable to say from direct and first-hand experiment.

The most common method of using a guide to excite a reflector is to place the axis of the guide parallel to the plane of the aperture and to bend the end of the guide through a right angle so that its open orifice faces the vertex of the parabola. We should say that the currents near the edge of the orifice induce currents in the reflector; that these induce currents in the outside wall of that part of the guide which is in front of the aperture; that these, in turn, are still more active in inducing currents in the reflector. We suspect that it is the currents induced on the outside of the walls of the guide which play the role of the aerial exciting the parabola. This is not the commonly accepted description; it may not be correct and it may not be the whole story.

The writer regards the parabolic reflector as a very complicated problem which is only partly solved. Parabolic reflectors were used very extensively in the period between 1942 and 1945, mostly at  $\lambda = 10$  cm. Optical methods were used as the basis of interpreting their observed behaviour: such methods turn on the distribution of electric field across the aperture and not on the currents induced in the metal

of the reflector and the wave guide. Thus they are only partly included in Maxwell's electromagnetic theory and hence do not fall properly within the ambit of this book. It is possible to find the distribution, in magnitude and phase, of the current in a flat sheet which is needed to produce a polar diagram of any desired shape. But the writer is not satisfied that the polar diagram can be predicted from measurement of the magnitude and phase distribution of electric field across the aperture of a parabolic mirror. The validity of the process turns on Kirchhoff's theorem, the correct and rigid use of which is not always easy. The writer will not feel the problem has been solved completely until the polar diagram is related to electric currents in the reflector or in the metal of the wave guide: and until it is known how to modify the exciting currents so as to produce any desired changes in the polar diagram. He does not feel it is necessary or desirable to recount here recognized techniques for analysis in terms of the distribution of electric field across the aperture: he has not sufficient first-hand experience of the agreement between 'practice and theory' to justify him in making a critical and systematic survey of their success or inherent validity. Until a purely electrical treatment has been evolved he feels it better to leave the problem *sub judice*.

### 13.6. Difficulties in understanding the optical behaviour of a parabola

In the beginning portions of this chapter it has been shown that the focus of a parabolic mirror, having an aperture of the order of  $10\lambda$ , is not a peculiarly favoured station for excitation by a single aerial. In the light of the earlier chapters of this book it would have been very surprising if the focus had possessed any peculiar properties. We have surely established that undue confidence has been placed in parabolic mirrors for radio use and that perhaps it shows some lack of understanding to set great store by this shape: so far all was in accordance with the knowledge and experience of an electrician. But now the converse problem obtrudes itself: why is the focus of a parabola peculiarly important in optical work? It will not do to dismiss the inquiry just because there is a change of scale of thousands to one: this vast change of scale does not in itself provide any obvious explanation. In optics the focus is a vast number of wavelengths from the vertex, and this is just the condition which we should expect to associate with a polar diagram having tens of thousands of very sharp beams, of the kind which have been likened previously to a porcupine's

spines. Indeed, if we could excite a parabola with a single source, whose volume was very much less than  $\lambda^3$ , then surely it is almost certain that the 'porcupine' diagram would exist, if means could be found for resolving one spine from its neighbours. If the focus still operated for a single oscillator then, presumably, at best we could expect to find the porcupine spines were grouped under an envelope which represents the

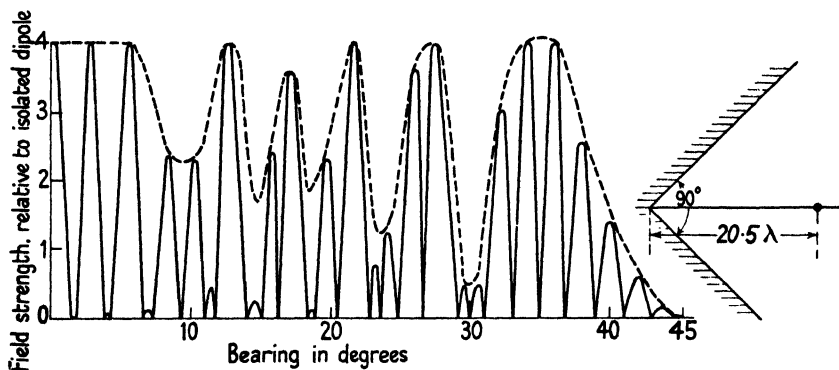


FIG. 13.13. Diffraction pattern for a  $90^\circ$  reflector when the aerial is distant  $20.5\lambda$  from its apex.

ghost of the very narrow beam which is experienced when a parabola is illuminated by a very small optical source. If we are correct in this surmise, then the virtue of parabolic shape must be that it has the property of grouping the 'spine lobes' under a central envelope, with very small envelopes representing side lobes. This idea at once raises the question as to whether the pattern for a Vee reflector tends to gather under an envelope which is itself reminiscent of a diffraction pattern, when the aerial is very far from the apex. We can scarcely hope to explore this possibility by direct appeal to the general Fourier expansion of the pattern, and the approach must be made from direct evaluation in particular cases. Thus Fig. 13.13 shows the equatorial pattern for a single aerial which is distant  $20.5\lambda$  from the apex of a  $90^\circ$  Vee; it is obvious that the maxima are tending to group themselves under an envelope curve which itself has the general character of a diffraction pattern. A very close examination of the pattern shows there are 29 maxima and 29 zeros in the range of  $\theta$  between  $0$  and  $45^\circ$ . A less close examination would show 6 maxima and 6 minima in this range. A very cursory examination would suggest a substantially constant illumination in the range between  $0$  and, say,  $40^\circ$ . Fig. 13.14 shows the equatorial pattern, between  $25^\circ$  and  $30^\circ$  for an aerial distant  $50\lambda$  from the apex of a right-angled Vee: here the envelope effect is

much more pronounced. There are 18 true maxima and 19 zeros in this range of  $13^\circ$ , but there are 4 pronounced maxima of the envelope curve. If this pattern were being explored experimentally, using a turn-table of ordinary construction, it is highly probable the true maxima and zeros would be missed and that the observer would record only the envelope curve and present it as the true diffraction pattern

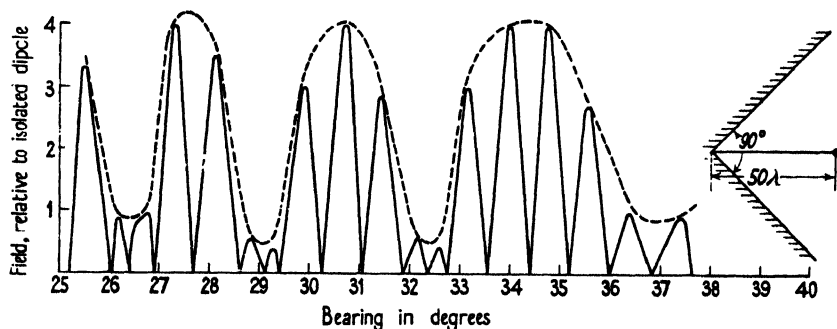


FIG. 13.14. Portion of diffraction pattern of a  $90^\circ$  reflector when the aerial is distant  $50\lambda$  from its apex.

for the Vee. We predict that if observations were made of the pattern resulting from a really large parabolic mirror, excited by a single aerial, then the recorded result would in fact be an envelope curve and that this envelope would be disclosed by making observations at intervals sufficiently close to reveal the 'spines of the porcupine'. Figs. 13.13 and 13.14 are reminiscent of a heterodyne effect of two sine curves of nearly equal period beating with one another. And indeed this is the true description of the pattern, as will be realized on reference to § 12.5, where it is shown that the pattern for a  $90^\circ$  Vee is the addition of the first  $45^\circ$  of the pattern for a like pair of filaments with the last  $45^\circ$  of that pattern; for example see Figs. 12.18 and 12.19.

Fig. 13.14 does not suggest that the maxima of the 'side lobe envelopes' would tend to decrease when  $k$  became very large indeed. We can predict the envelope or 'beating effect', and the unlikelihood that the envelope maxima tend to decrease as  $\theta$  increases, by looking at the problem from energy considerations. Thus, when  $k$  becomes very large the radiation resistance of the aerial must tend to the 'isolated value' because then the inphase component at it due to the three images will be negligible; then the output of work will be the same as if the aerial were in free space. But the forward field will be four times that of an isolated aerial when its distance from the apex is  $\frac{1}{2}\lambda$ ,  $\frac{3}{2}\lambda$ , etc. This would lead us to expect sixteen times the isolated output, but this



figure is reduced to four because field exists only in one quadrant of space. Each porcupine spine of the pattern is sensibly a sine curve and thus its mean square value is  $\frac{1}{2}$  and therefore the expected output would thereby be reduced to twice the isolated output. But the output is equal to the isolated output and so there must be some other feature in the pattern to account for a further halving of the output: doubtless that feature is the formation of the envelope curve, each of whose petals is sensibly a sine curve. When the angle between the sheets is  $60^\circ$  the field can be 5.2 times the isolated value: since the field occurs only in one-sixth of space and the mean square field of a porcupine spine is  $\frac{1}{2}$ , we might expect the output would be  $5.2^2/12 = 2.25$  times the isolated value, whereas it is equal to the isolated value. Hence now there must be a tendency for the 'side lobe envelopes' to decrease slightly. When  $\beta = 45^\circ$  the forward field attains 8 times the isolated value and then we can readily account for an output of  $64/(8 \times 2) = 4$  times the isolated output. Here it would seem the side-lobe envelopes must themselves tend to lie under an envelope which is substantially a sine curve.

Therefore may it not be that the peculiar virtue of parabolic shape is that the envelope curves group themselves under an envelope which is itself a sharp beam whose width is controlled dominantly by the aperture of the optical mirror? This is only a suggestion, but it does offer a possible way of reconciling the purely electrical approach with optical experience. According to this description the parabola would not exhibit its focal properties until there are enough zeros in the complete diffraction pattern to make the form of the envelope clearly apparent. The number of zeros depends on the distance of the aerial from the vertex. If about 100 zeros are required to allow the envelope to approach its limiting form, then the focal distance would need to be at least  $50\lambda$ , corresponding to aperture of at least  $200\lambda$ . If this rough guess is of the right order, then at  $\lambda = 10$  cm. the diameter of the mirror would need to be about 20 m. before it exhibited a behaviour which was becoming comparable with optical experience. And a sufficiently close examination would show the beam was an envelope covering a set of porcupine spines: an experience not realizable in optics, where the dimensions of the source are necessarily very large compared with  $\lambda$  and thereby the spines would be blurred out of existence by summation of the spines arising from different portions of the large source.

We suspect the parabola is a device for producing a narrow envelope

in circumstances when it is physically impossible to place the source within a few wavelengths of the reflecting surface. When this can be done a single beam (not envelope) two or three degrees wide can be produced by plane mirrors or by almost any concave shape. Parabolic shape is known to be reasonably effective, but it seems probable that its effectiveness is not *sui generis*. Possibly parabolic mirrors are an essential expedient when, as with light, we cannot construct focal distances which are not incomparably greater than  $\lambda$ .

It is proposed to leave the problem at this stage: it is left unsolved, but at any rate it has been pointed out that there appears to be a major problem awaiting solution, even though comparatively small parabolic mirrors are well established as a practical device. We close this chapter with some analyses which may possibly be helpful some day in attempting a quantitative solution.

### 13.7. The field of a semicircular cylinder

#### (a) Current density uniform

Let  $BAC$ , in Fig. 13.15, represent the cross-section of the semicircular cylinder, having centre at  $O$ . The current flow is perpendicular

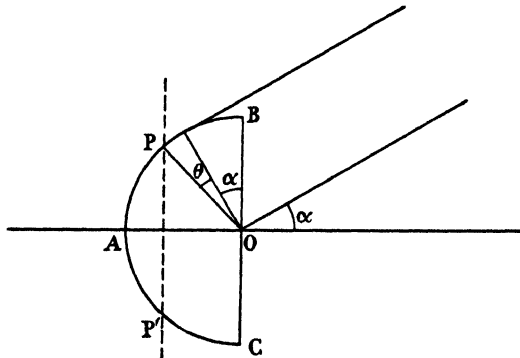


FIG. 13.15.

to the plane of the paper; the density is everywhere cophased and has the value  $I_0$ . Consider the field at a very distant point, on bearing  $\alpha$ , due to a current filament at  $P$ . The path difference, with respect to  $O$ , is  $R \sin \theta$ , and hence the phase angle is

$$\phi = \frac{2\pi R}{\lambda} \sin \theta \equiv k \sin \theta.$$

To obtain the field due to all filaments, typified by the one at  $P$ , we have to find the resultant of a series of equal vectors inclined to the

zero line at an angle  $\phi$  as defined above. Each vector will have a component  $\cos \phi$  in phase with the zero line and a component  $\sin \phi$  in quadrature thereto. We shall now calculate the field, on bearing  $\alpha$ , in terms of a component  $E_Q$  in phase with the field of a hypothetical element situated at  $O$  and a component  $E_P$  in quadrature thereto: in this  $E$  stands for the field, at the given distance, due to a filament of unit strength. Then

$$\frac{E_P}{I_0 R} = \int_{-\alpha}^{\pi-\alpha} \cos(k \sin \theta) d\theta, \quad \text{and} \quad \frac{E_Q}{I_0 R} = \int_{-\alpha}^{\pi-\alpha} \sin(k \sin \theta) d\theta.$$

We now use the Fourier expansion of  $\cos(k \cos \theta)$  and  $\sin(k \sin \theta)$  in terms of Bessel functions  $J_0, J_1$ , etc., and so obtain

$$\frac{E_P}{I_0 R} = \int_{-\alpha}^{\pi-\alpha} \{J_0(k) + 2J_2(k)\cos 2\theta + 2J_4(k)\cos 4\theta + \dots\} d\theta = \pi J_0(k),$$

and thus obtain the rather surprising result that  $E_P$  is independent of  $\alpha$ . Similarly,

$$\begin{aligned} \frac{E_Q}{I_0 R} &= 2 \int_{-\alpha}^{\pi-\alpha} \{J_1(k)\sin \theta + J_3(k)\sin 3\theta + \dots\} d\theta \\ &= 4 \left\{ J_1(k)\cos \alpha + \frac{J_3(k)}{3} \cos 3\alpha + \frac{J_5(k)}{5} \cos 5\alpha + \dots \right\}. \end{aligned}$$

For every filament such as  $P$  in Fig. 13.15 there is a similarly situated filament at  $P'$  and accordingly  $E_Q$  must be zero when  $\alpha = \frac{1}{2}\pi$ , and the general expression confirms it is then zero. The field at distance  $r$  from a filament of unit strength is given by

$$\frac{cE}{a\pi} = -J_0(ar) + jY_0(ar)$$

and hence

$$\begin{aligned} \frac{cE}{a\pi^2 I_0 R} &= \left[ J_0(k) - \frac{4}{\pi} j \left\{ J_1(k)\cos \alpha + \frac{J_3(k)}{3} \cos 3\alpha + \dots \right\} \right] \times \\ &\quad \times \{-J_0(ar) + jY_0(ar)\}. \end{aligned} \quad (13.1)$$

When  $ar \rightarrow \infty$  we may write  $Y_0 = J_1 = -J_3$ , etc., and  $J_0 = -Y_1 = Y_3$ , etc., and hence

$$\begin{aligned} \frac{cE}{a\pi^2 I_0 R} &= J_0(k) \{-J_0(ar) + jY_0(ar)\} - \frac{4}{\pi} \left[ \{-J_1(ar) + jY_1(ar)\} J_1(k) \cos \alpha - \right. \\ &\quad \left. - \{-J_3(ar) + jY_3(ar)\} \frac{J_3(k)}{3} \cos 3\alpha + \dots \right]. \end{aligned} \quad (13.2)$$

Since this is a solution of Maxwell's equation it must be valid for all values of  $r$  at which it is convergent. At  $r = 0$  it is obvious from Fig. 13.15 that

$$\frac{cE}{a\pi^2 I_0 R} = -J_0(k) + jY_0(k),$$

and this shows that when  $r < R$  it is necessary to interchange  $ar$  and  $k$ . At the surface of the cylinder  $r = R$ , and then

$$\frac{cE}{a\pi^2 I_0 R} = \{-J_0(k) + jY_0(k)\}J_0(k) - \frac{4}{\pi} \{[-J_1(k) + jY_1(k)]J_1(k)\cos\alpha - \dots\}. \quad (13.3)$$

There is no value of  $k$  for which this expression can be independent of  $\alpha$  and therefore it follows that a filament at the centre of a semicircular

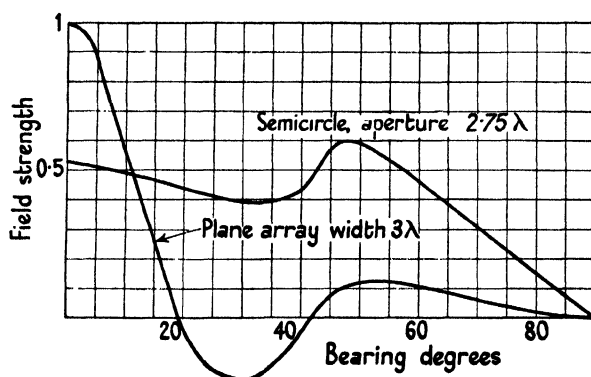


FIG. 13.16. Diffraction pattern for a certain semicircular array, with uniform current loading.

metal cylinder cannot induce a uniform and cophased current density in the reflector.

Equation (13.1) gives the diffraction pattern for a uniformly loaded semicircle. It will be noticed that there are necessarily two quadrature components of field and hence there cannot be any bearings on which the field is zero except possibly in the special cases where the radius is such as to make  $J_0(k) = 0$ . For example, Fig. 13.16 shows the pattern for a half-cylinder whose diameter is  $2.75\lambda$  (i.e.  $J_0(k) = 0$  for the third time) and compares it with the pattern for a uniformly loaded flat sheet of width  $3\lambda$  and which is carrying the same total current as the half-cylinder.

(b) *Sinusoidal distribution of current density*

Let the current density round the semicircle be  $i = I_1 \sin(\alpha + \theta)$ , see Fig. 13.15: then

$$\begin{aligned}
 \frac{E_P}{I_1 R} &= \int_{-\alpha}^{\pi-\alpha} \cos(k \sin \theta) \sin(\alpha + \theta) d\theta \\
 &= \int_{-\alpha}^{\pi-\alpha} \left\{ J_0(k) \sin(\alpha + \theta) + 2 \sum_1^{\infty} J_{2n}(k) \cos 2n\theta \sin(\alpha + \theta) \right\} d\theta \\
 &= 2J_0(k) - 4 \sum_1^{\infty} \frac{J_{2n}(k) \cos 2n\alpha}{(2n+1)(2n-1)}, \quad (13.4)
 \end{aligned}$$

$$\begin{aligned}
 \frac{E_Q}{I_1 R} &= \int_{-\alpha}^{\pi-\alpha} \sin(k \sin \theta) \sin(\alpha + \theta) d\theta \\
 &= 2 \int_{-\alpha}^{\pi-\alpha} \{ J_1(k) \sin \theta + J_3(k) \sin 3\theta + \dots \} \sin(\alpha + \theta) d\theta \\
 &= \sin \alpha \int_{-\alpha}^{\pi-\alpha} [J_1(k) \sin 2\theta + J_3(k) (\sin 4\theta + \sin 2\theta) + \dots] d\theta + \\
 &\quad + \cos \alpha \int_{-\alpha}^{\pi-\alpha} [J_1(k) (1 - \cos 2\theta) + J_3(k) (\cos 2\theta - \cos 4\theta) + \dots] d\theta \\
 &= \pi J_1(k) \cos \alpha. \\
 \therefore \frac{cE}{a\pi I_1 R} &= \left[ 2J_0(k) - 4 \left\{ \frac{J_2(k)}{1.3} \cos 2\alpha + \frac{J_4(k)}{3.5} \cos 4\alpha + \dots \right\} - j\pi J_1(k) \cos \alpha \right] \times \\
 &\quad \times \{ -J_0(ar) + jY_0(ar) \}.
 \end{aligned}$$

Proceeding as before we obtain

$$\begin{aligned}
 \frac{cE}{a\pi^2 I_1 R} &= \frac{2}{\pi} J_0(k) \{ -J_0(ar) + jY_0(ar) \} - J_1(k) \{ -J_1(ar) + jY_1(ar) \} \cos \alpha + \\
 &\quad + \frac{4}{\pi} \left[ \frac{J_2(k)}{1.3} \{ -J_2(ar) + jY_2(ar) \} \cos 2\alpha \dots \right]. \quad (13.5)
 \end{aligned}$$

To obtain the electric field at the surface of the half-cylinder put  $ar = k$  in (13.5).

(c) *Current density  $I_n \sin n(\alpha + \theta)$ , with  $n$  odd*

On using the previous methods it follows readily that

$$\frac{E_P}{I_n R} = \frac{2J_0(k)}{n} + 4n \left[ \frac{J_2(k) \cos 2\alpha}{(n+2)(n-2)} + \frac{J_4(k) \cos 4\alpha}{(n+4)(n-4)} + \dots \right] \quad (13.6)$$

and 
$$\frac{E_Q}{I_n R} = \pi J_n(k) \cos n\alpha. \quad (13.6a)$$

(d) *Current density  $I_n \cos n(\alpha + \theta)$ , with  $n$  even*

Now we obtain

$$\frac{E_P}{I_n R} = \pi J_n(k) \cos n\alpha$$

and 
$$\frac{E_Q}{I_n R} = -4 \left[ \frac{J_1(k) \cos \alpha}{(n+1)(n-1)} + \frac{3J_3(k) \cos 3\alpha}{(n+3)(n-3)} + \frac{5J_5(k) \cos 5\alpha}{(n+5)(n-5)} \dots \right]. \quad (13.7)$$

(e) *General expression for the electric force at the cylinder*

By means of (13.3)–(13.7) we now have an expression for the field at any point of a semicircle which carries any distribution of current, the said distribution having been expressed as a Fourier series. If the reflector is excited by a single filament, parallel to its axis, then the field of the said filament is known, in terms of a Fourier series, at all points of the reflector. By stating the condition that the net field at the surface is zero we can obtain a set of equations relating the amplitudes of the Fourier components of the induced current. By this means it ought to be possible to determine approximately the coefficients in the series representing the induced current. The labour of computation would be very severe and would be tolerable only for values of  $k$  which are not large. This is not a case of much practical interest, but some numerical solutions for small values of  $k$  might form a guide to the more general behaviour. The metal reflector must have finite thickness and there will be some current on the back of it: it would be necessary to make allowance for such currents in making an approximate numerical solution. The analysis is included here to assist anyone who cares to make the attempt.

(f) *The field of a circular arc with uniform density*

The equation of a circle referred to a point at the end of a diameter is  $y^2 = 2Rx\{(1-x)/2R\}$ , while that of a parabola is  $y^2 = 4ax$ , hence if  $x/2R$  is small, the circular arc does not differ much from a parabola whose focal length is  $\frac{1}{2}R$ . We shall take advantage of this approximation

to obtain the equation for the diffraction pattern of a parabolic array. If the chord of the arc subtends  $90^\circ$  at the centre, then the aperture of the arc is 0.854 of the aperture of the parabola and the sagitta of the bow is 0.586 of the focal length. If the arc subtends an angle  $2\phi$  at the centre of the circle, then we shall have for a uniformly loaded arc

$$\begin{aligned}\frac{\dot{E}_P}{I_0 R} &= 2 \left[ J_0(k)\phi - J_2(k)\sin 2\phi \cos 2\alpha + \frac{J_4(k)}{2} \sin 4\phi \cos 4\alpha \dots \right] \\ &= 2 \left[ J_0(k)\frac{1}{4}\pi - J_2(k)\cos 2\alpha + \frac{J_0(k)}{3} \cos 6\alpha - \frac{J_{10}(k)}{5} \cos 10\alpha \dots \right]\end{aligned}$$

if  $\phi = \frac{1}{4}\pi$ , and

$$\begin{aligned}-\frac{E_Q}{I_0 R} &= 2 \left[ J_1(k)\sin \phi \cos \alpha - \frac{J_3(k)}{3} \sin 3\phi \cos 3\alpha - \frac{J_5(k)}{5} \sin 5\phi \cos 5\alpha \dots \right] \\ &= \sqrt{2} \left[ J_1(k)\cos \alpha - \frac{J_3(k)}{3} \cos 3\alpha - \frac{J_5(k)}{5} \cos 5\alpha + \dots \right],\end{aligned}$$

if  $\phi = \frac{1}{4}\pi$ .

These two equations give the pattern for a uniformly loaded array whose contour is sensibly a parabola with the focus well in front of the aperture. The expression can readily be extended to include sinusoidal loading.

## XIV

### IN-LINE AND CURTAIN ARRAYS, YAGI AERIALS

#### 14.1. The performance of separately fed arrays

IN writing about the observed performance of separately fed arrays we must first discuss what features we are to look for in the experimental results. Provided the array is in the presence of a flat and perfectly conducting earth and has no reflector, the problem of predicting the pattern is completely soluble and the solution does not contain any idealizations. When flat sheets are used in combination with a single aerial we can predict the pattern only by means of the idealized pattern that would result if the sheets were infinite in extent: then the main purpose of experiment is to assess the degree of approximation to the ideal and to relate it to the size of the sheets. But when each member of an isolated array is fed with an assigned current the resulting pattern is known precisely, if the ground is flat: if the observed pattern does not agree with the calculated pattern, then the magnitude and phase of the currents in the members is not what it was intended to be. A discrepancy merely means a maladjustment somewhere and its appropriate correction is only indirectly a problem germane to aerials. If  $\lambda$  is greater than, say, 10 m., the current in each member can be measured by a conventional ammeter, but such a measurement will not disclose the phase: if  $\lambda$  is less than about 2 m. the current in each member cannot be measured directly. Due attention must be given to the layout of the feeding cables and to the design of the junction boxes so as to promote the desired distribution of current. These things having been done, the observed polar diagram must be regarded mainly as a means of checking that the current is in fact distributed among the members in the intended manner. Accordingly our task now is to learn to work back from the polar diagram to the current distribution, so that we shall know which cables need to be adjusted in order to bring the polar diagram into agreement with the one intended.

It is very difficult to devise a direct means of testing whether the feeding cables have the correct adjustment, even at wavelengths such that currents and impedances can be measured with tolerable accuracy. This is because the impedance of each member of an array depends upon all the other members and it does not suffice to adjust the cables so that they would feed similar currents into similar loads which had



no mutual interaction: uniform and cophased feeding will not result when all the cables have precisely similar adjustments. It would seem that the ultimate testing and adjustment ought to be made by exploring the electric field produced by the whole array: whether the exploration ought to be made near to the array or far away from it is a matter for further discussion.

With sufficient perseverance in adjustment of the cables the ideal pattern can be reproduced perfectly: the practical issue is to decide when the adjustment is good enough for the intended use of the array. If the array is to provide service to a fixed station, at, say,  $\lambda = 20$  m., then it is important to find out whether the main beam is centred on the correct bearing and has substantially its correct width; the exact size and bearings of the side lobes will not be very important provided they are not obviously very incorrect.† If the array is for Radar use, then it is usually very important to make the side lobes as small as possible and the main interest of the test will centre round these lobes. Thus it happens that a pattern (or degree of adjustment, call it which you will) which might well pass muster perfectly for fixed-station working could not be tolerated for Radar use. It is for Radar use that the pattern must agree very closely with the ideal and the difficulties of obtaining the agreement are very great because the wavelength will not be more than about 1 m.

We will now quote from an experiment which was designed to test how nearly the observed and the ideal pattern agreed, when the only preliminary adjustment had been to cut the feeding cables to equal length: the operating wavelength was 50 cm. Four well-made and apparently precisely similar dipoles, each 23 cm. long, were mounted on a wooden lath and arranged so that they could form either a four-element in-line array or a curtain array. The wooden lath was mounted horizontally on a wooden turn-table which stood in a large flat field; the receiver was about  $200\lambda$  distant from the array. The four concentric feeding-cables had been tested electrically and their lengths had been adjusted until all had the same electrical length: they were brought to a well-made junction box which had been constructed in a way which appeared to give every chance for equal division of current between the four outgoing branches. The centre distance between the dipoles was

† For observed patterns for arrays working at  $\lambda = 30$  m. see, for example, Figs. 17 and 20 of the paper 'Beam arrays and transmission losses' by Dr. T. Walmsley, *Journal I.E.E.* 69 (1931), 299: it will be noted in this Fig. 17 that the field strength does not fall to zero at  $\pm 18^\circ$  but only to a minimum. This shows the adjustment was imperfect, but it is an imperfection of no practical consequence in the use of that array.

$0.53\lambda$ . If the four currents are equal and cophased, then the field will be zero on bearing  $\theta$  when  $\sin \theta = \lambda/Ng$ ,  $2\lambda/Ng$ , etc.: here  $N = 4$  and  $g/\lambda = 0.53$ . Accordingly evaluation shows that the field should be zero when  $\theta = 28.1^\circ$  and  $70^\circ$ . Fig. 14.1 shows the observed pattern, and

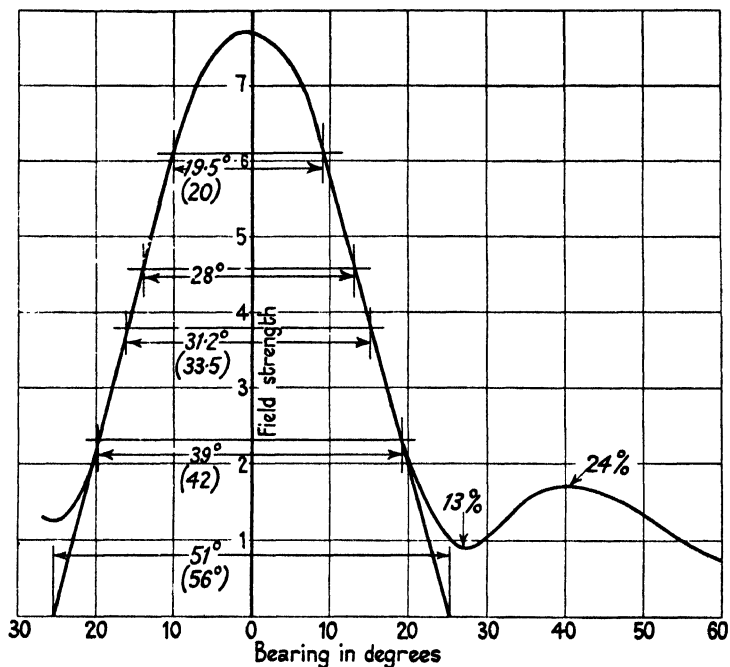


FIG. 14.1. Diffraction pattern of a certain 4-element in-line array,  $\lambda = 50$  cm.

it will be seen that the field does not fall to zero but falls to a minimum near  $\theta = 28^\circ$ . The straight sides of the main beam cut the bearing axis at  $\pm 25.5^\circ$ : the observed width at various heights is marked on the graph; the figures in brackets show the widths which the ideal beam should have: in every case the observed beam is narrower than the ideal. We will now attempt to deduce from the pattern the distribution of current which obtained in this array of four members. We shall presume the distribution is symmetrical about the mid-point of the array. The pattern is the sum of the patterns due to the inside pair  $A, A'$  and the outside pair  $B, B'$ . These are typified by the sketches in Fig. 14.2 (b) and (c) respectively. At some bearing  $OD$  the amplitude  $DE$  will equal the antiphase amplitude  $DF'$ ; hence at this bearing the field will be zero if all the currents are cophased.

The distance  $g$  between the members is likely to be about  $\frac{1}{2}\lambda$ : if  $d > \frac{1}{2}\lambda$ , there is some bearing  $\theta$  for which the path difference between  $A$  and  $A'$  is  $\frac{1}{2}\lambda$ , and on this same bearing the path difference between  $B$  and  $B'$  will be  $\frac{3}{2}\lambda$ . Hence, on this bearing the field must be zero no matter what the magnitude and phase of the currents in  $B$  and  $B'$  relative to the currents in  $A$  and  $A'$ . On bearing  $OK$  in Fig. 14.2 (c) the outside pair contribute nothing to the field, which is then due to the inside pair only; hence the observed field on this bearing is a measure of the current in the inside pair. In our example  $g/\lambda = 0.53$ , so

$$OD = \arcsin \lambda/6g = 18.3^\circ:$$

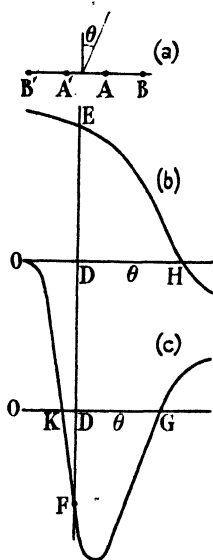
on this bearing the path difference for the inside pair is  $\frac{1}{2}\lambda$  and accordingly the field due to them is then  $2 \cos 30^\circ$  times the field due to one current alone. Hence if all four currents were equal and cophased, the fractional field on this bearing should be  $\frac{1}{2} \cos 30^\circ = 0.433$ ; but if the currents are equal and not truly cophased this ratio will be larger than 0.433. In Fig. 14.1 this ratio is  $\frac{26}{76} = 0.34$ ,

and thus it follows that the outside currents were larger than the inside currents. If the four currents are not cophased we can regard the

FIG. 14.2. Two component patterns for a 4-element array.

array as the superposition of two separate arrays; one 4-member array in which the currents are cophased but not necessarily equal and a pair of equal quadrature currents in the two outside members. Now let Figs. 14.2 (b) and (c) relate to cophased currents. Then we have seen already that the bearing for zero field would (with  $g/\lambda = 0.53$ ) be  $28^\circ$  if all currents were equal. If the current in the outside pair is greater than in the inside pair, then the vertical scale of the (c) figure will be increased relative to the (b) figure and it follows that the point  $D$  must be closer to  $K$  in order that  $DF$  shall equal  $DE$ . Since  $KF$  is nearly straight, it follows that if the outside currents are twice the inside currents  $DF$  will equal  $DE$  when  $KD$  is half the value it has for equal currents: and in this example this difference is  $(28^\circ - 18.3^\circ) = 9.7^\circ$ . Hence for currents in the ratio 2 to 1 the angle  $DK$  will be  $4.85^\circ$  and then the bearing for zero field will be

$$18.3^\circ + 4.85^\circ = 23.15^\circ.$$



Similarly for currents in the ratio 4 to 1 it would be

$$18.3^\circ + 2.42^\circ = 20.72^\circ.$$

We can approximate to the bearing for zero field of the cophased components of current by prolonging the straight sides of the main beam until they cut the bearing axis: this occurs at  $25.5^\circ$  in Fig. 14.1. Thus in our example  $DF = 25.5^\circ - 18.3^\circ = 7.2^\circ$ , and accordingly the ratio of the cophase components of currents is  $\frac{9.7}{7.2} = 1.35$ . If the quadrature component were zero the fractional field at  $\theta = 18.3^\circ$  would be  $\frac{1}{2.35} \cos 30^\circ = 0.37$ , and if there is a quadrature component this ratio will be smaller than 0.37. In Fig. 14.1 the ratio is 0.34 and thus accords with our prediction. If the contribution of the quadrature current to the R.M.S. field at  $\theta = 0$  be ignored, then we can find the relative value of the quadrature current from the relative field at the bearing at which the field is a minimum and this is about  $26^\circ$  in Fig. 14.1. At this bearing the path difference for the outside pair is  $3g \sin 26^\circ = 0.7\lambda$ . Hence, then, the field is proportional to  $2I_Q \cos 55 = 1.14I_Q$ ; at  $\theta = 0$  the field is proportional to  $4.6I_P$ , if the field due to  $I_Q$  is then ignored. At  $\theta = 26^\circ$  the fractional field in Fig. 14.1 is  $\frac{9}{78}$  and hence we deduce that  $I_Q/I_P = 0.47$ . Accordingly  $|I_B|/|I_A| = (1.35^2 + 0.47^2)^{\frac{1}{2}} = 1.43$  and the phase angle is about  $20^\circ$ . Although the observed pattern is in fairly good accordance with the ideal (for equal and cophased currents) it is clear that the currents are by no means equal and cophased. The precautions to make the feeding cables similar have not sufficed to make the currents equal: moreover, the currents would not have been equal even if the cables were similar, because the mutual impedances of the aerials are not equal in a 4-member in-line array. Thus, reference to § 2.19 will show that the middle member of a 3-element in-line array has a resistance of  $130\Omega$  and each of the two outer members a resistance of  $97\Omega$  when the three currents are equal. It is clear from this that the outer members have less resistance than the inner members and so the outer members will tend to carry a larger current than the inner ones. Possibly computation would show that the resistances are equal when the currents are in a ratio near 1:3.

When the axes of the dipoles were turned through  $90^\circ$  the main beam became wider than the ideal. On extending the straight sides of the beam to cut the bearing axis the width, at the base, was found to be  $60^\circ$ , in contrast to  $51^\circ$  in Fig. 14.1: the minimum field was 11 per cent.

(vice 13 per cent.) and the side-lobe maximum was 22 per cent. at  $45^\circ$  (vice 24 per cent. at  $40^\circ$ ). In the previous notation we now have  $DF = 30^\circ - 18.3^\circ = 11.7^\circ$ , and accordingly

$$\frac{I_A}{I_B} = \frac{11.7}{9.7} = 1.2.$$

Reference to § 2.14 will remind the reader that the current must tend to concentrate in the two inner members of a 4-element curtain. Let the current in the inner pair be  $x$  times the current in the outer pair. Then, following the process of working used in § 2.14, the condition for equal resistances is

$$0.6095x - \frac{1+x}{\pi^2} + \frac{1}{4\pi^2} = 0.6095 - \frac{x}{\pi^2} + \frac{x}{4\pi^2} - \frac{1}{9\pi^2},$$

whence  $x = 1.15$ .

We have estimated from the pattern that  $x = 1.2$ , and hence the distribution of current which did obtain is roughly that which would present equal loads at the ends of the four feeding cables.

These two examples should suffice to show how the approximate distribution of current can be deduced from the observed pattern: when this distribution is known, steps can be taken to force it nearer to uniformity and cophasedness. Clearly it is important to study the pattern very closely over a small range of bearing near the first minimum. Since the response of the galvanometer is usually proportional to the square of the field strength it is essential to provide the galvanometer with a variable shunt covering a very wide range of sensitivity. In practice this means that the galvanometer must be a very sensitive one, a reflecting type and not a unipivot. Analysis of the current distribution becomes impossibly involved when the array has many members, and then we must proceed by understanding what kind of disturbances in the pattern result from various kinds of current distribution. Although the main beam is usually substantially correct, the side lobes commonly differ widely from the ideal.

Thus consider Fig. 14.3, which is the observed pattern for an 8-element in-line array: the dipoles were 23 cm. long and were spaced 26.5 cm. apart,  $\lambda$  being 50 cm. Each dipole was fed through about 37 in. of cable and each cable had been cut so as to make the electrical length the same for all. The received field strength was measured by a thermocouple and galvanometer: the galvanometer was either a unipivot or a Cambridge portable reflecting instrument, whose sensitivity was about nine times as great as the unipivot. The available power was such that

field strengths less than about 15 per cent. of the maximum could scarcely be detected by the unipivot: with the reflecting instrument it was possible to detect a field if it was greater than about 4 per cent. of the maximum. The positions of the minima of field could be determined within about  $\pm 1^\circ$ .

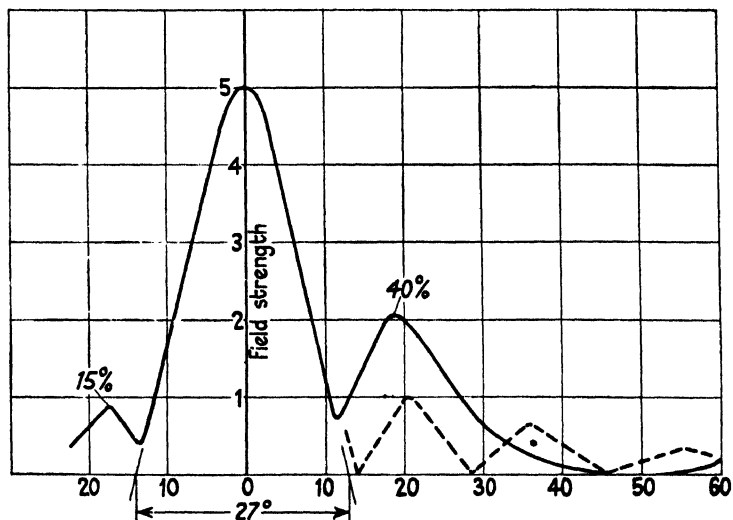


FIG. 14.3. Diffraction pattern of a certain 8-element in-line array,  $\lambda = 50$  cm.

If the eight currents were equal and cophased, then the maxima and minima and their bearings should be as recorded in Table 14.1.

TABLE 14.1

Bearing . (degrees)	0	13.8	20.5	28.5	36	45.5	56	72	80	90
Field .	100	0	20	0	13	0	7	0	2	0

On a bearing of  $72^\circ$  the path difference between any two consecutive dipoles is  $\frac{1}{2}\lambda$ , and hence the field will be zero on this bearing for any symmetrical loading. According to the above table the reflecting instrument should be incapable of detecting any field on bearings larger than about  $62^\circ$  if the currents are uniform and cophased.

The side lobes, according to Table 14.1, are shown dotted in Fig. 14.3. It is obvious that there is a hopeless discrepancy between the observed lobes and the lobes which would obtain if the loading was uniform. No field could be detected between  $44^\circ$  and  $54^\circ$ , or between  $76^\circ$  and  $90^\circ$ . There was a minimum between  $65^\circ$  and  $68^\circ$  and certainly not a zero at  $72^\circ$ . The width of the main beam, at its base, is  $27^\circ$  and this agrees

closely with the ideal width of  $27.4^\circ$ , but it is not quite symmetrical: the lobes are very unsymmetrical. The pattern is suggestive of a more or less progressive change of phase across the array, but that is about all that can be foretold about the distribution. Clearly it will be very hard to discover and locate the maladjustment: much time will be wasted in trying first this thing and then that—just fumbling in the dark. In Fig. 14.3 the field does not fall to zero at  $13.8^\circ$  but falls to a minimum near this bearing: this shows that the currents cannot all be cophased. The pattern is very far from symmetrical and this shows, almost certainly, that there is a more or less progressive change of phase along the array. In this particular example great care had been taken to make all the feeding cables similar: four consecutive members were fed from one junction box and the other half of the array from a similar box. These two boxes were fed through similar cables joined to a three-way box: it seems probable that the two last-mentioned cables were not in fact truly similar.

#### **14.2. Examples of patterns when the loading is symmetrical but not necessarily cophased**

It is proposed now to exhibit a family of patterns to show what results when the currents are not cophased. In particular it is desired to know whether the size of the side lobes is necessarily increased when the currents are not cophased. All the examples relate to a 16-member curtain because they were prepared to help analyse the performance of an existing 16-member curtain: but they may be regarded as generally typical. The patterns for certain cophased loading have been shown already in Figs. 2.2 to 2.7. If the current increases uniformly from zero at the middle to the greatest value at the outside members, then the size of the first lobe is 54 per cent. (see Fig. 2.5), in contrast to 21 per cent. when the loading is uniform. This shows the increase of current from the middle outwards must be very drastic in order to produce a very marked increase in the size of the lobes. Fig. 2.7 shows the pattern which results when the two middle currents are zero, the other fourteen being all equal. It is appropriate to describe this pattern as having only four lobes, where seven would have been expected: it is virtually as though the base line in Fig. 2.1 had been moved up about 12 per cent. Thus the existence of an unduly large first lobe together with half the correct number of lobes denotes that the currents are sensibly cophased but some central members have become disconnected.

Fig. 14.4 shows the pattern which results when the two outer quarters are in phase with one another but in phase quadrature with the middle half (the dotted pattern is for uniform cophased loading). Here again the number of lobes is halved. The main beam is twice its proper width at the base and it has a pronounced shoulder on it. The existence of this shoulder should tell the experimenter that large quadrature

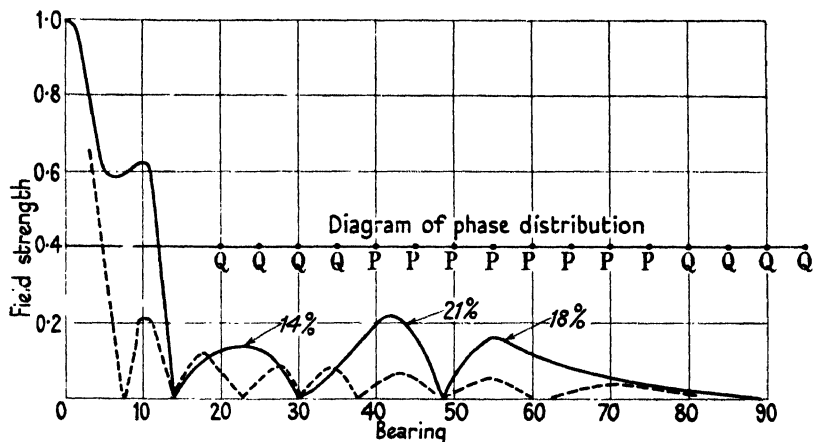


FIG. 14.4. Diffraction pattern for a 16-member curtain array, side spacing  $\frac{1}{2}\lambda$ . Current loading is uniform in R.M.S. value but the two outer groups of 4 are in phase quadrature with central group of 8. Power gain 12.2. Dotted pattern is for cophased currents.

currents exist; because the minimum at  $7^\circ$  is an attempt to produce the zero of field which would occur at  $7^\circ$  if the currents were cophased. The lobes have not become very large but they are halved in number.

Fig. 14.5 is the pattern which results when the R.M.S. current in the middle half is twice the current in the two outer quarters, the outer quarters being cophased with one another but in phase quadrature with the middle half. In general character Figs. 14.4 and 14.5 are not very dissimilar. Once more, the key to the distribution is that there are only half as many lobes as there ought to be.

Fig. 14.6 relates to a 1:2:2:1 cophased loading with a superposed quadrature loading in which the quadrature current increases uniformly from zero in the middle members to a value which makes the current in the outside members have a phase angle of  $45^\circ$ . The inset diagram shows the distribution of R.M.S. current across the curtain. If this had been obtained experimentally, from ammeter readings, it might well have been concluded that a very close approach had been obtained to a cophased loading described by the notation 1:1.4:1.4:1. It might well have been thought that the matching transformer feeding the



middle eight members had a ratio which increased their currents, relative to the two outside sets of 4, in the ratio 1:4:1, whereas it had

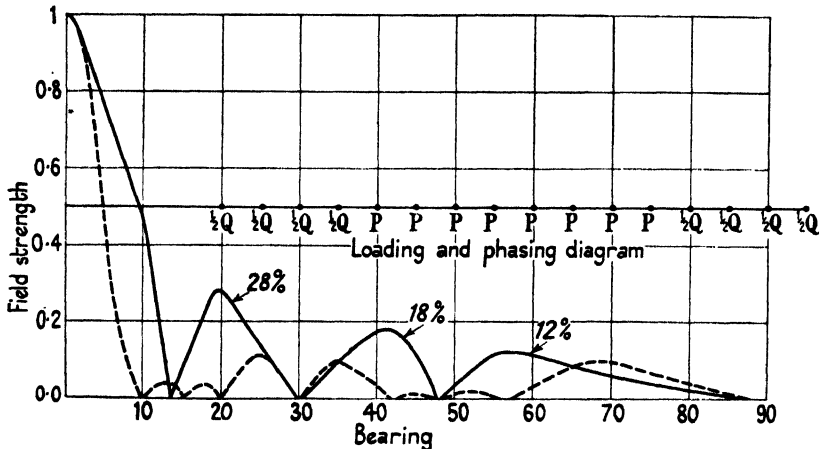


FIG. 14.5. Diffraction pattern for a 16-member curtain array, side spacing  $\frac{1}{2}\lambda$ , in which the current loading is 1:2:2:1 in R.M.S. value, but in which the currents in the two outer groups of four are in phase with one another but in phase quadrature with the central 8 currents. Power gain 10.5. Dotted pattern is for cophase currents.

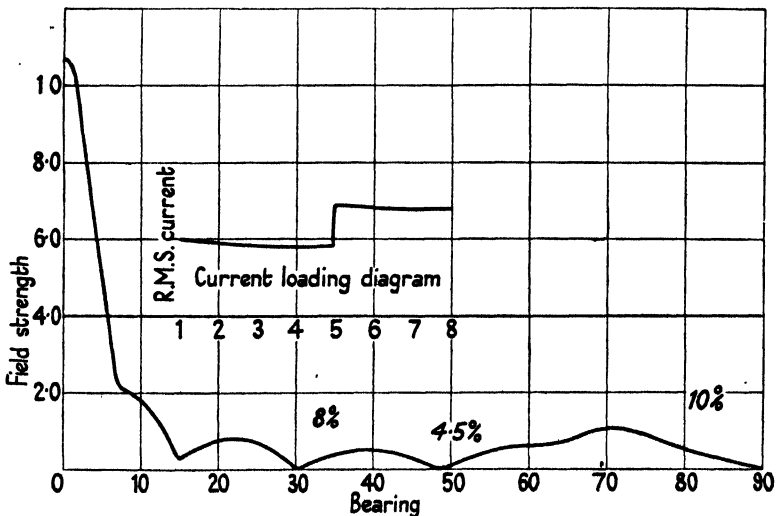


FIG. 14.6. Diffraction pattern for a 16-member curtain array, side spacing  $\frac{1}{2}\lambda$ . Current loading is 1:2:2:1 cophased, plus an outward triangular loading of quadrature component which makes phase angle of extreme members  $45^\circ$ . Power gain 17.

been intended to increase them in the ratio 2:1. The distribution test, made by ammeters only, might well appear to be satisfactory and might lead to the decision to leave well alone and not attempt to bring the

current loading more nearly in the ratio 2:1. The pattern, however, would show that the loading was not cophased, because there are only three lobes. This pattern should be compared with Fig. 2.3. There is a great contrast in detail, but from the practical point of view it is quite possible that Fig. 14.6 would be the preferable pattern because, on the whole, it has smaller lobes and fewer of them. Comparing

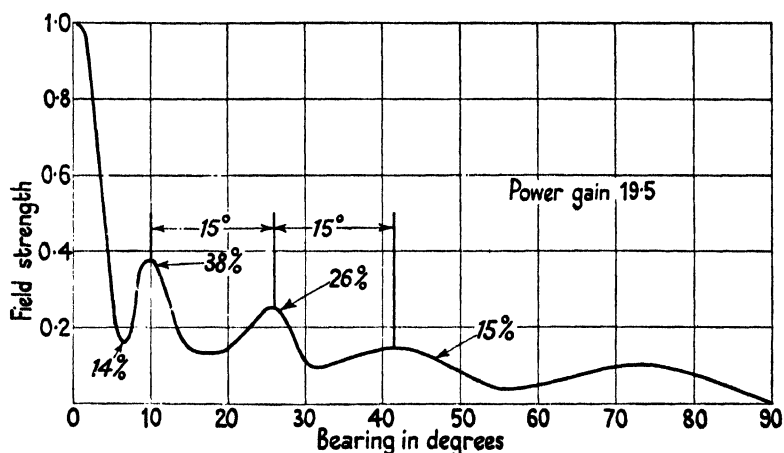


FIG. 14.7. Diffraction pattern for a 16-member curtain array, side spacing  $\frac{1}{2}\lambda$ . All currents equal in R.M.S. value but the middle pair are in phase quadrature with the other 14. Power gain 19.5.

Figs. 14.5 and 14.6 we conclude that a reasonable amount of progressive and symmetrical phase change, across the curtain, has not got much practical significance.

Fig. 14.7 shows the pattern which results when all members carry equal currents but when the current in the middle pair is in phase quadrature with the other fourteen cophased currents. This pattern is the vector sum of two components; one of them is the pattern shown in Fig. 2.7 and the other is the pattern for two equal currents separated by  $\frac{1}{2}\lambda$ . After due consideration, this description should make clear the structure of this pattern and show why it is virtually the same as Fig. 2.7 when pushed upwards by an amount which decreases smoothly to zero at  $\theta = 90^\circ$ . This figure is typical of many experimental patterns, in that it has unexpectedly large lobes which are too few in number and the field does not pass through zero but merely falls to minima. It is obviously the vector addition of a pattern having many lobes and a quadrature pattern which has only about one bearing for zero field. The obvious cause of a pattern such as Fig. 14.7 is a large quadrature

component of current in a pair of members which are not separated by more than one or two multiples of  $\frac{1}{2}\lambda$ .

An interesting case to consider is when the phase alternates by  $90^\circ$  from member to member. Suppose, for example, the array has 17 members. Then we have to combine the pattern for a 9-member array, whose side spacing is  $\lambda$ , with the pattern for an 8-member array, whose side spacing is  $\lambda$ ; the two arrays being coplanar and with a common centre point but having currents in phase quadrature. Since the side spacing is  $\lambda$ , consideration will show that the field on bearing  $90^\circ$  must be the same as the field on bearing zero. This alone would suffice to disclose the phase distribution if the array was a curtain. But if it was an in-line array the 'obliquity' effect would reduce the field to zero at  $\theta = 90^\circ$  and the phase distribution would disclose itself mainly by the last lobe being very large. The 'breadth factor' for an 8-member array with side spacing  $\lambda$  is

$$\text{B.F.} = \frac{\sin(8\pi \sin \theta)}{8 \sin(\pi \sin \theta)} = \frac{\sin(8\pi \sin \theta)}{16 \sin(\frac{1}{2}\pi \sin \theta) \cos(\frac{1}{2}\pi \sin \theta)}.$$

The obliquity factor for half-wave aerials is  $\cos(\frac{1}{2}\pi \sin \theta)/\cos \theta$ : hence if the array is to be in-line, its breadth factor becomes

$$\text{B.F.} = \frac{\sin(8\pi \sin \theta)}{16 \sin(\frac{1}{2}\pi \sin \theta) \cos \theta},$$

and this is the breadth factor for a 16-member curtain divided by  $\cos \theta$ . Hence the pattern can be derived by dividing the ordinates of Fig. 2.7 by  $\cos \theta$ . This counteracts the decreasing size of the side lobes: thus the lobe centred at  $56^\circ$  is increased from 5 per cent. to 9.2 per cent. and that centred at  $75^\circ$  is increased to 16 per cent. The resultant pattern for the 17-member array in which alternate currents are cophased and adjacent currents are in phase quadrature is shown in Fig. 14.8: it is characterized by a field which does not fall to zero anywhere but has a general level of about 10 per cent. in the range of bearing between  $15^\circ$  and  $65^\circ$ . The lobes are nowhere large, but the final lobe is surprisingly big for a final lobe, and this is the striking feature which discloses that it is alternate currents which are cophased, thereby producing an array whose spacing is  $\lambda$ .

Reviewing these examples, it becomes apparent that large side lobes are not a characteristic of currents which are imperfectly cophased: the characteristic of this is a reduced number of side lobes and probably minima rather than zero field on certain bearings. If the pattern of an existing array is to be analysed systematically it is the small values of

field which must be studied thoroughly, and this will involve a very sensitive galvanometer. It is the precise bearings of the minima or zeros of field which must be determined because it is the discrepancy between these bearings and the ideal which gives much information about the distribution of current, in both magnitude and phase.

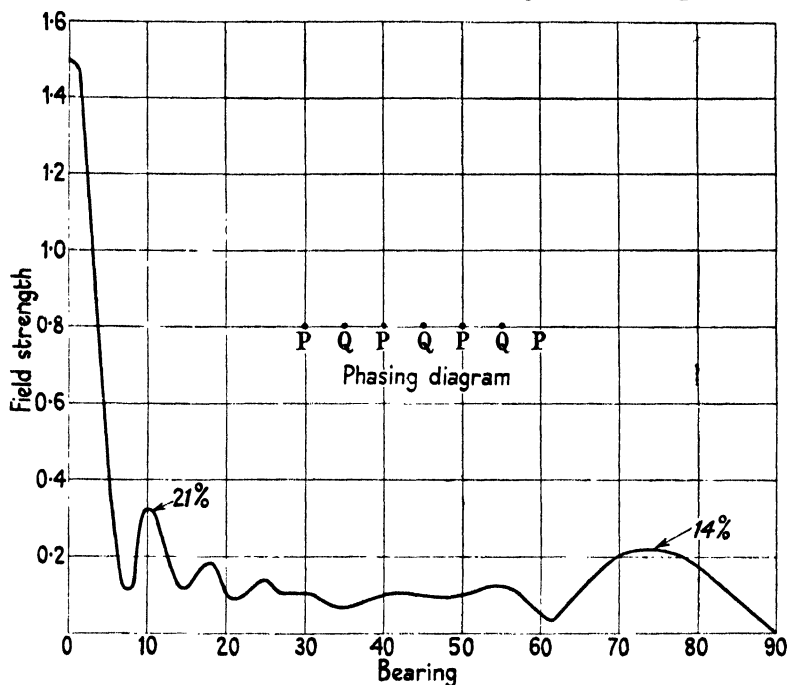


FIG. 14.8. Diffraction pattern for a 17-member curtain array, side spacing  $\frac{1}{2}\lambda$ . All currents equal in magnitude but phase alternates  $90^\circ$  from member to member.

Usually it is only in Radar applications that very close agreement is called for between the observed and the ideal pattern. Then it is that the very existence of side lobes may be a real nuisance. But even so it is very often the sharp maxima of side lobes which are more a nuisance than the mere existence of field on bearings well away from that of the main beam. But there is also the question of whether imperfect phasing decreases the power gain appreciably. Consideration will show that the power gain cannot depend much on the phasing because the main beam accounts for nearly all the power and the main beam is not much dependent on the phasing. The power gain has been evaluated, for all the examples we have given, on the supposition that each member of the curtain is a single half-wave aerial; the value of the gain is marked on each figure. For example, Fig. 2.3 records that the

gain for a 1:2:2:1 cophased loading is 17.3 and the gain for the loading to which Fig. 14.6 relates is 17.0; for uniform cophased loading the gain is 21.8 (Fig. 2.2) and in Fig. 14.7 the gain is 19.5. Imperfect adjustment of phase will not affect the gain appreciably unless the maladjustment is really gross.

### 14.3. Examples of patterns when the phase distribution is not symmetrical

In § 2.7 we studied the process of turning aside the main beam by making the phase change progressively across the curtain. When the array was wide we found that the amount of turning which could be produced was very small, of the order of two or three degrees. If only a few degrees of swing can be attained even when the phase changes progressively from leading in one extreme member to lagging in the other extreme member, then it follows that random and fortuitous maladjustments of phase cannot possibly swing the main beam by any significant amount.

It must be emphasized that because the main beam is found to be 'on centre', within the limits of ordinary measurements, then this is no indication that all the currents are cophased or that the phase distribution is symmetrical. It is a matter of experience that the main beam always is on centre and it does not demand a very deep understanding of the problem to realize that this result is inevitable.† It is an equally common experience that the side lobes are all wrong, in size and bearing: these two experiences are often thought to be contradictory, but of course they are not contradictory.

Fig. 14.9 shows the pattern for a curtain in which each of the 16 members carries the same R.M.S. current but when the two extreme currents are in antiphase with one another and in phase quadrature with the remaining 14 currents: it is the resultant pattern for which the two components have been recorded in Fig. 2.9. The main beam is about  $1^\circ$  off centre and its width at the base is about  $17.5^\circ$  (vice  $15^\circ$  for cophased loading). The outstanding feature is that the side lobes have become very unsymmetrical and also very large on the right-hand

† When we say the main beam is always on centre we are thinking of arrays which have at least 10 members: it is very easy to swing the beam when there are only about 4 members and this is very common practice in certain broadcast services. When engineers meet to discuss aerial problems it is common to hear views expressed which seem to be completely divergent. This divergence is not due to conflict of basic principles but arises because one man is accustomed to work at, say,  $\lambda = 15$  m. and another at, say,  $\lambda = 50$  cm.: one of them is apt to think of a typical array as having about 4 members while the other one thinks of it having about 24 members.

side of the diagram: thus the phase of the extreme members has had a profound effect on the side lobes and just that kind of effect which is experienced very commonly when an array is first tested. The same kind of effect is exemplified in Fig. 14.8. It is well to remember here that in plotting the experimental pattern the lobes would all be plotted

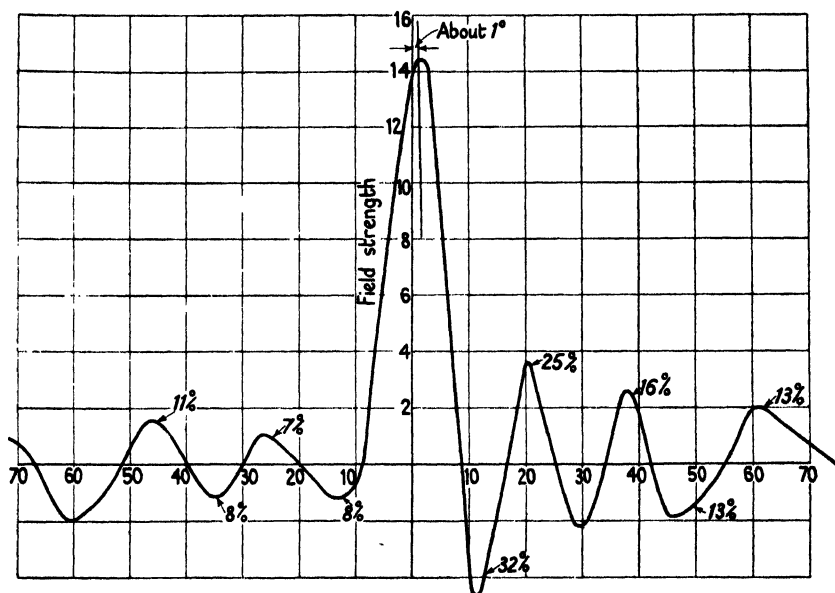


FIG. 14.9. Diffraction pattern for a 16-member curtain array, side spacing  $\frac{1}{2}\lambda$ . Current loading is uniform in magnitude but the two extreme members are in antiphase with one another and in phase quadrature with the central 14. Power gain 16.7.

above the base line. If this were done in Figs. 2.8 and 2.9 the lobes would be sensibly symmetrical in respect of amplitude and the dissymmetry would be mainly in their bearings. The feature which would strike the observer strongly is that the first pair of lobes have an amplitude of 37 per cent., instead of 21 per cent. for cophased loading.

Fig. 14.10 shows the pattern when one middle quarter of an array has its currents in phase quadrature with the other 12 equal and cophased currents. Here the main beam is turned off-centre by  $1^\circ$ : the side lobes are enormous and unsymmetrical. The arrowheads on the base line record the bearings for zero or maximum field when all the currents are cophased and they serve to indicate, for comparison, the features of the ideal pattern. This gross maladjustment of phase has devastated the ideal pattern and serves well to indicate the kind of

thing which can well result from a group of members being misphased: and a whole group may get misphased because the cable feeding their common junction box may be out of adjustment.

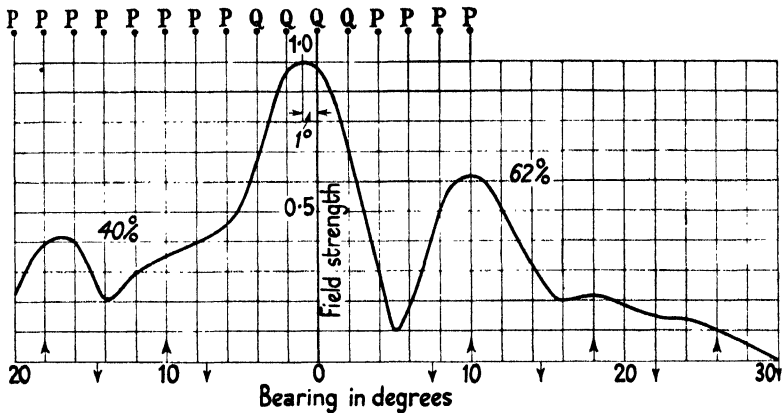


FIG. 14.10. Diffraction pattern for a 16-member curtain array, side spacing  $\frac{1}{2}\lambda$ . All currents equal in magnitude but the phase of one of the middle quarters is in quadrature with the other 12 cophased members. Power gain 13.6.

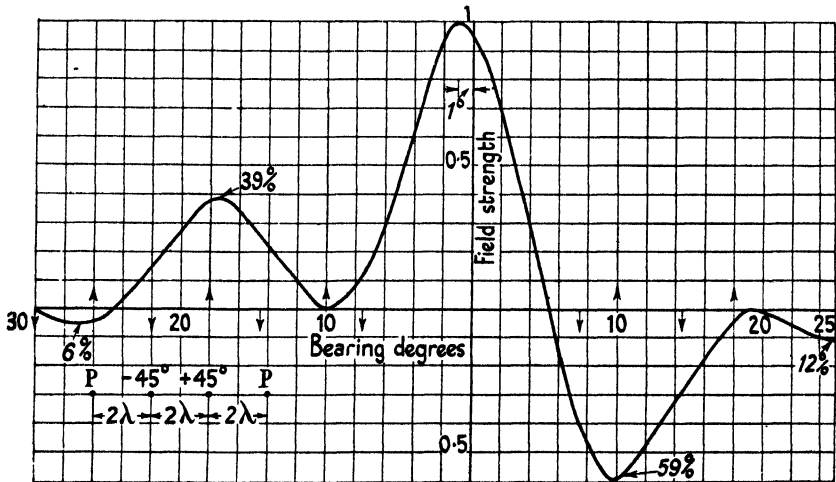


FIG. 14.11. Diffraction pattern for a 16-member curtain array, side spacing  $\frac{1}{2}\lambda$ . All currents equal in magnitude. The two middle quarters in quadrature with one another: the two outer quarters are cophased with one another but their phase differs  $45^\circ$  from the two middle quarters. Power gain 16.

Fig. 14.11 shows the pattern when the two middle quarters are in quadrature with one another and the two outer quarters are cophased but differ by  $45^\circ$  from the middle quarters. Here the side lobes are unsymmetrical, enormous, and reduced in number. The pattern is slightly reminiscent of Fig. 14.3.

It is hoped that the selection of examples which has been given will serve as templates with which to match and compare experimental patterns. Consideration of them, combined with judgement and experience, should enable engineers to recognize that a particular pattern (obtained experimentally) denotes that the maladjustment of phase resides in a determinable portion of the array and is of a recognizable kind. By the help of these templates it ought to be possible to proceed in a systematic way in correcting the cables: use of the templates ought to reduce the loss of time and patience which is attendant on blind experimentation.

#### 14.4. An example of a 16-member curtain in front of a flat reflector

Fig. 14.12 shows the observed pattern for a certain curtain array of 16 half-wave aeriels mounted in front of a flat copper sheet and operating at  $\lambda = 50$  cm. Each dipole was mounted on a brass tube, which was perpendicular to its axis, and the feeding cables passed up the centre of this tube. The tube passed through a bush in the copper back-plate and the distance between the dipoles and the back-plate could thereby be adjusted. The junction boxes for the feeding cables were provided with ' $\frac{1}{2}\lambda$  matching sections', and these had diameters such as to lead to the expectation that the two outer groups of 4 aeriels would be fed with half the current fed to the middle 8 aeriels. The radiation resistance of each member depends on the distance between the curtain and the back-plate; hence adjustment of this distance must affect the impedance which the group of 16 (together with their feeding cables, junction boxes, and matching sections) presents at the end of the main cable feeding the whole array. The match to the main feeding cable (70 ohms characteristic impedance) was most nearly correct when this distance was 11 cm.: and for this reason the distance 11 cm. was deemed to be the proper distance between the curtain and the back-plate.

To estimate the effect of the back-plate on the pattern we must derive the pattern due to the curtain together with its image distant 22 cm. ( $0.46\lambda$ ) from it. This amounts to multiplying the expression for the equatorial pattern, for the isolated curtain, by the factor

$$2 \sin(k \cos \theta),$$

where  $k$  is here equal to  $0.46\pi$ . Since the distance between the curtain and its image is here less than  $\lambda$  (it is less than  $\frac{1}{2}\lambda$ ), there is no bearing angle at which the field will be zero other than those angles when it



would be zero if the curtain were isolated. Thus the back-plate cannot produce any new lobes and can do no more than reduce the amplitude of the lobes: the said reduction will be appreciable only for the far-out lobes.

The sensitivity of the receiving apparatus did not suffice to show whether the field passed through zero or merely fell to a minimum.

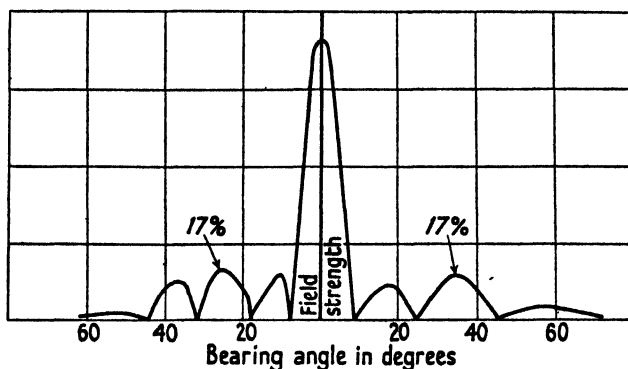


FIG. 14.12. Equatorial pattern of a certain 16-member curtain array, mounted in front of a flat reflector: and distant  $0.22\lambda$  from it:  $\lambda = 50$  cm.

Accordingly all the lobes in Fig. 14.12 are plotted on the same side of the base line. Indeed, field could not be detected if it was less than about 8 per cent. of the field at  $\theta = 0$ . Hence Fig. 14.12 purports to give more information than could be observed directly and, apart from the main beam, it was not possible to do much more than locate closely the five maxima from it and to find that on bearings greater than about  $45^\circ$  field could be detected only near  $+60^\circ$ .

If the currents had been cophased and the loading  $1:2:2:1$ , then the pattern should agree with Fig. 2.4, save that the 10 per cent. lobe centred on  $70^\circ$  would be reduced by the back-plate. Reference to Fig. 2.4 will show that a peak should have been observed at  $25^\circ$  and  $35^\circ$  and nowhere else: the observations do not agree with this prediction. Now compare the pattern with Fig. 14.5, in which there are maxima at  $20^\circ$  and  $42^\circ$  and with Fig. 14.6 in which there are maxima at  $22^\circ$  and  $42^\circ$ . Neither of these agrees with the observed pattern and yet, on the whole, the trend of the change of bearing is in the right direction. Fig. 14.12 shows that the phase distribution is not symmetrical and suggests that the outer members have an appreciable quadrature component of current. It would seem probable that the middle 12 members did in fact carry more current than the remainder because the width (at its base) of the main beam is about  $17^\circ$ , instead of  $14^\circ$  as it ought to be.

for uniform loading. The pattern is, perhaps, a little better than the ideal for uniform loading but very much worse than for cophased 1:2:2:1 loading. It is very doubtful if the extra complication of the matching lines, intended to produce 1:2:2:1 loading, was justified unless the pattern without them would have been worse than the ideal for uniform loading.

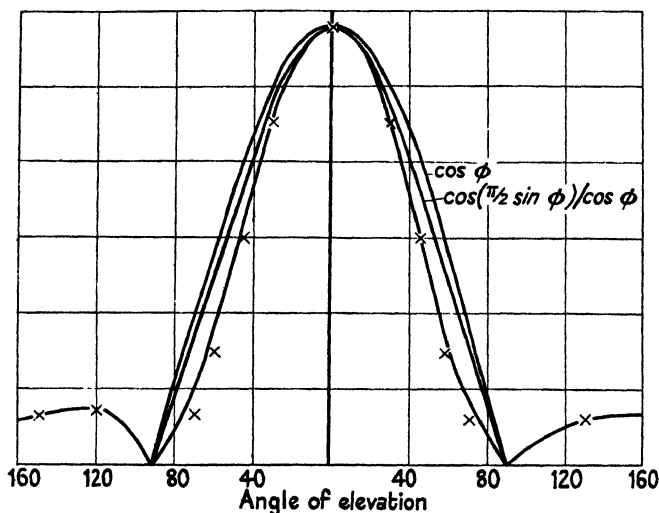


FIG. 14.13. Diffraction pattern in the other principal plane for same array as 14.12.

Fig. 14.13 shows the observed pattern in the other principal plane and is the only example, from experiment, of this pattern which we are able to give in this book. If the curtain consisted of 16 isolated doublets, then this pattern would vary as  $\cos \phi$ , where  $\phi$  is the angle of elevation. If it had consisted of isolated half-wave aerials, then it would have varied as  $\cos(\frac{1}{2}\pi \sin \phi)/\cos \phi$ . If it had consisted of half-wave aerials in front of an infinite plane, then this last factor should be multiplied by  $\sin(k \cos \phi)$ , where  $k$  is here equal to  $0.46\pi$ . The outside curve in Fig. 14.13 represents  $\cos \phi$ ; the middle curve represents  $\cos(\frac{1}{2}\pi \sin \phi)/\cos \phi$ , and the third curve is the second curve multiplied by the factor which allows for the array being distant  $0.22\lambda$  (i.e. 11 cm.) from an infinite flat plane. Twelve observed values of field strength are marked with a cross and these crosses lie very close indeed to the inside curve in the figure. This shows that all three expected corrections make successively closer approximations to reality. There is field in the range of  $\phi$  from  $90^\circ$  to  $180^\circ$  because the back sheet was not infinite (its width was about equal to  $\lambda$ ): the front-to-back ratio was about 9 to 1.

### 14.5. Measured performance of horizontal dipole arrays at $\lambda$ about 20 m.

We will now draw from the experience of Mr. H. Page† and explain first the excellent notation he uses for describing an array. If there are  $n$  rows, each consisting of  $m \frac{1}{2}\lambda$  aerials the lowest at height  $h\lambda$  above the ground, then the array is described by the symbols  $Hm/n/h$ . The letter  $H$  denotes that the polarization is horizontal: for example,  $H4/4/1$  denotes 4 rows of dipoles, the lowest of which is at height  $\lambda$  above the ground. Each row consists of 4 half-wave dipoles with small clearance between their tips and they are often fed as two columns of whole wave aerials. The letter  $R$ , before  $H$ , denotes that the array has a reflecting curtain: an additional letter  $S$  denotes that the column need not be fed cophasedly and thereby the beam can be 'slewed' to one side.

The vertical polar diagram was observed by measuring the e.m.f. induced in a loop carried by a balloon which was distant about 60 $\lambda$  from the array and could ascend to an angle of elevation of about 40°. The observed field strengths are reduced to mV/metre at a distance of 1 km., for an input of 1 kW.

Fig. 4 of Mr. Page's paper (*loc. cit.*) records the horizontal diffraction pattern for an H.R.S 4/4/1 array at a frequency of 15.31 Mc/s. The number of rows is not relevant to the horizontal pattern, which must be the same as for a single 4-element in-line array. It can readily be calculated that the first zero of a 4-element array occurs at  $\theta = 30^\circ$  if  $g/\lambda = \frac{1}{2}$  or  $\theta = 28.1^\circ$  if  $g/\lambda = 0.53$ . Mr. Page's figures give both the ideal and the observed pattern. The observed field strength falls to a minimum value, of about 2.5 per cent. at  $28.2^\circ$ : his ideal pattern falls to zero at  $30^\circ$ . Since there must have been some clearance between the tips of the dipoles it would seem that  $g/\lambda$  must have been greater than  $\frac{1}{2}$ , and hence it is not obvious why he makes his ideal pattern pass through zero at  $\theta = 30^\circ$ . It seems probable this array agreed more closely with the ideal than Mr. Page implies. The magnitude of the observed side lobe is in substantial agreement with the ideal. Since the field does not fall quite to zero at  $28^\circ$  it is to be inferred that the two outer columns were not precisely cophased with the inner two but that the discrepancy of phase was only of the order of  $2^\circ$ . His Fig. 5 shows the front-to-back ratio was about 14 to 1: there are indications that the field did not fall to zero at  $\theta = 90^\circ$  and this accords with expectation, since the reflecting screen had finite width.

His Fig. 3 records the vertical pattern on the centre line of the beam

† See *Journal I.E.E.* 92 (1945), Part III, 68.

and is reproduced here as Fig. 14.14: the full line curve in the figure is the ideal pattern for a 4-element array whose members carry equal cophased currents, and which is above a flat and perfectly conducting ground. It may be seen that there is very marked discrepancy between the observed and ideal patterns and it is necessary to discuss critically the reason for it. It is stated (*loc. cit.*) that the ground sloped down-

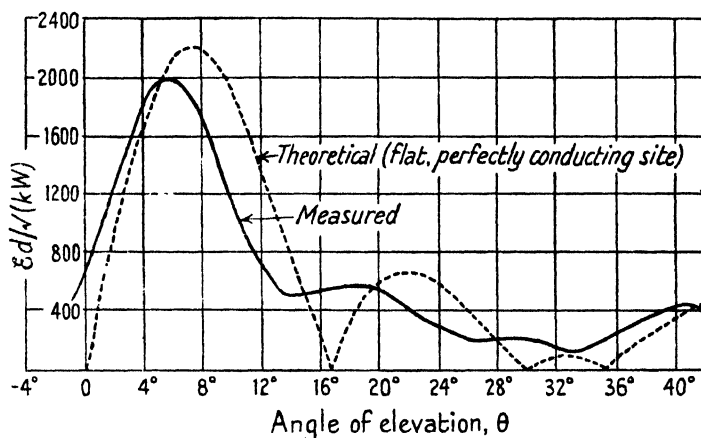


FIG. 14.14.

wards at a substantially constant slope of  $2.3^\circ$  for a distance of some  $50\lambda$  from the array. The figure shows the field does not fall to zero until an angle of depression of about  $2.7^\circ$  and doubtless this is accounted for by the ground slope. But it is very noticeable that the field does not pass through zero at any angle of elevation but passes only through minima whose fractional values are by no means small. Such minima are characteristic of an array in which the currents are not all cophased: the problem here is to decide whether the departure from cophasedness is in the currents, in the actual array, or in the currents induced in the sloping ground, which may possibly differ appreciably from a perfect conductor. In discussing the pattern in the horizontal plane (*loc. cit.*, Fig. 4) we have already decided that the four columns of the array were very closely cophased, and indeed suggested that the phase discrepancy was not more than  $2^\circ$ . It might perhaps seem, at first sight, that this showed that the discrepancies between the observed and ideal patterns in Fig. 14.14 are not due to incorrect phasing of the currents in the array and therefore must be due to effects of the ground. But careful consideration will show that this does not necessarily follow. The pattern in the horizontal plane shows the current is cophased

along each row of the array, but it does not show that the four rows are mutually cophased with one another. In other words, the pattern in the horizontal plane is the pattern of one horizontal 4-element in-line array at any distance above the ground: any number of such in-line arrays, acting simultaneously, will give the same pattern irrespective of the relative phase and magnitude of the current in them.

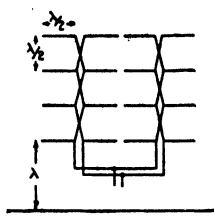


FIG. 14.15.

If all four rows are not mutually cophased, then the only effect will be that the absolute value of the field, on all bearings, will be less than if they had all been cophased. Fig. 14.15 (reproduced from Fig. 1 of Mr. Page's paper) shows that the half-wave elements were fed at one end (not from their mid-point) and thus each consecutive pair in a row formed what is called a whole wave aerial. Fig. 14.15 could be described as two columns of whole wave aerias fed by a pair of vertical cables, branching symmetrically from a central feeding cable. The feeding system has perfect symmetry about the mid-vertical line of the array: the observed pattern in the horizontal plane shows the current does in fact divide symmetrically between the two vertical feeding cables. But since the main feeder is connected at the bottom of the array and because the array is in the presence of the ground, the feeding system is not symmetrical about the mid-horizontal line of the array. It may well be that there is a progressive change of phase from row to row, and that the current in the top row is less than in the bottom row, since each vertical feeding cable has four loads (the four whole wave aerias) spaced at equal intervals along it.

It is helpful to consider the structure of the ideal pattern in Fig. 14.14. This pattern is the product of the pattern of an isolated 4-element curtain and the pattern of an unlike pair of currents separated by  $\frac{1}{2}\lambda$  (see Chapter II, p. 98). The field of a 4-element curtain (side spacing  $\frac{1}{2}\lambda$ ) carrying equal and cophased currents can be zero only when the path difference between alternate members is  $\frac{1}{2}\lambda$ . Since  $\sin 30^\circ = 0.5$  the field will be zero at an angle of elevation of  $30^\circ$ , no matter what is the height of the curtain above the ground. Accordingly the zero at  $\theta = 30^\circ$  in Fig. 14.14 is due to the array *per se*: the other two zeros in this figure are due to the height of the array above the ground (there is another such zero at  $58.2^\circ$ ). But it may be seen that the observed pattern is a maximum at  $\theta = 30^\circ$  and a minimum at  $33^\circ$  and this suggests that the currents in successive columns are neither equal nor cophased. The observed minimum at  $\theta = 26.2^\circ$  is presumably the attempt to produce

the zero at  $\theta = 30^\circ$  and if  $2.7^\circ$  be added, for the ground slope, then the bearing is very nearly correct. But still it is not a zero but only a minimum of 10 per cent. magnitude.

Fig. 14.16 is very instructive in demonstrating that the minima of the pattern are very sensitive to the relative phase of the current in the top row of the array. Curve *A* in this figure is the pattern for an H 4/4/1

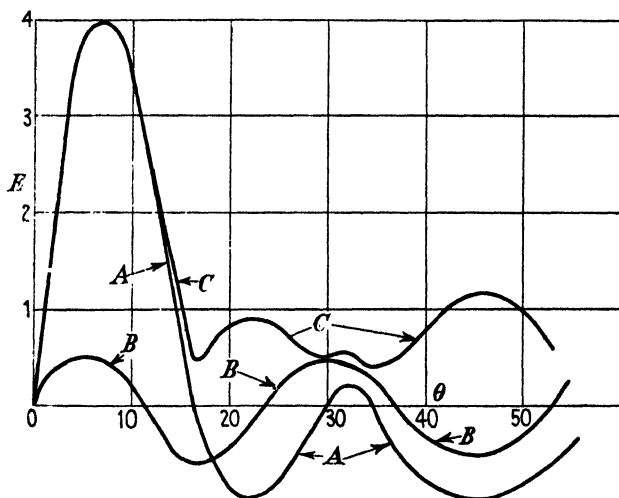


FIG. 14.16.

array in which all currents are equal and cophased, and it is the same as the dotted curve in Fig. 14.14. Curve *B* is the pattern for a single horizontal wire at a height  $2\frac{1}{2}\lambda$  above the ground and it may be called the pattern of an H 4/1/ $\frac{1}{2}$  array. Curve *C* is the pattern which would result if the patterns *A* and *B* coexisted in phase quadrature with one another. Thus it is the pattern of an H 4/4/1 array in which the current is cophased along every row, and in which the top row carries a current whose R.M.S. value is  $\{1 + (\frac{1}{2})^2\}^{\frac{1}{2}}$  times that in the other three rows and with a phase difference of  $7.1^\circ$  with respect to them. The shape of pattern *C* can be varied considerably by altering the relative magnitudes of curves *A* and *B*. However, the example chosen in Fig. 14.16 bears a strong resemblance to the observed pattern in Fig. 14.14 and serves to show that the discrepancy between the observed and ideal patterns, recorded there, may be due to a comparatively small change of phase from row to row and is not necessarily due to the slope or the imperfect conductivity of the ground.

It should be noted that Fig. 14.16 can be used to derive readily the

pattern which will result from any specified current in the top row. Thus, suppose its R.M.S. value is to be 0.71 of the other three currents and with a phase lag of  $45^\circ$ . First derive a curve  $D$  which is the difference between curves  $A$  and  $B$ ; then make a quadrature addition of curve  $B$  and curve  $D$ : the result will be the required pattern.

We have discussed at length the discrepancies between the observed and ideal patterns in Fig. 14.14 in order to make an exercise in analysing observed patterns. For many purposes these discrepancies are of no practical importance and the discussion may appear to be mere pedantry. The loss of power which results from the observed pattern in Fig. 14.14, as compared with the ideal pattern, is negligible and, in this respect, the observed pattern is very nearly as good as the ideal. The time and trouble required to bring the two into coincidence (always supposing the discrepancy is not due to the ground) by successive and systematic small changes in the feeding cable would not be justifiable.

Much of the writer's experience has been on Radar aerials in which special precautions had been taken to reduce the side lobes, and there it was important to try to make the observed side lobes agree with the ideal. They never did agree in the first instance, and the consequent adjustments were hampered and prolonged by inadequate knowledge of how to analyse an observed pattern. For Radar purposes the side lobes are very objectionable because of the spurious echoes they are liable to produce: the power wasted in them is never significant, *per se*. A reader who is concerned with Radar aerials, operating at a wavelength between 50 and 100 cm., may not feel this discussion has been mere pedantry. The response of a given person to a given discussion on aerials is coloured enormously by that person's particular needs of the moment: let his operational duties be changed slightly in respect of wavelength or kind of service and his response to the discussion of a given problem may well change out of all recognition.

## 14.6. Analysis of the effect of ground slope

### (a) *Uniform slope*

Masts are erected vertical, and not perpendicular to the surface of the ground on which they stand. We can simulate the conditions which arise from a uniformly sloping ground by solving the problem of a curtain whose plane is not perpendicular to an infinite conducting plane. This solution follows at once from the general solution of a current filament placed anywhere in a Vee and given in § 3.10. If we put  $n = 1$  in (3.20) we have the field of a wire parallel to a flat ground but referred

to an origin which is not at the foot of the perpendicular from the filament on to the plane. If there are several parallel filaments all in one plane, inclined at  $\alpha$  to the normal, which meets the infinite plane at the origin of polar coordinates, and if the distances of the successive filaments from the origin is denoted by  $k_1, k_2$ , etc., then (3.20) gives

$$\frac{E}{4E_0} = j\{\sum J_1(k)\cos\alpha\cos\theta - \sum J_3(k)\cos 3\alpha\cos 3\theta + \dots\} - \{\sum J_2(k)\sin 2\alpha\sin 2\theta - \sum J_4(k)\sin 4\alpha\sin 4\theta + \dots\}. \quad (14.1)$$

The form of (14.1) shows that  $|E|$ , the R.M.S. field, is symmetrical in both quadrants. This is immediately obvious since each component pattern is, by its very nature, symmetrical in both quadrants and hence the addition of the component patterns can be unsymmetrical only in phase: it also conforms with the general principle (see p. 163) that the beam cannot be turned off centre when  $n$  is an odd integer. Since both components in (14.1) will not pass through zero at the same value of  $\theta$  it follows that the pattern must have minima and not true zeros. Hence the experience recorded in Fig. 14.14 may have been due to the slope of the ground and not to lack of perfect cophase adjustment of the currents in the four rows of members. On substituting the numerical values appropriate to an H 4/ $\infty$ /1 array we have

$$\begin{aligned} \frac{E}{4E_0} = j\{-0.07 \cos\alpha\cos\theta + 0.13 \cos 3\alpha\cos 3\theta - 0.19 \cos 5\alpha\cos 5\theta - \\ - 0.34 \cos 7\alpha\cos 7\theta + 0.20 \cos 9\alpha\cos 9\theta - \dots\} - \\ - \{-0.13 \sin 2\alpha\sin 2\theta - 0.08 \sin 4\alpha\sin 4\theta + \\ + 0.40 \sin 6\alpha\sin 6\theta - 0.27 \sin 8\alpha\sin 8\theta + \dots\}. \end{aligned}$$

It would be necessary to go up to the term in  $\sin 21\theta$  in order to reduce the coefficients to less than 0.01 and the process of evaluation by this method would be intolerably laborious. Equation (14.1) has served its purpose by showing that a uniformly sloping ground will, *ipso facto*, convert the zeros into minima even if the currents are truly cophased. Thus, if a horizontally polarized array were mounted in a ship, then the pattern in the vertical plane would vary cyclically with the pitching of the ship, quite apart from the direct effect of the undulating surface of the ocean. Thus, with an H 4/ $n$ /1 array, if an aeroplane was flying at an angle of elevation near  $16^\circ$ , then its Radar echo would wax and wane with the pitching of the ship, being always a maximum when the ship was momentarily stationary.



*(b) Two uniform slopes*

Fig. 14.17 is the polar diagram (see Page, loc. cit., Fig. 9) in the vertical plane of an H 4/6/0.3 array, transmitting over ground which sloped downwards at an angle of  $3.5^\circ$  for a distance of  $6\lambda$ , when the slope changed quickly to  $7^\circ$  down. The feature of interest is the minimum at  $\theta = 4^\circ$ . Mr. Page obtains an interesting approximate

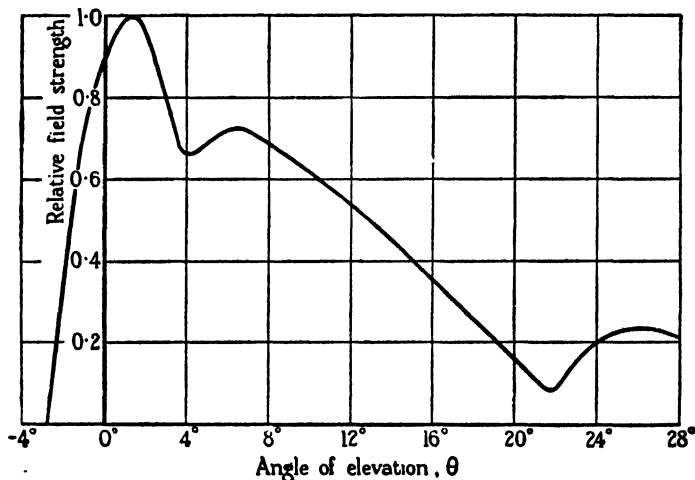


FIG. 14.17.

solution by means of ray-treatment; he points out that the portion of ground whose slope is  $-3.5^\circ$  will provide that part of the pattern which lies between  $\theta = 10.5^\circ$  and  $9^\circ$ . While the more sloping ground provides the portion of the pattern between  $\theta = -7.5^\circ$  and  $+3.5^\circ$ , in the range between  $\theta = 3.5^\circ$  and  $10.5^\circ$  there will not be any reflected ray (if the change of slope is abrupt) and accordingly the field strength will be half the maximum in this range. This general description accounts for the possibility of a minimum such as that at  $\theta = 4^\circ$  in Fig. 14.17 and no doubt the explanation is substantially correct.

However, the whole problem can be solved, at least formally, by classic methods and without ray-treatment. The ground can be regarded as a Vee having an angle of  $(180^\circ + 3.5^\circ) = 183.5^\circ$  and accordingly  $n = 0.982$ , and  $\alpha = (91.75^\circ - \arctan 0.25) = 77.75^\circ$  and

$$k = 2\pi \times \sqrt{17} \times 1.55 = 40.5.$$

The labour of evaluating the pattern from the Fourier series would be prohibitive; however, the full expression would consist of two component Fourier series in phase quadrature. Now examine Fig. 14.17 with the understanding that it is probably the quadrature addition of

two distinct patterns. It suggests strongly that one of these patterns has its first maximum near  $1.5^\circ$  and a zero near  $5^\circ$ , while the other has its first maximum near  $6^\circ$ . The quadrature addition of two such patterns would give a minimum, of large fractional value, near  $4^\circ$ . Thus it is not surprising, from the classical approach, that the pattern should have the general form of Fig. 14.17.

#### 14.7. The fields close to a curtain: method of estimating the power output

At a short distance from a wide curtain of high vertical wires the field must approach that of an infinite flat sheet and then be expressed by the equation

$$\frac{cE}{2\pi i} = -\cos ar + j \sin ar.$$

The field must approximate to a plane wave at short distances and to a spherical wave at large distances: our purpose now is to assess the range within which the field strength is approximately constant and independent of distance. It is necessary to give separate consideration to the inphase and the quadrature component of field. At the surface of a continuous sheet the quadrature component is zero, but this can scarcely be so in the plane of a curtain of separate wires. The quadrature component at the surface of each wire must be very dependent upon both the radius of the wire and the condition of tuning, presumably being zero if the wire is tuned precisely. We shall be content here with studying the field near a grid of  $N$  equal and cophased current filaments and shall not specify the quadrature field at points very close indeed to their plane. If each filament carries a current  $I$  and the side spacing is  $g$ , then the average current density over the plane of the grating will be  $i = I/g$ . If this density had been carried on a continuous sheet, then the field at its surface would have been given by the equation

$$\frac{cE}{2\pi i} = -1, \quad \text{whence} \quad -\frac{cE}{a\pi I} = \frac{2}{ag}.$$

But this is a grating, and not a continuous sheet, and therefore the inphase component of field at its middle wire is given by

$$-\frac{cE_P}{a\pi I} = 1 + 2\{J_0(ag) + J_0(2ag) + \dots\}.$$

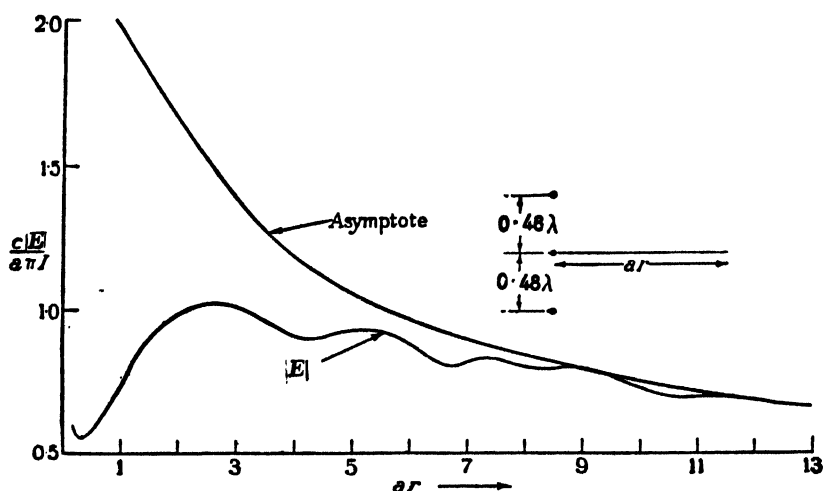
In most arrays the side spacing  $g$  is equal to  $\frac{1}{2}\lambda$ , which makes  $ag$  equal to  $\pi$ . We shall take  $ag = 3$  because doing so greatly facilitates the use of tables: it is near enough to the most common value, which is  $ag = \pi$ , to serve for the comparison we require. If  $ag = 3$ , then  $-cE/a\pi I = \frac{2}{3}$ ,

and this must give the limiting value to which  $E_P$  approaches at the middle wire of a grating in which  $ag = 3$ . Table 14.2 records the value of  $E_P$  at the mid-wire of gratings having 1, 3, 5, etc., wires and shows that a grating of 9 wires has approached very close indeed to a continuous sheet, in respect of the inphase field at the middle wire.

TABLE 14.2

Number of wires $\div cE_P/anI$	1	3	5	7	9	infinite sheet
	1.0000	0.4798	0.6004	0.6958	0.6674	0.6666

We now want to examine how the field strength depends on distance from the plane of the curtain and to assess the range in which it is

FIG. 14.18. Distribution of  $|E|$  in normal mid-plane of 3-wire grating.

substantially constant. Fig. 14.18 shows the distribution of  $|E|$  in the normal mid-plane of a 3-wire curtain and also the asymptote to which the field must approach when  $ar$  is large. It may be seen that  $|E|$  has reached the asymptotic value when  $ar$  exceeds about 9 and thus the wave front is virtually cylindrical when  $r/\lambda$  exceeds about  $\frac{3}{2}$ . But in the range of  $ar$  between about 2 and 6 the field strength is substantially constant and in this region the propagation is akin to a plane wave. Fig. 14.19 shows  $|E|$  in the normal mid-plane of a 7-wire grating and also the asymptote for  $ar$  large and the asymptote for a grating of infinite width. In the range of this figure  $|E|$  does not approach close to the asymptote for  $ar$  large but fluctuates about the asymptote for infinite width: with 7 wires the propagation is akin to a plane wave over about the first  $3\lambda$  of distance. So much for the distribution of  $|E|$

in the normal mid-plane, what of its distribution in planes which are parallel to the grating?

Fig. 14.20 supplies the answer to this question and shows the distribu-

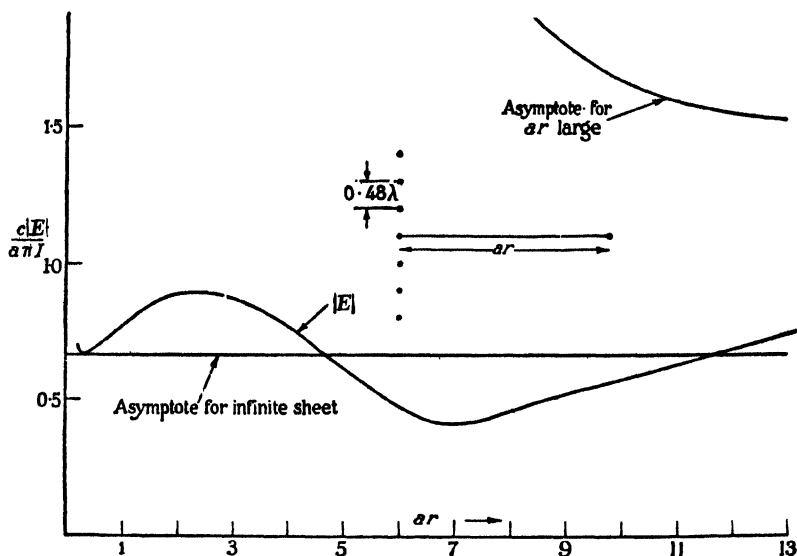


FIG. 14.19. Distribution of  $|E|$  in normal mid-plane of 7-wire grating.

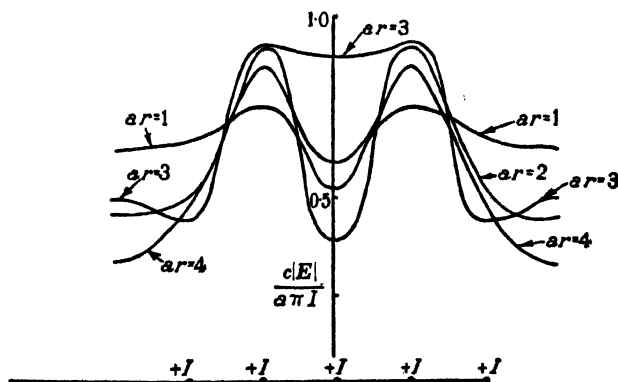


FIG. 14.20. Distribution of  $|E|$  in planes parallel to a 5-wire grating.

tion of  $|E|$  across various planes parallel to a grating of 5 wires. It shows that the value of  $|E|$  at a given distance from this grating is not constant, as it would be if the grating was propagating a plane wave. But it also shows that  $|E|$  is sensibly independent of distance in the normal planes which intersect the grating midway between the

component wires: it is in such planes that the field is most akin to a plane wave, and in them the figure shows that  $c|E|/(a\pi I)$  is very nearly equal to  $\frac{2}{3}$ , the value appropriate to a grid of infinite width.

This is a discovery which has an important bearing on the measurement of output by means of a monitor aerial. If output measurement by this means is to be reliable and trustworthy, then it must be insensitive to the exact position of the monitor and depend little on the width of the curtain. Near the beginning of § 9.2 we have likened the use of a monitor aerial to the use of a current transformer of large ratio and this is a very just and proper simile: the problem is to determine the magnitude of that ratio in any given application. Here we have shown that  $c|E|g/2\pi I = 1$  in a normal plane between two wires, and this gives the required ratio when it is combined with a monitor aerial designed in accordance with the principles explained in Chapter IX. In any given application in practice it will be desirable to explore, by means of the monitor aerial, the distribution of  $|E|$  in a normal plane between two wires near the middle of the curtain. Having proved, by experiment, that  $|E|$  is indeed constant over a considerable range of distance from the curtain it will remain only to choose some particular point, within that said range, which is convenient and suitable for the permanent location of the monitor. It is rare good fortune to be free to locate the measuring instrument at a point whose position is not dictated by electro-technical considerations and can be determined solely by convenience of mechanical construction. Having decided the distance between the monitor and the array it might be well to explore  $|E|$  as a function of position parallel to the array, in the manner corresponding to any two of the curves in Fig. 14.20: interpretation of the result of such a test would give a cross check that the spot chosen for the monitor was effectively situated in a mid-plane. In all this we are working on the justifiable assumption that the output of the uniformly loaded curtain was equal to the output from the same area of an infinite sheet. Accordingly the output is  $c|E|^2/2\pi$  per unit area of curtain, where  $|E|$  is the field strength deduced from the monitor aerial: hence the output in watts is

$$P = \frac{1}{60\pi} \times (\text{volts/m.})^2 \times (\text{area of curtain in square metres}).$$

Perhaps the reader may feel there is an unjustified step in passing to the output of the whole curtain from a field-strength measurement which must be on a mid-plane between two wires. But it is in these

planes that the field has the value corresponding to a plane wave, provided all the currents are equal and cophased. Perhaps the validity of the treatment will be justified more clearly by the help of Fig. 14.21, which relates to a sheet of total width  $1.9\lambda$  (i.e.  $ar = 12$  and thus corresponds to the 5-wire grid in Fig. 14.20) which is carrying a constant and cophased current density. The figure shows the distribution of  $E_P$  and

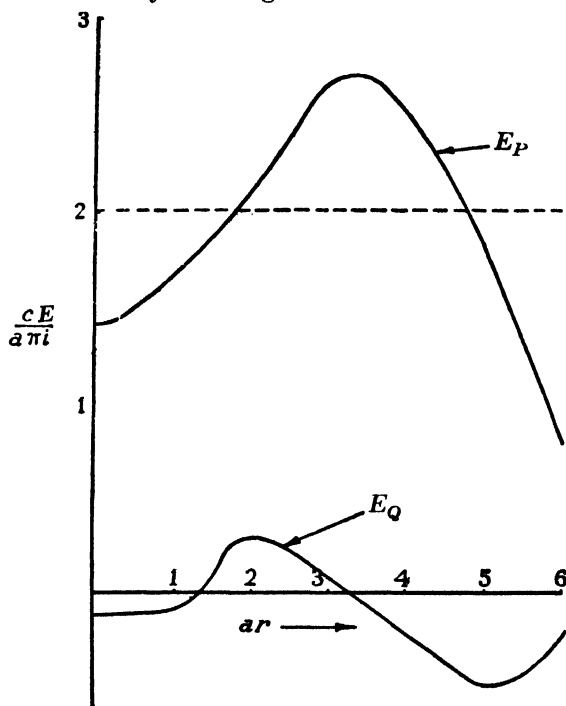


FIG. 14.21. Distribution of  $E_P$  and  $E_Q$  across a uniformly loaded sheet of width  $1.9\lambda$ .

$E_Q$ , across the half-width, at the surface of the sheet. If the sheet were infinitely wide, then  $E_Q$  would be zero and  $E_P$  would have the constant value shown by the dotted line. The output of work is given by

$$P = 2 \int_0^R E_P i \, dr = 2i \int_0^R E_P \, dr,$$

since  $i$  is constant, by hypothesis. It is obvious from the figure that the mean value of  $E_P$  across the sheet cannot be appreciably less than that shown by the dotted line: the output per unit width is not constant, but the fluctuations are above and below the output per unit area of a sheet of infinite width. It is interesting to note that  $E_Q$  twice changes sign across the sheet: this implies that the successive wires of a curtain

will require different tuning adjustments if the currents are to be equal and cophased.†

When the wavelength is such that a conventional ammeter cannot be used in each member of the curtain it is not easy to discover the relative currents carried by them. It is tempting and natural to attempt to use a monitor aerial to explore the current loading: and natural, at first sight, to place the monitor very close to each member in turn in the hope that its response will then be dominated by the current in that member. However, consideration will show this hope has no foundation. The quadrature component of field very close to the wire must be very small when the wire is correctly tuned and a small change of tuning must be competent to make a very large change in the quadrature component of field. The inphase component of field rises slowly to a finite value at the wire, and reference to Table 14.2 will show that the total value of  $E_P$  is due largely to the remainder of the curtain. Thus it is clear that the total field close to a wire will depend dominantly on the precise state of tuning of that wire, and accordingly the response of a monitor placed close to a wire is not likely to be a good measure of the R.M.S. current in it. The net quadrature field is brought to zero, by tuning, through the agency of the contribution from the charges distributed along the wire, and we need to eliminate the effect of the field due to these charges. Such fields, arising from charge distributions, have no curl; hence an indicator must be used which responds to the curl of the field and not to the field itself, and this means using a monitor loop rather than a monitor aerial. This can be put more directly as follows: the magnetic field at the surface of the wire, of radius  $b$ , must tend to the value  $H = 2I/b$  as compared with the value  $H = 2\pi I/g$  in the plane wave front. Thus the magnetic field near the surface of the wire must be dominated by the current in that wire, and accordingly it is the magnetic field which must be used to explore the current loading: the magnetic field can be measured by the e.m.f. it induces in a loop. A monitor loop is essentially the right tool and a monitor aerial essentially the wrong tool to use for exploring the current loading. If tests by a monitor loop have shown that all the currents are substantially equal to one another, then the response of a monitor aerial, placed close to each wire in succession, should be a sensitive test of the relative phase of the currents. The writer has vivid recollections of being called upon to test the current distribution across

† For a more complete treatment of all this section see *Journal I.E.E.* 91, Part III (1944), 23.

a 16-element curtain at  $\lambda = 50$  cm. and being provided with a primitive monitor aerial, colloquially called a 'probe', for the purpose. The factors governing the response of the probe, which have just been analysed, had not then been thought out. Tests by the probe showed that the response fluctuated by at least two to one, in a random manner, in passing from aerial to aerial across the curtain, even though it was fed through a cable system which had been designed and made with great care. It seemed highly probable that the probe tests gave a very wrong and pessimistic account of the current distribution. He noted that the response from any given aerial could be increased about twofold by lengthening it slightly, by slipping on a short length of copper gauze sleeving. These early and primitive tests now seem readily intelligible. The response of the probe was due mainly to  $E_Q$ , and this should be modified very much by adjusting the length of the aerial, even though such adjustment did not change the R.M.S. current very much. It was found that the main beam of the polar diagram of this array had substantially the correct width, and this showed the current distribution was very much more uniform than the probe tests had suggested. The moral is that a probe test shows up the phase and not the magnitude of the currents in the members. Thoughtful interpretation of the results of a systematic exploration by both monitor loop and by probe aerial should be capable of disclosing a great deal of information about the magnitude and phase of the current distribution across a curtain array and should help much with the final tuning adjustments of individual members. It is perhaps worth remarking here that it is a monitor aerial which ought to be used for measuring and monitoring the power output of the whole array. The loop is not suitable for this purpose because it is subject to an incalculable error resulting from 'aerial effect' and this would vitiate the absolute value of field strength deduced from the measured current in the loop.

#### 14.8. Measurement of the power output from a Vee reflector

We have discovered the region in which the field of a curtain differs insensibly from a plane wave and shown how the total output can be deduced from the field measured in this region. While we are on this subject it seems appropriate to discuss the corresponding problem of measuring the output from a single aerial in a Vee reflector. For this purpose it is required to know the distribution of field in the vicinity of the aerial and to discover a station where the field changes slowly with distance, because the monitor aerial must be placed at such a



station in order that its response shall not be unduly sensitive to its exact position in the Vee. In the idealized case of infinite sheets it is easy to calculate the field distribution when the source is either a current filament or a single doublet.

We will start with the case in which a doublet is on the bisector of a  $90^\circ$  Vee and distant  $\frac{1}{2}\lambda$  from its apex. The field at any point, in the

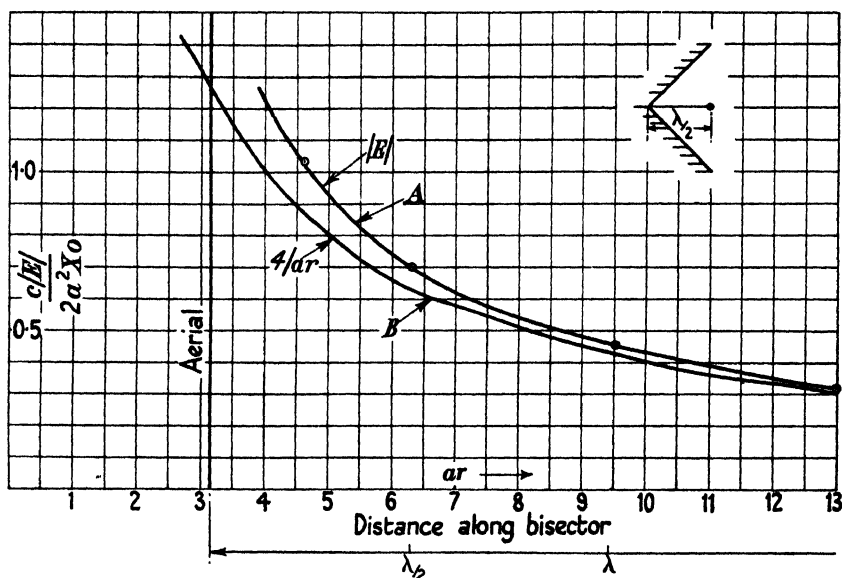


FIG. 14.22. Doublet in right-angled mirror,  $R/\lambda = \frac{1}{2}$ .

equatorial plane, can be found by adding the inphase components due to the doublet and its three equivalent images and likewise for the quadrature components: these two sums can then be added vectorially. When  $R/\lambda = \frac{1}{2}$  it has been shown that the power gain is 10 and it can readily be shown that the field at a very distant point on the bisector is the same as if a single doublet of fourfold strength were situated at the apex of the Vee, the Vee having been removed. Accordingly it is appropriate to compare the field distribution along the apex of the Vee with the curve  $c|E|/2a^2X_0 = 4/ar$ , since this curve must be the asymptote of the distribution along the said bisector. Curve A in Fig. 14.22 shows the calculated distribution along the bisector while curve B shows the asymptote over the same region. The difference between the two curves is not very considerable, and this is still another example showing that the modulus of the field very rapidly approaches the value corresponding to the asymptote at infinity. In Chapter XII we

decided it was unwise to place a monitor closer than about  $\frac{1}{2}\lambda$  from the excited half-wave aerial; for this reason the region between the aerial and the apex is forbidden territory. Accordingly the monitor would be placed at  $\frac{1}{2}\lambda$  in front of the aerial and at this point  $|E|$  is 1.12 times the value given by the asymptote curve. At this point  $|E|$  is varying sensibly as the inverse of the distance from the apex and accordingly

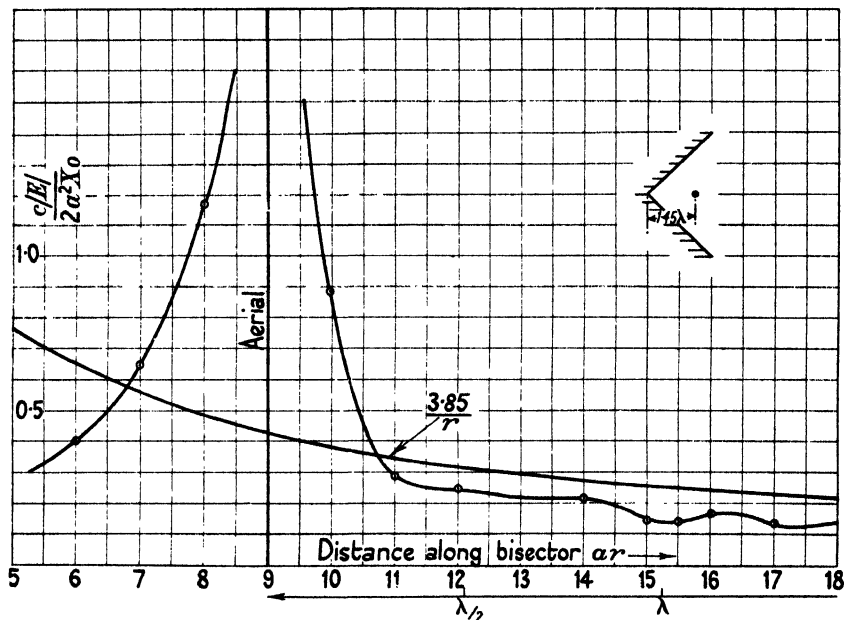


FIG. 14.23. Doublet in right-angled mirror,  $R/\lambda = 1.45$ .

a small and unsuspected displacement of the monitor would not affect its response very violently: in short, the field distribution is favourable for measuring the power output by a monitor aerial.

Fig. 14.23 shows corresponding graphs for a doublet at  $R/\lambda = 1.45$  ( $k = 9$ ) from the apex of a  $90^\circ$  Vee, a station where the forward power gain is near a maximum, having a value of about 20: our comments on the previous figure should suffice for this one.

The corresponding graphs for a doublet distant  $0.48\lambda$  from the apex of a  $60^\circ$  Vee shows that the curve of  $|E|$  oscillates slightly above and below the asymptote in the range of  $ar$  from 4.5 to 10; the general form of the distribution is well suited to the employment of a monitor aerial for measuring the power output.

It is much more simple to evaluate corresponding curves for a current filament because they are expressed in the Bessel series. It has been

done for a filament in a  $60^\circ$  Vee at  $R/\lambda = 0.48$  and the curve of  $|E|$  is found to lie everywhere slightly above the asymptote but has small undulations: the figure does not merit reproduction.

Fig. 14.24 shows corresponding graphs for a doublet  $\frac{1}{2}\lambda$  from the apex of a  $60^\circ$  Vee. The corresponding curves for a current filament were very

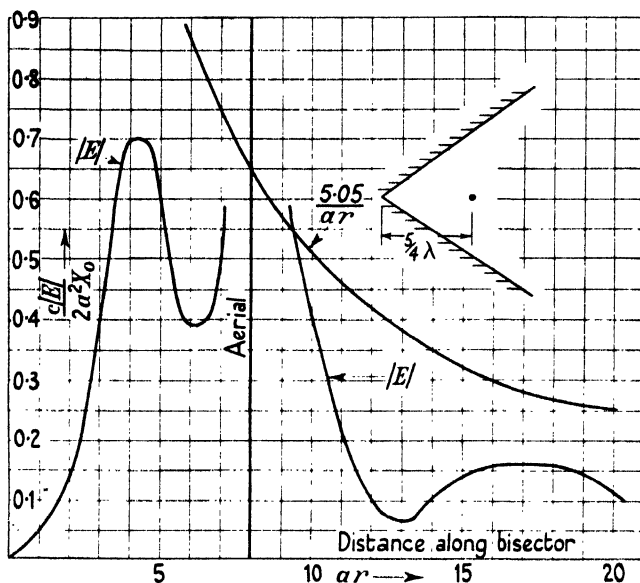


FIG. 14.24. Doublet on  $60^\circ$  mirror,  $R/\lambda = \frac{5}{4}$ .

similar to those for a doublet: the maxima and minima at  $ar = 4$  and  $6$  respectively were relatively larger and smaller with regard to the asymptote and the minimum at  $ar = 12$  was relatively larger. It is obvious from Fig. 14.24 that the monitor ought to be placed between the doublet and the apex and at  $ar = 4.5$ : it would be necessary to settle by experiment that the monitor had been stationed on the flat top of the maximum.

We must now find how to deduce the output from the field measured at any point in the forward direction and this will involve the calculated value of the gain  $G$ . The output of an isolated aerial is given by the formula

$$P = \frac{480\pi^2}{\lambda^2} k X_0^2 \text{ watts,}$$

where  $k$  is a factor depending on the length of the aerial and the current distribution along it. For a doublet  $k = 0.666$ , for a half-wave

aerial with sinusoidal distribution  $k = 0.6095$ , and for a half-wave aerial with triangular distribution  $k = 0.616$ . Accordingly for short aerials  $k$  is sensibly independent of length and distribution and so  $P$  is sensibly proportional to  $X_0^2$ . Again, for a short aerial

$$X_0^2 \doteq \frac{c^2 |E|^2}{4a^4} (ar)^2, \quad \text{if } ar > \pi,$$

$$\therefore P = 30c^2 |E|^2 r^2 k, \quad \text{if } r > \frac{1}{2}\lambda.$$

If the forward field of an aerial and reflector is  $F$  times that of the isolated half-wave aerial (having the same  $X_0$ ) and the gain is  $G$ , then

$$P = \frac{ck}{G} \{F|E|r\}^2,$$

where  $|E|$  is the measured field at a large distance  $r$  in the forward direction. But the system of measuring the power by a monitor aerial depends on measuring the field at a small distance: both because the field must be large enough to infer directly from the response of a thermocouple and because it is inconvenient to have the monitor at an appreciable distance from the aerial, especially when the aerial and reflector revolve on a turntable. Let  $\alpha$  be the ratio of  $|E|$  for an isolated doublet to  $|E|'$ , the field of that doublet in the given ideal reflector, at a given distance  $r$  from the isolated doublet or from the apex of the reflector: the value of  $\alpha$  is to be read from Figs. 14.22 to 14.24. Then we have

$$P = \frac{ck}{G} \{Fr\alpha|E|'\}^2.$$

Presuming that the monitor is placed at  $\frac{1}{2}\lambda$  in front of the aerial in the reflector then we have the values shown collected in the following table:

TABLE 14.3

	$F$	$G$	$\alpha$	$ar$	$(\alpha Far)^2/G$	Field for given $P$
Isolated half-aerial .	1	1	1	$\pi$	$\pi^2$	1
$90^\circ \left\{ \begin{array}{l} R/\lambda = \frac{1}{2} \\ R/\lambda = \frac{3}{2} \end{array} \right.$	4	10	0.9	$2.0\pi$	$5.20\pi^2$	0.44
	4	20	0.77	$4.0\pi$	$7.50\pi^2$	0.37
$60^\circ \left\{ \begin{array}{l} R/\lambda = \frac{1}{2} \\ R/\lambda = \frac{3}{4} \end{array} \right.$	3.7	16	1.1	$2.0\pi$	$4.20\pi^2$	0.44
	5	32	0.56	$5.4\pi$	$7.00\pi^2$	0.38

This table shows that, for a given power, the field at  $\frac{1}{2}\lambda$  in front of the aerial depends little on  $\beta$  or  $R/\lambda$ . But if the field is measured behind the aerial, at  $ar = 1.4\pi$ , in a  $60^\circ$  Vee in which  $R/\lambda = \frac{3}{4}$ , then the relative field per unit power is 1.2.

The values recorded in the above table relate to infinite sheets and

accordingly we must inquire how much they are likely to be affected by sheets of finite width, and this inquiry will require some experiments. For this purpose a pair of screens 8 ft. high were covered with copper gauze and used to form a Vee excited by a half-wave aerial, at  $\lambda = 125$  cm., on their bisector and parallel to their junction line: the screens were thus  $2\lambda$  high, in the direction parallel to the aerial. The screens were set at  $90^\circ$  to one another and then had a width of  $2\lambda$  and so the aperture was  $2.82\lambda$  wide and  $2\lambda$  high. A half-wave aerial was set at  $\frac{1}{2}\lambda$  from the apex (i.e. 62.5 cm.) and the monitor aerial ( $\frac{1}{2}\lambda$  long) was used to measure the relative values of  $|E|$  along the bisector in the range of distance between 100 and 250 cm. from the apex, and thus extended beyond the aperture plane. Taking  $r/\lambda = 1$  as the fiducial point (i.e.  $\frac{1}{2}\lambda$  in front of the aerial), it was found that the relative field strengths agreed perfectly with curve *A* in Fig. 14.22 in the range of  $ar$  between 5 and 13. The relative agreement being within the limits of experimental accuracy, it is not necessary to record these experiments in a figure, since Fig. 14.22 serves this purpose completely. Comparison of curves *A* and *B* in this figure shows that  $|E|$  departs appreciably from a  $1/ar$  law in this range. This experiment shows that, with  $R/\lambda = \frac{1}{2}$ , sheets  $2\lambda \times 2\lambda$  suffice to produce a field distribution along the bisector which has, in the range explored, just that departure from the  $1/ar$  law which would obtain if the sheets extended to infinity. Then presumably we may have confidence, in these circumstances, in the value deduced for *P* from a value of  $|E|$  derived from a monitor aerial.

The aerial was then placed at  $R/\lambda = \frac{3}{2}$  and the width of the screens was increased from 2 to  $3.5\lambda$ . The observed relation between current in the monitor aerial and distance along the bisector is shown by curve *A* in Fig. 14.25. Curve *B* in the same figure shows the current which would have obtained if the sheets had been infinite the current scale being chosen to make the two curves agree at  $r = 240$  cm. (i.e.  $0.42\lambda$  in front of the aerial). Here the plane of the aperture was 310 cm. from the apex and this was about one  $\lambda$  in front of the aerial. Taking the chosen fiducial point makes the agreement good on most of the region behind the aerial, and especially so at and near that maximum which occurs at  $ar = 50$  cm. The experimental curve passes through a maximum at  $ar = 140$ , whereas the calculated curve is shown as rising without limit. The discrepancy here is to be expected and doubtless arises mainly from the method of calculating the field of the doublet in the Vee. The field would rise to infinity at the doublet, but would attain a finite value very near the surface of the tuned half-wave

aerial. The discrepancy in the range between 140 and 160 cm. is due to the source being a half-wave aerial and not a doublet and is unlikely to be due to the finite size of sheets. On the other hand, the discrepancy in the range 240 to 320 cm. is almost certainly due to the finite size of the sheets, for we see that the field decreases much more rapidly with distance than it would do in the ideal problem. A general view of the

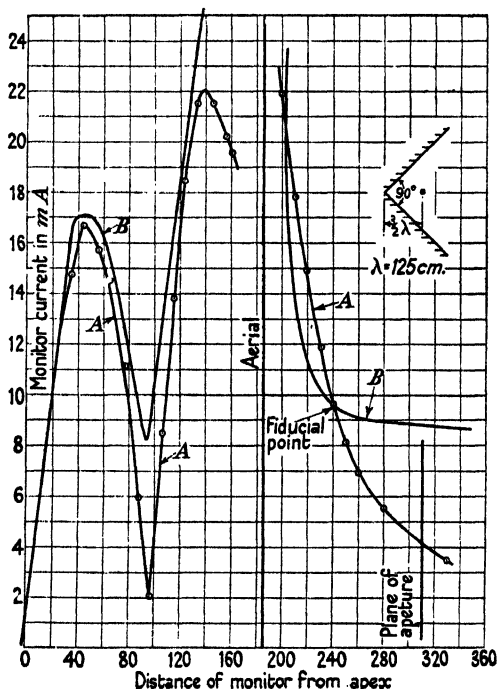


FIG. 14.25. Doublet in  $90^\circ$  mirror,  $R/\lambda = \frac{3}{2}$ ,  $\lambda = 125 \text{ cm.}$

comparison suggests that the relative distribution up to  $r/\lambda = 2$  is in substantial agreement with the distribution in the idealized problem and that, accordingly, a monitor aerial may be placed at any suitable point inside this range. Unquestionably the most suitable point is at the maximum at  $r = 50 \text{ cm.}$  It seems probable that the output of the aerial will then be the same as that of an aerial in an idealized  $90^\circ$  Vee and producing the same field strength at that point of maximum. This process will probably give the correct output of the aerial, but this will not suffice to give the correct value of the forward field at a distant point: indeed, this is shown up in the figure by the discrepancy in the range  $r = 240$  to  $320 \text{ cm.}$  If a measure is then made of the power required to produce the same forward field by an isolated aerial, then

the gain of the given reflector should equal the ratio of these two power measurements.

Screens  $2\lambda \times 2\lambda$  were then set at  $60^\circ$  to one another and excited by an aerial at  $\frac{1}{2}\lambda$  from the apex. The current induced in the monitor aerial was recorded as the monitor was moved continuously from 80 to 240 cm. from the apex, being then 30 cm. in front of the aperture plane. In the range of observation the current varied precisely in the inverse ratio of the distance from the apex. The test was repeated with the aerial distant  $0.42\lambda$  and  $0.58\lambda$  from the apex and in both cases the product of the monitor current and distance from the apex was constant. These last experiments show all that it is necessary to know about the dependence of the response on the position of the monitor, and it seems likely that the field strength has the value appropriate to infinite sheets and thus will serve for the purpose of deducing the output.

The width of the screens was then increased from  $2\lambda$  to  $3.5\lambda$  and the aerial was placed at  $\frac{3}{2}\lambda$  from the apex. The curve relating the observed values of monitor current and distance is reproduced in Fig. 14.26: this figure bears a marked resemblance to Fig. 14.24 which relates to  $r/\lambda = \frac{5}{4}$  (vice  $\frac{3}{2}$ ). The value of  $|E|$  was calculated for  $r/\lambda = \frac{1}{2}, \frac{3}{4},$  and 1, and these values are marked with crosses in the figure, the scale being chosen so as to fit the experimental value at  $r/\lambda = 2$ . Such points show that the relative agreement is well maintained over the scope of the figure. The proper place to locate the monitor is clearly at  $r/\lambda = 0.65$ , the exact location of the maximum being found experimentally in any given application.

When screens  $2\lambda \times 2\lambda$  were inclined at  $45^\circ$  to one another and the aerial was at  $r/\lambda = \frac{1}{2}$  the monitor current was found to vary precisely in the inverse ratio of the distance from the apex in the range of distance between  $0.60\lambda$  and  $2\lambda$ .

The analyses and experiments have disclosed much about the distribution of field in the vicinity of an aerial in a Vee and told us where an aerial ought to be situated for monitoring the power output. The existence of a maximum between the apex and the aerial, if this is more distant than  $\lambda$  from the apex, is very germane to our problem and requirement. For the flat top of a maximum is a very favourable spot at which to locate the monitor because then the response will be independent of small accidental displacements, such as may well occur in service. Moreover, the monitor will then be snugly housed in a place where it is very unlikely to be damaged or tampered with; its response should then be a very reliable measure of the temporal variations of

output, from any causes whatsoever, over a long period of time. It seems highly probable that the field at this point is independent of the size of the sheets, and accordingly the response of the monitor can be converted to read in terms of the total output, the conversion factor being calculable from the solution of the idealized problem.

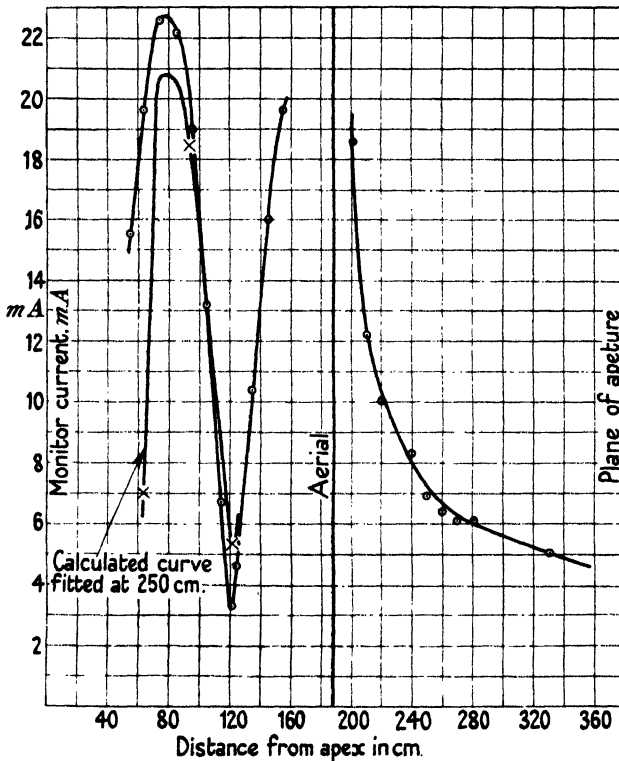


FIG. 14.26. Doublet in  $60^\circ$  mirror,  $R/\lambda = \frac{3}{2}$ ,  $\lambda = 125$  cm.

During recent years much good work has been done on the development of wattmeters for measuring the power passing along a coaxial cable. It would be very instructive to make a systematic comparison of the power supplied through the coaxial cable, feeding the half-wave aerial, and the output deduced from the response of the monitor aerial. Such an exercise should include an exploration of the effect of the height and width of the screen. If the work was carried out exhaustively it would ultimately make it possible to detect any unsuspected losses in the aerial mounting or in moisture films on the screens themselves. The time will come when it will be desired to specify 'acceptance tests' on the output from the aerial, and it seems likely such tests could be



based on the response of a suitably constructed and situated monitor aerial.

### 14.9. Yagi arrays

In § 2.21 we examined the pattern of a curtain in which adjacent currents are equal and opposite. In such circumstances the distant field along the normal to the curtain must be zero (if the number of members is even), and the field in the plane of the curtain will be  $N$  times that of one member alone if the side spacing is  $\frac{1}{2}\lambda$ . Equation (2.24) showed that the power gain tended to the limiting value of  $0.78N$  and the resistance of each member to  $93\Omega$ . The system commonly called a Yagi aerial is an attempt to excite a curtain in this manner by means of a single driven aerial, forming one of its members. Like reflecting screens it is a device for reducing the number of feeding cables demanded by a conventional broadside array.

If a curtain, of conventional form, has only its middle member fed with power, then experience shows that the dominant field strength is in the plane of the curtain, and this means that the driven aerial excites currents which are successively substantially in antiphase with one another. This being so it is natural to excite the end member of the curtain and to place a reflecting screen, or its equivalent, perpendicular to the plane of the curtain and near the driven member. Then the resulting pattern will be mainly in one sense only and in the plane of the array. The sharpness of the beam will increase with the number of members, but it is not surprising to find that a limit is approached, because the induced current is likely to diminish along the length of the curtain. The device was described by Hidetsugu Yagi in 1928† who referred to the row of aerials as a 'wave canal'. He records a polar diagram resulting from 20 undriven members (see Fig. 13, loc. cit.), and its beam width, at half-height, is about  $8^\circ$ .

Though the writer has often used Yagi aerials he has not had experience of developing them and therefore shrinks from writing much on the subject. The process of development must consist of an *ad hoc* determination of the length and spacing of the members to give the best over-all performance. He will draw from the experience of Mr. R. V. Alred.‡ Fig. 14.27 shows a drawing of an 8-member Yagi aerial developed for use in the Royal Navy at  $\lambda = 50$  cm. Polar diagram (b) in the same figure relates to the field strength in the equatorial plane

† See *Proc. Inst. Rad. Engrs.* **16**, 715.

‡ See *Journ. I.E.E.* **93** (1947), Part III.

and diagram (a) to the field in the plane of electric field. The first 'director rod' was distant  $0.28\lambda$  from the driven dipole and the distance between successive directors was  $0.37\lambda$ , these spacings having been found to give the best polar diagram: the length of the directors was  $0.40\lambda$  and it is said that this length was not very critical. The main beam was included within an angle of  $60^\circ$  and the pattern was very

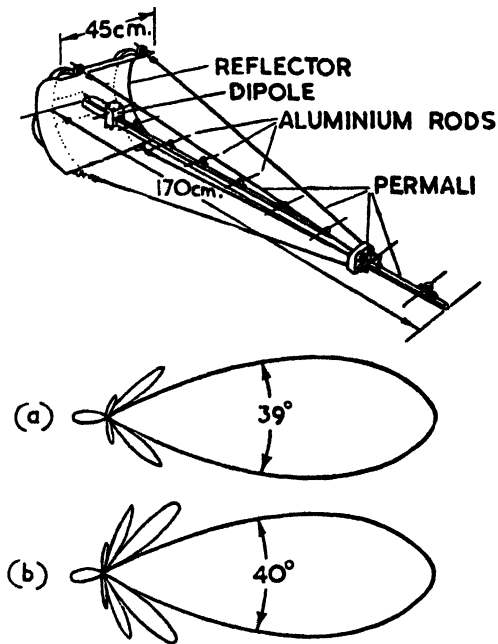


FIG. 14.27.

similar to what would have been obtained from a  $60^\circ$  Vee, or trough, with the aerial at  $\frac{1}{2}\lambda$  from the apex: the side lobes were larger than would have obtained with a Vee. The bearings for zero field were at  $30^\circ$ ,  $60^\circ$ , and  $80^\circ$  from the axis of the main beam. The equation for the pattern of a 9-member array with equal and opposite currents and  $\frac{1}{2}\lambda$  spacing is given in (2.22), and for it the bearings of zero field are  $39^\circ$ ,  $56^\circ$ ,  $70^\circ$ , and  $84^\circ$ . To allow for the reflector this pattern must be multiplied by the pattern for an unlike pair of currents separated by about  $4.5\lambda$ , and then the first zero of field would be at  $12^\circ$  from the plane of the array. Looked at in this way it would seem that the width of the main beam in the equatorial plane of a Yagi should depend very much on the size and position of the reflector.

The general principle of action of a Yagi aerial seems quite clear.

Basically it is a curtain array in which successive currents should be equal and opposite and spaced  $\frac{1}{2}\lambda$  apart: then the field will be zero along the normal to the curtain and  $N$  times that of one current in the plane of the curtain. A reflecting sheet, or its equivalent, at one end will restrict the field to one direction in the plane of the curtain. If the curtain is excited by only one driven aerial it is unlikely that successive

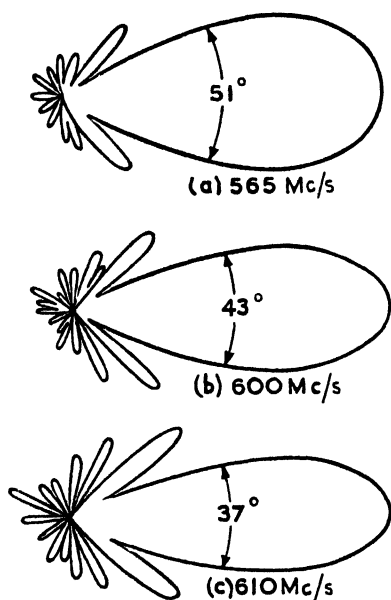


FIG. 14.28.

currents will in fact be equal even if they are substantially opposite, and the advantage of additional members is likely to be subject to diminishing returns: the optimum spacings and the total number of members must be determined by *ad hoc* experiment.

Fig. 14.28 (Alred, loc. cit.) is very instructive in showing the manner in which the equatorial pattern changes with frequency: Fig. (c) in it shows that a narrowing of the main beam is accompanied by an increase in the size of the first pair of side lobes, and doubtless this corresponds to an approach to a condition of zero forward field, when the main beam is replaced by a bifurcated beam. It suggests that (a) in this figure is the nearest approach to the pattern inherent to an ideal Yagi (i.e. successive currents equal and opposite), but that (b) might be deemed a preferable pattern for practical applications.

As a device for producing a reasonably sharp beam from one driven

aerial the Yagi system does not appear to offer any technical advantage over the use of reflecting sheets and it must require more development by process of blind experimentation. It does, however, offer an alternative method of mechanical construction which might offer advantages in some given application. However, it is worth remembering that a Vee in which the reflecting sheets are represented by a comb of rods (see Tables 11.2 and 11.3, pp. 396, 397) would have precisely the same mechanical construction as a Yagi and would not require any development by experimentation, since its behaviour is known to be very near that of an ideal Vee. Thus it would seem that the comb Vee is a better technical solution than the Yagi, while employing the same mechanical construction.

A metal tube is often used as the rod to support the members of a Yagi and then they are welded to it.

Alred (*loc. cit.*) describes experiments in which several parallel Yagi arrays were operated in parallel, and he shows that the resultant pattern is substantially the product of that for one isolated array with the pattern for a curtain having the same number of members as there were Yagi aerials. Thus his experiments were the counterpart of our experiments with two Vee's side by side and these are described in § 12.2.

For a valuable analysis of the design and behaviour of Yagi aerials, the reader is referred to a paper by R. M. Fishenden and E. R. Wiblin, *Proc. I.E.E.* 96 (1949), Part III, 5.

# TABLES OF BESSEL FUNCTIONS

From N. W. McLACHLAN, *Bessel Functions for Engineers*  
(Oxford: Clarendon Press, 1934)

## $J_0(z)$

$z$	0	0.1	0.2	0.3	0.4	0.5	0.6	0.7	0.8	0.9
0	1.0000	0.9975	0.9900	0.9776	0.9604	0.9385	0.9120	0.8812	0.8463	0.8075
1	0.7852	0.7198	0.6711	0.6201	0.5669	0.5118	0.4554	0.3980	0.3400	0.2818
2	0.2239	0.1666	0.1104	0.0655	0.0035	-0.0464	-0.0968	-0.1424	-0.1850	-0.2243
3	-0.2601	-0.2921	-0.3202	-0.3443	-0.3643	-0.3801	-0.3918	-0.3992	-0.4026	-0.4018
4	-0.3971	-0.3887	-0.3766	-0.3610	-0.3423	-0.3206	-0.2961	-0.2693	-0.2404	-0.2097
5	-0.1776	-0.1443	-0.1103	-0.0758	-0.0412	-0.0068	0.0270	+0.0599	0.0917	0.1220
6	0.1506	0.1773	0.2017	0.2235	0.2433	0.2601	0.2740	0.2851	0.2931	0.2981
7	0.3001	0.2991	0.2951	0.2882	0.2786	0.2663	0.2516	0.2346	0.2164	0.1964
8	0.1717	0.1475	0.1222	0.0960	0.0692	0.0419	0.0148	-0.0125	-0.0392	-0.0653
9	-0.0903	-0.1142	-0.1367	-0.1577	-0.1768	-0.1939	-0.2090	-0.2218	-0.2323	-0.2403
10	-0.2459	-0.2490	-0.2496	-0.2477	-0.2434	-0.2366	-0.2276	-0.2164	-0.2032	-0.1881
11	-0.1712	-0.1528	-0.1330	-0.1121	-0.0902	-0.0677	-0.0446	-0.0213	+0.0020	0.0250
12	0.0477	0.0697	0.0908	0.1108	0.1296	0.1469	0.1626	0.1766	0.1887	0.1988
13	0.3069	0.3129	0.3167	0.3183	0.3177	0.3150	0.3101	0.3032	0.2943	0.2836
14	0.1711	0.1570	0.1414	0.1245	0.1065	0.0875	0.0679	0.0476	0.0271	0.0064
15	-0.0142	-0.0346	-0.0544	-0.0736	-0.0919	-0.1092	-0.1263	-0.1401	-0.1533	-0.1660

When  $z > 15.9$ ,

$$J_0(z) \doteq \sqrt{\left(\frac{2}{\pi z}\right)} \left\{ \sin\left(z + \frac{1}{2}\pi\right) + \frac{1}{8z} \sin\left(z - \frac{1}{2}\pi\right) \right\} \\ \doteq \frac{0.7979}{\sqrt{z}} \left\{ \sin(57.296z + 45)^\circ + \frac{1}{8z} \sin(57.296z - 45)^\circ \right\}.$$

## $J_1(z)$

$z$	0	0.1	0.2	0.3	0.4	0.5	0.6	0.7	0.8	0.9
0	0.0000	0.0499	0.0895	0.1283	0.1660	0.2023	0.2367	0.2590	0.2688	0.4069
1	0.4401	0.4709	0.4983	0.5220	0.5419	0.5579	0.5699	0.5778	0.5815	0.5812
2	0.5787	0.5683	0.5560	0.5399	0.5202	0.4971	0.4708	0.4416	0.4097	0.3764
3	0.3391	0.3069	0.2618	0.2307	0.1792	0.1374	0.0955	0.0638	0.0128	-0.0372
4	-0.0660	-0.1033	-0.1386	-0.1719	-0.2028	-0.2311	-0.2566	-0.2791	-0.2985	-0.3147
5	-0.3276	-0.3371	-0.3432	-0.3460	-0.3453	-0.3414	-0.3343	-0.3241	-0.3110	-0.2961
6	-0.2767	-0.2559	-0.2329	-0.2081	-0.1816	-0.1538	-0.1250	-0.0955	-0.0653	-0.0349
7	-0.0047	+0.0252	0.0543	0.0826	0.1096	0.1352	0.1592	0.1813	0.2014	0.2192
8	0.2346	0.2476	0.2580	0.2657	0.2708	0.2731	0.2728	0.2697	0.2641	0.2559
9	0.2453	0.2324	0.2174	0.2004	0.1816	0.1613	0.1396	0.1166	0.0928	0.0684
10	0.0465	0.0184	-0.0068	-0.0313	-0.0555	-0.0789	-0.1012	-0.1224	-0.1422	-0.1603
11	-0.1768	-0.1913	-0.2039	-0.2143	-0.2225	-0.2284	-0.2320	-0.2333	-0.2323	-0.2290
12	-0.2324	-0.2157	-0.2060	-0.1942	-0.1807	-0.1655	-0.1487	-0.1307	-0.1114	-0.0919
13	-0.0703	-0.0489	-0.0271	-0.0052	+0.0166	0.0380	0.0590	0.0791	0.0984	0.1165
14	0.1334	0.1488	0.1636	0.1747	0.1820	0.1864	0.1909	0.2043	0.2066	0.2089
15	0.2081	0.2013	0.1955	0.1879	0.1784	0.1672	0.1544	0.1402	0.1247	0.1080

When  $z > 15.9$ ,

$$J_1(z) \doteq \sqrt{\left(\frac{2}{\pi z}\right)} \left\{ \sin\left(z - \frac{1}{2}\pi\right) + \frac{3}{8z} \sin\left(z + \frac{1}{2}\pi\right) \right\} \\ \doteq \frac{0.7979}{\sqrt{z}} \left\{ \sin(57.296z - 45)^\circ + \frac{3}{8z} \sin(57.296z + 45)^\circ \right\}.$$

$Y_0(z)$ 

$z$	0	0.1	0.2	0.3	0.4	0.5	0.6	0.7	0.8	0.9
0	$-\infty$	-1.534	-1.081	-0.8073	-0.6060	-0.4445	-0.3085	-0.1907	-0.0868	+0.0066
1	0.0883	0.1622	0.2281	0.2866	0.3379	0.3824	0.4204	0.4520	0.4774	0.4968
2	0.5104	0.5183	0.5208	0.5181	0.5104	0.4981	0.4813	0.4605	0.4359	0.4079
3	0.3769	0.3431	0.3071	0.2691	0.2296	0.1890	0.1477	0.1061	0.0645	0.0234
4	-0.0169	-0.0561	-0.0938	-0.1296	-0.1633	-0.1947	-0.2235	-0.2494	-0.2723	-0.2921
5	-0.3085	-0.3216	-0.3313	-0.3374	-0.3402	-0.3395	-0.3354	-0.3282	-0.3177	-0.3044
6	-0.2982	-0.2694	-0.2483	-0.2251	-0.1999	-0.1732	-0.1452	-0.1162	-0.0864	-0.0563
7	-0.0359	+0.0042	0.0339	0.0628	0.0907	0.1173	0.1424	0.1658	0.1873	0.2065
8	0.2235	0.2381	0.2501	0.2595	0.2663	0.2703	0.2715	0.2700	0.2659	0.2592
9	0.2499	0.2383	0.2245	0.2088	0.1907	0.1712	0.1502	0.1279	0.1045	0.0804
10	0.0557	0.0307	0.0056	-0.0193	-0.0487	-0.0675	-0.0804	-0.1122	-0.1336	-0.1516
11	-0.1688	-0.1843	-0.1977	-0.2091	-0.2183	-0.2262	-0.2399	-0.2522	-0.2622	-0.2798
12	-0.2252	-0.2184	-0.2095	-0.1986	-0.1858	-0.1712	-0.1551	-0.1375	-0.1187	-0.0989
13	-0.0782	-0.0669	-0.0532	-0.0434	+0.0085	+0.0301	+0.0512	0.0717	0.0913	0.1099
14	0.1372	0.1431	0.1575	0.1703	0.1812	0.1903	0.1974	0.2025	0.2056	0.2068
15	0.2055	0.2023	0.1973	0.1902	0.1813	0.1706	0.1584	0.1446	0.1295	0.1132

When  $z > 15.9$ ,

$$Y_0(z) \doteq \sqrt{\left(\frac{2}{\pi z}\right)} \left\{ \sin\left(z - \frac{1}{2}\pi\right) - \frac{1}{8z} \sin\left(z + \frac{1}{2}\pi\right) \right\}$$

$$\doteq \frac{0.7979}{\sqrt{z}} \left\{ \sin(57.296z - 45)^\circ - \frac{1}{8z} \sin(57.296z + 45)^\circ \right\}.$$

 $Y_1(z)$ 

$z$	0	0.1	0.2	0.3	0.4	0.5	0.6	0.7	0.8	0.9
0	$-\infty$	-6.459	-3.324	-2.293	-1.781	-1.471	-1.260	-1.103	-0.9781	-0.8731
1	-0.7812	-0.6981	-0.6311	-0.5485	-0.4791	-0.4133	-0.3476	-0.2847	-0.2337	-0.1644
2	-0.1070	-0.0617	+0.0015	+0.0623	0.1005	0.1459	0.1884	0.2276	0.2635	0.2959
3	0.2247	0.2496	0.2707	0.2879	0.4010	0.4102	0.4184	0.4167	0.4141	0.4078
4	0.2979	0.2846	0.2680	0.2484	0.2260	0.2010	0.2737	0.2445	0.2136	0.1812
5	0.1479	0.1137	0.0792	0.0445	0.0101	-0.0238	-0.0568	-0.0887	-0.1192	-0.1481
6	-0.1780	-0.1998	-0.2223	-0.2423	-0.2596	-0.2741	-0.2887	-0.2946	-0.3002	-0.3029
7	-0.3027	-0.2995	-0.2984	-0.2946	-0.2731	-0.2591	-0.2428	-0.2243	-0.2039	-0.1817
8	-0.1581	-0.1331	-0.1072	-0.0806	-0.0535	-0.0262	+0.0011	+0.0280	0.0544	0.0799
9	+0.1043	0.1375	0.1491	0.1691	0.1871	0.2032	0.2171	0.2287	0.2379	0.2447
10	0.2490	0.2508	0.2502	0.2471	0.2416	0.2337	0.2236	0.2114	0.1973	0.1813
11	0.1637	0.1446	0.1243	0.1029	0.0807	0.0579	0.0348	0.0114	-0.0118	-0.0347
12	-0.0571	-0.0787	-0.0994	-0.1189	-0.1371	-0.1538	-0.1689	-0.1821	-0.1935	-0.2028
13	-0.2101	-0.2182	-0.2182	-0.2190	-0.2176	-0.2140	-0.2084	-0.2007	-0.1913	-0.1798
14	-0.1666	-0.1520	-0.1389	-0.1186	-0.1003	-0.0810	-0.0612	-0.0408	-0.0203	+0.0006
15	0.0211	0.0413	0.0609	0.0799	0.0979	0.1148	0.1305	0.1447	0.1575	0.1686

When  $z > 15.9$ ,

$$Y_1(z) \doteq \sqrt{\left(\frac{2}{\pi z}\right)} \left\{ \sin\left(z - \frac{3}{2}\pi\right) + \frac{3}{8z} \sin\left(z - \frac{1}{2}\pi\right) \right\}$$

$$\doteq \frac{0.7979}{\sqrt{z}} \left\{ \sin(57.296z - 135)^\circ + \frac{3}{8z} \sin(57.296z - 45)^\circ \right\}.$$

## A SHORT LIST OF FORMULAE

(For a more complete list, see McLachlan, *Bessel Functions for Engineers*, p. 157)

1.  $J_{-n}(z) = (-1)^n J_n(z)$ ;  $J_n(-z) = (-1)^n J_n(z)$ ;  $J_{-n}(z) = J_n(-z)$ .
2.  $zJ'_\nu(z) = \nu J_\nu(z) - zJ_{\nu+1}(z)$ .
3.  $zJ'_\nu(z) = -\nu J_\nu(z) + zJ_{\nu-1}(z)$ .
4.  $2J'_\nu(z) = J_{\nu-1}(z) - J_{\nu+1}(z)$ , by addition from 2 and 3.
5.  $\frac{2\nu}{z} J_\nu(z) = J_{\nu+1}(z) + J_{\nu-1}(z)$ , by subtraction from 2 and 3.
6.  $Y_\nu(z)$  satisfies recurrence formulae of the type given in 2-5 inclusive;  $Y_n(z)$  satisfies the form given in 1.
7.  $I_\nu(z) = i^{-\nu} J_\nu(zi)$ ;  $I_n(z) = i^n J_n(-zi)$ .
8.  $zI'_\nu(z) = -\nu I_\nu(z) + zI_{\nu-1}(z)$ .
9.  $2I'_\nu(z) = I_{\nu-1}(z) + I_{\nu+1}(z)$ .
10.  $\frac{2\nu}{z} I_\nu(z) = I_{\nu-1}(z) - I_{\nu+1}(z)$ .
11.  $I'_0(z) = I_1(z)$ .
12.  $zK'_\nu(z) = \nu K_\nu(z) - zK_{\nu+1}(z)$ .
13.  $zK'_\nu(z) = -\nu K_\nu(z) - zK_{\nu-1}(z)$ .
14.  $2K'_\nu(z) = -[K_{\nu-1}(z) + K_{\nu+1}(z)]$ , from 12 and 13 by addition.
15.  $\frac{2\nu}{z} K_\nu(z) = K_{\nu+1}(z) - K_{\nu-1}(z)$ , from 12 and 13 by subtraction.
16.  $K'_0(z) = -K_1(z)$ .
17.  $J_\nu(z) = \frac{(\frac{1}{2}z)^\nu}{\Gamma(\nu+1)} \left\{ 1 - \frac{(\frac{1}{2}z)^2}{(\nu+1)} + \frac{(\frac{1}{2}z)^4}{2!(\nu+1)(\nu+2)} - \frac{(\frac{1}{2}z)^6}{3!(\nu+1)(\nu+2)(\nu+3)} + \dots \right\}$ .
18.  $J_{\frac{1}{2}}(z) = \sqrt{\left(\frac{2}{\pi z}\right)} \sin z = Y_{-\frac{1}{2}}(z) = H_{-\frac{1}{2}}(z)$ .
19.  $J_{-\frac{1}{2}}(z) = \sqrt{\left(\frac{2}{\pi z}\right)} \cos z = -Y_{\frac{1}{2}}(z) = -H_{\frac{1}{2}}(z)$ .
20.  $Y_0(z) = \frac{2}{\pi} \{ \gamma + \log(\frac{1}{2}z) \} J_0(z) - \frac{2}{\pi} \sum_{r=1}^{\infty} \frac{(-1)^r (\frac{1}{2}z)^{2r}}{(r!)^2} \left\{ 1 + \frac{1}{2} + \frac{1}{3} + \dots + \frac{1}{r} \right\}$ .
21.  $\cos(z \sin \theta) = J_0(z) + 2\{J_2(z) \cos 2\theta + J_4(z) \cos 4\theta + \dots\}$ .
22.  $\sin(z \sin \theta) = 2\{J_1(z) \sin \theta + J_3(z) \sin 3\theta + \dots\}$ .
23.  $\cos(z \cos \theta) = J_0(z) - 2\{J_2(z) \cos 2\theta - J_4(z) \cos 4\theta + \dots\}$ .
24.  $\sin(z \cos \theta) = 2\{J_1(z) \cos \theta - J_3(z) \cos 3\theta + \dots\}$ .
25.  $\cos z = J_0(z) - 2\{J_2(z) - J_4(z) + J_6(z) - \dots\}$ , from 21,  $\theta = \frac{1}{2}\pi$ , or from 23,  $\theta = 0$ .
26.  $\sin z = 2\{J_1(z) - J_3(z) + J_5(z) - \dots\}$ , from 24,  $\theta = 0$ , or from 22,  $\theta = \frac{1}{2}\pi$ .
27.  $z = 2\{J_1(z) + 3J_3(z) + 5J_5(z) + \dots\}$ .
28.  $J_{\nu+1}(z)Y_\nu(z) - J_\nu(z)Y_{\nu+1}(z) = 2/\pi z$ .
29.  $I_n(z)K_{n+1}(z) + I_{n+1}(z)K_n(z) = 1/z$ .
30.  $J_0(z)$  tends to  $-Y_1(z)$ , when  $z \rightarrow \infty$ .
31.  $J_1(z)$  tends to  $Y_0(z)$ , when  $z \rightarrow \infty$ .
32.  $J_{\nu+1}(z)$  tends to  $-J_{\nu-1}(z)$ , when  $z \rightarrow \infty$ .
33.  $J_n(z)Y_n(z) = -\frac{1}{n\pi}$ , when  $z$  tends to zero, for all values of  $n$  save  $n = 0$ .
34.  $I_1(z)K_1(z) \div \frac{1}{2}$ , when  $z$  tends to zero.

$$35. I_n(z)K_n(z) \doteq \frac{1}{2z} \left\{ 1 - \frac{(4n^2-1)^2}{64z^2} \right\}, \text{ for } z \text{ large.}$$

$$36. J_n^2(z) + Y_n^2(z) > \frac{2/\pi}{z} < \frac{2/\pi}{(z^2-n^2)^{\frac{1}{2}}}, \text{ for } z > n.$$

$$\frac{2/\pi}{(z^2-n^2)^{\frac{1}{2}}} > J_n^2(z) + Y_n^2(z) > \frac{2/\pi}{z}.$$

$$37. \int_0^\infty J_n(z) dz = 1; \quad \int_0^\infty Y_0(z) dz = 0; \quad \int_0^\infty \frac{J_n(az) dz}{z} = \frac{1}{n}, \quad n \neq 0.$$

$$38. \int_0^\infty J_0(az) \sin bz dz = \begin{cases} 0 \\ \infty \\ 1/\sqrt{(b^2-a^2)}. \end{cases}$$

$$39. \int_0^\infty J_0(az) \cos bz dz = \begin{cases} 1/\sqrt{(a^2-b^2)} \\ \infty \\ 0. \end{cases}$$

$$40. \int_0^\infty Y_0(az) \cos bz dz = 0.$$

$$41. \int_0^\infty K_0(az) \cos bz dz = \frac{1}{2} \pi / \sqrt{(a^2+b^2)}.$$

$$42. \int_0^\infty J_0(az) J_1(bz) dz = \begin{cases} 0 \\ 1/(2b) \\ 1/b. \end{cases}$$

$$43. J_0\{\sqrt{(x^2+y^2-2xy \cos \theta)}\} = J_0(x)J_0(y) + 2 \sum_1^\infty J_n(x)J_n(y) \cos n\theta.$$

$$44. Y_0\{\sqrt{(x^2+y^2-2xy \cos \theta)}\} = J_0(x)Y_0(y) + 2 \sum_1^\infty J_n(x)Y_n(y) \cos n\theta, \text{ for } y > x.$$

$$45. J_0\{\sqrt{(x^2+y^2)}\} = J_0(x)J_0(y) - 2J_2(x)J_2(y) + 2J_4(x)J_4(y) - \dots$$

$$46. J_0(x+y) = J_0(x)J_0(y) - 2J_1(x)J_1(y) + 2J_2(x)J_2(y) - \dots$$

$$47. J_1(x+y) = J_0(x)J_1(y) + J_1(x)J_0(y) - J_1(x)J_2(y) - J_2(x)J_1(y) + \dots$$

48. Interesting series are obtained by putting  $x = \pm y$  in 43-7. For example,

$$J_0(2z) = J_0^2(z) - 2J_1^2(z) + 2J_2^2(z) - \dots$$

$$\text{and} \quad 1 = J_0^2(z) + 2J_1^2(z) + 2J_2^2(z) + \dots$$

$$49. 1 = J_0(z) + 2J_2(z) + 2J_4(z) + \dots. \text{ Put } \theta = 0, \text{ in 21.}$$

$$50. 1 - 2J_0(z) + 2J_0(2z) - 2J_0(3z) + 2J_0(4z) \dots = 0, \text{ if } z < \pi.$$

$$51. \sum_0^\infty (-1)^n J_0(nz) = \frac{1}{\sqrt{\{1-(\pi/z)^2\}}}, \text{ for } z > \pi < 2\pi.$$

$$52. J_0(z) + J_0(2z) + J_0(3z) + \dots = \frac{1}{z} - \frac{1}{2}, \text{ if } z < 2\pi$$

$$\text{or} \quad = \frac{1}{z} \left\{ 1 + \frac{2}{\sqrt{\{1-(2\pi/z)^2\}}} \right\} - \frac{1}{2}, \quad \text{if } 4\pi > z > 2\pi.$$



# INDEX

- Aerials with large capacitance roof, 338-9.
- Alred, R. V., 91, 504, 506-7.
- Ampère, A. M., 2, 3, 7, 10, 12, 21-5, 27, 35.
- Array, curtain, 425-8, 470-6.
- alternate elements in antiphase, 111-12.
- of half-wave aerials, 105.
- , parallel to half-plane, 196-8.
- , pattern at any angle of elevation, 99.
- , power output, 489-95.
- , with binomial loading, 90-3.
- , with non-uniform cophased loading, 85-6.
- , with sinusoidal loading, 89-90.
- , with symmetrical but not cophased loading, 470-6.
- , with triangular loading, 86-9.
- , with uniform loading, 82-5.
- , high curtain, 110-11, 144.
- , horizontal dipole, 482-6.
- , in-line, 97-9, 106-10, 122, 145, 150, 154, 176, 241, 326, 465-70.
- in Vee reflector, 150-4.
- of Vee reflectors, 283-5.
- Back-to-front ratio, 193, 195, 215, 234, 235, 386-8, 396, 416, 421, 481-2.
- Baker, B. B., and Copson, E. T., 294.
- Ballantine, Stuart, 330.
- Barrow, W. L., and Lewis, F. D., 450-1.
- Bessel, F. W., 31.
- Bessel functions, general form, 137-9.
- tables, 508-9.
- series for forward field, 139-44.
- Bessel's equation, 31.
- Blodget, Miss, 294-5.
- Bouwkamp, C. J., 325, 327-8.
- Breadth factor defined, 83.
- , 83, 84, 88-91, 98.
- Coaxial tube resonator, 342.
- Comb aerial, 395-7.
- Cornu spiral, 194.
- Current components, distribution in a half-plane, 201-2.
- density, 199-203, 227-32, 237, 242-3, 252, 256, 258-65, 272-4, 280, 291, 296, 301-7, 423, 457-62.
- at Vee apex, 286-8.
- induced in flat infinite sheet, 122-5.
- induced in half-plane, 303-7.
- in semicircular cylinders, 457-62.
- variable across infinite plane, 58-62.
- Cylinder, current flowing round circumference, 258-61.
- Cylinder, external field of current, 263-4.
- perpendicular to electric vector, current in, 218-20.
- , plane wave incident on, 241-51, 261-3.
- , semicircular, 457-62.
- Cylinders, 218-20, 265-323.
- Darbord, R., 447.
- Diffraction pattern defined, 81.
- at finite distance, 165-7.
- patterns, 235, 238, 245, 263, 282, 316, 320, 391, 404-15, 418, 420, 425, 427, 428, 437-46, 454-5, 459, 465, 469-75, 477-8, 481.
- and polar diagrams, 81-117.
- Displacement current defined, 9-12.
- Doublet, electric, 324-9.
- , isolated, 66-70.
- line, 218-20, 260, 264.
- , field of, 54-5.
- , in Vee reflectors, 184-6.
- , parallel to flat sheet, 184-5.
- , ring, 78-80.
- Doublets, 121.
- in mirrors, 496-8, 501.
- Echoed field, 248, 250, 264.
- Edge effect, 199-203.
- Equipment for fieldwork, 341-62.
- Euler, L., 20, 30.
- Ewing, Sir J. A., 350.
- Faraday, M., 6, 7, 9, 10.
- Feeding cables, 144, 145, 217, 484.
- Filament between two parallel conducting planes, 64-6.
- carrying current  $I \cos(\pi y/g) \sin \pi t$ , 38-44.
- current, parallel to infinite plane, 119-25.
- , field of isolated, 28, 38.
- in presence of half-plane, 188-96.
- parallel to metal cylinder, 228-40.
- , isolated, origin not on wire, 50-1.
- Filaments, pair of, 45-8.
- , oppositely directed, 48-50.
- Firing through arrays, 206.
- Fishenden, R. M., and Wiblin, E. R., 507.
- Focus treatment, 249, 250.
- Folded roof aerials, 339.
- Forward field, 233, 234, 240-69.
- , Bessel series for, 128, 139-44.
- curves, 133-44, 225.
- of parabolic cylinders, 431-4.
- of trough reflector, 416.

- Forward field tests of Vee reflectors, 363-8.  
 — gain, *see* Power gain.  
 Fourier, J. B., 20, 21.  
 Franklin coils, 169, 214.  
 Fresnel, A. J., 20.  
 Fresnel's integrals, 142, 194, 308.
- Galvani, L., 2.  
 Galvanometers, experimental, 343-6, 357.  
 Gardiner, M., 34 n.  
 Gauss's theorem, 13.  
 Grating, 490-1.  
 —, infinite plane, 62-4.  
 Gray, A., and Matthews, G. B., 142.  
 Grids, currents induced in, 216-18.  
 Ground slope, effect of, 486-9.
- Half-wave aerial, 97, 100, 101, 105, 106-7, 145, 154, 171-87, 326-9, 431, 447.  
 — — —, field explored by monitor, 358-62.  
 — — — forward gain, 377.  
 — — — inphase component of electric force, 326.  
 — — — in plane of sheet, 389-92.  
 — — — in Vee reflector, radiation resistance, 172-5.  
 — — — opposite middle of rectangular sheet, 386-9.  
 — — — perpendicular to junction of reflecting sheets, 181.  
 — — —, power gain of, 175-7.  
 — — — radiation resistance, 70-2.  
 — — — resonant length, 332-8.  
 — — —, the  $Q$  of, 332-8.  
 Hallen, E., 325, 337.  
 • Harrison, C. W., 325, 338.  
 Heaviside, O., 3, 5.  
 Heaviside current element, 4, 5, 6, 9, 66.  
 Hedgehog patterns, 178, 179, 180, 282, 453-6.  
 Height factor, 330.  
 Hills, aerials on, 265-75.  
 Hipparchus, 19.  
 Huygens, C., 18-20.  
 Huygens' principle, 294.  
 Huygens-Fresnel technique, 275.
- Image systems, 121, 127, 130, 131, 163, 178.  
 Impedance of short thin aerial, 350-8.  
 Infinite sheet, 192, 195-8, 213, 302, 312, 318, 321-3.  
 — — —, field of, 55-62.  
 Isolated aerial, 324-40.
- Jeans, Sir J., 14 n., 113.
- Kelvin, Lord, 9.  
 King, L. V., 338.  
 King, R., 325, 338.  
 Kirchhoff, 294.  
 Kirchhoff's theorem, 453.  
 Kottler, 294.  
 Krauss, J. D., 395, 410.
- Lamb, Sir H., 206.  
 Langley, mean energy of sunlight, 258.  
 Larmore, Sir J., 206.  
 Lömmel, E. C. J. von, 142.  
 Long current filament, 188-96.  
 Lorentz, L., 17, 18, 25.  
 Lorentz's equations, 15.
- Macdonald, H. M., 335.  
 McLachlan, N., 34 n., 116, 272, 508, 510.  
 McPetrie, J. S., 349, 352, 355.  
 McPherson, W. L., and Ullrich, E. H., 447.  
 Maxwell, J. Clerk, 8, 10, 20, 21.  
 Maxwell hypothesis, 7-13, 36, 453.  
 — law, 9, 10, 11.  
 Maxwell's equations, 13-15, 31, 34, 129, 459.  
 Metre-amperes, 98.  
 Michelson, A. A., 91.  
 Monitor aerial, 349-62, 492, 494-504.  
 Morse, P. M., and Rubinstein, P. J., 321.
- Nagy, A. W., 395.  
 Netting sheets compared with continuous sheets, 393-7.  
 Network reflectors, 188-221.  
 Neumann, 6.  
 Newton, I., 19.  
 Non-reflecting chamber, 288-95, 298.
- Obliquity effect, 182.  
 Oersted, H. C., 2, 3.
- Page, H., 482, 488.  
 Page, L., and Adams, N. I., 324.  
 Parabola, 425.  
 — compared with trough reflector, 445-7.  
 — — — Vee reflector, 440-7.  
 Parabolic reflectors, 429-62.  
 Parasitic aerial, 389, 397-400, 405-6, 447-9.  
 — — —, improvement of pattern by, 160.  
 — — — with reflector, 447-9.  
 — rod, *see* Rod reflectors.  
 Pidduck, F. B., 351, 355-6.  
 Pierce, G. W., 339.  
 Pistolkors, A. A., 105.  
 Plane wave incident on cylinder, 241-51, 261-3.  
 — — — on half-plane, 300-1, 307-21.

- Poisson's equation, 17.  
 Polar diagram defined, 81.  
 — diagrams, 225, 226, 236, 245-6, 262-4, 270, 376, 378, 399, 453, 482.  
 Porcupine, *see* Hedgehog patterns.  
 Power gain defined, 100.  
 — —, 105, 211, 233-7.  
 — — of curtain of half-wave aerials, 105.  
 — — of half-wave aerial in Vee reflector, 175-7.  
 — — of high curtain, 110.  
 — — of in-line array in Vee reflector, 150-4.  
 — — of in-line arrays, 106-10.  
 — — of linear aerial, 330.  
 — — of non-uniform loading, 105.  
 — — of parallel half-wave aerials, 101-4.  
 — —, reciprocity in, 168-70.  
 Poynting's theorem, 62, 78, 106, 113-17, 127, 128, 151, 178, 183, 225, 235, 255-7, 291, 336.  
 Priestley, J., 10.  
 Proctor, R. Faraday, 125.
- Radiation resistance, 194, 226, 233, 234, 265.  
 — — of circle radius  $R$ , 72-8.  
 — — of filament in Vee reflector, 144-50.  
 — — of half-wave aerial in Vee reflector, 172-5.  
 — — of linear aerial, 329-32.
- Ratcliffe, J. A., 258.  
 Ray theory, 231, 232, 237, 240, 243, 301.  
 Reciprocal properties of cylinders, 240-1.  
 — — of Vee reflectors, 167-70.  
 Reflecting sheets at right angles, 125-7.  
 — — at any angle, 127-33.  
 — —, resistivity of, 124-5.  
 — —, semi-infinite, 130.  
 Reflector with convex back, 281-2, 421.  
 Retarded functions, 17.  
 Rod reflectors, 210-18.  
 Rods, comb of, 395-7.
- Screening properties of parallel wires, 203-7, 394-7.
- Screening properties of squirrel cage, 207.  
 Semi-infinite sheets, 188-221, 236, 304, 306, 309, 313-21, 388-9.  
 Shadow field, 247, 250-7, 264, 278, 319-21.  
 — ratio, 206, 393.  
 Shunt excitation, 331.  
 Side lobes, 444, 448, 452-6, 468, 470, 471, 473-8, 486.  
 — — flexibility, 97.  
 — — of curtain array, 425-8.  
 — —, power radiated in, 115.  
 — — rigidity, 97.  
 Solenoid, field of, 51-4.  
 Stokes, G. G., 20.
- Trough-shaped reflectors, 415-23, 445.  
 Tubes, *see* Cylinders.  
 Turning the main beam, 93-7, 401-9, 437, 476.  
 — — — — of Vee reflectors, 161-5.
- van der Pol, B., 329.  
 Vee reflectors, equatorial pattern, 369-85.  
 — —, pair of, 409-15.  
 — —, power output, 495-504.  
 — —, tests, 363-85.  
 — — with cylindrical back, 278-86, 423-5.  
 Voigt, 294.  
 Volta, A., 2.
- Walmsley, T., 464.  
 Watson, G. N., 34 n., 51 n., 63, 137, 142, 308.  
 Wave guide and parabola, 449-53.  
 — guides, cut-off property, 296-300.  
 — —, rectangular, 186-7, 295-300.  
 Wavemeters, 342.  
 Weber, 61.  
 Weber-Fechner law, 321.  
 Whittaker, E. T., and Watson, G. N., 51 n.  
 Wilmotte, R. M., 335.
- Yagi, H., 504.  
 Yagi arrays, 111-12, 410, 504-7.  
 Young, T., 19, 20.

PRINTED IN  
GREAT BRITAIN  
AT THE  
UNIVERSITY PRESS  
OXFORD  
BY  
CHARLES BATEY  
PRINTER  
TO THE  
UNIVERSITY

# DATE OF ISSUE

This book must be returned within 3, 7, 14 days of its issue. A fine of ONE ANNA per day will be charged if the book is overdue.

29 Sep 67

